SEQUENCE STRATIGRAPHY AND PALEOPEDOLOGY OF NONMARINE FORELAND BASINS: IGLESIA BASIN, ARGENTINA AND AXHANDLE BASIN, UTAH

A Dissertation

Presented to the Faculty of the Graduate School

of Cornell University

in Partial Fulfillment of the Requirements for the Degree of

Doctor of Philosophy

by

Brian G. Ruskin

August 2006

SEQUENCE STRATIGRAPHY AND PALEOPEDOLOGY OF NONMARINE FORELAND BASINS: IGLESIA BASIN, ARGENTINA AND AXHANDLE BASIN, UTAH

Brian G. Ruskin, Ph.D.

Cornell University 2006

Subdivision of strata into genetically related sequences reflects interaction between extrinsic and intrinsic processes affecting a basin's accommodation potential and environment. In nonmarine settings, sequence bounding surfaces are difficult to locate and several causal mechanisms (tectonism, climate change, and autogenic variability) combine in complex and still poorly-understood ways. However, integrating basin-scale analyses of subsurface and surface stratigraphy can promote interpretations about the magnitude of individual extrinsic forcings and suggest feedback mechanisms for sequence genesis. Extensive field measurements, seismic stratigraphy and facies analyses, and examination of fossil soils (paleosols) are utilized in the Miocene-Pliocene Iglesia wedgetop basin (Central Andean foreland, northwestern Argentina) and the Late Cretaceous-Early Eocene Axhandle wedgetop basin (Sevier foreland, central Utah, USA) to characterize extrinsic variability during nonmarine sequence deposition and refine general base level models.

Seismic stratigraphy of Iglesia Basin is reassessed and compared with correlative outcrops to evaluate tectonic and climatic control of sequence development. Intrabasinal deformation and surface uplift of the Frontal Cordillera of the Andes are documented. In basin-central outcrops, vertical transitions in lithofacies and paleosol characteristics demarcate seismic sequence boundaries. Paleosol profile measurements, stable isotopic ($\delta^{13}C$ and $\delta^{18}O$) time series, micromorphology and clay mineralogic analyses document paleoclimatic variability. Four sequence boundaries

are associated with climate shifts away from semiaridity. Increased aridity occurred at 9 Ma, 6.9 Ma and 5.2 Ma, concurrent with sequence boundary formation. At least three sequence boundaries formed during intervals of concurrent marginal surface uplift and climate shifts that worked in accord to starve the central basin of sediment.

Six stratigraphic sequences are defined between 76 – 49 Ma in Axhandle Basin, central Utah. Previous assessments of the basin's stratigraphy emphasized the role of tectonics. Herein, local paleoclimate variability is explored through analyses of paleosols and their relationship to the proposed stratigraphic sequences.

Previously proposed nonmarine systems tract models are compared with the Axhandle and Iglesia Basin sequences. Models characterized by lithofacies and sedimentary architecture are found to be incongruous with features observed and measured from the test basins' strata because of inadequate spatial, lithologic, aggradation rate and extrinsic mechanism definitions.

BIOGRAPHICAL SKETCH

Brian Ruskin was born December of 1979 in Pittsburgh, Pennsylvania. His early activities centered on art and science, including a short phase painting rocks, which may have suggested a future educational balancing act. This seemingly-incompatible combination of interests meant that Brian had difficulty deciding what he wanted to be when he grew up. For a while, becoming an astronaut was popular, replaced by a semi-serious attempt at cartooning. By high school, Brian became convinced that paleontology was the right field; meanwhile his parents wondered why their son had re-embraced dinosaurs many years after most kids outgrow them.

Weekends during high school, Brian volunteered at the Carnegie Museum of Natural History, sorting fossil fragments in the basement collections, or manning the "Paleo-Lab" exhibit while the professionals were on lunch break. Later, during college, this developed into a paying gig for Brian, and he inherited a back-log of unprepared specimens from the Wind River Basin of Wyoming, a place he would soon visit and love.

One particular weekend, a geologist from the University of Pittsburgh mentioned to Brian that geology was a solid foundation discipline for fledgling paleontologists. Since paleontology isn't a very common undergraduate degree program, Brian enrolled at the University of Pittsburgh in 1997 as a dual major in Geology and Studio Arts, still not willing to make up his mind and abandon either aptitude. This choice turned out to be a good one: it led to research involvements, challenging art projects, field work during two summers in Wyoming, and eventually the decision to pursue stratigraphy as a career. He received Bachelors degrees in Geology and Studio Arts in 2001.

Brian entered Cornell University in August of 2001. Ithaca proved a wondrous

setting in which to live and learn, and the years progressed surprisingly fast. He spent four field seasons in Argentina, two summers in Houston interning with Shell, and enjoyed learning from and with many extraordinary people. He still attempts the balancing act between the creative and scientific mindsets, and hopes to continue recognizing parallels between art and geology in the future.

ACKNOWLEDGEMENTS

Above all else, thanks be to God for the amazing gift of life and the opportunity to use and share His gifts. Without Him, I am nothing.

My deepest gratitude and love to my parents, Jack and Patricia Ruskin, for their constant love and support. They taught me the value of giving my best effort in whatever I attempt. Their selfless generosity while bringing up my brother and I is something I can never fully repay. Though my education has meant times of travel away from home, my parents always encouraged me to enjoy life's opportunities, and they patiently watched my cat until I returned. Also, when emotional difficulties and stresses became too much, they reinforced the value of keeping faith. I am also appreciative of my brother, John, for his friendship and for setting good examples.

My grandparents, James and Catherine Phillips and John and Mary Ruskin, understood the importance of a quality education and made many sacrifices to allow my brother and me to attend private grade school and high school. This provided a structure for conscientious learning and presented challenges and opportunities that directly influenced my future career choices. So, I thank my grandparents for building the framework for this dissertation and many other educational endeavors.

Great respect and appreciation goes to my advisor, Terry Jordan. Her invitation to be her graduate student afforded unimagined opportunities. She had confidence in me when I did not, allowed me to explore intellectual avenues of my choice, and when I was flat-out wrong, her words were always gentle, suggesting better alternatives. In the field, Terry's observational skills are second-to-none. She is also one of the kindest persons I've met, and sets an example of professional humbleness.

I'm also indebted to the wealth of knowledge of the Cornell faculty and members of the Cornell Andes Project. In particular, I'd like to acknowledge the

guidance of my additional committee members, professors Larry Brown and Kerry Cook.

There have been many other geologists and educators who have encouraged and inspired me to pursue research. Special thanks go to members of the University of Pittsburgh Department of Geology: Thomas Anderson (who first invited me to explore geologic research); Jack Donahue, Mark Evans, Bill Harbert, and Harold Rollins, all of whom allowed me to contribute in small ways to their projects. Annie Holmes' (University of Tennessee) passionate teaching of field geology and in particular stratigraphy at University of Missouri's Branson Field Lab in Wyoming definitely inspired my choice of earth science discipline.

Through five years at Cornell and two summers in Houston, I benefited immensely from the attentive ears and wise advice of Father Robert Smith, Phil Fiadino, John Wright and Scot Fraser. I thank them for their professional and spiritual encouragement.

My sincere gratitude and love go to Christina Bové, who has been incredibly patient with me during the last two and a half years, providing encouragement and a great example of dedication. Christina's company also helped me to enjoy life away from work.

For geologists, the term "fieldwork" is quite literal. Though I've heard that "the worst day in the field is still better than a day in the office", that's no consolation when you're lost, hungry and cold in the middle of nowhere! However, I was given opportunities to travel to Argentina four times, to conduct thesis research in some truly spectacular locales, and to broaden my cultural horizons through interactions with the very generous people listed below.

Federico Martina assisted during the 2002 field season, during which he helped dig the truck out of the sand and change flat tires more times than I want to remember!

His patience in the face of logistical nightmares and my limited grasp of Spanish was greatly appreciated and comforting during my first trip to Argentina. Federico and Soledad Dávila graciously opened their home to me during my stay in Córdoba, Argentina, 2002. Facundo Flores (a longtime friend of the Cornell Andes Project) provided excellent field vehicles three years in a row.

Rodrigo Morilla's help in the field went far beyond the call of duty. He served as translator, skilled off-road driver, and carbonate collector extraordinaire. His friendship made rough days in the dust storms and Zonda winds of Iglesia Basin, and long hours in the lab demagnetizing rocks much more enjoyable. I am also indebted to the Morilla family; their hospitality made Argentina feel much closer to home.

During my time at Cornell, I've had the privilege of interacting with fellow members of Terry Jordan's research group: Greg Hoke, Pete Nester, Katie Tamulonis, Juan Pablo Radíc, and Jose Rosario. Their insights and friendship were most appreciated as we together tackled the secrets of the Andes. Thanks also to my fellow graduate students, who provided support and reassurance that we're all in this together! Particular thanks to the following Snee Folks, all very unique and entertaining: Holly Caprio, Gaby Depine, Stephanie Devlin, Danielle Glasgow, Adam Goss, Meghan Herz, Greg Kirkpatrick, Amy Kwiatkowski, Jack Loveless, Neil McGlashan, Jacob "Cubbie" Moore, Herdis Schopka, Tiffany Tchakirides, and of course, Billy. Thanks also to Arthur Bloom for stimulating discussions, and Steve Gallow and Aaron Wade for computing assistance.

Lindsey Trachtenberg diligently separated clay size fractions and assisted with XRD analysis. Her patience saved me much time. Bruce Vaughn (INSTAAR, University of Colorado), Julie Cole (University of Arizona), and Arthur Kasson (Cornell) were very helpful in coordinating stable isotopic analyses. Terry

Spell (UNLV) kindly provided geochronological results. Tim Lawton (NMSU) was a wonderful guide in Axhandle Basin, central Utah. William Harbert (University of Pittsburgh) shared his expertise, guided our work as paleomagnetic technicians and came through with data in the eleventh hour!

Thanks to anyone I've forgotten who has been a friend and resource. You know who you are, and please know that you are appreciated.

TABLE OF CONTENTS:

LIST OF FIGURES:

LIST OF TABLES:

CHAPTER 1: SEQUENCE STRATIGRAPHIC CONCEPTS IN NONMARINE SETTINGS

Subdivisions of genetically related sedimentary rocks, or sequences, reflect the interaction of extrinsic and intrinsic processes within the accommodation space of a depositional basin. Accommodation space is the basin volume in which sediment may accumulate, and is determined by stratigraphic base level. Base level, the equilibrium surface between erosion and deposition, is continually modified through geologic time by changes in global sea level, subsidence, and sediment supply. Those modifications affect stratal geometries and generate sequences (Van Wagoner *et al.*, 1988). A sequence is a "relatively conformable succession of genetically related strata bounded by unconformities and their correlative conformities" (Mitchum *et al.*, 1977). Sequence stratigraphy strives to interpret the controls of stratigraphic base level and the genetic relations of stratigraphic intervals through the study of both the preserved rock units and the bounding surfaces. This technique emphasizes physical correlation of chronostratigraphic surfaces and integrates facies details in a detailed analytical method for ordering and interpreting the stratigraphic record (Shanley and McCabe, 1995). Seismic and stratigraphic techniques following the sequence concept have successfully predicted facies architecture in marginal marine settings, where relative sea level (the combination of eustatic sea level and local tectonic subsidence or uplift) may be equated with stratigraphic base level.

This dissertation analyzes facies architecture within nonmarine stratigraphic sequences and probes the genesis of the sequences. The proceedings of the 1991 NUNA conference on high-resolution sequence stratigraphy (summarized by Shanley and McCabe, 1994) revealed the difficulties inherent in applying sequence concepts to continental strata. Three significant problems raised by the conference still remain to be solved. First, how do fluvial systems correlate with changes in relative sea level?

Secondly, if correlation between coastal plain and marine systems can be established, what are the relative roles of eustatic, tectonic, and climatic variation on the resultant stratigraphy? Finally, and perhaps most problematic to the sequence stratigraphic model as a means of subdividing and interpreting stratal successions, is whether diagnostic surfaces or successions can confidently be located in nonmarine systems. This final concern is addressed in the following chapters using temporally and spatially well-calibrated test basins in northwestern Argentina and Central Utah.

This chapter serves as a summary of the principles of nonmarine sequence stratigraphy as well as the analytical methods utilized in subsequent chapters of this thesis. First, we briefly consider the conceptual controls of sequence genesis, with attention to the difficulties documenting these forcings in the stratigraphic record. Next, we address problems specific to nonmarine alluvial depositional systems. Finally, we outline the features of paleosols that can provide proxy information on the nature of sedimentary hiatuses, which can aid in the interpretation of how depositional controls varied through time, particularly across sequence boundaries.

I. *The concept of stratigraphic base level*

To accumulate sediment, there must be space available to be filled. Accommodation space (introduced by Jervey, 1988) is the volume available for sediment to accumulate in a depositional basin. Realms of accumulation and erosion are separated by a potential surface. This surface is referred to as base level (Figure 1.1). Deposition is possible (but not required) in the volume below base level, whereas erosion is possible (but not required) in the volume above base level. Discussion of base level must distinguish between the geomorphic and stratigraphic applications of the term. Geomorphic base level (*sensu* Davis, 1902) is simply sea level, or the geoidal projection of mean sea level around the Earth (Bloom, 1978). Stratigraphic base level (after Barrell, 1917) is a dynamic equilibrium surface below which

Figure 1.1: A**:** Cartoon of the interplay between stratigraphic base level and the geomorphic landscape, affecting the distribution of erosion and deposition in a given basin. B: Illustration of nonmarine stratigraphic sequence defined by sequence boundaries. The lower boundary is not erosional, but represents a facies change. The upper sequence boundary is erosional. Both boundaries are presumed to be regionally correlative and of significant magnitude to be recognized from autocyclic features.

A

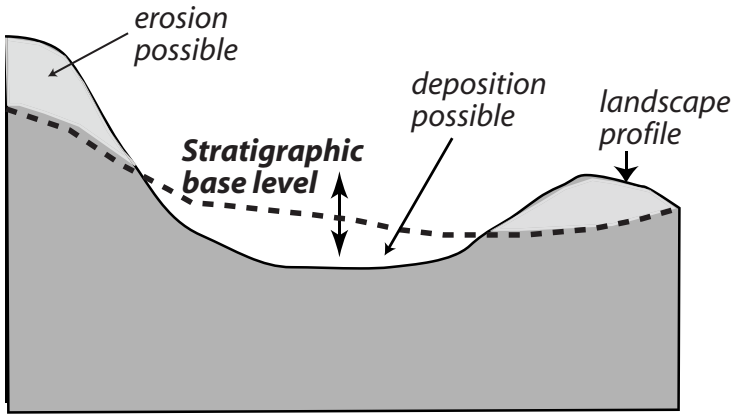
erosion
possible
deposition
possible
landscape
profile
Stratigraphic
base level

B

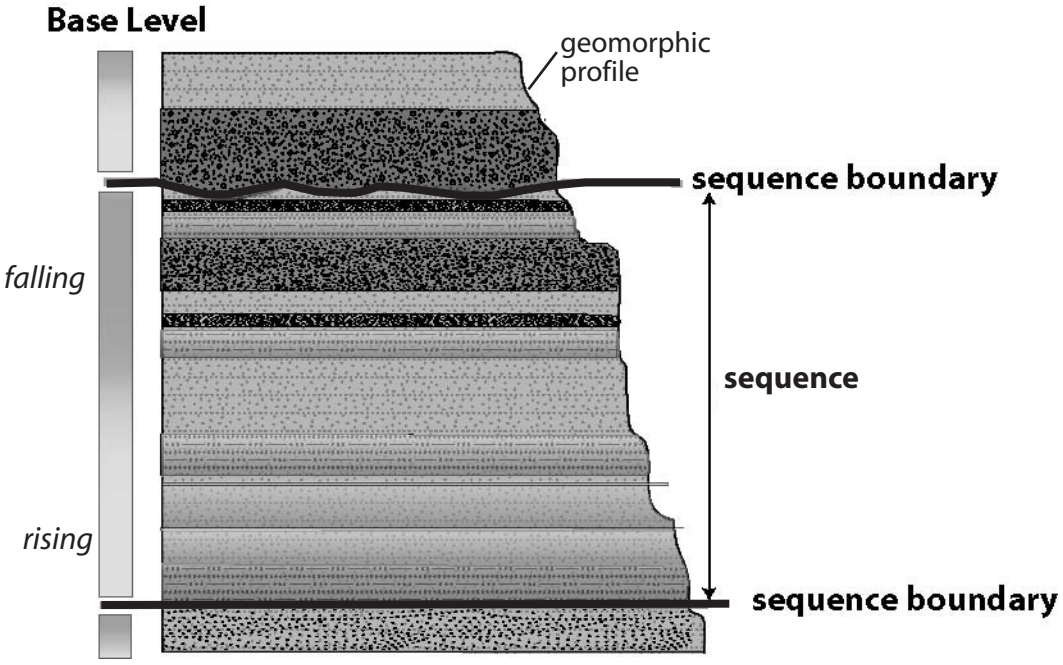
Base Level
geomorphic
profile
sequence boundary
falling
sequence
rising
sequence boundary

sediment may accumulate, and above which, erosion may occur. It is like a potential energy surface, undulating under the influence of tectonism, climate, eustasy, sediment delivery, etc. (Shanley and McCabe, 1994; Figure 1.2). Other definitions have confused the concept through the inclusion of both cause and effect of base level change (adjustment and erosion/deposition; see Sloss, 1962; Wheeler 1964; Schumm, 1993). For alluvial strata, Quirk (1996) suggested the concept of "base profile," essentially an extension of the graded river profile relative to some chronostratigraphic datum, including the effects of climate, sediment supply and hinterland tectonics. A related concept is the "stream equilibrium profile", a hypothetical graded river surface in 2D or depositional surface in 3D (Dalrymple *et al.*, 1998). However, the concept of a graded or equilibrium river profile may not be suitable for all depositional settings. Meanwhile, recent research in near-shore systems has shown fluvial profiles can adjust in complex and perhaps counterintuitive ways to external forcings (e.g. Muto and Swenson, 2006).

The stratigraphic application of base level is rendered abstract by a lack of physicality and also by superimposed variables affecting accommodation potential. Furthermore, Blum and Törnqvist (2000) suggested that stratigraphic base level, the upper limit of accommodation, is not a control of sedimentation but a consequence, and should be abandoned in preference for explicit description of sediment accumulation versus what is actually preserved. Similarly, Martinsen *et al.* (1999) propose an alternative formulation of base level fluctuation which compares accommodation, A (available space), with sediment supply, S as a ratio A/S. For A/S>1, the basin is underfilled. An A/S ratio of unity implies that all available space is filled, but this is an unstable equilibrium condition (flooding or underfilling can still occur). When sediment supply outpaces accommodation space generation (0<A/S<1), sediment accumulation is always possible (though not required), as well as the

Figure 1.2: Schematic representation of various relationships between mechanisms, magnitudes and rates affecting base level cyclicity. Sequence A is deposited during one base level cycle. Sequence B is deposited during one base level cycle, but under less variant conditions than Sequence A. Sequence C deposited under essentially the same magnitude of variability as Sequence A, but at a greater rate. Sequence D deposited under essentially the same magnitude and rate of extrinsic variability as A, but with added intrinsic variability. The more realistic case of Sequence E, deposited as extrinsic and intrinsic variables superimpose in space and time, with variant interference.

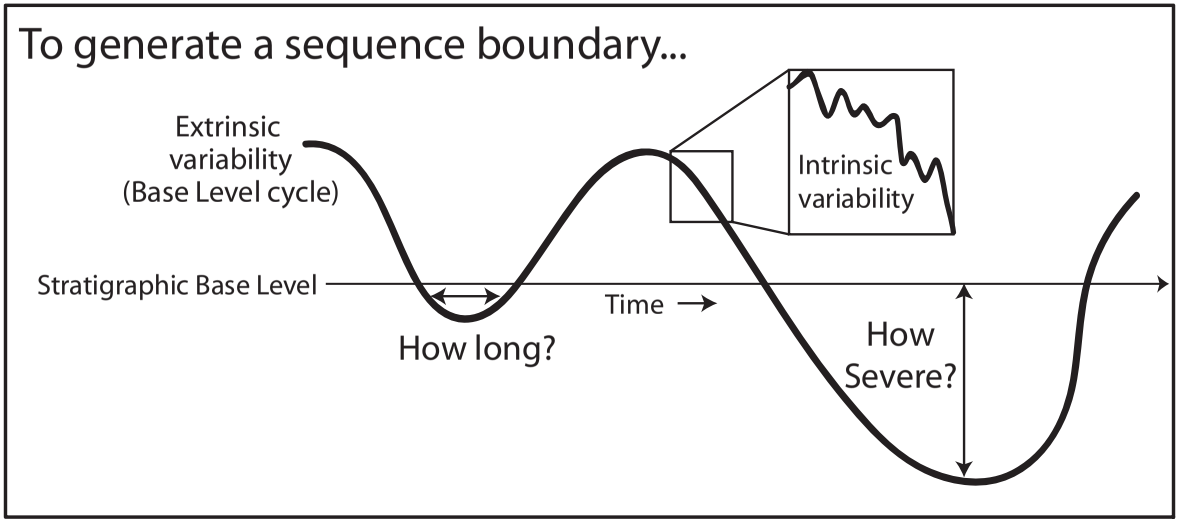
To generate a sequence boundary...
Extrinsic
variability
(Base Level cycle)
Intrinsic
variability
Stratigraphic Base Level
Time
How long?
How
Severe?

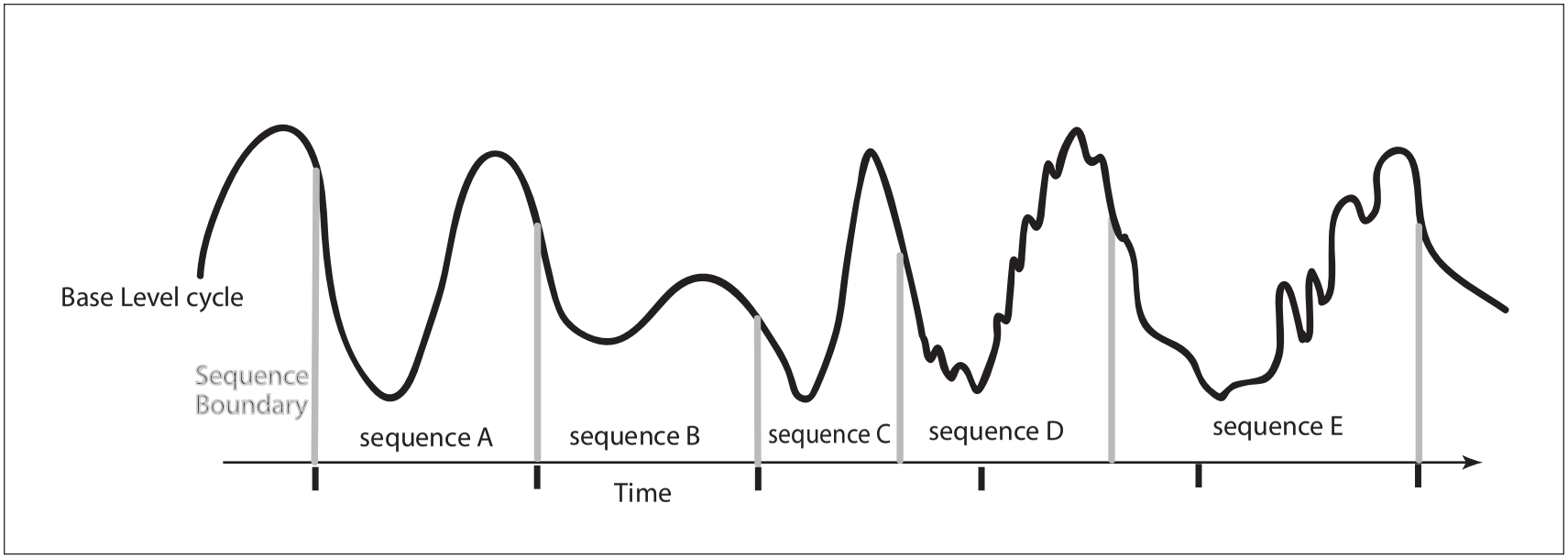
Base Level cycle
Sequence
Boundary
sequence A
sequence B
sequence C
sequence D
sequence E
Time

potential for sediment bypass out of the system. Finally, when no accommodation exists ($A/S \leq 0$), sediment is bypassed and previous deposits eroded (sequence boundary genesis).

II. C*ontrols of nonmarine accommodation:*

The question of what factor or factors provide the space and material necessary to accumulate stratigraphic successions carries with it an implicit concept of scale, both spatial and temporal. On the scale of an entire sedimentary basin, changes in tectonic uplift and subsidence probably exert fundamental control on the location and characteristics of continental (and in particular fluvial) strata (e.g. Sloss, 1991; Leeder, 1993). For foreland basins, the major trap for nonmarine sediments and the system considered in this thesis, tectonic subsidence creates accommodation for 2^{nd}-3^{rd} order sequences (1 Ma – 100 Ma, after Vail *et al.*, 1991). The meso-scale stratal architecture (i.e. individual outcrops) is more likely to reflect a combination of tectonic and climatic influences, superposed in both space and time (e.g. Leeder, 1993; Figure 1.2). For higher-frequency 4^{th} order cycles (0.1 – 1 Ma), other extrinsic and intrinsic variables are likely superimposed (Shanley and McCabe, 1994). As summarized by Ethridge *et al.* (1998), this superposition may lead to geologic "convergence", whereby different processes lead to similar results. Ideally, therefore, each potential control must be quantified and compared on similar spatial and temporal scales, and even then, feedback relationships should be expected.

A. Eustasy:

The role of eustatic control on coastal plain sediments and near-shore fluvial profiles has been greatly debated (e.g. Blum, 1993; Blum and Törnqvist, 2000). Primary effects of sea-level rise on the fluvial system are increased accommodation space, increased flooding of coastal fluvial channels, and vertical floodplain aggradation (Wright and Marriott, 1993). In some shoreline settings with low

topographic gradients, there is clear communication between the marine and nonmarine systems. Yet even along the coastal plain, eustatic variation probably exerts an effect on sedimentation processes only if the variability persists longer than the so-called "causal lag-time" (time difference between introduction of change and stream profile response) for that area (Dalrymple *et al.,* 1998). For wholly continental settings (e.g. closed intermontane basins, "hinterland sequences" of Mitchum, 1977), sea level fluctuations are of little or no relevance to alluvial sedimentation, the eustatic influence diminishing as a function of distance from the coast. In these wholly continental basins, alluvial successions record upstream controls on sediment supply and discharge which may not even be related to base level change, eustatic or otherwise (Shanley and McCabe, 1994; Blum and Price, 1998).

Distinguishing eustatic from other base level controls (e.g. tectonic subsidence, changes in sediment supply) on sequence deposition is possible in well-calibrated marine to marginal-marine systems, but the relative degree of each extrinsic forcing may be impossible to assign. In the Castlegate sandstone and Desert member of Blackhawk Formation, Book Cliffs, Utah, Van Wagoner (1995) characterizes fluvial deposits as 12 groups responding to 4 segments (systems tracts) on the base level curve. The attributes and associations of the strata are well-exposed in this locality, and the study benefits immensely from physical correlation of marine sequence boundaries to their fluvial counterparts. However, the observed alluvial cyclicity may be related to climate change rather than eustatic sea level. Even while favoring eustasy as a direct control, the author considers alluvial architecture to be closely tied to discharge (minimum during highstand, increasing during lowstand, decreasing during transgressive systems tract) which could be linked to climate control (e.g. global cooling; Van Wagoner, 1995).

A Quaternary example of the partitioning of glacio-eustatic and alluvial controls on stratigraphic architecture is the Colorado River system along the Texas Gulf Coast. Glacio-eustatic controls were determined to operate in downstream (i.e. nearshore) areas only, while independently-constrained climate-driven changes in discharge affected upstream deposition (Blum, 1993; Blum and Price, 1998). Eustatic base level falls apparently only directly affected deposits downstream of the apex of the subsiding alluvial-deltaic plain, causing composite unconformities in incised valleys. Upstream, no sequence boundaries tied to shoreline shifts were discernible. Instead, allostratigraphic units (e.g. stratal packages defined and identified on the basis of disconformible boundaries) throughout the upstream fluvial system responded to climate-driven changes in sediment supply.

B. Tectonism:

Tectonism exerts a primary control on accommodation space, chiefly through subsidence, but also via marginal uplift. Frostick and Steel (1993) outlined the main tectonic controls on sedimentary basin deposition, which include: (1) overall accommodation space, (2) direction of basin floor tilt (3) location and size of depocenter(s), (4) the character and orientation of basin margins (i.e. overall size and shape), (5) deflection of sediment delivery systems, and (6) the rate of sediment supply due to uplift and erosion. For foreland basins, flexural subsidence of the lithosphere in response to orogenic loading of the crust results in downward displacement of the earth's surface, creating space adjacent to the orogenic wedge that may be filled with sediment. The aerial extent of flexural subsidence is controlled by the elastic thickness of the deformed lithosphere. For foreland basins, downward deflection is greatest in areas closest to the load, and the deflection profile follows a dampened sinusoidal profile away from the load (e.g. Jordan, 1981). Meanwhile, the orogenic highland itself acts as both source and barrier to sedimentation. Tectonic

uplift also forms a boundary condition for climate through orographic effects on atmospheric circulation, glacial storage, etc. (Blum, 1993; Lenters and Cook, 1995).

For foreland basins, tectonic subsidence creates accommodation for 2^{nd}-3^{rd} order sequences (1 Ma – 100 Ma). However, many of the stratigraphic sequences explored in this dissertation occur on shorter time scales (0.1 – 1 Ma) and likely involve tectonic motions other than flexural subsidence alone. In Chapter 2, the aforementioned tectonic controls on sedimentation (Frostic and Steel, 1993) are each explored in turn and in combination.

C. Climate:

Climate is chiefly responsible for the transport of sediment to the depositional basin through its influence on erosion and discharge rates. The influence of variable discharge on alluvial sedimentary geometry has been extensively studied in modern, geologic, and synthetic examples (e.g**.** Milana, 1998**;** Milana and Tietze, 2002; Sheets *et al.,* 2002; Hickman *et al.,* 2005). However, determining the effect of climate on basin-scale deposition from the incomplete stratigraphic record is more tenuous. Qualitative assessment of syndepositional climate can come from the sediments themselves (e.g. lithofacies suggestive of humid or arid deposition), preserved organic traces, and the repetition or contrasts of lithofacies in stratigraphic succession (Cecil, 1990). Quantification of climate change relies instead on proxy datasets (e.g. stable isotopes of organic matter, mineralogic signals of weathering intensity, physiognomic reconstruction of fossil material, etc.). "Deep-time" paleoclimatologic assessments (e.g. over 10^4 – 10^6 year scales) remain qualitative to semi-quantitative (e.g. Rech *et al.,* 2003; Garzione *et al.,* 2006; this study, Chapters 3, 4 and 5), but are improving with advanced techniques and analogies to the complexities of the modern climate system.

D. Autocyclicity:

A final cautionary note is the role of autocyclic variability in continental, particularly fluvial, successions. Whereas allocyclic mechanisms (eustasy, climate, and tectonism) are changes outside a defined system, autocyclicity is a characteristic of the internal system. The term refers to how the system naturally responds to depositional or geomorphic thresholds. Features such as fluvial avulsions and alluvial or deltaic fan lobe switching that appear to represent, on a human time scale, intrinsic behavior might be misinterpreted in the stratigraphic record as responses to allocyclic forcing (Mohrig, 2000; Aslan *et al.*, 2005). It has also been suggested that patterns of vertical crustal movement and material addition (deposition) or removal (erosion) are roughly in balance when averaged over an appropriately long time scale (Paola, 2000). However, for shorter time scales, intrinsic mechanisms impacting the depositional system become apparent and may even dominate. A certain "unit stratigraphic interval" is thought to be the thickness necessary to average out autogenic processes and retain only extrinsic forcing, and is defined as the long-term sedimentation rate multiplied by the system's equilibration time or 1/e (Sheets *et al.*, 2002; David Mohrig, personal communication, 2005). Consideration of unit stratigraphic interval is of concern at the level of individual sedimentation events and high frequency cyclicity (e.g. Milankovich cycles). However, if the scales of consideration are sufficiently coarse, both temporally and spatially, intrinsic variations may be considered responses to larger-scale, extrinsic controls. Dalrymple *et al.* (1998) suggest that autocyclic effects on alluvial deposits only come into effect after the system has nearly equilibrated to the allocyclic forcing. For the basins considered in this thesis, it is expected that sequence boundaries and architecture observed at the basin-wide and 10^5-10^6 year scales reflect extrinsic forcing mechanisms. Autocyclic patterns may

occur within sequences but in terms of sequence genesis, they are not considered a likely mechanism.

III. ***Chronostratigraphy***

A further difficulty in nonmarine systems is limited chronostratigraphic resolution. Age control by paleontologic or interbedded igneous units is commonly coarser than the temporal scale of interest for 3rd, 4th or 5th order sequences (<1 M.y). Magnetostratigraphic dating has potential to provide highly precise temporal constraints on basin evolution and allow accurate characterization of the duration of nonmarine stratigraphic sequences. However, this method is not without its own quantitative uncertainties, such as nonunique correlation, field or analytical measurement error, fluctuations in sediment accumulation rates, and polarity zones missing from the local succession (Talling and Burbank, 1993). The latter problem is of particular import across sequence bounding unconformities, as well as unidentified disconformities.

IV. ***Difficulties with locating sequence boundaries in nonmarine settings***

Sequence stratigraphic concepts, as originally defined from seismic reflection profiles and applied to marine and marginal marine deposits, require the successful determination of key surfaces, related to points on the relative base level curve. These include (but are not limited to) the sequence boundary, surfaces of maximum flooding, transgression, ravinement, and downlap. For nonmarine deposits, multiple difficulties exist (outlined by Shanley and McCabe, 1994; 1995) which confound the search for such surfaces. First, ties to relative base level (the combined effect of eustatic and tectonic adjustments) in many continental basins are uncertain or, for intermontane basins hundreds of kilometers from the marine system, negligible. Nonmarine deposits, meanwhile, are often characterized by abrupt lateral facies changes and numerous internal erosion surfaces, such that it is difficult to distinguish extrinsically-

forced sequence boundaries from natural (intrinsic) hiatal surfaces or erosional surfaces in the alluvial system. This problem is compounded by discontinuous outcrop and the greater aerial extent of interfluves versus incised valleys where major unconformities are most likely to be recognized (see Aitken and Flint, 1996). Additionally, synthetic stratigraphic modeling and flume studies have shown that spatial variations in system dynamics (e.g. discharge rate, grain size, proximity to source area or tectonic input) could result in diachronous stratigraphic architecture or a zone where correlative unconformities are unrecognizable (e.g. Flemings and Jordan, 1990; Milana and Tietze, 2002).

Incised valleys in stratigraphic successions have been sought as indicators of nonmarine sequence boundaries formed in response to base level lowering (e.g. Dalrymple *et al*, 1998). Valleys initiate through incision in response to base level falls or perhaps uplift of the drainage headwaters (Schumm and Ethridge, 1994). Vertical aggradation in the channel may be the result of climate change and/or uplift-induced sedimentary production (Schumm and Ethridge, 1994). The rate of change is also important, as rapid base level fall favors valley incision whereas slower base level fall may favor regional flat surface erosion (Cant and Stockmal, 1993).

Conversely, it has been suggested that laterally continuous sequence boundaries (incisions and adjacent interfluvial disconformities) may form independent of base level changes, instead responding to upstream controls on sediment delivery (Shanley and McCabe, 1994). These upstream controls include lithology, topography, and particularly the density of vegetative cover (Weltje *et al.*, 1998), any of which may change through time. Again, scale of consideration is important when considering the relative importance of extrinsic controls. Schumm (1993) mentions that eustatic base level may exert an effect several hundred kilometers upstream, but changes in basin relief and climate are likely to affect the entire system. For entirely nonmarine

deposystems, Shanley and McCabe (1998) stressed that climate and tectonism exert controls on accommodation not only at the site of deposition, but also upstream (in the source area) and downstream (perhaps external to the system). Depending on the scale and tectonic setting of the basin, these zones may overlap or interchange through time.

Nonetheless, much recent work has been devoted to illustrating the potential to locate and interpret stratigraphic sequence boundaries or their "correlative conformities" in nonmarine strata (e.g. Aitken and Flint, 1996; McCarthy and Plint, 1998; Friedman and Sanders, 2000; Miall and Arush, 2001). Diagnostic features include abrupt changes in fluvial stacking patterns (e.g. degrees of sinuosity, amalgamation, coarseness, see Shanley and McCabe, 1995), presence of well-developed interfluvial paleosols or rooted exposure surfaces adjacent to an incised valley (Van Wagoner *et al.*, 1990; McCarthy and Plint, 1998) and systematic lateral and/or vertical changes in the above. Basins where subsurface geophysical and lithological data have been collected (e.g. reflection seismic profiles, well-logs, well cuttings) provide a four-dimensional framework for stratigraphic architectural characterization that may be lacking from outcrop-based analysis. Rarely are all components of a basin's chronostratigraphic, lithologic and structural evolution known. However, an integrated approach to sequence stratigraphic analysis will consider as many datasets as possible to better understand the complex interactions and most plausible responses in the sedimentary system.

V. *Systems tracts*

The concept of "systems tracts" has become entrenched in the sequence stratigraphic literature, but, as Van Wagoner (1995) points out, the usage is often incorrectly applied. These stratal bodies, as initially defined by Brown and Fisher (1977), are further subdivisions of sequences into contemporaneous depositional systems. They are defined by their position within a sequence, their bounding

surfaces, and stacking patterns between flooding surfaces ("parasequences"). Stratal geometries or lithofacies are often characteristic of a particular systems tract, and are given descriptive names in reference to their position in a sequence (e.g. "lowstand", "transgressive" and "highstand", see Van Wagoner *et al.*, 1988). However, this naming should not lead to direct interpretation of rock relationship to sea level or a portion of the sea level curve (Van Wagoner, 1995). Interpretations of systems tracts based on rock properties compared to those from inferred base level curves may be fundamentally different, and Van Wagoner (1995) advocates consistency in usage (e.g. rock properties for reservoir characterization and practical illustration, base level cyclicity for modeling).

Nonmarine systems tract models have been proposed to characterize base level cycles by common architectural elements (e.g. Legarreta *et al.*, 1993; Wright and Marriott, 1993; Van Wagoner, 1995; Currie, 1997; Dalrymple et al., 1998; Legarreta and Uliana, 1998; Plint *et al.*, 2001) although without appealing to a particular forcing mechanism. Martinsen *et al.*, (1999) and Anderson and Cross (2001) advocate the use of a simpler systems tract scheme for nonmarine strata, categorizing facies instead by their Accommodation / Sediment Supply (A/S) ratio. The features of these models are summarized in Table 1.1 and are discussed at length in Chapter 6**.** A mutual feature of these workers' models is the occurrence of pedogenic facies during the highstand period of the base level cycle, although disagreement exists concerning the amount of accommodation space available when those paleosols accumulate. The importance of interfluvial paleosols as sequence stratigraphic elements, particularly in demarcating times of fluvial incision elsewhere in the depositional system, is explored later in this thesis.

An important aspect of this dissertation is the documentation of the complexities and trends of nonmarine stratigraphic sequences based on well-calibrated

Table 1.1: Summary of previously-proposed models and characterizations of nonmarine sequences based on lithofacies and base level dynamics (systems tract models) and based on accommodation versus sediment supply rates.

Lithofacies-based classifications

1) Legarreta *et al*, 1993; Legarreta and Uliana,1998	2) Wright and Marriott, 1993	3) Van Wagoner, 1995
Aggradational Widespread suspended load deposits. Increased frequency of paleosols (upward maturing?) Landscape stability/reduced surface gradient (decelerating accommodation capacity)	***Highstand*** Reduced accommodation alllows well-developed floodplain soils. Higher rates of floodplain reworking, increased channel density. Low-gradient floodplains may develop shallow lakes.	***Highstand*** Muddy levee, crevasse splay, and lake margin deposits Broad interfluves. Interbedded single-story sandstone (low net:gross)
Backstepping Stepwise migration of coarsest facies toward basin margins. Mixed bedload and suspended load deposits. Upward fining grainsize (decreasing net:gross) Depositional response to increased accommodation potential (depositional area expands)	***Transgressive*** Multi-storey sandbodies, floodplain reworking, hydromorphic soils. Increased accommodation enhances floodplain storage (isolated channels, weakly developed, well-drained soils)	***Transgressive*** Thinner, single-story sandstone, moderate to low net:gross Mudstones dominate strata along with crevasse splays, lakes, soils Aggradational and upward-fining
Forestepping Upward coarsening channel fill complexes. Dominated by bedload transport Spatially restricted (near incised surface) Basinward shift of proximal deposits concurrent with marginal incision. Localized decrease in A/S ratio	***Lowstand*** Coarse-grained fluvial deposits/ Restricted low-sinuosity (braided) deposits Mature, well-drained soils on terraces	***Lowstand*** Multi-story, high net:gross, laterally continuous sandstones, filling updip end of incised valley. Braided crossbedded sands. No overbank accommodation. Upward fining.

4) Currie, 1997	5) Dalrymple*et al.*, 1998	6) Plint and McCarthy, 2001
Aggradational Abundant fine grained overbank and lacustrine deposits. Isolated, lenticular channels (anastamosing) transition to braided channel sandstones and conglomerates Increasingly mature paleosols as flood-plain aggradation decreases.	***Unconfined SEP Low*** Rate of aggradation lowered. Increased channel amalgamation. If elevation ~unchanged, extensive sheet sands deposited.	***Late Highstand-Lowstand-Early Transgressive*** Low accommodation, dominated by paleosols. The upper part of each sequence, followed by fluvial enrichment and sedimentary bypass.
Transitional Transitional from braided (laterally continuous) to meandering (isolated) channels. Increasing preservation of overbank sediment and paleosols. Coarse to fine grained.	***SEP High*** Rate of aggradation increases Channels more isolated within fine-grained floodplains. During low accommodation, soils develop. Minimal pedogenesis during high rates of aggradation.	***Late Transgressive - Early Highstand*** High accommodation, dominated by lacustrine facies and mud-enclosed ribbon channel sandstones, blanket interfluves and anastamosed rivers.
Degradational Coarse grained, braided channel sandstones and conglomerates. Laterally-continuous channel forms fill incised valleys. Thick paleosols adjacent to incised valleys.	***Confined SEP Low*** Sequence boundary or incised valley, with amalgamated channel sands within incised valley. Correlative floodplain soils (low preservation potential due to lateral channel switching/reworking).	***Early Transgressive*** Low accommodation, dominated by meandering multi-storey channels and valley fill

Accommodation/Sedimentation Supply-based Characterization:

Frostic and Steel, 1993	Martinsen*et al.*, 1999	Anderson and Cross, 2001
A>S: Fining upward succession	A/S >1: Sediment cannot fill available space. Flooding possible. A/S = 1: Expanded succession with high filling probability	Maximum A/S: distal facies, rise-to-fall turnaround Increasing A/S. Proximal to distal facies (contracting alluvial/ braidplain, expanding lakes); Base level rise
A<S: coarsening upward succession	0<A/S<1: Sediments always fill available space; Some sediment may bypass system A/S<0: No accumulation. Sediment bypass and/or erosion occurs !%Abrupt decrease in A/S: Sequence boundary generation !%Abrupt increase in A/S: Expansion surface generation !%Gradual increase in A/S: Expansion zones	Minimum A/S: proximal facies (maximum extent of alluvial fans; lacustrine facies may disappear); fall to rise turnaround Decreasing A/S: decreasing facies diversity (expanding alluvial/braidplain facies, contracting lakes); distal to proximal vertical facies succession; base level fall

field and laboratory datasets for a wholly nonmarine system. The test of any general model for sequence genesis is how well it conforms to what is represented in the geologic record. The reverse case is not applicable; real-world examples should not be forced into existing models if the preserved features do not agree. This work serves as a test of extant models and suggests ways to improve upon them.

VI. *Placing Constraints on Extrinsic Controls and Feedbacks*

Can the roles of tectonic variation and climate change be distinguished through the end-product stratigraphy? Both extrinsic variables may produce changes in the slope of alluvial fans and river profiles which will be expressed in stratigraphic architecture. Rivers are highly susceptible to changes in gradient via tectonic tilting, but respond in various ways, via avulsion, channel belt migration and changes in sinuousity, or by incision, all efforts to regain an equilibrium profile (Leeder, 1993). Schumm (1993) outlined the multiple controls (base level, geologic, and geomorphic) that affect fluvial systems (Fig. 1.3). Of ten explored variables affecting the broader controls, the most important for Schumm are the magnitude and rate of the base level change, the structure and bedrock over which the river flows, and the cohesiveness of the valley alluvium. Given the competition between tectonism and climate in the headwaters controlling sediment delivery, Schumm warns, almost any scenario of fluvial profile adjustment may be possible. Also, the upstream and downstream reaches of a fluvial profile may be out of phase with respect to aggradation/degradation, as well as with respect to the cause of profile adjustment (Ethridge *et al.,* 1998; Dalrymple *et al.,* 1998; van Heijst and Postma, 2001). It has also been suggested that fluvial response to climatic forcing may be nondeterministic and nonlinear (Blum and Törnqvist, 2000).

Given the multiple uncertainties and potential interactions of mechanisms controlling sediment accommodation, quantifying even some of these parameters

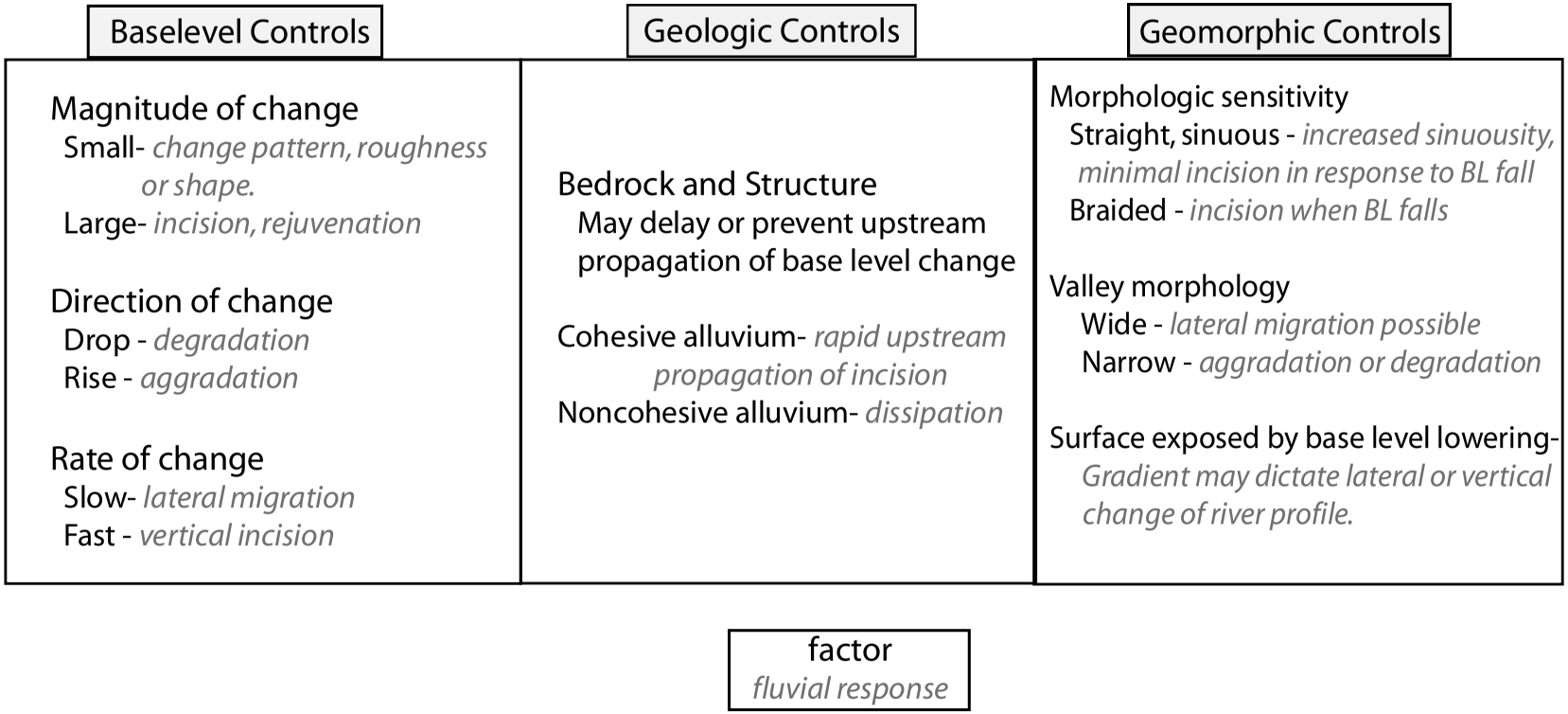

Figure 1.3: Variables affecting fluvial systems, as outlined by Schumm (1993).

appears a daunting task. One must be cognizant not only of the intricacies of the local system, but also the regional or even global boundary conditions that may have bearing on preserved or (in the case of sequence boundaries) unpreserved strata.

Parameterization of external forcing mechanisms, if the goal is to realistically model the depositional system, involves decisions concerning scale and combinations. First, one must apply an areal and temporal perspective: what are the boundary conditions most likely to act upon the depositional system over the time span and geographic area considered? Certain global changes (e.g. plate convergence rates, climatic optima or minima, long-duration trends or anomalies in either of these) may be sufficiently robust to be recorded in a local record, but regional changes are perhaps more interpretable and stand more chance of preservation. Next, one should consider the interactions that could potentially occur. If the goal is to understand stratigraphic architecture at the basin scale, certain complexities of the system may be of lesser importance. At the same time, parameterizing feedback relationships builds an appreciation for the complexity and nonexclusive nature of the sedimentary system from source to sink. The boundary conditions of climate and tectonism for the particular test basins considered in this thesis are discussed in following chapters.

The process-response view of sedimentology interpreted from preserved stratigraphy is not new (e.g. Sloss, 1962), but progressive refinements in quantitative basin analysis have indicated that sedimentary system response to variations, external and internal, is very complex and likely to involve dynamic feedback mechanisms. Coupling conditions in a sedimentary system, whether those conditions are shared physical laws, boundary conditions, or subsets of a deposystem, are often nonlinear and feature multidirectional feedbacks (e.g. Paola, 2000). Factors affecting sedimentary flux to the depositional basin are often coupled in complex feedback relationships. These factors include (a) climate, (b) relief, (c) episodic growth and

erosion of individual structures, (d) contrasts in exposed lithologic resistance, (e) changes in drainage basin size, (f) temporary sedimentary storage in intermontane basins and (g) natural geomorphic system lag time (Tucker and Slingerland, 1996).

An example of a sedimentary feedback system was outlined by Smith (1994) to show the difficulty of preserving high-frequency orbital ("Milankovitch") forcing in the stratigraphic record. A simplified feedback system for nonmarine deposition is presented in Figure 1.4, based on Smith's (1994) "stratigraphy machine". The directions of interactions between extrinsic variables and intrabasinal responses are depicted. The inference is that the stratigraphic record, though it may be "the only empirical record of global change" (Burke *et al.*, 1990), responds to multiple constructive and destructive forcings, such that attributing causal mechanisms must always include consideration of potential feedback relationships (Smith, 1994).

Tucker and Slingerland (1996)'s numerical model of an intermontane foreland basin between thrust ranges revealed a significant temporal asymmetry between thrust activity and sediment supply to the distal parts of the basin, particularly in cases of episodic source area tectonism. The magnitude of the "lag-time" between the initiation of thrust-induced subsidence in the foreland and subsequent deposition of the clastic wedge may be dependent on: (1) the tectonic setting of continental margin, (2) the period of "quiescence" between thrust events, (3) the rheology and strength of underlying lithosphere, (4) the position of sediment fill with respect to flexure-producing load and forebulge, and (5) the spatial partitioning of thrusts (Cant and Stockmal, 1993).

Another feedback system affecting alluvial deposition is between headwater geomorphology and discharge. Discharge is proportional to upstream catchment areas, and stream power is proportional to discharge as well as river slope. The implication is that, as the source area is uplifted and perhaps tilted to greater dip, there is a trade-off

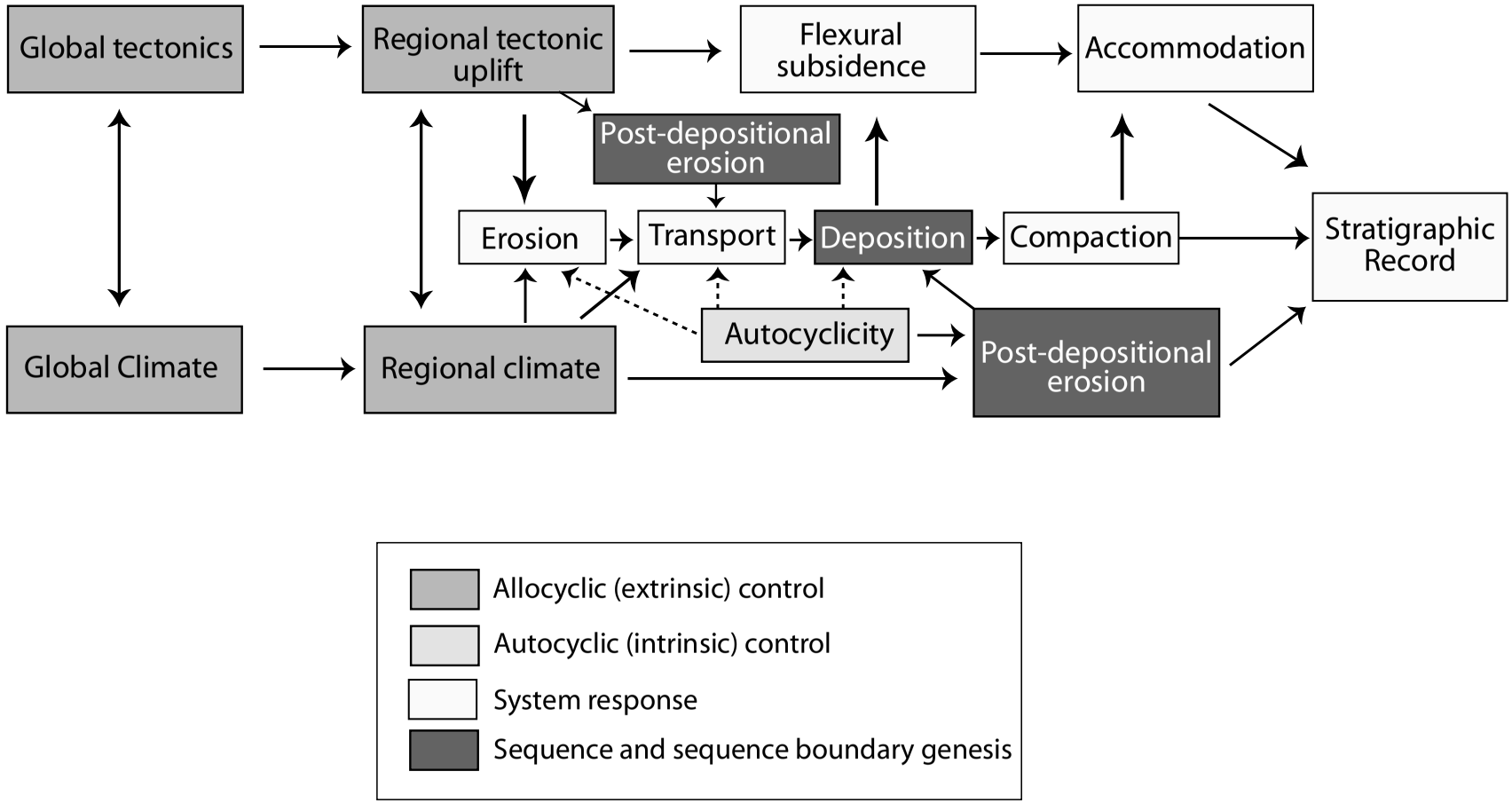

Figure 1.4: Nonmarine feedback system, representing some of the controls and responses for the depositional system (modified from Smith, 1994).

between decreasing catchment area (e.g. decreasing discharge) and fluvial profile slope increase on stream power (increasing discharge). A linear relationship between any two of the three variables (slope, area, and discharge) is not sufficient.

VII. *Sequence stratigraphic utilities of paleosols*

Soil formation (pedogenesis) reflects the combination of multiple environmental factors. Jenny (1941) attributed pedogenesis to five factors: climate, organic activity, relief, parent material, and time. These factors combine via physico-chemical processes (outlined by Schroeder, 1984) that lead to diagnostic soil properties (Figure 1.5). Interrelatedness of these processes and responses (observable properties) can facilitate interpretation of paleoenvironmental factors (e.g. Bronger and Catt, 1989).

The development of paleosols in stratigraphic successions is of significant value for interpreting depositional settings. Soil formation indicates a period of landscape stability, as well as temporally and spatially punctuated sedimentary deposition (Retallack, 1998; Birkeland, 1999). The nearly ubiquitous presence of soils in modern nonmarine landscapes of varied settings illustrates the interplay between geomorphic and pedogenic processes. Though they do represent "gaps in the sedimentary record of geological time" (Retallack, 1998), features of paleosols hold many clues as to what changes transpired during stratigraphic hiatuses. Fossil soil distribution in space and time can be used to document sedimentologic and topographic fluctuations, and suggest the degree to which extrinsic (tectonism and climate) and intrinsic (e.g. autocyclic and threshold-driven) mechanisms interact (Kraus, 1999). For example, laterally-continuous soil horizons reflect a tectonically undisturbed landscape.

The first-order relationship between climate and soil formation has long been recognized (Jenny, 1941) and some workers consider climate to be the most important

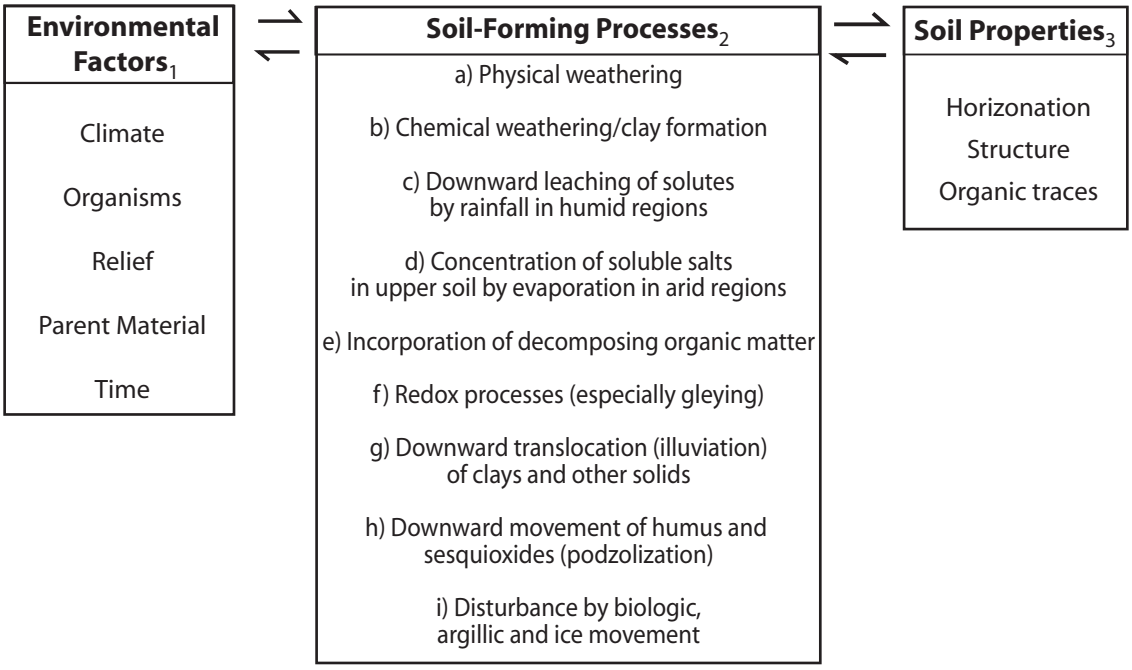

Figure 1.5: Relationship between factors, processes and properties of soils (after $_1$Jenny, 1941; $_2$Schroeder, 1984; $_3$Retallack, 2001).

factor affecting soil development (e.g. Birkeland, 1999). Various techniques are available to describe and attempt quantification of this association, including profile and micromorphologic measurements, clay mineral identification, and stable isotopic analysis of soil carbonates. The complex microclimate that exists within any given soil reflects local variability in any of the five environmental factors of soil formation (Fig. 1.5; Jenny, 1941), although for floodplain alluvial paleosols considered herein, the additional factor of relative soil humidity is considered to be important and to be a function of proximity to groundwater (via fluvial channels or topographic runoff) and regional climatology. For well-drained soils (e.g. oxidized, calcic paleosols) the microclimate may still retain a muted signal of the regional climate (Retallack, 2001), which is the signal of interest for these basin-scale studies. For these reasons, the utilization of paleosols as climatic and geomorphic proxies is complementary to the goals of nonmarine sequence stratigraphy.

A. *Soil formation:*

The parent materials of soils are minerals, either in combination and lithified as bedrock, or as unconsolidated sediments from physical weathering of pre-existing rocks. When exposed at the earth's surface, physical and chemical weathering processes occur, because of the interactions of the hydrosphere, atmosphere, and biosphere on the established topography, leading to soil development layered subparallel to the depositional surface and proceeding to progressively greater depths. If the rock is weathered in place, a layer of regolith may form, which is loose, unconsolidated material on which organic mater may accumulate. Bacteria and organic acids continue to chemically alter the regolith, and weathering proceeds to greater depths, such that the lower regolith becomes a C-horizon, which may or may not resemble the bedrock. As plants and animals inhabit the regolith, organic matter tends to accumulate, and an O horizon (organic-rich) is formed.

Infiltration of water leads to downward movement of organic compounds, dissolution of elemental compounds, and translocation or removal of the finer-sized minerals (leaching), resulting in structural segregation of the soil profile (Birkeland, 1999; Retallack, 2001; Figure 1.6A). As depth of weathering increases, an A horizon forms below the O horizon as a result of continued organic decomposition and loss of materials through leaching. Organic matter becomes less recognizable in the A horizon, and the texture of mineral grains is coarse and granular. Intense weathering in humid climates and in permeable, moist soils may result in an E horizon, where silicate clays, iron and aluminum oxides, and other solutes are flushed (eluviated) from upper layers in the soil to be redeposited at a lower position.

Clays, carbonates, evaporite minerals, and other solutes that have been entrained in the soil solution are moved downward (lixiviation) through the developing profile, and will accumulate in the B horizon. The B horizon represents the level of maximum accumulation (illuviation). Here, clays may expand and contract, become compressed by the overlying weight, as well as electrostatically attract, such that a soil structure might develop. Chemical alteration of various silicate clays in the B-horizon and elsewhere destroys the original mineralogy and structure of the parent material, as secondary clays are pseudomorphically substituted. When net evaporation exceeds net precipitation in the soil microclimate, accumulation of evaporite minerals (e.g. carbonate, gypsum, nitrates) may occur (Fig. 1.6A). Continued pedogenesis is limited by, among other factors, the permeability of the soil, and persistence of the climate. Theoretically, a soil profile will continue to grow from the top down through time, although subsequent burial by sediment effectively halts soil forming processes and, if the buried profile is lithified, it is termed a paleosol.

Figure 1.6: A) Floodplain pedosequence relationship to sedimentation rate and distance from fluvial channel (after Kraus, 1999). Arrows indicate increasing magnitude of feature. B) Catenary soil relationship with landscape (after Birkeland, 1999).

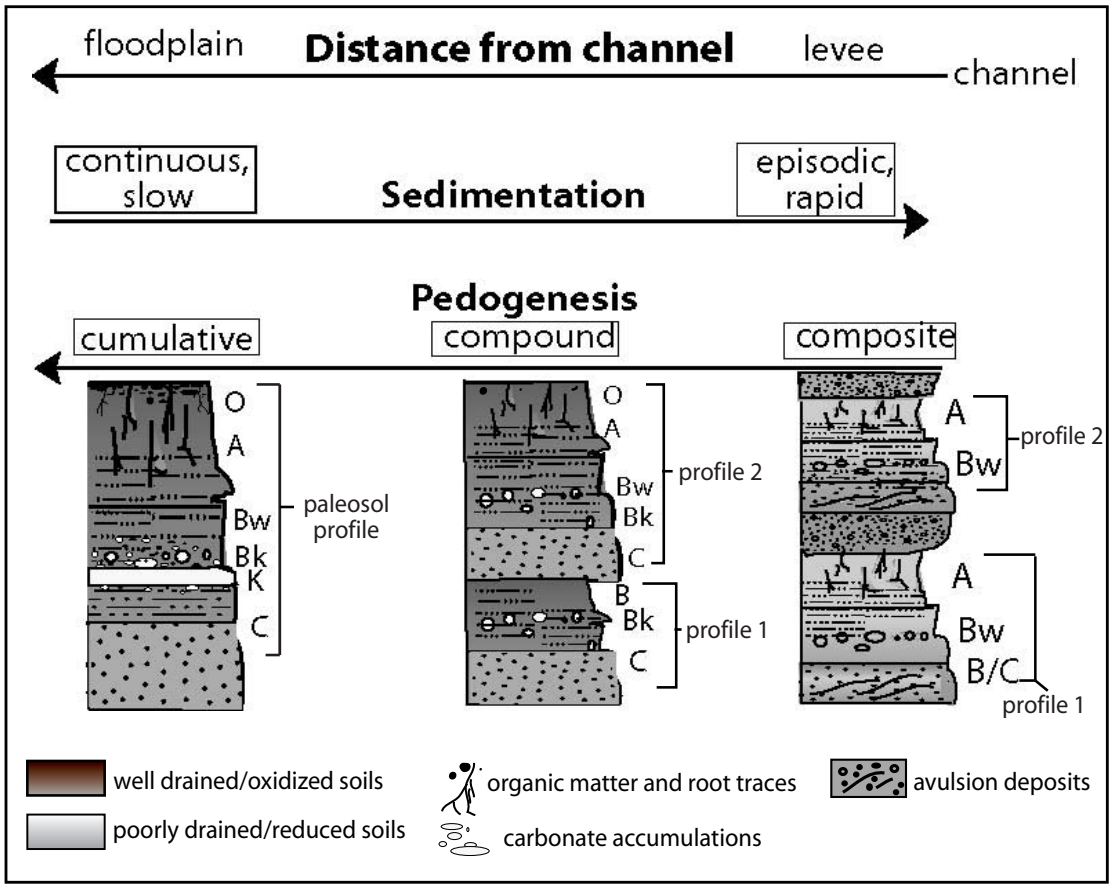
floodplain
Distance from channel
levee
channel
continuous, slow
Sedimentation
episodic, rapid
Pedogenesis
cumulative
compound
composite
O
A
Bw
Bk
K
C
paleosol profile
O
A
Bw
Bk
C
profile 2
B
Bk
C
profile 1
A
Bw
profile 2
A
Bw
B/C
profile 1
well drained/oxidized soils
poorly drained/reduced soils
organic matter and root traces
carbonate accumulations
avulsion deposits

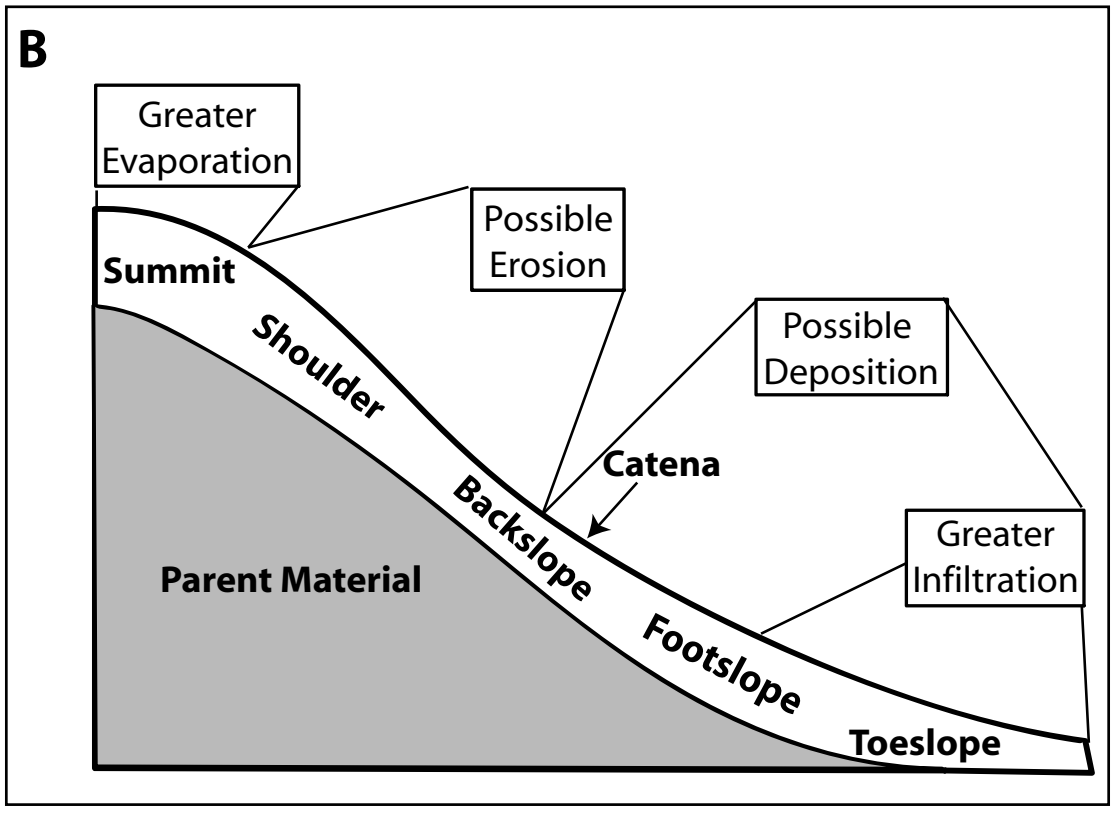
B
Greater Evaporation
Possible Erosion
Summit
Shoulder
Possible Deposition
Catena
Backslope
Greater Infiltration
Parent Material
Footslope
Toeslope

B. ***Rates of pedogenesis and sedimentation:***

In combination, the careful description of sedimentary facies and their associated fossil soils can provide a detailed record of the depositional environment. Kraus (1999) described stages of paleosol development in lateral and vertical succession as dependent on the interaction of the rates of pedogenesis and sedimentation. Consequently, documentation of the stages of paleosol development should allow for qualitative reconstruction of a basin's discharge history and accommodation potential (Figure 1.6). Bown and Kraus (1987) defined the concept of "pedofacies" as laterally adjacent bodies of sediment with fossil soils of variable maturity related to lateral differences in sedimentation rate (Fig. 1.6A). The term "maturity" is used to express the stage of soil development based on observable properties (e.g. horizonation, profile development/thickness, color, nodule development, mottling, contact relations) and does not signify an absolute age, as the maturation time is affected by many variables (e.g. Jenny, 1941; Bown and Kraus, 1993). Assessment of paleosol maturity is confounded by issues of preservation (e.g. erosional truncation, compaction) and post-depositional alteration. In general, however, an inverse relationship exists between soil maturity and rate of accumulation (e.g. low sedimentation rates on floodplains allow for well-developed soils, whereas in settings with high rates of sedimentation, such as adjacent to fluvial channels, soils will be immature; Fig. 1.6A).

Another general model of spatial differences in soil maturity is the catena model. A catena is a suite of soils developed along a topographic gradient, where soil features reflect slope-dependent differences in microclimate (Fig. 1.6B). Valentine and Dalrymple (1975) suggested that the catena concept is a meaningful test of pedogenesis versus diagenesis, as a complete catenary sequence is unlikely to form by post-pedogenic alteration. Floodplain catenas may develop due to microtopography

between the alluvial ridges, terraces and backswamps (Wright, 1992). Paleocatenas, however, are difficult to describe in ancient low-relief alluvial settings, especially among spatially restricted or separated geologic outcrops (Wright, 1992). Thus, we restrict our attention to the floodplain pedofacies model (Kraus, 1987) for cases in which lateral continuity and association of paleosols and adjacent fluvial deposits can be established.

Outcrop studies of vertical relationships of paleosol maturity in floodplain stratigraphic successions can allow the stratigrapher to better reconstruct the spatial and temporal characteristics of the depositional environment. Weak profile development (e.g. stacked B/C horizons, no A), and strong grain size contrasts may mean that sedimentation rate exceeded pedogenesis (Kraus and Aslan, 1993). Compound paleosol sequences (Fig. 1.6A) are tens of meters thick, often comprised of soil profiles of variable maturity, and are indicative of episodic sedimentation in a net aggradational system (Kraus, 1987). Soil maturity varies in a vertical succession in accord with proximity to channels as they migrate over the floodplain. These intervals are interpreted to be related to short-term changes in channel avulsion rate. Channel-belt avulsion deposits are meters-thick intervals of interbedded silt and sand with thin weakly-developed paleosol profiles (Fig. 1.6A, right column); overbank deposits are finer-grained, and contain thicker, more mature paleosols (Fig. 1.6A center and left columns; Kraus, 2002). Furthermore, a shift from numerous paleosols exhibiting variable drainage conditions to fewer, immature paleosols represents a decrease in avulsion frequency because of greater availability of fine-grained sediment between avulsion events (Kraus, 2002; White *et al.*, 2005). Megasequences include hundreds of meters of strata and possibly several compound sequences. The trends of soil development in the megasequence are largely controlled by external controls (climate

and tectonics), whereas extrachannel deposits in singular or compound paleosols reflect microclimate variability (Kraus, 1987).

Stable Isotopic Analysis of Pedogenic Carbonate:

Soil carbonates form where there is a net water deficit and carbonate super-saturation occurs, although increases in solution temperature or pH, partial pressure of CO_2 or solution composition change are also possible triggers of pedogenic carbonate (Chadwick and Graham, 1998). The precipitation reaction is given by:

$$Ca^{2+} + 2\ HCO_3^{1-} \leftrightarrow CaCO_3 + CO_2 + H_2O$$

Identification of the $CaCO_3$ source in soils must consider both detrital carbonate and atmospheric dust influx. Even in the presence of calcium-enriched parent material, Sr/Ca mixing calculations show that 95% or more of arid-region pedogenic carbon is atmospherically delivered, because of low weathering rates and high atmosphere-pedosphere dust cycling (Capo and Chadwick, 1999). Additionally, for Holocene pedogenic carbonates, Quade *et al.* (1989) showed no isotopic inheritance from limestone regolith, such that diffusion of soil respired CO_2 is likely the primary control of paleosol carbonate ^{13}C isotopic values (see below).

The depth and thickness of soil calcic (Bk or K) horizons (e.g. Fig. 1.6A) are generally related to the degree of soil wetting, and potentially to Mean Annual Precipitation (MAP) or seasonality (e.g. Retallack, 2001; 2005). Retallack (2005) compiled data for 675 modern post-glacial soils (<14 k.y.) and obtained empirical correlations between mean annual range of precipitation (highest mean monthly precipitation minus lowest mean monthly precipitation) and thickness of soil with carbonate (linear function, r^2=0.58) as well as thickness of Bk and MAP (exponential function, r^2=0.52). However, because of compaction and erosional truncation of paleosols, it is difficult to accurately measure the calcic horizon depth. Royer (1999) conducted a similar analysis of modern soils (n=1168) and found no correlation

between MAP and depth to Bk horizon (r_2=0.03). However, Royer's (1999) compilation included Pleistocene and Holocene soils in all catenary positions, the justification being that high-precision dating and issues of slope and drainage are difficult to constrain in paleopedologic studies. Furthermore, the large degree of scatter in modern data of both Royer (1999) and Retallack (2005) for depth versus precipitation precludes confident estimation of paleoprecipitation. A conservative and statistically significant correlation seems to be the presence of carbonate nodules and MAP<760 mm (Royer, 1999). The presence of other salts (e.g. sufates and nitrates) in paleosols can help constrain arid to hyperarid paleoclimatic conditions, although these minerals are highly soluble and are generally rarer in the fossil record than are calcic soils (e.g. Rech *et al.*, 2003). Thus, though the presence, depth and thickness of pedogenic carbonate accumulations permits general assessment of paleohumidity, caution must be applied to quantitative assessments of MAP and seasonality of precipitation from field measurements alone as carbonates can accumulate over a wide range of climatic conditions.

Carbonate morphology is another means by which to address soil maturity and pedologic processes. Machette (1985) identified six progressive stages of carbonate accumulation in paleosols developed on coarse and fine-grained parent materials (Table 1.2). Accumulation of carbonate progresses from filamentous cement to separate ("disorthic") or concentrated (Bk horizon) nodular forms, to coalescing layers ("caliche" or K horizons). Nodular carbonates (Stages II and III) are thought to reflect primary pedogenic processes and are often micritic in crystal form, whereas coalesced beds of carbonate (Stages IV and greater) are often sparitic and reflect groundwater diagenesis (e.g. Birkeland, 1999). Some efforts have been made to assess the time required for formation of the different accumulation stages in modern soils by means of radiocarbon dating (e.g. Gile, 1981; Birkeland, 1999; Retallack, 2005). For

Table 1.2: Stages of carbonate accumulation in soils (after Machette, 1985).

Stage	Soils in Gravel	Soils in sand, silt,clay
I	Thin discontinuous carbonate Coatings on/under clasts	Dispersed powdery and filamentous
II	Continuous coatings around and between clasts; discontinuous beyond main horizon	Few to common nodules and veinlets with powdery/filamentous carbonate between nodules.
III	Continuous layer enveloping clasts;	Continuous layer of coalescing nodules
	Less pervasive beyond main horizon	Some nodules/filamentous carbonate beyond main horizon.
IV.	Upper part of a solid layer with weakly developed platy or laminar structure capping less pervasively calcareous parts of the profile.	
V.	Platy or laminar structure cap strongly expressed, in places brecciated or with pisoliths of carbonate.	
VI.	Brecciation or recementation as well as pisoliths common in association with the laminar upper layer.	

paleosol analysis, such dating precision is not possible nor are the inputs of carbonate to the soil well quantified (e.g. Lal *et al.,* 2000). Thus, the stages of Machette (1985) must remain a relative rather than absolute sequence of development.

Isotopic analysis of soil carbonates is developing as a useful method of assessing paleoclimate variations through time. Based on comparison isotopic signatures of a 45 M.y. paleosol record and deep-sea cores, Retallack (2002) determined that significant global climate changes were accurately resolved in fossil soils. The challenge, however, is to discern regionally significant climatic forcing from the complications of the soil microclimate. The abundance of ^{13}C and ^{18}O isotopes represents only a small fraction of the sum of each element's isotopes (1.1% and 0.1905% respectively, Anderson and Arthur, 1983), but significantly reflect the behavior of biogeochemical systems. Carbon isotopic values are inherited from organic matter sources, atmospheric influx (e.g. Rech *et al.,* 2003), or diffusional mass transport of CO_2 in soil gas and reflect the dominant metabolic pathway of the soil ecosystem (Mermut *et al.,* 2000). Ratios of oxygen isotopes in soil carbonates are in equilibrium with soil water composition. Meteoric water composition, local evapotranspiration levels and soil temperatures directly influence soil water composition, such that oxygen isotopic ratios may denote important climatic transitions (Cerling and Quade, 1993). Less depleted values of $\delta^{18}O$ may be suggestive of high potential evapotranspiration, coupled with low precipitation (cf. enriched values of $\delta^{13}C$). However, without constraints on the factors affecting meteoric water composition, estimates of the cause of $\delta^{18}O$ shifts remain qualitative, but may be substantive in conjunction with $\delta^{13}C$ values (Wang *et al.,* 1993; Cerling and Quade, 1993).

The isotopic equilibration of authigenic soil carbonate can be modeled by diffusion mass transport of carbon dioxide in soil solution (Cerling and Quade, 1993). This relationship can be written as:

$$\frac{\partial C_s}{\partial t} = D_s \quad \frac{\partial^2 C_s}{\partial z^2} + \Phi_s(z)$$

(where C_s = concentration of CO_2 in soil, D_s = diffusion coefficient, Z = depth in soil, and $\Phi_s(z)$ = production of CO_2 as a function of depth). Diffusion theory also predicts a gradient of $\delta^{13}C$ values in Carbon dioxide for the upper 20-30 cm of a soil profile (a mix of atmospheric and biogenic CO_2), and stabilization below that level. The equilibrium value of ^{13}C below the shallow mixed layer is determined by the proportion of C_3 to C_4 plants comprising the biomass (Cerling and Quade, 1993). C_3 plants utilize the Calvin photosynthetic pathway, and include most trees, cool-season grasses, and shrubs. This older metabolic pathway developed under cooler Mean Annual Temperatures (M.A.T.) and higher atmospheric CO_2 partial pressure. Modern soil carbonates have $\delta^{13}C$ values ranging from -35‰ to -6‰**,** the less depleted values representing moisture-stressed conditions, warmer M.A.T., and the transition to the C_4 photosynthetic pathway (e.g. -12 ± 2‰, Fox and Koch, 2003, Latorre *et al.,* 1997). C_4 plants (Hatch Slack Cycle) include sedges and summer grasses better adapted to arid conditions, growth during the warm part of the year and greater insolation. Intermediate values of $\delta^{13}C$ are from CAM plants (Crassulacean Acid Metabolism), which include cacti and succulents, representing a minor proportion of global biomass (although for Iglesia Basin's semi-arid to arid depositional environment, CAM plants may have been a non-negligible component). The aforementioned model suggests that soil carbonates formed in the presence of pure C_3 or C_4 biomass have $\delta^{13}C$ values of -12‰ and -2‰, respectively (Wang *et al.,* 1993). However, arid conditions and low soil productivity can result in less depleted $\delta^{13}C$ values recorded in soil carbonates for the C_3 pathway (-14‰ to -8‰), such that pathway ranges may overlap, and mixed soil

ecologies are difficult to differentiate from arid environment C_3 biomass (Latorre *et al.,* 1997; Fox and Koch, 2003).

Oxygen isotopic ratios in pedogenic carbonates are controlled by the composition of soil water, which is related to climate for several reasons. In specific, meteoric water $\delta^{18}O$ values are strongly affected by temperature, evaporation, seasonality of precipitation, latitude, continentality and the contemporary ocean reservoir values of $\delta^{18}O$. Trends of $\delta^{18}O$ time series toward less negative values has been variously interpreted as reflecting (a) changes in temperature and precipitation patterns (e.g. seasonality of climate) that support C_4 plant growth (Amundson *et al.,* 1996) or (b) higher evaporation rates over grasslands relative to antecedent woodlands as radiative fluxes increase (Cerling and Quade, 1993). But it is often difficult to determine which factor or factors are responsible for shifts in the isotopic signature (Grootes, 1993; Mack and Cole, 2005). These multiple climatic and location controls, as well as diagenesis, may also combine such that $\delta^{18}O$ values 'homogenize' and show minimal change in response to major climatic variation (Pendall *et al.,* 1994; Wang and Cerling, 1994; Liu *et al.,* 1996). Nevertheless, regardless of the cause(s), major changes in soil carbonate $\delta^{18}O$ still may reflect climatic variability, particularly when covariant with $\delta^{13}C$ values (Wang *et al*., 1993). Scatter of oxygen isotopic values may represent differing water: rock ratios during diagenesis, possibly via variable permeability in the paleosol (e.g. Cerling, 1991; Driese and Mora, 1993).

It should be acknowledged that the stable isotopic composition of paleosol carbonates represents a "time averaged" signal of soil climate, due to overprinting or recrystallization during a prolonged period of formation leading to homogenization of isotopic values (e.g. Pendall *et al*., 1994). In contrast to postdepositional homogenization, isotopic heterogeneity of soil carbonates is a complex problem that persists even when nodules are microsampled (Deutz *et al.,* 2002). Isotopic

heterogeneity within a given soil profile may be due to (a) the diffusion of soil CO_2 which exponentially decreases with depth (Cerling and Quade, 1993), (b) differential infiltration and evapotranspiration of meteoric waters affecting $\delta^{18}O$ enrichment of soil water, (c) recrystallization reactions (e.g. diagenesis) or (d) argilloturbation, the intraprofile mixing and movement of soil carbonates via clay shrink-swell processes (Driese and Mora, 1993). Lateral variation in $\delta^{13}C$ may reflect shifting proportions of C_3 to C_4 biomass across a landscape. The isotopic values of a time series of homogenized bulk samples (e.g. single nodule or population of nodules from same depth in profile) however, do record the long-term soil climate (the desired signal for a basin-scale study and local complexities (soil microclimate) are "averaged out". Stable isotopic values of pedogenic carbonate nodules from three nonmarine foreland basins (Iglesia Basin and Lomas de las Tapias, Argentina and Axhandle Basin, Utah, USA) are presented and discussed in Chapters 3, 4 and 5 (see also Appendix i).

X-Ray Diffraction of pedogenic clays:

The identity of the clays in paleosol profiles is a consequence of the parent material and the degree of subsequent weathering. In arid climatic regimes, primary minerals such as biotite and plagioclase generally weather to smectite and kaolinite, respectively (Tardy *et al.*, 1973). Smectite (e.g. "montmorillonite") is less stable than kaolinite (owing to the latter's hydrogen-bonded, nonexpanding interlayer), and smectite forms under less-intense leaching (i.e. less humid) conditions. Thus, the presence of kaolinite in association with smectite may be suggestive of a formerly wetter climate that (gradually) became more arid (Birkeland, 1999) or of specific stability conditions (McBride, 1994). Given the complex chemical disequilibrium that can exist in the soil system, clay composition may depend more on the rate and intensity of weathering than on parent mineralogy (McBride, 1994). If clays are detrital, this may inform about weathering rates in the headwaters of the basin where

soils accumulate. General trends of clay mineral proportions have been shown to reflect variable weathering of igneous source rocks and climatic conditions in the upland source area (Barshad, 1966). Semi-quantitative assessment of smectite, illite, kaolinite and chlorite proportions (after Poppe *et al.*, 2001) provides information about weathering dynamics from source to soil. Paleosol clay mineralogy for the Miocene-Pliocene Iglesia Basin of northwestern Argentina is presented in Appendix iii.

Summary

Unlike the marine and coastal plain realms where relative base level oscillations yield predictable stratigraphic architectures, generalizations about controlling factors or predictable rock geometries are not yet established for continental settings. At present, improved understanding and quantification of the causative mechanisms of stratigraphic architecture in wholly nonmarine basins and especially the interactions among mechanisms remain portent goals for stratigraphic research.

The objectives of this dissertation are to fully document the stratigraphic characteristics of nonmarine sequences and constrain the extrinsic controls that may have formed them. To achieve these objectives, field methods are combined with laboratory analyses, all of which are constrained by previous chronostratigraphic documentation. Particular attention is paid to paleosols as a sequence stratigraphic element and recorder of processes and conditions that resulted in sedimentary hiatuses. Chapter 2 provides interpretation of reflection seismic profiles and outcrop-based sedimentologic features of the Miocene-Pliocene Iglesia Basin, San Juan Province, Argentina. Chapters 3, 4 and 5 utilize macroscopic, microscopic, mineralogic and geochemical data from paleosols as proxy information to assess changing climatic conditions concurrent with the development of nonmarine sequences in Andean and Sevier foreland basins (northwestern Argentina and Central Utah, respectively).

These investigations of sequence features and potential controlling mechanisms provide well-calibrated tests of general models for nonmarine systems tracts and sequence genesis (e.g. Legarreta *et al.*, 1993; Wright and Marriott, 1993; Van Wagoner, 1995; Currie, 1997; Dalrymple *et al*., 1998; Legarreta and Uliana, 1998; Martinsen *et al*, 1999; Anderson and Cross, 2001; Plint *et al.*, 2001). Subsequently, these models are assessed and refinements are suggested in Chapter 6. Finally, Chapter 7 discusses Tertiary stratigraphy of the central Sierras Pampeanas "broken foreland" of Argentina (Jordan, 1995), particularly regional pedogenic development and reassessment of previous correlations with a Miocene intercontinental seaway. It is hoped that these studies illustrate the necessity for integration of paleopedology, paleoclimatology, and seismic datasets with outcrop observations when analyzing nonmarine basins and their stratigraphic evolution.

References:

Aitken, J.F., and Flint, S.S., 1996, Variable expression of interfluvial sequence boundaries in the Breathitt Group (Pennsylvanian), eastern Kentucky, USA, *in* Howell, J.A., and Aitken, J.F. (eds), High Resolution Sequence Stratigraphy: Innovations and Applications: Geological Society Special Publication No. 104, p. 193-206.

Amundson, R., O.Chadwick, C. Kendall, Y.Wang, and M.DeNiro. 1996. Isotopic evidence for shifts in atmospheric circulation shifts during the late Quaternary in mid-North America.Geology 24:23-26.

Anderson, D.S. and Cross, T.A., 2001, Large-scale cycle architecture in continental strata, Hornelen basin (Devonian), Norway: Journal of Sedimentary Research, v. 21, p. 255-271

Anderson, T.F, and Arthur, M.A., 1983, Stable isotopes of oxygen and carbon and their application to sedimentologic and paleoenvironmental problems, *in* Arthur, M.A., Anderson, T.F., Kaplan, I.R., Veizer, J. and Land, L.S., eds., Stable Isotopes in Sedimentary Geology, SEPM Short Course, No.10, Dallas.

Aslan, A., Autin, W.J., and Blum, M.D., 2005, Causes of river avulsion: insights from the late Holocene avulsion history of the Mississippi River, U.S.A., Journal of Sedimentary Research, Vol. 75, p. 650-664.

Barrell, J, 1917, Rhythms and the measurements of geologic time: Geological Society of America Bulletin 28, p 745-904

Barshad, I., 1966, The effect of variation in precipitation on the nature of clay mineral formation in soils from acid and basic igneous rocks: Proc. Int. Clay Conf., 1:167- 173.

Birkeland, P. W., 1999, Soils and Geomorphology, 3rd Edition, Oxford University Press, 432 pp.

Bloom, A.L., 1998 Geomorphology: A systematic analysis of Late Cenozoic landforms, 3rd ed., Englewood Cliffs, New Jersey, Prentice-Hall 492 p.

Blum, M.D., 1993, Genesis and architecture of incised valley fill sequences: a Late Quaternary example from the Colorado River, Gulf Coastal plain of Texas: *in* Weimer, P. and Posamentier, H.W., eds., Siliciclastic sequence stratigraphy: Recent developments and applications, AAPM Memoir 58, p. 259-283.

Blum, M.D., and Price, D.M., 1998, Quaternary alluvial plain construction in response to glacio-eustatic and climatic controls, Texas Gulf Coastal plain: *in* Shanley, K.M., and McCabe, P.W., eds., Relative roles of eustasy, climate and tectonism in continental rocks: SEPM Special Publication No. 59, p. 31-48.

Blum, M.D. and Törnqvist, T.E., 2000, Fluvial responses to climate and sea-level change: a review and look forward: Sedimentology, Vol. 47, p.2-48.

Bown, T.M., and Kraus, M.K., 1987, Integration of channel and floodplain suites in aggrading fluvial systems. I: Developmental sequence and lateral relations of lower Eocene alluvial paleosols, Willwood Formation, Bighorn Basin, Wyoming: Journal of Sedimentary Petrology 57, p. 587-601.

Bronger, A. and Catt, J.A., 1989, Paleosols: Problems of definition, recognition and interpretation *in* Bronger, A. and Catt, J.A., eds., Paleopedology – Nature and Application of Paleosols, Cremlingen-Destedt: *Catena* Supplement 16, p. 1-8.

Brown, L.F., and Fisher, W.L., 1977, Seismic-stratigraphic interpretation of depositional systems: examples from Brazil rift and pull-apart basins in Peyton C.E., ed., Seismic Stratigraphy –Applications to Hydrocarbon Exploration: American Association of Petroleum Geologists Memoir 26, p. 213-248.

Burke, K., Francis, P., and Wells, G., 1990, Importance of the stratigraphic record in understanding global change: Palaeogeography, Palaeocimatology, and Palaeoceanography (Global Change Section), Vol. 89, p. 193-204.

Cant, D.J., and Stockmal, G.S., 1993, Some controls on sedimentary sequences in foreland basins; examples from the Alberta Basin *in* Frostick, L. E. and Steel, R. J (eds) Tectonic controls and signatures in sedimentary successions Special Publication of the International Association of Sedimentologists, 20, p.49-65

Capo, R.C. and Chadwick, O.A., 1999, Sources of strontium and calcium in desert soil and calcrete, Earth and Planetary Science Letters, v. 170, p. 61-72.

Cecil, C.B., 1990, Paleoclimate controls on stratigraphic repetition in chemical and siliciclastic rocks: Geology, Vol. 18, p.533-536.

Cerling, T. E., 1991, Carbon dioxide in the atmosphere: evidence from Cenozoic and Mesozoic paleosols. American Journal of Science 291: 377-400.

Cerling, T. E., and Quade, J., 1993, Stable carbon and oxygen isotopes in soil carbonates: *in* Stuart, P.K., Lohmann, K.C., McKenzie, J., and Savin, S., eds., Climate Change in Continental Isotopic Records, American Geophysical Union, Geophysical Monograph 78, 374 pp.

Chadwick, O.A. and Graham, R.C., 1998, Pedogenic processes *in* Sumner, M.E. ed., Handbook of Soil Science, CRC Publishing, 2148 p.

Currie, B. S., 1997: Sequence stratigraphy of nonmarine Jurassic-Cretaceous rocks, central Cordilleran foreland-basin system: Geological Society of America Bulletin, v.9., p 1206-1222.

Dalrymple, M., Prosser, J., and Williams, B., 1998, A dynamic systems approach to the regional controls on deposition and architecture of alluvial sequences, illustrated in the Statfjord Formation (United Kingdom, Norther North Sea) *in* Shanley, K.M., and McCabe, P.W., eds., Relative roles of eustasy, climate and tectonism in continental rocks: SEPM Special Publication No. 59, p. 65-81.

Davis, W.M., 1902, Base level, grade, and peneplain: Journal of Geology, p. 77-111

Deutz, P., Montañez, I.P., and Monger, H.C., 2002, Morphology and stable and radiogenic isotope composition of pedogenic carbonates in late Quaternary relict soils, New Mexico, U.S.A.: an integrated record of pedogenic overprinting: Journal of Sedimentary Research, v.72, p. 809-822.

Driese, S., G. and Mora, C.I., 1993, Physico-chemical environment of pedogenic carbonate formation in Devonian vertic palaeosols, central Appalachians, USA: Sedimentology, Vol. 40, p. 199-216.

Ethridge, F.G., Wood, L., and Schumm, S.A., 1998, Cyclic variables controlling sequence development: Problems and perspectives in relative role of eustasy, climate, and tectonism in continental rocks: SEPM, Spec. Pub. 59, p. 17-29

Flemings, P.B. and Jordan, T.E., 1990, Stratigraphic modeling of foreland basins: Interpreting thrust deformation and lithosphere rheology: Geology, Vol. 18, p. 430-434.

Fox, D.L., and Koch, P.L., 2003, Tertiary history of C_4 biomass in the Great Plains, USA: Geology, v. 31, p. 809-812.

Friedman, G.M., and Sanders, J.E., 2000, Comments about the relationships between new ideas and geologic terms in stratigraphy and sequence stratigraphy with suggested modifications: American Association of Petroleum Geologists Bulletin, v.84, p.1274-1280.

Frostick, L. E. and Steel, R. J, 1993, Tectonic signatures in sedimentary basin fills: an overview in Frostick, L. E. and Steel, R. J (eds) Tectonic controls and signatures in sedimentary successions Special Publication of the International Association of Sedimentologists, 20, p. 1-9

Garzione, C.N., Molnar, P., Libarkin, J.C., and MacFadden, B.J., 2006, Rapid late Miocene rise of the Bolivian Altiplano: Evidence for removal of mantle lithosphere: Earth and Planetary Science Letters, Vol. 241, p. 543-556.

Gile, L.H., Peterson, F.F., and Grossman, R.B., 1966, Morphological and genetic sequences of carbonate accumulations in desert soils: Soil Science, Vol. 101, p. 347-360.

Grootes, P.M., 1993, Interpreting continental oxygen isotope records: *in* Stuart, P.K., Lohmann, K.C., McKenzie, J., and Savin, S., eds., Climate Change in Continental Isotopic Records, American Geophysical Union, Geophysical Monograph 78, p. 37-46.

Hickson, T.A., Sheets, B.A., Paola, C, and Kelberer, M., 2005, Experimental test of tectonic controls on three-dimensional alluvial facies architecture: Journal of Sedimentary Research, Vol. 75, p. 710-722.

Jenny, H., 1941, Factors in Soil Formation: A System of Quantitative Pedology: McGraw-Hill, New York, 288 p.

Jervey, M.T., 1988, Quantitative geological modeling of siliciclastic rock sequences and their seismic expressions, *in* C.K. Wilgus *et al.*, eds., Sea level changes: an integrated approach: SEPM Special Publication 42, p. 47-69.

Jordan, T.E., 1981, Thrust loads and foreland basin evolution, Cretaceous, western United States: American Association of Petroleum Geologists Bulletin, Vol. 65, p. 2506-2520.

Kraus, M.J., 1987, Integration of channel and floodplain suites, II. Vertical relations of alluvial paleosols: Journal of Sedimentary Petrology, Vol. 57, p. 602-612.

Kraus, M.J., and Aslan, A., 1993, Eocene hydromorphic paleosols: significance for interpreting ancient floodplain processes: Journal of Sedimentary petrology, Vol. 63, p. 453-463.

Kraus, M. J., 1999, Paleosols in clastic sedimentary rocks: their geologic applications: Earth Science Reviews v. 47, p. 41-70.

Kraus, M.J., 2002, Basin-scale changes in floodplain paleosols: Implications for interpreting alluvial architecture: Journal of Sedimentary Research, vol. 72, p. 500-509.

Latorre, C., Quade, J., and McIntosh, W.C., 1997, The expansion of C_4 grasses and global climate change in the late Miocene: Stable isotope evidence from the Americas*:* Earth and Planetary Science Letters, v.146, p. 83-96.

Leeder, M. R., 1993, Tectonic controls upon drainage basin development, river channel migration and alluvial architecture: implications for hydrocarbon reservoir development and characterization *in* North, C.P. and Prosser, D.J., eds., Characterization of Fluvial and Aeolian Reservoirs, Geological Society Special Publication No. 73, p. 7-22.

Legarreta, L., Uliana, M.A., Laratonda, C.A. and Meconi, G.R., 1993, Approaches to nonmarine sequence stratigraphy- theoretical models and examples from Argentine basins *in*. Eschard, R., and Doligez, B., eds. Subsurface Reservoir Characterization from Outcrop Observations: Proceedings of the 7th IFP Exploration and Production Research Conference, p. 125-143

Legarreta, L. and Uliana, M.A., 1998, Anatomy of hinterland depositional sequences: Upper Cretaceous fluvial strata, Neuquen Basin, West-Central Argentina: *in* Shanley, K.M., and McCabe, P.W., eds., Relative roles of eustasy, climate and tectonism in continental rocks: SEPM Special Publication No. 59, p. 83-92.

Lenters, J.D. and K. H. Cook, 1995, Simulation and diagnosis of the regional summertime precipitation climatology of South America: *Journal of Climate*, Vol. 8, No. 12, p. 2988-3005.

Liu, B., Phillips, F.M., and Campbell, A.R., 1996, Stable carbon and oxygen isotopes of pedogenic carbonates, Ajo Mountains, southern Arizona: implications for paleoenvironmental change: Palaeogeography, Palaeoclimatology, Palaeoecology Vol. 124, p. 233-246.

Machette, M.N., 1985, Calcic soils of the southwestern United States *in:* Weide, D.L., ed., Soils and Quaternary Geology of the Southwestern United States: Geological Society of America Special Paper, 203, p. 10-21.

Mack, G.H. and Cole, D.R. 2005, Geochemical model of $\delta^{18}O$ of pedogenic calcite versus latitude and its application to Cretaceous paleoclimate: Sedimentary Geology Vol. 174, p. 115-122.

Martinsen, O.J., Ryseth, A., Helland-Hansen, W., Flesche, F., Torkilsden, G., and Idil, S., 1999, Stratigraphic base level and fluvial architecture: Ericson sandstone (Campanian), Rock Springs Uplift, SW Wyoming, USA: Sedimentology, v.46, p.235-259.

McBride, M.B., 1994, Environmental Chemistry of Soils: Oxford University Press, 406 p.

McCarthy, P.J., and Plint, A.G., 1998, Recognition of interfluve sequence boundaries: Integrating paleopedology and sequence stratigraphy: Geology, v. 26, p. 387-390.

Mermut, A.R, Amundson, R., and Cerling, T.E., 2000, The use of stable isotopes in studying carbonate dynamics in soils, *in* Rattan, L., Kimble, J.M., Eswaran, H., and Stewart, B.A., eds., Global Climate Change and Pedogenic Carbonates: Lewis Publishers. p. 65-85

Miall, A.D., and Arush, M., 2001, Cryptic sequence boundaries in braided fluvial successions: Sedimentology, v. 48, p. 971-985.

Milana, J.P., 1998, Sequence stratigraphy in alluvial settings: a flume-based model with applications to outcrop and seismic data: American Association of Petroleum Geologists Bulletin, v.82, p.1736-1753.

Milana, J.P. and Tietze, K.W., 2002, Three-dimensional analogue modeling of an alluvial basin margin affected by hydrological cycles: depositional processes, profiles and sequences: Basin Research, v. 14, p. 237-264.

Mitchum, R.M., Jr., 1977, Seismic stratigraphy and global changes of sea level, Part II: Glossary of terms used in seismic stratigraphy *in* Payton, C.E., ed., Seismic stratigraphy – Applications to hydrocarbon exploration: AAPG Memoir 26, p. 205-212.

Mohrig, D.C., Heller, P.L., Paola, C, and Lyons, W.J., 2000, Interpreting avulsion processes from ancient alluvial sequences: Guadalope-Matarranya system (northern Spain) and Wasatch Formation (western Colorado): Geological Society of America Bulletin, Vol. 112, p. 1787-1803.

Muto, T., and Swenson, J.B., 2006, Autogenic attainment of large-scale alluvial grade with steady sea-level fall: An analog tank-flume experiment: Geology, Vol. 34, p. 161- 164.

Paola, C., 2000, Quantitative models of sedimentary basin filling: Sedimentology, Vol. 47, p. 121-178.

Pendall, E.G., Harden, J.W., Trumbore, S.E., and Chadwick, O.A., 1994, Isotopic approach to soil carbonate dynamics and implications for paleoclimate interpretations: Quaternary Research, v. 42, p. 60-71.

Plint, A.G., McCarthy, P.J., and Faccini, U., 2001, Nonmarine sequence stratigraphy: Updip expression of sequence boundaries and systems tracts in a high-resolution framework, Cenomanian Dunvegan Formation, Alberta foreland basin, Canada: American Association of Petroleum Geologists Bulletin, v.85, p. 1967-2001.

Poppe, L.J., Paskevich, V.F., Hathaway, J.C., and Blackwood, D.S., 2001, A Laboratory Manual for X-Ray Powder Diffraction: U.S. Geological Survey Open-File Report 01-041, http://pubs.usgs.gov/of/of01-041/index.htm

Quade, J., Cerling, T.E., and Bowman, J.R., 1989, Systematic variations in the stable carbon and oxygen isotopic composition of pedogenic carbonate along elevation transects in the southern Great Basin, USA: Geological Society of America Bulletin, v. 101, p. 464-475.

Quirk, D.G., 1996, 'Base profile': a unifying concept in alluvial sequence stratigraphy *in* Howell, J.A. and Aitken, J.F., eds, High Resolution Sequence Stratigraphy: Innovations and Applications, Geological Society Special Publication No. 104, p. 37-49.

Rech, J.A., Quade, J., and Betancourt, J.L., 2003, Controls on the isotopic composition of soil carbonate in a hyperarid environment; a case study from the Atacama Desert, Chile: Geological Society of America, 2003 Annual Meeting, Abstracts with programs, v. 35, p. 408.

Retallack, G.J., 1998, Fossil soils and completeness of the fossil record: in Donovan, S.K. and Paul, C.R.C., eds., The Adequacy of the Fossil Record: John Wiley and Sons, United Kingdom, p. 133-164.

Retallack, G.J., 2001, Soils of the Past: an Introduction to Paleopedology, 2nd edition: Blackwell Science, 404 p.

Retallack, G.J., 2002, Paleosols compared with deep-sea records of Cenozoic global paleoclimatic change: Geological Society of America Abstracts with Program, v.34, p.63-64.

Retallack, G.J., 2005, Pedogenic carbonate proxies for amount and seasonality of precipitation in paleosols: Geology, v. 33, p. 333-336.

Royer, D.L., 2003, Depth to pedogenic carbonate horizon as a paleoprecipitation indicator: Geology Vol. 27, p. 1123-1126.

Schumm, S.A., 1993, River response to base level change: Implications for sequence stratigraphy: Journal of Geology, Vol. 101, p. 279-294.

Schumm, S.A. and Ethridge, F.G., 1994, Origin, evolution and morphology of fluvial valleys *in* Incised-valley systems: Origin and sedimentary sequences: Society for Sedimentary Geology Special Publication 51, p. 11-27.

Shanley, K.W., and McCabe, P.J., 1994, Perspectives on the Sequence Stratigraphy of Continental Strata: American Association of Petroleum Geologists Bulletin, v. 78, p 544-568.

Shanley, K.W., and McCabe, P.J., 1995, Sequence stratigraphy of Turonian-Santonian strata, Kaiparowits Plateau, Southern Utah, USA: Implications for regional correlation and foreland basin evolution: *in* Van Wagoner, J.C., and Bertram, G.T., eds., Sequence Stratigraphy of Foreland Basin Deposits - Outcrop and Subsurface Examples from the Cretaceous of North America: American Association of Petroleum Geologists Memoir 64, p.103-136.

Shanley, K.W., and McCabe, P.J. (eds), 1998, Relative role of eustasy, climate, and tectonism in continental rocks. SEPM Special Publication, vol. 59. Society for Sedimentary Geology, Tulsa, OK, USA. 234 pp.

Sheets, B.A., Hickson, T.A., and Paola, C., 2002, Assembling the stratigraphic record: depositional patterns and time-scales in an experimental alluvial basin: Basin Research, Vol 14, p. 287-301.

Sloss, L.L., 1962, Stratigraphic models in exploration: Journal of Sedimentary Petrology, Vol. 32., p. 415-422

Sloss, L.L., 1991, The tectonic factor in sea level change: a counter veiling view: Journal of Geophysical Research, Vol. 96, p. 6609-6617.

Smith, D.G., 1994, Cyclicity or chaos? Orbital forcing versus nonlinear dynamics *in* de Boer, P.L. and Smith, D.G., eds., Orbital forcing and cyclic sequences: Special Publication of the International Association of Sedimentologists 19, p. 531-544.

Talling, P.J., and Burbank, D.W., 1993, Assessment of uncertainties in magnetostratigraphic dating of sedimentary strata: *in* Aissaoui, D,M., McNeill, D.F, and Hurley, N.F., eds., Applications of paleomagnetism to sedimentary geology: SEPM Special Publication No. 49, p. 59-70.

Tardy, Y., Bocquier, G., Paquet, H., and Millot, G., 1973, Formation of clay from granite and its distribution in relation to climate and topography: Geoderma, v.10, p.271-284.

Tucker, G.E., and Slingerland, R., 1996, Predicting sediment flux from fold and thrust belts: Basin Research 8, p. 329-349.

Vail, P. R., F. Audemard, S. A. Bowman, P. N. Eisner, and G. Perez-Cruz. 1991. The stratigraphic signatures of tectonics, eustacy and sedimentology; an overview, p. 617-659. *In* G. Einsele, W. Ricken, and A. Seilacher, (eds.), Cycles and events in stratigraphy.

Valentine, K.W.G., and Dalrymple, J.B., 1975, The identification, lateral variation and

chronology of two buried paleocatenas at Woodhall Spa and West Runton, England: Quaternary Research Vol. 5, p. 551-590.

van Heijst, M. W. I. M.; Postma, G., 2001, Fluvial response to sea-level changes: a quantitative analogue, experimental approach: Basin Research 13, p. 269-292.

Van Wagoner, J.C., H. W. Posamentier, R. M. Mitchum, P. R. Vail, T. F. Sarg, T. S. Loutit, and J. Hardenbol. 1988, An overview of the fundamentals of sequencestratigraphy and key definitions, p. 39-45. *In* C. K. Wilgus, B.S. Hastings, C. G. St.G Kendall, H. Posamentier, C. A. Ross, and J. C. Van Wagoner, (eds.), Sea-Level Changes-- An Integrated Approach, Society of Economic Paleontologists and Mineralogists Special Publication, 42.

Van Wagoner, J.C., Mitchum, R.M., Campion, K.M., and Rahmanian, V.D., 1990, Siliciclastic sequence stratigraphy in well logs, cores, and outcrops: American Association of Petroleum Geologists Methods in Exploration 7, 63 p.

Van Wagoner, J.C., 1995, Sequence stratigraphy and Marine to Nonmarine Facies Architecture of Foreland Basin Strata, Book Cliffs, Utah, U.S.A., *in* Van Wagoner, J.C., and Bertram, G.T., eds., Sequence Stratigraphy of Foreland Basin Deposits - Outcrop and Subsurface Examples from the Cretaceous of North America: American Association of Petroleum Geologists Memoir 64, p. 137-223.

Wang, Y. Cerling, T. E. ; Quade, J. ; Bowman, J. R. ; Smith, G. A. ; Lindsay, E. H., 1993, Isotopes of paleosols and fossil teeth as paleoindicators: *in* Stuart, P.K., Lohmann, K.C., McKenzie, J., and Savin, S., eds., Climate Change in Continental Isotopic Records: American Geophysical Union, Geophysical Monograph 78, p. 241-248.

Wang, Y., and Cerling, T. E., 1994. A model of fossil tooth and bone diagenesis: Implications for paleodiet reconstruction from stable isotopes. *Palaeogeography, Palaeoclimatology, Palaeoecology*, 107: 281-289

Weltje, G.J., Meijer, X.D., and de Boer, P.L., 1998, Stratigraphic inversion of siliciclastic basin fills: a note on the distinction between supply signals from tectonic and climatic forcing: Basin Research, Vol. 10, p.129-153.

Wheeler, H.E., 1964, Base level, lithosphere surface and time-stratigraphy: Geological Society of America Bulletin, Vol. 75, p. 599-609

White, T., Witzke, B., Ludvigson, G., and Brenner, R., 2005, Distinguishing base-level change and climate signals in a Cretaceous alluvial sequence: Geology, Vol. 33, p. 13-16.

Wright, V.P., 1992, Paleopedology: stratigraphic relationships and empirical models *in* Martini, I.P. and Chesworth, W., eds., Weathering, Soils and Paleosols: Elsevier Science Publishers, p. 475-499.

Wright, V.P. and Marriott, S.B., 1993, The sequence stratigraphy of fluvial depositional systems: the role of floodplain sediment storage: Sedimentary Geology, Vol. 86, p. 203-210.

CHAPTER 2: NONMARINE SEQUENCE STRATIGRAPHY OF IGLESIA BASIN, NORTHWESTERN ARGENTINA: INTEGRATED SEISMIC AND OUTCROP INTERPRETATIONS.

Introduction:

The Iglesia Basin is a nonmarine Andean foreland basin ~75 km long and 40 km wide, consisting of approximately 3.5 km of Tertiary strata unconformably overlying Paleozoic basement. Best described as a wedge-top, or "piggyback", basin (see Ori and Friend, 1984), Iglesia Basin is located at S 30-31°, W 69-70° between the Frontal Cordillera (elevations to 6000 m above sea level) and westernmost range of the Precordillera thin-skinned thrust belt (maximum elevation ~3500 m; Figure 2.1). Previous interpretations of industry reflection seismic profiles from a basin-scale network combined with field reconnaissance had suggested the presence of basin-wide correlative stratigraphic sequences (Beer *et al.,* 1990; Fernandez-Seveso, 1993). Radiometric and magnetostratigraphic data constrained sequence deposition between approximately 20.2 and 4.3 Ma, with all but the lowest sequence forming between 9 and 4 Ma (Ré *et al.,* 2003). The quality and continuity of the seismic sequence boundaries as well as well-preserved outcrop belts make Iglesia Basin a remarkable test case for sequence stratigraphic principles within an entirely continental depositional environment (e.g. Milana, 1998; Den Bezemer *et al.,* 1999; Milana and Tietze, 2001). However, the fundamental question concerning the Iglesia Basin sequences remains unanswered, namely, "What factor or factors are responsible for sequence generation?"

Various genetic influences suggest themselves as causative agents in sequence generation, most probably tectonism and climate change for nonmarine settings. However, as suggested by Shanley and McCabe (1994), for a given basin, these extrinsic forces are likely to be superimposed (e.g. Figure 2.2). Therefore, an

Figure 2.1: Geographic position, bounding tectonic features, digital elevation model and seismic profile network for Iglesia Basin, San Juan Province, northwestern Argentina. Depth contours of Wadati-Benioff zone for Nazca oceanic plate subducting below South American continental plate (adapted from Cahill and Isacks, 1992).

Bolivia
Argentina
Chile
N
Chilean Flat-Slab Segment
Study Area
Peru- Chile Trench
Chile trench
400
300
200
150
100
50
S 22°
24°
26°
28°
30°
32°
64°
66°
68°
70°
W 72°
Contours of subducting Nazca Plate depth (km)
Precordillera
Frontal Cordillera
Iglesia Basin
Figure 2.2
W69°
W69°10'
W69°20'
W69°30'
W69°40'
W69°50'
S30°
S30°10'
S30°20'
S30°30'
S30°40'
5321
5322
5323
5324
5325
5326
5327
5328
5329
5330
5331
5332
5333
5334
5335
5336
5337
6500
5400
4300
3200
2100
1000
meters above sea level
0
10
km
20
30
Seismic profiles

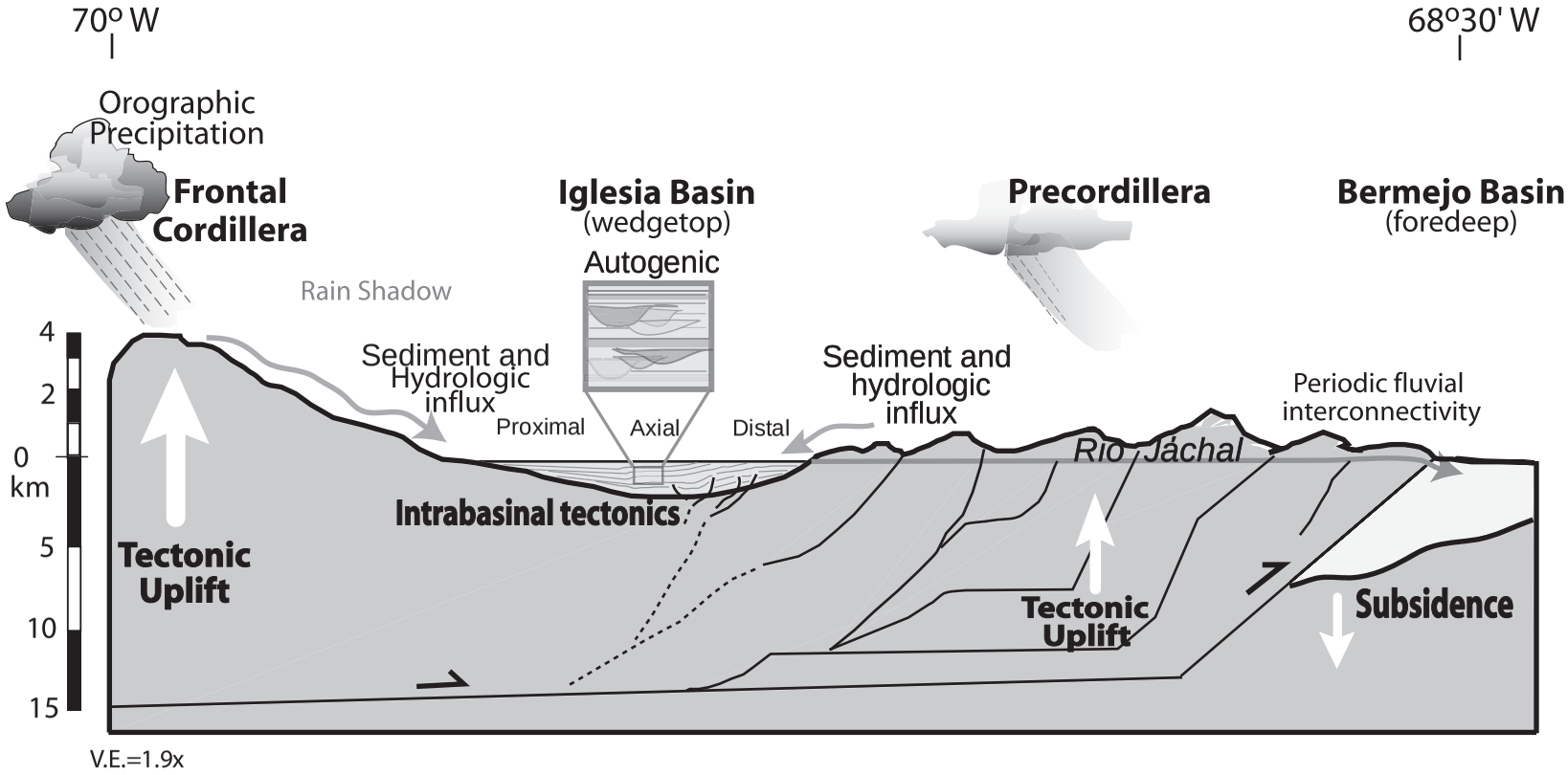

Figure 2.2: Simplified crustal scale cartoon of potential extrinsic and intrinsic (autogenic) controls on sedimentary deposition, erosion and transport affecting the Iglesia Basin. Cross section is at approximately S 30º15'. Topography is vertically exaggerated by 1.9x.

investigation of Iglesia Basin stratigraphic sequences must take into account: the timing and features of the regional orogenies, intrabasinal structures and active tectonics, the record of climate change (as gleaned from lithologic and isotopic signatures), and facies distributions that record variations in the drainage network and depositional environments.

The primary goal of this study is to test hypotheses about the factors controlling Iglesia Basin sequence development. Through integration of reinterpreted seismic reflection profiles and extensive outcrop-based observations, I provide a broadened perspective of the tectonic and climatic characteristics of Iglesia Basin. Special emphasis is placed on solving problems of stratigraphic correlation between subsurface and surface. Also, particular attention is paid to paleosols as sequence stratigraphic elements, which, along with associated lithofacies assemblages, function as sedimentologic and environmental indicators.

Tectonic Setting:

The Iglesia Basin is an intermontane nonmarine basin that formed by coupled uplift of the Frontal Cordillera and Precordillera fold-thrust belt. The Frontal Cordillera represents a broad crustal-scale fault-bend fold anticline and is linked to the Precordillera by a decollement ~16-18 km below the Iglesia-Calingasta Valley (Allmendinger *et al.,* 1990). As such, the Iglesia Basin represents the wedgetop (i.e. “thrust-top” or “piggyback”) depozone of the Andean foreland, with the more extensive Bermejo foredeep depozone to the east (Fig. 2.2). DeCelles and Giles (1996) defined the wedge-top depozone as the frontal portion of the orogenic wedge, whose deposits are characterized by extremely coarse and immature sediment, growth structures, and an abundance of unconformities. In Iglesia Basin, the latter two properties characterize the entire basin, and as shall be discussed, such unconformities are variably expressed in seismic profiles and outcropping strata. For subsequent

discussion, the region S 30°-30°65', W 69°-69°45' is referred to as Iglesia basin, as this is the seismically-defined depositional area for the majority of Tertiary strata.

The Iglesia-Calingasta Valley (~S 30° – 32°, W 69°- 70°), of which Iglesia Basin comprises the northern half, is geographically positioned in a notable area with respect to plate dynamics and inherited basement geology. Beneath the South American continental plate the subducting Nazca Plate dips <30°, which is somewhat shallower than typical subduction angles of 45° or greater (Uyeda, 1982). Additionally, the portion of the Nazca plate from S 28° -33° flattens to a subhorizontal bench at ~250 km inboard of the Chilean trench, and this "Central Chilean flat-slab" subduction extends under the continent for >400 km before steepening again (Cahill and Isacks, 1992; Figure 2.1). The Iglesia-Calingasta Valley is positioned directly above the transition zone between 30° dip and subhorizontal dip of the subducting plate. The valley also represents the proposed suture zone between the Devonian (?) "Chilenia terrane" with the Cambro-Ordovician "Precordillera terrane" (Ramos *et al*., 1986; Thomas and Astini, 2003). A suture is not exposed or seismically imaged, but is inferred on the basis of Ordovician ophiolites (Yerba Loca Formation) that crop out fairly continuously along the eastern valley margin and accompany Late Ordovician deep marine units (Ramos *et al*., 1986).

At about 26 Ma, convergence between the Nazca oceanic plate and South American continent changed from oblique to orthogonal and subsequently increased in velocity (Pilger, 1984). Convergence rates since 26 Ma have averaged ~110 mm/yr along the South American plate boundary between S 10 ° and S 40° (Pardo-Casas and Molnar, 1987). Based on GPS velocity solutions, the current plate convergence vector for the Nazca plate at S 33.63° W 78.84° is measured as 63 mm/year trending 083° (Kendrick *et al.,* 2003). Nazca plate velocity modeled from geodetic estimates of Euler

rotational poles gives a range of values from ~63-66 mm/yr at S 30° W 72.4°, trending 080° (Kendrick *et al.,* 2003).

A thickened crust and thinned, hydrated mantle lithosphere characterize the Central Chilean flat-slab region (Kay *et al.,* 1999). From depth-phase conversion using pmP (Mohorovicic discontinuity) reflectors, the crust below Iglesia Basin is estimated to be ~56 km thick (McGlashan *et al.,* 2006). This result is comparable to results from Pn phase velocity modeling using broadband stations installed at S 30° that suggest 60-65 km thick crust beneath the Iglesia Basin and its margins (Fromm *et al.*, 2004).

The Iglesia-Calingasta Valley is structurally fragmented by the north-south trending El Tigre fault system (26°-36° S, 69° W, Bastías, *et al.*, 1997). At least six blind thrusts are imaged in seismic which offset Neogene strata. The ages of activity of the El Tigre thrusts are younger than ages of initiation of the thin-skinned Precordillera thrust belt (Jordan *et al.,* 1993). Fault-bend folding above the El Tigre faults has exposed portions of Paleozoic metasedimentary basement rocks and Miocene-Pliocene sedimentary units. Uplift and folding associated with the thrusts had the effect of shifting the eastern boundary of sedimentary deposition progressively toward the west through time, occurring most significantly after 5 Ma (Ré *et al.*, 2003). The kinematics of displacement of the El Tigre fault set is documented only for Quaternary deformation. Quaternary motion along El Tigre fault is fragmented; in the area of Iglesia Basin, east-west extension dominates (e.g. Bastías *et al.,* 1984; Bastías *et al.*, 1997), although a 120-km-long segment of the fault south of the Iglesia Basin (~S 31°) shows minor right-lateral strike-slip motion estimated at 1 mm/yr via cosmogenic dating of abandoned alluvial fan surfaces (Siame *et al.,* 1997). Quaternary right-lateral offset along the El Tigre fault is also inferred north of Iglesia (Bastías *et al.,* 1997).

Various authors have inferred a number of faults in Iglesia Basin based on perceived lineations and structural trends (e.g. Furque, 1979; Ragona *et al.,* 1995). Some of these are imaged in seismic and interpreted as splays of El Tigre fault system (Figure 2.3). Others, however, are not well resolved or crossed by seismic profiles, and lack stratigraphic or structural criteria to infer their origin or relationship to El Tigre thrusts. Subsequent discussion of intrabasinal structures (chiefly fault-bend folds and blind thrusts) is limited to those clearly imaged in seismic profiles.

Tectonic mechanisms affecting accommodation:

Wedgetop or "piggyback" foreland basin deposits reflect the competition between tectonic uplift and regional subsidence (Figure 2.2). Such basins form in interior portions of a thrust belt as a result of the step-wise propagation of thrust-sheets toward the foreland. As successive thrust sheets become inactive, they and adjacent structural lowlands commonly are passively carried toward the foreland by the next active thrust (Ori and Friend, 1984). In addition, in some cases, thrust activity in the internal part of a thrust belt may post-date initial migration of the thrust front, in which case this “out-of-sequence” internal thrusting may result in subdivision of a pre-existing wedgetop basin (e.g. Burbank *et al.,* 1999). Beer *et al.* (1990) and Talling *et al.* (1995) outlined possible causes of subsidence (expressed as accumulation) and uplift (expressed as incision) within wedgetop basins, illustrating the potential competition between uplift and subsidence, thus affecting sediment deposition and preservation patterns. Several scenarios presented by these workers are addressed below and summarized in Figures 2.4, 2.5 and 2.6.

The wedgetop depozone differs from other parts of a foreland basin in that crustal-scale loads and local-scale structural relief exist on both sides of the valley, such that both margins likely contributed to the basin’s subsidence history. To a first degree, the entirety of the orogenic wedge and the decollement below are subject to

Figure 2.3: Iglesia Basin outcrop belts, major structural features, and northern portion of seismic reflection profile grid. Labeled localities and measured sections are referenced in text. Splays of El Tigre fault system are those imaged in seismic profiles.

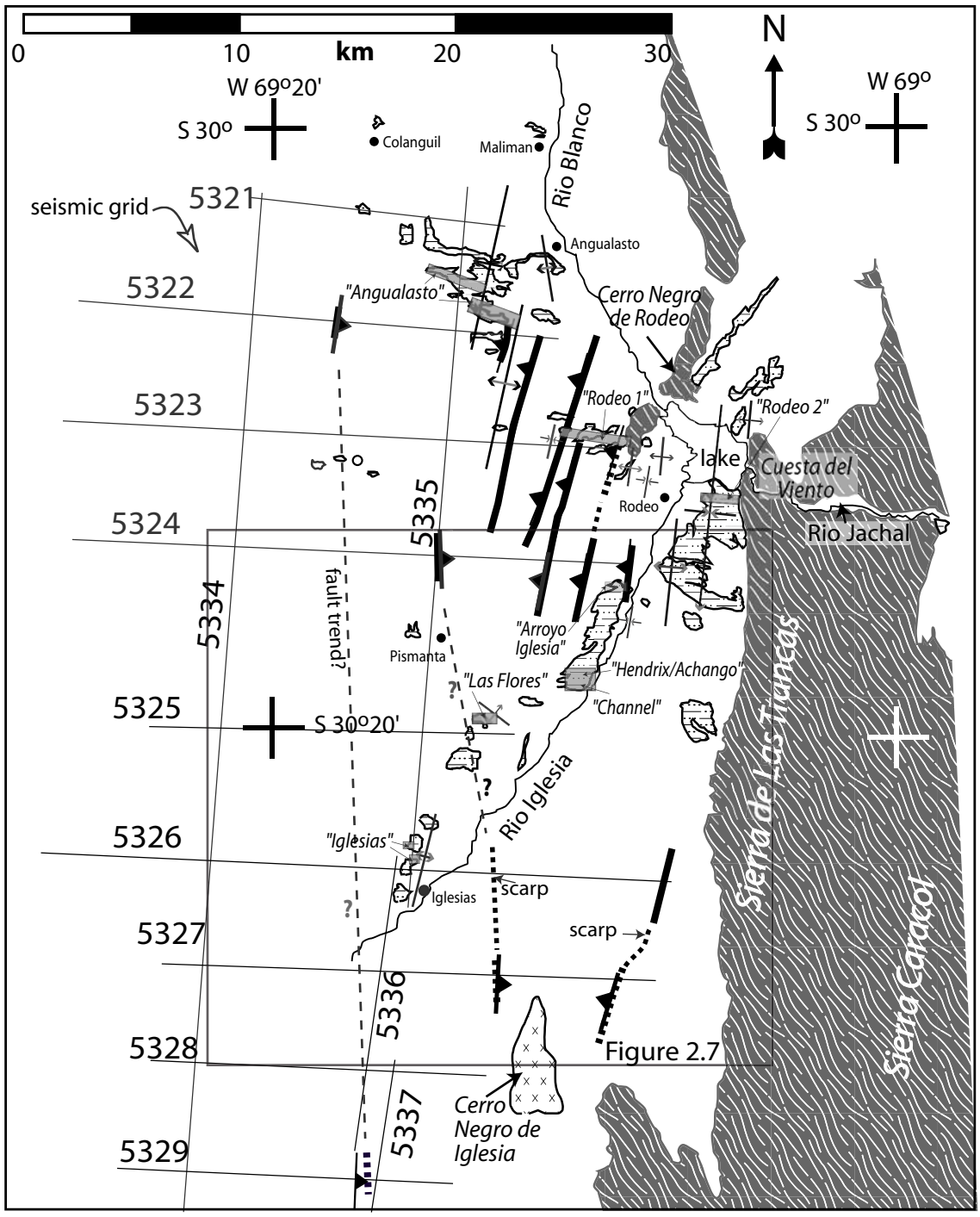
0
10
km
20
30
N
W 69º20'
S 30º
W 69º
S 30º
Colanguil
Maliman
Rio Blanco
seismic grid
5321
5322
5323
5324
5325
5326
5327
5328
5329
5334
5335
5336
5337
Angualasto
"Angualasto"
Cerro Negro de Rodeo
"Rodeo 1"
"Rodeo 2"
lake
Cuesta del Viento
Rodeo
Rio Jachal
fault trend?
Pismanta
"Arroyo Iglesia"
"Hendrix/Achango"
"Las Flores"
"Channel"
S 30º20'
Rio Iglesia
"Iglesias"
Iglesias
scarp
scarp
Sierra de Las Tranca
Sierra Caracol
Cerro Negro de Iglesia
Figure 2.7
Neogene outcrops
Post Pliocene alluvium
Thrust fault imaged in seismic
Fault inferred from outcrop
Miocene intrusives
Paleozoic metasediments/ intrusives
Measured section
Town/locality

long-wavelength isostatic compensation (subsidence) due to crustal thickening. If crustal temperatures are low, isostasy will be regional and flexural, the wavelength of flexure dependent on the elastic thickness of the crust (Jordan, 1981). Additionally, since flexural deformation of the crust follows a sinusoidal profile which dampens away from the load, subsidence adjacent to the load is coupled with a distal, smaller amplitude uplift called the "forebulge". Superposition of flexural deformation profiles from each margin may result in destructive interference (see Figure 2.4A), particularly adjacent to the narrower load (e.g. Precordillera).

The topographic expression of intrabasinal folds may have affected adjacent syntectonic deposition. The folds themselves would have become local source areas or barriers to sedimentation, as well as interacting with pre-existing drainage. A common result of folding is deflection or diversion of pre-existing drainages, resulting in the establishment of axial or strike-parallel drainage systems (e.g. Burbank *et al.*, 1999; Fig. 2.5). Also, during active uplift of the fold, the footwall subsides and fluvial channels may be "dammed" allowing for upstream aggradation (Talling *et al.*, 1995; Fig. 2.4B). Tectonic quiescence permits channel profile reequilibration, probably leading to incision of the aggraded strata and/or the fold itself (Figure 2.6C).

Basin uplift is also possible in the wedgetop depozone if the underlying decollement linking the thrust belt dips away from the foreland. In this case (Fig 2.4C), the vector of thrust motion has a component of vertical motion and the overlying strata may uplift as well as translate in the direction of thrust propagation. For the coupled Frontal Cordillera – Precordillera system, the basal detachment is presumed to be 16-18 km deep under Iglesia Basin at S 30°, versus 15 km deep at the eastern edge of the thrust belt, ~60 km to the east (i.e. a decollement dip of 0.38° to 1.15° west; Allmendinger *et al.*, 1990). If the Iglesia Basin translated east by ~70 km in the past 20 Ma (based on minimum estimates of movement, e.g. Jordan *et al.*, 1993;

Zapata and Allmendinger, 1996), cumulative uplift would be as little as 500 m to a maximum of 1400 m, equal to rates of 0.003-0.007 cm/yr. These uplift rates are an order of magnitude lower than one-dimensional (i.e. stratigraphic column) rates of sedimentary accumulation for Mio-Pliocene strata in Iglesia Basin (as much as 0.1 cm/yr). Thus, this mode of uplift probably has minimal effect on the basin's subsidence profile through time.

It is noteworthy that crustal loading adjacent to Iglesia Basin may not be flexurally, but rather locally, compensated by isostasy. 2-D and 3-D mechanical modeling by Cardozo and Jordan (2001), assuming an infinite elastic lithosphere, failed to accurately model the Iglesia Basin geometry (i.e. topographic profile). Furthermore, modern regional gravity surveys (Stewart and Watts, 1997) suggest local compensation of the Frontal Cordilleran crustal load.

Beer *et al.* (1990) suggested a model by which sequences are generated by episodic Precordillera thrust events (Fig. 2.6). During thrusting, enhanced relief between the Precordillera and Iglesia Basin would result in restriction of the wedgetop-draining river, the Rio Jáchal, causing fluvial deposition throughout the basin (Fig 2.6 b). Then, when structural uplift ceased, the river would adjust to a lower baselevel within the Bermejo foreland basin to the east, downcutting through the Precordillera bedrock and Iglesia sedimentary units (Figure 2.6c). Sedimentary deposition at Huaco, Argentina, where the Río Jáchal exits the Precordillera, has included clasts of Frontal Cordilleran provenance since at least 13.7 Ma (after Jordan *et al.,* 2001), suggesting periodic drainage connectivity between wedgetop and foredeep depozones. Additionally, the river valley follows a major east-trending structural discontinuity at S 30° (Jordan *et al.,* 1993), suggesting structural pinning of the Rio Jáchal at this latitude. Episodic changes between internal and external drainage is inferred for Iglesia Basin from changes in clast composition percentages at Huaco

Figure 2.4: General cartoon models of isostatic crustal subsidence and uplift for wedgetop basins (after Talling *et al.*, 1995) adapted to structural geometry of Iglesia Basin. A: Internal flexural subsidence profile of basin as result of crustal loading of margins (Frontal Cordillera to west, Precordillera fold-thrust belt to east). B: Local subsidence of footwall of intrabasinal thrust faults. C: Uplift associated with dip of underlying decollement of the orogenic wedge.

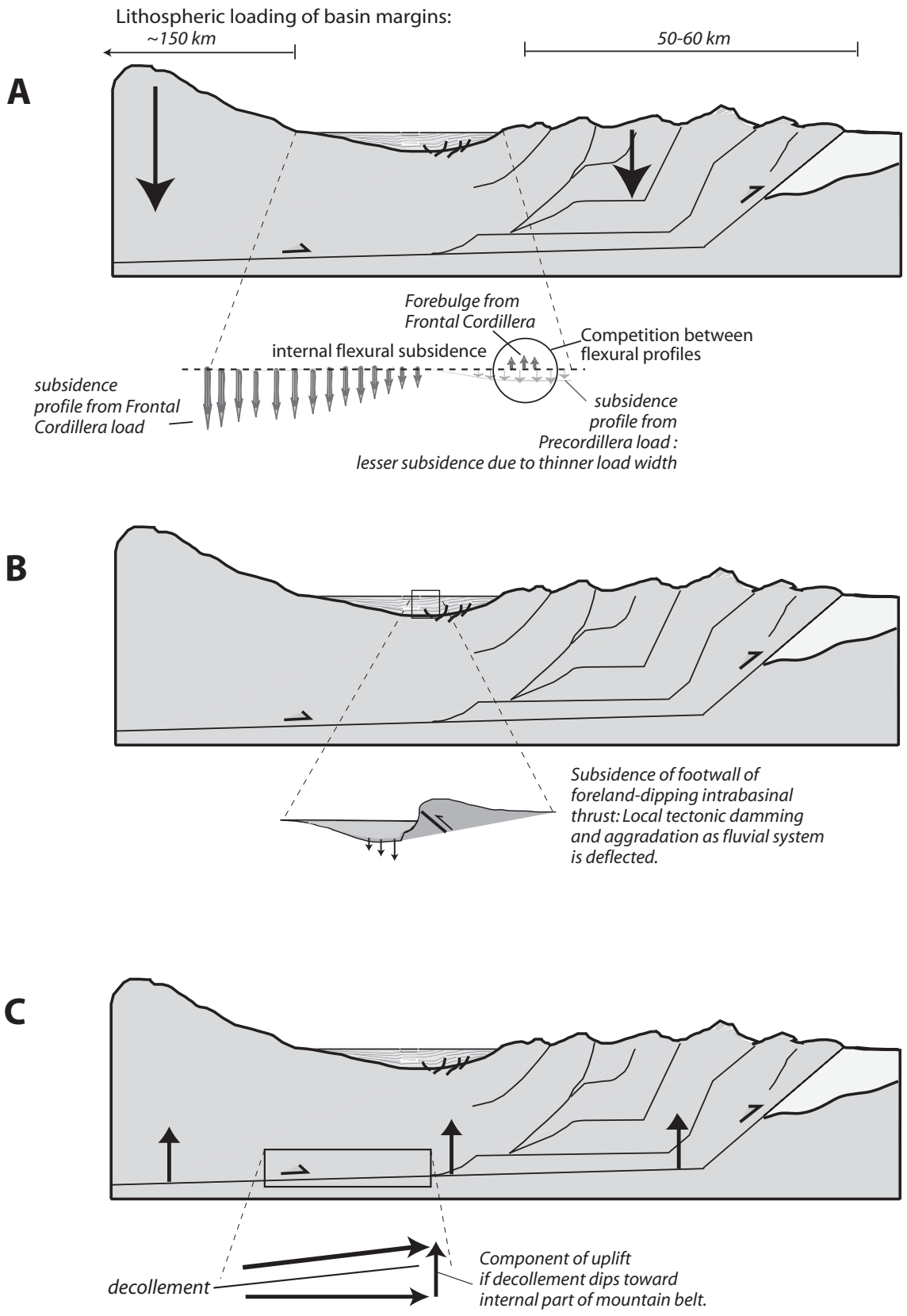
Lithospheric loading of basin margins:
~150 km
50-60 km
A
Forebulge from
Frontal Cordillera
Competition between
flexural profiles
internal flexural subsidence
subsidence
profile from Frontal
Cordillera load
subsidence
profile from
Precordillera load :
lesser subsidence due to thinner load width
B
Subsidence of footwall of
foreland-dipping intrabasinal
thrust: Local tectonic damming
and aggradation as fluvial system
is deflected.
C
decollement
Component of uplift
if decollement dips toward
internal part of mountain belt.

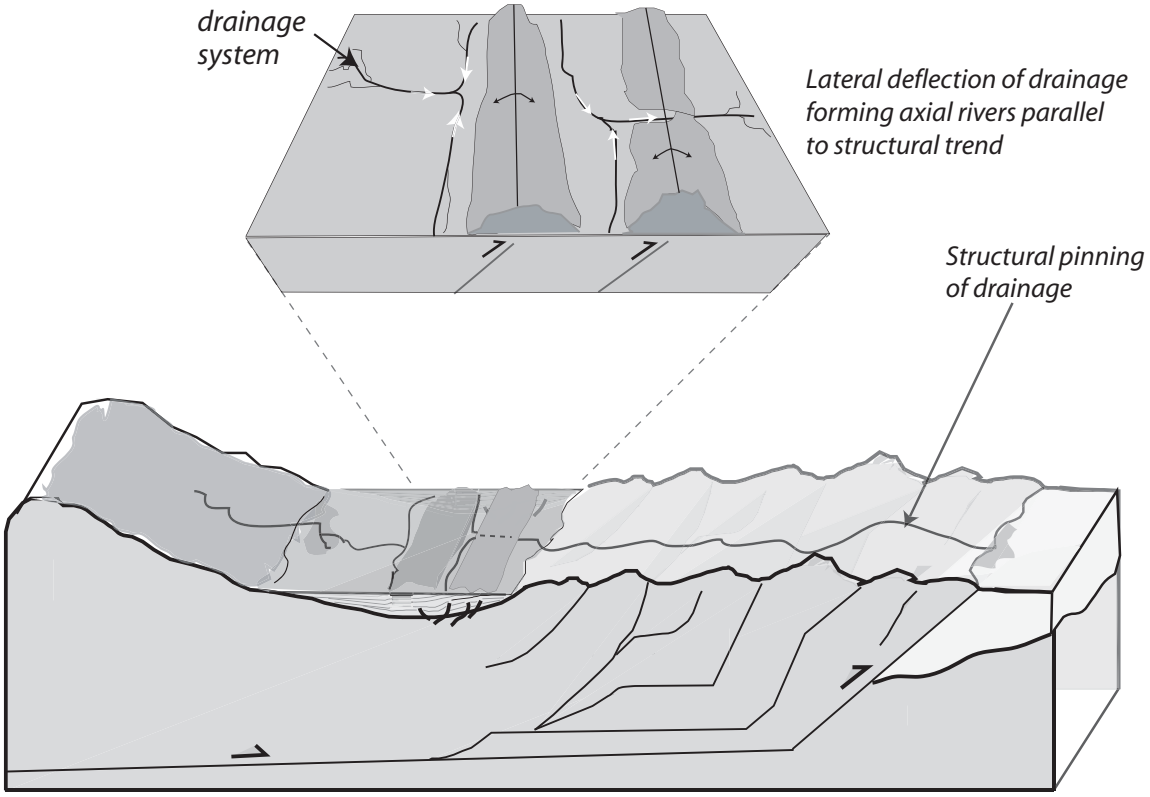

Figure 2.5: Deflection of wedgetop fluvial system via intrabasinal thrust-parallel structures; External drainage established and maintained by thrust-perpendicular structural discontinuity.

(e.g. Damanti, 1989; Fernández, 1996; Jordan *et al.*, 1997). However, despite detailed individual temporal constraints of grain provenance and Precordilleran thrust events, correlation of these with times of Iglesia Basin sequence accumulation and erosion is poor (see also Jordan *et al.*, 2001). Thus, Beer *et al.*'s (1990) model for sequence accumulation and incision in response to episodic Precordilleran thrusting is plausible, but not independently confirmed.

Patterns of onlap and growth stratal geometries imaged in seismic profiles (see below) indicate that intrabasinal folds in the Iglesia Basin were active during Tertiary sedimentary deposition. These folds and associated faults may have affected surface gradients near the basin axis, with consequent changes of accommodation space and streamflow, or may have forced rerouting and/or capture of particular channel systems (Fig. 2.5), leading to localized erosion and altered patterns of fluvial architecture.

Uplift history of Frontal Cordillera and Precordillera:

Though subsidence along the Chilean coast of South America and associated Andean orogenesis has occurred since the Jurassic, the current phase of Andean uplift ("Quechua phase") began in the early Miocene (e.g. Jordan *et al.*, 1983; Mégard *et al.*, 1984). The exact timing of spatially distinct episodes as well as approximate elevations is less well known. Because the same decollement that links the Precordillera thrusts also controls uplift of the Frontal Cordillera, then timing constraints of fault motion may be applied to both structural boundaries of the Iglesia basin (Cardozo and Jordan, 2001).

At S 30°, 130-170 km of upper crustal shortening have been accommodated by thrust faulting in the Precordillera and Frontal Cordillera of the Andes, with 60-75% of the shortening accommodated by the Precordillera (Allmendinger *et al.*, 1990). Six major east-verging thrust sheets have been mapped (Fig. 2.2) and their relative timing of motion conforms to that of a critically deforming orogenic wedge (Jordan *et al.*,

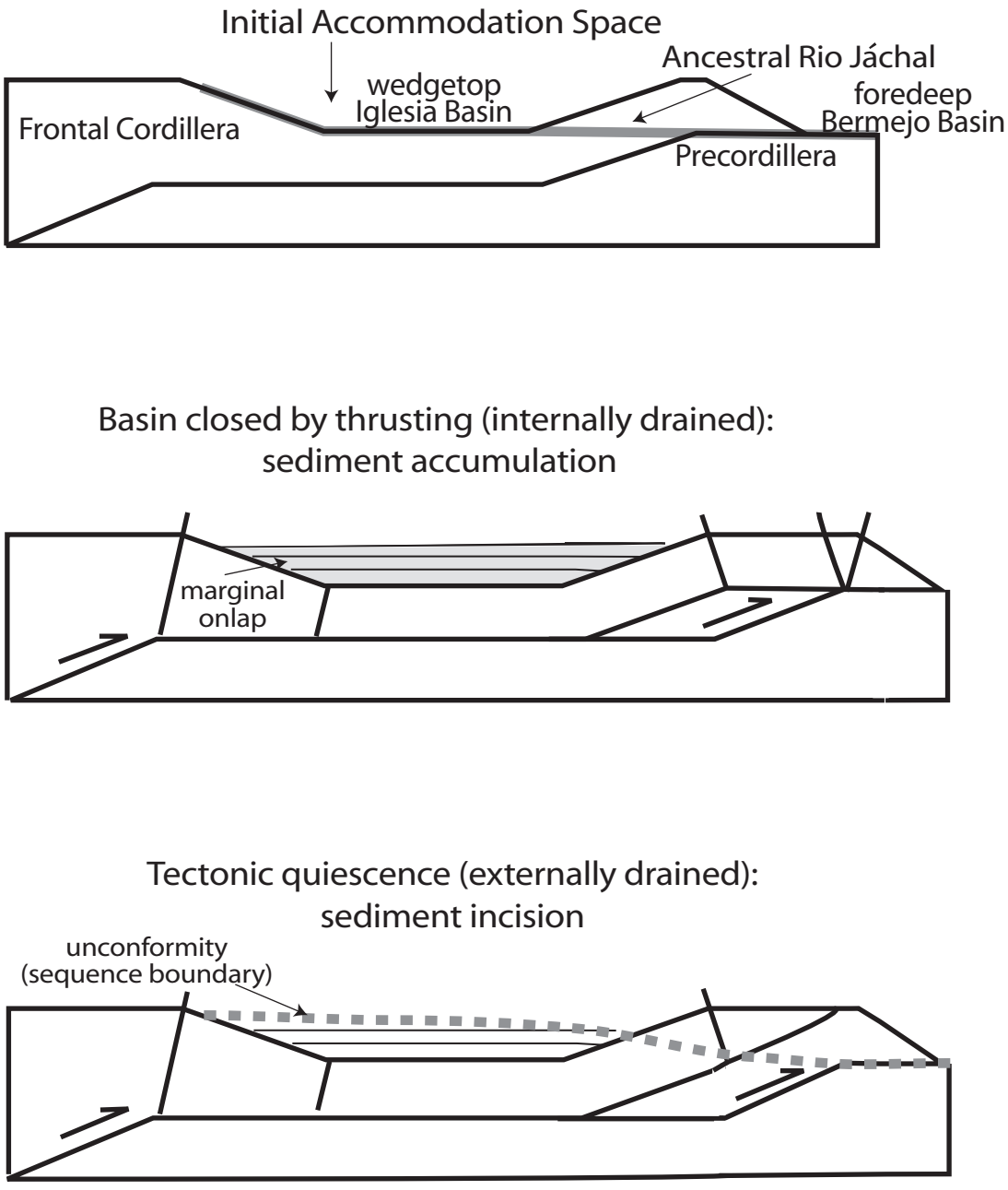

Figure 2.6: Tectonic model of sequence development in Iglesia Basin via creation of relative relief between basin floor and Precordillera fold-thrust belt, and internal versus external drainage of wedgetop depozone (after Beer *et al*., 1990).

1993; 2001). The westernmost of the Precordillera thrusts (Rio las Trancas thrust plate) experienced movement by ~21 Ma, providing a topographic barrier to the east side of Iglesia basin, which continued to develop throughout the Tertiary (Jordan *et al.*, 2001).

North of Iglesia Basin, Riquelme (2003) documented Frontal Cordillera elevation in excess of 2 km prior to 17 Ma. On the basis of radiometric, magnetostratigraphic and petrographic studies in adjacent basins, the Frontal Cordillera was actively uplifting between S 30° and S 33° from15-12.5 Ma (Jordan *et al.*, 1996; Irogoyen, 1997; Cristallini and Ramos, 2000). Additional evidence for episodic Frontal Cordilleran uplift comes from foreland lithofacies information (e.g. clast provenance, paleocurrents, relative ages; Irogoyen, 1997) angular unconformities and pedipain surfaces in the Frontal Cordillera, recognized near the El Indio copper prospect (along the Chile-Argentina border between S 29°20' and S 30°30'; Ramos *et al.*, 1987; Bissig *et al.*, 2001, 2002). Three planar surfaces, named Frontera-Deidad, Azufrera-Torota and Los Rios, are separated in elevation by 200-400 m and interpreted as erosive events corresponding with pulses of uplift at 17-15 Ma, 14-12.5 Ma, and 10-6 Ma, respectively. Two of these pedimentation events correspond with regional inter-formational angular unconformities (between Escabrosos and Cerro de las Tórtolas Formations, 17.5 – 17 Ma; between Cerro de las Tórtolas and Vacas Heladas Fomations, 14-12.7 Ma; Ramos *et al.*, 1987; Bissig *et al.*, 2001; see below). The above mentioned datasets, as well as reflector rotations against the western margin of the Iglesia Basin (discussed below), permit a general summary of Miocene-Pliocene episodes of Frontal Cordilleran and Precordilleran uplift (Table 2.1).

Neogene volcanic history of the Central Andes near Iglesia Basin:

Although little discussed in previous evaluations of Iglesia Basin's stratigraphy, volcanic eruptions in nearby areas of the Central Andes may have

Table 2.1: Timing of uplift of Iglesia Basin margin structures, S 28º - 33º. Sources: [1]: Ramos *et al.*, (1987) [2]: Jordan *et al.* (1993); [3]: Zapata and Allmendinger (1996); [4]:Irogoyen (1997); [5]:Bissig *et al.*, (2001); [6]:Bissig *et al.* (2002); [7]: Ruskin (2006).

Frontal Cordillera		Precordillera	
Age (MA)	**Evidence**	**Evidence**	**Age (MA)**
5.2 to 4.5	Rotations of Iglesia Basin seismic reflector[7]		
>6.9	Rotation of Iglesia Basin seismic reflector[7]		
10 to 6	Los Rios peneplain surface[5,6]	Maximum rate of Precordillera shortening[3]	11.3 to 9.5
11.7 to 9	Foreland basin provenance, facies[4]		
14 to 12.5	Azufrera-Torota peneplain surface[5,6]		
	Cerro de Las Tortolas- Vaca Helada unconformity[1]	western and central Precordillera thrusting[2,3] (minimum duration)	14.7 to 2.6
16	Syntectonic foreland basin strata[4]		
17 to 15	Frontera-Deidad peneplain surface[5,6]		
	Escabrosos-Cerro de Las Tortolas unconformity[1]	Initial thrusting of western Precordillera (Trancas thrust)[2,3]	~21 to 18.5

affected drainage basins and influenced sediment flux rates to Iglesia Basin. Though the Iglesia-Calingasta valley is along strike with the Miocene volcanic arc of the Central Andes, the Central Chilean flat-slab segment is relatively nonvolcanic at present and has been for the past 5 Ma (Kay *et al.*, 1999). With the exception of an andesitic-dacitic intrusion (see below) and thin ash deposits of indeterminate source, there are no post-Miocene volcanic rocks in Iglesia Basin (Leveratto, 1976; Bercowski, 1993). However, as shall be discussed below, the Miocene basin fill includes volcaniclastic deposits, notably as voluminous rhyolites and associated andesitic clasts deposited sometime between 20-12 Ma (Figure 2.7). Interbedded volcanics post 9 Ma are generally rhyolitic ash fall deposits less than one meter thick or fluvially-recycled tuffaceous sandstones.

Eight stages of Neogene arc volcanism have been recognized in the Frontal Cordillera from S 29° - 31°, five of which are concurrent with Iglesia basin accumulation (Kay *et al.,* 1999; Bissig *et al.,* 2001). Dacitic to mafic andesitic lava flows and subordinate tuffs and volcaniclastic breccias characterized the Escabroso Group (21-17.5 Ma; Bissig *et al.,* 2001), these units formerly referred to as late Doña Ana stage volcanism (e.g. Kay *et al.*, 1999). Volcanic activity in the arc over the Chilena flat-slab gradually diminished after 17 Ma (Bissig *et al.,* 2001). The Cerro de Las Tórtolas Formation silicic andesitic stratovolcanoes erupted (17-14 Ma) followed by Vacas Heladas Formation dacitic eruption (12.7 – 11 Ma). Andesitic arc volcanism terminated in the Frontal Cordillera by 9 Ma (Kay *et al.*, 1999). The Pascua Formation (8-7.5 Ma) consists of isolated dacitic dikes and tuffs. Larger, more rhyolitic eruptions followed during the Vallecito stage (7-5.5 Ma, Kay *et al.,* 1999; 6.2 – 5.5 Ma, Bissig *et al.*, 2001).

An intrabasinal andesitic to dacitic volcanic center is located in the southern Iglesia Basin (S 30°30', W 69°10'), referred to as Cerro Negro (Fig. 2.9). Leveratto

(1976) obtained a K/Ar age of 17±5 Ma from biotites in a dacite sample from this center. Ruskin resampled the unit for $^{40}Ar/^{39}Ar$ dating of plagioclase, yielding very discordant $^{40}Ar/^{39}Ar$-age spectrum (i.e. no isochron or plateau age assigned) with low radiogenic yields (see Appendix B). An age range of 12 ± 3.7 Ma is a conservative estimate. The overlap of age ranges obtained by Leveratto (1976) and Ruskin suggests that Cerro Negro was active ~12 - 16 Ma, contemporaneous with the Cerro de las Tórtolas Formation of the Frontal Cordillera.

Deposits from the Cerro Negro center are thought to be localized in the adjacent southern portion of the basin. Bercowski (1993) mapped various volcaniclastic facies north of Cerro Negro (see Fig. 2.7) and interpreted them to be locally sourced. However, the nature of the volcanic source is ambiguous. Volcanic facies suggestive of fissure eruptions are found to the northeast (near Cuesta del Viento), and Cerro Negro is flanked by traces of El Tigre fault splays, suggesting possible fault-control of volcanic eruptions (Bercowski, 1993). Conversely, Bercowski (1993) also suggested a caldera-like ring structure just north of Cerro Negro which may have sourced some of the igneous units. Reconnaissance of this feature is inconclusive; there is not clear evidence of continuous caldera-rim fault scarps and the deposits are very dispersed and weathered, confounding clear stratigraphic relationships. It is equally likely that the "caldera" feature is actually formed by splays of the El Tigre faults, as the structural trend can be traced north and south of the proposed caldera.

General stratigraphy:

The Tertiary sediments of Iglesia Basin have been variously divided into formations and sequences with some disagreement. Wetten (1975) originally proposed the name Iglesia Group, composed of two formations: 1) Lomas del Campanario Formation, the lower unit, comprised of a basal agglomeratic member and an upper

Figure 2.7: Lithofacies and radiometric ages associated with igneous deposits in southern Iglesia Basin, near Cerro Negro andesitic-dacitic center (after Leveratto, 1976; Tabbutt *et al.*, 1989; Kay *et al.*, 1996; this study). Location is marked as rectangle on Figure 2.3.

Volcanic bombs
Mixed sediments (volcanic and Iglesia Group sediments)
Lahar facies
Volcanic detritus/ avalanche
Seismic line
5327
Mapped trace of El Tigre faults
Dated sample locality
proposed caldera (Bercowski, 1993)
5326
5327
5334
5336
37
69 10'
69 20'
30°20'
30°30'
Las Flores
BR03-26
6.54 +/- 0.03 Ma
BR03-33B
6.26+/-0.09 Ma
Lomas del Campanario
Iglesias
Bella Vista
Cerro Negro
BR0328
12+/- 3.7 Ma
11+/- 0.5 (Kay et al., 1999)
10.2+/- 1.4 Ma (Tabbutt et al., 1989)

conglomeradic member, and 2) Las Flores Formation, also subdivided into two members, the lower being volcaniclastic and the upper member dominantly sedimentary. Subsequently, Furque (1979) mapped all Tertiary sediments as Rodeo Formation, consisting of basal conglomerates and calcareous and sulfate-rich sandstones above. To the north of the town of Rodeo, the Tertiary sediments tectonically overlie the Devonian Punilla Formation, while along the eastern basin margin Tertiary strata unconformably overlie the Ordovician Yerba Loca Formation (Furque, 1979). Later stratigraphic summaries reinstated the Lomas del Campanario and Las Flores names as unconformity-bound members of the Rodeo Formation (Beer *et al.*, 1990) or Iglesia Group (Contreras *et al.*, 1990; Ré *et al.*, 2003). Gagliardo *et al.* (2001) argued that the Lomas del Campanario and Las Flores names should be abandoned in favor of an all-encompassing Rodeo Formation, on the basis of lithologic similarity between type sections and a perceived tectonic rather than erosive contact between members. For the level of detail required of sequence stratigraphic analysis (e.g. stratal thicknesses of tens of meters, localized or subtle unconformable surfaces), this study will not further consider formation names. Tertiary basin fill is herein referred to collectively as the Iglesia Group *sensu* Wetten (1975).

Previous Work in Iglesia Basin:

During the past three decades, stratigraphic studies in Iglesia Basin have provided evidence that the region presents ample possibilities to test sequence stratigraphic concepts in a nonmarine framework. Iglesia Basin's general stratigraphy and diatomite deposits were documented by Wetten (1975). Furque (1979) mapped the Iglesia Valley and west-central Precordillera and briefly discussed regional geologic history, climate and economic mining potential. Fieldwork by Johnson *et al.* (1987) and Beer (1989) led to detailed, but still localized descriptions of strata in the northern basin. Using industry-grade seismic reflection data from a basin-scale network of 14

lines, Snyder (1988) inferred the presence of nonmarine sequences within the Tertiary fill. Beer (1989) subsequently documented five seismic sequences, based on onlap and truncation patterns. Later, the seismic data were reinterpreted by Fernández-Seveso (1993) to include additional sequences bringing the total to eleven. Detailed but localized field campaigns and magnetic polarity studies increased understanding of basin features and their temporal ranges on the local scale while attempting to establish sequence boundaries (very well-imaged in the basin-scale seismic network) in outcrop (e.g. Johnson *et al.*, 1987, Ré and Barredo, 1993; Ré, 1994; Ré and Stein, 1994; Jordan *et al*, 1997). This study reports on information gathered during four field seasons in Argentina, during which almost eleven weeks were spent in the Iglesia Basin. These campaigns included observations at additional outcrop localities and reassessed previous interpretations of the characteristics of the seismic sequence boundaries in exposed strata, allowing a more complete discussion of basin deposition.

Iglesia Basin seismic sequence stratigraphy:

This study benefits from having a basin-scale industry-quality seismic network from which to interpret the subsurface depositional architecture (Fig. 2.1). Seventeen 48-channel active (primacord explosive) source reflection seismic profiles from Argentine oil company Yacimientos Petrolíferos Fiscales (YPF) were collected in Iglesia Basin in 1980-1981. The profiles were processed by Horizons Consulting for YPF in the early 1980's and several lines (5324, 5326 and 5333) were reprocessed by Snyder (1988) in an effort to better image sub-basinal structures. Thirteen west-east profiles are approximately 25-35 km in length, while four north-south tie lines range from 15-75 km long. The total profile length of the network is in excess of 950 km. The resultant seismic grid covers the majority of the longitudinal dimension of the Iglesia Valley (~2600 km^2). However, the eastern portion of the basin (5-10 km west of the Sierra de Las Trancas) is not imaged in seismic. Five seconds of two-way travel

time (TWTT) are recorded in the unmigrated sections, although reasonably continuous reflectors are common only in the upper 2 seconds of data.

The first detailed interpretation of the reflection geometries was conducted by Beer (1989), who denoted five mostly-conformable intervals separated by sequence boundaries that can be correlated between profiles throughout the basin. The sequence boundaries were defined by reflector onlap to the west and local truncation of underlying reflectors. The overall lenticular geometry of the basin fill was noted, with the thickest Tertiary basin fill near the center of the seismic network and younger sequences restricted to the western part of the basin (Beer *et al.,* 1990). By converting the position of the land surface into the time domain and tracing reflections across folds, seismic sequence boundaries were extrapolated to the surface for general comparison to outcrop characteristics (Beer *et al*., 1990).

The Iglesia Basin seismic network was subsequently reassessed by Fernandez-Seveso (1993), who increased the number of seismic sequences to eleven. Subdivision of the Tertiary basin fill permitted finer observations of variation in tectonically-controlled accommodation space through time. However, with finer subsurface subdivision came the need for greater precision in extrapolation to surface outcrops, which was challenged by the gentle dips in the near-surface seismic mute zone as well as complex folds and faults in the central basin. Nonetheless, the eleven sequence framework formed the basis for subsequent field assessment of sequence boundary characteristics as well as the chronology of accumulation. Radiometric, magnetostratigraphic, and biostratigraphic dating (Johnson *et al.,* 1987, Ré and Barredo, 1993; Ré, 1994; Ré and Stein, 1994; Jordan *et al*, 1997, Ré *et al*, 2003) constrain sequence deposition between approximately 20.2 and 4.3 Ma; all but the lowest sequence formed between ~9 and 4.3 Ma. The two intervals of accumulation

(20.2 to >9 Ma, <9 – 4 Ma) correspond with intervals of diminished shortening rate in the adjacent Precordillera fold-thrust belt (Jordan *et al.,* 1993; Ré *et al.,* 2003).

Hypotheses for sequence generation:

Proposed origins of the sequences emphasize one extrinsic mechanism as dominant (e.g. purely-tectonic or purely-climatic control). These models have not been rigorously tested against subsequent field observations, nor have more likely alternative, combined models been considered. Each end-member model is discussed and critiqued below.

Beer *et al.* (1990) suggested a tectonic model for Iglesia Basin sequence genesis corresponding to the thrust history of the Precordillera fold and thrust belt (Figure 2.6). The role of thrusting in creating accommodation space has already been discussed. A variation on this model is that, downstream of Iglesia Basin, the foreland-draining Rio Jáchal River was dammed by small-scale topographic barriers formed by thrusting, causing base level rise and fluvial deposition throughout Iglesia basin. Then, when erosion broke through the structural dam, the river could readjust its profile to the baselevel within the Bermejo foreland basin to the east, downcutting through the Precordillera bedrock and Iglesia sediments. Clast composition data which suggest cyclic changes of provenance from the Frontal Cordillera to the Precordillera on the 10^5 year scale can be interpreted to be consistent with Beer *et al.*'s models (Jordan *et al.,* 1997). However, the Beer *et al.* (1990) model assumes that climate was semi-arid throughout sequence deposition and that the Frontal Cordilleran headwater lithologies are homogeneous and respond uniformly to erosion, resulting in the overly-simplified case of constant sediment supply. Later, when additional age constraints became available to test the model, it became apparent that the ages of the five main Precordillera thrust events are not the same as the ages of the Iglesia sequences (Jordan *et al.*1993). Furthermore, as shown by Ruskin and Jordan (2006; Chapter 3),

paleoclimate actually varied between relatively more humid and more arid states across several sequence boundaries and during sequence deposition.

Numerical modeling of the Iglesia Basin sedimentary patterns (as reported by Beer *et al.*, 1990) was attempted by Den Bezemer *et al.* (1999). Their model advects pre-tectonic and syn-tectonic strata through a velocity field with vectors parallel to the underlying fault and kink domains. Fold kink axes are fixed to the footwall of the modeled fault segments. Overall, mass is conserved in a transport-limited system, with different erosive diffusivity functions for 'gravel', 'sand', pre-tectonic 'basement' and eroded sediment. To test the Beer *et al.* (1990) hypothesis of prograding unconformities during periods of tectonic quiescence, displacement rates were varied through time over a two-step decollement with some times of instantaneous drop of displacement rate to zero. The western fault-bend fold ("Frontal Cordillera" proxy) is considered to be a constant sediment source, and climate (i.e. sediment delivery) remains unchanged throughout the model runs. Unconformity generation was found to be related to basinward progradation of coarse-grained sediment, while marginal onlap (retrogradation) coincided with fine-grained deposition.

The above numerical model yielded three results that are not consistent with Beer *et al.'s* (1990) tectonic models of sequence development. First, without an external control other than tectonism (i.e. variable climate or sedimentation), the model produces a coarsening-upward grain size succession, as opposed to the long-term fining-upward gradation observed from outcrops. Second, modeled basin-center outcrops are fine-grained as are observed central outcrops. In contrast, Beer *et al.*'s (1990) tectonic model predicts progradation toward the basin axis of coarse grained deposits at each sequence boundary, and this is generally not witnessed in outcrop. Finally, Den Bezemer *et al.*'s (1999) modeled grain sizes suggest that the eastern margin (i.e. "Precordillera") would occasionally contribute coarse clasts to the basin**.**

With the exception of a basal brecciated unit related to initial tectonic movement in the Precordillera, sediment shed from the east is generally sand-sized or finer. An important implication of Den Bezemer *et al.*'s (1999) numerical modeling is that tectonic activity alone cannot explain the sedimentation patterns and boundaries of the Iglesia Basin.

Climate change is the other external forcing factor likely to impact sequence deposition and was modeled by Milana (1998) as a control of Frontal Cordillera discharge cycles. Milana (1998) envisioned discharge variations related to glaciations in the Frontal Cordillera source area. He hypothesized that, during periods of low stream discharge (while ice volumes were accumulating), a low-efficiency transport system deposited alluvium in areas proximal to the Frontal Cordillera. Increasing discharge (during deglaciation) would re-transport sediment to distal positions with concurrent proximal incision.

Milana (1998) reported on two ramped flume experiments, run with constant sediment supply but fluctuating discharge, which mimic the proposed Iglesia system. Both flume simulations exhibited depositional geometries characteristic of "proximal incision cycles", the cyclic change of the boundary position between erosion and deposition. Increasing and then maintaining steady stream discharge generated sequential basinward progradation, an overall reduction in slope, and a truncation surface with slow deposition in proximal areas, characterized as the High Discharge Systems Tract (HDST). Decreasing and then maintaining steady discharge in the flume simulation led to rapid onlap and fining-upward trends, a distal condensed section, and later progradation with distal downlap geometries and coarsening-upward deposits, described as the Low Discharge Systems Tract (LDST). A recently developed 3D model of these cycles (Milana and Tietze, 2002) provides insights about the lateral variability of sequence boundaries, a fact that was originally observed by

Beer *et al.* (1990) for the Iglesia basin and which must be carefully considered. While an excellent basis for comparison to new seismic mapping (see below), this climatic model is probably insufficient to fully characterize Iglesia deposits for two reasons. First, tectonic input was not considered, though both margins of the basin certainly uplifted during sequence deposition (Table 2.1). Secondly, though increasing water discharge can do significant work in semi-arid to arid systems (e.g. Molnar, 2001), it has been shown that the ratio of water discharge to sediment supply is an important factor in modeled alluvial processes (e.g. Weissmann *et al.*, 2002; Hickson, 2005). The other factors that affected sediment supply (Chapter 1) are not integrated into Milana's (1998) conceptual or Milana and Tietze's (2002) flume modeling. As a cautionary note, the assumption that there were mountain glaciations in the Frontal Cordillera during sequence deposition must be carefully examined. Bissig *et al.* (2002) noted that glacial erosion features are largely absent from Upper Miocene geomorphic surfaces in the Frontal Cordillera near the Chile-Argentina border, just west of Iglesia. At present, clear evidence for Miocene-Pliocene glaciations in Argentina is limited to Patagonian deposits far to the south and younger than most of the Iglesia Group (~S 47°, <5.8 Ma, Rabassa *et al.*, 2005), so the premise of discharge variability related to glacial cycles concurrent with basin filling remains speculative.

Latest seismic interpretation and integration with field observations:

Reinterpretation of the Iglesia basin seismic profiles became necessary for several reasons. A fundamental goal of this dissertation is to document the impact of extrinsic variables during sequence deposition. The end-member models described above do not realistically describe the intricacies of the natural system and do not agree with more recent observations. As such, reconsideration of the 3-D network of seismic profiles at the basin-scale and the scale corresponding to individual outcrop belts was required. Further attention in seismic interpretation was paid to intrabasinal

structures, facies changes, and the sequence framework in the subsurface as it relates to newly-considered outcrop localities. This study also includes three previously uninterpreted profiles in the southernmost part of the basin (5331-33, see Fig. 2.1), permitting for the first time documentation of the southern terminus of the Iglesia Basin (cf. Snyder, 1988; Beer *et al.*, 1990). Finally, interpretation was performed in digital format; the paper copies were scanned, permitting manipulation of spatial dimensions and image enhancement with graphical software.

The procedure for seismic interpretation of the Iglesia Basin seismic network is as follows. (1) Identify and mark reflector terminations as onlap, erosive truncation, toplap or downlap, interpreting interfaces at which those terminations occur as unconformities. (2) Trace each unconformity surface over the complete basin, parallel to conformable reflectors, tying between parallel profiles using longitudinal tie-lines. (3) Ascertain if sequence interpretation is congruent among all lines in network and correct as necessary. (4) Create a chronostratigraphic history for sequence deposition. This procedure generally follows that recommended by Vail (1987). Note that, ideally, seismic sequence interpretation involves calibration of the reflectors with geophysical or petrographic information gleaned from well logs, which are unavailable for Iglesia Basin. However, as will be discussed below, the ability to locally correlate seismic reflectors with basin center outcrop belts permits some prediction of subsurface depositional trends.

Table 2.2 and Figure 2.8 summarize the reflection characteristics and criteria used for this seismic stratigraphic interpretation. The number of sequences that can be correlated throughout the network of seismic lines remains at eleven, although there is evidence for a younger twelfth sequence in profiles 5325 and 5327. These will be referred to as Sequences 1 (oldest) to 11 (youngest). Reflector onlap (Fig. 2.8A) is the most commonly observed termination geometry, chiefly occurring along the western

Table 2.2: Reflector characteristics and sequence synthesis of Iglesia Basin seismic stratigraphic interpretation.

Line	Sequence Boundary	Onlap	Truncation	Toplap	Amplitude	Continuity	Rotation along west margin
5321	8--> 9		Y		High	High	
5322	9-->10	Y			Medium	Low to Medium	
	8-->9	Y		Y	High	Medium	Y
	7-->8	Y	Y	Y	Medium	Low to Medium	Y
	6-->7	Y	Y		Medium	Medium	Y
	5-->6	Y			High	High	
	4-->5	Y			High	High	
	3-->4	Y			Medium	Medium	
	2-->3		Y		Low to Medium	Low to Medium	
	1-->2	Y	Y		Medium to High	Medium to High	
	Basement-->1	Y	Y		Medium to High	Medium to High	
5323	10-->11		Y		Medium	Medium	Y
	9-->10	Y			Medium to High	Medium	Y
	8-->9	Y			Medium	Medium	Y
	7-->8	Y			Low to Medium	Low to Medium	
	6-->7	Y			High	Medium to High	
	5-->6	?		?	High	Medium to High	
	4-->5	Y			Medium	Medium to High	Y
	3-->4	Y	Y		Medium	Medium	Y
	2-->3	Y			Medium to High	Medium	
	1-->2	Y	Y	Y	Medium to High	Medium to High	
	Basement-->1	Y	Y		High	High	
5324	9-->10	Y			Medium to High	High	Y
	8-->9	Y	Y		Medium to High	High	
	7-->8	Y	Y		Medium to High	High	
	6-->7	Y	Y		Medium to High	Medium	
	5-->6	Y			Medium	Medium	
	4-->5	Y	Y		Medium to High	High	Y
	3-->4	Y			Low to High	Medium	
	2-->3	Y		Y	Low to High	Medium	
	1-->2	Y			High	High	Y
	Basement-->1	Y			Medium	Medium	
5325	9-->10	Y		Y	High	Medium to High	
	8-->9			Y	High	Medium	
	7-->8	Y			High	Medium	
	6-->7	Y	Y		Low to High	Medium	
	5-->6		Y	Y	Medium to High	High	
	4-->5	Y			High	Medium to High	
	3-->4	Y			Low to High	Medium	
	2-->3	Y			Medium to High	Medium	
	1-->2	Y			Medium	Medium	
5326	10-->11	Y			Medium to High	Medium to High	
	9-->10	Y	Y	Y	Medium to High	Medium	Y
	8-->9	Y	Y		Medium to High	Medium	
	7-->8	Y	Y		High	Medium to High	
	6-->7	Y			Medium to High	Medium	
	5-->6	Y	Y		Medium to High	Low to Medium	Y
	4-->5	Y		Y	Medium to High	High	
	3-->4	Y			Low to Medium	Medium	
	2-->3	Y			High	Medium to High	
	1-->2	Y			Medium	Medium	Y
5327	10-->11	Y			Low to High	Medium	
	9-->10	Y	Y		Medium to High	Low to Medium	
	8-->9	Y			Low to High	Low to Medium	Y
	7-->8		?	Y	Medium	Low to Medium	
	6-->7		?		Medium	Low to Medium	
	5-->6		Y	Y	Medium to High	Medium to High	Y
	4-->5	?			Medium to High	Medium	
	3-->4	Y		Y	High	Medium	
5328	10-->11				Low to Medium	Low to Medium	
	9-->10	Y			Medium to High	Medium to High	
	8-->9		Y		Medium to High	High	
	7-->8	?		Y	Medium to High	Medium to High	Y
	6-->7	Y		?	Medium	Medium	
	5-->6	?			Medium to High	High	
	4-->5	Y		Y	Medium to High	Medium to High	
	3-->4	Y	Y		Medium to High	Medium to High	
5329	7-->8		Y		Medium	Medium to High	
	6-->7		Y		Medium	High	
	5-->6		Y		Medium	Medium to High	
	4-->5	Y	Y		Medium	Medium to High	
	3-->4	Y	Y		Medium to High	Medium to High	Y
	2-->3		Y	Y	High	Medium to High	
	1-->2		Y		Medium to High	Medium to High	
	Basement-->1	Y	Y		Medium to High	Medium	Y
5330	7-->8			Y	High	High	
	6-->7	Y	Y		Medium to High	Medium to High	Y
	5-->6	Y			Medium to High	Medium	
	4-->5	Y			Medium	Medium	Y
	3-->4	Y		?	Medium to High	Medium to High	
	2-->3	Y			Medium to High	Medium to High	
	1-->2	Y		Y	Medium	Low	
	Basement-->1	Y			Medium to High	Low to Medium	

Summary

Boundary	# Lines Present	Onlap	Truncation	Toplap	Rotation along western margin
10-->11	3	2	1	0	1
9-->10	7	7	2	1	3
8-->9	8	5	4	1	2
7-->8	9	5	4	4	2
6-->7	9	7	5	0	1
5-->6	9	4	4	2	1
4-->5	9	8	2	2	2
3-->4	9	9	3	1	1
2-->3	7	5	2	2	
1-->2	7	6	3	2	1
Basement-->1	5	5	3	0	1

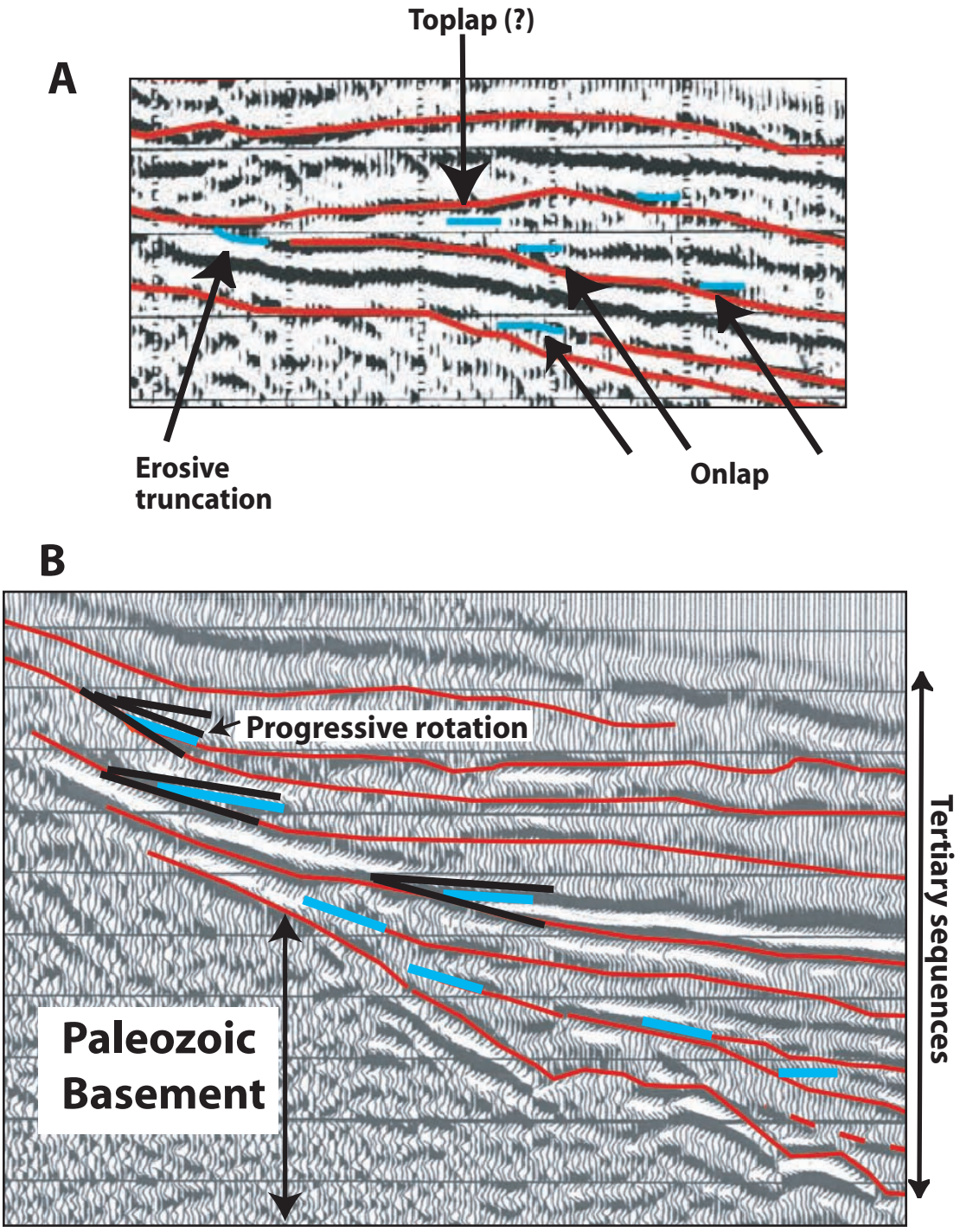

Figure 2.8: A: Examples of seismic reflection termination geometries interpreted for Iglesia Basin profiles. B: Onlap onto western margin and examples of rotated reflectors onlapped by overlying Tertiary strata. Red lines are mapped seismic sequence boundaries. Blue lines indicate reflector termination.

basin margin where Tertiary strata contact Paleozoic basement rocks of the Frontal Cordillera. Onlap across Tertiary sequences is also common, constituting the main criteria for sequence boundaries, and reveals progressive rotation of the subsurface strata by marginal and intrabasinal thrusting (Fig. 2.8B). Other reflector terminations are interpreted as erosional truncation and toplap (Fig. 2.8A). Truncation is more common near the western margin, but locally extends up to 8 km eastward from the intersection of strata with basement that defines the contemporaneous basin margin. Reflector downlap was not observed on any of the profiles.

With respect to the assumptions implicit in seismic sequence interpretation, Thorne (1992) notes that the interpreter assumes that reflection terminations can be unambiguously classified (e.g. toplap, downlap, onlap). However, as a result of the westward convergence of reflectors in the Iglesia Basin latitudinal lines, this assumption is likely violated. In many cases, toplap cannot be distinguished from apparent truncation. This may reflect depositional or erosional thinning of strata such that the unit is too thin to be resolved by the seismic wave (Sheriff and Geldart, 1983; Vail, 1987).

Simplified summaries of the upper one to two seconds of each seismic line are presented for west-east (dip-parallel) profiles (Figures 2.9 and 2.10) and north-south (strike-parallel) profiles (Figure 2.11) and illustrate the basin-scale geometries of the stratigraphic sequences. Also represented is an onlap map (Figure 2.12) of the western terminus of seismic sequence boundaries against the Frontal Cordillera basement rock. The basement topography has a north-northwest trend which results, from north to south, in progressive eastward displacement of Tertiary stratal onlap. Disparity between the axis of the depocenter and the axis of the modern valley increases from north to south (Fig. 2.12) and this trend continues into the Calingasta Valley (Snyder, 1988).

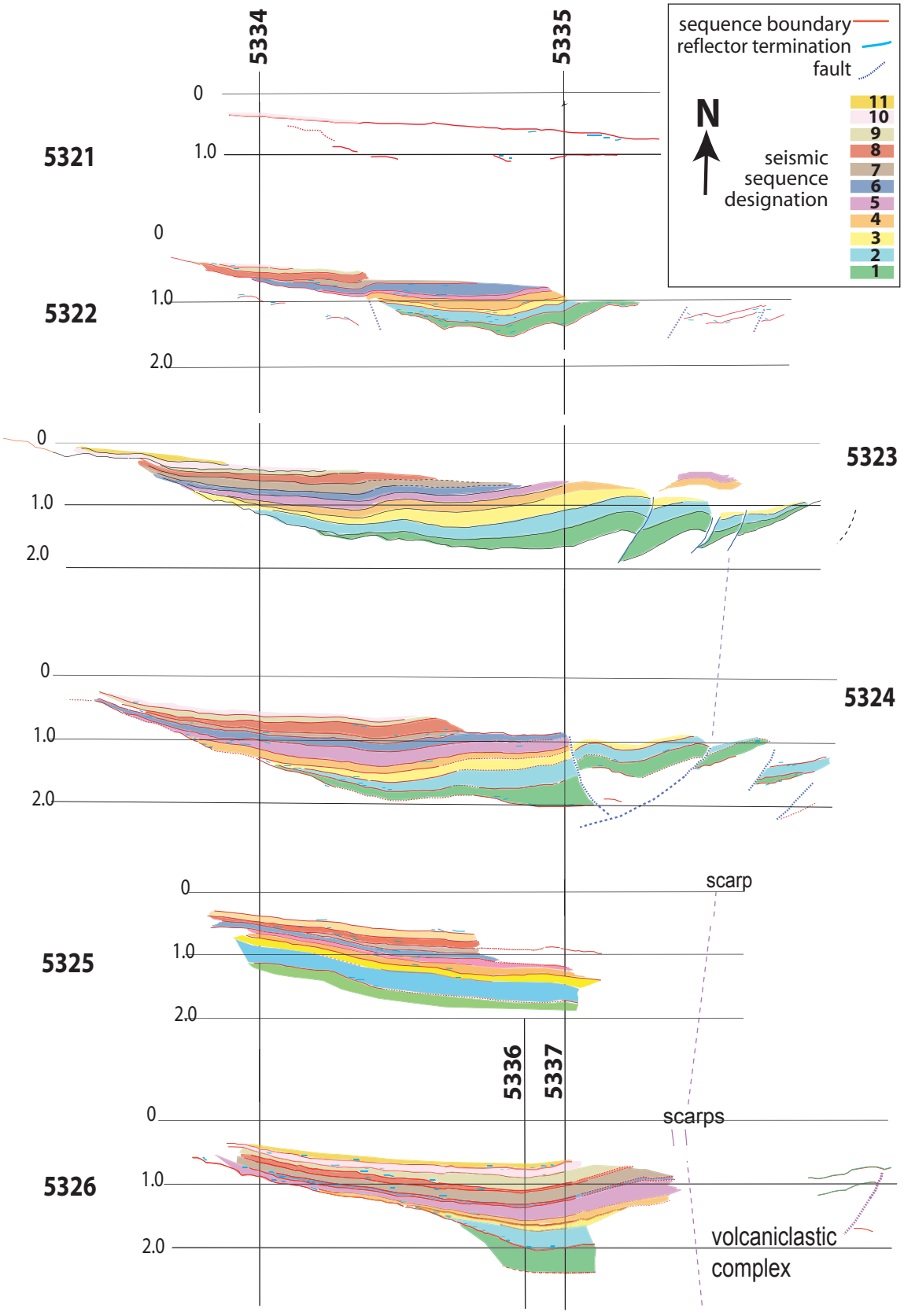

Figure 2.9: Interpreted northern half of Iglesia Basin seismic network.

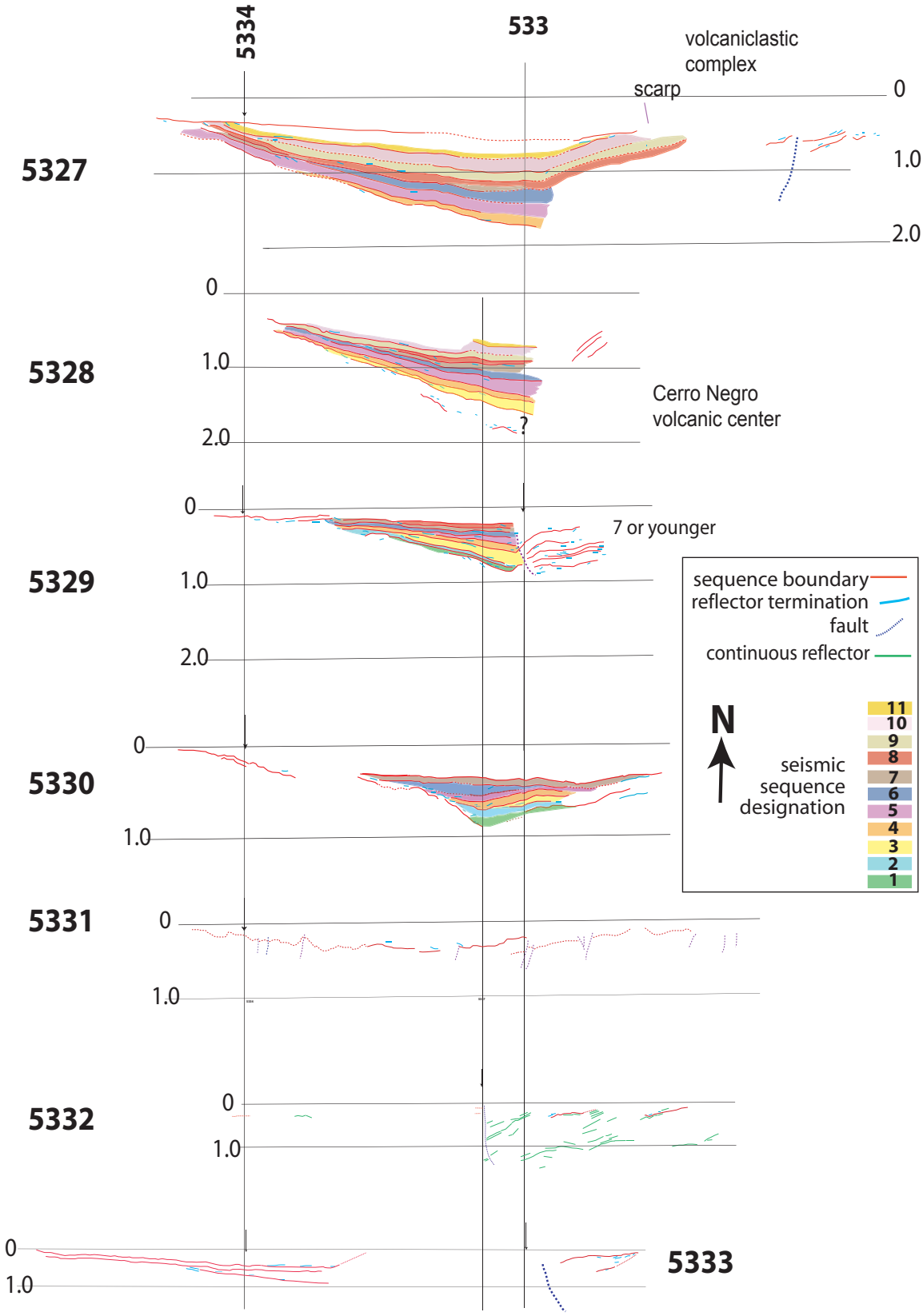

Figure 2.10: Interpreted southern half of Iglesia Basin seismic network.

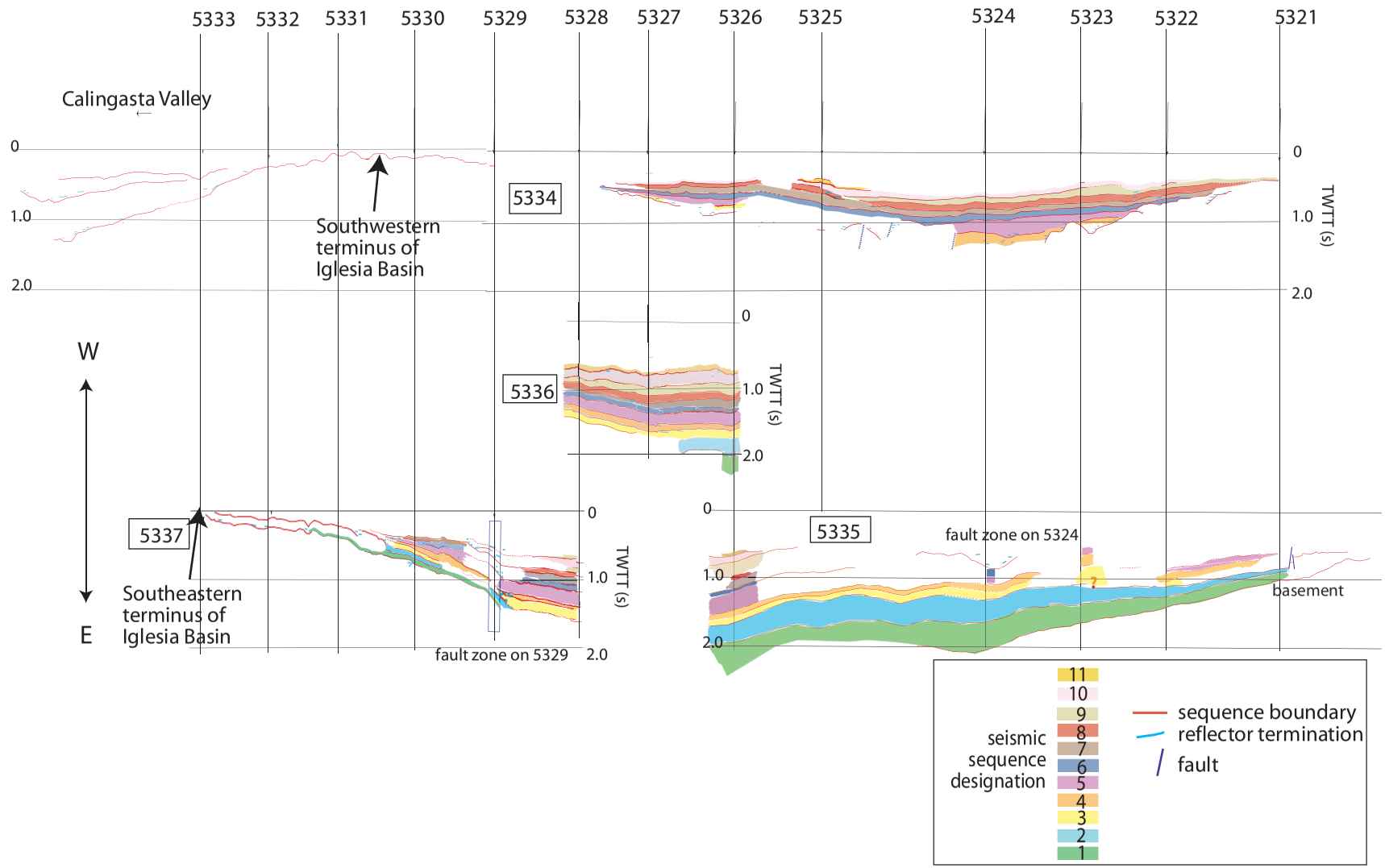

Figure 2.11: Interpreted sequence stratigraphy for north-south seismic profiles, Iglesia Basin

Figure 2.12: Maximum western extent of Iglesia Basin sequences, inferred from reflector onlap. Profiles and mapped onlap positions have been rotated parallel to latitude and longitude. Dashed lines indicate profiles in which western terminus of sequence boundary could not be interpreted.

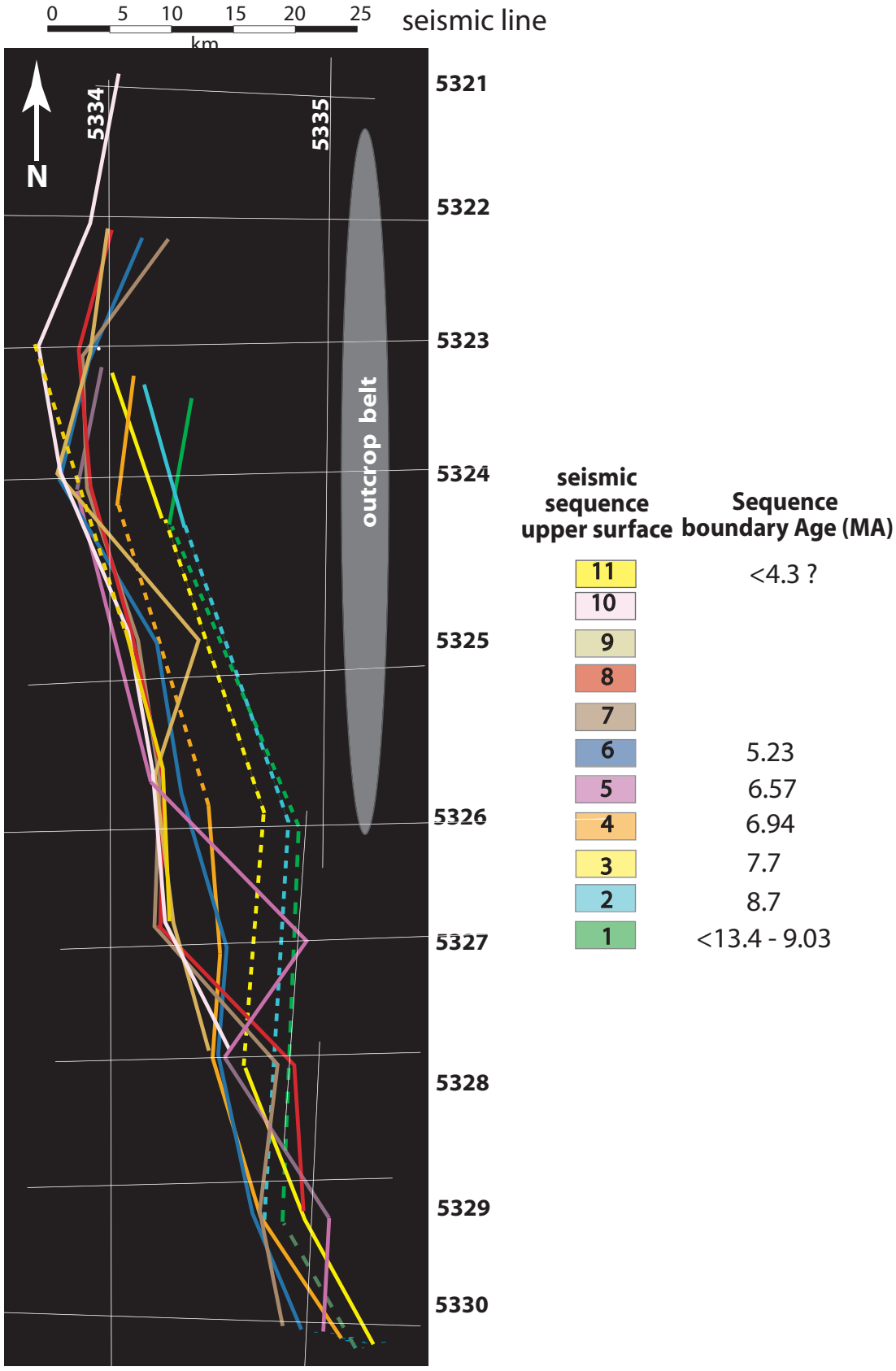
0 5 10 15 20 25
km
seismic line
N
5334
5335
outcrop belt
5321
5322
5323
5324
5325
5326
5327
5328
5329
5330
seismic sequence upper surface
Sequence boundary Age (MA)
11
<4.3 ?
10
9
8
7
6
5.23
5
6.57
4
6.94
3
7.7
2
8.7
1
<13.4 - 9.03

The overall geometry of the basin is lensoid. However, the basin is subdivided by El Tigre thrust faults and folds, resulting in as many as six sub-basins in the north. In the region of profiles 5322-24, sequences 6 and younger are restricted to the westernmost subbasin (see following discussion of growth strata). In contrast, to the south of profile 5324, the youngest sequences extend farther eastward than their northern counterparts (Figs. 2.8 and 2.12). In the vicinity of lines 5326 and 5327, sequence 11 onlaps onto sequence 10 to the east, but even so, extends further into the basin center than it does to the north (Fig 2.12).

Westward broadening through time is generally the case (successive sequences onlapped farther west than those below). Also evident from the reflector geometries is a basinward fanning (divergence) of strata (Figs. 2.8B, 2.9, 2.10). A notable exception to this progressive onlapping trend is evident on profiles 5327 and 5329, wherein sequence 5 (both lines) and sequence 6 (5327) retrograde eastward (Fig. 2.12). This relative offlap may signal a period of increasing uplift in the Frontal Cordillera, or alternatively a local change in sediment supply or accommodation space.

The southern terminus of Iglesia Basin deposition can be addressed for the first time by the inclusion of three previously-uninterpreted lines (5331-5333) Along the western longitudinal line (5334), the upper basement reflector is strongly imaged and is very close to the ground surface north of line 5331 (Fig. 2.11). This basement high defines the southwestern terminus of Iglesia basin strata. However, sequence 1 and possibly sequence 2 or younger can be traced along line 5337 as far south as line 5333. Therefore, although sequence designations are uncertain for west-east profiles 5332-33, their eastern portions do include Tertiary fill from Iglesia Basin. In contrast, the western portion of line 5333 seems to image Calingasta basin strata. Two seismic sequences can be distinguished above the basement in the Calingasta basin on the basis of reflector onlap and erosional truncation (line 5333, Fig 2.11). A seismic

profile in the eastern Calingasta Valley near S 31.5° may contain three Tertiary sequences (Snyder, 1988). Limited exposure and scant description of Oligocene-Miocene conglomerates, sandstones and siltstones (>200 m according to Stipanicic, 1979) in the Calingasta valley precludes interpretation of genetic connectivity between the basins.

Splays of the El Tigre fault system are clearly imaged in the central Iglesia basin, where they appear as mostly blind thrusts offsetting and folding the Tertiary sequences. At least six east-vergent fault splays are interpreted in the northern basin (lines 5322-24). High angle west-vergent faults (opposite to sense of motion of major thrusts in the Precordillera) are imaged locally in profiles 5322, 5324, 5329 and 5333. At least two splays with west vergence are inferred, both of which are to the west of the east-vergent fault system (see Figs. 2.3, 2.9 and 2.10). The western of the two splays corresponds to the Colangüil fault described by Snyder (1988) and the site of minor fault array measurements by Allmendinger *et al.* (1990). It is uncertain how these zones connect with the El Tigre thrust faults in the central portions of the seismic network.

Growth strata are recognizable in seismic profiles, providing relative constraints on the timing of intrabasinal deformation. Growth strata develop on the limbs of active fault-bend folds provided that sedimentation rate is comparable to (or greater) than the rate of tectonic uplift. The syntectonic strata accumulate within triangular zones concordant with respect to prekinematic strata. Ré *et al.* (2003) recognized growth stratal geometries in one latitudinal profile, 5322. They suggested that uplift of the westernmost fault-bend anticline of the El Tigre set occurred during deposition of Sequences 2-4 as well as sequence 7 (sequence interpretation of Fernández-Seveso, 1993). Reinterpretation of this profile in terms of sequence boundaries and projection of reflectors through kink bands of homogeneous dip

suggests that the western fault was active midway through seismic Sequence 2 through lower Sequence 8 (Figure 2.13A). In seismic line 5323, an additional upward-narrowing growth triangle is witnessed in the west-central portion of the profile, unrelated to the main east-vergent splays of El Tigre fault (Fig. 2.13B). The package of growth strata here initiates within Sequence 5 and projects upward at least through lower Sequence 10 (the growth triangle apex is not resolvable). A minor degree of thinning (in time domain) occurs over the fold crest. Finally, reflector onlap onto dipping underlying seismic sequence boundaries is commonly observed in basin-center positions (e.g. Fig 2.13A, seismic inset, base of sequence 5, 7, and 8; Fig. 2.13B, seismic inset, base of sequence 5 and 6), implying syndepositional uplift of these folds. Therefore, intrabasinal deformation of shifting loci likely occurred throughout Mio-Pliocene sequence deposition and may have affected formation of the sequence boundaries themselves.

The basinward divergence of seismic reflectors is accompanied by interpreted progressive onlap of certain sequence-bounding reflectors, perhaps representing episodic uplift of the Frontal Cordillera. However, if the Frontal Cordillera is considered a crustal scale fault-bend fold (e.g. Allmendinger *et al.*, 1990), Iglesia Basin strata accumulate against the fold's forelimb where geometric models of fault-bend folding preclude progressive stratal rotation (e.g. Suppe, 1983). In such models, apparent rotation is a consequence of variations in sediment compaction or depositional slopes from proximal to distal areas. Yet, geometric models (e.g. reliant on kink-band folding and self-similar fold amplification) may not accurately reflect rheological complexities of syntectonic strata (e.g. Salvini *et al.*, 2001). In fact, the production of wedges of progressively-rotated syntectonic strata have been numerically modeled for fault-bend fold systems (Salvini *et al.*, 2001). Also, Rafini and Mercer (2002) modeled forelimb growth stratal geometries which are akin to

Figure 2.13: Growth stratal geometries associated with fault bend folding in A: seismic profile 5322 and B: profile 5323. Axial surfaces for kink bands have been interpreted and define backlimb growth triangles. Inset seismic reflector examples show evidence of stratigraphic thinning and/or onlap onto the backlimb of a fault-bend fold that is not associated with the main splays of El Tigre Fault System to the east.

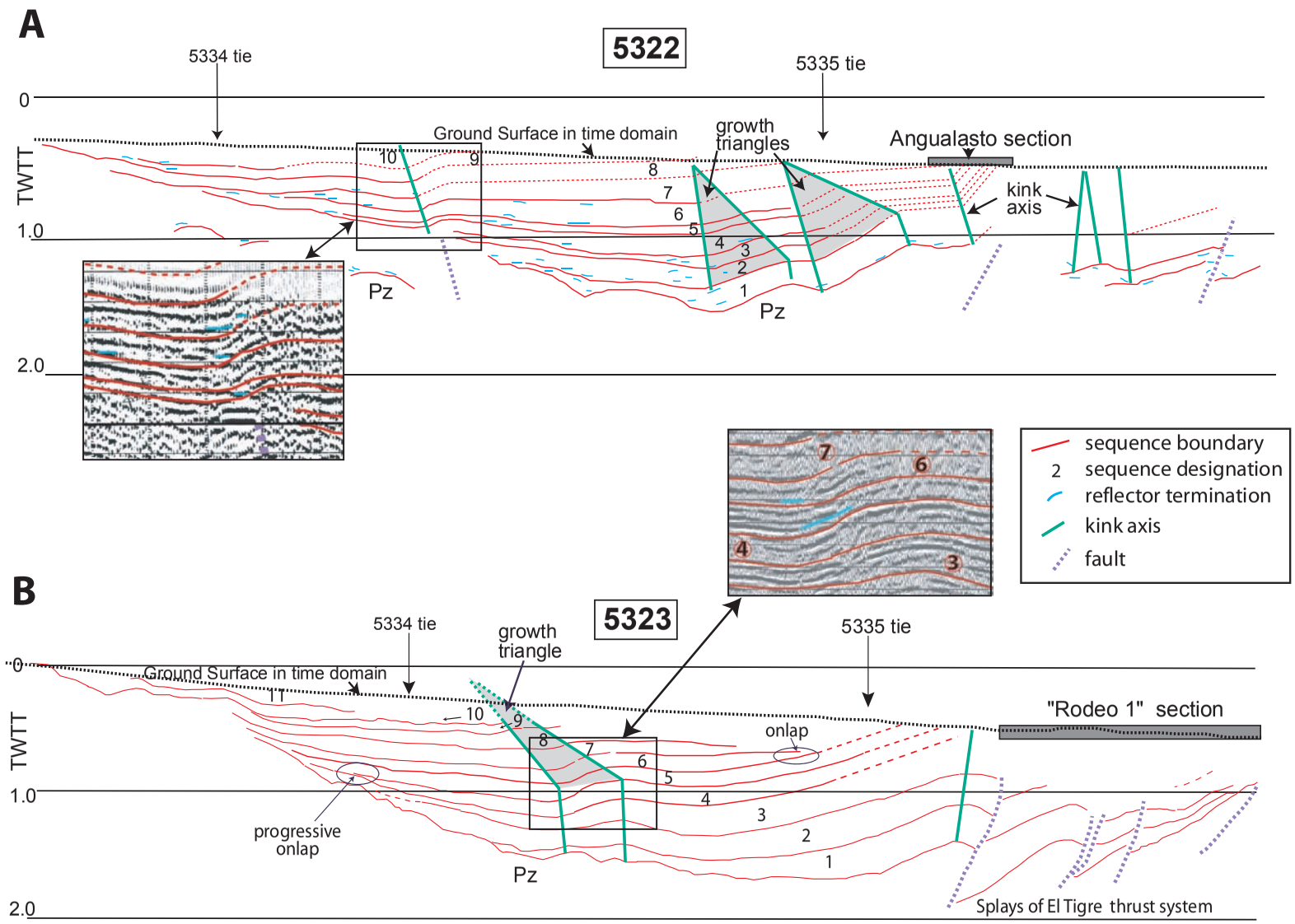
A
5322
5334 tie
5335 tie
0
TWTT
1.0
2.0
Ground Surface in time domain
growth
triangles
Angualasto section
kink
axis
10
9
8
7
6
5
4
3
2
1
Pz
Pz
B
5323
5334 tie
growth
triangle
5335 tie
0
Ground Surface in time domain
11
10
9
8
7
6
5
4
3
2
1
TWTT
1.0
2.0
"Rodeo 1" section
onlap
progressive
onlap
Pz
Splays of El Tigre thrust system
sequence boundary
2 sequence designation
reflector termination
kink axis
fault

Iglesia Basin's seismic reflections by altering the ratio between rates of uplift and sedimentation changes and permitting erosional events. Differential compaction between the proximal and distal areas could result in overall fanning and divergence of the strata. However, the observed rotation and progressive onlapping occur over a small spatial scale (near the western margin), where differential compaction is probably minimal (e.g. similar lithologies, densities and bulk porosities).

If the progressive rotation of reflector onlap witnessed in dip-parallel seismic profiles (Figs. 2.8-2.10) does represent growth strata, these rotations provide relative temporal constraints on the timing of Frontal Cordilleran uplift. As summarized in Table 2.2, sequence boundary (SB) rotation is apparent at a number of stratigraphic intervals, but is only observed with some regularity in the seismic network at SB 4-5, 7-8, 8-9 and especially SB 9-10. From these rotations, we infer that Frontal Cordilleran uplift was more pronounced relative to sediment supply rates prior to the time represented by western reflections of sequences 5, 8, 9 and 10, possibly even influencing the hiatuses that terminated the underlying sequences.

Basement faults in a different orientation to the north-south trending El Tigre thrusts are also imaged in longitudinal profiles (Fig. 2.11). Longitudinal profile 5334 exhibits several faults which likely disrupt sequences 4-5. A number of faults offset the upper basement reflector on latitudinal line 5331. However, uncertainties of sequence correlation between the faulted areas prohibit confident interpretation of the sense of structural offset.

The eastern segments of three of the west-east profiles (5326-28, Fig. 2.9-2.10) transect areas mapped as volcaniclastic facies associated with the Cerro Negro de Iglesia andesitic-dacitic center as well as topographic lineaments interpreted as scarps of El Tigre fault system (Bercowski, 1993; Ragona *et al.*, 1995). The eastern portions of these profiles are almost devoid of continuous reflectors, likely due to the velocity

difference between the volcanic deposits (surficial and intruded) and the surrounding Tertiary sediments. However, to the east of the volcaniclastic complex, a west-dipping splay of El Tigre fault is imaged in lines 5326-27 (Fig. 2.9-2.10). No fault is imaged on the west side of the volcanic center, although on profile 5328, reflectors are rotated to a westward dip. This deformation may be due to volcanic inflation or alternatively via an unimaged fault.

Seismic Facies Analysis:

Seismic facies analysis may be employed in order to infer gross aspects of lithofacies and depositional history. Seismic facies (Vail, 1987) are mappable, three-dimensional intervals of seismic reflections with distinct reflection characteristics. The most commonly employed reflection characteristics for seismic facies analysis are overall configuration, continuity, amplitude, frequency and sonic velocity, from which general aspects of the depositional system may be inferred (see Table 2.3). After seismic facies are demarcated, other pertinent seismic, geophysical or lithologic data are considered (e.g. from seismic processing, boreholes or outcrop) to facilitate interpretation of the seismic facies' stratigraphic significance.

A rare published example of nonmarine seismic facies interpretation is for the Paleocene Fort Union Formation in west-central Wyoming (Ray, 1982). Three seismic facies were defined on the basis of reflection continuity, amplitude and frequency, which could be related to three general lithofacies observed in outcrop or boreholes. When all three parameters were low, the seismic facies represented laterally discontinuous fluvial sandstones amid generally shaly intervals. In the case of high values of all parameters, heterogeneously interbedded sandstones and shales were inferred. Low amplitudes and frequency combined with moderate continuity corresponded to massive lacustrine shales.

Table 2.3: Typical parameters and geologic significance for seismic facies analysis (after Vail, 1987).

Seismic Facies Parameters	Geologic Interpretation
" **Configurations:**	Depositional processes; paleotopography/erosion; fluid content
o Parallel	Stable basin
o Divergent	
o Prograding (inc. sigmoidal, oblique, hummocky)	Lateral outbuilding
o Chaotic	Variable or high-energy deposition
" **Reflection Continuity**	Bedding continuity; depositional processes
Continuous	
Truncated (onlap, offlap, toplap, downlap, truncation)	Unconformity
" **Reflection Amplitude**	Velocity-density contrast; bed spacing; fluid content
" **Reflection Frequency**	Bed thickness; fluid content
" **Internal velocity**	Lithology/porosity/fluid estimations

Legarreta *et al*. (1993) outlined the lithologic nature of mostly nonmarine seismic facies in the Mesozoic San Jorge basin in central Patagonia, Argentina. They found that the highest amplitude reflectors corresponded to high proportions of sandstone and conglomerate in well logs. The weakest areas of seismic reflection were associated with mudrocks. Intermediate reflector continuity and amplitude correspond with a variable mix of sandstones and shales.

Field interpretation of lithofacies along seismic line 5322 (Fig. 2.3) permitted Beer (1989) and Beer *et al.* (1990) to recognize three general facies to guide subsurface seismic facies analysis. In general, conglomerates, sandy units, and muddy facies were described, interpreted as concentric facies belts of sequentially finer particle size, from proximal alluvial fans to sand-flats to distal playa lakes, respectively. Projecting outcrop characteristics into seismic reflectors, three seismic facies were defined on the basis of reflector amplitude and continuity. The "conglomeratic" facies consisted of discontinuous, low amplitude reflections, "sandy" facies were represented by continuous, high amplitude reflections and "muddy" facies were reflections of moderate continuity and low amplitude. However, based on his measured section along 5322, Beer (1989) predicted a constant distance of facies transition from the paleomargin (westernmost onlap position of reflections): conglomerates extended up to 7 km from the margin, sands from 7 to 13 km, and at distances further than 13 km, muddy facies dominated. Based in this scaling of facies, predicted and observed seismic facies generally correspond (Beer, 1989), but not completely. Reassessment of the entire seismic profile network (discussed below) leads to many refinements to this simple depositional zonation.

Seismic facies interpretation was conducted throughout the Iglesia Basin network by recognizing differences in reflection continuity and amplitude. Three qualitative seismic facies (SF) assemblages were considered: (SF-1) high continuity,

Seismic Facies 1:
High Amplitude
High Continuity

Seismic Facies 2:
Medium Amplitude
Medium Continuity

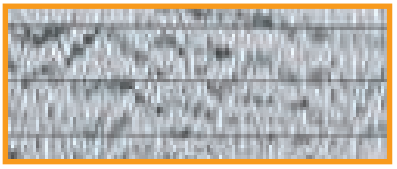

Seismic Facies 3:
Low Amplitude
Low Continuity

Figure 2.14: Characteristic examples of seismic facies utilized for interpretation of Iglesia Basin seismic reflection profiles.

high amplitude areas, (SF-2) medium continuity, medium amplitude areas; and (SF-3) low continuity, low amplitude (or chaotic, reflection- free) areas (Figure 2.14). These facies were mapped without regard for previously-defined sequence boundaries and are discussed in turn below. Because frequency of reflections is similar throughout the time sections, it was not considered as a facies attribute.

Two notes of caution should be applied to seismic reflection interpretation. First, the interpretive process for paper or scanned seismic lines is subjective, in that the interpreter qualitatively judges what areas consist of increase or decrease of each reflector characteristic. Such choices may be defensible if an automated seismic facies program is utilized with digital data, but this is not possible for interpretation of paper copies of seismic profiles. Secondly, and related to the above, seismic attributes may vary from profile to profile as a result of different processing schemes. For example, varying the velocity-depth model and gain control fundamentally changes the resolvability and amplitude of the reflectors considered. Therefore, unless identical processing and display are used in the entire seismic network, inter-profile variations in reflection attributes are to be expected. These variations will affect seismic facies interpretations.

Areas of reflections with high continuity and amplitude (Seismic Facies 1) are widely distributed about the profile network and suggest several three-dimensional attributes (Figures 2.15-2.17). In the western longitudinal profile (5334, Fig. 2.17), distribution of SF-1 is patchy and only locally correlates with the latitudinal profiles (Figure 2.15-2.16). Several wedge-like bodies of this facies are defined, most notably in the northwestern network (lines 5322 through 5325), exhibiting aspect ratios (TWTT to horizontal distance based on scaling of Figs. 2.15-2.16) of 2.4-5.6. Along the eastern longitudinal profiles (5336, 5337), the facies appears more linear than to the west (aspect ratio: 3 to 11.3) and correlates well with lines 5326-5331 (Fig. 2.16).

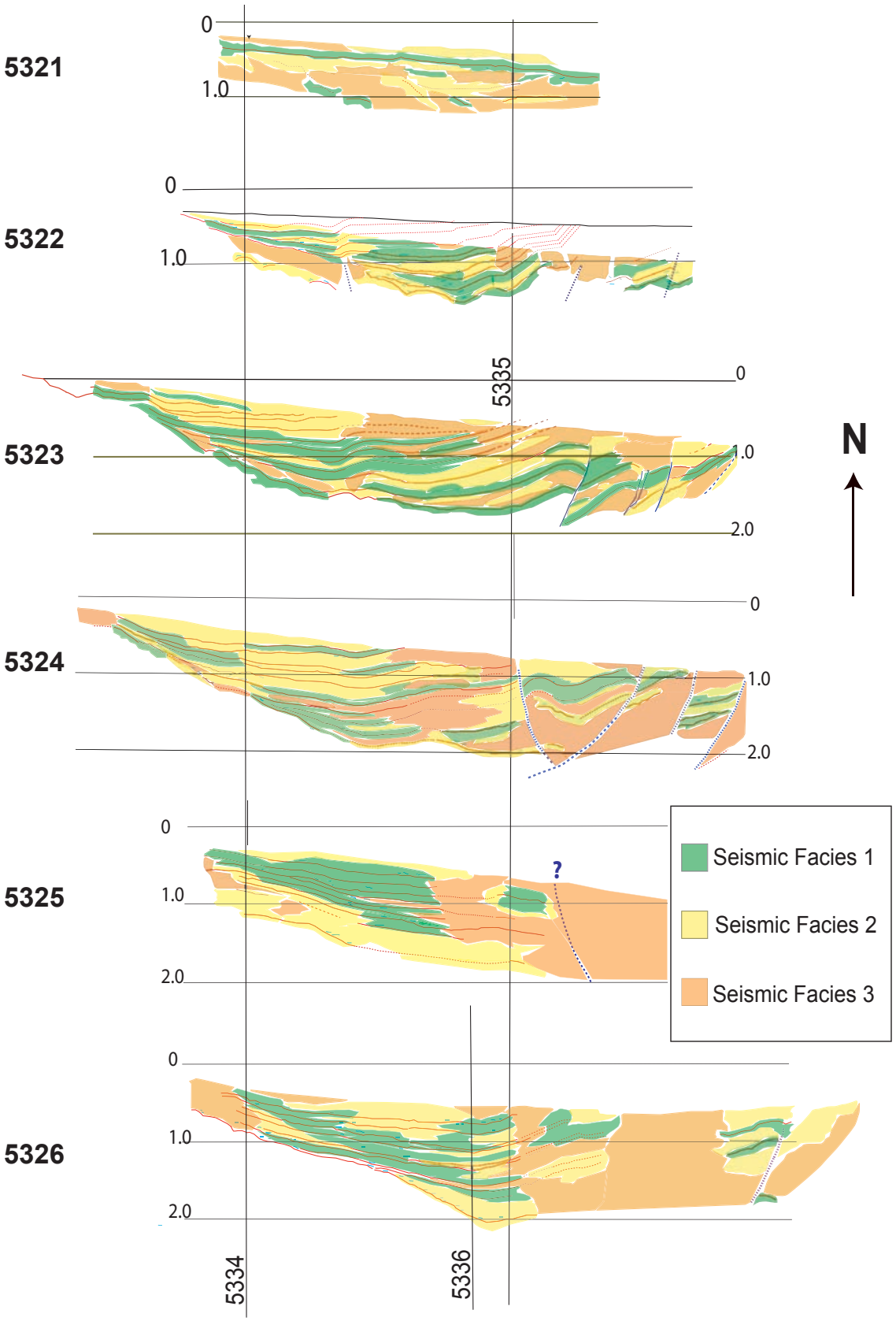

Figure 2.15: Seismic facies interpretation of northern Iglesia Basin seismic network

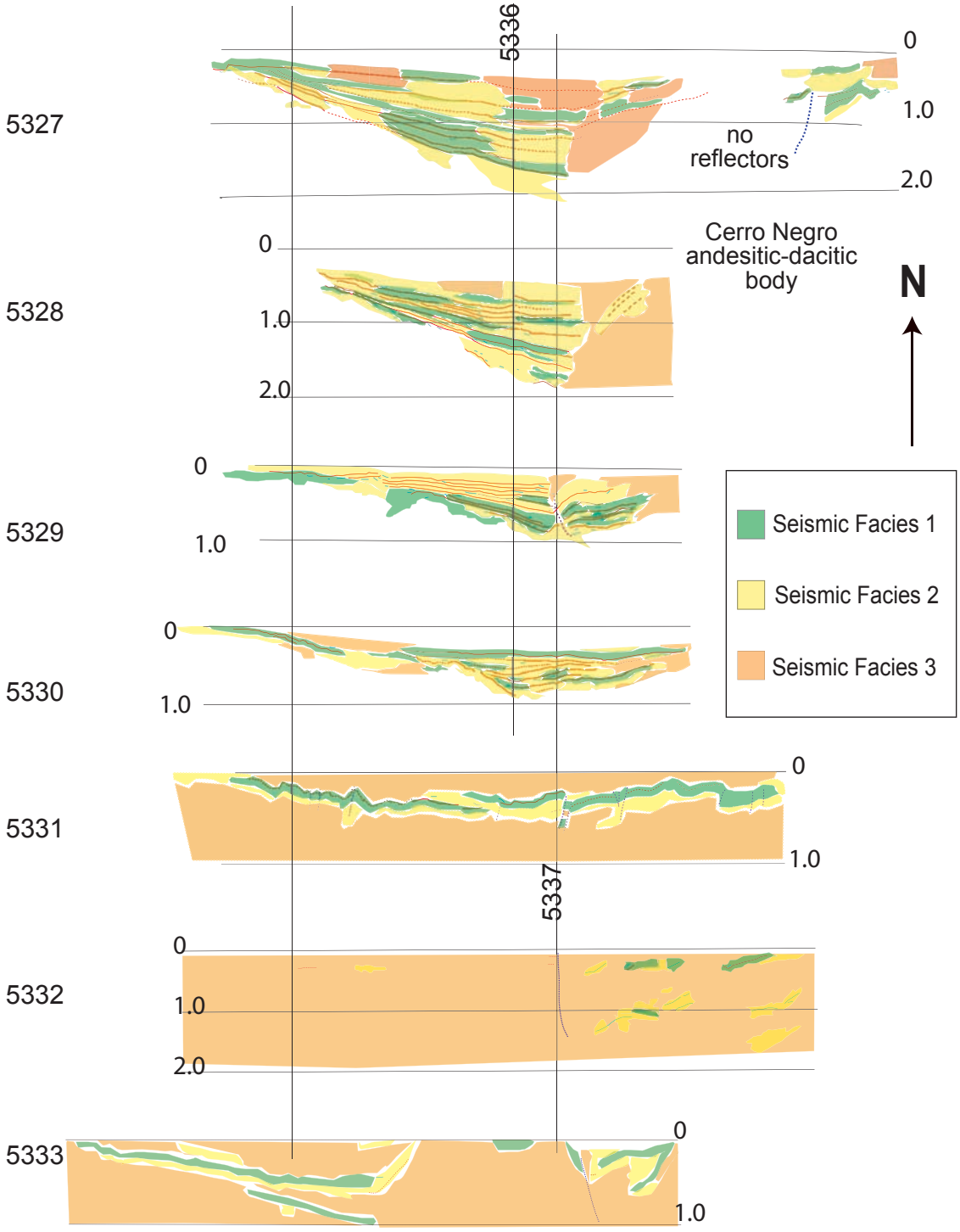

Figure 2.16: Seismic facies interpretation for southern half of Iglesia Basin seismic network

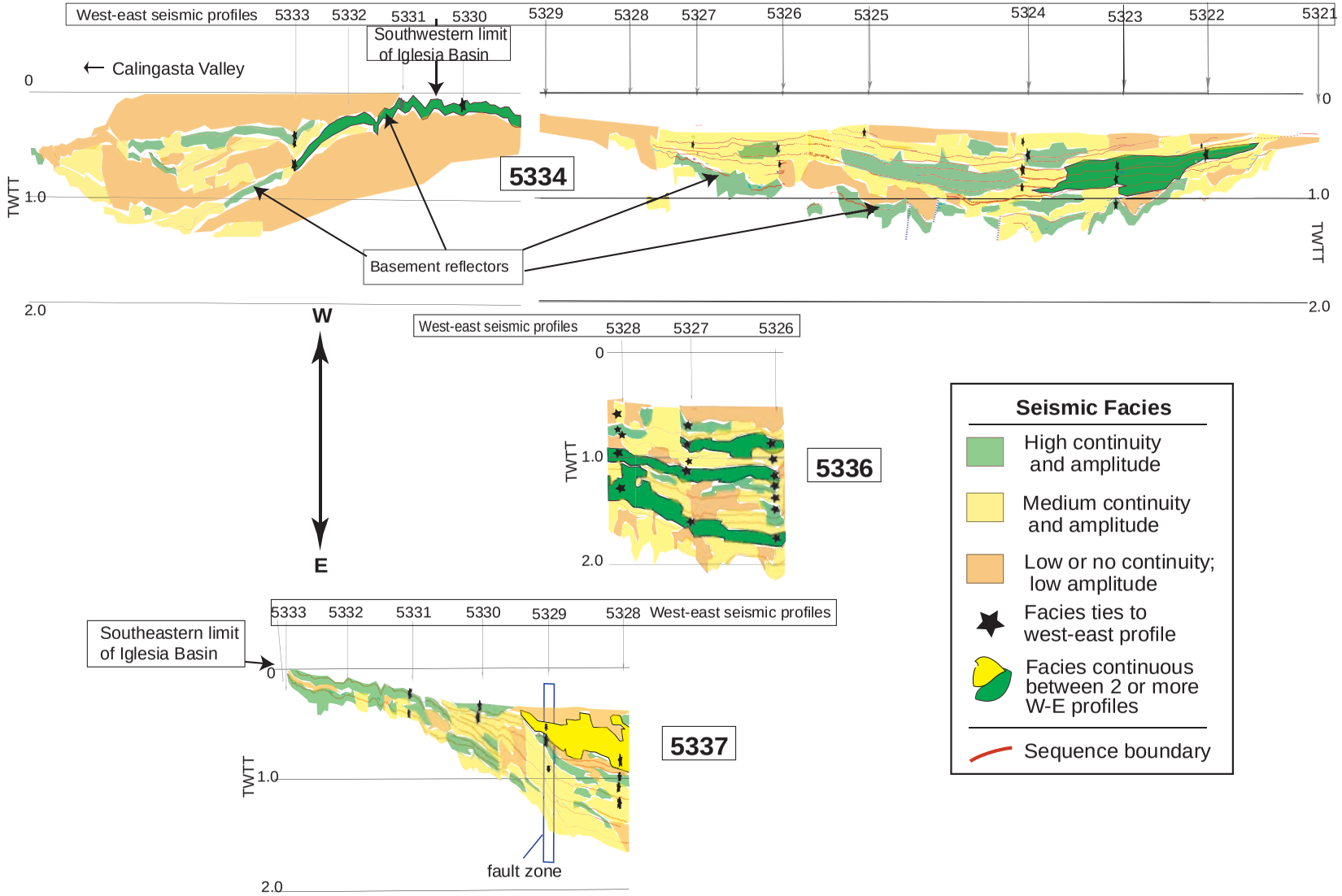

Figure 2.17: Seismic facies interpretation for north-south profiles of Iglesia Basin. Vertical scale is two-way travel time (in seconds).

Several of the SF-1 areas can be tied amongst two or three west-east profiles, suggesting sheet geometries. In latitudinal profiles, SF-1 also exhibits sheet-like organization (aspect ratio 2.6 to >32), mainly distributed in the western and center portions of the profiles (Figs. 2-15-2.16). Additionally, the facies appears to oscillate in eastern extent through time, though generally retrograding toward the west shallower in the profiles.

The high amplitude and high continuity facies is strongly associated with the unconformable contact between Paleozoic "basement" and the Tertiary sequences. This is especially true of the southwestern portion of the network (lines 5330-34, Fig. 2.16), where SF-1 coincides with the top of a basement high marking the boundary between the Iglesia and Calingasta basins.

Many of the sequence boundaries are associated with reflectors of high continuity and amplitude (Figs. 2.15-2.17). This relationship is pronounced in profiles 5322-24 (Fig. 2.15), where long portions of certain sequence boundaries are mapped as seismic facies 1. In particular, SB 1-2, 4-5 and 5-6 correspond with long areas of SF-1 on three or more latitudinal lines, while SB 7-8 coincides with this facies over the majority of longitudinal line 5336 (Fig. 2.17). However, many of the lower aspect-ratio facies areas cross-cut seismic sequence boundaries.

Seismic facies 1 can be interpreted in terms of lithologic discontinuities. Seismic reflection principles dictate that the greater the acoustic impedance (seismic wave velocity multiplied by rock density), the stronger the reflection. Thus, the highest amplitudes in the seismic grid should reflect strong lithologic discontinuities. Furthermore, greater reflector continuity suggests continuous, widespread strata deposited under similar energy conditions (e.g. Sangree and Widmier, 1977), although care must be taken in interpreting horizontal resolution because of the effects of noise and frequency attenuation, resulting in horizontally smeared reflections (e.g. Sheriff

and Geldart, 1983). However, assuming the above principles hold, it is not surprising that seismic facies 1 corresponds with the contact of sequence 1 with the basement and with SB 1-2, both of which are basin-scale hiatuses (at least 4 M.y.) with field-observed erosional contacts and strong lithologic contrasts (e.g. basement metasediments vs. sequence 1 rhyolitic volcanics vs. sequence 2 boulder conglomerates). The above-mentioned coincidence of certain younger sequence boundaries with SF-1 probably results from lithologic rather than erosional discontinuity, as erosional contacts are not prevalent in basin-center outcrops.

Seismic facies 2, defined as reflections of medium amplitude and continuity, is prevalent in western and central portions of the seismic network (Figs 2.15 and 2.16). In many cases, SF-1 laterally transitions into areas mapped as SF-2. Spatially, this facies covers a significant proportion of individual profiles, but lacks distinct geometric arrangement; it appears as broad, irregular patches. In some of the northern latitudinal profiles, SF-2 is associated with sequence boundaries, but typically as correlative conformable portions of the reflectors. It is also fairly common in the younger sequences (e.g. lines 5323, 5324, 5326, 5327 & 5329; Figs. 2.15-2.16). Comparison of the longitudinal cross sections (Fig. 2.17) reveals that SF-2 is somewhat more prevalent in the center of the basin (lines 5336-37) than towards the western margin (5334).

The final seismic facies, SF-3 is characterized by areas of low reflection continuity and amplitude, or by areas of chaotic, non-parallel reflection geometries. In almost all profiles, SF-3 is almost ubiquitous beneath the basement-Tertiary contact. Also, SF-3 typifies the shallowest areas of the seismic lines, near the mute zone, where reflector multiples (“ghosts”) are commonly observed. However, the facies is also commonly observed toward the central and eastern portions of the profiles, as well as in the vicinity of the thrust splays. The southernmost profiles (5331-5333) are also of

poor reflection continuity, and thus are largely designated as SF-3 (Fig. 2.17). A few patchy areas of SF-3 can also be discerned near the western margin (lines 5322-26, Fig. 2.15). The low amplitude suggests the seismic waves traveled through relatively homogeneous media.

It is noteworthy that while some of the seismic facies units parallel the sequence boundaries, many other areas cross-cut the unconformity surfaces. This carries chronostratigraphic significance, as the sequence boundary-parallel facies are roughly time lines, whereas the cross-cutting (i.e. thicker) facies units are diachronous, suggesting the nature of sediment deposition at the basinal scale. For example, SF-1 and SF-2 are often parallel with sequence boundaries, and confined to relatively thin zones in the TWTT profiles. The stratigraphic nature of these seismic facies is more likely a regional disconformity. In the alternative case of facies cross-cutting sequence boundaries, SF-1 grades laterally into SF-2, and both facies units retrograde toward the west through time. This corresponds to Walther's Law of vertical and lateral succession and suggests variable sedimentary distribution from the Frontal Cordillera source area through time, comparable to the interpretation of Beer (1989).

Comparison of this seismic facies analysis to previous workers' analyses (Ray, 1982; Beer *et al.*, 1990; Legarreta *et al.*, 1993) reveals additional caveats to direct lithofacies interpretation. A major difference between my facies interpretation and that of Beer *et al.* (1990) is that I do not recognize facies 3 near the western basin margin, nor is proximal to distal facies zonation apparent in all of the profiles. Where it is possible to infer progradation or retrogradation away from the paleomargin (e.g. profiles 5322, 5324, and 5326), if Beer's (1989) lithologic interpretations were applied to this study's seismic facies, the lithologic gradation would be (proximal to distal): sandy to muddy to conglomerate. This gradation is very unlikely for intermontane alluvial basins, as depositional energy should decrease with increasing distance from

the source ranges. Comparison with Ray's (1982) seismic facies is possible only on the criteria of reflection continuity, as Ray does not include a medium grade of amplitude. Nonetheless, Iglesia Basin lithofacies would grade (proximal to distal) from interbedded sandstones and shales to massive lacustrine shales to laterally discontinuous fluvial sands and shales using Ray's (1982) scheme. This, too, is an unusual assemblage, as the facies of lowest depositional energy (lacustrine shales) is expected to occur in the basin center or in closed-drainage areas, although there is indication that the basin axis shifted through time. More likely is the association related by Legarreta *et al.*, (1993), whereby a diminution of reflector amplitude and continuity coincides with decreased grain size.

Recognizing seismic reflectors and sequence boundaries in outcrop:

Synthetic seismograms from outcrop-based data are sometimes used for comparison to actual seismic profiles. Typically, subsurface lithologic information is gleaned from borehole geophysical logs. Knowledge of the density and sonic velocity variations with depth permits creation of synthetic vertical traces to correlate between depth and travel time. In the absence of well logs, one could substitute appropriate sonic velocity values for the lithologies observed in measured stratigraphic sections. This requires approximating intervals of the stratigraphic column as a single rock type. Such "depth averaging" is essentially what the seismic source wave does as it propagates downward. Although fine subdivisions of the stratigraphic section enhance the realism of the synthetic seismogram, any lithologic unit less than ~20 m thick would not have been imaged by reflections in a seismic survey of comparable quality to Iglesia Basin. A severe limitation of this method is the nonuniqueness of compressional seismic velocities (v_p) for various sedimentary units. Common sedimentary rock types often have overlapping velocity ranges (e.g. v_p of Tertiary sandstones = 2 - 2.5 km/s; v_p of shale = 2.1 - 2.6 km/s; Kearey *et al.*, 2002). The

values are nonunique because of variable fluid content, mineralogy, grain sorting, and degree of compaction/cementation. Lithostatic compaction may be especially important, as the Bulk Modulus term in v_p measures uniaxial compressional strain, causing v_p to increase with burial depth.

Nonetheless, synthetic seismic modeling of alluvial facies was conducted by Fernández (1996) for the foreland Bermejo Basin east of Iglesia Basin and the Precordillera in order to compare seismic facies attributes to outcrop-based facies interpretations (Milana, 1991). He found that variations in lithologic unit thickness and lithologic stacking patterns had a larger effect on seismic facies response than did specific lithologies. As such, various combinations of common alluvial lithologies (e.g. conglomerates and sandstones) can yield similar seismic reflection responses. For this reason and those mentioned above, synthetic seismic modeling for Iglesia Basin would provide little additional information to interpret subsurface lithologies and was not attempted. Therefore, analysis of the nature of the clearly imaged seismic sequence boundaries must move to detailed documentation of their surface expression.

Identification in outcrop of rocks that constitute reflectors or sequence boundaries is complicated by the differences between the spatial scales of outcrop and seismic observations. The maximum vertical resolution for seismic reflection surveys is on the order of 1/4 to 1/8 of the source wavelength (Sheriff and Geldart, 1983). Because high-frequency attenuation and velocity increase with depth, resolution will correspondingly degrade deeper in the seismic profile. For Tertiary strata of Iglesia Basin, interval seismic velocities average 2.8 km/s (Snyder, 1988). Applying a bandpass filter of 16-48 Hz (typical of Iglesia basin's processing parameters), each reflector may be optimistically expected to represent 10-20 of meters of strata, and potentially several tens of meters. Lateral and vertical variations in the substrate's

seismic velocity only add to the fact that the spatial and temporal range of strata depicted by seismic reflections is hardly constant.

In order to assess the outcrop expression of the seismic sequence boundaries, it is pertinent to ask the question "What degree of lithologic change, and over what thickness, is necessary in outcrop to generate the acoustic impedance contrast revealed by the strong subsurface seismic reflectors?" Because of the spatial resolution of seismic waves, it is doubtful that a seismic sequence boundary represents a discrete contact (i.e. bedding plane) but rather is the average of stratigraphic variability occurring over thicknesses >20 m. Earlier studies in Iglesia Basin lead to the expectation that it is improbable that sequence boundaries younger than the SB 1-2 are manifest as multi-meter erosive discontinuities, at least not where exposed at basin center or distal positions relative to the Frontal Cordillera (Ré *et al.*, 2003). Likewise, angular unconformities near the basin margins (denoted by seismic reflector onlap and/or truncation) cannot be examined in outcrop because they are obscured by Quaternary gravel deposits. To identify rock properties corresponding to seismic sequence boundaries, lithofacies and structures in all sequences (but particularly sequences 1 through 7) were mapped during eleven weeks of field study with attention to outcrop-scale vertical variations that have along-strike continuity.

Six composite stratigraphic columns of the best exposured Tertiary sections (Figures 2.18 through 2.22**,** locations noted on Figure 2.3) show that major erosional surfaces (e.g. >10 m of relief) are very rare. Instead, lithofacies variations and paleosol intervals are observed in the Tertiary strata over vertical scales of a few meters to ~50 m. This suggests that the continuous medium-to-high amplitude reflectors that are mapped as seismic sequence boundaries based on reflection geometries near the basin margins commonly correspond in distal parts of the basin to relatively conformable lithologic contrasts rather than erosive surfaces.

Figure 2.18: Stratigraphic column for Angualasto measured section (Fig. 2.3), with references to sequence boundary intervals, chronostratigraphy and sample locations. Magnetostratigraphic interpretation after Ré *et al*., 2003.

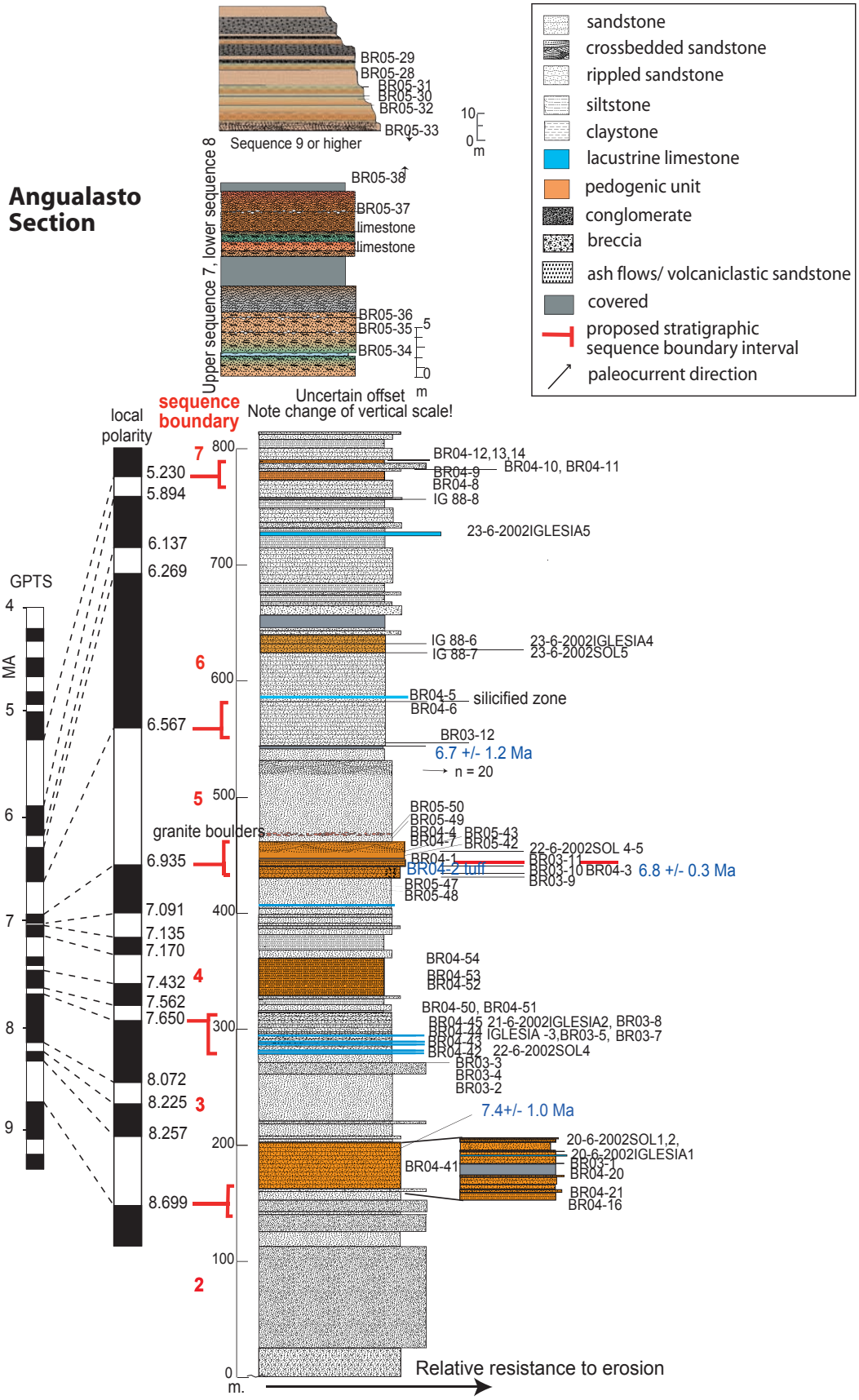
Angualasto Section
BR05-29
BR05-28
BR05-31
BR05-30
BR05-32
BR05-33
Sequence 9 or higher
10
0
m
BR05-38
BR05-37
limestone
limestone
Upper sequence 7, lower sequence 8
BR05-36
BR05-35
BR05-34
5
0
m
Uncertain offset
Note change of vertical scale!
sandstone
crossbedded sandstone
rippled sandstone
siltstone
claystone
lacustrine limestone
pedogenic unit
conglomerate
breccia
ash flows/ volcaniclastic sandstone
covered
proposed stratigraphic sequence boundary interval
paleocurrent direction
local polarity
sequence boundary
GPTS
MA
4
5
6
7
8
9
5.230
5.894
6.137
6.269
6.567
6.935
7.091
7.135
7.170
7.432
7.562
7.650
8.072
8.225
8.257
8.699
7
6
5
4
3
2
800
700
600
500
400
300
200
100
0
m.
granite boulders
BR04-12,13,14
BR04-9
BR04-10, BR04-11
BR04-8
IG 88-8
23-6-2002IGLESIA5
IG 88-6
IG 88-7
23-6-2002IGLESIA4
23-6-2002SOL5
BR04-5
BR04-6
silicified zone
BR03-12
6.7 +/- 1.2 Ma
n = 20
BR05-50
BR05-49
BR04-4, BR05-43
BR04-7, BR05-42
22-6-2002SOL 4-5
BR04-1
BR03-11
BR04-2 tuff
BR03-10 BR04-3
6.8 +/- 0.3 Ma
BR03-9
BR05-47
BR05-48
BR04-54
BR04-53
BR04-52
BR04-50, BR04-51
BR04-45 21-6-2002IGLESIA2, BR03-8
BR04-44 IGLESIA -3,BR03-5, BR03-7
BR04-43
BR04-42 22-6-2002SOL4
BR03-3
BR03-4
BR03-2
7.4+/- 1.0 Ma
20-6-2002SOL1,2,
20-6-2002IGLESIA1
BR03-1
BR04-20
BR04-41
BR04-21
BR04-16
Relative resistance to erosion

Figure 2.19: Stratigraphic column for Rodeo 1 measured section (Fig. 2.3), with references to sequence boundary intervals, chronostratigraphy and sample locations. Magnetostratigraphy interpretation (Ré *et al*., 2003) modified in light of new $^{40}Ar/^{39}Ar$ radiometric data (Appendix B)

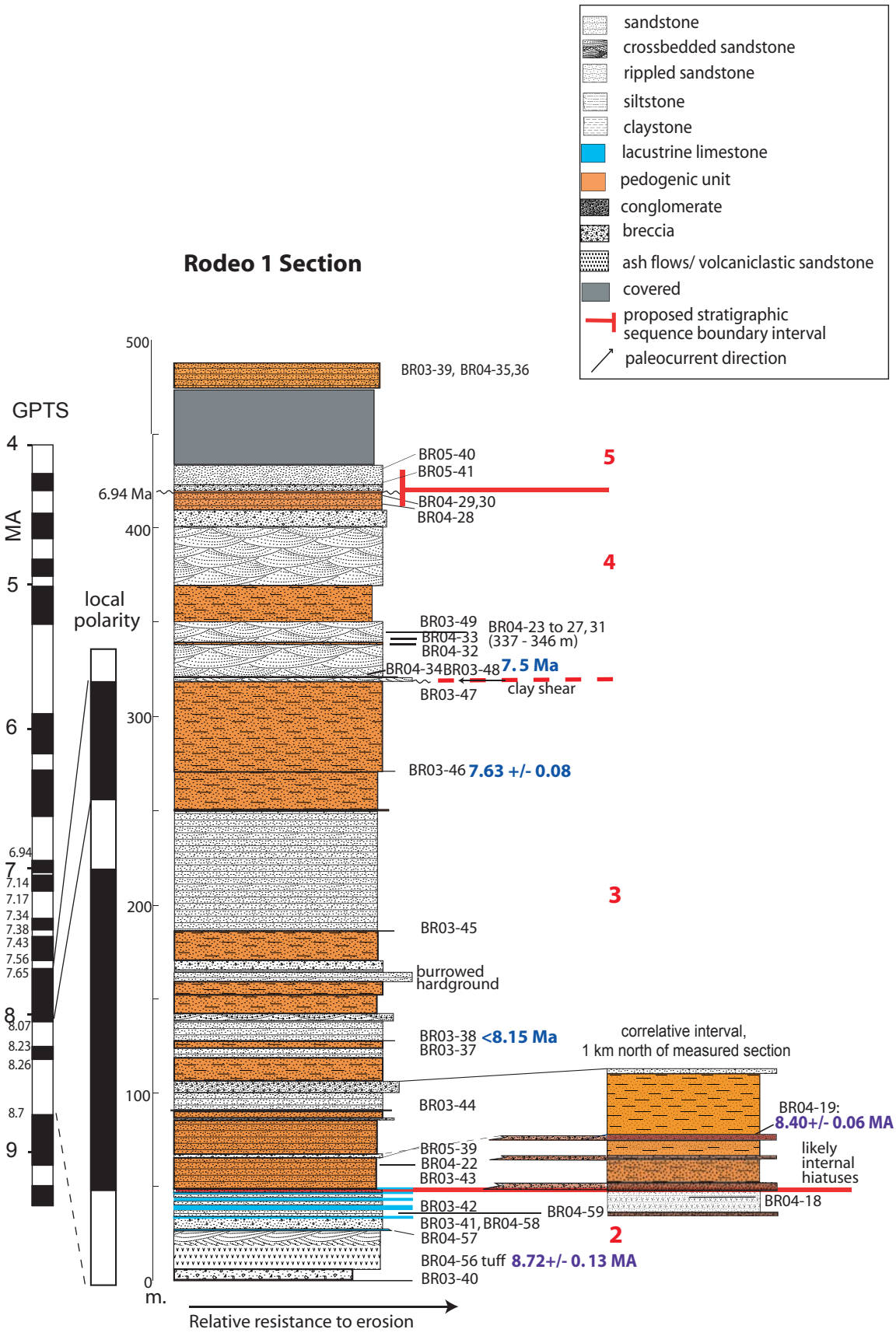
Rodeo 1 Section
sandstone
crossbedded sandstone
rippled sandstone
siltstone
claystone
lacustrine limestone
pedogenic unit
conglomerate
breccia
ash flows/ volcaniclastic sandstone
covered
proposed stratigraphic sequence boundary interval
paleocurrent direction
GPTS
MA
local polarity
500
400
300
200
100
0
m.
6.94 Ma
BR03-39, BR04-35,36
BR05-40
BR05-41
BR04-29,30
BR04-28
5
4
BR03-49
BR04-33
BR04-32
BR04-23 to 27, 31 (337 - 346 m)
BR04-34
BR03-48
7.5 Ma
clay shear
BR03-47
BR03-46
7.63 +/- 0.08
3
BR03-45
burrowed hardground
BR03-38
<8.15 Ma
BR03-37
correlative interval, 1 km north of measured section
BR03-44
BR04-19:
8.40+/- 0.06 MA
BR05-39
BR04-22
BR03-43
likely internal hiatuses
BR03-42
BR04-59
BR04-18
BR03-41, BR04-58
BR04-57
2
BR04-56 tuff
8.72+/- 0.13 MA
BR03-40
Relative resistance to erosion

Figure 2.20: Stratigraphic column for Rodeo 2 measured section (Fig. 2.3), with references to sequence boundary intervals, chronostratigraphy and sample locations. Magnetostratigraphy (Ré *et al*., 2003) modified in light of new $^{40}Ar/^{39}Ar$ radiometric data (Appendix B)

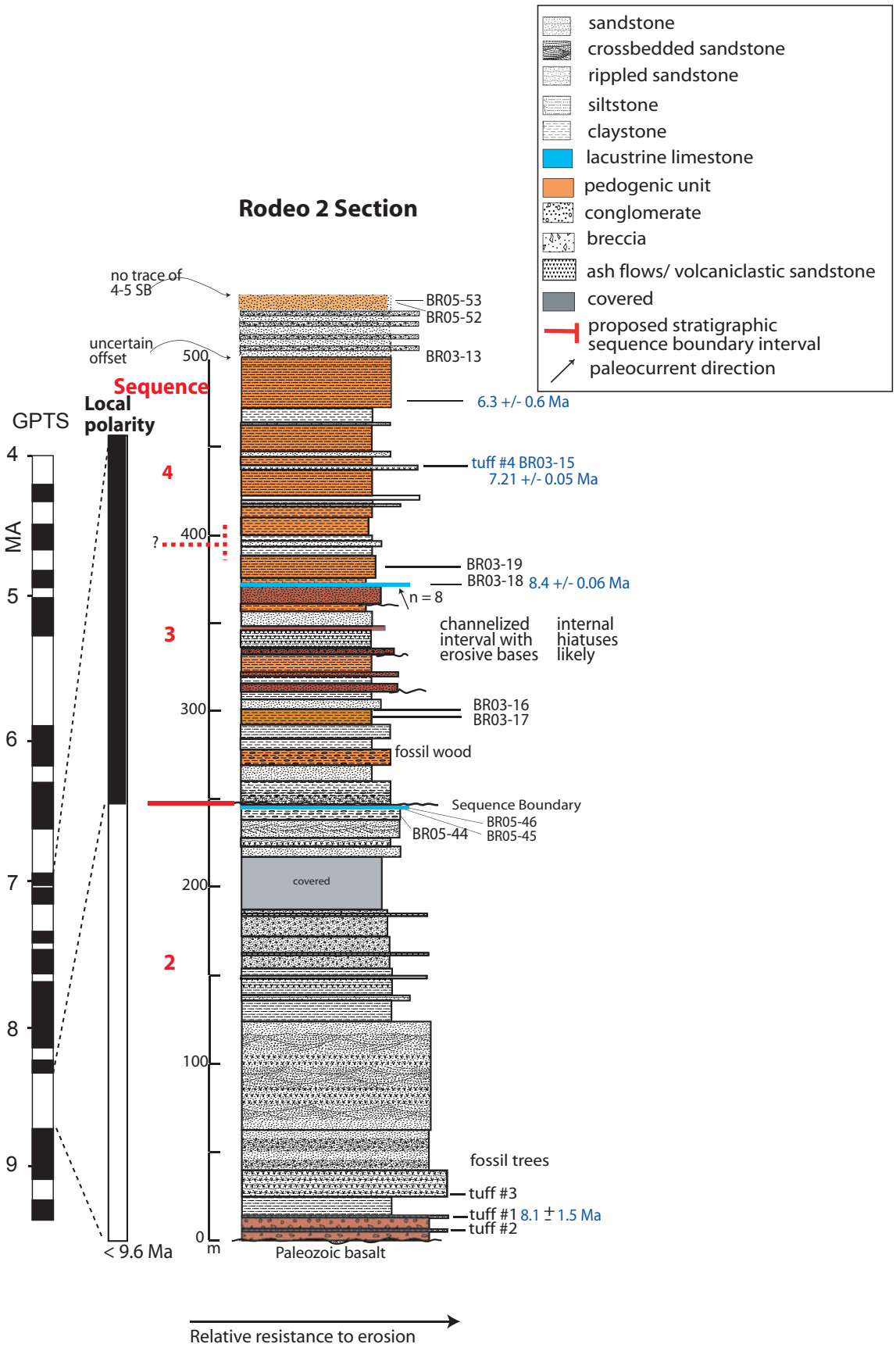
Rodeo 2 Section
sandstone
crossbedded sandstone
rippled sandstone
siltstone
claystone
lacustrine limestone
pedogenic unit
conglomerate
breccia
ash flows/ volcaniclastic sandstone
covered
proposed stratigraphic sequence boundary interval
paleocurrent direction
no trace of 4-5 SB
uncertain offset
Sequence
Local polarity
GPTS
MA
4
5
6
7
8
9
500
400
300
200
100
0
m
?
4
3
2
BR05-53
BR05-52
BR03-13
6.3 +/- 0.6 Ma
tuff #4 BR03-15
7.21 +/- 0.05 Ma
BR03-19
BR03-18
8.4 +/- 0.06 Ma
n = 8
channelized interval with erosive bases
internal hiatuses likely
BR03-16
BR03-17
fossil wood
Sequence Boundary
BR05-46
BR05-45
BR05-44
covered
fossil trees
tuff #3
tuff #1
8.1 ± 1.5 Ma
tuff #2
< 9.6 Ma
Paleozoic basalt
Relative resistance to erosion

Figure 2.21: Stratigraphic columns along Arroyo Iglesia measured sections (Fig. 2.3), with references physical correlation horizons, chronostratigraphy and sample locations. Sequence assignment based on comparison with Rodeo 2 section, seismic framework and new radiometric ages (Appendix B).

Arroyo Iglesia Sections

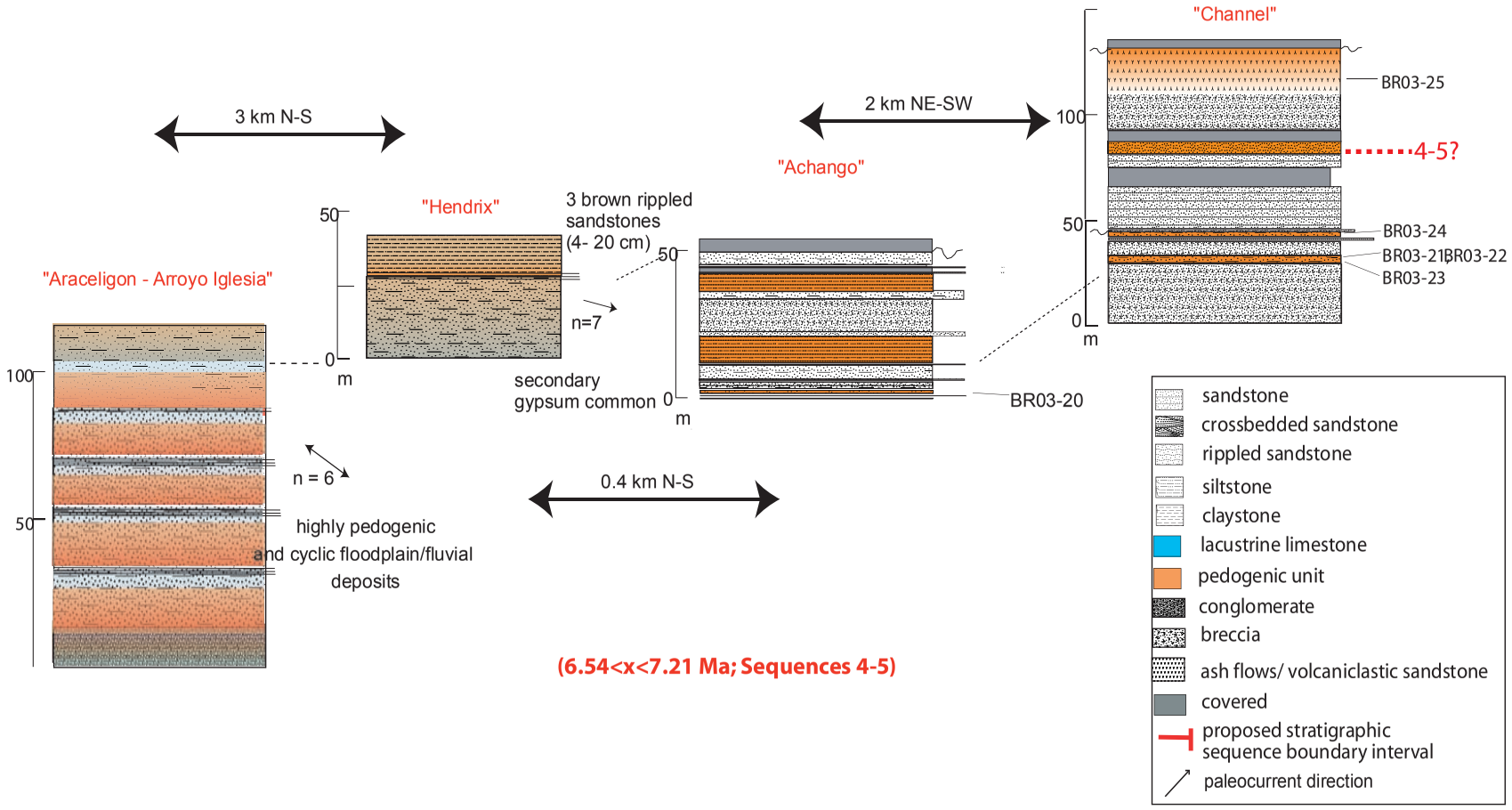

(6.54<x<7.21 Ma; Sequences 4-5)

Figure 2.22: Stratigraphic columns for Las Flores and Iglesias measured sections (Fig. 2.3), with references to chronostratigraphy and sample locations. Sequence assignment based on comparison with seismic framework and new radiometric ages (Appendix B).

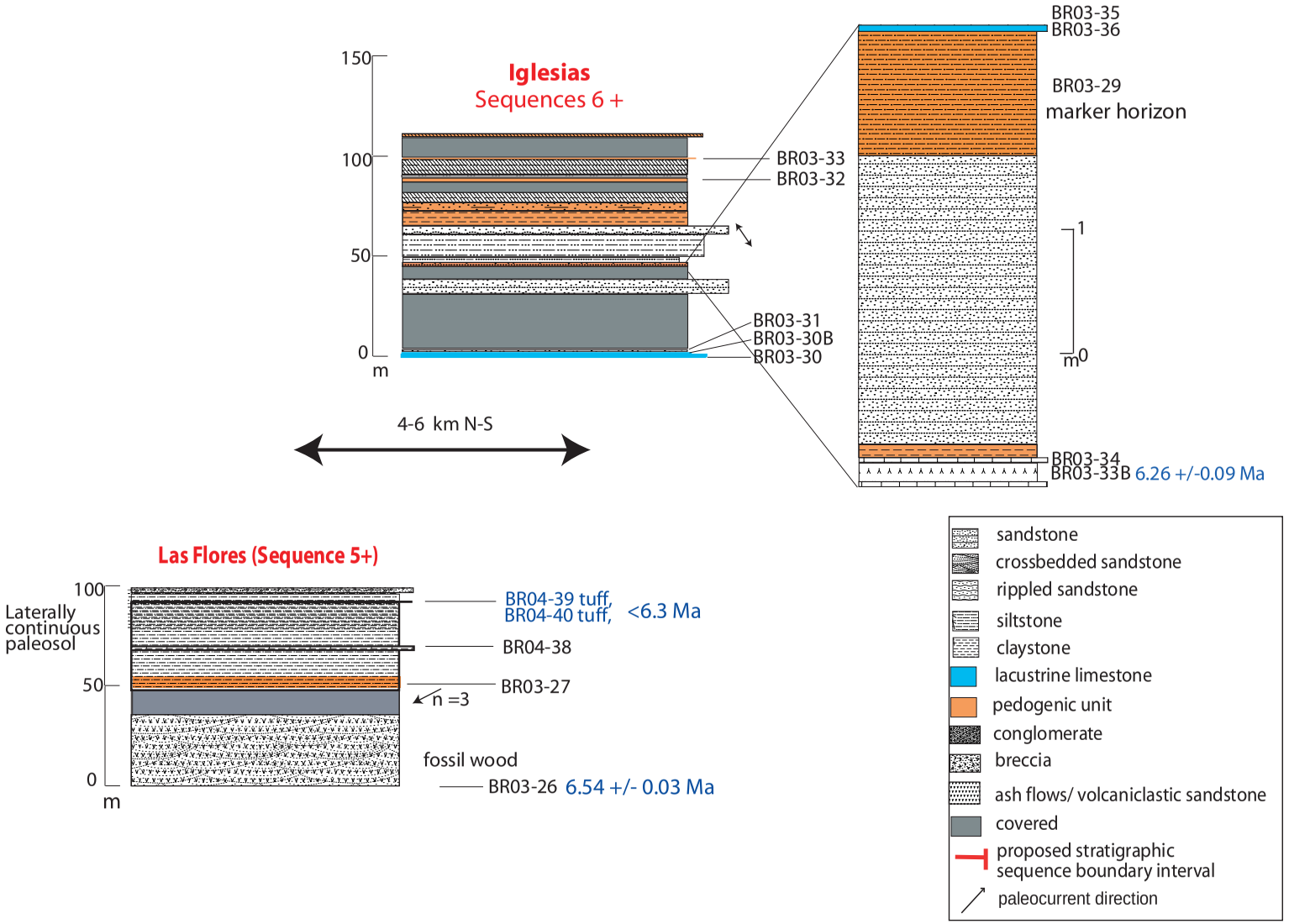
Iglesias
Sequences 6 +
150
100
50
0
m
BR03-33
BR03-32
BR03-31
BR03-30B
BR03-30
4-6 km N-S
BR03-35
BR03-36
BR03-29
marker horizon
1
m0
BR03-34
BR03-33B 6.26 +/-0.09 Ma
Las Flores (Sequence 5+)
100
Laterally
continuous
paleosol
50
0
m
BR04-39 tuff,
BR04-40 tuff, <6.3 Ma
BR04-38
BR03-27
n =3
fossil wood
BR03-26 6.54 +/- 0.03 Ma
sandstone
crossbedded sandstone
rippled sandstone
siltstone
claystone
lacustrine limestone
pedogenic unit
conglomerate
breccia
ash flows/ volcaniclastic sandstone
covered
proposed stratigraphic
sequence boundary interval
paleocurrent direction

Nevertheless, the most recognizable sequence boundary in outcrop is in fact an incision surface separating Sequence 1 (<20.2 – 13.4? Ma) from Sequence 2 (>9 – 8.7 Ma). The >4 million year hiatus is exposed at the core of a fault-bend anticline overlying the westernmost of the east-vergent El Tigre splays. Several U-shaped gullies with ~20 m of relief are found in the uppermost Sequence 1 light gray and violet ignimbrites with poorly rounded dacitic clasts (<15 cm diameter). Filling the gullies are cross-stratified greenish conglomeratic channel deposits of Sequence 2, with well-rounded boulders up to 2 m in diameter. Flow direction was directed toward the southeast from clast imbrications at the base of sequence 2 (n=31, Beer *et al.*, 1990; this study). This sequence boundary is the only one characterized by appreciable erosive relief in the basin-center outcrops. Though velocity-depth conversion suggests that Sequence 1 achieves almost 1800 m thickness in the subsurface, its characteristics and upper unconformable surface are known primarily from this single anticlinal outcrop that is <1 km^2 in spatial extent and <100 m in exposed vertical height.

Another seismic sequence boundary whose nature is clearly defined by surface exposures is the seismic sequence 4-5 boundary, at which there is a mature pedogenic interval followed by a regional facies change. Within seismic sequence 4 (~7.7-6.9 Ma), fairly mature, commonly calcic paleosols are abundant, interbedded with thin sheet sandstones or trough-crossbedded sandstones. Corresponding to the projection of the seismic 4-5 SB are two mature, orange (10R 5/3; 5YR 5/6), meter-thick calcic paleosols. These beds are conspicuous in hue compared with surrounding strata and are easily traced for 10-15 km horizontal distance and in several of the structural sub-basins (Fig. 2.3). These are also the most developmentally mature and recognizable paleosols of the Tertiary fill. Above the paleosols, sequence 5 strata are predominantly composed of grouped trough-crossbedded sandstones (foreset dips 10°-25°), some exhibiting soft-sediment deformation features and generally lacking paleosols.

Associated with the 4-5 SB is a 1.5-m-thick bed of granite boulders, whose maximum boulder size approaches 70 cm. Although very discontinuous in outcrop expression, the boulder bed has been recognized in four distinct locations, always within 5 m above the sequence boundary paleosols.

A particular lithofacies that appears to coincide with projections into outcrop of seismic sequence boundaries is palustrine carbonate. Sequence 3 (8.7 – 7.7 Ma) is comprised primarily of sheet sandstones with interbedded immature paleosols (becoming more mature upsection). Previously, the 3-4 SB was interpreted to correspond with a change from pinkish-orange pebbly sandstones (i.e. containing volcanic clasts from the Frontal Cordillera) into greenish strata (i.e. sedimentary clasts from the Precordillera), interpreted to reflect a change in drainage orientation or paleogeography. Also at the 3-4 SB is an increased contribution of calcareous paleosol horizons and a paleomagnetic reversal (7.7 Ma; Ré *et al*., 2003). Newly mapped in sequence 3 are at least seven calcareous sandstone beds (10-30 cm thick) within 50 m of the polarity reversal that form resistant benches which can be correlated over distances of up to 5 km. Each carbonate bed exhibits evidence of bioturbation, upper-surface burrowing and crawling traces, and slight pedogenic overprinting. Together the composition and sedimentary structures suggest a low-energy and occasionally-subaerially exposed shallow-water "palustrine" depositional environment (Esteban and Klappa, 1983; Platt and Wright, 1992). It is suggested that this 50-m–thick interval in which a minority of the bulk rock consists of these calcareous strata combined with the more subtle change in sandstone clast composition presents an acoustic impedance contrast sufficient to create the seismic reflection corresponding to SB 3-4. Though palustrine limestones are seen elsewhere in the basin, they are abundant and widely distributed only at this seismic sequence boundary (3-4) and at SB 2-3 (described below).

Most of the remaining seismic sequence boundaries, when projected to outcrop, are subtly expressed, but several significant lithofacies changes are herein postulated to represent hiatus intervals. The first is an abrupt facies change at the top of seismic sequence 2. In detail, the lower sequence contains primary tuffs (<20 cm thick), crossbedded tuffaceous sandstones, thin carbonate-cemented sandstones (<50 cm thick, interpreted as pond deposits; see below and Appendix F) and the lower two of a series of 5 reddish pebble conglomerate channel deposits. Sequence 2 is interpreted to conclude with the uppermost of the series of carbonate benches (46 m height in Fig. 2.19), the overlying sediments comprised of nonvolcanic sandstones, aquic Inceptisols and lacking prominent carbonate beds (Rodeo 1 section; Figure 2.19). Exposures of the same stratigraphic level along the eastern basin margin (correlated across the intrabasinal faults by tracing the 5 reddish conglomerate beds) indicate that similar environmental changes in the late Miocene are stratigraphically preserved over >5 km distances (Fig. 2.20). A magnetic reversal coincides with this facies transition at two measured sections that cross this boundary, which is also suggestive of a hiatus (Johnson *et al.*, 1987; Ré and Stein, 1994). This sharp and regionally recognizable facies change is interpreted to represent seismic sequence boundary 2-3. The 2-3 SB as exposed in the Angualasto section (Fig 2.18) also roughly corresponds with another pebble provenance change, from ~40% green sedimentary clasts (i.e. Precordillera source) in sequence 2 to ~70% orange igneous clasts (i.e. Frontal Cordillera source or Colangüil batholith 30 km to NW) in sequence 3 along with the appearance of carbonate paleosol horizons (Ré *et al.*, 2003). In addition, I would add that a change in grain caliber may also contribute to the seismic SB. Sequence 2, though fining upward, is distinct in its generally conglomeratic texture near Angualasto. Similarly, sequence 3 is macroscopically characterized as

sandstone, much of which has a color banded appearance related to redoximorphic paleosol horizons (Figs 2.19-2.20).

The other seismic sequence boundaries that can be projected into outcrops (5-6 and 6-7) have also been better characterized with emphasis on the vertical scale resolvable in seismic reflectors. They are discussed in turn below:

The location as well as the characteristics of the 5-6 sequence boundary has been reconsidered in light of recent field campaigns. Previously, the boundary was described as an angular discordance with several meters of inclined sandstones between parallel, shallowly dipping beds. Erosional truncation of only three meters was noted, but no accompanying lithologic change (Ré *et al.,* 2003). However, structural measurements and graphical tracing of bedding contacts explains this interval as planar crossbedded sandstone bedforms of various thicknesses and angular foreset contacts (Figure 2.23). Surrounding strata are also siltstones and crossbedded sandstones (flow direction NE to E, n=20), interbedded on the meter scale and sometimes locally deformed by load structures, suggesting rapid delivery of fluvial sediments. In the 25 m of strata overlying the "former SB" crossbeds, vertical changes in grain size and bed thickness are witnessed. Sandstone bedding becomes more massive and sheetlike, lacking crossbedding, and finer-grained interbeds decrease in thickness and abundance. I suggest that this interval of increasing bed thickness and fluctuating depositional energy represents a change in depositional energy related to upstream forcing and is a stronger candidate for the seismic sequence boundary than the swift and autocyclic deposition of crossbedded sandstones below. At the top of this interval, one observes a unique zone of siliceous beds (~580 m, Fig 2.18). A 15-cm thick amorphous silica bed with iron oxide inclusions forms a local bench. Surrounding sandstones also are conspicuously recemented with silica along joints and bedding planes. Just above the silica bed is a 10-cm thick carbonate bench as well as

Figure 2.23: Graphical tracing of outcrop previously interpreted as angular unconformity associated with seismic sequence 5-6 (Ré et al., 2003). Light lines denote angular to tangential foreset terminations of planar crossbed set.

several bentonitic seams. The siliceous interval may reflect paleogroundwater flow at this horizon, or alternatively, may result from ash accumulation in a water body (cf. zeolites formed by cation-leaching of ash in alkaline groundwater). In either case, the zone is unique among observed Iglesia Group strata and is coincident with the projection of the 5-6 seismic sequence boundary.

Increased pedogenesis marks the transition between outcrops of seismic sequences 6 and 7. Ré *et al.* (2003) located the boundary at an erosive surface (~3 m relief) filled with reddish crossbedded pebble conglomerate. The conglomerate's coloration (via granitic clasts and hematite staining) is locally distinct, but there is little primary lithologic change and the degree of erosion is minor when compared to the vertical resolution of seismic, such that the erosive contact and the several conglomerate beds are unlikely to be imaged in seismic. However, akin to the 2-3 and 3-4 boundaries, strata overlying the red conglomerates are strongly pedogenic for >20 m observable before the section is covered with terraces. The paleosol profiles are oxidized, clay-rich (argillic) and contain abundant carbonate accumulations (nodules and horizons), which are very rare in sequence 6 below. This change in lithofacies occurs over a thicker vertical distance than the previous SB candidate (Ré et al., 2003), likely represents a diminishment of sedimentation rate (e.g. mature paleosols) and is hereby proposed as the outcrop characterization of seismic SB 6-7.

Table 2.4 summarizes the compositional and erosional features as well as the correspondence with magnetostratigraphic reversals (summarized in Ré *et al.*, 2003) of seismic sequence boundaries 1-2 through 6-7 (~9 – 5.2 Ma). For the Angualasto section (Fig. 2.18), note the remarkable correspondence between paleomagnetic polarity reversals and sequence boundaries. Assuming that the Angualasto section captures all global reversals ("polarity completeness" *sensu* Beer, 1990), it is suggested that the sequence boundaries represent longer hiatuses than those

Table 2.4: Nonmarine Iglesia Basin outcrop characteristics of projected seismic sequence boundaries.

Seismic Boundary	Age (Ma)	Outcrop Characteristics at Boundary				
		Erosion (>3 m)	Change in clast composition	Vertical change in lithofacies (<40 m interval)	Change in pedogenesis	Magnetic Reversal
6-7	5.2	Locally 3 m		X	X	X
5-6	6.6			X		X
4-5	6.9			X	X	X
3-4	7.7		X	X		X
2-3	8.7		X	X		X
1-2	9.03<x<13.4	X	X	X		X

represented by pedogenesis and autocyclic erosion or bedding contacts. This is not the case for the Rodeo 1 and 2 paleomagnetic sections (Figs. 2.19 and 2.20), where radiometric age constraints and observed disconformities (e.g. channel erosion, hardgrounds, and compound pedogenesis) preclude correlations to the magnetic timescale without inferring several missing polarity zones at sequence boundaries or within the extensively pedogenic and channelized sections.

Structural measurements and stratigraphic correlation have better established sequence continuity across the El Tigre intrabasinal thrust faults. Because of variable reflector resolution in the vicinity of the faults, assessing vertical offset and designating sequences is problematic, especially across the multiple fault splays. Moreover, overlying fault-bend folds often cannot be traced through the near-surface mute zone on the seismic profiles. Finally, there are very few exposures of strata over the main fault system (northern basin; see Figure 2.3). For these reasons, previous field campaigns found it difficult to correlate between the sequence-calibrated Angualasto section and the Rodeo 2 section (Figs. 2.18 and 2.20) along the eastern basin margin. Vestiges of the five distinct reddish channel deposits had been recognized west of the Rodeo 2 section (T.E. Jordan, personal communication). More recently, exposures of all five redbeds and associated volcaniclastic and pedogenic facies were observed north of the Rodeo 1 section (north of reservoir at Dique Cuesta del Viento dam), tightly folded and onlapping both flanks of Cerro Negro de Rodeo (Figure 2.3 and 2.24), as well as in strata correlative with the lower Rodeo 1 section. Expansion of the mapped extent of these facies provides solid evidence that sequences 2 and 3 correlate across the eastern and central El Tigre thrusts, although the volcaniclastic character of sequence 2 differs from its alluvial conglomeratic appearance west of the fault train (Angualasto section, Fig. 2.18; see below).

Figure 2.24: Outcrops of five reddish conglomeratic channels associated with the 2-3 sequence boundary, recognized on both sides of fault-bend fold train. Upper photo is view south toward synclinal Rodeo 2 section. Lower photo is 5.5 km NE of upper photo, looking southwest toward Cerro Negro de Rodeo basement uplift. Rodeo 1 measured section begins on opposite flank of basement to west. Locations referenced in Fig 2.3.

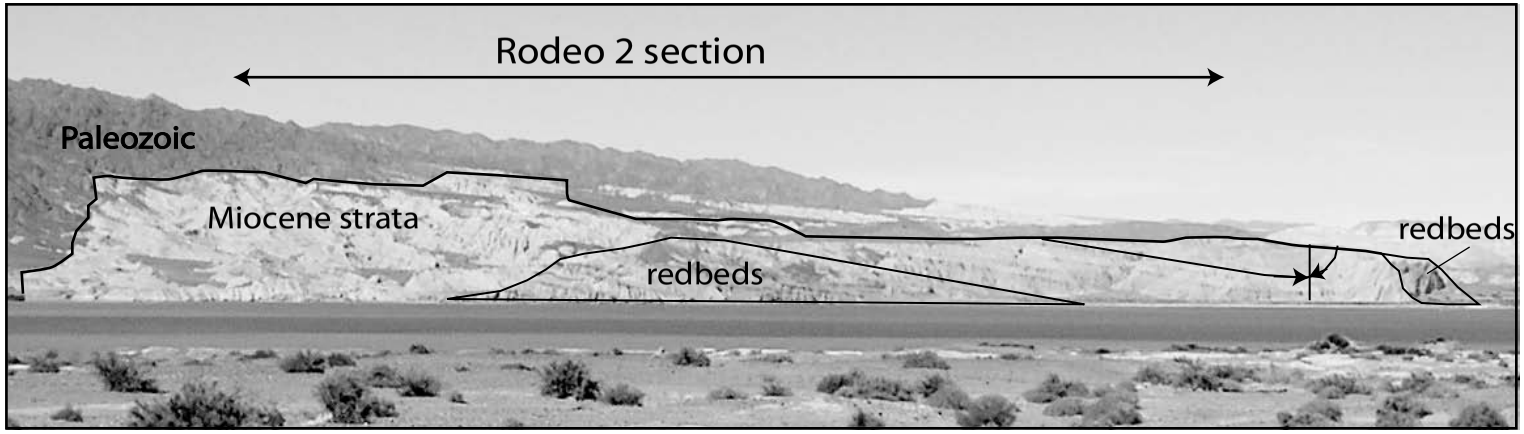
Rodeo 2 section
Paleozoic
Miocene strata
redbeds
redbeds


redbeds
Paleozoic
Cerro Negro
de Rodeo

Seismic interpretation suggests a degree of lithologic thinning and erosion at certain sequence boundaries (4-5, 5-6, 6-7, 7-8; Fig. 2.13) associated with fault bend folding in the west-central basin. In outcrop, folding associated with the El Tigre thrusts is commonly fully definably in outcrop scale, characterized by dipping axial surfaces and closed to tight interlimb angles, though fold crests in the basin center have been erosively removed. Such folds likely had topographic significance during sequence deposition. For example, the above-described difference in lithofacies of Sequence 2 implies a barrier to deposition between western alluvial and eastern volcaniclastic sediment. An axial drainage during sequence 4 deposition (see Appendix D) suggests drainage was strike-parallel with the fault train and associated folds. Other folds, however, lacked significant relief (see below, with respect to SB 4-5) and none of the observed tight folds are accompanied by facies or grain size zonation. Thus, though seismic onlap onto basin-center fold limbs does correspond with sequence boundaries, it is uncertain from the outcrops as to what extent intrabasinal tectonics affected sequence boundary development.

Recent fieldwork has extended the sequence framework stratigraphically calibrated along profile 5322 (Angualasto section) to outcrops along profile 5323 (Rodeo 1 section). Although seismic sequence 1 and the boulder-laden lower sequence 2 are not observed along line 5323, lithofacies comparable to sequences 3 and 4 are exposed. A sequence stratigraphic link between sections was established upon recognition of the 4-5 SB paleosol couplet in the remeasured Rodeo 1 section. The paleosols are remarkably consistent in terms of horizonation, structure, hue and lithologic assemblage between the Angualasto and Rodeo 1 sections, although they thin slightly to the south. This is noteworthy because the paleosols are observed in disparate structural subbasins separated by anticlinal axes (see Figs 2.3 and 2.9). Regional mature pedogenesis such as this implies landscape stability (Birkeland,

1999). Therefore, significant intrabasinal folding either post-dates the 4-5 sequence boundary (not likely considering growth stratal relationships observed in seismic profile 5322; Fig. 2.13A) or syndepositional fold-related topography was not a significant control on pedogenic development at this boundary.

Additional outcrops, some previously undescribed, were measured and sampled, enhancing the characterization of the basin-scale depositional system. Of particular note is the description of the northernmost basin deposits (near Colangüil and Maliman, Fig. 2.3) beyond the seismic network, as well as rare exposures of the youngest sequences (Sequences 8-11). Also noteworthy is evidence of basin axial drainage and cyclic fluvial avulsion and compound floodplain pedogenesis, spatially akin to the modern axial drainage (Arroyo Iglesia; Fig. 2.3). These stratigraphic features do not inform directly about sequence formation, but are described and interpreted in greater detail in Appendix D.

Discussion:

1. *Overall basin evolution:*

With respect to other intermontane wedgetop basins, Iglesia Basin is an example with nonerosive sequence boundaries preserved in relatively fine-grained sedimentary units. Recall that DeCelles and Giles (1996) characterized wedge-top deposits as extremely coarse and immature with an abundance of unconformities. While seismic sequence boundaries are certainly continuous at the basin scale, coarse grained (nonvolcaniclastic) deposits are only common in sequence 2 (~9 to 8.7 Ma) and the youngest sequences, and in both cases these deposits are in the westernmost subbasin. Yet, as has been discussed, sequence boundaries are more subtly expressed in outcrop as lithofacies changes often corresponding with variable degrees of pedogenesis and shifting depositional environments (Table 2.4). Also, despite the constant presence of marginal topography (source area for sediment) as well as the

aforementioned evidence for pulses of uplift (i.e. changing gradients, increased stream power), Iglesia Basin exhibits a fining- and thinning-upward stratigraphy. Interestingly, this trend holds even as depositional loci shifted toward the west after sequence 6 (<6.5 Ma). This reduction in grain size, accompanied by lithologic indicators of low-energy deposition (e.g. laminated mudstones, paleosols, paludal limestones with trace fossils suggesting subaerial exposure), implies an overall waning of depositional energy through time. However, estimated stratigraphic thickness and seismic volumes for sequences 7 through 11 suggest that the volume of sediment per unit time actually increased compared with the older sequences (Fernández, 1996; Table 2.5). These volumes are poorly constrained, however, because of poor seismic resolution in the eastern part of the basin. The rates are estimates, since the temporal history of the youngest sequences is extrapolated from a fission track ash dated 5.1± 0.8 Ma (Ré *et al.*, 2003), so sequence deposition is assumed to have concluded by ~4.3 Ma. Yet, because only the western sector of the basin is included in Fernández's volumes, such an increase in sediment volume/time is expected because of restriction of the depocenter to the western subbasin post sequence 7.

2. *Tectonic Controls*

From field and seismic interpretations, the means by which tectonism affected Iglesia Basin sequence deposition can be summarized. Frostick and Steel (1993) outlined what they perceive as main tectonic controls on sedimentary basin deposition: (1) overall accommodation space, (2) direction of basin floor tilt (3) location and size of depocenter(s), (4) the character and orientation of basin margins (i.e. overall size and shape), (5) deflection of sediment delivery systems, and (6) the rate of sediment supply due to uplift and erosion. Each of these controls can be addressed for Iglesia Basin.

Table 2.5: Estimated sediment volume per unit time for seismic sequences, based on geometric estimation of Fernandez, 1996. Durations of sequences 7-11 are unconstrained, so time has been partitioned equally between them based on radiometric and magnetostratigraphic contraints on the base of sequence 7 and minimum age of sequence deposition.

Sequence	Age (Ma)[1]	Duration[2]	Compacted Volume (km^3)[3]	Volume/Time (km^3/Ma)	median age of sequence (Ma)
11	>4.3 Ma	Average duration: 1.86×10^5 years	53.27	286.398	4.3
10	5.1 +/- 0.8		61.31	329.624	4.486
9	5.1?		154.82	832.366	4.672
8	<5.23		99.9	537.097	4.858
7	5.230 - ?		113.62	610.860	5.044
6	6.57 - 5.23	1.337×10^6 yrs	123.9	92.670	5.8835
5	6.94 - 6.57	3.68×10^5 yrs	163.06	443.098	6.7535
4	7.7 - 6.94	7.15×10^5 yrs	187.31	261.972	7.32
3	8.7 - 7.65	1.049×10^6 yrs	109.62	104.500	8.175
2	9.03 - 8.7	3.26×10^5 yrs	159.4	488.957	8.865
1	17.2+/-3.8	$<6.8 \times 10^6$ yrs	181	26.618	17.2

1: As correlated to Global Magnetic Polarity Time Scale (Cande and Kent, 1995), utilizing radiometric constraints

2: Duration of lacunas unknown

3: From Anibal Fernandez, 1996

First, and paramount to basin evolution, is the availability of accommodation space in Iglesia Basin since at least 20 Ma, as suggested by western margin onlap of seismic sequence 1 (17.2±3.8 Ma) and the measured onset of thrusting in the western Precordillera (Jordan *et al.*, 1993; 2001). Accommodation space was also created during or after the hiatus associated with SB 1-2 incision and continued to be available 9-4 Ma, although punctuated by base level falls at the sequence boundaries (see Chapter 1).

Geometric effects of tectonism, such as the direction of basin floor tilt, location and size of depocenter(s) and orientation of basin margins (controls 2-4 of Frostic and Steel, 1993) can each be observed in Iglesia Basin's seismic reflection profiles and have been described above. These features fundamentally affect sediment distribution and thus may result in sediment accumulation in one place versus starvation (hiatus) in another.

Deflection of sediment delivery systems (control 5 of Frostic and Steel, 1993) is speculated to have occurred in response to fault-bend folding over the intrabasinal El Tigre thrusts. The generally NW-SE paleocurrent measurements and cyclicity of fluvial sediments and floodplain paleosols above and east of the El Tigre thrust splays (see Appendix D) suggests that syndepositional folding enhanced development of an axial drainage system, similar to the modern configuration of the Río Blanco and Río Iglesia rivers. Major differences in the lithologic nature of Sequence 2 deposits (conglomeratic to the west, volcaniclastic and calcareous to the east) suggest a degree of topographic restriction of deposition amid the various subbasins of the fault train. Finally, the large-scale restriction of deposition to the westernmost subbasin (Sequence 7 and younger) implicates a change in depositional gradients and positive relief due to fault bend folding.

Tectonic control of sediment flux (control 6 of Frostick and Steel, 1993) occurred at both Iglesia Basin's margins and internally as a result of fault-bend folding. The interpreted progressive rotation of seismic reflectors against the western margin and the independently-constrained chronology of the linked Frontal Cordillera-Precordillera system (Table 2.1) argue for a semi-continuous degree of marginal uplift since 20 Ma, but occurring at varied rates and spatial positions. Rotation of reflectors against the western margin, however, is not robust in terms of timing or continuity from profile to profile, and does not correspond with all sequence boundaries. Therefore, marginal uplift along the entire length of the Iglesia Basin is not considered the driving force of sequence boundary genesis. Rather, locally variant uplift would have affected local sediment delivery.

Contingent on lithologic resistivity and availability of water for sediment transport, it is likely that periods of enhanced uplift rate (Table 2.1) generated more stream power (via stream profile rotation) for marginal incision (sequence boundary generation?) and ultimately sediment transport into the central basin (Hilley and Strecker, 2005). In chapter 3, the interpreted variations in paleoclimate in both the headwaters area and Iglesia Basin are combined with tectonic uplift to better explain sediment delivery and stratigraphic organization.

Finally, the longevity and relative spatial stasis of external drainage to the Bermejo foredeep via the Río Jáchal River is probably structurally controlled at crustal discontinuity through the Precordillera at ~S 30° 10' (cf. Allmendinger *et al.,* 1990; Talling *et al.,* 1995; Jordan *et al.,* 2001). Other Andean intermontane basins (e.g. Toro basin, eastern Puna margin and Santa Maria valley; Hilley and Strecker, 2005) exhibit outlets to the foreland through structurally complex parts of the orogen where along-strike discontinuities direct drainage patterns from wedgetop to foredeep (cf. Talling *et al,* 1995; Burbank *et al*., 1999). As postulated by Beer *et al.* (1990) and supported by

clast composition studies in the Bermejo foredeep (e.g. Damanti, 1989; Fernández, 1996), this river played an important role in both basins' evolution, although the temporal history of external drainage does not correlate well with sequence development or tectonic thrust events (discussed above and in Chapter 3).

For Iglesia, intrabasinal faulting and associated folding were active concurrent with sequence deposition, although the location of deformation may have varied through time. Sequences 2 through 8 were deformed by the El Tigre thrust system (Fig. 2.11A). In southern lines, faulting and folding affected sequences 7 and younger (Fig. 2.8). To the west, strata were folded from sequence 5 through at least sequence 10 (Fig. 2.11B).

3. *Climatic (hydrologic) Control:*

The climatic model for sequence origin proposed by Milana (1998) can be reappraised via seismic interpretation. An outcome of the seismic grid reinterpretation was the determination that no reflectors exhibit downlap terminations. This is an important feature of Milana's (1998) model of hydrologic (climate-driven) variability. In flume models of an alluvial system, downlap geometries were generated during periods of low discharge. The lack of downlapping reflectors in the Iglesia basin seismic lines may reflect spatial aliasing failure of the seismic network to characterize the 3-dimensional complexity of the depositional system (cf. Milana and Tietze, 2002). While the lack of downlap is an inconsistency of model and observation, variable hydrology or climatic control may be nevertheless a cause of sequence formation; in chapter 3, I document evidence from paleosols and lithofacies for significant changes in relative humidity during deposition of sequences 2-7.

4. *Seismic Facies*

Some attention should be paid to the high amplitude, continuous facies (SF-1), as it exhibits characteristic geometries both within and between profiles (2-3 lines, ~5

to 10 km) as well as representing the greatest contrasts in lithology. Ray (1982) identified this facies as “interbedded sandstones and shales”. Beer (1989) considered the same reflector characteristics as “sandy”, although this is observed in outcrop as a diverse assemblage of coarse sandstone, crossbedded sandstone, poorly- sorted mudstones and paleosols. Strong seismic reflectors are also promoted by high clay content (Sheriff and Geldart, 1995), such as may be found on floodplains where depositional energy is low, and as horizons in floodplain paleosols. Furthermore, Hanneman *et al*. (1994) recognized that intervals of calcic paleosols appear in seismic reflection data as high amplitude continuous reflectors, confirmed by well cuttings and geophysical log correlation. Iglesia Basin strata contain several intervals (>50 m) of compound paleosols, notably during late sequence 3 and sequence 4, as well as at and above SB 6-7, where the composite effect of pedogenic carbonate and clay horizons may be imaged in seismic profiles. Similarly, the SB 2-3 and SB 3-4 each are associated with repetition of palustrine limestones. These beds are lithologically similar to pedogenic K horizons (indeed, palustrine units are often mistaken as soil calcretes). The acoustic impedance contrast of these units (averaged over a depth range of 30-50 m) with surrounding strata could be akin to that recognized by Hanneman *et al.* (1994).

Based on the spatial relationships and lateral extent of SF-1, it is suggested that the facies corresponds either to fluvial sheet sandstones (high aspect ratio) and discrete channel sand bodies (low aspect ratio) or intervals (tens of meters thick) containing calcic and argillic (clay-rich) paleosols. The latter are common in sequences 3 and 4 as well as above sequence 7 (discussed in Chapter 3). Projecting these outcrop positions back into the subsurface, they compare favorably with sequence intervals and boundaries mapped as SF-1, especially where this facies extends farthest into the center of the seismic profiles (Fig. 2.25 profiles 5322, 5323, 5326).

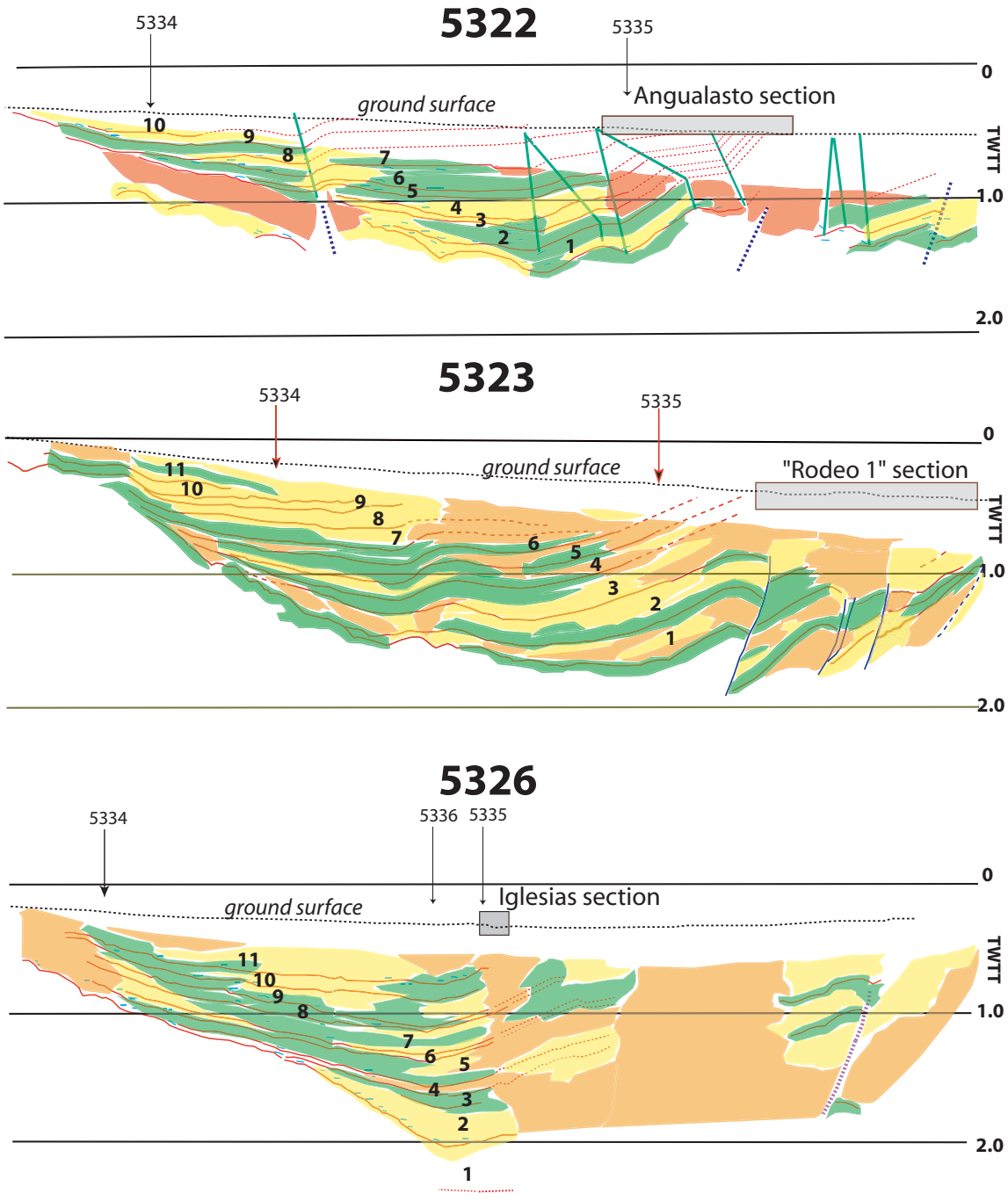

Figure 2.25: Seismic facies with respect to projections into outcrop.

5. ***Sequence boundary interpretation:***

The causes of the most readily recognized sequence boundaries (1-2 and 4-5) can be generally interpreted. Valley incision into Sequence 1 occurred in response to relative base level fall, due to either (1) uplift of the drainage headwaters (see Table 2.1), (2) drop in base level downstream in the foreland or (3) a change in headwater discharge following cessation of explosive volcanism in the drainage basin. Subsequent aggradation of sequence 2 multi-storey boulder-cobble conglomerates within the channels could have resulted from either climate change or uplift-induced sediment production (Schumm and Ethridge, 1994). A notable change in depositional energy occurred at the 4-5 sequence boundary (6.94 Ma, Ré *et al.,* 2003), coincident with interpreted uplift of the western margin (Table 2.1 and Fig. 2.8). Increased short term sedimentation rate during early Sequence 5 is presumed on the basis of the replacement of uppermost Sequence 4's mature floodplain paleosols by tens of meters of trough-crossbedded sandstone, which often exhibited flaser or load deformation, suggesting rapid sedimentation. A major increase in headwater discharge is also implicated by the discovery of a bed of granitic boulders directly above the 4-5 SB in at least 3 separate localities, separated by up to 5 km along-strike. The pedogenic impact of this transition is discussed in Chapter 3. However, these lithologic features support the premise of basin-scale (tectonic?) interruption of what was previously a stable landscape at this seismic sequence boundary.

Similar changes in depositional energy, though not recorded as dramatically in the basin-center outcrops as the 1-2 SB and 4-5 SB, likely occurred at the other seismic sequence boundaries. Seismic sequence boundaries projected into outcrops corresponding with lithofacies changes (2-3 SB), unique lithologies (2-3 and 3-4 SB palustrine carbonates; Appendix F) or compound paleosols (4-5 and 6-7 SB) implicate environmental changes in excess of those expected from autocyclic variability. These

features are distinct in vertical succession and are continuous along-strike for several kilometers and, as will be described in chapter 3, are the basin-central to distal disconformities correlative with proximal unconformities imaged in seismic.

Summary

Integration of interpretations from the complete Iglesia Basin seismic network provides a basin-scale appreciation of the tectonic and sedimentologic complexities of this wedgetop nonmarine foreland basin. At least eleven seismic sequences are confirmed, nine of which have been described in outcrop (see Figs. 2.18-2.22 and Appendix D). At least four episodes of western margin (Frontal Cordilleran) uplift (prior to 6.9 Ma and between 5.2-4.3 Ma) are inferred from seismic reflector rotation. Seismic growth strata suggest that intrabasinal syntectonic deformation accompanied sequences 2 through 10, locally coincident with sequence boundaries 4-5, 5-6, 6-7 and 7-8. Thus, tectonism clearly played a role in the development of these younger sequence boundaries. In outcrop, sequence boundaries 1-2 through 6-7 have been located in basin central locations and correlated amongst disparate exposures as well as across thrust-fault bend folds. While the oldest sequence boundary is clearly erosional (as well as the longest in duration, up to 4.4 Ma) and temporally coincident with multiple uplift events in the basin margins (Table 2.1), the overlying higher-frequency sequence boundaries correspond in basin-center positions to lithofacies transitions occurring at the scale of tens of meters and related to changing depositional energy. On the basis of stratigraphic architectural elements, lithofacies associations, paleosol development and seismic facies interpretation, a fining-upward trend is supported, corresponding with a general reduction in depositional energy, even as the depositional locus shifted toward the Frontal Cordillera source area. Thus, intra- and extra-basinal tectonism influenced many of the sequence boundaries and the depositional evolution of the Iglesia Basin. In the following chapter, these seismic and

outcrop observations are integrated with paleoclimate proxies to better describe the likely interactions between extrinsic variables affecting sequence genesis.

Acknowledgements:

Funding for fieldwork was provided by American Chemical Society Petroleum Research Fund grant 39557-AC8 to T.E. Jordan as well as Geological Society of America and American Association of Petroleum Geology Graduate Research Grants to B.G. Ruskin. Greg Hoke, Federico Martina and Facundo Flores assisted with field work and logistics. In particular, my gratitude goes to Rodrigo Morilla and his family for their assistance and hospitality.

References:

Allmendinger, R.W., Figueroa, D., Snyder, D., Beer, J., Mpodozis, C., and Isacks, B.L., 1990, Foreland shortening and crustal balancing in the Andes at 30ºS latitude: Tectonics, v.9, p. 789-809.

Bastías, H., Weidmann, N.E., and Pérez, A.M., 1984, Dos zonas de fallamiento Pliocuaternario en la Precordillera de San Juan: Noveno Congreso Geologico Argentino, Actas II, p. 329-341.

Bastías, H., Perucca, L., Paredes, J.D., and Tello, G., 1997, El Tigre Quaternary fault system, Argentina: Geological Society of America Abstracts with Programs, A-443.

Beer, J.A.., 1989, Magnetic polarity stratigraphy and depositional environments of the Bermejo Basin, and seismic stratigraphy of the Iglesia Basin, Central Andes: Ph.D. Dissertation, Cornell University, Ithaca, NY, 195 p.

Beer, J.A., 1990, Steady sedimentation and lithologic completeness, Bermejo Basin, Argentina: *Journal of Geology*, Vol. 98, p. 501-517.

Beer, J.A., Allmendinger, R.W., Figueroa, D.E., and Jordan, T.E. 1990, Seismic stratigraphy of a non-marine piggyback basin, Central Andes: American Association of Petroleum Geologists Bulletin, v.74, p.1183-1202.

Bercowski, Felisa, 1993, Facies piroclasticas en el Terciario del valle de Iglesia, Prov. de San Juan, Argentina: XII Congreso Geológico Argentino y II Congreso de Hidrocarburos, Actas IV, p. 206-215.

Birkeland, P. W., 1999, Soils and Geomorphology, 3rd Edition, Oxford University Press, 432 pp.

Bissig, T., Lee, J.K.W., Clark, A.H., and Heather, K.B., 2001, The Cenozoic history of Volcanism and hydrothermal alteration in the Central Andean Flat-Slab region: New ^{40}Ar-^{39}Ar constraints from the El Indio-Pascua Au (-Ag, Cu) Belt, 29° 20' – 30° 30' S: International Geology Review, Vol. 43, p. 312-340.

Bissig, T., Clark, A.H., and Lee, J.K.W., 2002, Miocene landscape evolution and geomorphic controls on epithermal processes in the El Indio-Pascua Au-Ag-Cu belt, Chile and Argentina: Economic Geology, Vol. 97, p. 971-996.

Burbank, D.W., McLean, J.K., Bullen, M., Abdrakhmatov, K.Y., and Miller, M.M., 1999, Partitioning of intermontane basins by thrust-related folding, Tien Shan, Kyrgyzstan: Basin Research 11, p.75-92.

Cahill, T., and Isacks, B.L., 1992, Seismicity and shape of the subducting Nazca Plate: Journal of Geophysical Research, Vol. 97, p. 17503-17529.

Cardozo, N. and Jordan, T. 2001, Causes of spatially variable tectonic subsidence in the Miocene Bermejo Foreland Basin, Argentina: Basin Research, v.13, p. 335-357.

Contreras, V., Damiani, O., Milana, J., Bracco, A., and Barrera, A., 1990, Paleogeno y Neogeno de San Juan. Decimo Congreso Geológico Argentino, Relatorio, p. 154-185.

Cristallini, R. and Ramos, V.A., 2000, Thick-skinned and thin-skinned thrusting in the La Ramada fold and thrust belt: crustal evolution of the High Andes of San Juan, Argentina: Tectonophysics, Vol. 317, p. 205-235.

Damanti, J., 1989, Evolution of the Bermejo foreland basin; provenance, drainage development and diagenesis, PhD Dissertation, Cornell University, Ithaca, NY, 191 p.

DeCelles, P.G. and Giles, K.A., 1996, Foreland basin systems: Basin Research, v.8, p. 105-123.

Den Bezemer, T, Kooi, H., and Cloetingh, S., 1999, Numerical modelling of fault-related sedimentation *in*: Numerical Experiments in Stratigraphy: Recent Advances in Stratigraphic and Sedimentologic Computer Simulations, SEPM Special Publications No. 62, p.177-196.

Fernández, A.E., 1996, Seismic analysis, paleoclimatology and fluvial architecture of the Bermejo Basin, Central Andes, Western Argentina: Ph.D. Dissertation, Cornell University, Ithaca, NY, 270 p.

Fernández-Seveso, F., 1993, Sismoestratigrafia de la Cuenca Iglesia: Informe de actividades en la Universidad de Cornell, Informe interno No. 10.408: 20 pp.

Flemings, P.B. and Jordan, T.E., 1990, Stratigraphic modeling of foreland basins: Interpreting thrust deformation and lithosphere rheology: Geology, Vol. 18, p. 430-434.

Fromm, R., Zandt, G., and Beck, S.L., 2004, Crustal thickness beneath the Andes and Sierras Pampeanas at 30°S inferred from Pn apparent phase velocities: Geophysical Research Letters, Vol. 31, L06625.

Furque, G., 1979, Descripción geológica de la hoja 18c, Jáchal. Dirección Nacional de Geología y Minería, Boletín 125, 79 p.

Gagliardo, M.L., A.T. Caselli, C.O. Limarino, F. Colombo Pinol, and A. Tripaldi, 2001, “Las unidades terciaras de la Cuenca Rodeo-Iglesia: validez y correlación de las unidades formacionales”: *Revista de la Asociacion Geologica Argentina* 56 (1), p. 121-125.

Hanneman, D.L., Wideman, C.J., and Halvorson, J., 1994,Calcic paleosols: their use in subsurface stratigraphy: American Association of Petroleum Geologists Bulletin, v. 78, p. 1360-1371.

Heller, P.L., Angevine, C.L., Winslow, N.S., and Paola, C., 1988, Two-phase stratigraphic model of foreland-basin sequences: Geology, v. 16, p.501-504.

Hickson, T.A., B.A. Sheets, C. Paola, and M. Kelberer, 2005, Experimental test of tectonic controls on three-dimensional alluvial facies architecture, Journal of Sedimentary Research, v. 75, p. 710-722.

Hilley, G. E., Strecker, M. R., 2005, Processes of oscillatory basin filling and excavation in a tectonically active orogen: Quebrada del Toro Basin, NW Argentina. Bulletin, Geological Society of America, 117, 887-901.

Johnson A.T., Jordan, T.E., Johnson, N.M., and Naeser, C., 1987, Cronologia y velocidad de sedimentacion en una secuencia volcaniclastica, Rodeo, Provincia de San Juan, Argentina: Decimo Congreso Geologico Argentino, Actas II: p. 87-90

Jordan, T.E., 1981, Thrust loads and foreland basin evolution, Cretaceous, western United States: American Association of Petroleum Geologists Bulletin, Vol. 65, p. 2506-2520.

Jordan, T.E., Isacks, B.L., Allmendinger, R.W., Brewer, J.A., Ramos, V.A., and Ando, C.J., 1983, Andean tectonics related to the geometry of subducted Nazca plate: Geological Society of America Bulletin, Vol. 94, p. 341-361.

Jordan, T.E., Allmendinger, R.W., Damanti, J.F., and Drake, R.E., 1993, Chronology of motion in a complete thrust belt: The Precordillera, 30-31˚ S, Andes Mountains: Journal of Geology, Vol. 101, p. 135-156.

Jordan, T.E., Fernández, A., Fernández-Seveso, F., Ré, G., and Milana, J.P., 1996, Asymmetric durations of sequences and their boundaries in the Mio-Pliocene nonmarine Iglesia Basin, Argentine Andes: Geological Society of America, Abstracts with Programs, v. 28: A-186.

Jordan, T.E., Tamm, V., Figueroa, G., Flemings, P.B., Richards, D., Tabbutt, K., and Cheathan, T., 1996, Development of the Miocene Manantiales foreland basin, Principal Cordillera, San Juan, Argentina: Revista Geológica de Chile, Vol. 23, p. 43-79.

Jordan, T.E., Kelley, S., Fernandez, A., Fernandez-Seveso, F., Ré, G., and Milana, J.P., 1997, Relaciones entre las historias evolutivas de las cuencas de Iglesia y Bermejo, Prov. de San Juan, Argentina: Actas de las segundas jornadas sobre geologia de Precordillera, p.142-147.

Jordan, T.E., Schlunegger, F. and Cardozo, N., 2001, Unsteady and spatially variable evolution of the Neogene Andean Bermejo foreland basin, Argentina: Journal of South American Earth Sciences, v.14, p. 775-798.

Kay, S.M, Mpodozis, C., and Coira, B., 1999, Neogene magmatism, tectonism, and mineral deposits of the Central Andes (22° to 33° S latitude) *in* Skinner, B.J., ed., Geology and Ore Deposits of the Central Andes: Society of Economic Geology Special Publication (SEG) No. 7, p. 27-59.

Kearey, P., Brooks, M., and Hill, I., 2002, An Introduction to Geophysical Exploration 3rd Ed.: Blackwell Science, 262 p.

Kendrick, E., Bevis, M., Smalley Jr., R., Brooks, B., Vargas, R. B., Lauría, E., and Fortes, L.P.S., 2003, The Nazca-South American Euler vector and its rate of change: Journal of South American Earth Sciences, Vol. 16, p. 125-131.

Legarreta, L., Uliana, M.A., Laratonda, C.A. and Meconi, G.R., 1993, Approaches to nonmarine sequence stratigraphy- theoretical models and examples from Argentine basins *in*. Eschard, R., and Doligez, B., eds. Subsurface Reservoir Characterization from Outcrop Observations: Proceedings of the 7th IFP Exploration and Production Research Conference, p. 125-143

Leveratto, M.A., 1976, "Edad de intrusivos Cenozoicos en la Precordillera de San Juan y su implicancia estratigrafica": Asociación *Geológica Argentina Revista*, XXI (1) p. 53- 58.

McGlashan, N.A., Brown, L.D., and Kay, S.M., 2006, Crustal thickness in the Andes from teleseismically recorded depth-phase precursors: Geological Society of America: Backbone of the Americas – Patagonia to Alaska, abstract. 3-7 April, 2006.

Mégard, F., Noble, D.C., McKee, E.H., and Bellon, H., 1984, Multiple pulses of Neogene compressive deformation in the Ayacucho intermontane basin, Andes of Central Peru: Geological Society of America Bulletin, Vol. 95, p. 1108-1117.

Milana, J.P., 1991, Sedimentología y magnetoestratigrafia de formaciones Cenozoicas en el area de Mogna y su insercion en el marco tectosedimentario de la Precordillera oriental: Tesis de doctorado, Universidad de San Juan, Argentina, 273 p.

Milana, J.P., 1998, Sequence stratigraphy in alluvial settings: a flume-based model with applications to outcrop and seismic data: American Association of Petroleum Geologists Bulletin, v.82, p.1736-1753.

Milana, J.P. and Tietze, K.W., 2002, Three-dimensional analogue modeling of an alluvial basin margin affected by hydrological cycles: depositional processes, profiles and sequences: Basin Research, v. 14, p. 237-264.

Molnar, P., and H. Lyon-Caen, 1988, Some simple physical aspects of the support, structure, and evolution of mountain belts, in: Clark, S.P., Jr., Burchfiel, B. C., and Suppe, J., eds, *Processes in Continental Lithospheric Deformation, Geological Society of America Special Paper 218*, p. 179

Molnar, P., 2001, Climate change, flooding in arid environments and erosion rates: Geology, Vol. 29, p. 1071-1074.

Ori, G.G. and Friend, P.F., 1984, Sedimentary basins formed and carried piggyback on active thrust sheets: Geology, v. 12, p. 475-478.

Pardo-Casas, F. and Molnar, P., 1987, Relative motion of the Nazca (Farallon) and South American plates since Late Cretaceous time: Tectonics, Vol. 6, p. 233-248.

Posamentier, H.W. and Allen, G.P., 1999, Siliciclastic sequence stratigraphy: Concepts and Applications, SEPM Concepts in Sedimentology and Paleontology 7, 210 p.

Rabassa, J., Cronato, A.M., and Salemme, M., 2005, Chronology of the Late Cenozoic Patagonian glaciations and their correlation with biostratigraphic units of the Pampean region (Argentina): Journal of South American Earth Sciences, Vol. 20, p. 81-103.

Ragona, D. and 23 others, 1995, Mapa geológico de la provincial de San Juan, República Argentina: Ministerio de Economía y Obras y Servicios Públicos.

Rafini, S. and Mercier, E., 2002, Forward modeling of foreland basins progressive unconformities: Sedimentary Geology Vol. 146, p. 75-89.

Ramos, V.A., Jordan, T. E., Allmendinger, R. W., Kay, S. M., Mpodozis, C., Cortés, J. M., and Palma, M , 1986, Paleozoic terranes of the central Argentine-Chilean Andes: *Tectonics*, Vol. 5, No. 6, p. 855-880.

Ramos, V.A., Page, R.N., Kay, S., Lapido, O., and Delpino, D., Geologia de la region del volcan Tórtolas, Valle del Cura – Provincia de San Juan: Decimos Congreso Geologico Argentino, 4, p. 260-263.

Ray, R.R., 1982, Seismic stratigraphic interpretation of the Fort Union Formation. Western Wind River Basin: example of subtle trap exploration in a nonmarine sequence *in:* Halbouty, M.T., ed., The Deliberate Search for the Subtle Trap: AAPG Memoir 32. p.169-180.

Ré, G. H. and Barredo, S.P., 1993, Estudio magnetoestratigrafico y tasa de sedimentacion del Grupo Iglesia, en sus afloramientos aledaños a la localidad de Angualasto (Prov. de San Juan): XII Congreso Geológico Argentino y II Congreso de Exploración de Hidrocarburos, Actas II, p. 148-155.

Ré, G.H., 1994, Magnetoestratigrafia de la secuencia Neogenica aflorante en Arroyo Chaleta (Angualasto, San Juan); Implicancias tectonosedimentarias: Actas V Reunión Argentina de Sedimentología, p. 205-209

Ré, G. H. and Barredo, S.P., 1994, La secuencia volcaniclastica Neogenica de Rodeo y su correlacion con el volcanismo Andino a partir de estudios magnetoestratigraficos: Actas V Reunión Argentina de Sedimentología, p. 211-216.

Ré, G. H. and Stein, J.E., 1994, Estudio magnetoestratigrafico del Grupo Iglesia (Prov. De San Juan): Implicancias neotectonicas: XIII Congreso Geológico Argentino y III Congreso de Exploración de Hidrocarburos, Actas II: p. 491

Ré, G.H., Jordan, T.E., and Kelley, S., 2003, Cronologia y paleogeografia del Teriario de la cuenca intermontana de Iglesia septentrional, Andes de San Juan, Argentina: Revista de la Asociación Geológica Argentina, v. 58, p. 31-48.

Riquelme, R., 2003. Évolution géomorphologique néogène des Andes Centrales du Desert d'Atacama (Chili): interaction tectonique-érosion-climat. PhD Thesis, Univ. Toulouse III-Paul Sabatier, 258 pp.

Salvini, F., Storti, F., and McClay, K., 2001, Self-determining numerical modeling of compressional fault-bend folding: Geology, Vol. 29, p. 839-842.

Sangree, J.B., and Widmier, J.M., 1977, Seismic stratigraphy and global changes of sea level, part 9: Seismic interpretation of clastic depositional facies *in* Payton, C.E, ed., Seismic Stratigraphy – applications to hydrocarbon exploration: American Association of Petroleum Geologists Memoir 26, p. 165-184.

Shanley, K.W., and McCabe, P.J., 1994, Perspectives on the Sequence Stratigraphy of Continental Strata: American Association of Petroleum Geologists Bulletin, v. 78, p 544-568.

Sheriff, R.E., and Geldart, L.P., 1983, Exploration Seismology Vol. 2: Data-Processing and Interpretation: Cambridge University Press, Cambridge, 592 p.

Sheriff, R.E., and Geldart, L.P., 1995, Exploration Seismology 2nd Ed., Cambridge University Press, Cambridge, 592 p.

Snyder, D.B., 1988, Foreland crustal geometries in the Andes of Argentina and the Zagros of Iran from seismic reflection and gravity data: PhD thesis, Cornell University, Ithaca, NY, 196 p.

Stewart, J., and Watts, A.B., 1997, Gravity anomalies and spatial variations of flexural rigidity at mountain ranges: Journal of Geophysical Research, Vol. 102, p. 5327-5353.

Stipanicic, P.N., 1979, El Triasico del valle del rio de los Patos *in* Segundo Simposio de Geología Regional Argentina, Academía Nacional de Ciencias, Córdoba, 1, p. 695-744.

Suppe, J., 1983, Geometry and kinematics of fault-bend folding: American Journal of Science, Vol. 283, p. 684-721.

Talling, P.J., Lawton, T.F., Burbank, D.W., Hobbs, R.S., 1995, Evolution of the latest Cretaceous-Eocene nonmarine deposystems in the Axhandle piggyback basin of central Utah: GSA Bulletin, v. 107, p. 297-315.

Thomas, W. A., and Astini, R. A., 2003, Ordovician accretion of the Argentine Precordillera terrane to Gondwana: A review: Journal of South American Earth Sciences, v. 16, p. 67-79

Thorne, J.A., 1992, An analysis of the implicit assumptions of the methodology of seismic sequence stratigraphy *in* AAPG Memoir 53: Geology and Geophysics of Continental Margins, p. 375-394.

Uyeda, S, 1982, Subduction zones: An introduction to comparative subductology: Tectonophysics, Vol. 81, p. 133-159.

Vail, P.R., 1987, Seismic stratigraphy interpretation using sequence stratigraphy *in* Bally, A.W. (ed.), Seismic stratigraphy: American Association of Petroleum Geologists Studies in geology No. 27.

Weissmann, G.S., Mount, J.F., and Fogg, G.E., 2002, Glacially-driven cycles in accumulation space and sequence stratigraphy of a stream-dominated alluvial fan, San Joaquin Valley, California, U.S.A. , Journal of Sedimentary Research, v. 72, p. 240-251.

Wetten, Cristian, 1975, "Estudio geologico economico de un yacimiento de diatomite y analisis de Mercado": II *Congreso Ibero-americano deGeología Económica*, V: p. 513-529.

Zapata, T. R., and Allmendinger, R. W., 1996, The thrust front zone of the Precordillera, Argentina: a Thick-skinned triangle zone: American Association of Petroleum Geologists Bulletin, v. 80, p. 359-381.

CHAPTER 3: CLIMATE CHANGE ACROSS NONMARINE SEQUENCE BOUNDARIES: PALEOPEDOLOGY AND LITHOFACIES OF IGLESIA BASIN, NORTHWESTERN ARGENTINA

Abstract

Subdivision of sedimentary rocks into genetically related sequences reflects interaction between the extrinsic and intrinsic processes that affect a basin's accommodation potential as well as its environment. In nonmarine settings, sequence bounding surfaces are often difficult to locate and several causal mechanisms for sequences (e.g. tectonism, climate change, and autogenic variability) combine in complex and still poorly-understood ways. Here we draw upon paleosols as sources of evidence for causes of sequence boundaries in the upper Miocene-lower Pliocene nonmarine Iglesia wedgetop basin (S 30°-31°, W 69°-70°), San Juan Province, Argentina. Stable isotopic compositions (δ^{13} C and δ^{18}O), clay mineralogy, inorganic carbon weight percentages, and micromorphic features of paleosols that span 9.3 – 4.6 Ma reveal environmental conditions concurrent with the development of ten nonmarine stratigraphic sequences. Compound pedofacies and regionally recognizable, abrupt lithofacies changes inform about fluctuations in both accumulation rate and climate across sequence boundaries and between structural sub-basins. Isotopic ratios and soil inorganic carbon weight percentages indicate increased aridity at 6.9 and 5.2 Ma, both times of sedimentary hiatus. Notable enrichment of δ^{13}C signal at 6.9 Ma also suggests dominance of C_4 plant biomass in northwestern Argentina. We interpret that the Iglesia basin strata accumulated under conditions that were generally semi-arid with seasonal precipitation, and that at least three of the 10 sequence boundaries formed during intervals of marginal surface uplift concurrent with greater aridity that eroded proximal strata and starved the central basin of sediment input, resulting in hiatuses in sediment accumulation.

Introduction:

Whereas the natural packaging of strata into unconformity-bounded stratigraphic sequences is a source of considerable information about paleogeography and history of a marine sedimentary basin (e.g. Miall, 1997; Posamentier and Allen, 2000), in nonmarine systems it is commonly difficult to locate and interpret stratigraphic sequence boundaries or their "correlative conformities" (e.g. Shanley and McCabe, 1994; Aitken and Flint, 1996; McCarthy and Plint, 1998; Friedman and Sanders, 2000; Miall and Arush, 2001). Incised valleys have generally been interpreted as erosive surfaces formed in response to base level lowering and utilized as nonmarine sequence boundaries (e.g. Shanley and McCabe, 1994; Schumm and Etheridge, 1994); however these erosive surfaces are spatially limited and may not be recognized. Other characteristic features of nonmarine sequence boundaries include abrupt changes in fluvial stacking patterns (e.g. degrees of sinuosity, amalgamation, coarseness, see Shanley and McCabe, 1995), presence of well-developed interfluvial paleosols or rooted exposure surfaces adjacent to the incised valley (e.g. Van Wagoner *et al.*, 1990; McCarthy and Plint, 1998), and systematic lateral changes in the above features. Some of these features prove elusive, given the often discontinuous nature of continental strata in both time and space. Nonetheless, recent work has illustrated the potential to locate and interpret nonmarine stratigraphic sequences, particularly through recognition and analysis of paleosols. In this paper we utilize paleosols to analyze the environment of a nonmarine intermontane sedimentary basin in the Argentine Andes, and in particular to identify the reasons that the strata are organized into large-scale unconformity-bounded stratigraphic sequences.

Soil formation ("pedogenesis") indicates a period of landscape stability, as well as temporally and spatially punctuated sedimentary deposition (Retallack, 1998; Birkeland, 1999). Paleosols are essentially hiatal in nature; thus their recognition is a

key to understanding accumulation rates. An inverse relationship exists between soil maturity and rate of accumulation, both laterally across the interfluve and in vertical succession, as a consequence of floodplain relief, drainage and sedimentation gradients (Bown and Kraus, 1987**;** Kraus, 1987; Wright, 1992). In alluvial settings, it has been suggested that the time represented by pedogenesis is very large compared to both deposition and erosion (Bown and Kraus, 1993). The characteristics and distribution of fossil soils in space and time can therefore be used to document sedimentation and topographic fluctuations, and suggest the degree to which extrinsic (tectonic and climatic) and intrinsic (e.g. autogenic and/or threshold-driven) mechanisms interact (e.g. Ethridge *et al.*, 1998; Kraus, 1999).

One attribute of any terrestrial depositional environment is climate control on erosion and sediment transport; hence knowledge of paleoclimate is invaluable to the correct sequence stratigraphic interpretation of the reasons for spatial and temporal variability of sediment accumulation and facies. But because sedimentary facies record hydrology, a result of an entire drainage basin rather than local atmospheric conditions, facies are not robust proxies for paleoclimate at the site of deposition. In contrast, a first-order relationship between climate and soil formation has long been recognized (Jenny, 1941), and various techniques are available to describe and quantify this association, including profile and micromorphologic measurements, clay mineral identification, and stable isotopic analysis of soil carbonates. The complex "micro-climate" that exists in any given soil may be treated (at least for well-drained soils) as a muted version of the regional climate (Retallack, 2001). Therefore, the utilization of paleosols as climatic proxies is complementary to the goals of nonmarine sequence stratigraphy.

The nonmarine Iglesia foreland basin of NW Argentina (San Juan Province, 30-31° S, 69-70 ° W, Figure 3.1) affords ample opportunities to evaluate

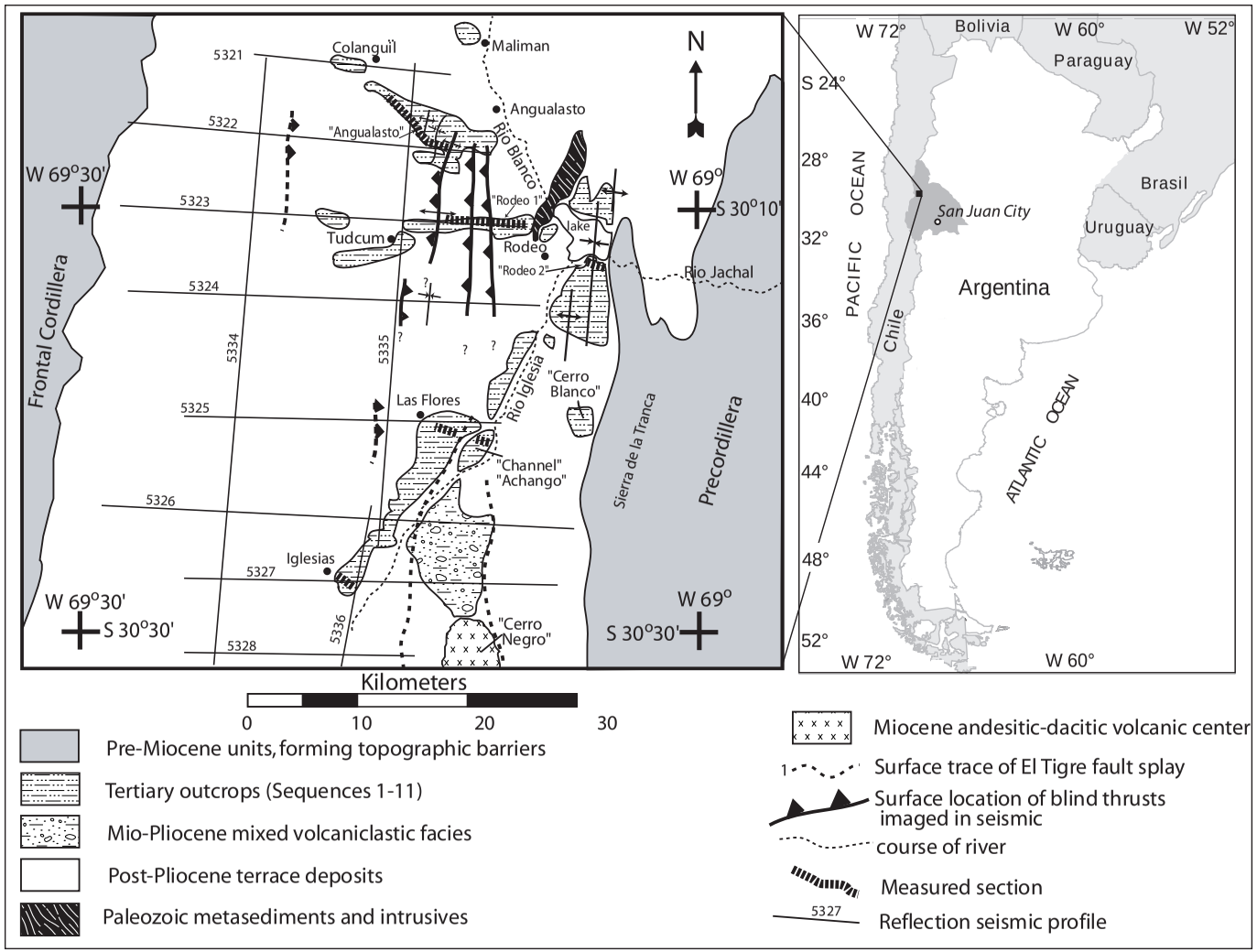

Figure 3.1: Geographical position, major tectonic features, outcrop belts and seismic reflection profile grid for Iglesia Basin, San Juan Province, Argentina. Labeled localities and measured sections are referenced in text.

syndepositional climatic variation, geomorphologic responses, and the stratigraphic sequence outcomes, through integration of surface, subsurface, and geochemical datasets. The Tertiary basin developed between the Frontal Cordillera of the Andes (western margin) and Precordillera thin-skinned thrust belt (eastern margin), and comprises the northern 70 km of the more extensive Iglesia-Calingasta Valley. Translated passively on top of the westernmost ("Las Trancas") thrust sheet, Iglesia Basin is classified as the "wedgetop" or "piggyback" component to the more extensive Bermejo foredeep depozone preserved largely on the eastern side of the Precordillera (Ori and Friend, 1984; Allmendinger *et al*., 1990; DeCelles and Giles, 1996; see Chapter 2). Interpretation of a basin-scale network of 1980's industry-grade seismic reflection profiles suggests the presence of up to eleven stratigraphic sequences defined by reflector geometries (e.g. onlap, toplap, and truncation) within 3.5 km thickness of the dominantly fluvial Miocene-Pliocene Iglesia Group (Beer *et al.,* 1990, Fernandez-Seveso, 1993; Ré *et al.,* 2003, Figure 3.2; Table 3.1). Because the eastern half of the basin fill is inclined gently, the seismic sequences are physically continuous with the surface outcrops (Fig. 3.2), which permits radiometric and magnetostratigraphic dating of surface strata to serve as constraints on the ages of seismic sequences. Along profiles 5322 and 5323, the full duration of sequence deposition was approximately 20.2 to 4.3 Ma, and all but the lowest sequence formed between ~9 and 4.3 Ma (Ré and Barredo, 1993; Ré and Stein, 1994, Jordan *et al.*, 1997; Ré *et al.,* 2003). The two intervals of Iglesia Basin accumulation (Sequence 1 and Sequences 2-11) correspond with intervals of diminished shortening rate in the Precordillera thrust belt (Jordan *et al.,* 1993).

Overall basin geometry, a north-trending lens reaching 3.5 km in thickness near its axis (Fig. 3.2b), was controlled by tectonic movement on both margins as well as out-of-sequence intrabasinal thrusting. Blind thrust faults of El Tigre fault system

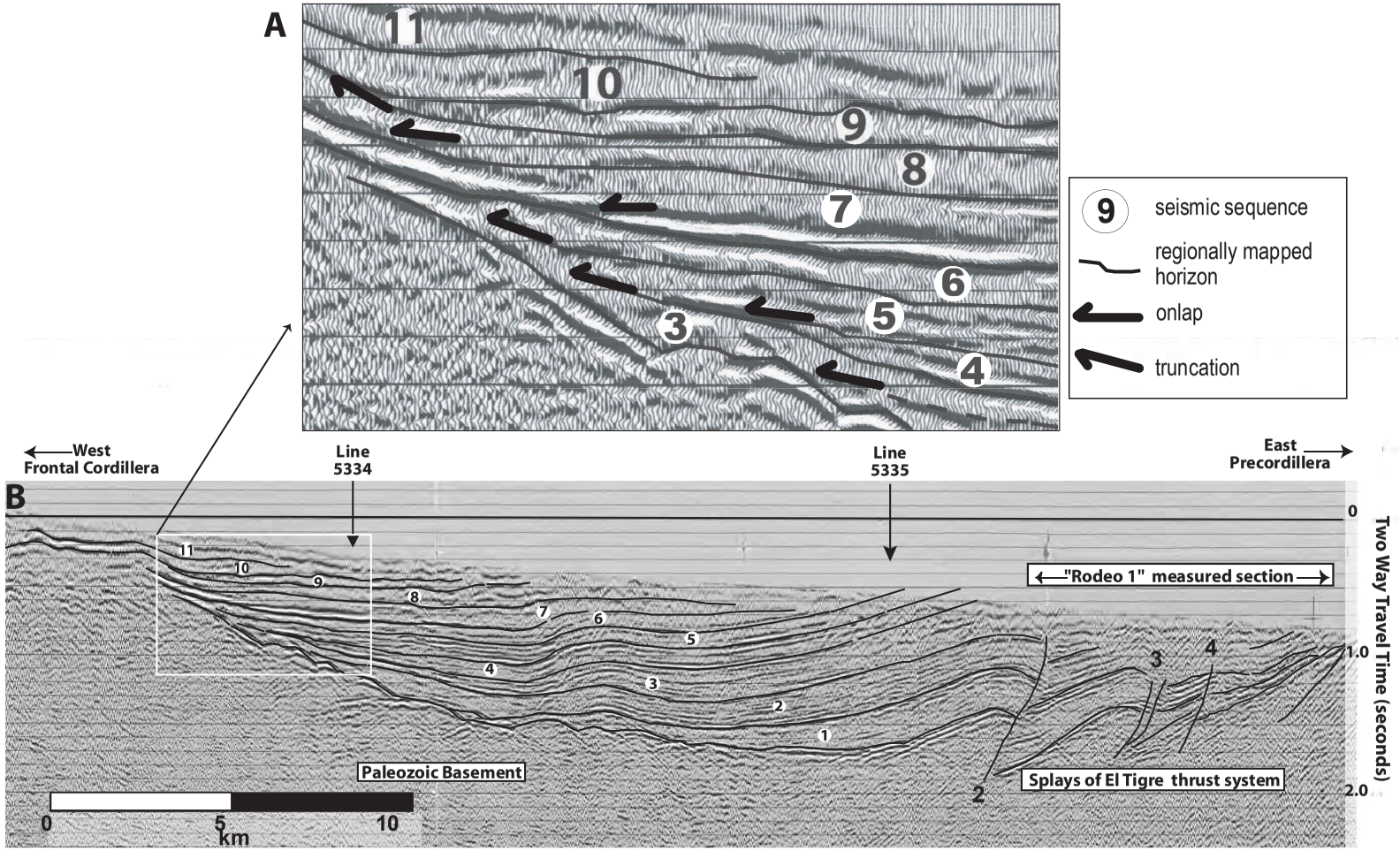

Figure 3.2: Representative seismic profile illustrating nature of seismic sequence boundaries in Tertiary sedimentary fill of Iglesia Basin. (A) Detail of western margin and common reflector geometries. (B) Full length of seismic profile, showing sequences correlated among seismic network as well as intrabasinal thrusts. Seismic profile is parallel with Rodeo 1 outcrop measured section.

Table 3.1: Summary of seismic reflection geometric criteria for sequence boundary interpretation for Iglesia Basin, Argentina. Line numbers correspond to seismic profiles illustrated in Figure 3.1, as well as several additional profiles to the south of studied outcrops. Western rotation refers to cases where sequence boundaries are noticeably inclined with respect to overlying (often onlapping) reflectors, or cases where entire sequence packages of reflectors are inclined relative to their position in undisturbed central basin positions.

Line	Sequence Boundary	Onlap	Truncation	Toplap	W Rotation
5321	8--> 9		Y		
5322	9-->10	Y			Y
	8-->9	Y		Y	
	7-->8	Y	Y	Y	
	6-->7	Y	Y		Y
	5-->6	Y			
	4-->5	Y			
	3-->4	Y			
	2-->3		Y		
	1-->2	Y	Y		
	Basement-->1	Y	Y		
5323	10-->11		Y		
	9-->10	Y			Y
	8-->9	Y			Y
	7-->8	Y			Y
	6-->7	Y			Y
	5-->6	?		?	Y
	4-->5	Y			Y
	3-->4	Y	Y		Y
	2-->3	Y			
	1-->2	Y	Y	Y	
	Basement-->1	Y	Y		
5324	9-->10	Y			
	8-->9	Y	Y		
	7-->8	Y	Y		
	6-->7	Y	Y		Y
	5-->6	Y			
	4-->5	Y	Y		Y
	3-->4	Y			
	2-->3	Y		Y	
	1-->2	Y			Y
	Basement-->1	Y			
5325	10-->11		Y		
	9-->10	Y			
	8-->9	Y	Y		
	7-->8		Y	Y	
	6-->7		Y		
5326	8-->9	Y	Y		Y
	7-->8	Y	Y		Y
	6-->7	Y			Y
	5-->6		Y		
	4-->5	Y			Y
	3-->4	Y			Y
	2-->3	Y	Y		
	1-->2	Y			
	Basement-->1	Y			
5327	7-->8	Y			Y
	6-->7	Y	Y		Y
	5-->6	Y	Y		
	4-->5				
	3-->4		Y		
	2-->3	Y			
	1-->2	Y	Y		
5328	8-->9				
	7-->8	Y			
	6-->7		Y		
	5-->6	Y	Y		Y
	4-->5	Y			Y
	3-->4		Y	Y	
	2-->3	Y		Y	
	1-->2		Y		
	Basement-->1	Y	Y		
5329	7-->8		Y		
	6-->7		Y		
	5-->6		Y		
	4-->5	Y	Y		
	3-->4	Y	Y		
	2-->3		Y	Y	
	1-->2		Y		
	Basement-->1	Y	Y		
5330	3-->4	Y	Y		
	2-->3	Y		Y	
	1-->2	Y	Y		
	Basement-->1	Y		Y	

Summary				
Boundary	**Present**	**Onlap**	**Truncation**	**Toplap**
10-->11	2	0	2	0
9-->10	4	4	0	0
8-->9	7	5	4	1
7-->8	8	6	5	2
6-->7	8	5	6	0
5-->6	7	4	4	0
4-->5	7	6	2	0
3-->4	8	6	5	1
2-->3	8	6	3	4
1-->2	8	6	6	1
Basement-->1	7	7	4	1

(26°-36° S, ~69° 10’ W) offset the strata at depth and divide the basin into at least six north-trending structural sub-basins (Figs. 3.1 and 3.2). The stratigraphic sequences are brought to surface levels by fault-propagation folds, some exhibiting growth-stratal relations in the subsurface. The prevalence of folds over faults facilitates tracing units among discontinuous outcrops and from seismic to outcrop. The structural relief that separates the Iglesia basin from both the Frontal Cordillera and the western ranges of the Precordillera increased during the general time interval of accumulation in the Iglesia basin, through folding rather than across basin-bounding faults (Allmendinger *et al*., 1990). The basin broadened (in east-west dimension) during deposition of the lower seven sequences, followed by restriction of the youngest four sequences to the westernmost structural sub-basin (Ré *et al.*, 2003; Fig. 3.2). Most exposures are confined to longitudinal belts parallel to the structural trend and in axial positions. Nonetheless, well exposed sections have also been measured and dated along the eastern margin (Rodeo 2 section, Fig. 3.1).

End-Member Models of Iglesia Basin Sequence Genesis:

A tectonic model for Iglesia Basin sequence generation has been suggested, but does not completely explain observed characteristics of the stratigraphy. The model includes two states, one enhancing sediment accumulation and the other creating unconformities between sequences, which would result from tectonically-mediated base level changes of the latitudinal drainage, Río Jáchal (~30° S) (Beer *et al.*, 1990). In the first state, Precordillera thrust events closed drainage from the wedgetop depozone, leading to sequence accumulation in a basin ponded west of the thrust-induced blockage. In the second state, tectonic quiescence allowed the drainage to reequilibrate with the Bermejo Basin base level to the east, excavating Iglesia Basin and generating sequence boundaries. The role of tectonism on large-scale basin accommodation is not in doubt. However, the number and timing of seismic sequence

boundary formation as initially interpreted by Beer *et al.,* (1990) does not correlate well with Precordillera fault motions (Jordan *et al*., 1993).

The role of external climate forcing on Iglesia Basin sequence generation was explored by Milana (1997, 1998), who envisioned discharge variations related to glacial cycles in the Frontal Cordillera source area. Seismic observation suggests a hierarchy of proximal incision (sequence boundaries). Milana (1998) and Milana and Tietze (2002) explored the likely architecture and facies of discharge-induced sequences through examination of one Iglesia Basin seismic profile and flume models in two and three dimensions. Sediment transport in these flume models is clearly linked to variable discharge: during periods of low stream discharge, a low-efficiency transport system deposits alluvium in areas proximal to the source (along the basin margins), whereas increasing discharge re-transports sediment to distal positions and is accompanied by proximal incision. However, our evaluation of outcrops and the entire seismic network do not reveal downlapping geometries as Milana's (1998) flume model prescribes for low discharge periods (see Chapter 2). Although the experimental models assist in interpretation of sedimentary architecture that one could expect by discharge variability, the simplifying assumptions, that sedimentary supply and tectonic environment are fixed, are inappropriate for the active orogenic margins of Iglesia Basin.

We acknowledge the difficulties of discriminating between climate and tectonic forcing mechanisms from the inherently incomplete sedimentary record. The end-member models proposed above are too simple to reflect the intricacy of the Iglesia Basin wedgetop depositional setting, wherein sedimentation was likely affected by multiple forcing mechanisms. In this paper, it is not our intention to rule out the influence of tectonic base level control, or to generalize sequence concepts for all nonmarine settings. Rather, through field documentation of lithofacies variations and

field, geochemical and isotopic characterization of the paleosols, we strive to document the degree and nature of climate change across nonmarine stratigraphic sequence boundaries.

Modern Climate and Soils of Iglesia Basin:

San Juan Province, Argentina currently experiences a semi-arid climate with seasonal precipitation, controlled by both its latitudinal position and its location in the rainshadow of the Andes ranges to the west. The majority of precipitation in northwestern Argentina during occurs during the austral summer, December-February (Ambrizzi *et al.*, 2005). During the period 1981-1990, mean annual precipitation (MAP) at San Juan City (31° 30' S, 68°42' W, 630 m elevation) was 92.3 mm/year (Servicio Meteorológico Nacional de Argentina, 2005). Precipitation near San Juan City is seasonal, with 90% of annual rainfall occurring between October and March, the austral summer (Perucca and Paredes, 2004).

Within the Iglesia Basin, west of the Precordillera range and at ~2000 m elevation, there are no official rain gauges, but climate characteristics can be approximated using regional climate models. The International Water Management Institute models mean annual temperatures (MAT) of 10-13°C and MAP of 50-100 mm/year (IWMI World Water and Climate Atlas, 2005, data compiled every 5' from 30°0'0"S, 69°0'0" W through 30° 30' S, 69° 30' W). This model also reveals seasonality: Iglesia Basin precipitation is greatest during January and February, with a secondary maximum during June-August (Figure 3.3). Annual temperatures appreciably decrease and winter precipitation values increase with elevation in the Frontal Cordillera to the west (Fig. 3.3), in which much of the Iglesia Basin drainage catchment is located. These measured and modeled results permit Iglesia Basin to be considered a "steppe" semi-arid climatic zone by both the Köppen and Trewartha climate classification schemes (McKnight and Hess, 2000)

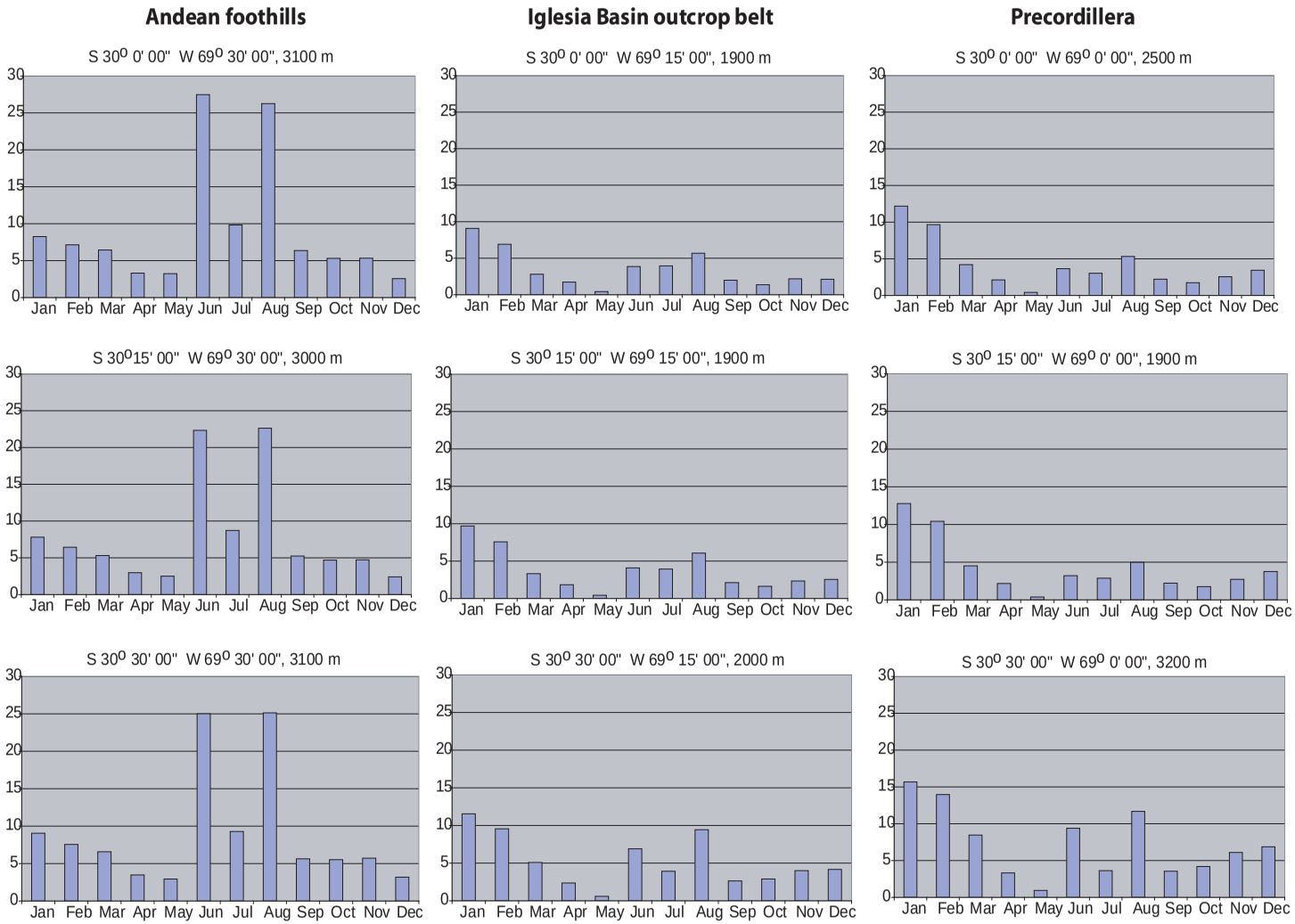

Figure 3.3: Monthly precipitation (mm) for Iglesia Basin and margins, from IWMI Climatology 1961-1990. Positions are relative WGS-84 datum and elevations are given in meters above sea level (from SRTM dataset).

The controls on modern climate may be clues to controls on the Mio-Pliocene climates of interest to this study. One system that contributes to semi-aridity in the Iglesia Basin is the Hadley Circulation cell. This thermal circulation transfers sensible and radiative heat from equatorial to higher latitudes. At its latitudinal position (S 30-31°), Iglesia Basin is located in a zone of high pressure where the Hadley cell drives descent of dry air which hinders precipitation and drives evaporation. Past positions of the sinking air of Hadley circulation have been explored using a general circulation model (GCM) to explore the global effects of changes in the latitudinal sea surface temperature gradient, as well as global climate change (Rind, 1998; Rind and Perlwitz, 2004). If the meridional temperature gradient increased during the late Tertiary (with or without global climate change), the model predicts increased Hadley cell intensity (*i.e.* increased stream function of the zonal mean meridional wind circulation). Also, GCMs suggest that numerous factors influence the poleward extent of Hadley circulation, including topography and seasonality (Cook, 2004; Rind and Pelwitz, 2004). Both of these could have profoundly affected Iglesia Basin climate during sequence formation concurrent with Andean uplift, as shifts in the poleward extent of Hadley circulation would impact the regional climate of deposystems on the fringe of the circulation cycle. Another strong contributor to the local climate is the orographic effect of the adjacent Andes. Climate modeling has shown that a primary control of Central Andean precipitation patterns is the Andean orogen (Lenters and Cook, 1995). The appreciable topography of the Frontal Cordillera (elevations up to 6200 m to west of Iglesia Basin) focuses precipitation on its western slope and creates a corresponding rain shadow in the eastern foreland (the Iglesia catchment). The orographic precipitation minimum is compounded by the dry adiabatic descent of high-velocity hot air down the leeward slope, the "Foehn Effect". These warm, dry winds, locally called "zonda winds", are frequent during the Austral winter in conjunction with low-

pressure systems that approach from the west, and can raise temperatures by up to 15°C while depressing dewpoints by 20°C in a few hours (Puliafito *et al.*, 2002; Seluchi *et al.*, 2002). The combination of (a) persistence of the Central Andes as a topographic high since at least 15 Ma (Irogoyen, 1997) and (b) minimal latitudinal drift of South America during the intervening time (Hartley *et al.*, 1992), allows us to speculate that the Mio-Pliocene Iglesia valley existed in a rain shadow and was influenced by atmospheric circulation patterns similar to present.

Modern soils near the Iglesia valley are classified as Entisols or "other" (INTA, 1990; Moscatelli and Puentes, 1998). Entisols are considered incipient soils in their overall development as a consequence of unfavorable local conditions (Retallack, 2001). This statement does not implicate a climatic or geomorphic regime, because slope, humidity and parent materials are nonunique for Entisol classification. In the case of Iglesia Basin, present semiaridity and geomorphically young surfaces may be responsible for the generally poor soil formation. As a consequence, agriculture (e.g. small vineyards and croplands) is limited to well-irrigated lands adjacent to streams and rivers (Baudino *et al.*, 2002). Recent pedogenesis is visible chiefly along road cuts and ephemeral drainages in the Iglesia Basin, where soils are characterized by redoximorphic bands and mottles as well as illuviation of clay and minor horizonation.

Iglesia Basin sequences:

Iglesia Group strata from ~20.2 - 4.3 Ma constitute a fining-upward succession of nonmarine units punctuated by depositional hiatuses of varied outcrop expression. General lithologic features and chronostratigraphy of the sequences is presented in Figure 3.4. The lower section (sequences 1-2) has a notable volcaniclastic component (e.g. tuffs and reworked tuffaceous sandstone), but volcanic influence decreases upsection, such that ash interbeds are generally <30 cm thick and infrequent in sequences 3-11. A lengthy hiatus exists between sequences 1 and 2 (duration ≥4.4

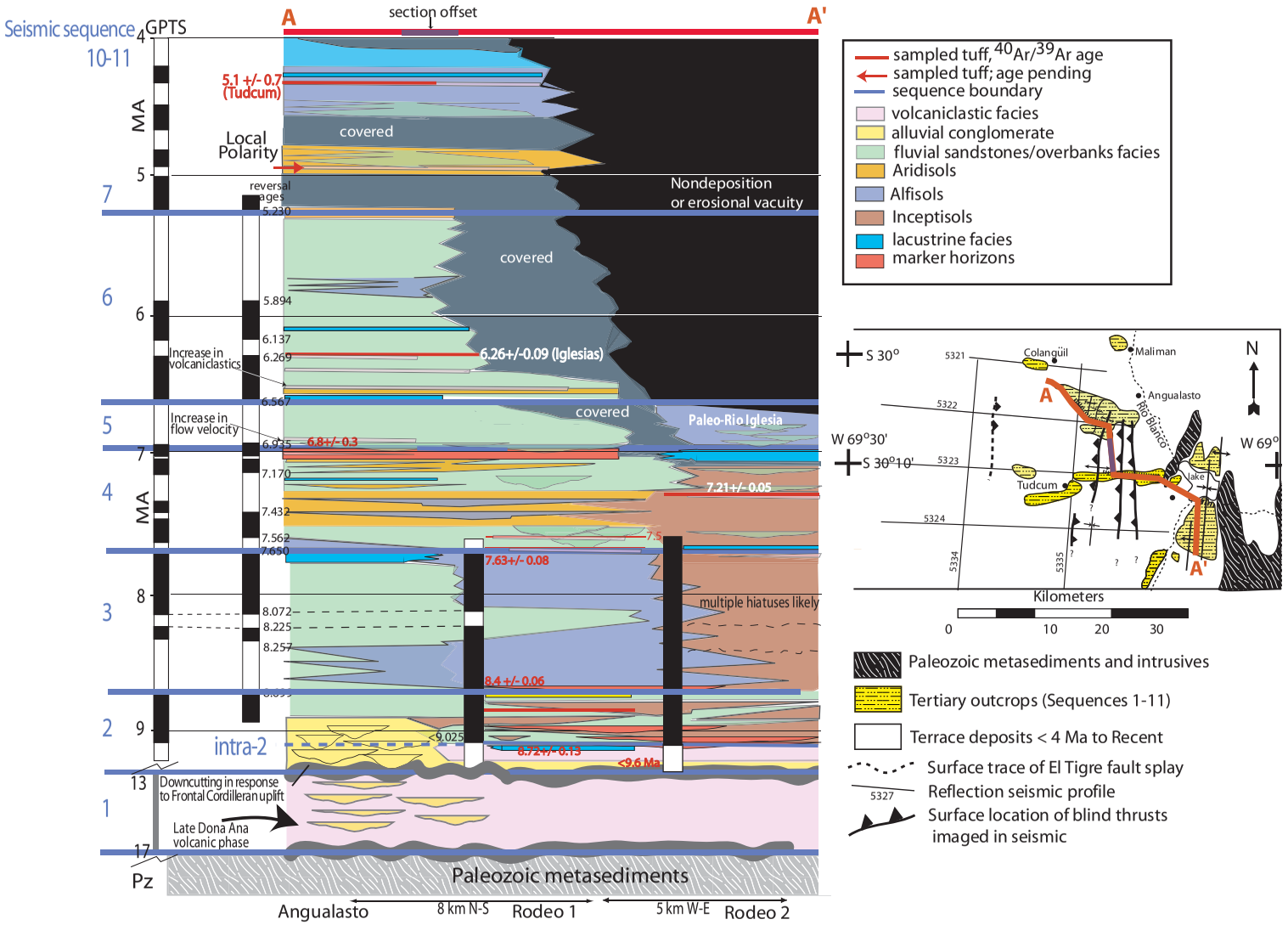

Figure 3.4: Chronostratigraphic fence diagram of Miocene-Pliocene sequences, Iglesia Basin, Argentina.

million years), but the hiatuses at all other sequence boundaries in axial positions are less than 1 million years. The long-term progression of the sedimentary environments was from initial alluvial deposits with the coarsest-grained incised valley fill at the base (seismic sequence 2), to sheet and channel sandstones interbedded with fine grained overbank deposits (sequences 3-7) and finally to a system dominated by fine-grained (low-energy) overbank and backswamp deposits (seismic sequences 10-11, ~ 4.3 Ma). Sequences 8-9 are poorly exposed, due to outcrop weathering and post-Pliocene terrace cover. With the exception of the Sequence 1-2 boundary, field characteristics of the seismic sequence boundaries are typically subtle, characterized by localized incision (a few meters depth), changes in clast provenance, or vertical changes in lithofacies, some slight, but others quite prominent (see Chapter 2). The ages and durations of the seismic sequence boundaries are revealed by paleomagnetic polarity stratigraphy (Ré *et al.*, 2003, Fig. 3.4).

A. *Pedogenic component of sequences:*

Upper Miocene-Lower Pliocene paleosols were recognized in outcrops following the criteria presented by Retallack (2001), namely the development of soil horizons (e.g. illuvial, eluvial, and calcic layers), diagnostic structures (peds, glaebules, etc.), and root traces or biological alteration or destruction of original sedimentary textures. Other features such as gley coloration and mottling, slickensides, and carbonate layers were carefully examined and interpreted, as these features may be related to diagenesis or compaction. Profiles and nodules were measured with a metric tape, principal dry-condition colors recorded using a Munsell Soil Color chart (1973 edition), and carbonate accumulations tested with dilute HCl acid (10%). Soil carbonate accumulations were classified following stages described by Machette (1985) for non-gravel soils (I: dispersed, II: nodular, III:

layered/coalesced nodules, IV: solid horizon, etc). Observed features are summarized in Appendix A, Table A.2.

Iglesia Group fossil soils are typically exposed as truncated compound successions wherein multiple, incomplete paleosol profiles are bounded by nonpedogenic sheet or channel sandstones (Wright, 1992; Kraus, 1999). Individual profiles commonly consist of an upper argillic B-horizon with subangular-blocky to granular ped structure, Stage II or III carbonate glaebules 2-6 cm in diameter (Machette, 1985), and gradation into a C-horizon and/or nonpedogenic sediment downward in the profile. Upper organic-enriched paleosol horizons (O and/or A) are always absent (save sparse charcoal residue). In some cases, fluvial channels locally eroded the underlying paleosol to depths of as much as 0.5 m. Inter-horizon boundaries and transitions to nonpedogenic sediments occur gradually (over 5 to 15-cm depth range, Soil Survey Staff, 1993). Other notable features are redoximorphic mottles or color banding (aquic features) and compaction structures (i.e. compressed peds, flaser bedding, minor slickensides), that suggest that groundwater influence and sedimentation rate, respectively, often fluctuated during or immediately after the pedogenic time interval. The aquic bands occur on a variety of scales (mm to tens of cm in vertical dimension, hundreds of m along-strike) and are common in Sequence 3 deposits (~8.7-7.7 Ma) and in the eastern sub-basins. Soils containing carbonate nodules commonly have orange hues to their B or Bk horizons or are associated with oxidized floodplain silts or (more rarely) trough-crossbedded sandstones. Observed paleosols are classified as Inceptisols (comparable to the modern Entisols of Iglesia Basin), Alfisols, and Aridisols (after Retallack, 1993, cf. Protosols, Argillosols and Calcisols of Mack *et al.*, 1993). Calcic paleosols are largely absent from outcrops of both the western and easternmost sub-basins as well as outcrops ~7.2 – 6.5 Ma along the modern axial drainage, Arroyo Iglesia (Fig. 3.1). These intervals exhibit extensive

compound pedogenesis, but lack significant development of stage II or greater carbonates.

B. ***Recognition of sequence boundaries in seismic and outcrop:***

In the Iglesia Basin, identification in outcrop of the features corresponding to the well-imaged seismic sequence boundaries has proven difficult despite repeated field campaigns (e.g. industry short courses 1988 & 1990; Beer *et al.,* 1990; Milana, 1998; Ré *et al.,* 2003). There are a set of causes of this difficulty (summarized below; see also Chapter 2). First, the continuity of exposures, while good, is imperfect (post-Pliocene terrace deposits cover much of the basin's Mio-Pliocene sequences). Second, the seismic data mute zone creates a data gap several hundred meters thick between the seismic information and the outcrops, a critical gap because the variable angles of dip of the limbs in individual folds lead to multiple possible choices for the projection of subsurface fold limbs to surface exposures. The combination of mute zone and variable dips result in horizontal uncertainties on the order of 100-200 m in the projected positions of seismic sequence boundaries to exposed beds. Third, the seismic sequence boundaries reflect changes in physical properties across a thickness of >20 m (Sheriff and Geldart, 1983), whereas outcrops permit resolution of characteristics to a scale of centimeters. Fourth, in some sectors of the basin the seismic sequences are not physically continuous with the outcrops because of intrabasinal thrust faults, and elsewhere (e.g. the eastern part of the basin) there are exposed strata but no seismic data. Nonetheless, several surfaces or intervals of strata have been interpreted to be the evidence of abnormally long hiatuses or marked changes in the history of the sedimentary basin, and are therefore considered to be the outcrop expressions of the seismic stratigraphic sequence boundaries.

The only sequence boundary that is easy to recognize because it is a major erosional boundary is SB 1-2 (Chapter 2 and Ré *et al.,* 2003; Figure 3.5 A). As there

Figure 3.5: Outcrop expression of nonmarine seismic sequence boundaries, recognized by (A) valley incision with notable hiatus and lithofacies change (SB 1-2); (B) Regional mature paleosol couplet (marked with arrows; SB 4-5). Across this boundary, sediment accumulation rate increased from 10 cm/ka to 48 cm/ka; (C) Abrupt, regional facies change and corresponding paleomagnetic reversal within seismic sequence 2 ("Intra-2" of Fig. 4). Coarse-grained oxidized channels ("redbeds") are marker horizons labeled 'rb". Thin palustrine limestones are labeled 'ls'. Gray box shows portion of section illustrated in photo D. (D) Outcrop expression of facies change at ~9.0 Ma in Rodeo 1 section. Persons in photos are ~1.9 m tall for scale.

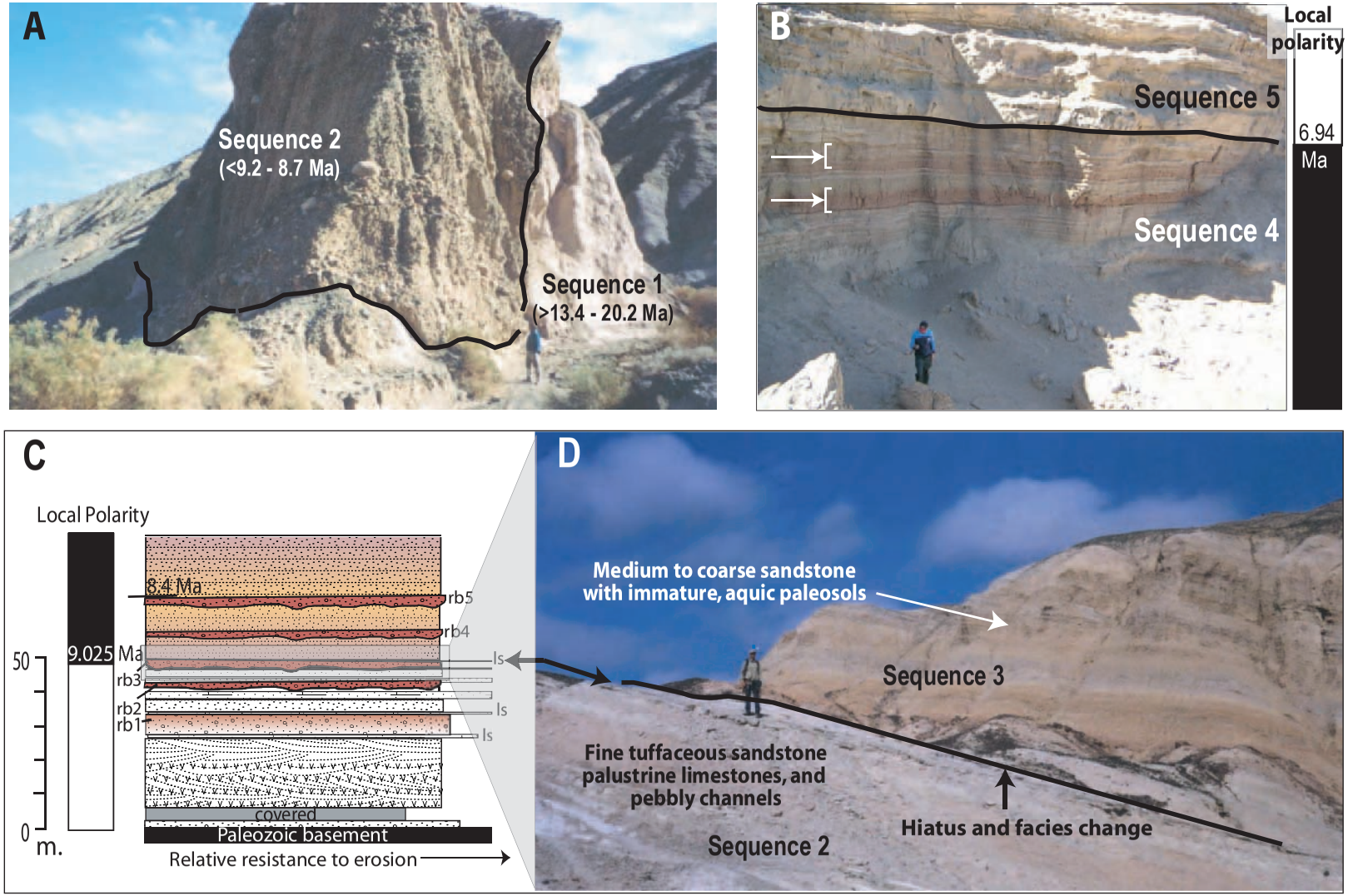
A
Sequence 2
(<9.2 - 8.7 Ma)
Sequence 1
(>13.4 - 20.2 Ma)
B
Local polarity
Sequence 5
Sequence 4
6.94
Ma
C
Local Polarity
8.4 Ma
9.025 Ma
rb5
rb4
rb3
rb2
rb1
ls
ls
ls
covered
Paleozoic basement
50
0
m.
Relative resistance to erosion
D
Medium to coarse sandstone
with immature, aquic paleosols
Sequence 3
Fine tuffaceous sandstone
palustrine limestones, and
pebbly channels
Sequence 2
Hiatus and facies change

are no recognized paleosols in sequence 1 or lowermost sequence 2 and thus little information about the nature of the environmental change across the >4 Ma SB hiatus, we do not discuss this feature further.

Sequences 2 through 7 all contain local paleosols. Because the sequence boundaries between all of these sequences are subtly expressed in outcrop, we rely heavily on their paleosols to reveal environmental changes through time, particularly those that may have accompanied sequence boundary formation. Macroscopic paleosol properties are listed in Appendix A, TableA.2.

The single seismic sequence boundary whose nature is clearly defined by surface exposures is the seismic sequence 4-5 boundary, at which there is a mature pedogenic interval followed by a regional facies change to channelized fluvial deposition (Fig. 3.5 B). In seismic data, the sequence 4-5 boundary is conformable in the great majority of the basin (with occasional truncation), but along the western basin margin (Fig. 3.2) the top of sequence 4 dips more steeply to the east than do reflectors in sequence 5, and sequence 5 onlaps the top of sequence 4. Given that onlap omits the lower half of seismic sequence 5 and in the basin center, S5's duration is ~370,000 years (Ré *et al.*, 2003), the hiatus between S4 and S5 is roughly 150,000-200,000 years in the western zone. In the basin center, within seismic sequence 4 (~7.7-6.9 Ma), fairly mature, commonly calcic paleosols are abundant. Two mature, orange (10R 5/3; 5YR 5/6), meter-thick calcic paleosols (Fig. 3.5 B) at the top of sequence 4 are easily traced for >10 km along strike, maintaining a similar degree of pedogenic development (e.g. horizonation, clay ped structure, nodules, coloration and distinctness of boundaries with surrounding nonpedogenic sediment; see Table 3.2). These are the most developmentally mature and recognizable paleosols of the Tertiary fill. The lithofacies and pedogenesis of the strata differ above and below these two principal paleosols. Below, compound calcic, oxidized paleosols are interbedded with

thin sheet sandstones and pebble-laden channels with <0.5 m erosional relief. In contrast, above the pair of orange paleosols, in sequence 5, overlying strata are predominantly composed of grouped trough-crossbedded sandstones (foreset dips 10°-25°), some exhibiting soft-sediment deformation features and generally lacking paleosols. The upper part of the sequence-bounding paleosol couplet is cross-cut by a broad channel that locally cuts out 0.5 to 1 m. Associated with the pair of orange paleosols that constitute the 4-5 sequence boundary is a 1.5 m thick bed of granite boulders, whose maximum boulder size approaches 70 cm. Although very discontinuous in outcrop expression, the boulder bed has been recognized in four distinct locations, always within 5 m above the sequence boundary paleosols.

Most of the remaining seismic sequence boundaries, when projected to outcrop, are subtly expressed, but several significant lithofacies changes are herein postulated to represent hiatal intervals (see also Chapter 2). An abrupt facies change from volcaniclastic fluvial deposits and interbedded thin carbonate beds to finer-grained and pedogenic, nonvolcanic sandstones above characterizes the 2-3 SB on both sides of the intrabasinal thrust belt (Figs. 3.1 and 3.5C and D). Upsection, the 3-4 SB is characterized by a 30 m thick interval containing at least 7 regionally correlated calcareous sandstone beds (10-30 cm thick). These carbonates are interpreted as palustrine (Esteban and Klappa, 1983; Platt and Wright, 1992; see Appendix F) and although seen infrequently in overlying strata, they are abundant only at the 2-3 and 3-4 SB.

C. ***Macroscopic Interpretations of Environmental Changes that Accompany Sequence Boundaries:***

Utilized in conjunction with accumulation rate information obtained from magnetostratigraphy (Ré *et al.*, 2003) and seismic interpretation, pedogenic facies and stark lithofacies changes assist greatly in describing basin-scale changes in

environment during deposition of sequences 2-7 (9 – 5.2 Ma). Pedogenic outcrops of seismic sequences 3 and 4 (8.7 – 6.9 Ma) together represent a "pedofacies megasequence" (Kraus, 1987) comprised of multiple compound pedo-sequences, each tens of meters thick. The trends of soil development and isotopic variability (see below) in the megasequence are more likely controlled by extrinsic forcing than microclimate, which affects individual soils on a shorter time scale (Kraus, 1987). Sequence 3 (8.7 - 7.7 Ma) paleosols are commonly aquic and lack Stage II or greater carbonate nodules. In contrast, paleosols of sequence 4 (7.7 – 6.9 Ma) are more commonly oxidized and calcic. As soil carbonates require a net water deficit for formation, it is postulated that for soils lacking calcic horizons (Argillisols and Inceptisols), it was proximity to near-surface groundwater (e.g. in internally-drained sub-basins or in positions adjacent to basin margins experiencing greater runoff) and/or fluvial channels that precluded significant carbonate accumulation. The presence of calcite nodules in conjunction with oxidized paleosols suggests soil-drying or falling ground-water levels during sequence 4 deposition (Kraus and Aslan, 1993). The simplest interpretation of these features is an increase in soil drainage through time, perhaps reflecting increasingly arid or seasonal climate for the sequence 4 interval relative to sequence 3, allowing oxidation and carbonate production (Miall, 1996; Retallack, 2001).

The especially mature paleosols at the 4-5 sequence boundary, consistent in thickness and maturity for 5-10 km distance along strike, reflect a period of unusual landscape stability even though measured sediment accumulation rates had increased upward in sequence 4 (Figure 3.6). Conditions appropriate for extensive floodplain pedogenesis during late sequence 4 deposition are compatible with the slow or null accumulation that one expects at a stratigraphic sequence boundary. However, magnetostratigraphic age constraints from the measured sections reveal that

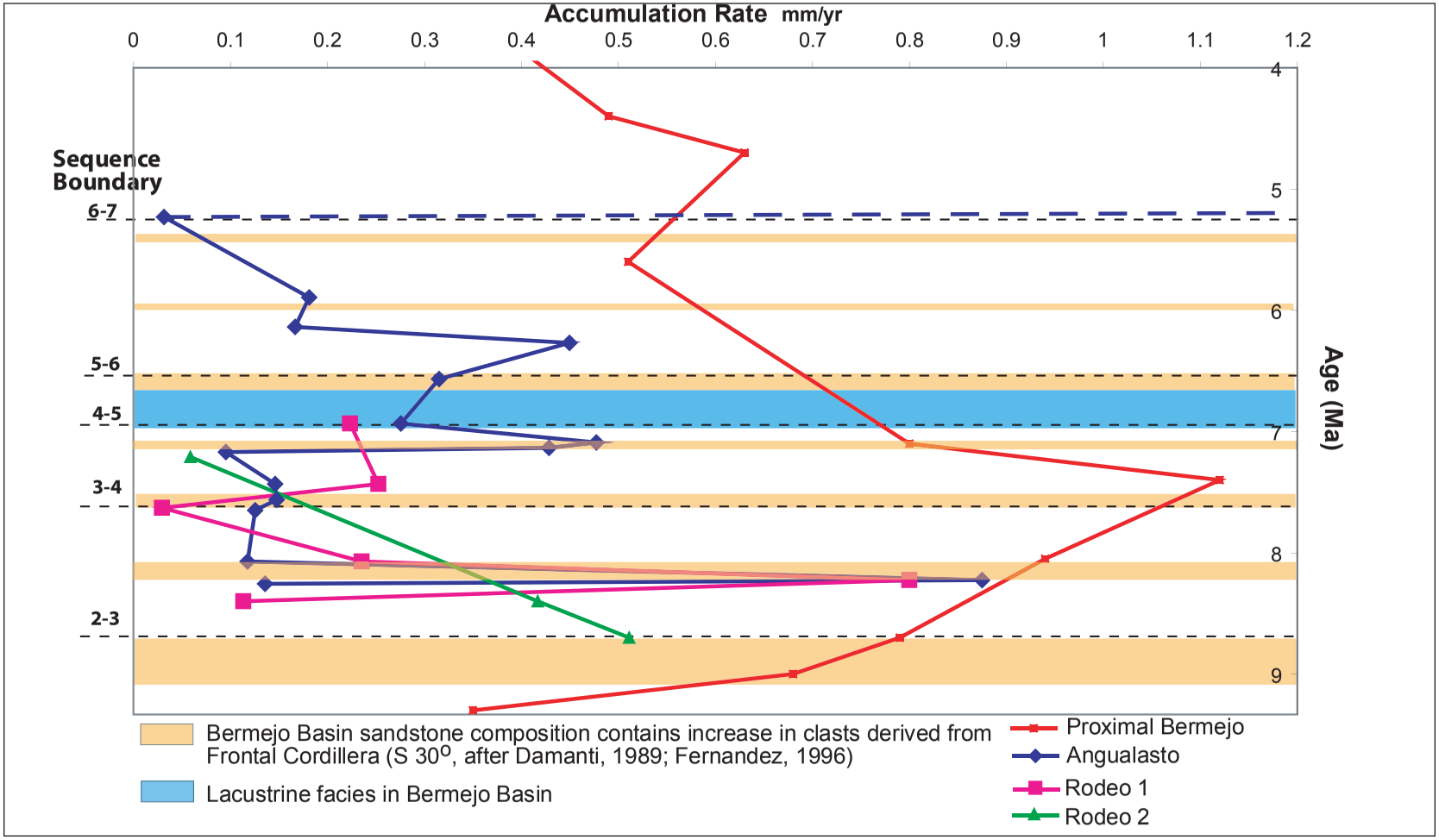

Figure 3.6: Accumulation rate histories and clast provenance interpretations for Iglesia Basin and western Bermejo Basin. Locations of Iglesia sections are shown in Figure 3.1. Accumulation rates are based on magnetostratigraphy of Jordan et al., (2001), Ré et al., (2003) and this study.

sedimentation rates were on the increase during sequence 4, beginning at 7.6 Ma in the Rodeo 1 section and 7.2 Ma in the Angualasto section 10 km to the north (see Fig. 3.1 and Figure 3.6). Furthermore, seismic volume estimates by Fernández (1996) reveal a 69% increase in accumulated volume/time (km^3/Ma) from sequence 4 to sequence 5. Based on the steeper inclination of the seismic sequence boundary 4-5 along the western basin margin relative to reflectors of sequence 5, we infer that the slope of the Frontal Cordillera headwater drainages increased across the sequence boundary in response to orogenic uplift. This uplift would have increased flow velocities, providing sufficient stream power to transport observed granite boulders to basin-center positions. Together, the increased depositional energy and higher rate of accumulation disturbed the stability of soil development, such that during sequence 5 (~6.9 – 6.5 Ma), sedimentation rate outpaced the rate of pedogenesis.

Isotopic, mineralogic, chemical and micromorphic analyses of paleosols

A. ***Materials and Methods:***

Samples were collected of pedogenic carbonates and clays as well as palustrine limestones. In all cases, samples were obtained from freshly exposed surfaces or minimally weathered outcrops. Wherever possible, pedogenic carbonates were sampled >30cm below the upper boundary of the corresponding paleosol to minimize the effect of atmospheric diffusion on $\delta^{13}C$ values (Cerling and Quade, 1993). Preference was given to Stage III carbonates (coalesced layers of nodules, after Machette, 1985) and five to ten individual nodules were collected from each Bk horizon. Stage I or II carbonates were sampled only if reactive to dilute HCl acid (e.g. audible fizzing with numerous bubbles, >5% carbonate, after Retallack, 1997). More pervasive calcretes (Stages IV and greater) were avoided, as the likelihood of post-pedogenic groundwater influence could not be discounted. Carbonate mineralogy was studied in representative thin sections that were stained with alizarin dye to facilitate

differentiation of calcite from other birefringent matrix minerals. Carbonate occurs chiefly as micritic matrix and ovoid, concentric aggregates set in clay groundmass. The nucleus of such concentrations is commonly dissolved or contains quartz grains. Diagenetic sparite is rare, occurring only as vug filling. The micritic calcite crystal form and lack of recrystallization textures support a pedogenic interpretation of the carbonate concentrations, a requisite condition to isotopic analysis and paleoclimate interpretations (e.g. Garzione *et al.*, 2006).

We report isotopic compositions of C and O as well as weight percent of inorganic carbon obtained from pedogenic carbonate nodules 9.0 – 4.7 Ma, summarized in Table 3.2. The stable isotopic composition of paleosol carbonates represents a "time averaged" signal of soil climate, due to overprinting or recrystallization during a prolonged period of formation (e.g. Pendall *et al.*, 1994). Additionally, it has been shown that isotopic heterogeneity of soil carbonates is a complex problem that persists even when nodules are microsampled (Deutz *et al.*, 2002). For our purpose, which is to characterize large spatial and temporal ranges of surface conditions by representing an average isotopic signal for a given paleosol horizon, the time-averaged signal is desirable rather than problematic. Nodules from each sample horizon were homogenized to a fine powder using a mortar and pestle. Isotopic analyses were chiefly conducted at the Cornell Stable Isotope Laboratory with a dual inlet Finnegan MAT Delta Plus mass spectrometer. Subsidiary analyses are from the Institute of Arctic and Alpine Research, University of Colorado and the University of Arizona Stable Isotope Laboratory. Results are given in delta notation relative to the Vienna Pee Dee Belemnite standard (V-PDB, where $\delta_{sample} = [(R_{sample} / R_{V\text{-}PDB})\text{-}1] \times 100$), with precision better than 0.1 per mil for both $\delta^{13}C$ and $\delta^{18}O$. Ages were assigned to each sample by linear interpolation between correlation points using

Table 3.2: Isotopic and weight percent inorganic carbon for Iglesia Basin pedogenic carbonates. Ages assigned by linear interpolation to magnetostratigraphy of Ré et al. (2003) and new radiometric data (see Appendix B). Gray boxes represent samples derived from same paleosol horizon or interval.

Sample	Age (Ma)	Section	$\delta^{13}C$	$\delta^{18}O$	%C
BR05-28	4.6	South Colanguil	-7.596	-6.990	2.10
BR05-29	4.7	South Colanguil	-2.591	-4.686	2.07
BR05-30	4.8	South Colanguil	-6.524	-7.182	2.36
BR04-17	5	Tudcum	-8.503	-8.083	1.03
BR05-33	5	South Colanguil	-8.571	-5.140	1.79
BR05-38	5.11	Angualasto	-9.123	-3.652	1.35
BR05-37	5.12	Angualasto	-6.792	-2.630	1.28
BR05-36	5.14	Angualasto	-6.788	-2.142	1.30
BR05-35	5.15	Angualasto	-6.482	-6.368	2.09
BR04-14	5.18	Angualasto	-6.992	-5.355	0.46
BR04-13	5.19	Angualasto	-4.421	-9.572	0.85
BR04-12	5.2	Angualasto	-2.345	-5.434	0.15
BR04-10	5.22	Angualasto	-7.603	-6.711	0.54
BR04-11	5.22	Angualasto	-8.006	-7.953	0.32
BR03-27	6	Las Flores	-5.515	-10.859	
BR03-33	6.12	Iglesias	-2.944	-6.024	0.51
BR03-32	6.13	Iglesias	-4.278	-7.290	0.52
BR03-29	6.17	Iglesias	-9.459	-9.242	
BR02-SOL5	6.45	Angualasto	-4.597	-7.685	
BR04-35	6.5	Rodeo 1	-13.235	-8.647	0.35
BR04-36	6.5	Rodeo 1	-11.280	-5.298	0.50
BRO3-39	6.5	Rodeo 1	-8.238	-4.662	
BR03-12	6.6	Angualasto	-4.425	-7.399	0.53
BR05-53	6.61	Cuesta del Viento	-4.196	-2.920	0.33
BR05-52	6.62	Cuesta del Viento	-7.916	-2.072	0.51
BR03-25	6.7	Channel	-5.149	-5.539	
BR03-24	6.85	Channel	-3.948	-8.541	
BR03-21	6.87	Channel	-4.408	-8.318	
BR03-22	6.87	Channel	-3.043	-7.761	
BR03-23	6.88	Channel	-4.680	-8.289	
BR05-50	6.89	Angualasto	-10.945	-2.717	0.73
BR04-4	6.9	Angualasto	-5.545	-8.129	0.54
BR05-49	6.9	Angualasto	-8.963	-1.653	0.42
BR05-40	6.92	Rodeo 1	-9.751	-3.571	2.15
BR04-30	6.93	Rodeo1	-7.330	-6.338	0.51
BR04-7	6.93	Angualasto	-6.323	-8.987	0.45
BR05-41	6.93	Rodeo 1	-9.570	-2.008	1.34
BR05-43	6.93	Angualasto	-3.168	-2.096	1.56
BR04-1	6.935	Angualasto	-6.688	-8.160	1.16
BR04-29	6.935	Rodeo 1	-8.231	-7.715	0.45
BR05-42	6.935	Angualasto	-3.207	-2.736	3.06
BR03-10	6.95	Angualasto	-6.824	-4.812	
BR04-3	6.95	Angualasto	-6.914	-7.515	1.07
BR03-9	6.96	Angualasto	-7.386	-6.190	
BR05-47	6.97	Angualasto	-8.006	-3.952	0.83
BR05-48	6.98	Angualasto	-9.739	-2.017	0.85
BR04-28	7	Rodeo 1	-8.023	-6.658	0.42
BR03-49	7.1	Rodeo 1	-8.631	-5.039	
BR03-49 duplicate	7.1	Rodeo 1	-8.594	-5.013	
BR04-54	7.2	South Angualasto	-6.319	-8.157	0.67
BR04-27	7.29	Rodeo 1	-9.142	-7.756	0.64
BR04-26	7.3	Rodeo 1	-8.590	-9.122	0.63
BR04-25	7.31	Rodeo 1	-10.206	-9.603	0.53
BR04-31	7.31	Rodeo 1	-8.987	-6.778	0.54
BR04-24	7.32	Rodeo 1	-8.172	-9.065	0.64
BR04-23	7.33	Rodeo 1	-8.465	-8.986	0.64
BR04-33	7.35	Rodeo 1	-8.271	-6.408	0.55
BR04-32	7.4	Rodeo 1	-9.352	-7.257	0.57
BR04-53	7.4	South Angualasto	-6.764	-8.630	0.57
BR04-52	7.45	South Angualasto	-8.453	-10.256	0.34
BR04-34	7.5	Rodeo 1	-8.373	-7.568	0.57
BR04-50	7.6	South Angualasto	-7.332	-9.211	0.98
BR04-51	7.6	South Angualasto	-9.424	-7.533	0.38
BR03-47	7.65	Rodeo 1	-9.303	-5.405	
22-6-2002 SOL4	7.8	Angualasto	-7.660	-4.750	
22-6-2002 SOL4 Duplicate	7.8	Angualasto	-7.710	-4.600	
BR03-3	7.8	Angualasto	-7.761	-6.030	
BR03-3 duplicate	7.8		-7.701	-6.016	
BR03-4	7.8	Angualasto	-7.908	-6.931	
BR03-45	7.96	Rodeo 1	-6.612	-9.410	0.54
BR03-2	8	Angualasto	-7.208	-5.906	
BR03-2 Duplicate	8	Angualasto	-7.098	-6.454	
BR03-19	8.19	South of Rodeo 2	-4.995	-2.378	
BR03-37	8.21	Rodeo 1	-6.296	-2.685	
BR02-SOL3	8.25	Angualasto	-5.872	-8.753	0.56
BR03-44	8.34	Rodeo 1	-6.428	-6.881	
BR04-41	8.35	Angualasto	-6.818	-8.704	0.74
BR04-20	8.4	Maliman	-6.956	-10.408	0.64
BR04-21	8.5	Maliman	-5.854	-7.998	0.69
BR03-17	8.58	Rodeo 2	-6.439	-7.753	
BR04-22	8.62	Rodeo 1	-7.627	-7.894	0.55
BR03-16	8.7	Rodeo 2	-5.942	-8.780	0.44
BR04-16	8.7	East of Rio Blanco	-5.500	-8.285	0.95
BR04-59	8.75	South of Rodeo 1	-5.877	-4.455	0.56
BR05-39	8.85	Rodeo 1	-3.117	-3.938	1.88
BR04-18	9.03	East of Rodeo 1	-8.043	-8.085	0.79
BR05-44	9.06	Rodeo 2	-6.165	-2.654	1.32
BR03-13	6.3 +/- 0.6	Cerro Blanco	-6.932	-9.096	

the magnetostratigraphic framework constructed by Ré *et al*. (2003), as well as additional radiometric dates (Appendix B).

Clay mineralogy of paleosols was also identified, although abundances of constituent clays are only semi-quantitative. Mineral separates were prepared by gravitational and centrifugal force settling following procedures of Moore and Reynolds (1994). Size accuracy of grain size classes was confirmed by SEM. Fine clay dispersions (<0.2 μm) were placed onto glass slides and oven-dried at 90°C for one hour immediately prior to X-Ray diffraction analysis. XRD analysis was performed at the Cornell Center for Materials Research with a Scintag Theta-Theta Diffractometer. Mineralogy was qualitatively assessed by interpreting diffractograms (after Chen, 1977; Moore and Reynolds, 1994; Bouchet *et al.*, 2000; Poppe *et al.*, 2001) and comparison with lab-run clay standards. When permissible by interpreted mineral assemblages and spectra, proportions of smectite, illite, kaolinite and chlorite were semi-quantitatively assessed by applying empirical factors, for comparative purposes rather than absolute values (Poppe *et al.*, 2001).

B. Isotopic data:

Stable isotopic values of pedogenic carbonates are a proxy for syndepositional climatic conditions. Below about 30 cm depth in the soil profile, the carbon isotopic composition of pedogenic carbonates primarily reflects fractionation by respiration of the dominant biomass (Mermut *et al.*, 2000). As different biomass fractions utilize water with differing efficiency, characterizing the paleopedologic ecosystem can help determine relative humidity of the local climate. C_3 plants (trees, cool-season grasses, and most shrubs) use more water than C_4 plants (e.g. summer-growing prairie and savannah grasses), which are better adapted to high light and water stressed conditions (Cerling and Quade, 1993). If only C_3 plants were present in the soil, resultant pedogenic carbonate $\delta^{13}C$ values should be -14‰ to -12‰ (versus PDB). Values

above -8‰ reflect a mixed biomass, and values of about +2‰ indicate the presence of pure C_4 ecosystems (Wang *et al.*, 1993; Kleinert and Strecker, 2001).

Oxygen isotopic ratios in pedogenic carbonates are controlled by the composition of soil water, which is related to climate for several reasons. In specific, meteoric water $\delta^{18}O$ values are strongly affected by temperature, evaporation, seasonality of precipitation, latitude, continentality and the contemporary ocean reservoir values of ^{18}O. But it is often difficult to determine which factor or factors are responsible for shifts in the isotopic signature (Grootes, 1993; Mack and Cole, 2005). These multiple climatic and location controls, as well as diagenesis, may also combine such that $\delta^{18}O$ values 'homogenize' and show minimal change in response to major climatic variation (Pendall *et al.*, 1994; Wang and Cerling, 1994; Liu *et al.*, 1996). Nevertheless, regardless of the cause(s), major changes in soil carbonate $\delta^{18}O$ still may reflect climatic variability, particularly when covariant with $\delta^{13}C$ values (Wang *et al*., 1993).

Here we present $\delta^{13}C$ and $\delta^{18}O$ analyses from 92 pedogenic carbonate samples spanning 9.0 – 4.6 Ma, representing a proxy record of basin climate during deposition of sequences 2 through 7 (Figures 3.7 and 3.8). Of particular interest is the variability in the isotopic signals across seismic sequence boundaries. Also of interest is whether the basin-scale record shows the influence of the perceived global-scale Late Miocene expansion of C_4 plants (attributed to greater aridity, seasonality of precipitation, and/or decreasing atmospheric CO_2), which has been recognized in other South American basins (Cerling *et al.*, 1997; Latorre *et al*, 1997; Kleinert and Strecker, 2001).

The isotopic values of homogenized bulk samples reveal that the variability among multiple samples at single stratigraphic horizons is less than the variability through time of the series of horizons (Figs 3.7 and 3.8). The range of values from all

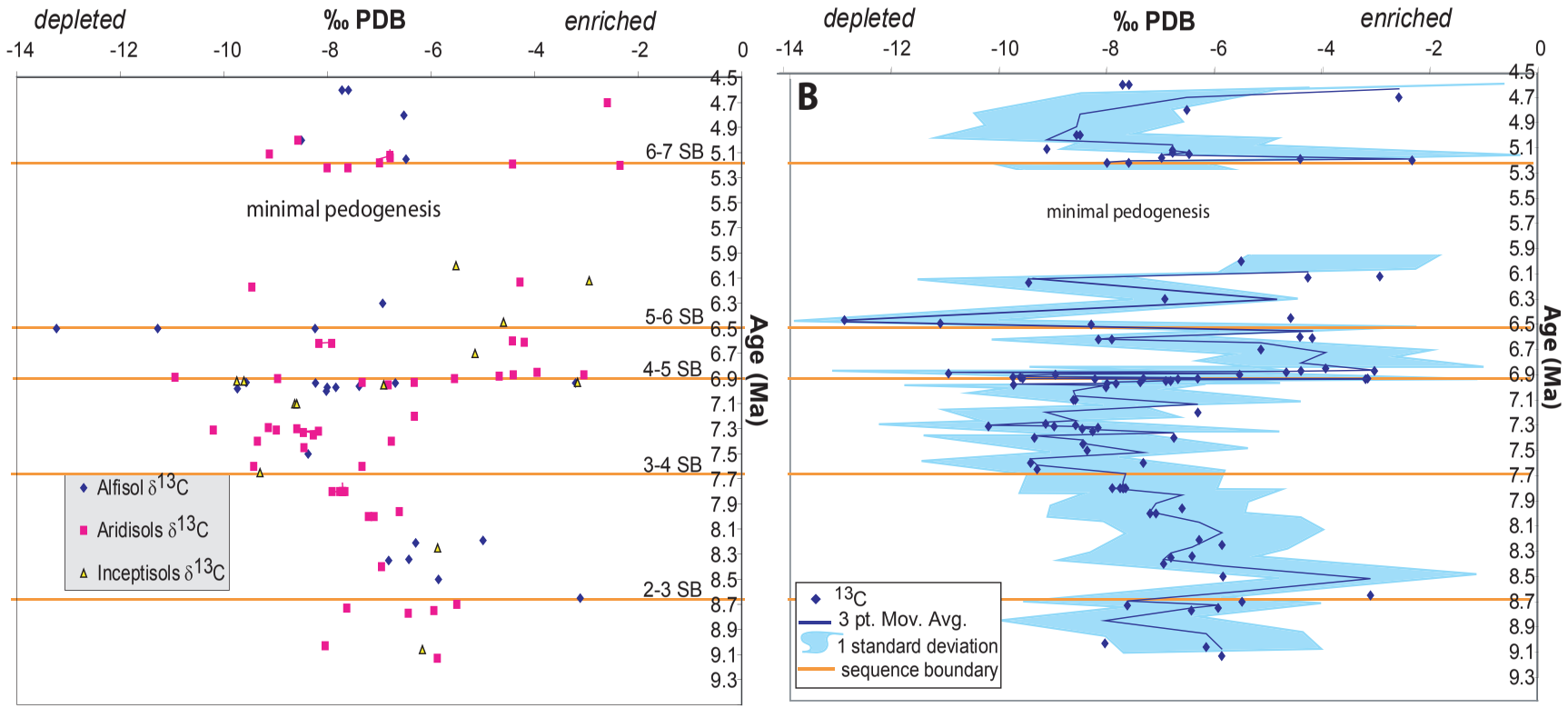

Figure 3.7: (A) Iglesia Basin δ13C time series from pedogenic carbonates, grouped by paleosol classification (n=92, s.d=2.05). (B) Time series of all paleosol types. Blue line represents 3 point moving average and blue envelope represents one standard deviation for all data.

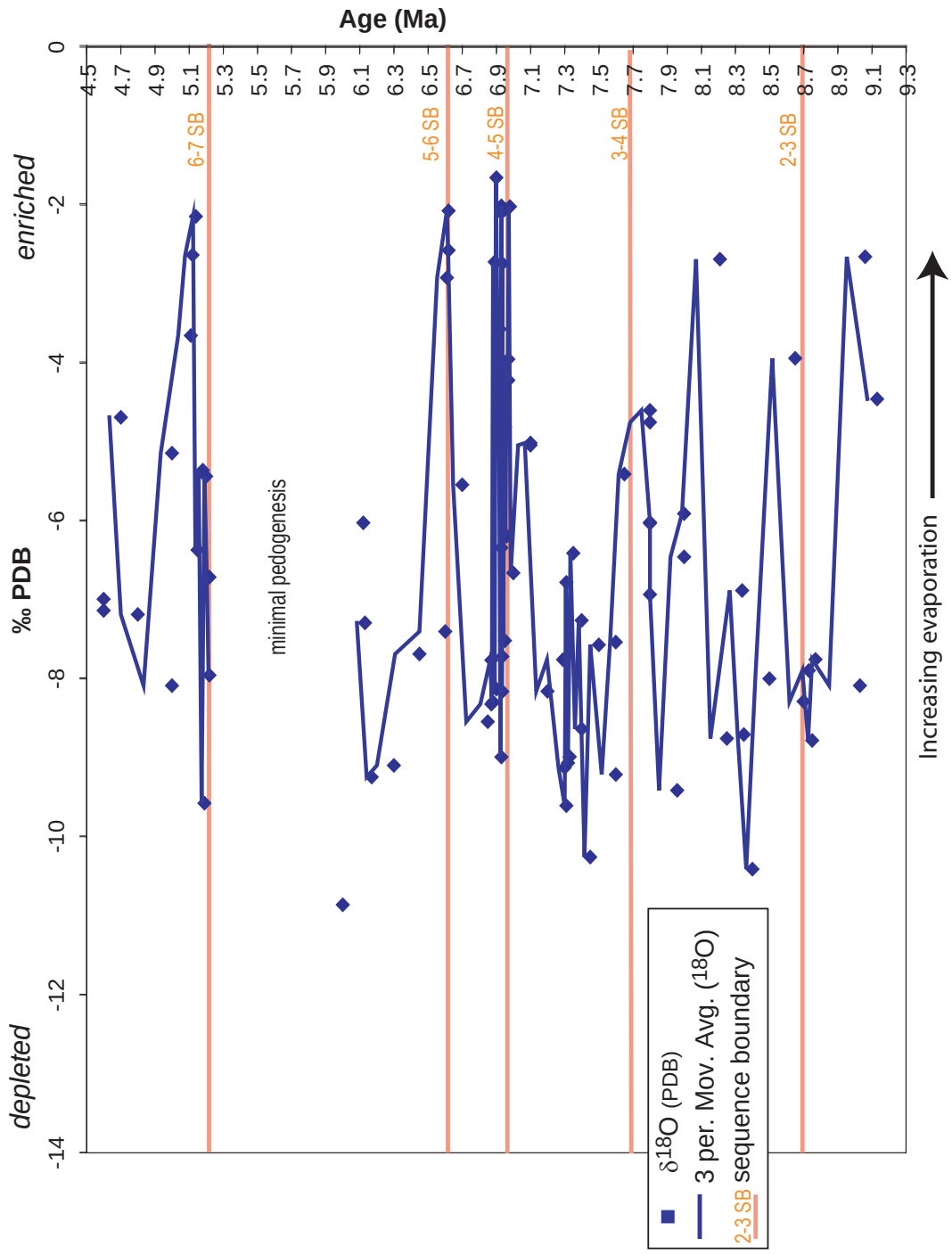

Figure 3.8: Iglesia Basin d 18O time series in relation to sequence boundaries (n=92, s.d=2.36).

samples between 9.0-4.6 Ma is 10.9 ‰ $\delta^{13}C$ and 9.2‰ $\delta^{18}O$ (the $\delta^{13}C$ range decreases to 8.6‰ when 4 diagenetically-altered samples are removed). Where single paleosols could be confidently physically correlated over several km distances, isotopic ranges of multiple samples from multiple sites are within 1.5‰ $\delta^{13}C$ and 2.6‰ $\delta^{18}O$. For similar compilations of pedogenic isotopes, internodular variations of 1-3‰ are common, (e.g. Latorre *et al.,* 1997; Deutz *et al.,* 2002; Blisniuk *et al.* 2005; Garzione *et al.,* 2006). From such comparisons, we conclude that natural microclimate variability introduced several per mil of variance at individual times, but that this variance is less that the magnitude of trends and abrupt shifts in the isotopic time series (i.e. on scale of a pedofacies megasequence) that reflect regionally significant climate changes.

C. ***Discussion of isotopic values:***

Several trends are evident from the $\delta^{13}C$ record (Fig. 3.7 A and B). First, there is a steady trend toward more depleted (negative) values during Sequence 3 and early Sequence 4 deposition (progressing from 8.7 Ma to 7.31 Ma, linear $r^2 = 0.595$, n=32), which accompanies the macroscopic aquic nature of these paleosols (significant redoximorphic mottling and/or banding, extensive illuviation and clay segregation in the profile). No overall trend but greater $\delta^{13}C$-signal variability are evident during late Sequence 4 (7.3 – 6.9 Ma), an interval with increasingly important carbonate in Aridisols, and which culminates in the extensive mature Aridisols at the 4-5 sequence boundary. At and shortly above the 4-5 boundary (~6.9 Ma), variability of the $\delta^{13}C$ signal is extreme, with variations between -10.9‰ and -3‰, in the same interval whose sedimentology and paleosols reflect the change from conditions well suited to soil formation to conditions of increased discharge and higher sediment accumulation rates. At ~6.5 Ma a set of Alfisols yield especially negative ^{13}C values (-8‰ to –13‰; see Table 3.2), in comparison to horizons with Aridisols and Inceptisols. These

samples were collected near a tight fold associated with a blind thrust fault (Figs. 3.1 and 3.2), where local hydrology and soil moisture may have been wetter due to local relief. Whether these Alfisol carbonate nodules represent regional climate or local hydrology is unclear. Continuing up-section, much of sequence 6 is devoid of paleosols, so the isotopic record is sparse. However, pedogenesis resumed in conjunction with the 6-7 sequence boundary (~5.2 Ma), and short periods of extremely high $\delta^{13}C$ values (-4 to -2‰) interrupt otherwise intermediate (-9 to -6‰) values.

Some of the Iglesia Basin sequence boundaries play distinctive roles in the stable isotope history. Progressive depletion of $\delta^{13}C$ values initiates at the Sequence 2-3 boundary. Note that two of the stratigraphic sequence boundaries, the 4-5 boundary (6.9 Ma) and the 6-7 boundary (5.2 Ma), are associated with paleosols that registered anomalously large swings in $\delta^{13}C$ values.

With respect to the global evolution of C_4 grasses, several interpretations of the Iglesia Basin carbon isotopic record are possible, depending on the threshold value utilized. It was originally proposed that C_4 biomass expanded globally at ~ 8 to 5 Ma in response to global climate change, perhaps triggered by a decrease in atmospheric CO_2 concentrations or increased aridity (e.g. Cerling *et al.,* 1997; Cerling *et al.,* 1998). But a cautionary note to biomass partitioning was raised by Fox and Koch (2003), who noted that, even for C_3 dominated ecosystems, arid conditions and low soil productivity result in less depleted $\delta^{13}C$ values than previously indicated. As a result, pedogenic $\delta^{13}C$ values of C_3 and C_4 communities may overlap, and mixed soil ecologies are difficult to differentiate. As a result of this complexity, various authors have proposed different thresholds as guides to interpretation. For example, Latorre *et al.,* (1997) suggested that -8‰ $\delta^{13}C$ is representative of the threshold between C_3 and C_4 plants in semi-arid environments of the Central Andes. If this value is accepted for Iglesia Basin, sampled paleosols seem to record a C_4–enriched biomass from 9.2 to

around 7.5 Ma (Figure 3.7), prior to Cerling *et al.'s* (1997) postulated global transformation. This is slightly earlier than similarly derived global and Argentine paleosol records that suggest C_4 plants expanded post 8 Ma (Cerling *et al.*, 1997; Latorre *et al*, 1997; Kleinert and Strecker, 2001). However, the less-depleted $\delta^{13}C$ values may represent aridity and low soil productivity of a dominantly C_3 ecosystem (Fox and Koch, 2003). An alternative isotopic spectrum was proposed by Wang *et al.* (1993) for $\delta^{13}C$ values between -12‰ (pure C_3) and +2‰ (pure C_4), such that -5‰ $\delta^{13}C$ represents a median value and values within the range represent mixed C_3 and C_4 biomass (Figure 3.9). This helps to distinguish the most arid intervals in a signal that may be significantly affected by microclimatic variations in humidity. Whether interpreted based on the Latorre *et al.* (1997) or Wang *et al.* (1993) criteria, the Iglesia Basin $\delta^{13}C$ signal is spiky and reveals short-lived arid intervals occurring ~6.9-6.7, 6.2, and 5.2 Ma. Aridification and/or warm-seasonal precipitation at 6.9, 6.2 and 5.2 Ma is interpreted from the isotopic proxies for biomass, corresponding well with two sequence boundaries (SB 4-5 and 6-7) as well as with increasing values of inorganic carbon elemental percentages and $\delta^{18}O$ (see below).

The $\delta^{18}O$ signal (Figure 3.8) varies complexly, likely due to the sensitivity of this isotopic system to multiple variables (e.g. Mack and Cole, 2005). Nevertheless, its trends are somewhat like those of the $\delta^{13}C$ values. For example, sequence boundaries 4-5 and 6-7 are intervals of extreme variability of the signal, exhibiting some of the most enriched values of the sample series, also true of the $\delta^{13}C$ signal. However, the $\delta^{18}O$ values reveal a trend that was not evident in the C isotopes: each seismic stratigraphic sequence experienced first increasingly depleted $\delta^{18}O$ and then increasingly enriched $\delta^{18}O$ values, interrupted by changes in trends at the sequence boundaries. Some published studies of paleosol carbonate stable isotopes reveal that $\delta^{13}C$ and $\delta\ ^{18}O$ vary with similar trends through time, likely due to decreasing

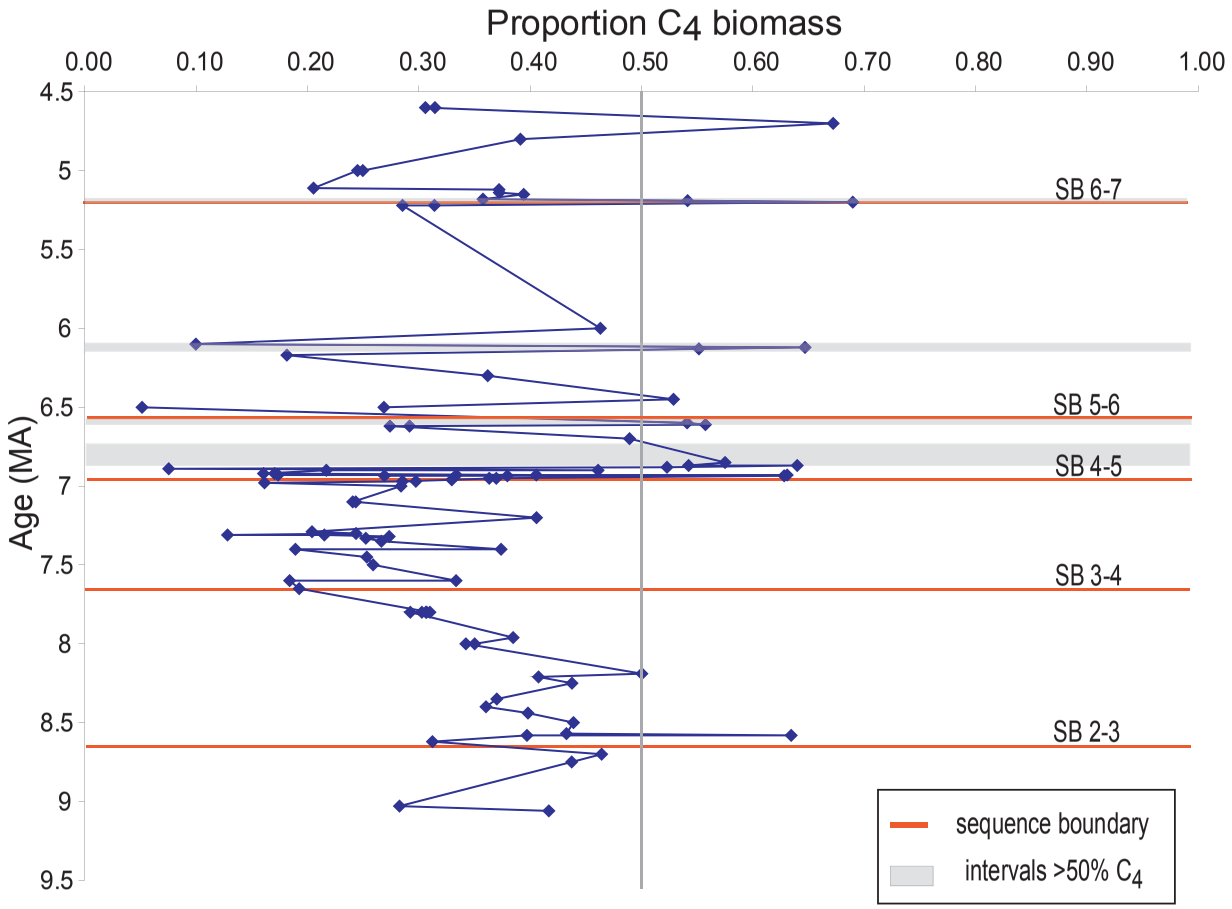

Figure 3.9: Interpretation of biomass contributions from pedogenic carbonate $\delta^{13}C$ record compared to threshold values for C4 plant appearance. Biomass partitioning uses threshold values of Wang et al., 1993. Grey horizontal areas denote times of dominantly C4 plants (where constrained by 2 or more datapoints).

temperatures which depletes both isotopic systems (Cerling and Quade, 1993; Latorre et al., 1997; Kleinert and Strecker, 2001). With only the exception of the upper half of sequence 3, similarity of $\delta^{13}C$ and $\delta^{18}O$ trends is also the case for the Iglesia basin paleosol carbonates; though the correlation is not linear, the most pronounced trends agree in both isotopic series

We anticipated that the $\delta^{18}O$ data would contain a long-term trend toward increased depletion (more negative values), because we expected that progressive topographic uplift of the Frontal Cordillera to the west might have enhanced Rayleigh distillation and orographic rain-out of ^{18}O prior to precipitation reaching the Iglesia valley. However, there is no overall trend in these data for the time interval 9.3-4.6 Ma. The lack of such a trend does not constitute proof that there was no increased orographic effect, however, because the isotopic fractionation of pedogenic calcite also depends on temperature. Deep ocean sediment $\delta^{18}O$ values (summarized by Zachos *et al.*, 2001) indicate isotopic enrichment in conjunction with global cooling and west Antarctic ice sheet expansion since ~7.5 Ma. It is plausible this Late Miocene-Early Pliocene global cooling might have counteracted a simple elevation-related depletion of meteoric $\delta^{18}O$ (Poage and Chamberlain, 2001).

Paleoclimate inferences can be drawn by comparing the Mio-Pliocene $\delta^{18}O$ record with modeled modern isotopic values. Because of the difficulty constraining the many variables affecting oxygen isotopic fractionation, Mack and Cole (2005) modeled modern pedogenic carbonate $\delta^{18}O$ as a function of (absolute) latitude, taking into account meteoric water composition, soil temperature (including South American MAT compiled by Hoffmann, 1975), and evaporation (Fig. 3.10). One significant finding of their study is that, regardless of seasonality of precipitation or latitude, pedogenic carbonate $\delta^{18}O$ values are increasingly enriched with increasing soil water evaporation. Relative enrichment of $\delta^{18}O$ values for Iglesia Basin paleosols occurs at

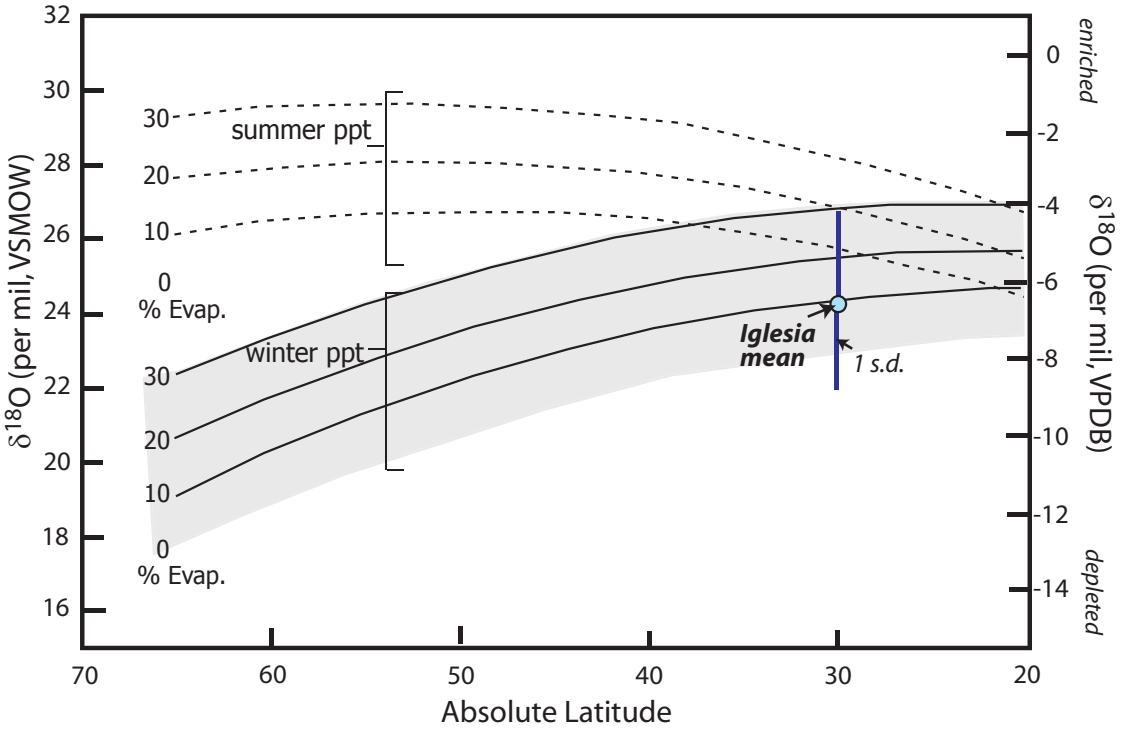

Figure 3.10: Comparison of predicted modern pedogenic carbonate $\delta^{18}O$ (solid and dashed lines) to measured values from Iglesia Basin Mio-Pliocene palesols. The predicted modern $\delta^{18}O$ values are functions of latitude, seasonality, ambient soil temperature and evaporation. It is assumed that site latitudes have not changed significantly since the Late Miocene. The modeled soil temperature includes South American climatology of Hoffmann (1975). Iglesia mean $\delta^{18}O_{SMOW}$= 24.35, S.D. =2.36 (n=92), where $\delta^{18}O_{SMOW} = (1.03092 * \delta^{18}O_{PDB}) + 30.92$. Redrafted from Mack and Cole, 2005, Fig. 1B.

the 3-4, 4-5, 5-6 and 6-7 sequence boundaries. This implies that periods of sequence boundary genesis may coincide with times of increased aridity. Since Argentina has maintained approximately the same latitude during the late Cenozoic (e.g. Hartley *et al.*, 1992), the Iglesia Basin $\delta^{18}O$ record can be compared readily with Mack and Cole (2005)'s geochemically modeled results to address seasonality of precipitation (Fig. 3.10). Our mean $\delta^{18}O$ value (24.26‰ versus standard mean ocean water, SMOW) plots within the modern winter-precipitation field experiencing 10% evaporative loss of soil water (a reasonable value for dry soils, e.g. Jones, 1992). Indeed, values plotting within the winter season precipitation field dominate the time series, save the most enriched periods (Fig. 3.8). But the range of data could indicate a mixture of both summer and winter precipitation, as occurs in the modern Iglesia climate regime (Fig. 3.3).

Of additional note are dramatic increases in percentage of soil inorganic carbon ($\%C_{inorganic}$), which occur ~8.6 Ma, 6.9 Ma, and post-5.2 Ma (Fig. 3.11). In general, the source of soil inorganic carbon is dust-borne material or detrital carbonate in the soil matrix (Lal and Kimble, 2000). The earliest increase in $\%C_{inorganic}$ slightly post-dates the 2-3 Sequence boundary (8.7 Ma), the next increase occurs at the 4-5 Sequence boundary (6.9 Ma) and the youngest $\%C_{inorganic}$ increase began with the 6-7 boundary (5.2 Ma). Increased $\%C_{inorganic}$ values persist post 5.2 Ma, as deposition was restricted to the western half of the Iglesia valley (See also Fig. 3.2). A modest, but discernible increase in carbon content at 7.6 Ma occurs just after t the 3-4 sequence boundary (7.7 Ma). We interpret the marked increases in soil inorganic carbon percentage as a record of increased delivery of dust-derived Ca and Mg ions during arid periods (e.g. Gile *et al*, 1966; Mayer *et al.*, 1988; Capo and Chadwick, 1999). This interpretation reinforces the $\delta^{13}C$-based interpretation of greater aridity at the 4-5 and 6-7 sequence boundaries.

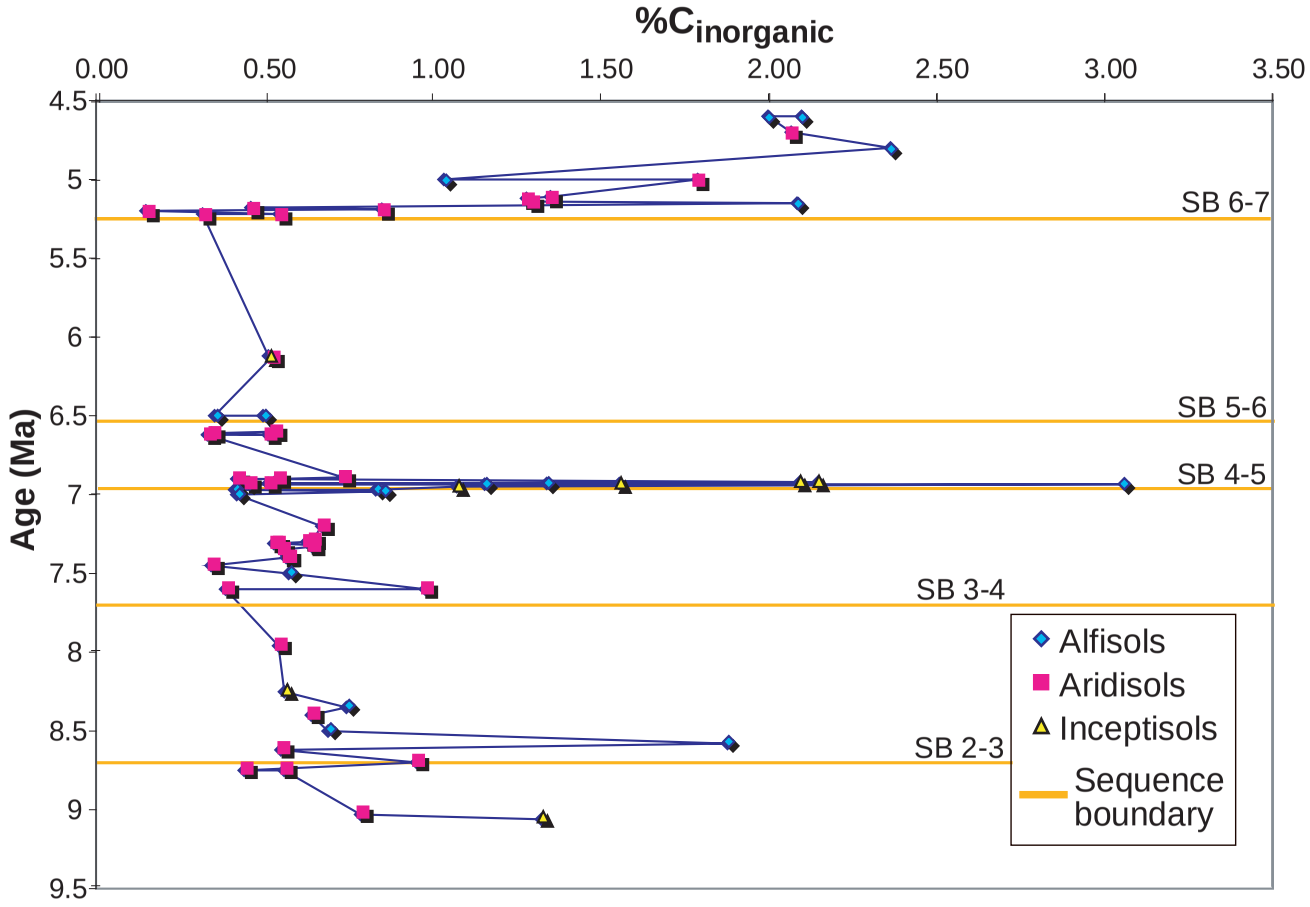

Figure 3.11: Soil inorganic carbon content of Mio-Pliocene Iglesia Basin paleosols in relation to sequence boundaries. Data points are identified by paleosol classification (see also Table 3.3).

D. ***Micromorphology and clay mineralogy:***

McCarthy and Plint (1998) noted that, while field observations may be sufficient to satisfactorily demarcate a nonmarine sequence boundary, careful micromorphic analysis of paleosols is needed to determine the genetic significance of the boundaries. Thin section description followed guidelines summarized by FitzPatrick (1993). Microfabrics are generally asepic (argillasepic, silasepic and calcisepic depending on percentage of clay, silt, or carbonate), with porphyroskelic to agglomeroplasmic texture. Calcite textures are micritic, with only minor sparitic vein accumulations or secondary replacement of mineral grains with sparite. Abundance of quartz (of grain size <2 microns) ranges from a few percent in floodplain soils, to 10-15% in soils collected from tuffaceous sandstone successions, and to as much as 20% in limestone samples. Quartz grains vary from subrounded to angular, and are occasionally highly fractured or exhibit zoned extinction. Feldspar grains are rare and generally of poor quality. Unaltered mica grains and opaque minerals comprise <1% of the sections.

Common micromorphic features include clay films (cutans), hematite mottles and concentrations, and pseudo-grains (grain-shaped patches of clay matrix and carbonate). Representative features are illustrated in Figure 3.12**.** Void spaces commonly retain partial outlines of crystal forms. The clay proportion ("matrix") is weakly oriented and represents >70% of the area of the thin-section of all sampled paleosols (Fig. 3.12 A, B, and C). Clay films are in general local features confined to grain margins (Fig. 3.12 B and C). Carbonate occurs either as micritic matrix or as ovoid, concentric aggregates set in clay groundmass (Fig. 3.12 A). The nucleus of such concentrations is commonly dissolved or contains quartz grains. Iron oxides are often confined to pore spaces and fractures, although less porous samples exhibit

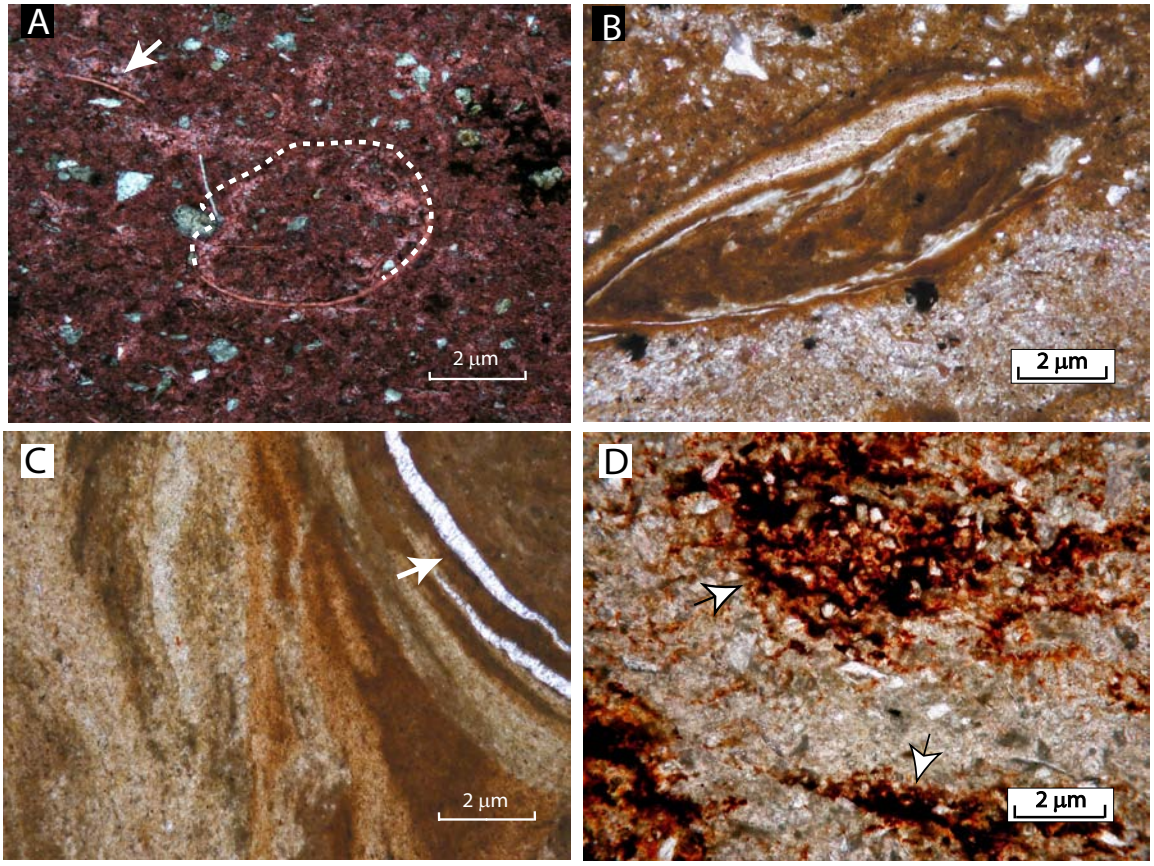

Figure 3.12: Photomicrographs of representative micromorphic features of Iglesia basin paleosols. All photos are magnified 10x under nonpolarized light.(A) Calciasepic fabric comprised largely of clay-sized minerals and micritic calcite (stained red with alizarin dye). Dotted line shows approximate outline of nodular calcite form, arrow demarcates needle-shaped calcite (sample 22-6-02 SOL 4, 7.8 Ma). (B) Ferric clay cutan formed by intraprofile translocation and redoposition of clay particles (sample22-6-02 SOL4-5SB, 6.94 Ma). (C) Argillasepic fabric formed by pedogenic disruption of sedimentary bedding. Arrow points to vein of sparite, likely due topost-pedogenic precipitation (sample BR03-12, 6.6 Ma). (D) Ferric mottles (with arrows) in soil formed in fluvially reworked tuffaceous sandstone (sample BR03-17, 7.5 Ma)

diffuse hematite mottling in the groundmass (Fig. 3.12 D). For soil profiles examined in multiple samples, clay mineral and hematite abundances increase with soil depth.

With the understanding that micromorphic analyses represent spatially limited samples of the complex soil microclimate, what generalities about paleoclimate can be drawn? First, the micromorphic features reveal that pedogenic alteration was an important process in the late Miocene to early Pliocene environment of the Iglesia basin. The distribution of clays reflects extensive illuviation. Both the replacement of framework grains by secondary minerals and the fact that pore boundaries in some cases mimic primary grains, imply rather extensive dissolution of siliciclastic minerals, especially feldspar, in the weathering environment. The clay film distribution reflects occasional wetting and drying cycles. The down-profile movement of clays and subsequent clay film ("cutan") formation requires sufficient water infiltration, but not so much as to preclude carbonate translocation. Hematite was abundant in soil matrices, either as discrete concentrations or in microstructural association with clay minerals. This was the case even in paleosols that were not readily classified as "oxidized" in outcrop, which may indicate near-surface early diagenetic alteration in a semi-arid climate (e.g. Schöner and Gaupp, 2005). Certainly many soils (particularly in Sequence 3 and along the eastern margin) experienced periodic waterlogging and reducing conditions, but the near ubiquity of hematite and common carbonate accumulations suggests net water deficit. Finally, the micritic crystal form of observed calcite supports the pedogenic origin of the mineral, rather than diagenetic formation.

Clay mineralogy was identified by X-Ray Diffraction for 30 pedogenic samples ranging in age from ~9.2 - 5 Ma collected from multiple localities in the basin (See Appendix C). Qualitative assessment of diffractograms indicates that smectite and illite are nearly ubiquitous in the paleosols. Four main associations are present: (a)

smectite, illite, and kaolinite (b) smectite, illite, and chlorite, (c) smectite with illite and (d) illite with chlorite. No distinct correlation between isotopic values and clay assemblage is evident. In general, these are common associations for clay-rich paleosols, and smectite has been shown to be the dominant clay mineral for soils receiving <500 mm/year of precipitation (Retallack, 2001). Primary diffractogram peaks for smectite were commonly broad, reflecting a range of mineral spacing due to interlayer hydration and/or variations in ionic charge (McBride, 1994). Chlorite and kaolinite are also common in Iglesia clays, occurring respectively in 9 and 12 of the diffractograms. Rarer minerals were palygorskite (an indicator of pedogenesis in climates with MAP<400 mm/yr, Singer, 1984), laumontite, and a mica-montmorillonite mixture. Calcite is the prominent carbonate mineral in two palustine samples studied (with associated illite), and calcite also appears in the <0.2 μm size fraction of seven of the paleosol samples.

Semi-quantitative assessment of smectite, illite, kaolinite and chlorite proportions (after Poppe *et al.,* 2001) provides information about weathering dynamics from source to soil (Figure 3.13 A). There are significant variations in the relative mineral percentages in the <0.2 μm fraction from their mean values of 57% smectite, 29% illite, 13% chlorite, and 1% kaolinite. Smectite and illite populations are correlated in an inverse manner (linear r^2 = 0.98, n=14). The largest relative shifts in smectite/illite percentages occur 8.0 – 6.7 Ma. Samples outside of this temporal range show more gradual trends in composition, which persist among samples collected from disparate parts of the basin. The proportions of smectite and chlorite are also inversely related (linear r^2=0.84, polynomial r^2=0.87, n=18), with smectite completely absent in samples from ~8.8 to 8.5 Ma wherein chlorite is most abundant (63-66%). However, since chlorite diffraction peaks (14.3-14.0 angstroms) occur within the range for air-dried smectite (15.4-13.2 angstroms); it is possible that mixed-layer

Figure 3.13: Semi-quantitative estimates of clay mineralogy and source area climatology for Iglesia Basin paleosols. (A) Estimates for paleosols containing smectite, illite, kaolinite, and chlorite, following method of Poppe et al., 2001. For samples 9.2 - 8.25 Ma, it is uncertain from X-ray diffractograms whether smectite is completely replaced by chlorite or the two coexist as a mixed-layer phase. (B) Plot of variations in the abundance of several clay mineralsderived from weathering of igneous rocks as a function of mean annual precipitation, MAP (after Barshad, 1966). Note coincidence of Iglesia Basin smectite and illite abundance data, which suggest MAP <350 mm/yr.

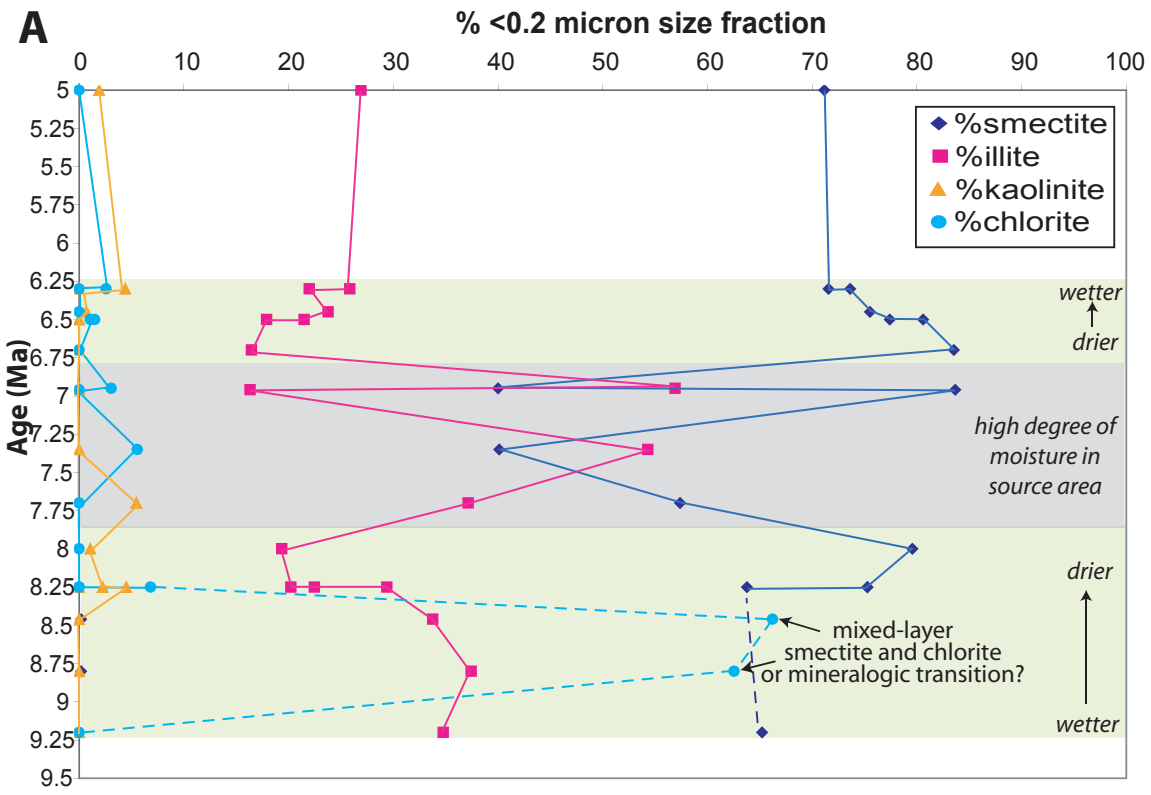
A
% <0.2 micron size fraction
0
10
20
30
40
50
60
70
80
90
100
Age (Ma)
5
5.25
5.5
5.75
6
6.25
6.5
6.75
7
7.25
7.5
7.75
8
8.25
8.5
8.75
9
9.25
9.5
%smectite
%illite
%kaolinite
%chlorite
wetter
drier
high degree of moisture in source area
drier
wetter
mixed-layer smectite and chlorite or mineralogic transition?

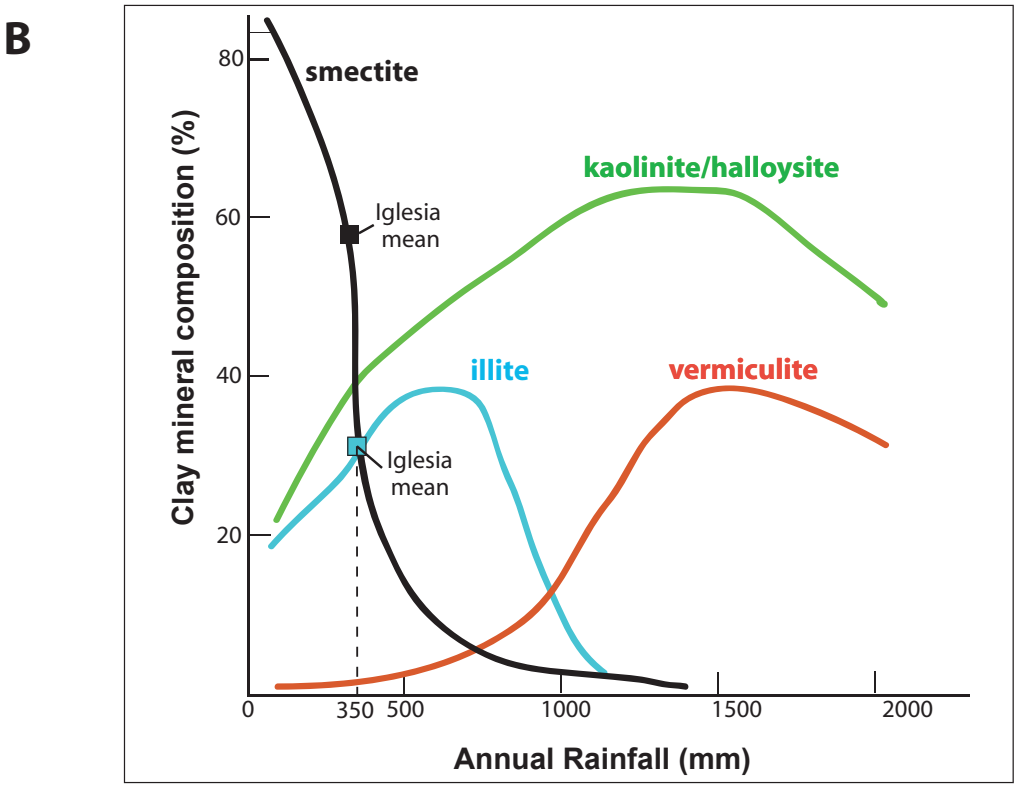
B
Clay mineral composition (%)
80
60
40
20
smectite
kaolinite/halloysite
illite
vermiculite
Iglesia mean
Iglesia mean
0
350
500
1000
1500
2000
Annual Rainfall (mm)

smectite/chlorite is present instead of chlorite. Also, the transition from smectite to chlorite is very common in shallow crustal very-low-grade metamorphism, and usually associated with geothermal fluid flow (Aguirre *et al.,* 2000; Robinson *et al.,* 2001). The higher concentrations of chlorite or mixed-phase smectite/chlorite occurring in Sequence 2 and early Sequence 3 paleosols probably reflects sediment provenance from the east, chlorite derived from Paleozoic marine siliciclastics, limestones and ophiolitic rocks (e.g. Net *et al.,* 2002).

If syndepositional paleoclimate was semi-arid within Iglesia Basin, as the $\delta^{13}C$ data suggest, it is likely that a significant portion of the paleosol clay minerals are detrital in origin, derived from weathering of igneous rocks in the Frontal Cordillera (and Precordillera for the older sequences) drainage basin. General trends of clay mineral proportions have been shown to reflect variable weathering and climatic conditions in the upland source area (Barshad, 1966; Fig 3.13 B). Smectite is the most abundant species in the most arid regimes, followed by illite and kaolinite as chief species in semi-arid environments, and finally kaolinite and vermiculite as precipitation increases (Barshad, 1966; McBride, 1994; Retallack, 2001). Using the semi-quantitative mean estimates from XRD analysis of Iglesia Basin paleosols, it is plausible that detrital clays formed in parts of the drainage basin experiencing ≤350 mm/yr rainfall (Figure 3.13 B). Also, because climatically-driven weathering results in an inverse relationship between smectite and illite abundance, the time series of clay composition shows: (a) increasing source area aridity 9.2 – 8.0 Ma; (b) marked variation in weathering and/or moisture post 8.0 Ma until ~6.9 Ma, and (c) relatively consistent weathering conditions 6.7 – 5.0 Ma. It is acknowledged that some of the variation may reflect true authigenic clay formation within complex soil microclimates due to chemical disequilibria in soil waters (McBride, 1994) and that this method provides only an estimate of mineral abundances. However, we argue that trends

evident among a range of sample localities represent an integrated record of headwater climatic variability, which impacted both the types of clays generated as well as their transport into the basin. The period of clay percentage variation (7.8 – 6.9 Ma; Sequence 4) corresponds with climatic variability revealed by the $\delta^{13}C$ data.

Discussion:

As a rule, it is difficult to decipher the separate tectonic and climatic influences on sedimentation and sequence boundary generation. Yet careful consideration of the timing and spatial scale of independently determined variations in tectonic activity and climate characteristics can help one to distinguish the relative importance of these extrinsic variables. These boundary and intrabasinal conditions are summarized in Figures 3.6 and 3.14.

There was tectonic input to creation of the basin, prior to and during accumulation of the sequences considered here. Considering tectonism at a very large spatial scale, the slope of the Nazca Plate 27°-33° S subducting under South America began to shallow by ~10 Ma and reached "flat-slab" geometry by ~8 Ma (Cahill and Isacks, 1992; Kay *et al.*, 1999; Kay and Mpodozis, 2002), with uncertain consequences in long-wavelength subsidence in the Iglesia Basin above. Regionally, the Frontal Cordillera had ≥2 km relief prior to 17 Ma and was actively uplifting ~15 Ma (Irogoyen, 1997; Riquelme, 2003) while the Precordillera fold and thrust belt propagation began ~20 Ma and deformation continued throughout the Tertiary, with times of slow or null shortening 18-16 Ma and 9 – 5.5 Ma (Jordan *et al.*, 1993; Irogoyen, 1997, see also Table 2.1). Also, as documented by Ruskin (2006; chapter 2) through seismic interpretation, relative relief between the Frontal Cordillera and Iglesia Basin increased during deposition of the Tertiary basin fill, most notably before deposition of Sequences 5, 6, 7 and afterward (see Fig. 3.14).

Concurrently, climate varied during Iglesia Basin sequence deposition. After the middle Miocene climatic optimum, rapid global cooling began ~14 Ma, coincident with expansion of the Antarctic Ice Sheet, and persisted as a general trend through the rest of the Neogene (Raymo and Ruddiman, 1992; Zachos *et al.*, 2001). The specific time interval of interest for comparison to Iglesia Basin sequences (9 to 4 Ma) was characterized by a first interval (~9- 6 Ma) during which global temperature fluctuated slowly between colder (9-8.2 Ma; 7.6 – 6 Ma) and warmer (8.2-7.6 Ma) conditions, followed by a period of persistent global cooling beginning around 6 Ma (Zachos *et al*., 2001). Latitudinal temperature gradients may have increased during the Late Tertiary concurrent with establishment of the West Antarctic ice sheet and changes in deep-ocean circulation, which would have strengthened Hadley Cell circulation (Flower and Kennett, 1994; Rind, 1998; Hartley, 2003). This might have resulted in greater aridity at the latitude of Iglesia Basin. Several South American paleoclimate records, however, exhibit contrasting regional humidity trends during the Miocene-Pliocene (e.g. Alonso *et al.*, in press). This lack of regional coherence illustrates that it is difficult to separate paleoclimate responses to global climate change from paleoclimate changes forced by uplift of the Andean topographic barrier (*e.g.* Blisniuk et al., 2005; Garzione *et al*., 2006). For example, in northwesternmost Argentina and southern Bolivia, a shift from arid climate to more humid conditions beginning ~10-7 Ma has been inferred from lithologic and paleontologic proxies (Hernández *et al.*, 1996; Stark and Anzótegui, 2001; Uba *et al.*, 2005). But for the Andean foreland near the Iglesia basin, generally cool and dry conditions from 19 – 2.5 Ma have been recognized from lithofacies characteristics (*e.g.* Jordan *et al.*, 2001). A departure from this trend may be expressed in the development of lacustrine facies in the Bermejo foreland east of Iglesia from ~7 Ma- 6.6 Ma (Fernandez, 1996; Fig. 3.6). Rather than a

climatic change, alternatively this lacustrine facies may reflect closure of the Bermejo drainage system due to tectonic variance (7.3 – 6.5 Ma; Jordan *et al.,* 2001).

Changing headwater hydrology can be inferred from clast provenance and accumulation rate data for the Bermejo and Iglesia Basins (Figure 3.6). Note that the Bermejo accumulation rates are generally much higher than those of Iglesia. Episodic drainage connectivity between the basins is inferred from increased proportions of volcanic detritus sourced in the Frontal Cordillera that reached the foreland depozone (Damanti, 1989; Jordan *et al*, 1993, 1996; Fernández, 1996). At least seven intervals (<0.4 M.y.) of increased proportions of Frontal Cordilleran (igneous) clasts reaching the Bermejo Basin occur between 9-5.5 Ma. Two of these peak intervals correspond with sequence boundaries (3-4 and 5-6), but the rest do not. Increased delivery of sediment from the headwaters to the foredeep could represent a change in hydrology, such that either more stream power was available for transfer of sediment or that basin connectivity was enhanced. The accumulation rate response, however, is more difficult to interpret, particularly from spatially limited column accumulation rate data. Increased discharge from the Frontal Cordillera might be expected to be stratigraphically represented by lesser accumulation rates in Iglesia (sedimentary bypass) and by higher rates of accumulation in the proximal Bermejo Basin. This is the case from ~8.2 – 7.3 Ma (Sequences 3 and 4), during which time Iglesia accumulation rates are diminished versus peak accumulation in Bermejo. Conversely, if accommodation space was sufficient in the Iglesia Basin, the wedgetop depozone could continue to accumulate sediment despite (point-source) drainage connectivity with the foredeep (e.g. Damanti, 1989). In two cases (~8.2 and 7.1 Ma), Iglesia column accumulation rates are high in correspondence with increased headwater clast delivery. Overall, we lack the spatial and temporal precision to quantify or fully characterize headwater discharge variability. Qualitatively, however, changing

sediment delivery from headwaters through the wedgetop depozone probably occurred repeatedly during sequence deposition and affected sediment supply to the basin central outcrops. The role of this discharge variability on sequence genesis is discussed below.

With the above global and regional conditions in mind, the summary of paleoclimatic proxies for Iglesia Basin (Fig. 3.14) suggests several strong associations between sequence genesis and extrinsic variability. At least four of the sequence boundaries (2-3, 4-5, 5-6 and 6-7) are strongly associated with relative aridity within the basin. Additionally, the 3-4 sequence boundary is related to a change from humid to more arid environments in overlying sediments. Finally, at least four sequence boundaries (4-5, 5-6, 6-7, and one or more boundaries post 5.2 Ma) show tectonic influence on their origin, based on rotation and geometries of seismic reflectors (Table 3.1; see also Chapter 2). In summary, then, we have shown climatic influence at five sequence boundaries, tectonic influence at three SB's and likely interacting extrinsic influence at three SB's. This is in contrast to previous interpretations of sequence genesis that discounted climate (e.g. Beer *et al.*, 1990) or tectonics (Milana, 1998), as factors in Iglesia Basin sequence genesis.

Quantifying the role of tectonically-induced versus climatically-induced sedimentation may be impossible to determine in an ancient alluvial setting. For example, precipitation-related (climatic) changes in discharge may affect sediment delivery rates depending on the direction and severity of the climate change (e.g. Langbein and Schumm, 1958; Dendy and Bolton, 1976), and also the seasonality of precipitation and associated vegetation cover (e.g. Weldje *et al.*, 1998; Hooke, 2000; Molnar, 2001). Similarly, tectonic uplift increases relief and slopes, thus generating sediment (via denudation) and aiding its transport (e.g. Bridge, 2003; Riebe *et al.*, 2004), the amount and longevity of sediment flux dependent on lithologic resistance to

Figure 3.14: Summary of climatic and tectonic variability during deposition of Iglesia Basin stratigraphic sequences 2 - 11. Superscripts: [1]After Jordan *et al*. (2001); [2]Trend line from Zachos *et al*. (2001).

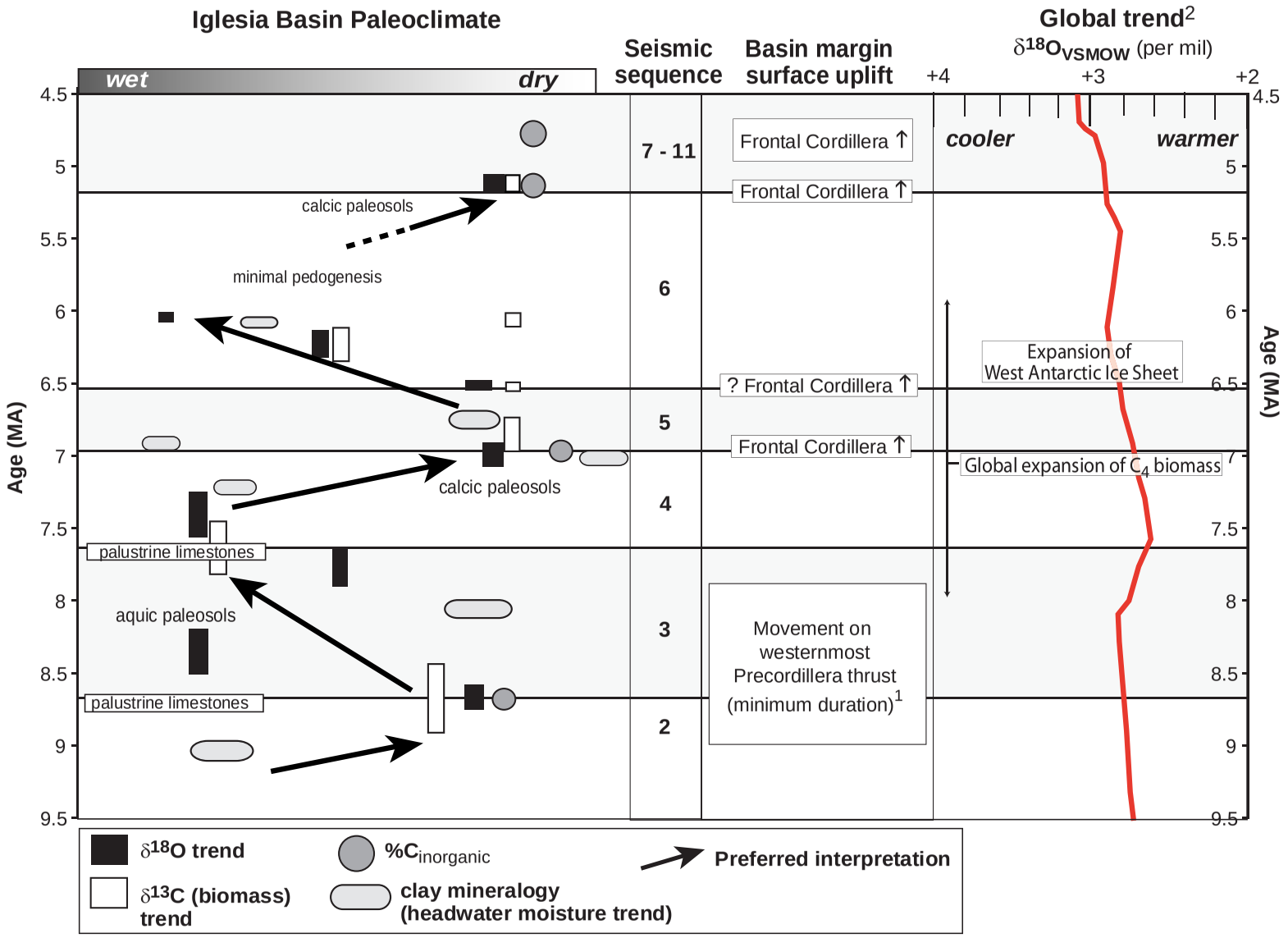
Iglesia Basin Paleoclimate
wet
dry
Seismic sequence
Basin margin surface uplift
Global trend2
δ18OVSMOW (per mil)
+4
+3
+2
cooler
warmer
Age (MA)
7 - 11
6
5
4
3
2
Frontal Cordillera ↑
Frontal Cordillera ↑
? Frontal Cordillera ↑
Frontal Cordillera ↑
Movement on westernmost Precordillera thrust (minimum duration)1
Expansion of West Antarctic Ice Sheet
Global expansion of C4 biomass
calcic paleosols
minimal pedogenesis
calcic paleosols
palustrine limestones
aquic paleosols
palustrine limestones
δ18O trend
δ13C (biomass) trend
%Cinorganic
clay mineralogy (headwater moisture trend)
Preferred interpretation

erosion and configuration of the drainage area (Schumm, 1993; Tucker and Slingerland, 1996). Few of these factors or their likely feedbacks have been accurately constrained (in time or magnitude) in the geologic past without implicit assumptions (e.g. Hooke, 2000; Riebe *et al.,* 2004), hence the continued need for numeric and kinematic models which can control or vary certain parameters in scaled, realistic ways (e.g. Johnson and Beaumont, 1995; Milana and Tietze, 2002; Hickson, 2005). These and many other scaled models reveal the range of natural variation that precludes simple linear relationships between the variables and stratigraphic architecture.

Acknowledging the above limitations, we can still intuit how climatic and tectonic variability (or both) may have affected sediment delivery to the Iglesia basin. For example, this study indicates certain sequence boundaries formed during periods of enhanced aridity (2-3, 4-5, 6-7; Fig. 3.14). Arid conditions in the basin need not require low discharge from the headwaters, however; Weissmann *et al.* (2002) showed that alluvial sequence boundaries marked by proximal incision and distal hiatus/paleosols occur when sediment: water ratios are low (e.g. high discharge) following a glacial episode. Several seismic sequence boundaries correspond with basin margin surface uplift (4-5, 5-6, 6-7; Table 3.1). Cooler global temperatures during the late Tertiary (e.g. Zachos *et al.,* 2001) and uplift of the Frontal Cordillera would have promoted periodic mountain glaciations, contributing to hydrologic variability and sediment delivery fluctuations. We can therefore postulate that, in cases where marginal uplift and climatic aridity are synchronous (boundaries 4-5, 5-6 and 6-7), rotation of headwater drainages probably enhanced marginal incision via increased slope and stream power, but far distal positions were correspondingly sediment-starved, creating the hiatal intervals recognized in seismic and outcrop.

As a means of assessing this interpretation of sequence boundary formation, we consider the individual and combined effects of climatic and tectonic variation on sediment delivery. Based on the climatic trends interpreted from this study (Fig. 3.14), and assuming that humidity changes represent departures from semiaridity, we apply the simple relationships between mean annual precipitation and sediment yield measured by Langbein and Schumm (1958) and Dendy and Bolton (1976). Semiarid climate (MAP of 300-500 mm/yr) maximizes sediment yield. More humid climates have less sediment yield because of greater vegetative cover, whereas arid climates deliver less sediment because of diminished runoff (Bridge, 2003). For periods of marginal uplift (Fig. 3.14), we assume that at the onset of uplift, proximal incision occurs, followed by denudation during uplift and a slow waning of sediment delivery between uplift events (e.g. Ahnert, 1970; Schumm, 1993; Riebe *et al.*, 2004). The sediment delivery trends are predicted for climate and tectonism separately and then summed as a qualitative "net sedimentation flux" (Figure 3.15). Treating climate and tectonism as independent is probably not realistic, and each variable's role on sediment delivery is simplified (e.g. Hooke, 2000), but this provides a point of departure for considering the likely feedback between marginal uplift and climatic shifts on nonmarine stratigraphic architecture. These simple predictions can be compared with measured rates of sediment accumulation from the Angualasto and Rodeo stratigraphic sections, and several intervals of predicted and measured net sedimentation do correspond.

Conclusions:

As a result of integrated fieldwork, seismic interpretation and geochemical analysis of paleosols, we show that climate was a significant contributor to subdivision of the nonmarine Iglesia Basin into stratigraphic sequences. This study demonstrates first that paleoclimate signal can be recognized in nonmarine strata and at sequence

Figure 3.15: Predicted sediment delivery response to variations in climate and marginal surface uplift inferred from Iglesia Basin strata. These trends from climate and tectonic effects are summed to predict a “net sedimentation” state which can be compared to sequence boundaries and measured rates of sediment accumulation from the Angualasto and Rodeo 1 sections.

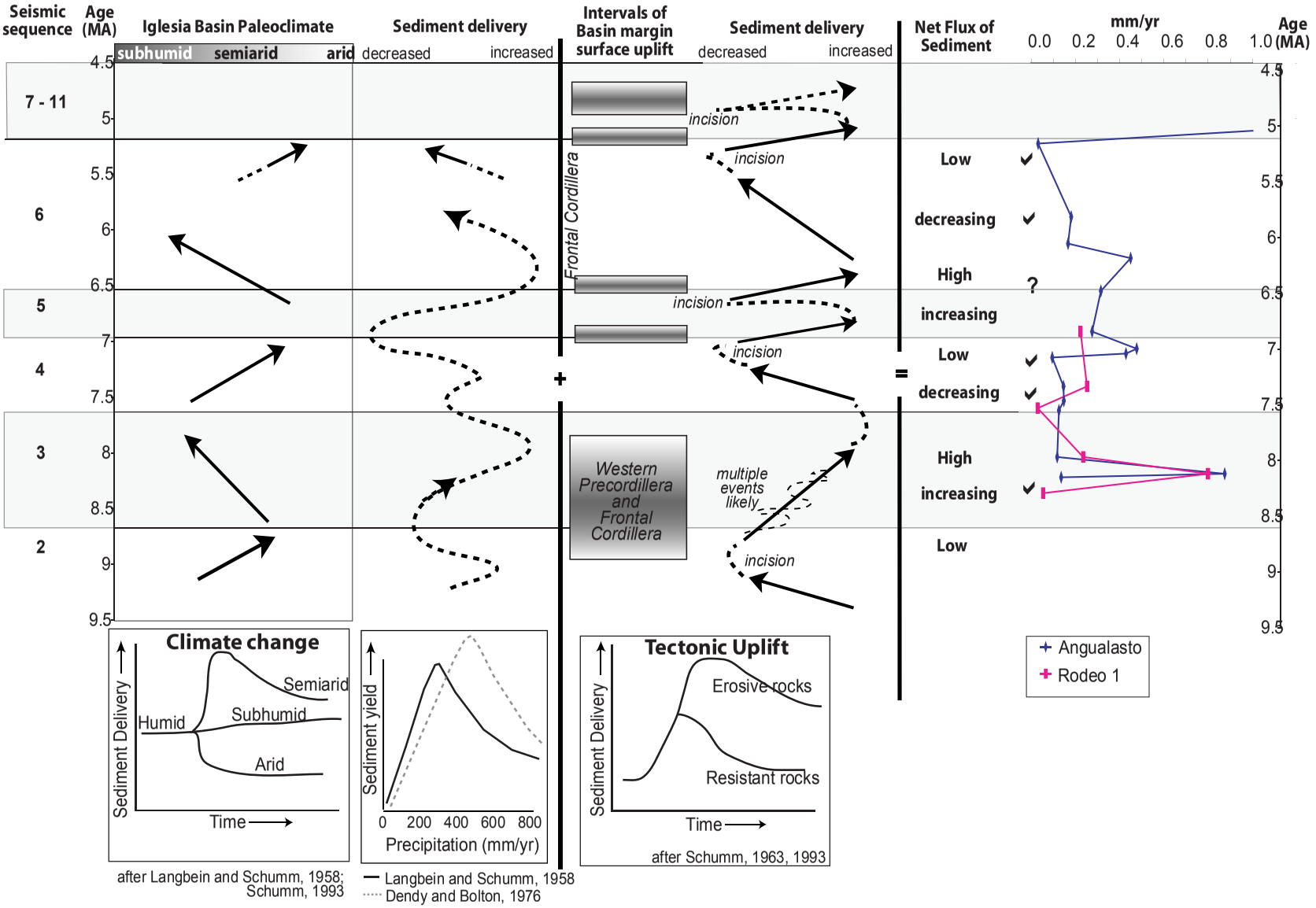
Seismic sequence
Age (MA)
Iglesia Basin Paleoclimate
subhumid
semiarid
arid
Sediment delivery
decreased
increased
Intervals of Basin margin surface uplift
Sediment delivery
decreased
increased
Net Flux of Sediment
mm/yr
0.0 0.2 0.4 0.6 0.8 1.0
Age (MA)
7 - 11
6
5
4
3
2
4.5
5
5.5
6
6.5
7
7.5
8
8.5
9
9.5
Frontal Cordillera
incision
incision
incision
incision
Western Precordillera and Frontal Cordillera
multiple events likely
incision
+
=
Low
decreasing
High
increasing
Low
decreasing
High
increasing
Low
?
Angualasto
Rodeo 1
Climate change
Sediment Delivery
Humid
Semiarid
Subhumid
Arid
Time
after Langbein and Schumm, 1958; Schumm, 1993
Sediment yield
0 200 400 600 800
Precipitation (mm/yr)
Langbein and Schumm, 1958
Dendy and Bolton, 1976
Tectonic Uplift
Sediment Delivery
Erosive rocks
Resistant rocks
Time
after Schumm, 1963, 1993

boundaries even within the active tectonic setting of the Central Andes and Precordillera fold-thrust belt. Vertical lithofacies transitions that correspond to sedimentary hiatuses and seismic sequence boundaries which are regionally continuous are shown to be characterized by varying degrees of pedogenesis which record evidence of paleoclimate fluctuations. The basin climate was generally semi-arid in the Late Miocene and Pliocene, punctuated by times of particularly pronounced increased aridity at ~9 Ma, 6.9 Ma and 5.2 Ma. From this result, we propose that a combination of tectonic uplift and climate variability in the Frontal Cordillera resulted in marginal incision and concurrent distal sediment starvation, which generated sequence geometries observed in seismic profiles as well as the associated lithologic features recognized in outcrop. Finally, stable isotopic and geochemical analyses support the expansion of C_4 biomass to northwestern Argentina by ~9 Ma, earlier than previously recognized, and C_4 dominance by 6.9 Ma.

Acknowledgements:

Funding for fieldwork and analyses was provided by American Chemical Society Petroleum Research Fund grant 39557-AC8 to T.E. Jordan. Additional support provided by AAPG Grants-in-Aid and a GSA graduate reseach grant to B. Ruskin. Rodrigo Morilla assisted greatly during field campaigns in 2003-2005. Lindsey Trachtenberg prepared clay separates, and Maura Weathers, William Bassett and Gregory Hoke facilitated XRD analyses and interpretation. Correspondence with Louis Derry and Greg Mack aided geochemical interpretations. Thanks also to Bruce Vaughn (INSTAAR Univ. of Colorado), Julie Cole (Univ. of Arizona) and Arthur Kasson (COIL, Cornell University) for coordinating stable isotopic analyses. Terry Spell (UNLV) provided labwork and consultation concerning radiometric analyses. Critical reviews by Andres Aslan, Michael Blum and Brian Willis greatly improved the quality and focus of this manuscript.

References:

Ahnert, F., 1970, Functional relationships between denudation, relief, and uplift in large mid-latitude drainage basins: American Journal of Science, Vol. 268, p. 243-263.

Aitken, J.F., and Flint, S.S., 1996, Variable expression of interfluvial sequence boundaries in the Breathitt Group (Pennsylvanian), eastern Kentucky, USA, *in* Howell, J.A., and Aitken, J.F. (eds), High Resolution Sequence Stratigraphy: Innovations and Applications: Geological Society Special Publication No. 104, p. 193-206.

Allmendinger, R.W., Figueroa, D., Snyder, D., Beer, J., Mpodozis, C., and Isacks, B.L., 1990, Foreland shortening and crustal balancing in the Andes at 30ºS latitude: Tectonics, v.9, p. 789-809.

Alonso, R., Carrapa, B., Coutand, I., Haschke, M., Hilley, G., Schoenbohm, L., Sobel, E.R., Strecker, M.R., Trauth, M.H., and Villanueva, A., 2006, Tectonics, climate, and landscape evolution of the Southern Central Andes: The Argentine Puna Plateau and adjacent regions between 22 and 28° S lat: *in review*

Ambrizzi, T., de Souza, E.B., and Pulwarty, R.S., 2005, The Hadley and Walker regional circulations and associated ENSO impacts on South American seasonal rainfall *in* Diaz, H.F., and Bradley, R.S., eds., The Hadley Circulation: Present, Past and Future, Kluwer Academic Publishers, p. 203-235.

Anderson, T.F, and Arthur, M.A., 1983, Stable isotopes of oxygen and carbon and their application to sedimentologic and paleoenvironmental problems, *in* Arthur, M.A., Anderson, T.F., Kaplan, I.R., Veizer, J. and Land, L.S., eds., Stable Isotopes in Sedimentary Geology, SEPM Short Course, No.10, Dallas.

Barshad, I., 1966, The effect of variation in precipitation on the nature of clay mineral formation in soils from acid and basic igneous rocks: Proc. Int. Clay Conf., 1:167-173.

Baudino, O.M., Suero, E.A., Augusto. M, Gimenez, M.E., and Flores, N., 2003, Monitoring organochlorine pesticides in surface and ground water in San Juan Argentina: Journal of the Chilean Chemical Society, Vol. 48, p.7-12. ISSN 0717-9707

Beer, J.A., Allmendinger, R.W., Figueroa, D.E., and Jordan, T.E. 1990, Seismic stratigraphy of a non-marine piggyback basin, Central Andes: American Association of Petroleum Geologists Bulletin, v.74, p.1183-1202.

Birkeland, P. W., 1999, Soils and Geomorphology, 3rd Edition, Oxford University Press, 432 pp.

Blisniuk, P.M., Stern, L.A., Chamberlain, C.P., Idleman, B., and Zeitler, P.K., 2005, Climatic and ecologic changes during Miocene surface uplift in the Southern Patagonian Andes: Earth and Planetary Science Letters, 230, p. 125-142.

Blum, M.D., 1993, Genesis and architecture of incised valley fill sequences: a Late Quaternary example from the Colorado River, Gulf Coastal plain of Texas: *in* Weimer, P. and Posamentier, H.W., eds., Siliciclastic sequence stratigraphy: Recent developments and applications, AAPM Memoir 58, p. 259-283.

Bouchet, A., Meunier, A., and Sardina, P, Clay Minerals: Crystal structure X-ray diffraction identification, Bull. Centre Rech. Elf Exploration Production, Memoir 23, 136 p.

Bown, T.M., and Kraus, M.K., 1987, Integration of channel and floodplain suites in aggrading fluvial systems. I: Developmental sequence and lateral relations of lower Eocene alluvial paleosols, Willwood Formation, Bighorn Basin, Wyoming: Journal of Sedimentary Petrology 57, p. 587-601.

Bown, T.M., and Kraus, M.J., 1993, Time-stratigraphic reconstruction and integration of paleopedologic, sedimentologic, and biotic events (Willwood Formation, Lower Eocene, Northwest Wyoming, USA): Palaios, Vol. 8, p. 68-80.

Bridge, J.S., 2003, River and Floodplains: Forms, Processes, and Sedimentary Record: Blackwell Publishing Ltd., 491 p.

Cahill, T., and Isacks, B.L., 1992, Seismicity and shape of the subducting Nazca Plate: Journal of Geophysical Research, Vol. 97, p. 17503-17529.

Cardozo, N. and Jordan, T. 2001, Causes of spatially variable tectonic subsidence in the Miocene Bermejo Foreland Basin, Argentina: Basin Research, v.13, p. 335-357.

Capo, R.C. and Chadwick, O.A., 1999, Sources of strontium and calcium in desert soil and calcrete, Earth and Planetary Science Letters, v. 170, p. 61-72.

Cecil, C.B., 1990, Paleoclimate controls on stratigraphic repetition in chemical and siliciclastic rocks: Geology, Vol. 18, p.533-536

Cerling, T. E., and Quade, J., 1993, Stable carbon and oxygen isotopes in soil carbonates: *in* Stuart, P.K., Lohmann, K.C., McKenzie, J., and Savin, S., eds., Climate Change in Continental Isotopic Records, American Geophysical Union, Geophysical Monograph 78, 374 pp.

Cerling, T.E., Harris, J.M., MacFadden, B.J., Leakey, M.G., Quade, J., Eisenmann, V., and Ehleringer. J.R., 1997, Global vegetation change through the Miocene/Pliocene boundary: *Nature*, 389, p. 153-158.

Cerling, T.E., Ehleringer, J.R., and Harris, J.M., 1998, Carbon dioxide starvation, the development of C_4 ecosystems, and mammalian evolution: Phil. Trans. R. Soc. London B. 353: 159-171.

Chen, P-Y, 1977, Table of key lines in X-ray powder diffraction patterns of minerals in clays and associated rocks: Indiana Geological Survey, 67 p.

Chivas, A.R, Cali, J. A., Chapman, A., Shelley, J. M.G., and De Dekker, P., 1993, Coupled stable-isotope and trace-element measurements of carbonates as

paleoclimatic indicators: *in* Stuart, P.K., Lohmann, K.C., McKenzie, J., and Savin, S., eds., Climate Change in Continental Isotopic Records, American Geophysical Union, Geophysical Monograph 78, 374 pp.

Cook, K.H., 2004, Hadley circulation dynamics: seasonality and the role of continents: *in* Diaz, H.F. and Bradley, R.S., eds., The Hadley Circulation: Present, Past and Future Advances in global Change Research Vol. 21, Kluwer Academic Publishers, p. 61-84.

Dalrymple, M., Prosser, J., and Williams, B., 1998, A dynamic systems approach to the regional controls on deposition and architecture of alluvial sequences, illustrated in the Statfjord Formation (United Kingdom, Norther North Sea) *in* Shanley, K.M., and McCabe, P.W., eds., Relative roles of eustasy, climate and tectonism in continental rocks: SEPM Special Publication No. 59, p. 65-81.

Damanti, J., 1989, Evolution of the Bermejo foreland basin; provenance, drainage development and diagenesis, Ph.D. dissertation, Cornell University, Ithaca, NY, 191 p.

DeCelles, P.G. and Giles, K.A., 1996, Foreland basin systems: Basin Research, v.8, p. 105-123.

Dendy, F.E. and Bolton, G.C., 1976, Sediment yield-runoff-drainage area relationships in the United States: Journal of Soil and Water Conservation, Vol. 32, p. 264-266.

Deutz, P., Montañez, I.P., and Monger, H.C., 2002, Morphology and stable and radiogenic isotope composition of pedogenic carbonates in late Quaternary relict soils, New Mexico, U.S.A.: an integrated record of pedogenic overprinting: Journal of Sedimentary Research, v.72, p. 809-822

De Wet, C.B., Yocum, D.A., and Mora, C.I., 1998, Carbonate lakes in closed basins: sensitive indicators of climate and tectonics: an example from the Gettysburg Basin (Triassic), Pennsylvania, USA, in Shanley, K, W. and McCabe, P.J., eds., Relative Role of Eustasy, Climate and Tectonism in Continental Rocks: SEPM Special Publication, No. 59, p. 191-212.

Esteban, M and Klappa, C.F., 1983, Subaerial exposure environment, *in* Scholle, P.A., Bebout, D.G., and Moore, C.H., *eds.* "Carbonate Depositional Environments, American Association of Petroleum Geologists Memoir 33, p.1-96.

Ethridge, F.G., Wood, L., and Schumm, S.A., 1998, Cyclic variables controlling sequence development: Problems and perspectives in relative role of eustasy, climate, and tectonism in continental rocks: SEPM, Spec. Pub. 59, p. 17-29

Fernández-Seveso, F., 1993, Sismoestratigrafia de la Cuenca Iglesia: Informe de actividades en la Universidad de Cornell, Informe interno No. 10.408: 20 pp.

FitzPatrick, E.A., 1993, Soil Microscopy and Micromorphology: John Wiley and Sons, 304 p

Flower, B.P. and Kennett, J.P., 1994, The Middle Miocene climatic transition: East Antarctic ice sheet development, deep ocean circulation and global carbon cycling: Palaeogeography, Palaeoclimatology, Palaeoecology Vol. 108, p. 537-555.

Fox, D.L., and Koch, P.L., 2003, Tertiary history of C_4 biomass in the Great Plains, USA: Geology, v. 31, p. 809-812.

Friedman, G.M., and Sanders, J.E., 2000, Comments about the relationships between new ideas and geologic terms in stratigraphy and sequence stratigraphy with suggested modifications: American Association of Petroleum Geologists Bulletin, v.84, p.1274-1280.

Garzione, C.N., Molnar, P., Libarkin, J.C., and MacFadden, B.J., 2006, Rapid late Miocene rise of the Bolivian Altiplano: Evidence for removal of mantle lithosphere: Earth and Planetary Science Letters, Vol. 241, p. 543-556.

Gile, L.H., Peterson, F.F., and Grossman, R.B., 1966, Morphological and genetic sequences of carbonate accumulations in desert soils: Soil Science, Vol. 101, p. 347-360.

Grootes, P.M., 1993, Interpreting continental oxygen isotope records: *in* Stuart, P.K., Lohmann, K.C., McKenzie, J., and Savin, S., eds., Climate Change in Continental Isotopic Records, American Geophysical Union, Geophysical Monograph 78, p. 37- 46.

Hartley, A.J., Jolley, E.J., and Turner, P., 1992, Paleomagnetic evidence for rotation of the Precordillera of Northern Chile: structural constraints and implications for the evolution of the Andean forearc: Tectonophysics, 205, p. 49-64.

Hartley, A.J., 2003, Andean uplift and climate change, *Journal of the Geological Society of London*, Vol. 160, p. 7-10.

Hickson, T.A., Sheets, B.A., Paola, C, and Kelberer, M., 2005, Experimental test of tectonic controls on three-dimensional alluvial facies architecture: Journal of Sedimentary Research, Vol. 75, p. 710-722.

Hoffmann, J.A.J., 1975, Climatic Atlas of South America, UNESCO

INTA, 1990, El Atlas de Suelos de la República Argentina, Tomos I y II,Buenos Aires, 677 p.

International Water Management Institute World Water and Climate Atlas, 2006: http://www.iwmi.cgiar.org/WAtlas/atlas.htm

Irogoyen, M.V., 1997, Magnetic polarity stratigraphy and geochronological constraints on the sequence of thrusting in the Principal and Frontal cordilleras and the Precordillera ofthe Argentine central Andes (33°S latitude): PhD Dissertation, Carleton University, 392 p.

Jenny, H., 1941, Factors in Soil Formation: A System of Quantitative Pedology: McGraw-Hill, New York, 288 p.

Johnson A.T., Jordan, T.E., Johnson, N.M., and Naeser, C., 1987, Cronologia y velocidad de sedimentacion en una secuencia volcaniclastica, Rodeo, Provincia de San Juan,Argentina: Decimo Congreso Geologico Argentino, Actas II: p. 87-90.

Johnson, D.D. and Beaumont, C., 1995, Preliminary results from a planform kinematic model of orogenic evolution, surface processes and the development of clastic foreland basin stratigraphy *in*: Dorobek. S.L. and Ross, G.M., eds., Stratigraphic Evolution of Foreland Basins: SEPM Special Publication No. 52, p. 3-24.

Jones, H.R., 1992, Plants and microclimate: a quantitative approach to environmental plant physiology, 2nd Edition; Cambridge University Press, 428 p.

Jordan, T.E., Allmendinger, R.W., Damanti, J.F., and Drake, R.E., 1993, Chronology of motion in a complete thrust belt: The Precordillera, 30-31˚ S, Andes Mountains: Journal of Geology, v. 101, p. 135-156.

Jordan, T.E., Kelley, S., Fernandez, A., Fernandez-Seveso, F., Ré, G., and Milana, J.P., 1996, Relaciones entre las historias evolutivas de las cuencas de Iglesia y Bermejo, Prov. de San Juan, Argentina: Actas de las segundas jornadas sobre geologia de Precordillera, p.142-147.

Jordan, T.E., Schlunegger, F. and Cardozo, N., 2001, Unsteady and spatially variable evolution of the Neogene Andean Bermejo foreland basin, Argentina: Journal of South American Earth Sciences, v.14, p. 775-798.

Kay, S. M., C. Mpodozis, and B. Coira, 1999, Magmatism, tectonism, and mineral deposits of the Central Andes (22°-33°S latitude. In Skinner, B. (ed.), Geology and Ore Deposits of the Central Andes, Society of Economic Geology Special Publication (SEG) No. 7, 27-59.

Kay, S. Mahlburg and C. Mpodozis, 2002, Magmatism as a probe to the Neogene shallowing of the Nazca plate beneath the modern Chilean flatslab, Journal of South American Earth Science, 15, 39-59.

Kleinert, K., and Strecker, M.R., 2001, Climate change in response to orographic barrier uplift: paleosol and stable isotope evidence from the late Neogene Santa María basin, northwestern Argentina: GSA Bulletin, Vol. 113, p. 728-742.

Kraus, M.J., 1987, Integration of channel and floodplain suites, II. Vertical relations of alluvial paleosols: Journal of Sedimentary Petrology, Vol. 57, p. 602-612.

Kraus, M.J., and Aslan, A., 1993, Eocene hydromorphic paleosols: significance for interpreting ancient floodplain processes: Journal of Sedimentary petrology, Vol. 63, p. 453-463.

Kraus, M. J., 1999, Paleosols in clastic sedimentary rocks: their geologic applications: Earth Science Reviews v. 47, p. 41-70.

Lal, R., and Kimble, J.M., 2000, Pedogenic carbonates and the global Carbon cycle *in* Lal, R., Kimble, J.M., Eswaran, H., and Stewart, B.A, eds., Global Climate Change and Pedogenic Carbonates, Lewis Publishers, p. 1-14.

Langbein, W.B., and Schumm, S.A., 1958, Yield of sediment in relation to mean annual precipitation: American Geophysical Union Trans., Vol 39, p. 1076-1084.

Latorre, C., Quade, J., and McIntosh, W.C., 1997, The expansion of C_4 grasses and global climate change in the late Miocene: Stable isotope evidence from the Americas: Earth and Planetary Science Letters, v.146, p. 83-96.

Lenters, J.D. and K. H. Cook, 1995, Simulation and diagnosis of the regional summertime precipitation climatology of South America: *Journal of Climate*, Vol. 8, No. 12, p. 2988-3005.

Liu, B., Phillips, F.M., and Campbell, A.R., 1996, Stable carbon and oxygen isotopes of pedogenic carbonates, Ajo Mountains, southern Arizona: implications for paleoenvironmental change: Palaeogeography, Palaeoclimatology, Palaeoecology Vol. 124, p. 233-246.

MacBeth Division of Kollmorgen Instruments Corp., Munsell Soil Color Charts, 1973 edition. Baltimore, MD.

MacFadden, B.J., Wang, Y., Cerling, T.E., and Anaya, F., 1994, South American fossil mammals and carbon isotopes: a 25 million-year sequence from the Bolivian Andes: Palaeogeography, Palaeoclimatology, Palaeoecology, Vol. 107, p. 257-268.

Machette, M.N., 1985, Calcic soils of the southwestern United States *in:* Weide, D.L., ed., Soils and Quaternary Geology of the Southwestern United States: Geological Society of America Special Paper, 203, p. 10-21.

Mack, G.H., James, W.C., and Monger, H.C., 1993, Classification of paleosols: Geological Society of America Bulletin, v. 105, p. 129-136.

Mack, G.H. and Cole, D.R. 2005, Geochemical model of $\delta^{18}O$ of pedogenic calcite versus latitude and its application to Cretaceous paleoclimate: Sedimentary Geology Vol. 174, p. 115-122.

Marriot, S. B., 1999, The use of models in the interpretation of the effects of base-level change on alluvial architecture. In: Fluvial Sedimentology VI (Eds N.D. Smith and J. J. Rogers), Spec. Publ. Int. Assoc. Sediment., 28, 333-346.

Mayer, L., McFadden, L., and Harden, J.W., Distribution of calcium carbonate in desertsoils: a model: Geology, Vol. 16, p. 303-306.

McBride, M.B., 1994, Environmental Chemistry of Soils: Oxford University Press, 406 p.

McCarthy, P.J., and Plint, A.G., 1998, Recognition of interfluve sequence boundaries: Integrating paleopedology and sequence stratigraphy: Geology, v. 26, p. 387-390.

McCarthy, P.J., and Plint, A.G., 2003, Spatial variability of paleosols across Cretaceous interfluves in the Dunvegan Formation, NE British Columbia, Canada: palaeohydrological, palaeogeomorphological and stratigraphic implications: Sedimentology, Vol. 50, p. 1187-1220.

McKnight, T.L andHess, D., 2000, Climate Zones and Types: Dry Climates (Zone B): *Physical Geography: A Landscape Appreciation*, Upper Saddle River, NJ: Prentice Hall. pp. 212-19,

Mermut, A.R, Amundson, R., and Cerling, T.E., 2000, The use of stable isotopes in studying carbonate dynamics in soils, *in* Rattan, L., Kimble, J.M., Eswaran, H., and Stewart, B.A., eds., Global Climate Change and Pedogenic Carbonates: Lewis Publishers. p. 65-85

Miall, A. D., 1997, The geology of stratigraphic sequences: Springer-Verlag, Berlin, 433 p.

Miall, A.D., 1999, The Geology of Fluvial Deposits: Sedimentary facies, Basin analysis and petroleum geology: Springer-Verlag, 582 p.

Miall, A.D., and Arush, M., 2001, Cryptic sequence boundaries in braided fluvial successions: Sedimentology, v. 48, p. 971-985.

Milana, J.P., 1991, Sedimentología y magnetoestratigrafia de formaciones Cenozoicas en el area de Mogna y su insercion en el marco tectosedimentario de la Precordillera oriental: Tesis de doctorado, Universidad de San Juan, Argentina, 273 p.

Milana, J.P., 1997, Sequencias aluviales asociadas a variaciones hidrológicas: consideraciones teóricas y ejemplos: Asociación Argentina de Sedimentología Revista Vol 1, p. 103- 124.

Milana, J.P., 1998, Sequence stratigraphy in alluvial settings: a flume-based model with applications to outcrop and seismic data: American Association of Petroleum Geologists Bulletin, v.82, p.1736-1753.

Milana, J.P. and Tietze, K.W., 2002, Three-dimensional analogue modeling of an alluvial basin margin affected by hydrological cycles: depositional processes, profiles andsequences: Basin Research, v. 14, p. 237-264.

Molnar, P., 2001, Climate change, flooding in arid environments, and erosion rates: Geology, Vol. 29, p. 1071-1074.

Moore, D.M. and Reynolds, R.C., Jr., 1997, X-Ray Diffraction and the Identification and Analysis of Clay Minerals, 2nd Ed: Oxford University Press, New York, 332 p.

Moscatelli, G. y Puentes, M.I. 1998, Suelos Argentinos. In: Conti, M. (Coord.) *Principios de Edafología con énfasis en suelos argentinos.* p. 334-350.1ra. Ed., Orientación Gráfica Editora. Buenos Aires, Argentina.

Net, L.I., Alonso, M.S., and Limarino, C.O., 2002, Source rock and environmental control on clast mineral associations, Lower Section of Paganzo Group

(Carboniferous), Northwest Argentina: Sedimentary Geology, Vol. 152, p. 183-199.

Ori, G.G. and Friend, P.F., 1984, Sedimentary basins formed and carried piggyback onactive thrust sheets: Geology, v. 12, p. 475-478.

Pendall, E.G., Harden, J.W., Trumbore, S.E., and Chadwick, O.A., 1994, Isotopic approach to soil carbonate dynamics and implications for paleoclimate interpretations: Quaternary Research, v. 42, p. 60-71.

Perucca, L.P., and Paredes, J., 2004, Alluvial fan flooding in the Department of Pocito, Province of San Juan, Argentina, Episodes, Vol. 27, No. 3, p. 190-194

Platt, N.H., and Wright, V.P., 1992, Palustrine carbonates and the Florida Everglades-Towards an exposure index for the fresh-water environment?: Journal of Sedimentary Petrology, Vol. 62, p. 1058-1071

Poage, M.A. and Chamberlain, C.P., 2001, Empirical relationships between elevation and the stable isotope composition of precipitation and surface waters: considerations for studies of paleoelevation change: American Journal of Science, v. 301, p. 1-15.

Poppe, L.J., Paskevich, V.F., Hathaway, J.C., and Blackwood, D.S., 2001, A Laboratory Manual for X-Ray Powder Diffraction: U.S. Geological Survey Open-File Report 01- 041, http://pubs.usgs.gov/of/of01-041/index.htm

Posamentier, H.W. and Allen, G.P., 2000, Siliciclastic sequence stratigraphy: Concepts and Applications: SEPM Concepts in Sedimentology and Paleontology Series 7, 204 p.

Puliafito, C., Puliafito, S.E., and G.K. Hartmann, 2002, Observations of large stratospheric ozone variations over Mendoza, Argentina: *Atmospheric Chemistry and Physics Discussions*, 2, p. 507-523.

Quade, J., Cerling, T.E., and Bowman, J.R., 1989, Systematic variations in the stable carbon and oxygen isotopic composition of pedogenic carbonate along elevation transects in the southern Great Basin, USA: Geological Society of America Bulletin, v. 101, p.464-475.

Raymo, M.E. and W.F. Ruddiman, 1992, Tectonic forcing of late Cenozoic climate: *Nature*, 359, p.117-122.

Ré, G. H. and Barredo, S.P., 1993, Estudio magnetoestratigrafico y tasa de sedimentacion del Grupo Iglesia, en sus afloramientos aledaños a la localidad de Angualasto (Prov. de San Juan): XII Congreso Geológico Argentino y II Congreso de Exploración de Hidrocarburos, Actas II, p. 148-155.

Ré, G. H. and Stein, J.E., 1994, Estudio magnetoestratigrafico del Grupo Iglesia (Prov. De San Juan): Implicancias neotectonicas: XIII Congreso Geológico Argentino y III Congreso de Exploración de Hidrocarburos, Actas II: p. 491

Ré, G.H., Jordan, T.E., and Kelley, S., 2003, Cronologia y paleogeografia del Teriario de la cuenca intermontana de Iglesia septentrional, Andes de San Juan, Argentina: Revista de la Asociación Geológica Argentina, v. 58, p. 31-48.

Retallack, G.J., 1993, Classification of paleosols: discussion: Geological Society of America Bulletin, v. 105, p. 1635-1637.

Retallack, G.J., 1997, A Colour Guide to Paleosols, John Wiley and Sons, Chichester, 175 p.

Retallack, G.J., 1998, Fossil soils and completeness of the fossil record: in Donovan, S.K. and Paul, C.R.C., eds., The Adequacy of the Fossil Record: John Wiley and Sons, United Kingdom, p. 133-164.

Retallack, G.J., 2001, Soils of the Past: an Introduction to Paleopedology, 2nd edition: Blackwell Science, 404 p.

Riebe, C.S., Kirchner, J.W., and Finkel, R.C., 2004, Erosion and climatic effects on long-term chemical weathering rates in granitic landscapes spanning diverse climate regimes: Earth and Planetary Science Letters, Vol. 224, p. 547-562.

Rind, D., 1998, Latitudinal temperature gradients and climate change: Journal of Geophysical Research, v.103, p. 5943-5971.

Rind, D., and Perlwitz, J., 2004, The response of Hadley Circulation to climate changes, past and future *in* Diaz, H.F., and Bradley, R.S., eds., The Hadley Circulation: Present, Past and Future, Kluwer Academic Publishers, p. 399-435.

Riquelme R., 2003. Evolution Géomorphologique Néogène des Andes Centrales du Désert d'Atacama (Chili): Interaction Tectonique-Erosion-Climat. PhD Thesis, Université Paul Sabatier-Toulouse III, France, 258 p.

Schumm, S.A., 1993, River response to base level change: Implications for sequence stratigraphy: Journal of Geology, Vol. 101, p. 279-294.

Seluchi, M.E., Norte, F.A., Satyamurty, P., and S.Chan Chou, 2002, Analysis of three situations of the Foehn Effect over the Andes (Zonda Wind) using the ETA-CPTEC Regional Model: *Weather and Forecasting*, Vol. 18, No. 3, p. 481-501.

Servicio Meteorológico Nacional de Argentina, 2005, http://www.meteofa.mil.ar/

Schöner, R. and Gaupp, R., 2005, Diagenetic reactions of Fe-species pre- and post petroleum migration: Examples from Permian sandstone reservoirs in northern Germany, Central European Basin System: abstract, European Geosciences Union, Geophysical Research Abstracts, Vol. 7, 08628.

Shanley, K.W., and McCabe, P.J., 1994, Perspectives on the Sequence Stratigraphy of Continental Strata: American Association of Petroleum Geologists Bulletin, v. 78, p 544-568.

Shanley, K.W., and McCabe, P.J., 1995, Sequence stratigraphy of Turonian-Santonian strata, Kaiparowits Plateau, Southern Utah, USA: Implications for regional correlation and foreland basin evolution: *in* Van Wagoner, J.C., and Bertram, G.T., eds., Sequence Stratigraphy of Foreland Basin Deposits - Outcrop and Subsurface Examples from the Cretaceous of North America: American Association of Petroleum Geologists Memoir 64, p.103-136.

Sheriff, R.E., and Geldart, L.P., 1983, Exploration Seismology Vol. 2: Data-Processing and Interpretation: Cambridge University Press, Cambridge, 592 p.

Schumm, S.A., 1963, Disparity between modern rates of denuadation and orogeny: U.S. Geological Survey Professional Paper 454-H, 13 p.

Schumm, S.A., 1993, River response to base level change: Implications for sequence stratigraphy: Journal of Geology, Vol. 101, p. 279-294.

Schumm S. A. & Ethridge F. G. 1994. Origin, evolution and morphology of fluvial valleys *In:* Dalrymple, R.W., Zaitlin, B.A., and Scholle, P.A., eds., Incised-valley systems: Origin and sedimentary sequences, Society for Sedimentary Geology Special Publication 51. pp. 11–27.

Singer, A., 1984, Pedogenic palygorskite in the arid environment *in* Singer, A. and Galan, E., *eds*., palygorskite-Sepiolite: occurrences, genesis and uses: Developments in Sedimentology 37, El Sevier, p. 169-175.

Soil Survey Staff, 1993, Soil Survey Manual, Handbook, US Department of Agriculture, 18.

Tucker, G.E. and Slingerland, R., Predicting sediment flux from fold and thrust belts: Basin Research, Vol. 8, p. 329-349.

Uba ,C.E., Heubeck, C., and Hulka, C., 2005, Facies analysis and basin architecture of the NeogeneSubandean synorogenic wedge, southern Bolivia: Sedimentary Geology, Vol. 180, p. 91-123.

Van Wagoner, J.C., Mitchum, R.M., Campion, K.M., and Rahmanian, V.D., 1990, Siliciclastic sequence stratigraphy in well logs, cores, and outcrops: American Association of Petroleum Geologists Methods in Exploration 7, 63 p.

Wang, Y. Cerling, T. E. ; Quade, J. ; Bowman, J. R. ; Smith, G. A. ; Lindsay, E. H., 1993, Isotopes of paleosols and fossil teeth as paleoindicators: *in* Stuart, P.K., Lohmann, K.C., McKenzie, J., and Savin, S., eds., Climate Change in Continental Isotopic Records: American Geophysical Union, Geophysical Monograph 78, p. 241-248.

Wang, Y., and Cerling, T. E., 1994. A model of fossil tooth and bone diagenesis: Implications for paleodiet reconstruction from stable isotopes. *Palaeogeography, Palaeoclimatology, Palaeoecology*, 107: 281-289

Weissmann, G.S., Mount, J.F., and Fogg, G.E., 2002, Glacially-driven cycles in accumulation space and sequence stratigraphy of a stream-dominated alluvial

fan, San Joaquin Valley, California, U.S.A., Journal of Sedimentary Research, v. 72, p. 240-251.

Weltje G.J., X.D. Meijer, P.L. de Boer; Stratigraphic inversion of siliciclastic basin fills: a note on the distinction between supply signals resulting from tectonic and climatic forcing. In: Basin Research, Jaargang: 1998, Vol. 10, no. 1, 1998, p. 129-153

Wright, V.P., 1992, Paleopedology: stratigraphic relationships and empirical models *in* Martini, I.P. and Chesworth, W., eds., Weathering, Soils and Paleosols: Elsevier Science Publishers, p. 475-499.

Zachos, J., Pagini, M., Sloan, L., Thomas, E., and Billups, K., 2001, Trends, rhythms, and aberrations in global climate 65 Ma to present: Science, v. 292, p. 686-693.

CHAPTER 4: MAGNETOSTRATIGRAPHY AND PALEOPEDOLOGY OF THE MOGNA AND EL CORRAL FORMATIONS, LOMAS DE LAS TAPIAS, SAN JUAN, ARGENTINA

Abstract:

New paleomagnetic analyses extend the chronostratigraphy at Lomas de las Tapias (Ullum department, San Juan, Argentina, S 31.5°, W 68.6°) from 9.0 Ma to 2.6 Ma. This is an interval of interest for the documentation of paleohydrologic variation through a valley that traverses the Precordillera fold-thrust belt. At Lomas de Las Tapias, strata exposed on the banks of the modern San Juan River reveal a transition between channelized deposits of the paleo-San Juan River (Mogna Formation) and unconfined bajada facies (El Corral Formation). New magnetic polarity data, correlated to the global magnetic polarity time scale, reveal that the transition occurred at approximately 2.6 Ma, as the course of the river shifted northward. Options for the location of the river system are considered. Interbedded paleosols dated 6.37 – 2.9 Ma exhibit characteristics and stable isotopic ($\delta^{13}C$ and $\delta^{18}O$) values that suggest shifts through time in relative soil humidity as a function of their proximity to the paleo-river. In addition, similarity of the pedogenic carbonate $\delta^{18}O$ trends with respect to contemporaneous paleosols in the Iglesia Basin suggests changes in headwater discharge from the Frontal Cordillera that fed both the proximal Iglesia-Calingasta Valley and the distal Lomas de las Tapias site.

Introduction:

The discharge history of the Frontal Cordillera may be deduced from deposits of the paleo-San Juan River. This paper focuses on this record from Ullum, in San Juan Province, Argentina, located adjacent to the course of the modern San Juan River. The San Juan River drainage basin neighbors and is similar to the Jáchal River basin to the north (Fig. 4.1). These rivers drain the Frontal Cordillera and Principal

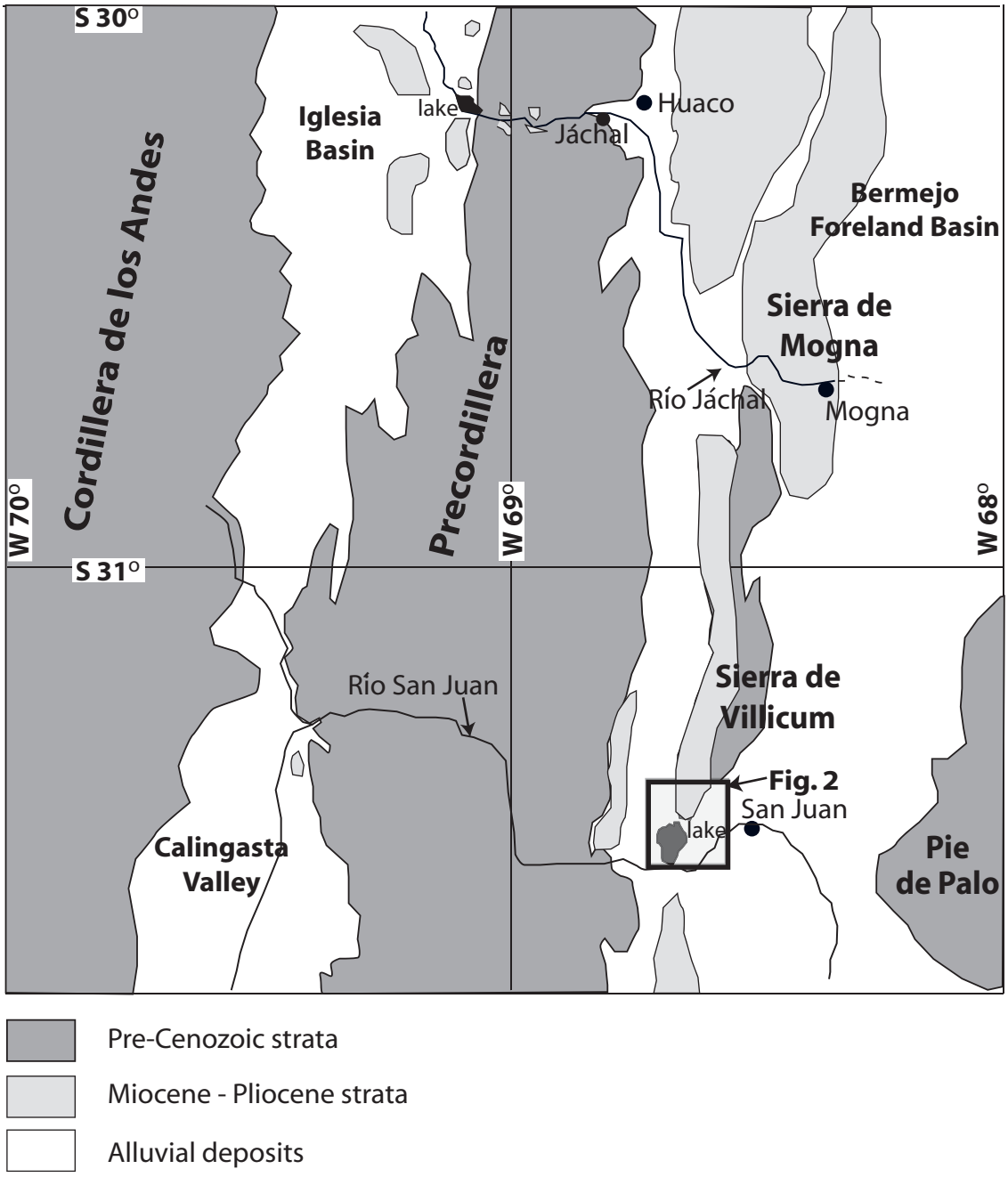

Figure 4.1: Generalized geologic framework and location map of northwestern Argentina localities referenced in text. Rectangular in lower right demarcates study area, shown in detail in Figure 4.2.

Cordillera east of the continental drainage divide (Chile-Argentina border), as well as large tracts of the Precordillera thrust belt, before entering foreland basins east of the Andes. Each river passes through a broad valley that separates the Frontal Cordillera and Precordillera ranges, the Calingasta Valley for the San Juan and the Iglesia Valley for the Jáchal. To a first order, we presume that the history of fluctuations in surface water input to the Calingasta Valley from the Frontal Cordillera was likely very similar to the history of surface water input from the Frontal Cordillera to the Iglesia basin. However, the Calingasta Valley trapped strata only in isolated depositional centers (<2000 m combined Mesozoic and Cenozoic subsurface thickness), whereas the Iglesia valley became a major basin in which up to 3.5 km of strata accumulated during the Miocene-Pliocene alone (Stipanicic, 1979; Snyder, 1988; Chapter 2). Thus, a key distinction between these rivers is that the San Juan River exported water and sediment to the foreland at approximately the same rate that it was discharged from the Frontal Cordillera, whereas the Jáchal River system left much of its sediment load trapped in the Iglesia basin. Therefore, some insight to hydrologic changes in the Frontal Cordillera can be obtained by comparing contemporaneous Iglesia Basin strata (e.g. Ré *et al*., 2003, Ruskin, 2006) and strata exposed at Ullum.

To better understand local and regional hydrologic variability of the San Juan River drainages, such as first described by Milana (1991), we paleomagnetically constrain the timing of changes in fluvial architecture within the upper ~650 m of the Ullum section. The chronological study builds on work done in the lower 1000 m by Bercowski *et al.* (1986). Additionally, the abundant paleosols of the Mogna Formation are described for the first time and pedogenic carbonate nodules analyzed for stable isotopic values of ^{13}C and ^{18}O, providing information in addition to textural, architectural and fabric data (Bercowski *et al.*, 1987; Milana, 1997) about variations in relative humidity through time. We use $\delta^{13}C$ values as a proxy for dominant biomass

(via plant-respired CO_2) and thus relative water stress of the paleovegetation (e.g. Cerling and Quade, 1993). Values of $\delta^{18}O$ reflect isotopic fractionation of soil water and respond to many factors (e.g. continentality, seasonality of precipitation, evapotranspiration, and altitude, among others; see Mermut *et al.*, 2000), which can be used in combination with $\delta^{13}C$ data to detect environmental changes. Here we consider the $\delta^{18}O$ record of Iglesia Basin and Ullum to fundamentally reflect changing regional hydrology. Additionally, we utilize weight percentages of soil inorganic carbon as a record of influx of Ca and Mg through dust which may aid the accumulation of soil carbonates (Lal and Kimble, 2000), and whose variations through time may demarcate periods of changing aridity.

Prior work:

In the Lomas de Las Tapias syncline, quebrada de Ullum (~10 km NW of San Juan City, Argentina), approximately 1500 m of Neogene nonmarine strata are exposed (Figures 4.1 and 4.2). Contreras (1981) defined these outcrops as the Ullum Formation, an upward-coarsening three-member succession of basal silty claystones, overlain by interbedded sandstones and conglomerates with tuffaceous and faunal material, and concluding with nonfossiliferous sandstones and conglomerates. On the basis of the "Chasicoan" land mammal fossil assemblage, Contreras (1981) assigned an age to the lower two member of Ullum Formation of middle to late Pliocene. However, the Chasicoan mammalian stage has been subsequently recalibrated to 10-9 Ma (Gradstein *et al*, 2004), or Late Miocene. Magnetostratigraphic analyses and ash chronology by Bercowski *et al.* (1986) constrained the age of the lower and middle portions of the outcrop to Late Miocene, 9.025 - 5.89 Ma (their correlation, ages adjusted to geomagnetic polarity time scale of Cande and Kent, 1995). Detailed sedimentologic measurements by Bercowski *et al.* (1987) in the lower 1000 m of section distinguished 12 lithofacies in two associations: an anastamosed, high to low

Figure 4.2: Satellite image of study area (enlarged from Figure 4.1), the Lomas de Las Tapias, Departamento de Ullúm, northwest of San Juan City. Image from Google Earth © 2006.

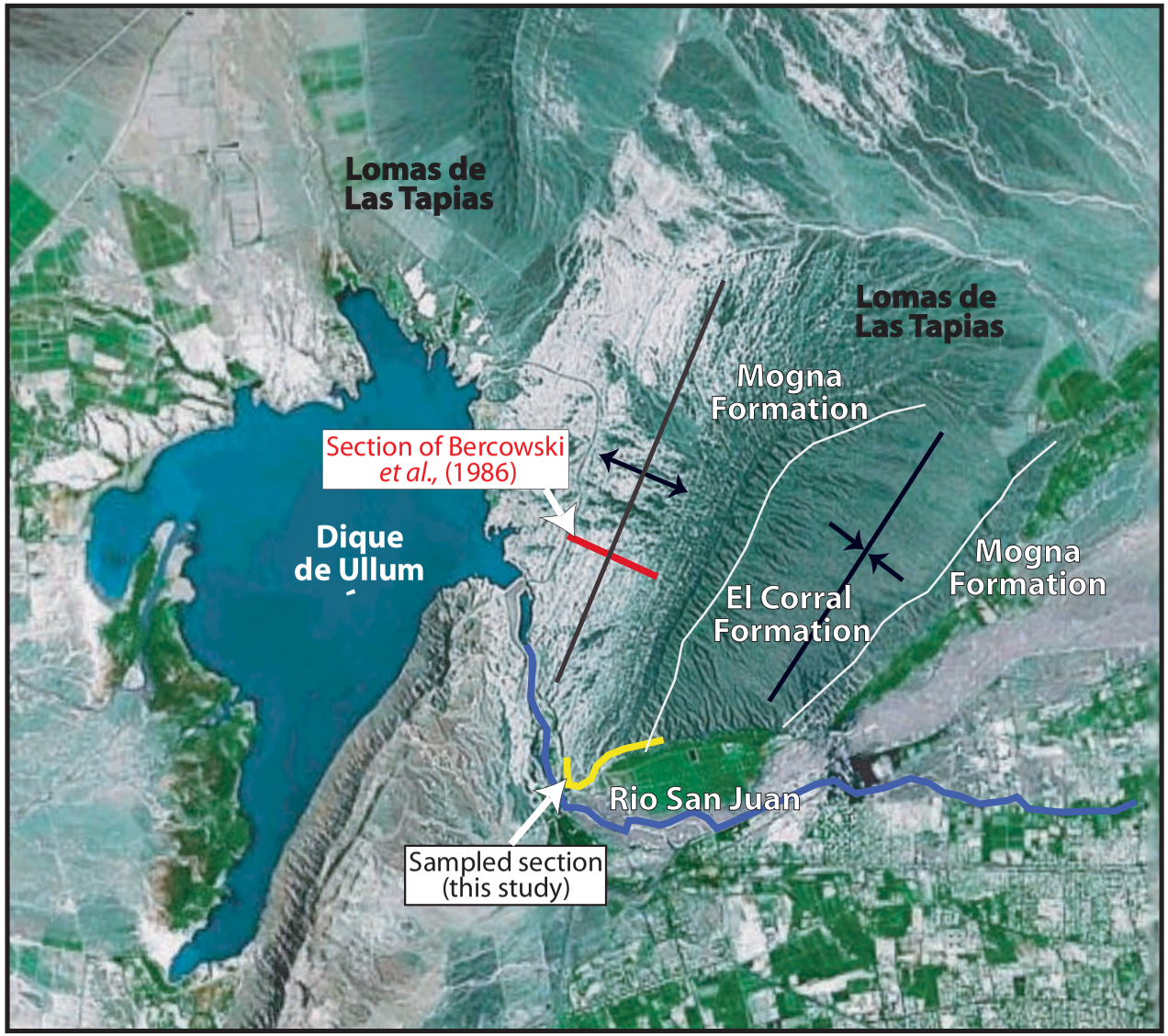
Lomas de
Las Tapias
Lomas de
Las Tapias
Mogna
Formation
Section of Bercowski
et al., (1986)
Dique
de Ullum
El Corral
Formation
Mogna
Formation
Rio San Juan
Sampled section
(this study)

sinuosity fluvial facies and an overlying prograding distal alluvial fan assemblage with low sinuosity braided channels. On the basis of lithologic and temporal similarity, the upper ~700 m of Lomas de Las Tapias outcrops correlate with the Mogna and El Corral Formations as defined at Mogna, Argentina, ~90 km to the NNE (Milana, 1991, 1997; Milana *et al.,* 2003). The lower 650 m of outcrop east of the San Juan River at Lomas de las Tapias is hereafter considered the Lomas de Las Tapias Formation (Contreras *et al.*, 1990; See Figure 4.3).

Mio-Pliocene sedimentary units exposed along the eastern margin of the Precordillera fold-thrust belt (Fig. 4.1) can be interpreted with respect to variations through time in the courses of the San Juan River (exposures at Sierra de Mogna and Ullum) and Jáchal River (outcrops at Huaco; e.g. Jordan et al, 1993; Milana, 1991, 1997; Milana *et al.,* 2003). In the proximal Bermejo foreland basin, the Río Jáchal Formation is identified by finely laminated siltstones and sandstones grading upward into planar bedded conglomerates (Contreras *et al,* 1990). The overlying Mogna Formation is characterized by well-sorted conglomerates. The upward passage from the Río Jáchal to Mogna Formation represents a marked hydrologic change indicative of a shift from ephemeral alluvial and floodplain deposition to high-energy, river-dominated facies. Milana (1991) hypothesized that the abrupt textural and facies changes at the base of the Mogna Fm. (4.0 Ma by linear interpolation to magnetostratigraphy of Milana *et al.,* 2003) represented the introduction of a perennial river at Mogna, Argentina, probably the paleo-San Juan River which presently exits the Central Precordillera at Ullum (Fig. 4.1). Changes occurred again, when fluvial deposition was replaced at Mogna ~1.6 Ma by poorly sorted and unchannelized conglomerates of the El Corral Formation, interpreted as bajada deposits (Milana *et al.,* 2003). Temporal correlations between the Mogna and Ullum paleomagnetic sections revealed depositional diachronism of the Mogna Formation, which initiated

progressively later in the north (4.0 Ma) than in the south (6.6 Ma; Bercowski *et al.*, 1986; Milana *et al.*, 2003). This suggested to Milana (1991,1997) that the course of the San Juan River shifted to the north of its current position at 4 Ma, accumulating riverbed strata at Mogna before shifting back to the south ~1.6 Ma. However, the magnetostratigraphy of the Ullum section was incomplete, only extending as young as 5.89 Ma and thus the timing of the shifts in the river could not be tested at the southern site.

At Ullum, the Lomas de Las Tapias and Mogna Formations exhibit marked changes in clast provenance and depositional facies suggestive of changing local paleohydrology (Fig. 4.3). The lower section comprises the Lomas de las Tapias Formation (~9.0 – 6.6 Ma, Bercowski et al., 1986) and consists mostly of unconfined (tabular) sandstones with interbedded well-laminated silty sandstones and rare conglomerate lenses. These deposits were interpreted as those of an anastamosing river with variable sinuosity (Bercowski *et al*, 1987). Coinciding with the first multi-meter-thick conglomerate beds (tabular or with minor basal erosion) of the Mogna Formation (~6.6 Ma), fine-grained interbeds become strongly pedogenic and contain abundant carbonate nodules. The section coarsens upward, such that erosional-based, well-sorted conglomerates become thicker and comprise an increasing percentage of the preserved stratigraphy. The dominantly conglomeratic section was interpreted as braided Donjek-type distal alluvial fan deposits of a major paleodrainage crossing the Precordillera (Bercowski *et al.*, 1987; Miall, 1996; Milana, 1997). The composition of gravel clasts in the fluvial channels varies between dominantly volcanic (e.g. Frontal Cordillera source) and sedimentary lithic (e.g. Precordillera source). These provenance variations are multicyclic, occurring both within and between individual conglomerate units (Milana, 1991). Such alternations in dominant clast provenance suggest that

Figure 4.3: Simplified chronostratigraphic section for Lomas de Las Tapias, San Juan Province, Argentina (S 31.5° W 68.5°) showing general lithologies, sampling sites and preferred correlation to GPTS (Cande and Kent, 1995). Column on left shows entirety of Bercowski *et al.* (1986) section as well as base of this study's sampled section. Right-hand column shows sites of paleosols and paleomagnetic samples for this study and the transition between Mogna and El Corral Formations. Note change of vertical scale between columns.

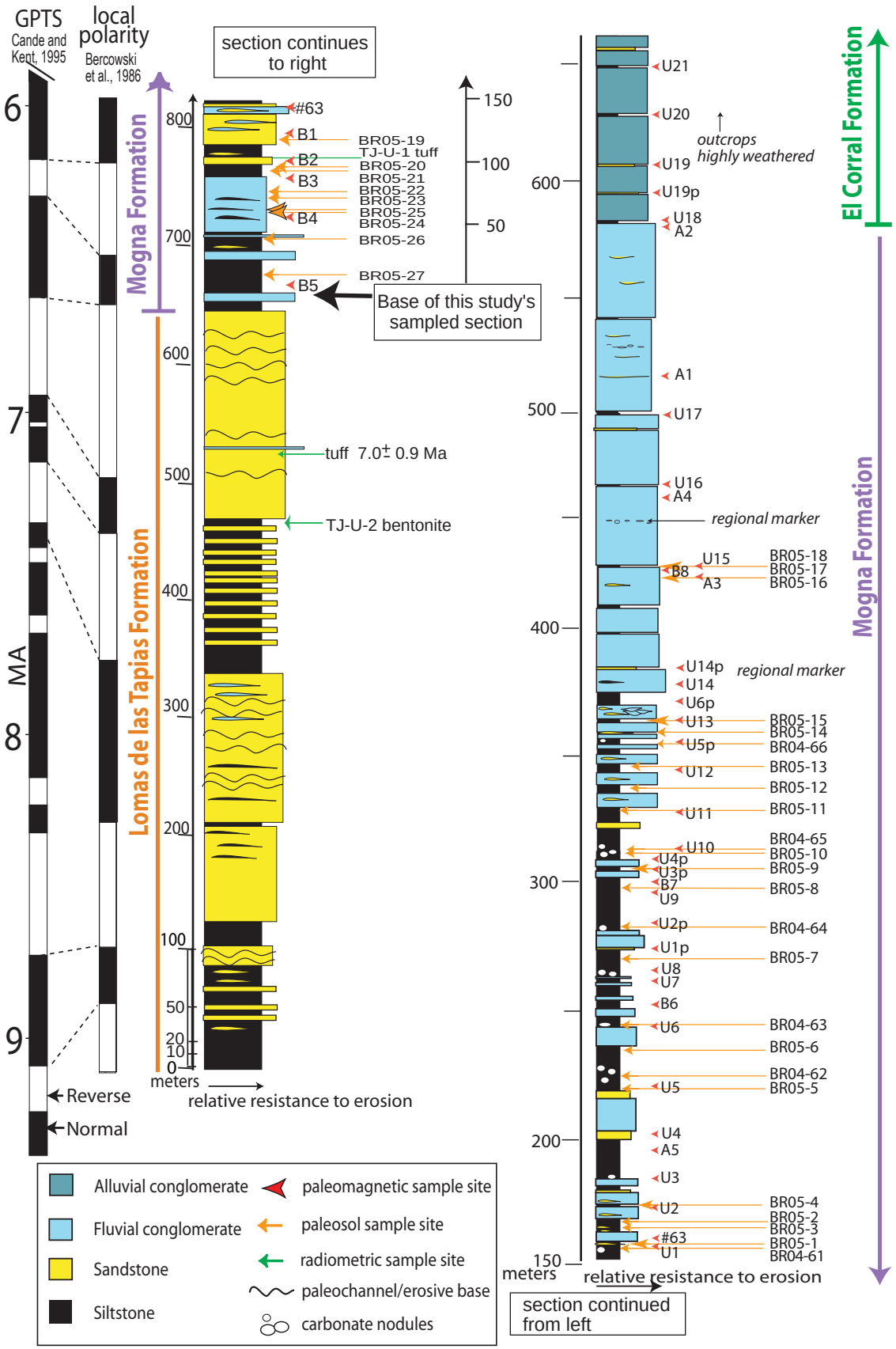
GPTS
Cande and Kent, 1995
local polarity
Bercowski et al., 1986
section continues to right
Mogna Formation
Lomas de las Tapias Formation
El Corral Formation
Mogna Formation
MA
6
7
8
9
Reverse
Normal
meters
relative resistance to erosion
#63
B1
B2
B3
B4
B5
BR05-19
TJ-U-1 tuff
BR05-20
BR05-21
BR05-22
BR05-23
BR05-25
BR05-24
BR05-26
BR05-27
Base of this study's sampled section
tuff 7.0± 0.9 Ma
TJ-U-2 bentonite
outcrops highly weathered
regional marker
regional marker
U21
U20
U19
U19p
U18
A2
A1
U17
U16
A4
U15
B8
A3
BR05-18
BR05-17
BR05-16
U14p
U14
U6p
U13
U5p
U12
U11
U10
U4p
U3p
B7
U9
U2p
U1p
U8
U7
B6
U6
U5
U4
A5
U3
U2
#63
U1
BR05-15
BR05-14
BR04-66
BR05-13
BR05-12
BR05-11
BR04-65
BR05-10
BR05-9
BR05-8
BR04-64
BR05-7
BR04-63
BR05-6
BR04-62
BR05-5
BR05-4
BR05-2
BR05-3
BR05-1
BR04-61
Alluvial conglomerate
Fluvial conglomerate
Sandstone
Siltstone
paleomagnetic sample site
paleosol sample site
radiometric sample site
paleochannel/erosive base
carbonate nodules
section continued from left

de Las Tapias Formation and lower 150 m of the Mogna Formation increase from about 19 cm/ky to 50 cm/ky, well above the slow rates about which Talling and Burbank (1993) cautioned. Ultimately, the resultant average accumulation rates for the upper Mogna and El Corral Formations must be defensible based on the lithologies and unconformities observed in the section (discussed below).

Field and Laboratory Procedure:

A: ***Paleomagnetic analysis***

Hand block samples for paleomagnetic analysis were collected from the entire Mogna Formation (580 m thick) and lower 70 m of El Corral Formation exposed at Lomas de las Tapias (S 31° 30', W 68° 38') during three separate field seasons. The preferred lithology for paleomagnetic samples was minimally weathered and well-consolidated siltstone, although in the coarser upper section, fine-grained sandstone was sampled by necessity. Intervals with evidence of oxidation and/or recementation were avoided. Three or four samples, each oriented with respect to the earth's magnetic pole with a compass, were withdrawn from each horizon. A total of 137 samples were collected from 42 horizons at approximately 20 m stratigraphic increments (greater or lesser spacing depending on lithology and general polarity scheme from preliminary laboratory analyses conducted in 2004). These were subsequently prepared by grinding to cubic forms to fit in 5.8-cm^3 plastic containers for placement in the laboratory's automated sample handler.

For proper calibration of the local paleomagnetic section to the global geomagnetic polarity time scale (GPTS), our section overlaps with the upper 150 m of the section of Bercowski *et al.* (1986). The Bercowski *et al.* (1986) magnetic polarity correlation was anchored by the date of one interbedded ash, and spans 9.03 Ma to 5.89 Ma (Cande and Kent, 1995). Furthermore, two volcaniclastic units (a crystalline 15-cm-thick tuff and a 27-cm-thick green and brown biotite-bearing bentonite) were

also collected for $^{40}Ar/^{39}Ar$ radiometric age determination (see Figure 4.3 for locations). Age determination for these extrusive units is pending.

Incremental thermal demagnetization and analysis of paleomagnetic vectors were conducted at the University of Pittsburgh Paleomagnetic Laboratory. The lab houses a three-axis 2-G cryogenic superconducting rock magnetometer (SRM) with an automated sample handler system in a magnetically shielded environment (maximum field <300 nT). The natural remanent magnetism (NRM) for each sample was recorded first, after which we applied a thermal demagnetization sequence (200°, 400°, 450°, 500°, 550°, and 600°C) to each sample (Figure 4.4) using a large-capacity furnace with shielded (<4 nT) cooling area. This stepwise thermal treatment is in accord with the progression used by Bercowski *et al.* (1986) and, consistent with magnetic signal decay upon heating (see below), assumes that magnetite is the dominant ferromagnetic mineral carrier. Samples were heated in quartz boats for one hour and cooled for an additional hour prior to analysis. Several coarser-grained samples disintegrated during the thermal demagnetization procedure. However, 36 of the 42 sampled sites retained at least 3 samples throughout thermal demagnetization.

B: *Pedogenic carbonate samples*

Carbonate nodules were collected from 33 paleosol horizons in ~490 m of the Mogna Formation (Figure 4.3). We preferentially selected discrete nodules (2-20 cm in diameter) where concentrated in horizontal bands (Bk horizons, stage II and III carbonate accumulations of Machette, 1985). We avoided coalesced carbonate layers, as a nonpedogenic origin for such accumulations cannot be discounted. Three to ten individual nodules were collected from the same depth level for an individual paleosol profile, taken >30 cm below the top of the preserved profile to minimize isotopic fractionation from atmospheric diffusion (see Cerling and Quade, 1993). Nodules

from single horizons were subsequently homogenized to a powder with mortar and pestle.

Ratios of carbon and oxygen isotopes were analyzed at Cornell University Stable Isotope Laboratory (COIL) using a Finnegan MAT Delta Plus mass spectrometer. For each horizon, 40 mg of powder were massed into tin thimbles and introduced to the mass spectrometer via a NC2500 Elemental Analyzer with an oxidation column containing chromium and copper oxide at 1000°C. The carrier gas between equipment was ultra high purity helium introduced at a rate of 120 ml/min.

Paleosol characteristics:

Pedogenic siltstones and sandstones are plentiful in the lower half of the Mogna Formation (Fig. 4.3). Almost all fine-grained intervals contain some evidence of pedogenesis (e.g. ped structure, clay illuviation and horizonation, carbonate accumulations, disruption or destruction of primary sedimentary bedding). Furthermore, calcic paleosols (those with significant nodular or coalesced carbonate accumulations) comprise a significant proportion of the pedogenic facies. The oldest carbonate nodule-bearing paleosols are younger than 6.6 Ma (based on paleomagnetic correlation of Bercowski *et al.*, 1986; level BR05-27 on Fig.4.3). Paleosols continue upsection in the channel-dominated interval, but their thickness and development diminish accordingly, restricted to thin siltstone and mudstone interbeds.

Paleosols commonly occur at Ullum as compound profiles 2-20 m thick in fine-grained sediments. Individual profiles are typically less than 1 meter in thickness, consisting of an upper Bt (clay-rich, structural) horizon, one or more Bk (calcic) horizons, and a lower C horizon (altered sedimentary units). The upper boundary of compound paleosol intervals is usually eroded, exhibiting relief of 0.5 – 5 m. The depth of erosion increases upward in the stratigraphic column corresponding with thicker channel conglomerate bodies. Intraprofile horizon boundaries are laterally

smooth to wavy and vertical transitions are gradual (e.g. 5-15 cm; Retallack, 2001). Carbonate accumulations are commonly discrete ("disorthic") Stage II (nodular) forms or Stage III (congealed nodular) forms (after Machette, 1985). Rootlets and burrows are rare, but where present are filled by fine sand or, more rarely, by carbonate ("rhizoliths"). Redoximorphic banding and/or mottling are uncommon, but occur locally in the lowermost 100 m of the Mogna Formation (see Fig. 4.3). Characteristics of sampled paleosols are summarized in Table 4.1.

Though existing lithofacies models for the Lomas de Las Tapias strata discuss the characteristics of the fluvial and alluvial deposits (Bercowski *et al.,* 1997; Milana, 1997), these lack incorporation of the sizeable proportion of interbedded paleosols into a complete landscape description. The initial multi-meter channelized conglomerates at the base of the Mogna Formation (~6.6 Ma in Bercowski *et al.*, 1986) signal the arrival of a major river that periodically avulsed. Based on the lithologic association of the overlying Mogna Formation, we infer alternation of overbank and stable floodplain deposits with channel avulsions, the latter becoming more frequent through time. Between avulsions, fine-grained sediments were deposited on floodplains, where sedimentation rates were sufficiently low to allow for soil formation (e.g. Kraus, 1987). These floodplains were well-drained, evidenced by the calcic accumulations and lack of redoximorphic features. In the upper Mogna Formation (e.g. 450 m and higher, right hand column, Fig. 4.3), pedogenesis was minimal or soils were subsequently eroded, perhaps due to an increase in floodplain sedimentation rates, river avulsion rates or both. The recognition of abundant mature floodplain paleosols is useful in understanding the initial characteristics of the paleodrainage: avulsion was for a time infrequent and overbank sedimentation slow. Furthermore, the floodplain was sufficiently broad that paleosols did not become indurated by a near-surface water

Table 4.1: Characteristics of sampled paleosols, Mogna Formation, Lomas de Las Tapias, San Juan Province, Argentina.

Sample ID	Age (Ma)	Paleosol description	Carbonate Stage	Max. nodule size (cm)	Depth of Bk (cm)	Thickness of Bk (cm)
BR04-61	6.06	Compound paleosols in siltstone-sandstone.	II	4		
BR04-62	5.51	Compound paleosols in siltstone-sandstone.	II	10		
BR04-63	5.36	Pedogenic siltstone with Bk horizon and elongate disorthic carbonate nodules. Well formed ped structure	II-III			
BR04-64	4.87	Pedogenic siltstone with disorthic carbonate nodules	II			
BR04-65	6.64	Pedogenic siltstone with abundant disorthic carbonate nodules	II	8		
BR04-66	4.32	Greenish siltstone with disorthic carbonate nodules	II	10		
BR05-1	6.05	Compound paleosols in siltstone-sandstone. Elongate carbonate nodules, parallel to bedding	III	4		12
BR05-2	5.92	4 m compound soil interval, with Bt and Bk horizons,	II	4	40	
BR05-3	5.94	Elongate carbonate nodules, blocky peds, sandy base	II	4		
BR05-4	5.88	1m thick clay-rich reddish paleosol, with subrounded interlocking peds, irregular carbonate nodules	II	3		
BR05-5	5.54	Mudstone paleosol with multiple Bk horizons, elongate carbonate nodules	III	15	30	
BR05-6	5.43	Interbedded sandstone and pink pedogenic mudstone, multiple Bk horizons, dense with spheroid to elongate carbonate nodules	III	20		
BR05-7	5.11	Compound sandy paleosols; lacks ped structure some intraprofile carbonate dislocation possible	II-III	5		40
BR05-8	4.73	Silty paleosol, lacks ped structure and carbonate nodules are disorthic/dispersed	II	6		70
BR05-9	4.69	Sandy, some incipient ped structure, no discernible Bk, Carbonates disorthic, very hard, egg-shaped	II	10		
BR05-10	4.64	Interbedded pebby conglomerates and sandy paleosols; Carbonates in laterally-continuous Bk horizons and disorthic	II-III	4		20
BR05-11	4.54	Compound paleosol, two Bk horizons within 20 cm	III		100	8
BR05-12	4.49	Clayey, red, ped-rich paleosol with Bk, interbedded with reddish coarse sand-pebble units	III			15
BR05-13	4.41	4-m silt-fine sand interval with compound paleosols; Numberous disothic carbonates (ovoid to irregular)	II-III	3	100	10
BR05-14	4.27	Sand paleosol with thin (<2-cm) red clay laminations and clay peds. Disorthic carbonate nodules (rare)	II	2		
BR05-15	4.22	Silty paleosol with irregular carbonate forms, some coalesced Possibly rhizoliths?	II-III			30
BR05-16	3.82	Sandy nodular paleosol with carbonate cement, yellow iron-oxide weathering; Oblate disorthic nodules.	I-II	15		
BR05-17	3.8	Poorly sorted pebbly sandstone with concretionary carbonates (some with pebble nucleii); Pedogenic?	II		100	
BR05-18	3.8	Sandy paleosol with small, irregular disorthic carbonates	II	3	50	
BR05-19	6.18	Compound paleosols in siltstone-sandstone. Multiple Bk horizons (thin stringers); Horizonation excellent	III			6
BR05-20	6.35	Sandy paleosol with disorthic and layered carbonates	II-III			
BR05-21	6.46	Sandy oxidized paleosol with layered carbonates	III		90	8
BR05-22	6.57	Grey and red silty paleosol with thin Bk; blocky ped structure	III			
BR05-23	6.58	4 m thick redozimorphic silty paleosol. Reddish clay interbeds	II			
BR05-24	6.59	Pedogenic sandstone with Bk at base	III			
BR05-25	6.59	Fine sand paleosol with disorthic ovoid nodules	II			
BR05-26	6.62	8 m interval of interbedded planar sandstone and paleosols (<1 m) Carbonate nodules alligned in Bk.	III			
BR05-27	6.65	Interbedded pedogenic silt and sandstone. Disorthic carbonate nodules	II			

table as might be expected if the river was nearby during pedogenesis (cf. Kraus and Aslan, 1993).

The transition between the Mogna and El Corral Formations at Ullum is evidenced by changes in sedimentary architecture and by a thin sandstone bed at the base of the El Corral Formation. Like the upper Mogna Formation, the El Corral Formation is also predominantly conglomeratic. But architecturally, the deposits are unconfined (i.e. nonchannelized) and texturally they are poorly sorted. This formation's lithofacies were interpreted as deposits of an alluvial bajada (Milana, 1997). This transition was studied in detail for evidence of pedogenesis or significant depositional hiatus. Between the two formations appears a pebbly sandstone bed about 0.6 – 1 m thick with subrounded lithic clasts (≤ 3 cm in diameter). No characteristic pedogenic structures were observed. There is only minor erosional relief (<1 m) at the base of the El Corral Formation. The maximum clast size and lack of pedogenic features suggests a reasonably high depositional energy associated with this transition sandstone, albeit of lesser energy than the overlying and underlying strata. Finer-grained mud drapes above and below this interval were sought for paleomagnetic analysis, but these are rare and poorly lithified in the uppermost Mogna and the lower El Corral Formations. A similar sandy interval is present at the base of El Corral Formation at Sierra de Mogna (Milana *et al.,* 2003).

Paleomagnetic Analysis:

The magnetic declination and inclination as well as remanent intensity for each sample were recorded during thermal demagnetization (see Appendix for data summary). Figure 4.4 shows examples of Zidjerveld, Lambert equal area and intensity diagrams for better-behaved samples following the demagnetization procedure. Principal component analysis (PCA) was applied to preferred sequential thermal steps to assess the mean direction of the paleomagnetic field for a given site. For most

Figure 4.4: Representative Zidjerveld, equal area and intensity diagrams for paleomagnetic analyses of Upper Mogna Formation. Stratigraphic position of sample shown in Figure 4.3.

◇ horizontal plane
○ vertical plane

Site U14
Sample C

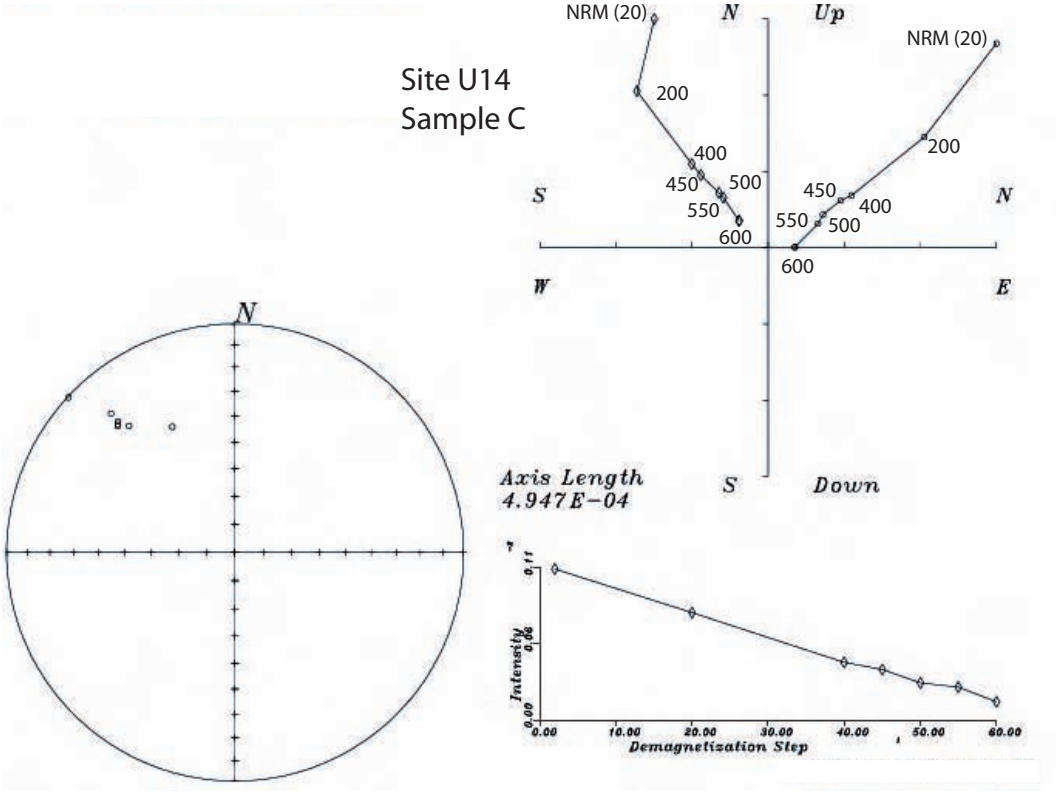

Site U11
Sample A

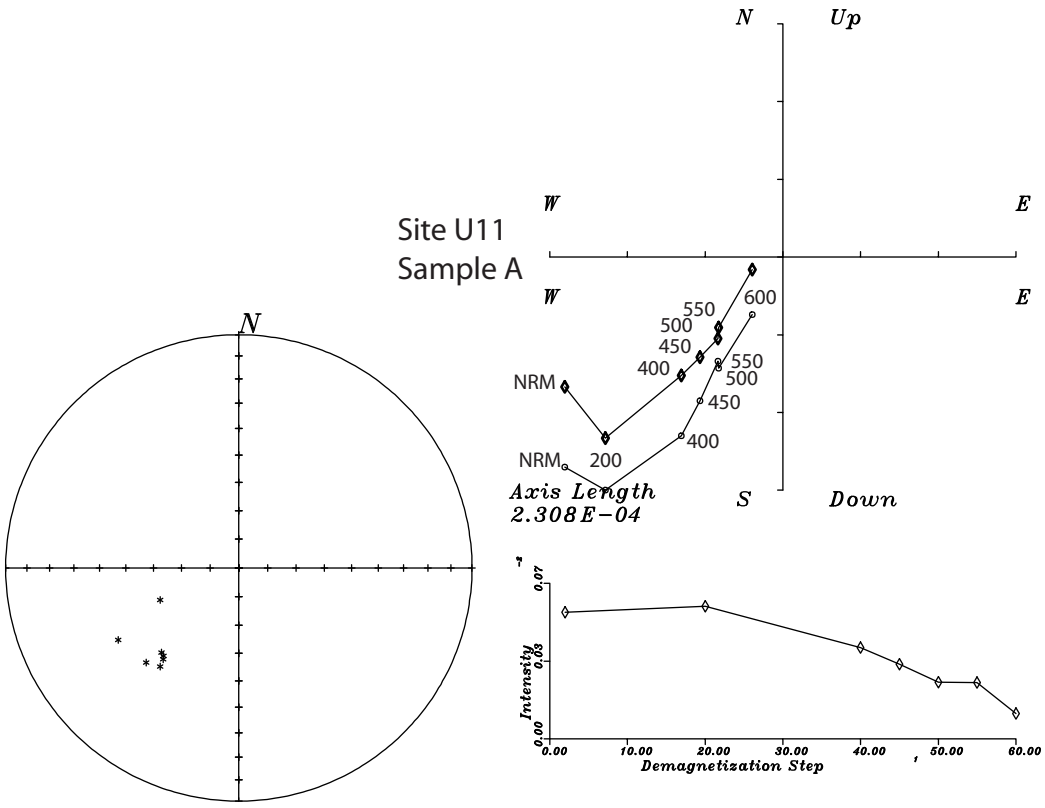

samples, a low stability discordant component was evident between the Natural remanent magnetism (NRM) and 200°C heating step (e.g. Fig. 4.4 lower sample), which was not included in PCA. Occasionally, a secondary vector component was observed in later thermal heating steps, often corresponding with an increase in total intensity. This may represent the formation of ferromagnesian minerals during the thermal cleansing process**,** and was also not considered in the PCA. The maximum angular deviation (MAD) of the best-fitting line was calculated as a measure of the precision of PCA. Samples with MAD>20° (n=6) were considered to be of questionable precision and subsequently not included in statistical classification (c.f. Butler, 1992). Stepwise data for each sample is given in appendix iv.

Site-mean paleomagnetic vector directions were calculated for samples with small maximum angular deviations from the preferred linear segment by employing Fisher probability distribution (Fisher, 1953). The resultant vector length (R), Watson (1956) criteria for non-randomness, and vector orientation from visual inspection of Zidjerveld diagrams were used to classify sample sites according to the following scheme: Class 1: $N \geq 3$, $R \geq 2.62$; Class 2a: $N=3$, $R<2.62$, but sample orientation not in doubt; Class 2b: $N=2$, $R>1$, vectors oriented to same polarity; Class 3: $N \leq 3$, one sample is discordant; and Class 4: data inconsistent between samples. Out of the 42 sampled sites, 18 sites are class 1, 8 sites are class 2, and 10 sites are class 3. The remaining sites gave ambiguous results, were designated as class 4 and rejected from further consideration.

Virtual geomagnetic pole (VGP) latitude was calculated from mean principal magnetic vector directions, assuming a site paleolatitude of S 31.5° (e.g. South American latitudes have not significantly varied since the Miocene, cf. Hartley *et al.*, 1992). Table 4.2 summarizes the resultant paleomagnetic statistics for the sites,

including the estimated precision parameter (k) and α_{95} confidence limit (after Butler, 1992).

It is noteworthy that the statistical significance of the Mogna and El Corral Formation magnetic samples diminishes upsection corresponding with decrease in fine-grained interbeds suited for sampling. From the base of the Mogna Formation until ~300 m in the section (see Table 4.2), most of the sample sites are class 1 quality. Above ~300 m, a greater percentage of class 2 and 3 samples are observed. One possible explanation for the discordance of some samples from a univectorial decay of NRM toward the origin is pedogenic overprinting. For example, Ojha *et al.* (2000) found that paleosols and sandstones of the Neogene of western Nepal gave erratic vector results during thermal demagnetization in comparison to well-laminated, nonpedogenic siltstone. As mentioned, pedogenic alteration affected virtually all of the finer-grained interbeds of the lower Mogna Formation, and the thin, nonpedogenic mud drapes of the uppermost section lack adequate lithification for paleomagnetic sampling. Paleosols may not be typically preferred for paleomagnetic analysis, but Tauxe and Badgley (1988) obtained coherent data from hematite-rich Neogene paleosols from Pakistan, and suggested that the paleosols' hematite pigment is an effective carrier of chemical remanent magnetism. Unfortunately, the paleosols of Lomas De Las Tapias are not abundantly oxidized, suggesting a low level of hematite. This is supported by the intensity decay behavior of the samples, which was almost zero by 600°C, below the Curie temperature of hematite (680°C).

Another possible source of randomness in the upper Mogna Formation paleomagnetic analyses is the inclusion of sand- or small granule-size grains in some of the upper section's sampled interbeds. Each clast has its own characteristic remanent magnetism inherited from its own lithification and subsequent exposure history. These upper Mogna interbeds are also more weathered and may contain more

Table 4.2: Summary of paleomagnetic data for Mogna and lower El Corral Formations, Lomas de las Tapias, Ullúm, Argentina. Classification based on criteria of Fisher (1953) and Watson (1956).

Sample	Meters from base	N	R value	K value	alpha 95	Class	VGP latitude	Polarity
B5	0	4	3.92	39.18	11.18	1	7.85	N
B4	61	4	3.88	24.16	14.24	1	-14.95	R
B3	94	4	3.64	8.23	24.40	1	-25.37	R
B2	111	4	3.83	17.73	16.62	1	27.42	N
B1	131	4	2.85	2.60	43.40	1	28.04	N
U1	153	3	2.87	15.48	20.54	1	-55.07	R
U2	170	3	0.99	0.99	81.06	3	-74.68	R
A5	195	3	2.79	9.64	26.04	1	8.38	N
U5	221	3	2.92	26.00	15.85	1	6.03	N
U6	243	3	2.97	58.11	10.60	1	23.50	N
B6	251	4	3.94	53.10	9.61	1	-78.33	R
U7	260	3	1.31	1.18	74.29	3	-12.77	R
U8	266	3	2.75	8.11	28.38	1	2.07	N
U2P	286	3	2.66	5.91	33.24	1	33.34	N
U9	299	3	1.18	1.10	77.12	3	-24.44	R
B7	302	4	3.97	111.50	6.63	1	-35.24	R
U3P	309	3	0.38	0.76	92.43	3	-11.70	R
U10	318	2	1.98	61.49	12.62	2b	-51.71	R
U11	333	3	1.02	1.01	80.33	2a	-6.61	R
U12	345	3	0.42	0.77	91.88	3	26.16	N
U5p	362	3	2.05	2.10	55.74	3	-4.70	R
U13	372	2	1.89	9.36	32.36	2b	-31.60	R
U6P	380	2	1.89	9.40	32.28	2b	-25.25	R
U14	388	3	0.97	0.98	81.53	3	-53.54	R
U14P	402	3	2.63	5.41	34.74	1	32.32	N
A3	433	3	2.90	19.07	18.51	1	-64.71	R
U15	437	3	2.42	3.47	43.39	3	22.10	N
A4	463	3	2.95	43.67	12.23	1	8.11	N
U16	472	2	1.91	11.68	28.97	2b	-10.57	R
U17	501	3	1.37	1.23	72.92	2a	4.45	N
A1	517	4	3.92	39.50	11.14	1	28.66	N
A2	581	3	1.78	1.63	63.22	3	39.71	N
U18	584	3	0.71	0.87	86.53	2a	-84.47	R
U19p	595	2	1.99	195.17	7.09	2b	-84.80	R
U19	607	3	1.43	1.28	71.53	3	-18.75	R
U20	628	4	3.15	3.53	37.26	1	-18.85	R

Class 1	18
Class 2a	3
Class 2b	5
Class 3	10
Class 4	0

oxidized ferromagnesian minerals or chemical remanent magnetism, interfering with the determination of the rock's primary magnetic component (Butler, 1992).

Preferred correlation:

The previous local polarity section at Ullum (Bercowski *et al.*, 1986) was anchored by a tuff dated 7.0± 0.9 Ma by fission track analysis of zircon grains, and these workers' preferred correlation generally matches the reversal pattern of the GPTS between 9.0 and 5.89 Ma (Fig. 4.3). However, several global reversals were not observed in the local section. This is probably due to the coarse sample spacing (20-30 m) and relatively coarse grain size as well as observed unconformities (channel bases) within the sandy Lomas de las Tapias Formation. We collected bentonite in the stratigraphic vicinity of the 7.0± 0.9 Ma tuff (Figure 4.3) in the hopes of future improved confidence in the Bercowski *et al.* (1986) correlation.

The local polarity reversals of the Mogna and lower El Corral Formations are shown in Figure 4.5. Polarity was assigned by assessing the sign as well as the magnitude of calculated VGP latitude and by consideration of site class. Calibration to the previous magnetostratigraphy is straightforward, because our sampled section overlaps with the upper 150 m of the Bercowski *et al*. (1986) section and the lowest three polarity zones are coincident. Thus, the base of our section is correlated to normal chrons 3An.1n and 3An.2n of the GPTS (6.57 – 6.27 Ma and 6.14-5.89 Ma). The remainder of our section reveals a pattern of reversals comparable to the GPTS pattern. A short normal excursion between 339 and 354 m in the section (Fig. 4.5) was not correlated to the GPTS because it is defined by a single Class 3 site. Similarly, a reversal at 480 m, defined by only one Class 2 site with low VGP latitude, is not considered in the local pattern. Most informative, however, is the recognition of a long normal chron between 435 m and 583 m in the section (Fig. 4.5; reversals assigned halfway between sites of opposite polarity). This normal zone and the four reversals

tributaries within the Precordillera contributed variable amounts of sediment to the trunk streams through time (Milana, 1991 and unpublished data).

Magnetic polarity stratigraphy has been a very effective chronologic tool in the Andean foreland basins of Argentina (Johnson *et al.*, 1986; Beer, 1990; Jordan *et al.*, 1990; Reynolds *et al.*, 1990; Ré *et al.*, 2003). Accurate detection of polarity reversals for stratigraphic age correlation depends foremost on preservation and recovery of natural remanent magnetism in sediments at the time of their lithification. Definition of the magnetic polarity history also depends on availability of samples spaced in a stratigraphic column such that the positions of all (or most) polarity reversals are well located. Typically, reconnaissance sampling of relatively unweathered fine-grained sediments at fixed intervals through a stratigraphic column is conducted for preliminary magnetostratigraphy. Subsequently, sampling between selected initial sites provides higher-resolution polarity determination. Logistically, these steps are not always possible, as outcrops may be inaccessible or of unsuitable lithology or quality for sampling. The coarsening-upward nature of the Ullum section (Mogna and El Corral Formations) largely dictates the sampling scheme: fine-grained units low in the section are more suitable for paleomagnetic analysis than are the conglomeratic upper Mogna and El Corral Formations, which consist of minimal and often unconsolidated inter-channel mudstone, confounding uniform spacing. Whether or not a high percentage of the earth's changing magnetic polarity is captured in the local strata ("polarity completeness", e.g. Beer, 1990) depends on stratigraphic completeness (e.g. minimal erosion, net aggradation), but more so on accumulation rate. Talling and Burbank (1993) warned that for low rates of sediment accumulation (e.g. <5 cm/ky), shorter-duration subchrons (<100 ky) of the Geomagnetic Polarity Time Scale (GPTS) may not be represented in the local magnetostratigraphy. Based on the magentostratigraphy of Bercowski *et al.* (1986), accumulation rates for the Lomas

Figure 4.5: Preferred correlation of upper Mogna and lower El Corral Formations at Ullúm, Argentina to GPTS of Cande and Kent (1995).

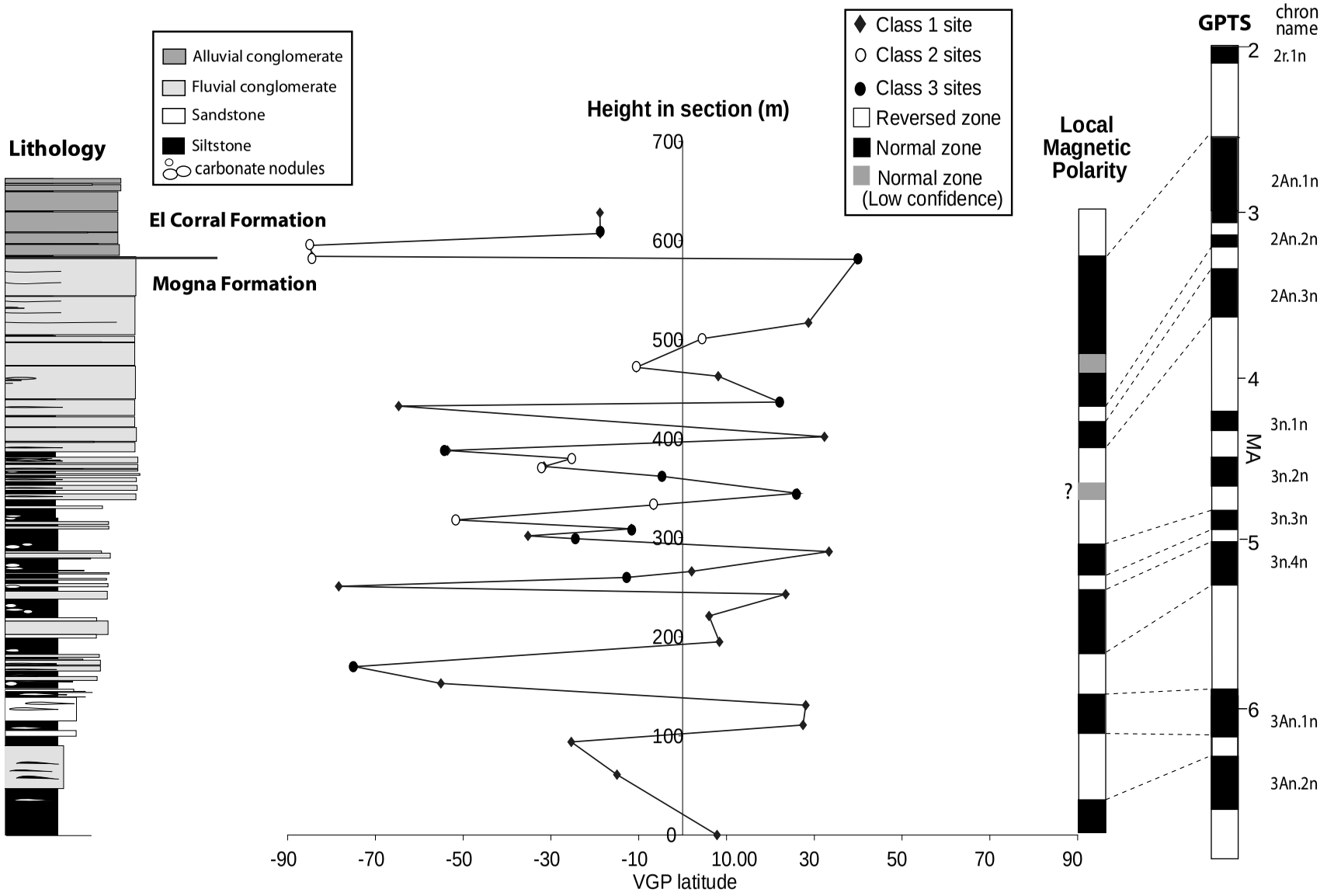
Lithology
Alluvial conglomerate
Fluvial conglomerate
Sandstone
Siltstone
carbonate nodules
El Corral Formation
Mogna Formation
Height in section (m)
700
600
500
400
300
200
100
0
-90
-70
-50
-30
-10
10.00
30
50
70
90
VGP latitude
Class 1 site
Class 2 sites
Class 3 sites
Reversed zone
Normal zone
Normal zone (Low confidence)
Local Magnetic Polarity
?
GPTS
chron name
2
2r.1n
2An.1n
3
2An.2n
2An.3n
4
3n.1n
3n.2n
3n.3n
5
3n.4n
6
3An.1n
3An.2n
MA

below it are comparable to GPTS chrons 2An.3n through 2An.1n. Our local polarity section concludes in a reversed zone. Thus, the upper limit of correlation is at the top of normal chron 2An.1n, or 2.58 Ma, which occurs at the base of the El Corral Formation and is well constrained between samples only 3 meters apart (A2 and U18, see Table 4.2) with highly opposed VGP latitudes.

Accumulation rates for Mogna Formation:

An outcome of this magnetostratigraphy is the determination of a near-constant long-term rate of sediment accumulation, despite the observed degree of lithologic variability. Figure 4.6 illustrates the age of global polarity reversals compared with their correlated height in the section as well as the positions of major lithologic changes. This rate of accumulation (from compacted column heights) is remarkably linear with respect to time over the period 9 – 2.8 Ma, averaging 19 cm/k.y. (R^2=0.93). Rates were somewhat higher between 7.3 and 6.1 Ma, averaging ~41 cm/k.y. during that time interval. During the stratigraphic interval characterized by mature calcic pedogenesis (6.6 – 4.8 Ma), rates of accumulation slowed somewhat, averaging 17 cm/ky before accelerating with the onset of stacked channelized conglomerates ~4.8 Ma. However, variations in rate are not pronounced, despite the major transitions in sedimentation upsection. This is in accord with the observations of Beer (1990) from highly complete stratigraphic and paleomagnetic sections in the proximal Bermejo Basin: lithofacies changes and sedimentation rates need not be related. Though potential exists for circular arguments, it is suggested that the local polarity correlation with the GPTS represents a "best-fit accumulation rate-dependent correlation", assuming that the least variant accumulation rate trend is probably correct (Talling and Burbank, 1993).

The decrease in paleosol thickness and calcareous accumulations upsection amid thicker conglomerate beds appears to be consistent with the expected inverse

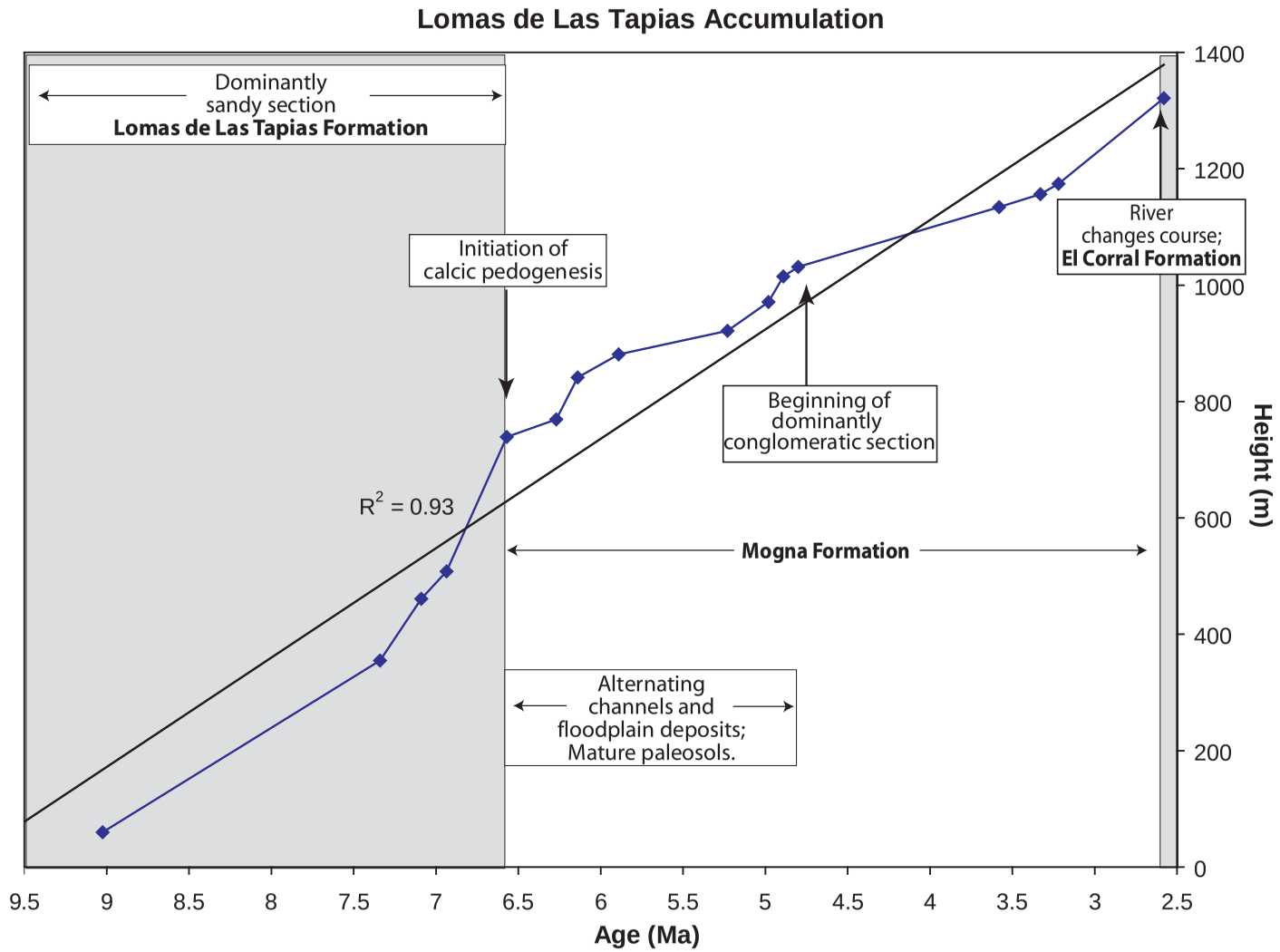

Figure 4.6: Accumulation rate curve for Mogna and lower El Corral Formations at Lomas de Las Tapias.

relationship between rate of fluvial accumulation and pedogenesis (e.g. Kraus, 1987), and the onset of calcic pedogenesis in the lower Mogna formation corresponds with a decrease in accumulation rate (Fig. 4.6). The chronologic data, however, show that the rate of accumulation of the lower paleosol-rich interval was slightly faster than the upper paleosol-poor interval.

Paleosol Carbonate Stable Isotopes:

Based on the preferred paleomagnetic correlation (Figure 4.5), the sampled pedogenic interval corresponds to the time range 6.37 to 2.9 Ma. This duration represents the extent of calcic pedogenesis observed at Lomas de Las Tapias. The $\delta^{13}C$, $\delta^{18}O$ and weight percent inorganic carbon data are summarized in Table 4.3 and Figure 4.7.

Both isotopic series for the Mogna Formation paleosol carbonates are depleted relative to the Peedee belemnite (PDB) standard. Pedogenic $\delta^{13}C$ values range widely from -14.34‰ to -4.17‰. The range of $\delta^{18}O$ values is slightly less, from -11.74‰ to -3.93‰ (Table 4.3).

Two trends are evident in the $\delta^{18}O$ time series: pronounced isotopic depletion from 6.37 to 5.38 Ma and subsequent gradual enrichment (Fig. 4.7). The $\delta^{18}O$ values markedly decrease from -3.93 to -11.74‰ (linear R^2=0.84). Except for a brief period of enrichment (5.0-4.95 Ma), the long-term trend from 5.38-2.9 Ma is slow enrichment of ~2‰.

The $\delta^{13}C$ time series exhibits a degree of cyclicity (Fig. 4.7). The series displays two intervals of marked depletion (6.0 – 5.7 Ma, 5.0 – 4.2 Ma) prior to re-enrichment to values generally between -8 and -5‰. Arguably, the period and degree of depletion of the cycles decreases through time, although this may be an artifact of the coarse sample spacing upsection. Whereas the $\delta^{18}O$ time series exhibits marked enrichment at 4.95 Ma, $\delta^{13}C$ values underwent concurrent depletion.

Table 4.3: Stable isotopic and weight percent inorganic carbon from pedogenic carbonates, Mogna Formation, Ullúm, Argentina. Ages assigned by linear interpolation with magnetostratigraphy of Bercowski *et al.* (1986) and this study. Height in section refers to start of this study's measured section, labeled in Figure 4.3

SAMPLE ID	Age (MA)	Height (m)	δ^{13}C (PDB)	δ^{18}O (PDB)	Wt. %C
BR05-18	2.90	508.5	-10.391	-9.498	3.915
BR05-17	2.90	508	-6.293	-8.721	3.850
BR05-16	2.92	504	-9.533	-7.941	3.220
BR05-16 dup	2.92	504	-9.765	-7.954	3.475
BR05-15	3.26	428	-5.609	-9.291	4.812
BR05-14	3.31	421	-8.238	-9.864	5.911
BR04-66	3.37	414	-4.172	-6.060	N/A
BR05-13	3.49	403	-11.389	-9.244	4.378
BR05-12	3.60	393	-8.882	-9.604	5.615
BR05-11	3.72	383	-10.554	-9.946	5.016
BR04-65	3.96	363	-5.815	-7.592	N/A
BR05-10	3.97	362	-6.979	-10.529	5.514
BR05-9	4.12	350	-7.373	-10.447	3.752
BR05-8	4.21	342	-11.146	-10.113	1.476
BR04-64	4.50	318	-6.916	-8.701	N/A
BR05-7	4.85	299	-14.336	-10.834	5.819
BR04-63	4.95	270	-8.353	-5.177	N/A
BR05-6	4.95	258	-13.142	-11.369	4.522
BR04-62	5.00	243	-5.431	-7.271	N/A
BR05-5	5.01	238	-6.252	-10.996	4.574
BR05-4	5.29	179	-7.064	-9.427	4.103
BR05-2	5.38	173	-9.612	-11.738	5.056
BR05-3	5.43	170.4	-7.360	-10.848	5.433
BR05-1	5.68	155	-13.591	-11.422	6.129
BR04-61	5.71	153	-8.152	-9.809	N/A
BR05-19	5.97	129	-14.331	-8.157	4.204
BR05-20	6.15	96	-6.085	-7.574	3.048
BR05-21	6.17	87	-9.203	-7.920	3.360
BR05-22	6.18	77	-7.581	-8.009	3.304
BR05-23	6.20	71	-5.790	-7.121	5.253
BR05-25	6.21	63	-4.959	-8.851	2.668
BR05-24	6.21	62	-8.759	-5.423	2.515
BR05-26	6.24	45	-7.489	-6.601	3.279
BR05-27	6.37	20	-6.941	-3.929	1.728

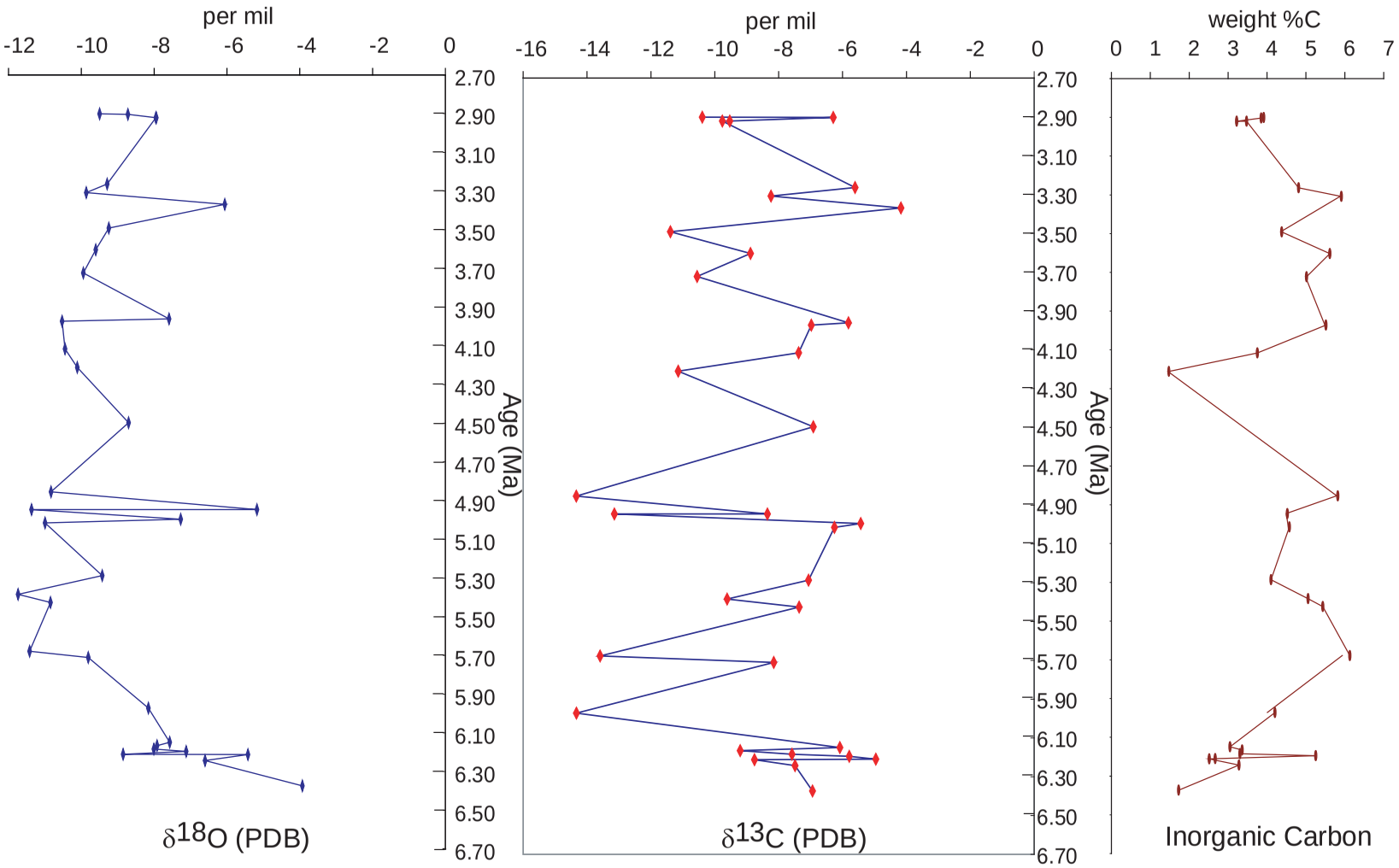

Figure 4.7: Stable isotopic time series and weight percentage of inorganic carbon from pedogenic carbonates, Mogna Formation, Lomas de Las Tapias, Argentina.

Finally, the weight percent of inorganic pedogenic carbonate also displays a cyclic trend, although poorly correlated with the stable isotopic time series. Between 6.4 and 5.6 Ma, the elemental abundance increases steadily from 1.7 to 6.1% (Fig. 4.7). This may suggest greater atmospheric or detrital influx of carbonate dust. With the exception of a large decrease at 4.2 Ma, values from 5.6 to 2.9 Ma are close to the mean value of 4.1%.

Discussion

A challenge for interpreting paleoclimate from the proxy data from paleosol analyses is distinguishing the source of signal variation. The preserved paleoclimate signal from Mogna Formation paleosols may reflect one or several of three controls: (1) Local hydrologic variability related to proximity to and longevity of stable trunk drainages; (2) Regional hydrologic variability ultimately related to uplift of the Frontal Cordillera; (3) Global climate change. The evidence for or against these controls are discussed below.

1. *Local climate control:*

The degree of pedogenesis within Mogna Formation (e.g. compound, calcic soils) implies periods of landscape stability on a well-drained floodplain experiencing low rates of sedimentation. This was the case between times of avulsions of the main drainage, reflected by channelized conglomeratic lenses. However, floodplain sediments and soils were undoubtedly impacted by groundwater fluctuations and variable sedimentation rates as the river system evolved, fluctuations that are likely to be reflected in the stable isotopic time series.

The Ullum $\delta^{13}C$ time series suggests fluctuating biomass and by inference, local humidity. Periods of depleted values (<-8‰) were likely periods of mixed C_3 and C_4 biomass (Wang *et al.,* 1993) and thus variable soil humidity on the floodplains, probably reflecting proximity of the groundwater level. The brief excursions toward

$\delta^{13}C$ values >-8‰ reflect increased proportions of C_3 biomass adapted to arid conditions and an increased proportion of C_4 biomass. As mentioned, shifts in $\delta^{13}C$ values from their mean are less pronounced through time. It is suggested that as the drainage system became better established in space, the local groundwater and soil water conditions correspondingly became more homogeneous, resulting in a more stable local ecology. This is supported by time series of $\delta^{18}O$ values (whose fractionation reflects local variables such as soil temperature, evaporation and differential infiltration) and the weight percentages of inorganic carbon of the carbonate nodules, both of which appear to homogenize upsection.

2. *Regional climate control:*

A region's climate includes not only the absolute values of temperature and precipitation, but also how they are seasonally distributed (seasonality). Restricting our discussion to precipitation, both the amount and seasonality of precipitation reflect boundary conditions such as latitude, prevailing wind directions, moisture sources and barriers to atmospheric circulation. Variable discharge could be purely tectonic (as a result of uplift and reconfiguration of the drainage divide between Atlantic and Pacific basins), purely climatic (e.g. glacial cyclicity), or more likely, a combination of the two (e.g. increased orographic precipitation and mountain glacier formation in response to tectonic increases in elevation). These features are regional and thus one might attempt comparison to extrabasinal paleoclimate proxies.

For Ullum, we have at our disposal information from contemporaneous strata of the Iglesia Basin which probably responded similarly to source area hydrologic variability (see above). In both basins, calcic paleosol development diminished through time, reflecting either locally high rates of sedimentation compared to rates of pedogenesis or regional climates under which precipitation exceeded evapotranspiration (e.g. Kraus and Aslan, 1993; Retallack, 2001). Causes of

sedimentation rate change, however, can be difficult to correlate between stratigraphic sections and basins. Therefore, a more informative comparison is the basins' $\delta^{18}O$ time series.

The pedogenic carbonate $\delta^{18}O$ time series from Ullum is compared regionally with that obtained from calcic paleosols of the Iglesia Basin during the time interval 6.4 to 4.6 Ma (Figure 4.8; see also chapter 3). The two $\delta^{18}O$ time series display similar long- term cycles. Both basins reveal a trend toward greater depletion from 6.4 to ~5.4 Ma. Note that this is prior to the spatial establishment of the trunk river at Ullum (sometime between 4.8 and 3.6 Ma). After 5.4 Ma, both time series show progressive enrichment of $\delta^{18}O$. Long-term enrichment continues for the Ullum isotopic record until the youngest calcic paleosols at 2.9 Ma.

The dynamics of $\delta^{18}O$ fractionation can reflect large-scale features affecting meteoric water such as continentality, latitude, air temperature and seasonality of precipitation (Mermut *et al.,* 2000; Nordt *et al*., 2003). The combined effect of these variables was geochemically modeled by Mack and Cole (2005) whereby $\delta^{18}O$ of pedogenic carbonate is a function of absolute latitude. Though the suitability of this geochemical model for paleoclimate reconstruction is not well established, it provides a starting point for comparison of present and past $\delta^{18}O$ systems. Assuming that the paleolatitudes of the sample sites were similar to the present (~S 30° for Iglesia, S 31.5° for Ullum), we can compare the measured $\delta^{18}O$ mean and range of values to Mack and Cole's (2005) modeled fields of summer and winter precipitation (Figure 4.9). The mean value for the 34 Ullum samples is -8.76‰ vs. PDB (standard deviation = 1.91‰) and is firmly within the field of winter season precipitation. However, the most enriched values (~6.4-6.2 Ma, ~5.0 Ma) overlap with the summer precipitation field. Similarly for Iglesia, the mean value of -6.49‰ vs. PDB (n=92, s.d. =2.34‰) implies winter precipitation but the range of data could indicate a

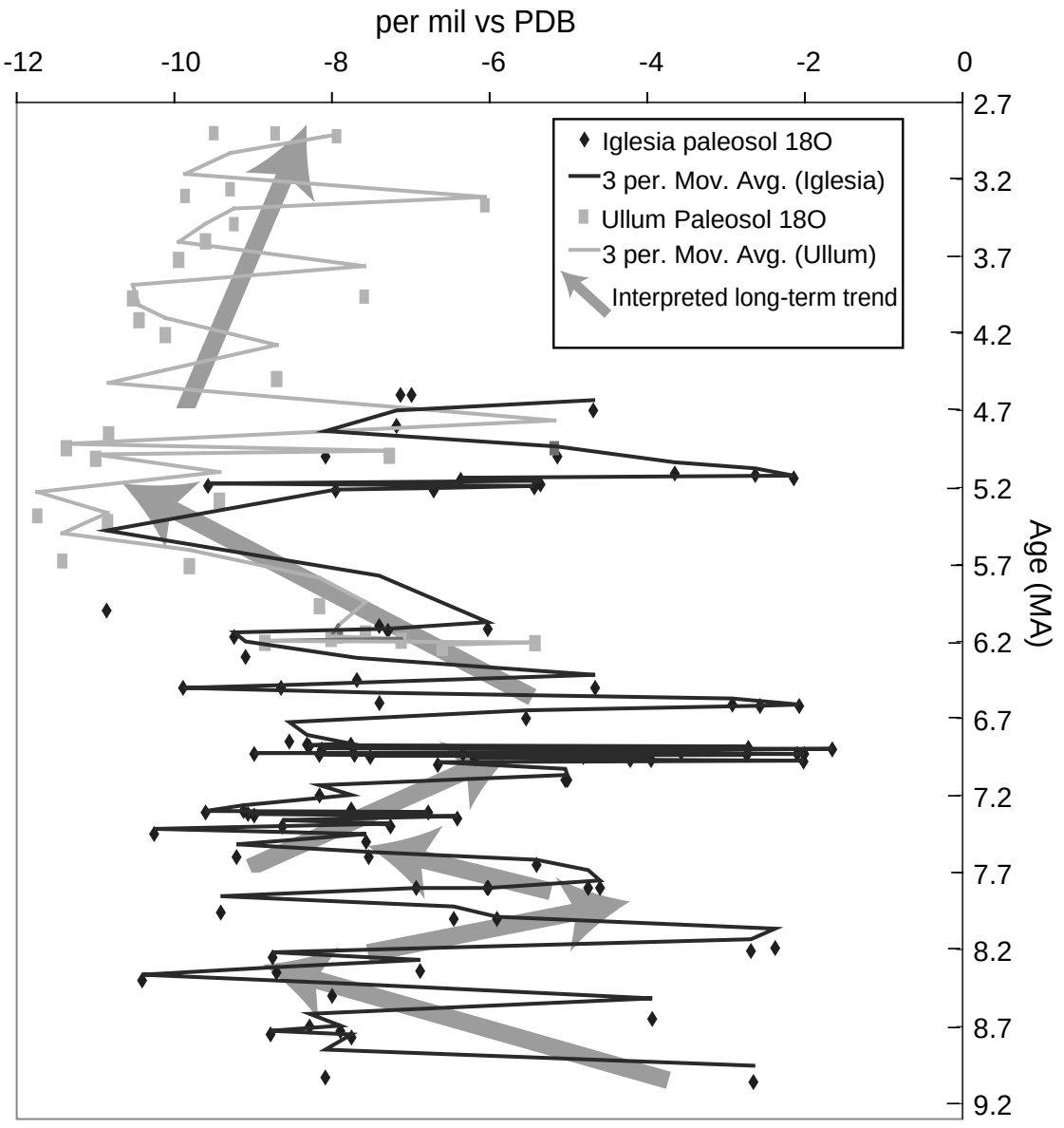

Figure 4.8: Comparison of pedogenic carbonate stable isotopic values from Iglesia Basin (S 30° - 30.5°, W 69° - 69.5°) and Ullum section (S 31.5° W 68.5°). Lines between data points represent three-point moving averages. Arrows indicate interpreted trend.

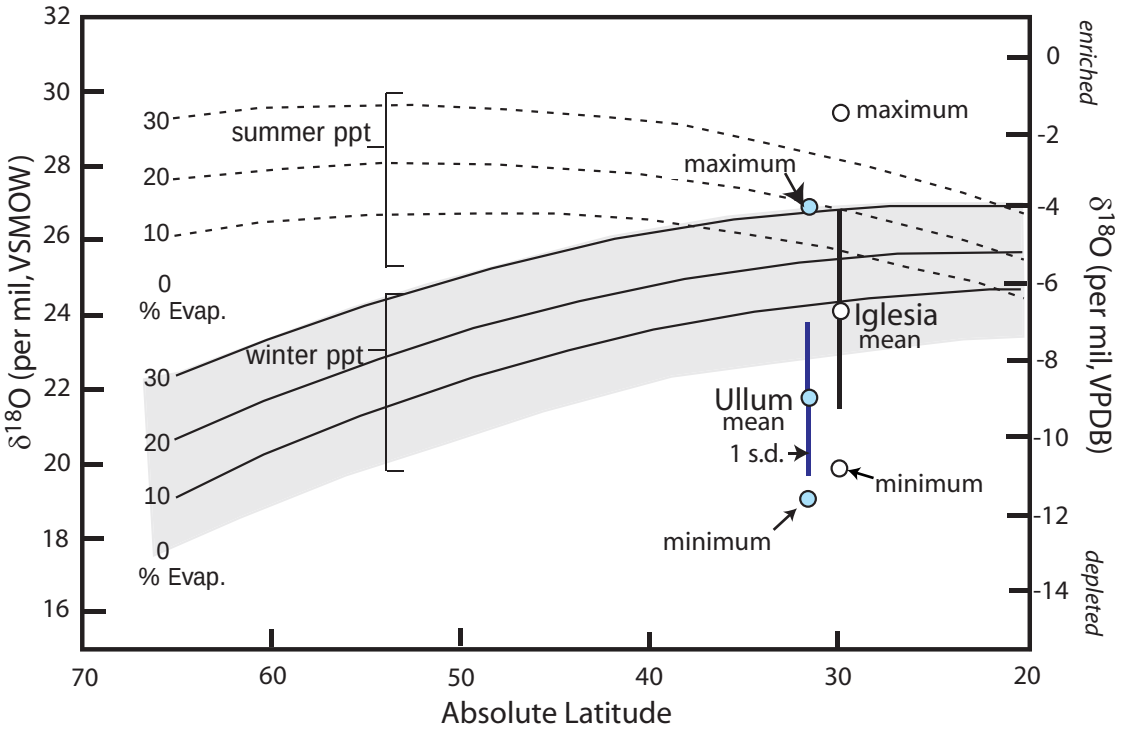

Figure 4.9: Comparison of observed $\delta^{18}O$ values from Mogna Formation pedogenic carbonates of Ullum locality and Iglesia Group pedogenic carbonates from Iglesia Basin with latitudinally-dependent geochemical model of Mack and Cole (2005; modification of Fig. 1B).

mixture of both summer and winter precipitation (see also Chapter 3). It is plausible that through time the seasonality of precipitation changed from dominantly summer season to winter season (Fig. 4.8).

Topographic uplift of the Frontal Cordillera during the Late Miocene and Pliocene (see Table 2.1) would have uplifted air and the Pacific-derived moisture, enhancing Rayleigh distillation and orographic rain-out of ^{18}O of precipitation falling in the Andean headwaters area, and resulting in a depleted ^{18}O signal in the pedogenic carbonate time series (e.g. Poage and Chamberlain, 2001). Relative abundances of detrital clay minerals from Iglesia Basin paleosols implicate a period of increased weathering in the source area 6.75-5.2 Ma (see chapter 3),and by inference, increased precipitation, which could also have affected the $\delta^{18}O$ depletion in the interval 6.4 to 5.4 Ma at Ullum and Iglesia Basin (Fig. 4.8). Variable discharge in the headwaters could be purely tectonic (as a result of uplift and reconfiguration of the drainage divide between Atlantic and Pacific basins), purely climatic (e.g. glacial cyclicity), or more likely, a combination of the two (e.g. increased orographic precipitation and mountain glacier formation in response to tectonic increases in elevation).

However, after 5.4 Ma, the long-term trend is enrichment of $\delta^{18}O$ (less negative values). This enrichment can be interpreted as climatic aridification or evaporative enrichment (e.g. Cerling and Quade, 1993; Grootes, 1993). This is supported by the preservation of Late Neocene geomorphic features without evidence of glacial erosion in the Frontal Cordillera between S 29° 20’ and S 30° 30’, suggesting that the area was an arid intermontane plateau during the Late Miocene (Bissig *et al.*, 2002).

3. *Global climate change:*

Global climatic variation during the Late Cenozoic may also have led to the observed long-term $\delta^{18}O$ enrichment of Ullum paleosols younger than 5.4 Ma.

Isotopic fractionation of pedogenic calcite responds to mean annual air temperature and seasonal insolation and precipitation (e.g. Nordt *et al.*, 2003). These conditions were likely changing during the Late Miocene and Pliocene, as inferred from sea surface temperature records (Zachos *et al.*, 2001). A $\delta^{18}O$ enrichment of about 3‰ relative to modern ocean water has been attributed to global cooling, which led to expansion of ice in West Antarctica (Zachos *et al.*, 2001). Closer to the study sites, global cooling may have also triggered South American glaciations recognized by deposits in Patagonia, Argentina (~47°S) and Bolivia (~16°S) during the past 6 Ma (e.g. Mercer, 1983; Rabassa *et al.*, 2005). Though Miocene and Pliocene mountain glaciations in the Central Andes are purely speculative, it is probable that the global cooling reflected by glaciations north and south of the study sites also affected the paleoclimate signal of the pedogenic carbonates. During glaciations, delivery of water from the headwaters to the Río Jachal and Río San Juan would have been impeded, perhaps reflected in the enriched $\delta^{18}O$ values from pedogenic carbonates which suggest drier conditions at Ullum and in Iglesia Basin.

Paleoclimate synthesis:

On the basis of the above macroscopic and isotopic datasets, it can be argued that the Mogna Formation paleosols reflect aspects of the global and regional paleoclimate signal concurrent with their deposition. Yet the dynamics of the local hydrologic system were clearly changing (e.g. Milana *et al.*, 2003) and certainly affected pedogenic development. The coincidence of isotopic homogenization and decreasing paleosol maturity with the spatial stabilization of the main paleodrainage post 4.8 Ma suggests, therefore, that the main paleoclimatic signal is that of local variation in humidity related to fluvial dynamics of the paleo-San Juan. Note that enrichment at Ullum is remarkably regular despite the multiple interactions affecting $\delta^{18}O$ fractionation. This contrasts with the signal from Iglesia basin, which, while

coincidentally enriched, is enriched by a greater extent over a shorter period and exhibits greater intersample variability (Fig. 4.8).

Paleo-drainage system:

The new paleomagnetic data refines the temporal history of the shifting location of the paleo-San Juan river system. At 6.6 Ma, the river exited from the Central Precordillera at a position similar to today, ~30 km west-southwest of Ullum. However, due to the distal position on the alluvial fan system, the channel in the vicinity of Ullum varied markedly through time, until after 4.8 Ma (e.g. 390-450 m in right-hand column, Figure 4.3) when isolated channels and interbedded mature floodplain lithofacies transition to nested conglomeratic channel successions. At Sierra de Mogna, thin conglomeratic beds suggested initial encroachment of the braided river ~4.0 Ma (Milana *et al.*, 2003; Figure 4.10). This synchroneity of deposition of similar architecture at both Mogna and Ullum suggests multiple outlets from the Precordillera during the interval 4.0-2.6 Ma. Such a configuration represents an added complexity to the hydrologic model of Milana (1997) in which the paleo-San Juan River course was interpreted to shifted north through the Central Precordillera at ~4 Ma and deposit a point source alluvial fan at Sierra de Mogna.

At 2.6 Ma, Ullum's alluvial fan gravels (El Corral Formation) prograded over the abandoned fluvial channels of the upper Mogna Formation, concurrent with complete northward shift of the paleo-river to Mogna (Fig. 4.10). Although the Ullum section is not complete younger than 2.6 Ma, the Mogna location returned to bajada conditions <1.6 Ma, signaling the return of the Río San Juan to the Ullum area.

The cause of the shifting course of the paleo-San Juan River is uncertain, partially because its exact course through the Central Precordillera is unknown. Milana (1991 and unpublished data, 1996) postulated that the drainage reconfiguration and changes in clast provenance represent the tectonic evolution of the Precordillera

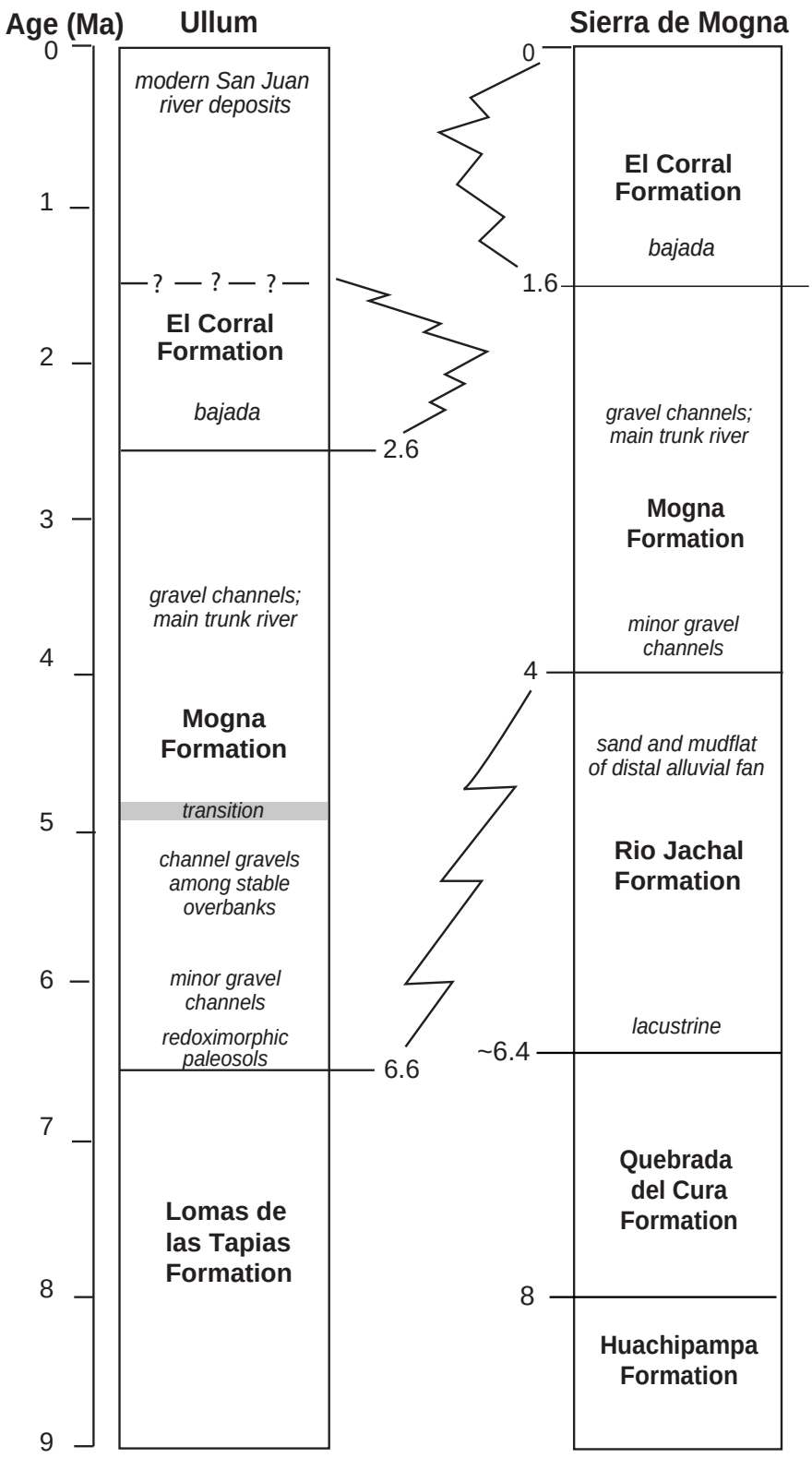

Figure 4.10: Temporal relationships of lithofacies between Ullum and Sierra de Mogna, San Juan Province, Argentina

and foreland basin system whereby thrust events would close drainage passes and change the course of the river through intermontane valleys while tributaries would be progressively captured and only a few trunk rivers (e.g. Rio Jachál and Rio San Juan) would exit the thrust belt. Yet, the contributions of such drainages to Mogna Formation deposition are uncertain. One option is that the initial conglomeratic deposits at Sierra de Mogna (~4.0 Ma) represent a drainage independent to the San Juan River system (possibly even the ancestral Río Jachál). This is proposed because of the considerable temporal overlap of supposed Rio San Juan deposition at both Sierra de Mogna and Ullum (4.0 – 2.6 Ma) which does not fit well with a thrust-related or geomorphic diversion of the trunk river at 4 Ma (cf. Milana *et al.*, 2003). Alternatively, on the basis of lateral interfingering of Mogna Formation deposits at sections along Sierra de Mogna (Milana *et al.*, 2003), it is possible that 4.0 – 2.6 Ma, a large alluvial fan centered near Ullum contributed variable amounts of sediment to northern distributary channels near Sierra de Mogna. In this case, a parallel river system through the Precordillera exiting near Sierra de Mogna is unnecessary, though a large-scale shift (probably tectonically-related) of the trunk stream's course at 2.6 Ma is still required.

Conclusions:

New paleomagnetic analyses of the Mogna and El Corral Formations exposed in the Lomas de Las Tapias (Departamento de Ullum, San Juan Province, Argentina) expand and complete the temporal record of this section from 9.0 Ma to 2.6 Ma, longer than previously interpreted (c.f. 4 Ma, Milana *et al.*, 2003). The transition between Mogna and El Corral formations is correlated as 2.6 Ma, and corresponds with the termination of paleo-Rio San Juan River at Ullum. Characteristics of interbedded paleosols and stable isotopic values of pedogenic carbonate nodules reveal fluctuations in local and perhaps regional hydrology through the Iglesia-

Calingasta Valley from 6.4 to 2.9 Ma. For strata representing 6.4 to 4.8 Ma, paleosol maturity and association with fluvial lithofacies suggest a period of landscape stability and hydrologic variability. Between 4.8 and 3.6 Ma, the main trunk stream of the fluvial system and local ecology became spatially established and paleoclimate variability correspondingly diminished.

Acknowledgements:

Financial support for this project was provided by American Chemical Society Petroleum Research Fund grant #39557-AC8 to T.E. Jordan. Laboratory usage and paleomagnetic expertise kindly provided by William Harbert. Rodrigo Morilla conducted invaluable fieldwork and was of great assistance during paleomagnetic measurements. Juan Pablo Milana guided sedimentologic observations in the field and established the physical stratigraphic ties between previous sections and our own. Thanks to Arthur Kasson (Cornell University Stable Isotope Laboratory) for coordinating analyses.

References:

Beer, J.A., 1990, Steady sedimentation and lithologic completeness, Bermejo Basin, Argentina: *Journal of Geology*, Vol. 98, p. 501-517.

Bercowski, F., Berenstein, L.R. de, Johnson, N. and C. Naeser, 1986, Sedimentología, magnetoestratigrafia y edad isotópica del Terciario en Lomas de las Tapias, Ullum, Provincia de San Juan: *Primero Reunión Argentina de Sedimentología*, La Plata, Actas, 169-172.

Bercowski, F., Ruzycki, L., and N.M. Johnson, 1987, Litofacies y paleoambiente del Terciario en Lomas de las Tapias, Ullum, Prov. de San Juan, Argentina: *Decimo Congreso Geologico Argentino,* San Miguel de Tucuman, Actas II, p. 101-104.

Bissig, T., Lee, J.K.W., Clark, A.H., and Heather, K.B., 2001, The Cenozoic history of Volcanism and hydrothermal alteration in the Central Andean Flat-Slab region: New ^{40}Ar-^{39}Ar constraints from the El Indio-Pascua Au (-Ag, Cu) Belt, 29° 20' – 30° 30' S: International Geology Review, Vol. 43, p. 312-340.

Bissig, T., Clark, A.H., and Lee, J.K.W., 2002, Miocene landscape evolution and geomorphic controls on epithermal processes in the El Indio-Pascua Au-Ag-Cu belt, Chile and Argentina: Economic Geology, Vol. 97, p. 971-996.

Butler, R.F., 1992, Paleomagnetism: magnetic domains to geologic terranes: Blackwell Scientific Publications, Boston, 319 p.

Cande, S.C., and D.V. Kent, 1995, Revised calibration of the geomagnetic polarity timescale for the Late Cretaceous and Cenozoic: *Journal of Geophysical Research*, v. 100, No. B4, p.6093-6095.

Cerling, T. E., and Quade, J., 1993, Stable carbon and oxygen isotopes in soil carbonates: *in* Stuart, P.K., Lohmann, K.C., McKenzie, J., and Savin, S., eds., Climate Change in Continental Isotopic Records, American Geophysical Union, Geophysical Monograph 78, 374 pp.

Contreras, V.H., 1981, Caracteristicas bioestratigraficas del Terciario de Lomas de las Tapias, Departamento Ullum, Provincia de San Juan: *VIII Congreso Geológico Argentino*, San Luis, Actas IV, p. 813-822.

Contreras, V.H., Damiani, O., Milana, J.P., Bracco, A., and Barrera, O.M., 1990, Paleógeno y Neógeno de San Juan: Relatorio de Geologica y Recursos Naturales de la Provincia de San Juan, Decimo Primer Congreso Geologico Argentino, San Juan, p. 154-187.

Fisher, R.A., 1953, Dispersion on a sphere: Proceedings of the Royal Society of London, Vol. A217, p. 295-305.

Gradstein, F.M., Ogg, J.G., Smith, A.G. et al., 2005, A Geologic Time Scale 2004: Cambridge University Press, 610 p.

Grootes, P.M., 1993, Interpreting continental oxygen isotope records *in* Stuart, P.K., Lohmann, K.C., McKenzie, J., and Savin, S., eds., Climate Change in Continental Isotopic Records, American Geophysical Union, Geophysical Monograph 78, 374 pp.

Hartley, A.J., Jolley, E.J., and Turner, P., 1992, Paleomagnetic evidence for rotation of the Precordillera of Northern Chile: structural constraints and implications for the evolution of the Andean forearc: Tectonophysics, 205, p. 49-64.

Irogoyen, M.V., 1997, Magnetic polarity stratigraphy and geochronological constraints on the sequence of thrusting in the Principal and Frontal cordilleras and the Precordillera of the Argentine central Andes (33°S latitude): Ph.D Dissertation, Carleton University, 392 p.

Johnson, N.M., Jordan, T.E., Johnsson, P.A., and Naeser, C.W., 1986, Magnetic polarity stratigraphy, age and tectonic setting of fluvial sediments in an eastern Andean foreland basin, San Juan Province, Argentina *in* Allen, P. and Homewood, P., eds, Foreland Basins: International Association of Sedimentologists, Special Publication, Vol. 8., p. 63-75.

Jordan, T. E., Rutty, P. M., McRae, L. E., Beer, J. A., Tabbutt, K., and Damanti, J. F., 1990, Magnetic polarity stratigraphy of the Miocene Rio Azul section, Precordillera thrust belt, San Juan province, Argentina: Journal of Geology, v. 98, p. 519-539.

Jordan. T.E, Drake, R.E., and Naeser, C.W., 1993, Estratigrafia del Cenozoico Medio en la Precordillera a la latitude del Rio Jachal, San Juan Argentina: XII Congreso Geológico Argentino, Actas Tomo II, p. 132-141.

Kraus, M.J., 1987, Integration of channel and floodplain suites, II. Vertical relations of alluvial paleosols: Journal of Sedimentary Petrology, Vol. 57, p. 602-612.

Kraus, M.J., and Aslan, A., 1993, Eocene hydromorphic paleosols: significance for interpreting ancient floodplain processes: Journal of Sedimentary Petrology, Vol. 63, p. 453-463.

Lal, R., and Kimble, J.M., 2000, Pedogenic carbonates and the global Carbon cycle *in* Lal, R., Kimble, J.M., Eswaran, H., and Stewart, B.A, eds., Global Climate Change and Pedogenic Carbonates, Lewis Publishers, p. 1-14.

Machette, M.N., 1985, Calcic soils of the southwestern United States *in:* Weide, D.L., ed., Soils and Quaternary Geology of the Southwestern United States: Geological Society of America Special Paper, 203, p. 10-21.

Mercer, J.H., 1983, Cenozoic glaciations in the Southern Hemisphere: Annual review of Earth and Planetary Sciences, Vol. 11, p. 99-132.

Mermut, A.R, Amundson, R., and Cerling, T.E., 2000, The use of stable isotopes in studying carbonate dynamics in soils, *in* Rattan, L., Kimble, J.M., Eswaran, H., and Stewart, B.A., eds., Global Climate Change and Pedogenic Carbonates: Lewis Publishers. p. 65-85

Miall, A. D., 1996, The geology of fluvial deposits. Sedimentary facies, basin analysis, and petroleum geology. Springer: Berlin

Milana, J.P., 1991, Sedimentología y magnetoestratigrafia de formaciones Cenozoicas en el area de Mogna y su insercion en el marco tectosedimentario de la Precordillera oriental: Tesis de doctorado, Universidad de San Juan, Argentina, 273 p.

Milana**,** J.P., 1997, El significado tectosedimentario de la formaciones Mogna y El Corral. *II Jornadas de Geología de Precordillera*, San Juan, pp. 148–153.

Milana, J.P., Bercowski, F., and Jordan, T.E., 2003, Paleoambientes y magnetoestratigrafía del Neógeno de la Sierra de Mogna, y su relación con la Cuenca de Antepaís Andina: Revista de la Asociación Geológica Argentina, Vol. 58, p. 447-473.

Nordt, L., Atchley, S., and Dworkin, S., 2003, Terrestrial evidence for two greenhouse events in the Latest Cretaceous: GSA Today, Vol. 13, p. 4-9.

Ojha, T.P., Butler, R.F., Quade, J., DeCelles, P.G., Richards, D., and Upreti, B.N., 2000, magnetic polarity stratigraphy of the Neogene Siwalik Group at Khutia Khola, far western Nepal: Geological Society of America Bulletin, Vol. 112, p. 424-434.

Poage, M.A. and Chamberlain, C.P., 2001, Empirical relationships between elevation and the stable isotope composition of precipitation and surface waters: considerations for studies of paleoelevation change: American Journal of Science, v. 301, p. 1-15.

Rabassa, J., Cronato, A.M., and Salemme, M., 2005, Chronology of the Late Cenozoic Patagonian glaciations and their correlation with biostratigraphic units of the Pampean region (Argentina): Journal of South American Earth Sciences, Vol. 20, p. 81-103.

Ré, G.H., Jordan, T.E., and Kelley, S., 2003,Cronologia y paleogeografia del Teriario de la cuenca intermontana de Iglesia septentrional, Andes de San Juan, Argentina: Revista de la Asociación Geológica Argentina, v. 58, p. 31-48.

Retallack, G.J., 1998, Fossil soils and completeness of the fossil record: in Donovan, S.K. and Paul, C.R.C., eds., The Adequacy of the Fossil Record: John Wiley and Sons, United Kingdom, p. 133-164.

Retallack, G.J., 2001, Soils of the Past: an Introduction to Paleopedology, 2nd edition: Blackwell Science, 404 p.

Reynolds, J. H., Jordan, T. E., Johnson, N. M., Damanti, J. F., and Tabbutt, K. T., 1990, Neogene deformation of the flat-subduction segment of the Argentine-Chilean Andes: Magnetostratigraphic constraints from Las Juntas, La Rioja Province, Argentina: Geological Society of America Bulletin, v. 102, p. 1607-1622.

Rodríguez, D.J., 2004, Estudio sedimentologico y estratigrafico del Neogene Superior de Lomas de Las Tapias, con el fin de interpreter la evolucion del antiguo Río San Juan: unpublished thesis, Universidad Nacional de San Juan.

Ruskin, B.G., 2006, Sequence stratigraphy and paleopedology in nonmarine foreland basins: Iglesia Basin, Argentina and Axhandle Basin, Utah: Ph.D Dissertation, Cornell University, Ithaca, NY, USA.

Ruskin, B.G. and Jordan, T.E., 2006, Climate change across nonmarine sequence boundaries: paleopedology and lithofacies of Iglesia Basin, northwestern Argentina: *in press,* Journal of Sedimentary Geology

Snyder, D.B., 1988, Foreland crustal geometries in the Andes of Argentina and the Zagros of Iran from seismic reflection and gravity data: PhD thesis, Cornell University, Ithaca, NY, 196 p.

Stipanicic, P.N., 1979, El Triasico del valle del rio de los Patos *in* Segundo Simposio de Geología Regional Argentina, Academía Nacional de Ciencias, Córdoba, 1, p. 695-744.

Talling, P.J., and Burbank, D.W., 1993, Assessment of uncertainties in magnetostratigraphic dating of sedimentary strata *in* Aissaoui, D.M., McNeill, D.F., and Hurley, N.F., eds., Applications of paleomagnetism to sedimentary geology: SEPM (Society for Sedimentary Geology) Special Publication, No. 49, p. 59-69.

Tauxe, L., and Badgley, C., 1988, Stratigraphy and remanence acquisition of a paleomagnetic reversal in alluvial Siwalik rocks of Pakistan: Sedimentology, Vol. 35, p. 697-715.

Wang, Y. Cerling, T. E. ; Quade, J. ; Bowman, J. R. ; Smith, G. A. ; Lindsay, E. H., 1993, Isotopes of paleosols and fossil teeth as paleoindicators: *in* Stuart, P.K., Lohmann, K.C., McKenzie, J., and Savin, S., eds., Climate Change in Continental Isotopic Records: American Geophysical Union, Geophysical Monograph 78, p. 241-248.

Watson, G.S., 1956, A test for randomness of directions: Monthly Notices Geophysical Journal of the Royal Astronomical Society, Vol. 8, p. 160-161.

Zachos, J., Pagini, M., Sloan, L., Thomas, E., and Billups, K., 2001, Trends, rhythms, and aberrations in global climate 65 Ma to present: Science, v. 292, p. 686-693.

CHAPTER 5: NONMARINE SEQUENCE STRATIGRAPHY AND PALEOCLIMATE INTERPRETATIONS FOR AXHANDLE BASIN, CENTRAL UTAH, U.S.A.

Abstract:

Six unconformity-bound stratigraphic sequences are defined within Campanian to Upper Eocene (76 – 49 Ma) nonmarine strata of the Axhandle wedgetop basin, Central Utah. Sequences are characterized by distinct lithologic assemblages, paleocurrent directions, clast provenance and drainage conditions, as well as different degrees of paleosol development. These features can be correlated with confidence for up to 10 km horizontal distances. Detailed stratigraphic sections and magnetostratigraphy (Lawton *et al*., 1993; Talling et al., 1994) present tremendous possibilities to document the spatial and temporal distribution of sequence stratigraphic features and also the relative roles of tectonism and climate on nonmarine sequence genesis. Previous assessments of the Axhandle stratigraphy (e.g. Talling *et al*., 1995) emphasized the role of tectonics on the evolution of the depositional system. Herein, the role of local climate variability is explored in greater detail through a preliminary suite of stable isotopic analyses from interbedded paleosols and their relationship to the proposed stratigraphic sequences. In particular, we reassess and dismiss a proposed Paleocene-Eocene humidity spike reported by Retallack (2005).

I. Introduction:

The Campanian to Eocene Axhandle basin (central Utah) represents a wedgetop depositional zone of the Sevier foreland basin system (Figure 5.1). This region of Utah lies between the Basin and Range Province and the Colorado Plateau, and was the leading edge of Sevier thrusting during the Late Cretaceous (Lawton and Weiss, 1999). About 1.2 km thickness of alluvial and lacustrine strata, represented chiefly by the Paleocene North Horn Formation, spans the time range from 76 to 51 Ma (Talling

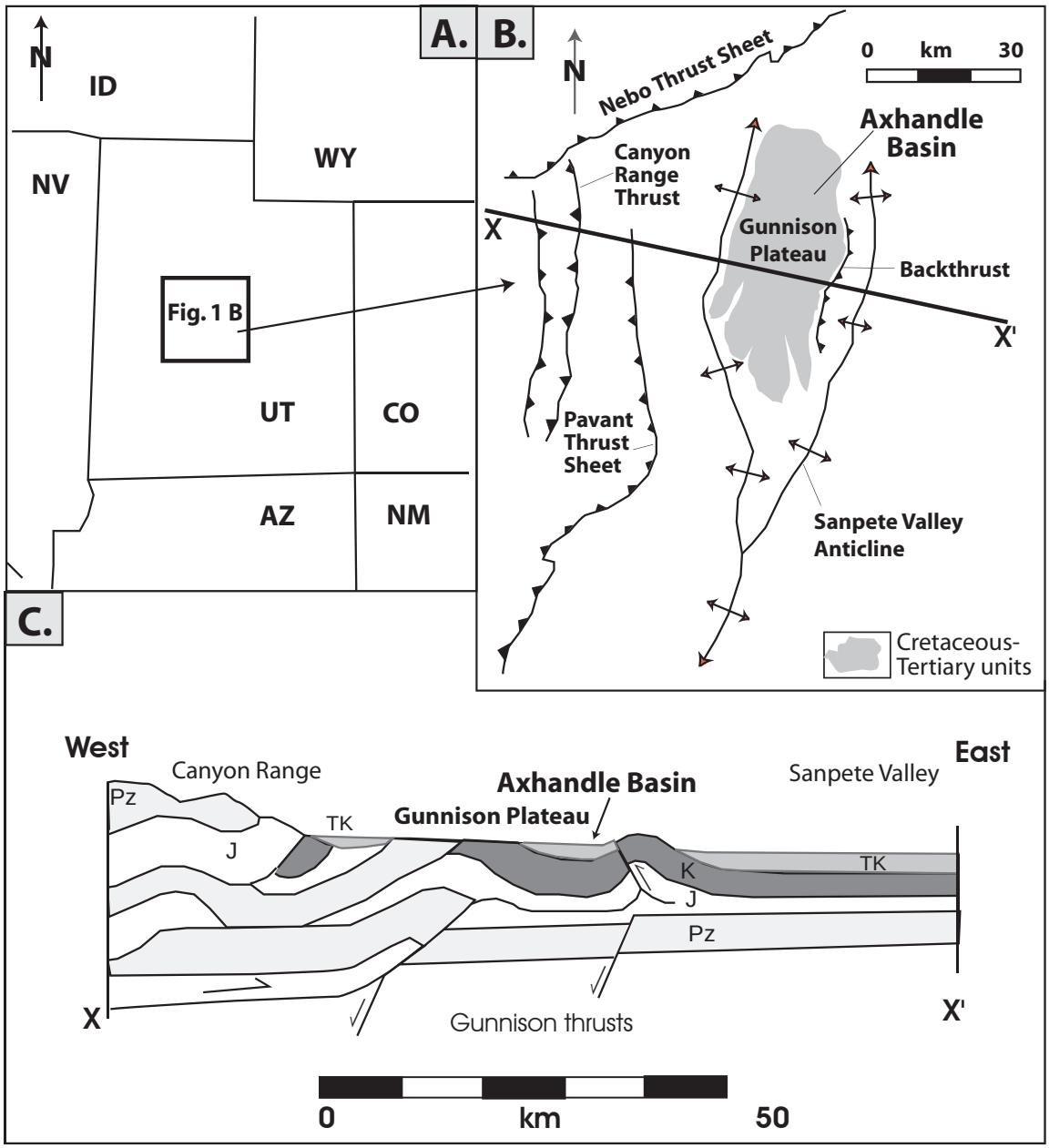

Figure 5.1: Location map and generalized structural cross section of Sevier foreland and Axhandle wedgetop basin. A: Regional map, western United States, with square denoting area of Figure 5.1B: B: Schematic map of Sevier foreland structures bounding the Late Cretaceous - Eocene Axhandle Basin. Cross section line X-X' corresponds with Figure 5.1C. C: Regional cross section of early Tertiary structural and topographic setting of Axhandle wedgetop basin. Pz: Paleozoic units; J:Jurassic units; K:Cretaceous units; TK: Cretaceous and Tertiary units, undifferentiated. Figures redrafted after Talling et al. (1995).

et al., 1994; 1995). The eastern margin of the basin is very well exposed along the eastern flank (backthrust) of the San Pitch Mountains, also known as the Gunnison Plateau (Figure 5.2).

The Axhandle Basin fill has been used to better understand the syntectonic evolution of the Gunnison Thrust system. Wedgetop depositional zones of foreland basin systems are often characterized by unconformities and growth stratal relationships that reflect sedimentary response to active thrusting and may constrain the timing and/or magnitude of tectonic events (DeCelles and Giles, 1996). Talling *et al.* (1995) documented lithofacies characteristics and architecture, depositional chronology (based on magnetostratigraphy and biostratigraphic markers), provenance and drainage patterns to reveal several episodes of thrusting and uplift (described below). Two intervals of comparatively rapid aggradation, interrupted by an interval of slow accumulation including multiple hiatuses, were revealed by extensive along-strike magnetostratigraphic sampling; the interval of slow accumulation is characterized by soil formation (Talling *et al.*, 1994). Changes in drainage configuration, bulk lithology and caliber have been used as evidence of an episodic deformation history. Retallack (2005) documented the nature and evolution of abundant floodplain paleosols in one stratigraphic section to discern climatic conditions from ~64 – 50 MA, a time range corresponding with one or several episodes of uplift along the eastern margin of the basin (Talling *et al*., 1994).

The purpose of this study is to assess variability of sedimentary rock properties as a function of climatic change. Many modern, published models consider sedimentary rock variability in the context of sequence stratigraphy (e.g. Legarreta *et al.*, 1993; Wright and Marriott, 1993; Van Wagoner, 1995; Currie, 1997; Dalrymple *et al.*, 1998; Legarreta and Uliana, 1998; Plint et al., 2001; see Chapter 6). My approach is detailed examination of case studies in the Iglesia basin, Argentina (Chapters 2 and

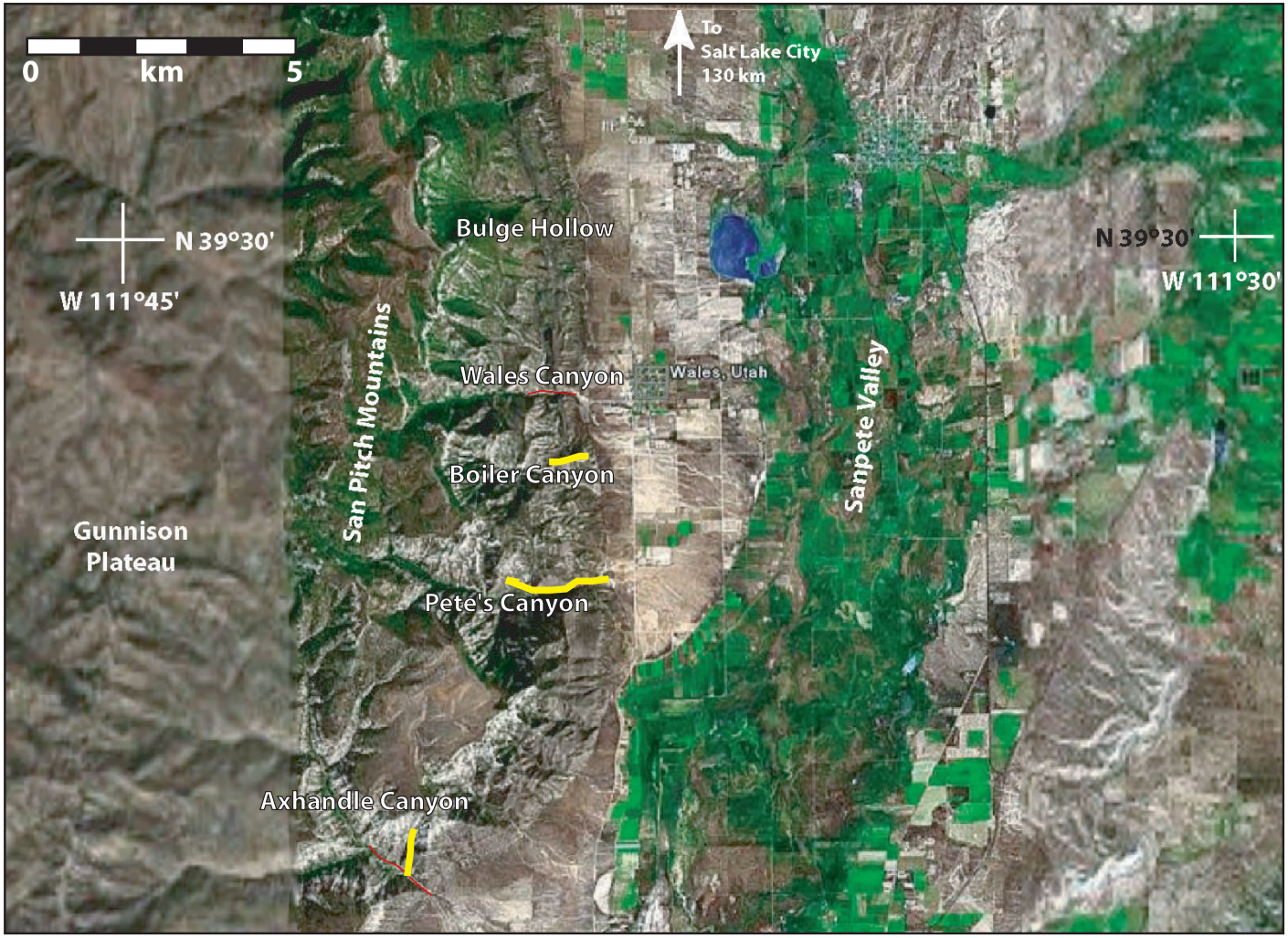

Figure 5.2: Satellite image of study area, the eastern escarpment of the Gunnison Plateau where Jurassic - Eocene strata outcrop. Stratigraphic sections considered in this study are marked in yellow. Image modified from Google Earth, 2006.

3), and Axhandle basin, Utah. For Axhandle, it is well documented that the abovementioned periods of tectonic activity greatly affected accommodation space and resultant sedimentary deposits (see below). However, prior workers did not address syndepositional climate conditions or climate variability in the Late Cretaceous through Eocene Axhandle example, nor did they consider syntectonic sedimentation within a sequence stratigraphic framework.

The tools used in this study to identify the roles of climatic and/or tectonic change include paleosol analysis in addition to tools relied upon for previous detailed studies in Axhandle basin (e.g. sediment accumulation rates, geometrical evidence of syntectonic deposition in outcrop, detrital clastic petrology, paleocurrent analysis, and stable isotopic analysis of paleosols). The Axhandle basin has laterally extensive and vertically compound clay-rich paleosols interbedded with tabular sandstone bodies (Lawton et al., 1993; Talling et al., 1995). In some cases, paleosol characteristics are useful in identifying and interpreting nonmarine stratigraphic sequence boundaries (e.g. McCarthy and Plint, 1998; Plint et al., 2001; Weissmann et al., 2002; Ruskin and Jordan, 2006). These fossil soils provide excellent opportunity to address regional paleoclimatology concurrent with tectonic activity. The Axhandle outcrops have excellent chronostratigraphic control via paleomagnetic data, with supplementary paleontologic data (Talling *et al.*, 1994). Another advantage of the Axhandle basin for sequence stratigraphic analysis is continuity of along-strike exposures of the North Horn Formation, in which channel density, channel stacking and interconnectedness, and the relations of paleosols to channels can be mapped and interpreted in a nonmarine stratigraphic sequence framework.

Stable isotopic analysis of pedogenic carbonates has been proven useful in understanding both the temporal and spatial dynamics of the ancient soil system in response to climate (e.g. Cerling and Quade, 1993; Cerling *et al.*, 1997; Koch *et al.*,

2003). As a first assumption, pedogenic carbon (PC) isotopic composition reflects that of soil CO_2 supplied by decay of organic matter and, at depths less than 30 cm in the soil profile, from atmospheric input (Cerling and Quade, 1993). Thus, $\delta^{13}C$ values of PC supply proxy information about the synpedogenic ecosystem. Oxygen isotopic composition for PC is controlled by soil water, which itself reflects meteoric water isotopic compositions and is affected by temperature, evaporation, elevation, seasonality, continentality, etc. Since such factors (and their combined effects) are difficult to account for in the geologic record, changes in $\delta^{18}O$ PC are commonly considered in conjunction with other paleoclimate proxies (e.g. Wang *et al.*, 1993).

Mack and Cole (2005) demonstrated a method to interpret seasonality of precipitation based upon modeled $\delta^{18}O$ isotopic composition as a function of latitude. Today, the $\delta^{18}O$ composition of pedogenic carbonate between 20° and 60° of the equator varies as a function of latitude, because geographic position incorporates gradients of ambient soil temperature, meteoric water $\delta^{18}O$ isotopic composition, and soil evaporation, all of which exert strong influence on the soil isotopic system (Cerling and Quade, 1993; Fricke and O'Neill, 1999). At present, there is not a systematic global database of modern pedogenic carbonate $\delta^{18}O$ values with which to infer paleoclimate from paleosol $\delta^{18}O$ values, such that modeling is a necessary substitute (Mack and Cole, 2005). Though the suitability of this model for paleoclimate reconstruction is not well established, especially given the number of unconstrained factors influencing paleosol $\delta^{18}O$, it provides a starting point for comparison of present and past $\delta^{18}O$ systems. We consider this model because Mack and Cole (2005) utilized paleosols of Axhandle Basin, providing a means of comparison to $\delta^{18}O$ values obtained in this study. Inferred seasonality of precipitation that may result from Mack and Cole's (2005) model can be compared with other macroscopic features of paleosols for more robust paleoclimate assessment.

II. General Stratigraphy and Tectonics

a) Previous stratigraphic nomenclature:

The nonmarine sedimentary fill of the Axhandle Basin has been informally divided into eight named intervals, arranged into three members on the basis of distinctness of facies associations, clast composition, and paleocurrents (Table 5.1 and Figure 5.3; Lawton *et al*., 1993; Talling *et al*., 1995; Lawton and Weiss, 1999). The Lower Member is characterized by basal conglomerates, silty "redbeds" interfingering with amalgamated sandstone bodies, and finally, coal-bearing siltstone. The Lower Member transitions sharply to the overlying extensive conglomerate and fluvial sandstones and overbank paleosols of the Middle Member. The Middle Member is characterized by extensive pedogenesis in northern sections, whereas stacked paleochannels interpreted as incised valley deposits occur contemporaneously to the south. Sediment accumulation was sufficiently slow during Middle Member deposition that the magnetic polarity record is incomplete, consistent with compound hiatuses which sum to several million years in duration (Talling *et al.*, 1994). The Upper Member is interpreted as lacustrine delta deposits, with abundant calcareous siltstones and a 60-120 m thick limestone unit, the Wales Tongue of the more extensive Eocene Flagstaff Formation limestone. An additional and stratigraphically important sedimentary division can be made on the basis of general grain size: coarse grained facies are vertically stacked in the southern basin and fine-grained facies are dominant to the north (Talling *et al*., 1995). For the purpose of greater detail, I refer to the eight interval names in subsequent discussion (see Table 5.1)

At least four episodes of thrusting in the Gunnison thrust system have been inferred, based on angular and progressive unconformities and shifts in lithofacies and paleocurrents (Talling *et al*., 1994; Table 5.1 and Figure 5.3). The main interval of shortening on the eastern margin backthrust occurred during 83-75 MA (based on

Table 5.1: Lithostratigraphic summary of Late Cretaceous - Eocene Axhandle Basin deposits (after Lawton and Weiss, 1999).

	Age	Named Interval	Lithology	Depositional Interpretation	Deformation features
Upper Member	Early Eocene	Flagstaff Limestone	Light grey-to-light yellow limestone and dolostone, calcareous claystone	Extensive shallow freshwater marsh ("palustrine")	
	Early Eocene	Upper Redbed	Red and brown mottled siltstone and lesser sandstone.	Low-gradient, well-drained floodplain deposits	
	Late Paleocene	Wales Tongue	Distinct orange-weathering sandy carbonate	Marginal to open lacustrine deposits	
	Paleocene	Coal Canyon	Stacked tabular pebbly sandstone and conglomerate	West to Northwest-flowing lacustrine deltas	Reversal of paleocurrent implies uplift to east
Middle Member	Late Cretaceous-Paleocene	Calcareous Siltstone	North: Calcareous pedogenic siltstone and mudstone, weathers blocky. Massive purple-red-grey paleosols with calcic nodules/tubules . Subordinate upward-coarsening /thickening sandstone. South: lenticular sandstone and conglomerate, oncolitic/stromatolitic caps	North: Well-drained floodplains and lake margins; South: Lacustrine deltas and adjacent fluvial systems	
	Late Cretaceous	Big Mountain	Interbedded conglomerate and sandstone, 4 submembers: Lower Sandstone; Lower Conglomerate (50% limestone and dolostone clasts); Upper Sandstone;	Incised valley fill(s); east-flowing sandy and gravelly braided rivers	
			Upper Conglomerate (80% limestone and dolostone clasts). Lower Sandstone, Lower Conglomerate (50%limestone and dolostone clasts)		
Lower Member	Maastrichtian	Coal-bearing	olive-grey siltstone with abundant, thin coalbeds (<1.3 m), plant fragments, upper micritic beds interbingered with coal	Marshy bogs and poorly drained floodplains	Basal angular unconformity, eastern margin
	Late Campanian-Maastrichtian	Sheet Sandstone	Tabular fine-to-coarse grained sandstone with large-scale trough crossbedding; interbedded carbonaceous siltstone	Meanderbelt and floodplain with marsh deposits	
	Late Campanian-Early Maastrichtian	Lower Redbed	Reddish-brown poorly sorted/bioturbated siltstone; lesser pebbly sandstone and conglomerate. Siltstones are 1-2 m thick, often pedogenic, with micritic nodules (2-4 cm).	Ephemeral fluvial system of distal alluvial fan with well-drained interfluves	Basal angular unconformity
	Late Campanian	Basal Conglomerate 2	Horizontally laminated sandstone and conglomerate Beds 1-2 m thick; increasing clast size/angularity upsection	Westward-shed alluvial fan deposits	Progressive rotation and intraformational angular unconformities
	Late Campanian	Basal Conglomerate 1	clast-supported boulder to pebble conglomerate trough crossbedded sandstone; Beds 2-10 m thick	East-flowing braided fluvial deposits	Progressive rotation and intraformational angular unconformities

Figure 5.3: Sequence stratigraphic fence diagram of North Horn Formation and Flagstaff Limestone outcrops along eastern margin of Axhandle Basin (after Talling *et al.*, 1994, Fig. 3; Talling *et al.*, 1995, Fig. 5; Lawton and Weiss, 1999, Fig. 2). Periods of tectonic movement are based on above workers' documentation. Isochrons (black lines) based on magnetostratigraphy of Talling *et al.*, 1994, and have been recalibrated to global geomagnetic polarity time scale of Cande and Kent, 1995.

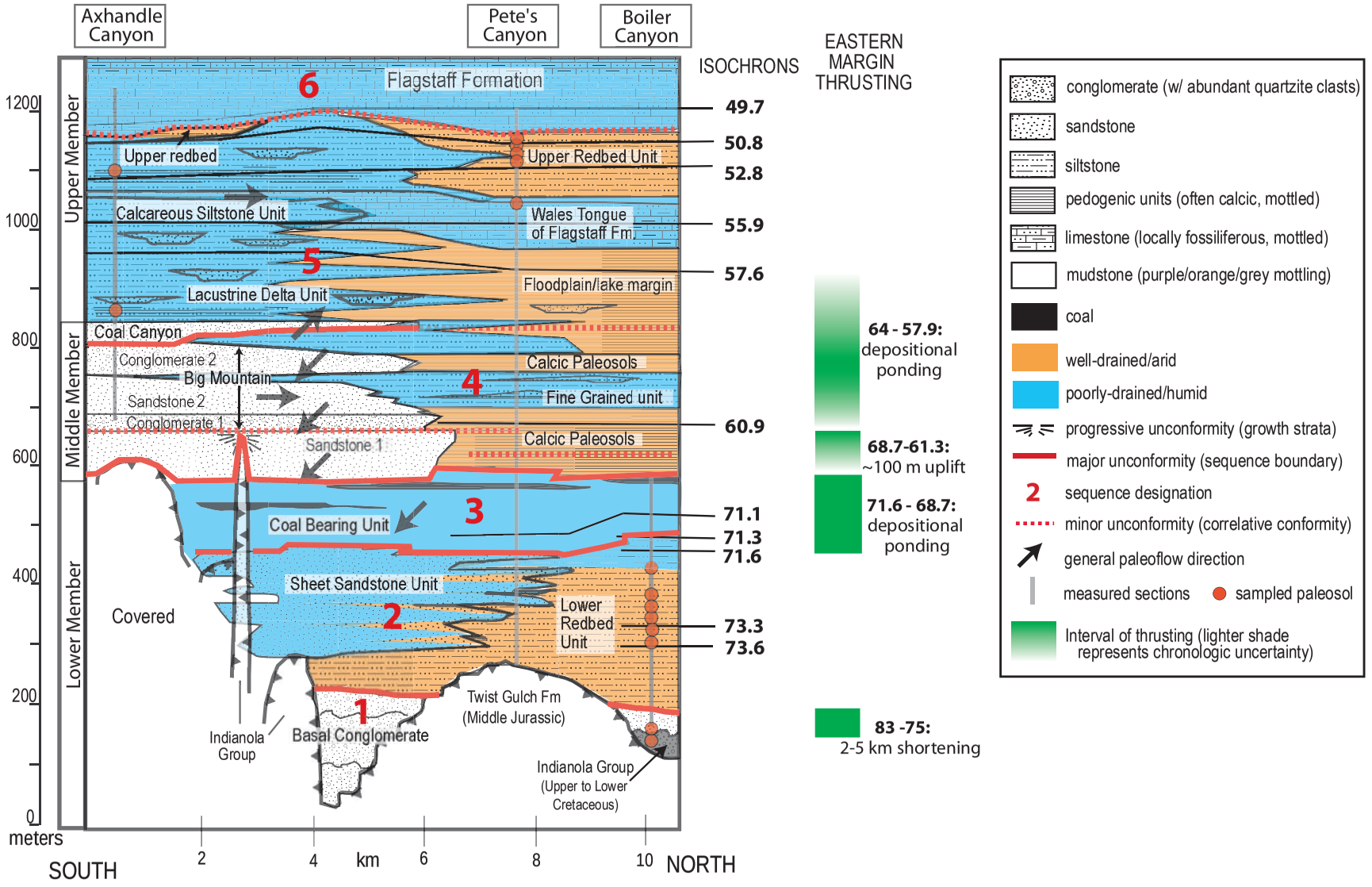
Axhandle Canyon
Pete's Canyon
Boiler Canyon
ISOCHRONS
EASTERN MARGIN THRUSTING
Flagstaff Formation
Upper Member
Middle Member
Lower Member
Upper redbed
Upper Redbed Unit
Calcareous Siltstone Unit
Wales Tongue of Flagstaff Fm.
Lacustrine Delta Unit
Floodplain/lake margin
Coal Canyon
Conglomerate 2
Big Mountain
Sandstone 2
Conglomerate 1
Calcic Paleosols
Fine Grained unit
Sandstone 1
Calcic Paleosols
Coal Bearing Unit
Sheet Sandstone Unit
Covered
Lower Redbed Unit
Twist Gulch Fm (Middle Jurassic)
Indianola Group
Basal Conglomerate
Indianola Group (Upper to Lower Cretaceous)
1
2
3
4
5
6
49.7
50.8
52.8
55.9
57.6
60.9
71.1
71.3
71.6
73.3
73.6
64 - 57.9: depositional ponding
68.7-61.3: ~100 m uplift
71.6 - 68.7: depositional ponding
83 -75: 2-5 km shortening
conglomerate (w/ abundant quartzite clasts)
sandstone
siltstone
pedogenic units (often calcic, mottled)
limestone (locally fossiliferous, mottled)
mudstone (purple/orange/grey mottling)
coal
well-drained/arid
poorly-drained/humid
progressive unconformity (growth strata)
major unconformity (sequence boundary)
sequence designation
minor unconformity (correlative conformity)
general paleoflow direction
measured sections
sampled paleosol
Interval of thrusting (lighter shade represents chronologic uncertainty)
1200
1000
800
600
400
200
0
meters
SOUTH
2
4
km
6
8
10
NORTH

biostratigraphic correlation) and resulted in >2 km of erosion and 2-5 km of shortening structurally accommodated by Cretaceous units. A second interval of shortening, inferred from depositional ponding and paleocurrent measurements, occurred between 71.6 – 68.7 MA (these and subsequent ages based on magnetostratigraphy of Talling *et al.*, 1994, recalibrated to Cande and Kent, 1995). Sometime between 68.7-61.3 MA, approximately 100 m of eastern margin uplift caused a progressive unconformity along strike of the backthrust. A fourth stage of shortening in the Gunnison thrust system is revealed by an interval of depositional ponding and eastward paleoflow of 64-57.9 MA units, although with considerable uncertainty in the paleomagnetic correlation (Talling and Burbank, 1993).

Previous workers do not speak directly of stratigraphic sequences in Axhandle Basin, instead referring to informal units or members, but the features they describe are akin to unconformity-bounded stratigraphic sequences. Dramatic facies changes occur north to south along the mountain front exposures, but internal unconformities are also pronounced (Lawton and Weiss, 1999). At least six intervals of strata are separated by four eastern margin angular unconformities and one regional disconformity. Each interval exhibits distinct changes in lithofacies and architecture which can be recognized in vertical section (i.e. at the scale of single outcrops) as well as being traceable for several kilometers along strike (N-S) (Figure 5.3). Some of these features have been attributed to episodes of uplift on the backthrust that defines the eastern basin margin (Figure 5.1; Talling *et al.*, 1994; 1995). However, other features may reflect sedimentary response to variable discharge, possibly controlled by changing climatic conditions (discussed below).

b) Proposed sequence stratigraphy of North Horn and Flagstaff Formations:

On the basis of documented regionally continuous stratigraphic disconformities, North Horn and Flagstaff Formation outcrops along the Eastern Gunnison Plateau can

be subdivided into six nonmarine sequences. In early descriptions of the Axhandle stratigraphy (see Lawton and Trexler, 1991), six unconformity-bounded units were recognized in the eastern Gunnison Plateau, with only four discernible to the west. Unconformable contacts in Lawton and Trexler's (1991) early scheme were erosive surfaces in the incised valley fill of the Middle Member. The sequence stratigraphy proposed herein (see Figure 5.3 and Table 5.2) follows Lawton and Trexler (1991) in subdivision of the valley fill complex (at the erosive base of the Big Mountain and Coal Canyon Members). However, I also extend sequence boundaries into the correlative section to the north of the incised valley (e.g. fine-grained pedogenic section with >5 M.y. hiatus). Additional sequences are defined at the base of the North Horn Formation and the base of the interfingered Lower Redbed/Sheet Sandstone Member, as well as at the base of the Flagstaff Formation. These stratigraphic contacts are at least locally unconformable and separate packages of strata with dramatically different facies characteristics (described below).

In subsequent discussion, the components of this sequence framework are referred to as Proposed Sequences (PS). Sedimentary and structural characteristics described in this section are based on previous extensive mapping (Lawton *et al*., 1993; summarized in Lawton and Weiss, 1999), and these features were observed in the field by the author under the guidance of Lawton:

1) The basal sequence (PS-1, 83-75 MA) consists predominantly of conglomerate and overlies thrust-bounded Mid-Jurassic through Upper Cretaceous units across an angular unconformity. Growth strata occur throughout PS-1 as a result of progressive deformation and uplift of the basin's eastern margin, a west-vergent thrust fault.

2) An angular unconformity separates PS-1 and PS-2 (75 – 71. 3 MA), the latter consisting of interbedded sheet sandstones (dominant to the south) and reddish pedogenic sandstones and siltstones (principally in northern sections). The southern

Table 5.2: Sequence stratigraphic framework for Axhandle Basin. Age assignments based on Talling et al., 1994, recorrelated to Cande and Kent, 1995. Members correspond with those described by Lawton and Weiss, 1999, summarized in Table 5.1. See text for discussion of interpreted forcings.

Proposed Sequence	Age (MA)	Component Members	Nature of basal contact; *Internal hiatuses*	Interpreted Forcing(s)
PS-6	<50	Flagstaff Formation	Disconformity (east)	Climate
PS-5	<60.9 - 50	Conglomerate 3, Calcareous Siltstone; Wales Tongue; Upper Redbed	Incised valley; *intense pedogenesis to north; Multiple flooding episodes.*	Climate (late) Climate; Tectonism
PS-4	<68.7- <60.9	Sandstone 1, lower Calcareous Siltstone; Conglomerate 1	Incised valley; *multiple paleosol horizons >5 MA paleomagnetic gap*	Climate; Tectonism
PS-3	71.3 - 68.7(?)	Coal Bearing Unit	Angular unconformity (east) Correlative comformity (west)	Climate; Tectonism
PS-2	75 - 71.3	Lower Redbed; Sheet Sandstone	Angular unconformity	Climate
PS-1	83 - 75	Basal Conglomerate 1 and 2	angular unconformity; *intraformational progressive bed rotation*	Tectonism

units are interpreted as an amalgamated braidplain, while northern sections are less-channelized floodplains. Localized intrasequence rotational unconformities are also present in PS 2.

3) The third sequence (PS-3, 71.3 – 68.7? MA) commences with a slight and local angular discordance (~4°) with underlying units, as well as a change in lithofacies. Basal sandstone in PS-3 is present above the angular unconformity, which includes angular clasts derived from the "Sheet Sandstone Member" (see Lawton et al., 1993; Lawton and Weiss, 1999). Overlying beds are olive-gray siltstones, interbedded with thin coal seams and fossiliferous micrite. Channel bodies are more isolated in PS-3 than those in PS-2. These lithologies and the reduction coloration also contrast sharply with the coarser, generally oxidized units below (PS-2).

4) Coarse-grained and compositionally-distinct channel deposits of the Middle Member (Talling *et al.*,1995) or the Big Mountain Member (Lawton and Weiss, 1999) comprise PS-4 (<68.7 - <60.9 MA). Vertical stacking of these deposits in the south and central sections suggests they represent incised valley deposits (Talling *et al.*, 1995). However, to the north, strata interfinger with finer-grained pedogenic overbank units which overlie the coal-bearing unit without apparent unconformity. This sequence is less well constrained by magnetostratigraphy than all the other units, likely because of unrecognized internal unconformities or pedogenic hiatuses (age uncertainties discussed by Talling and Burbank, 1993).

5) A regional erosive surface initiates PS-5 (<60.9 – 50 MA), the thickest and the most lithologically-varied subdivision of the North Horn Formation. The sequence initiates with basal conglomerate over an erosive surface ("Big Mountain Member" of Lawton *et al.*, 1993) which shows a 180° change in paleocurrent direction. Overlying the conglomerate in southern sections are calcareous siltstone and interbedded channel deposits. Pedogenesis is marked to the north, where calcareous siltstones and thin

sandstones dominate. A paludal limestone unit 60-120 m thick (the "Wales Tongue Member" of Lawton *et al*., 1993) and a conspicuous redbed are present in uppermost PS-5, each of which thicken substantially to the north and west.

6) The uppermost sequence, PS-6 (<50 Ma), consists of the Eocene Flagstaff Formation. This lacustrine limestone is present throughout central and eastern Utah, and the portion outcropping in Axhandle Basin (the Cove Mountain Member) represents a regional base level low stand in response to Sevier foreland thrusting (Stanley and Collinson, 1979; Lawton and Weiss, 1999). The basal contact has been mapped as locally unconformable, based on the distinctness of its lower contact with the underlying redbeds (Lawton and Weiss, 1999).

It is likely that Sequence 4 may contain additional major unconformities that would justify subdivision of the valley fill complex into several more sequences, as there are at least 4 local incision surfaces within the Middle Member's stacked valley complex (Big Mountain and Coal Canyon Members of Lawton et al., 1993; see also Table 5.1). These incision events are potentially correlative with pedogenic hiatuses to the north. However, uncertainty regarding the spatial extent of these incision events prevents further subdivision at present. Consequently, only the first and last incision events are presently considered sequence boundaries, based on other supporting criteria (e.g. stark vertical and lateral facies changes, 180° paleocurrent reversal).

c). Tectonic versus climatic control of sequences:

Determination of distinct "climate-controlled" or "tectonically-controlled" deposits from foreland basin strata poses a major challenge to stratigraphers, as the records are inherently incomplete, nonexclusive and biased by scale. On the scale of an entire sedimentary basin, changes in tectonic uplift and subsidence probably exert fundamental control on the location and characteristics of continental (and in particular fluvial) strata (e.g. Sloss, 1991; Leeder, 1993). For foreland basins, the

major trap for nonmarine sediments and the Axhandle basin deposystem considered herein, tectonic subsidence creates accommodation for 2^{nd}-3^{rd} order stratigraphic sequences (1 Ma – 100 Ma, after Vail *et al*., 1991). The meso-scale stratigraphic architecture (i.e. individual outcrops) is more likely to reflect a combination of base level, tectonic, and climatic influences, superposed in both space and time (Leeder, 1993). Feedback relationships should also be expected in the deposystem, as tectonism and climate both influence sediment flux (e.g. relief, episodic growth and erosion of individual structures, contrasts in exposed lithologic resistance, changes in drainage basin size, etc; see Tucker and Slingerland, 1996). The result is a situation in which the stratigrapher must seek an interpretation of sequence genesis that is most consistent with available data from multiple data sets and proxies, despite the strong probability of convergent responses to multiple forcing mechanisms (e.g. Schumm, 1993).

Although some Axhandle basin strata record syntectonic deposition during thrust events in the eastern Cretaceous Sevier foreland, we can qualitatively identify certain intervals for which climate change may have influenced the stratigraphy to an equal or greater extent as did tectonism. Four intervals of eastern margin deformation (described above) were identified from North Horn Formation strata (Talling *et al.*, 1994; see "eastern margin thrusting" column, Figure 5.3). Previously, uplift-induced incision and thrust-load flexural subsidence were suggested as the dominant controls of Axhandle basin stratigraphy (Talling *et al*., 1995). Lithofacies and paleocurrent information also permitted qualitative interpretation of drainage conditions (well-drained vs. poorly drained) of the named intervals and members (Talling *et al*., 1995; Figure 5.3). Within the framework of the proposed sequence stratigraphy, one can identify intervals temporally correlative with episodic tectonism: PS-1, PS-3 and portions of PS-4 and 5. In contrast, the majority of PS-2 (<75 Ma) and strata younger

than ~57.9 Ma of PS-5 and PS-6 accumulated during tectonically-quiescent periods and on low-gradient landscapes (Talling *et al*., 1995). It is during these intervals that a pure climatic signal stands the best chance of being discerned, and are the intervals where paleosols were sampled for proxy records of paleoclimate variation (see below). On the basis of timing of tectonic deformation and changes in characteristics of lithofacies assemblages, the relative role(s) of tectonism and climatic variation on sequence boundary formation are listed in Table 5.2.

It is worth stating again that a significant magnetostratigraphic hiatus (>5 Ma) was identified within pedogenic strata of PS-4. These paleosols are along-strike with the stacked valley-fill deposits seen in southern sections. Eastern margin uplift of ~100 m was inferred from progressive rotations within the channel fill complex and from eastward-draining paleocurrents. Marginal uplift may be responsible for erosive removal of correlative paleosols to the north. Alternatively, this uplift may have localized to the south of the eastern margin, not affecting the northern well-drained pedogenic floodplain. The abundance of paleosols implies at least an episodically stable landscape north of the incised channels. As such, joint tectonic-climatic influence on PS-4 deposition is suggested.

A particular interval when paleoclimate control on nonmarine sequence generation might be expected is the Paleocene-Eocene Epoch boundary, preserved in late PS-5 of Axhandle basin strata. The Paleocene-Eocene boundary coincides with a short-lived, but dramatic global climate change that is well-resolved in both the marine and terrestrial stratigraphic records. Oxygen isotopic data from marine microfossils 59 to 50 Ma (summarized by Zachos *et al*., 2001) exhibit a positive anomaly, the largest of the Cenozoic, indicating warming of mid-to-high latitude surface waters as well as deep ocean waters. Also, at ~55 Ma, isotopic peaks occur in both the $\delta^{18}O$ (sharp increase) and δ^{13} C (sharp decrease) benthic foraminifera records, referred to as the

Paleocene Eocene Thermal Maximum (PETM; Zachos *et al*., 2001). This global warming event coincides with a marked faunal transition, with many vertebrate taxa appearing for the first time at the Paleocene-Eocene boundary (e.g. Clarkforkian-Wasatchian land-mammal age boundary; Gingerich, 2003). On land, the PETM and Eocene warming trend has been globally identified in high-resolution stable isotopic time series from paleosol carbonates as major δ^{13} C depletion (Cojan *et al*., 2000; Koch *et al*., 2003) and modest enrichment of δ^{18}O (Koch *et al*., 2003). In Axhandle Basin, Retallack (2005) utilized paleosol geometric transfer functions to assess paleoprecipitation and suggested increased humidity at the Paleocene-Eocene boundary, within PS-5 (discussed below).

III Paleosols in Axhandle Basin sequence stratigraphy

Talling *et al*. (1995) demonstrated that paleosol-rich intervals of Paleocene strata can be traced for up to 5 km of lateral continuity and they provide a high-resolution chronostratigraphy for the paleosols. To analyze the paleosols within the proposed sequence stratigraphy, field reconnaissance was conducted by the author in October 2005, with guidance from Timothy Lawton (University of New Mexico, Las Cruces), who conducted geologic quadrangle mapping of the area (Lawton *et al*., 1993; Lawton and Weiss, 1999) as well as subsequent basin analyses (Talling *et al*., 1994, 1995). The purpose of the new fieldwork was to examine relations among paleosols and fluvial facies, and to obtain samples of paleosol carbonates of sufficient number and appropriate locations to test for isotopic and paleoenvironmental variability both along-strike and through time. Attention was paid to channel belt architecture (single-storey, multi-storey, facies variability), in the context of the drainage changes and climate variations documented by Talling *et al*. (1995) and Retallack (2005).

All North Horn Formation paleosols that we recognized in the field possess at least two of the following characteristics: horizonation (e.g. argillic, calcic), structural development (e.g. vertic and/or ped structures), root traces in the sedimentary matrix or filled with carbonate minerals (rhizoliths), destruction of primary sedimentary bedding ("pedoturbation", often in association with trace fossils), and color banding/mottling (Working Group on the Origin and Nature of Paleosols, 1971; Retallack, 2001, Soil Survey Staff, 2003). Calcic soils typically have Stage II carbonate accumulations (i.e. distinct nodules; after Machette, 1985), though Stage I (filamentous) and Stage III (coalescing nodules) are also present. We found that many paleosol units would have required trenching to accurately assess profile thickness and characteristics, which was not feasible with the available time and tools.

Measured stratigraphic sections and field reconnaissance of Axhandle Canyon, Pete's Canyon and Boiler Canyon (along with its neighboring canyon, Deer Gulch) (Lawton *et al*., 1993; Fig.5.2) permit assessment of the spatial and temporal abundance of paleosols in the proposed sequence framework. It has been suggested that in alluvial settings, the proportion of geologic time represented by pedogenesis is very large compared to the amount of time devoted to both deposition and erosion (Bown and Kraus, 1986). Although thickness of paleosol profiles does not scale directly with duration of pedogenesis, the relative abundance and maturation characteristics of paleosols do permit qualitative assessment of sedimentation vs. pedogenesis rates (e.g. Bown and Kraus, 1993). The logged sections (Lawton *et al*., 1993) include features characteristic of paleosols (e.g. rootlet traces, rhizoconcretions, in situ carbonate nodules, burrows, and mottles). Lawton *et al*.'s (1993) logged thicknesses of fine-grained strata with one and commonly more of these features were summed as a first approximation of maximum thickness of paleosols. Each of these sections was visited by the author for visual confirmation of the degree of

pedogenesis, and suggests that the column measurements (Table 5.3) serve as an upper limit of total paleosol thickness. Even based on this crude assessment of pedogenic abundance, it is clear that paleosols comprise a large proportion of the exposed strata. Considered by cumulative thickness, the pedogenic intervals are thickest in the southern and central sections, Axhandle Canyon and Pete's Canyon. In terms of pedogenic development, however, paleosols are more mature in central and northern sections. In Pete's Canyon and Boiler Canyon, individual paleosol profiles are generally thicker and separated by lesser amounts of nonpedogenic sediment than in Axhandle Canyon. These northern and central paleosols exist as "cumulative" (e.g. superimposed) and "compound" (separate but numerous soils in tens of meters of strata) profiles (Kraus, 1987). Temporally, pedogenesis is dominant during PS-2, 4, and 5 (75 – 71.3 MA, <68.7 Ma – 50 Ma).

A reconnaissance suite of 17 pedogenic carbonate samples was obtained from the Boiler Canyon/Deer Gulch (PS-2), Axhandle Canyon (PS-5) and Pete's Canyon (PS-5) sections. Each sample's location was specified relative to Lawton *et al*.'s (1993) paleomagnetic sample horizons specified in measured sections of Lawton *et al*. (1993) and documented by Talling *et al*. (1994). The soil carbonate samples were collected from Stage II or, when available, Stage III accumulations, preferably from >30 cm depth below the paleosol top, to minimize the effect of atmospheric CO_2 diffusion on their carbon isotopic values (Cerling and Quade, 1993). In most cases, a minimum of 5 nodules could be obtained from a single depth level in the paleosol. Sample ages were assigned by linear interpolation of the magnetostratigraphic sections, with errors taking into account potential stratigraphic misplacement. The pedogenic interval of PS-4 in Pete's Canyon was not sampled, as the magnetostratigraphic correlation is most uncertain in this interval, prohibiting confident age assignments. Nodules were homogenized by crushing to a fine powder

Table 5.3: Estimated vertical percentage of paleosols in Axhandle Basin measured sections, based on stratigraphic logs of Lawton et al., (1993). Exposed thickness refers to uncovered strata.

Section	Total height (m)	(Exposed)	Cumulative paleosols (m)	Paleosol %
Axhandle Canyon:	500	(464)	130	26 (28)
Pete's Canyon:	987	(817)	152	15 (19)
Boiler Canyon/ Deer Gulch:	363	(341)	61	17 (18)

with mortar and pestle. Isotopic analyses were conducted at the Cornell Stable Isotope Laboratory with a dual inlet Finnegan MAT Delta Plus mass spectrometer. Values are reported as per mil differences relative to the Peedee Belemnite standard (PDB). The lithofacies associations and paleosol characteristics of the 17 pedogenic carbonate samples are described below and data summarized in Table 5.4.

a) Deer Gulch/Boiler Canyon sections:

Deer Gulch and Boiler Canyon are the third and fourth major valleys encountered, respectively, as one progresses south along the Eastern San Pitch Mountains (Fig. 5.2). To the north, Wales Canyon and Bulge Hollow also expose Upper Cretaceous- Eocene strata, but paleosol exposure and development are less impressive. Both Deer Gulch and Boiler Canyon have been magnetostratigraphically correlated (Talling *et al.*, 1994) and feature thick exposures of the Lower Member of the North Horn Formation, which unconformably overlies faulted Middle Jurassic Twist Gulch Formation and Cretaceous Indianola Group (Lawton and Weiss, 1999).

The oldest sampled paleosols from the Axhandle basin are in the Lower Cretaceous Cedar Mountain Formation (Indianola Group), below the base of the measured section of Talling *et al.*, (1994) (Fig. 5.3). This alluvial, fluvial and lacustrine formation contains common pedogenic calcretes throughout northeast and central Utah (Woods *et al.*, 2003). In the vicinity of the Gunnison Plateau, the formation is Barremian through Middle Albian in age, or approximately 127-100 Ma (Utah Geological Survey, 1999). In Boiler Canyon, the Lower Cretaceous Cedar Mountain Formation is overturned and dipping to the southeast, overlain across a thrust fault by the Jurassic Twist Gulch Formation redbeds (Lawton and Weiss, 1999). The exposure is <10 m in stratigraphic thickness, confined to the south side of an ephemeral stream valley. The outcrop consists of brightly mottled (purple, orange and grey) pedogenic siltstone and fine sandstone with disorthic micritic carbonate nodules

to 10 cm in diameter. Redoximorphic features and carbonate accumulations are of greater dimension in the Cedar Mountain Formation than in any paleosols observed in the overlying North Horn Formation.

Two pedogenic carbonate samples were obtained 10 m below the base of the Boiler Canyon paleomagnetic section, within PS-2 (Fig. 5.3, Table 5.2). Within a sandy purple and grey mottled paleosol, a locally continuous, 20-cm-thick K horizon (Stage IV of Machette, 1985) and subvertical rhizoconcretions were sampled. These samples were collected to provide a basis for isotopic comparison of these types of carbonate accumulations with the lower-stage carbonate nodules that are plentiful in the overlying units.

The "Lower Redbed Unit" of the North Horn Formation's Lower Member (PS-2) was the source of an additional six carbonate samples (Figures 5.3 and 5.4). These were obtained from an interval correlated from 73.1 to 72.4 Ma (age error ±0.03 Ma). The sampled interval is 41 m thick, comprised of greenish-white pedoturbated and bioturbated concretionary sandstone beds 20-30 cm thick that are separated by several meters of compound paleosols, reddish in coloration and containing multiple stringers of irregularly-shaped sandy micrite nodules (<4 cm diameter). Lighter coloration in the concretionary sandstones relative to pedogenic units is continuous into the outcrop (i.e. not surficial weathering), and may reflect either a compositional change to the sandstone (e.g. lesser clay concentration via eluviation) or perhaps post-depositional alteration via fluid flow (T. Lawton, personal communication, 2005). An additional textural and color change occurs near the top (39 m height) of the local section (Fig. 5.4). At this stratigraphic level, the unit transitions from clay-rich red soils with diffuse nodular carbonates (stage II) to ochre-grey incipient soils with filamentous (stage I) carbonates.

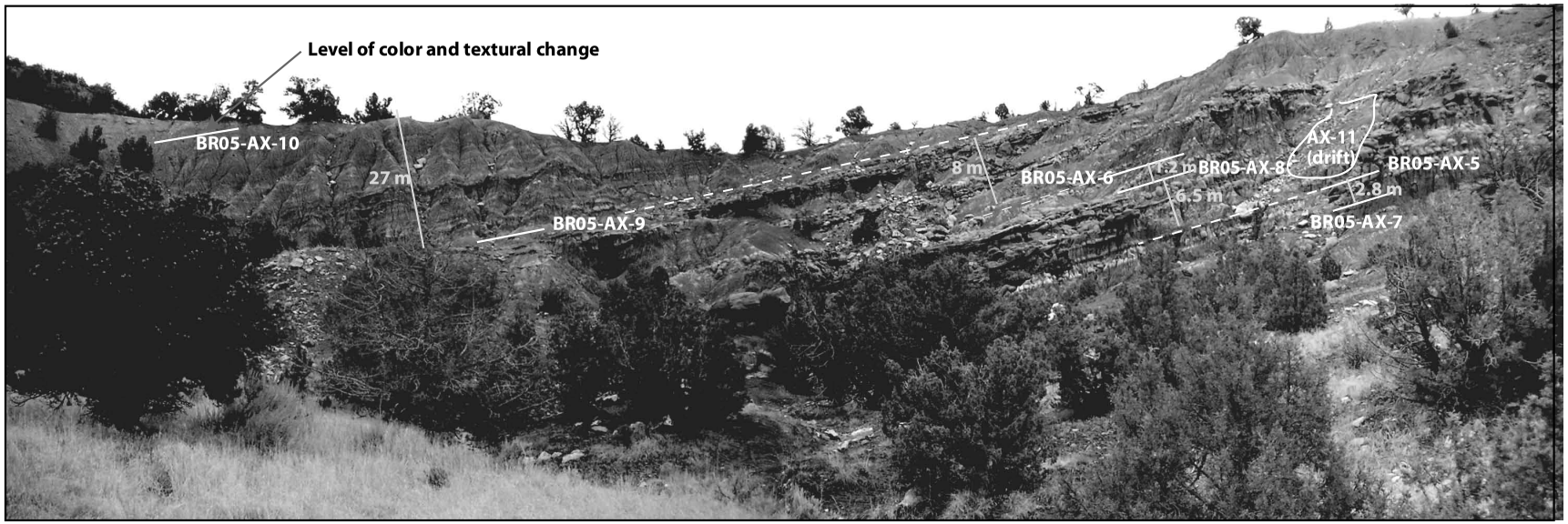

Figure 5.4: Boiler Canyon sampled section, eastern San Pitch Mountains, Axhandle Basin. Pedogenic carbonate samples were obtained from the Lower Redbed Unit (after Lawton and Weiss, 1999), North Horn Formation, 72-74 Ma. View is to the North.

b) Pete's Canyon section:

The gorge known as Pete's Canyon (2.5 km south of Boiler Canyon) is the location for one of the most extensive stratigraphic sections (following location and vertical log of Lawton *et al*., 1993), spanning the entirety of the North Horn Formation, and providing the clearest exposures of the pedogenic PS-4 and PS-5. Outcrops along the canyon walls are prone to coverage by modern soil slumping and erosion, but are macroscopically identifiable as paleosols by their intense red, purple and grey color banding and, after trenching, their extensive mottling, blocky ped structure, horizonation and fibrous to nodular carbonate accumulations (see Figure 5.5). Pedogenesis persists into the overlying calcareous siltstone unit (the palustrine Wales Tongue Member), where gleyed soils are interbedded with thin limestones, transitioning upsection to more oxidized paleosols in the Upper Redbed Member (e.g. Lawton *et al*., 1993) just below the Flagstaff Formation (PS-5; Fig. 5.5).

Though the stratigraphic interval outcropping at Pete's Canyon is strongly pedogenic, and previous workers note abundant nodular carbonates in the measured section, access to fresh exposures of paleosols proves difficult. The preliminary suite of 5 samples were obtained from the uppermost Wales Tongue and Upper Redbed Members (PS-5) and required trenching to obtain what was considered "primary" carbonates, generally Stages I and II. Where disorthic carbonates were present, they were small (<4 cm) and dispersed within the profile. Pedogenic intervals are highly mottled and consist of compound profiles. Many of the observed paleosols and surrounding strata are the source materials for modern soils, such that isotopic values should be interpreted with caution, as they may represent inheritance from multiple sources. Despite this uncertainty, these samples' isotopic values are of particular interest because they represent the time interval at or just after the Paleocene-Eocene transition (55.8 ± 0.2 Ma, Gradstein *et al*., 2005).

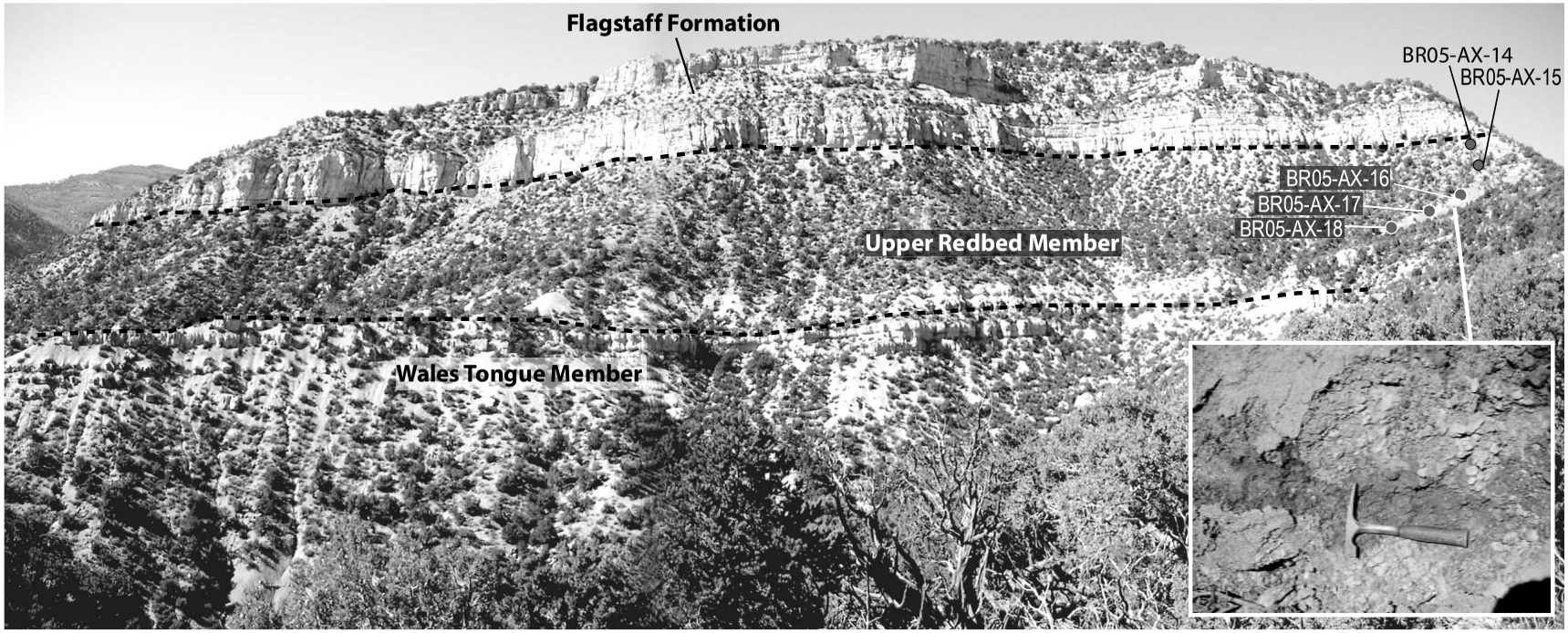

Figure 5.5: Pete's Canyon sample section, eastern San Pitch Mountains, Axhandle Basin. Dashed lines mark approximate contact between informal members. Red circles denote sample locations (see also Table 3). Sampled units are approximately 55.4 -51.4 Ma. Inset photo shows characteristic color mottling and subrounded ped structure of trenched paleosols. View is toward the Northwest.

c) Axhandle Canyon section:

The Middle and Upper Members of the North Horn Formation, including the Wales Tongue limestone, a thin Upper Redbed unit, and the ridge-capping Eocene Flagstaff Formation limestone (PS-4, 5 and 6) are well exposed in the bifurcating Axhandle Canyon, about 7 km south of Pete's Canyon. Field observations and sampling followed the original magnetostratigraphic section up the northeastern canyon wall, such that lithostratigraphic, isotopic, and chronostratigraphic data are very well correlated.

The upper portions of the 530-m-thick section are characterized by vertic paleosols (i.e. with subvertical cracks related to shrink-swell of clays via seasonal drying). These calcareous-cemented sediments are generally fine-grained and their variable degrees of Vertic pedogenesis can lead to general interpretations of environmental conditions. Unfortunately, few units contain stage II or III carbonate nodules that would be suitable for interpretation of Carbon isotopic data.

Two paleosols that possess clear Bk (i.e. calcic) horizons were recognized at 176 m and 360 m in the paleomagnetic section of Lawton *et al.*, (1993) (59.7 Ma and 52.8 Ma, respectively; PS-5; Fig. 5.3). In the paleosol at 176 m in the section, the Bk horizon is ~30 cm below the upper contact of the paleosol profile and an overlying oncolitic/algal limestone. Fossil material and sparitic calcic nodules in the Bk horizon result in uncertainty as to whether carbonate in the Bk horizon is truly pedogenic. Minor erosive relief does occur at the top of this paleosol, below the limestone. The paleosol at 360 m height contains a >40 cm thick interval of very sparitic carbonate nodules, concentrated >90 cm below the top of the exposed paleosol. The overlying 7 to 8 m of section, and perhaps some of the sampled paleosol profile, is covered.

d) Stable Isotopic Analyses:

The $\delta^{13}C$ and $\delta^{18}O$ values as well as percent inorganic carbon for all 17

samples are summarized in Table 5.4 and as time series and section-specific isotopic ranges in Figure 5.6. The limited sample suite precludes detailed assessment of paleoclimatic changes, but some qualitative interpretations of the soil system are possible.

The oldest North Horn Formation samples (~76-72 Ma, PS-2), collected from Boiler Canyon/Deer Gulch, are closely clustered in space and time but exhibit a wide range of isotopic values (Figure 5.6A). Values of $\delta^{13}C$ range from -6 to -13.3 ‰ while $\delta^{18}O$ ranges from -1.6 to -10.1‰. Both isotopic series fluctuate in accord, save the youngest two samples. No overall trend is evident from this low-resolution sample suite, although the coincidence of variability between Carbon and Oxygen series may suggest an external rather than microclimate forcing. Interestingly, the percent inorganic carbon ($\%C_{inorganic}$), here used as a proxy for atmospheric dust influx/aridity (e.g. Capo and Chadwick, 1999; Lal and Kimble, 2000) sharply declines at ~72.6 Ma, coincident with depleted $\delta^{13}C$ and $\delta^{18}O$ values.

Samples from PS-5 (at and above the Paleocene-Eocene boundary) exhibit slightly less variable isotopic values compared with older sampled paleosols (Fig. 5.6A). Values of $\delta^{13}C$ range from -4.98 to -10.2 ‰ while $\delta^{18}O$ ranges from -1.6 to -8.5‰. As with samples from PS-2, both isotopic series in PS-5 samples change in general accord. The $\delta^{18}O$ values for three distinct soils 52 – 51.4 Ma agree within 0.3‰. Pedogenic carbonate oxygen isotopic values are sometimes 'homogenized' by diagenesis, such that the sampled soils may show minimal change in response to major climatic variation (Pendall *et al*., 1994; Liu *et al*., 1996). The sample just after the Paleocene-Eocene boundary (BR05-AX-18; 55.4 Ma) exhibits enrichment in both isotopic series by 1.7 – 4 ‰ relative to older and younger samples as well as a 2% decrease in $\%C_{inorganic}$. Comparing the mean isotopic values for PS-2 and PS-5 samples (Fig. 5.6B), the younger sequence is slightly enriched in both δ^{13} C and $\delta^{18}O$.

Table 5.4: Pedogenic carbonate samples and stable isotopic results for Axhandle Basin deposits ordered by age. Heights correspond to paleomagnetic sections of Lawton et al. (1993). Ages assigned by linear interpolation, using Talling et al. (1994) magnetostratigraphy recorrelated with global polarity timescale of Cande and Kent (1995).

SAMPLE	AGE (Ma)	age error	%C	13C pdb	18O pdb	Section	height in section (m)	height error	Comments
br05-ax-14	51.41	0.31	4.378	-8.564	-8.432	Pete's Canyon	850	10	overprinted limestone?
br05-ax-15	51.72	0.16	5.911	-4.983	-8.456	Pete's Canyon	840	5	trenched paleosol
br05-ax-16	52.03	0.16	4.812	-9.726	-8.173	Pete's Canyon	830	5	trenched paleosol
br05-ax-17	52.34	0.16	3.220	-5.975	-1.623	Pete's Canyon	820	5	trenched paleosol
br05-ax-3	52.78	0.02	5.817	-10.231	-3.765	Axhandle Canyon	360	2	sparitic
br05-ax-18	55.41	0.33	3.850	-6.203	-1.982	Pete's Canyon	725	10	filamentous carbonate
br05-ax-4	59.65	2.05	5.654	-9.003	-4.363	Axhandle Canyon	176	2	associated with stromatolitic layer
br05-ax-10	72.44	0.03	5.514	-7.154	-9.997	Boiler Canyon/ Deer Gulch	182	2	
br05-ax-9	72.8	0.03	3.752	-7.241	-8.506	Boiler Canyon/ Deer Gulch	159.5	2	
br05-ax-6	72.93	0.03	4.522	-12.918	-10.054	Boiler Canyon/ Deer Gulch	151.75	2	
br05-ax-8	72.95	0.03	1.476	-10.976	-8.076	Boiler Canyon/ Deer Gulch	150.5	2	
br05-ax-5	73.04	0.03	4.574	-6.096	-1.562	Boiler Canyon/ Deer Gulch	144.75	2	
br05-ax-7	73.1	0.03	5.819	-13.286	-9.765	Boiler Canyon/ Deer Gulch	141	2	
br05-ax-1	76.4	2.75	5.672	-12.571	-5.736	Boiler Canyon/ Deer Gulch	-10	5	rhizolith
br05-ax-2	76.4	2.75	5.486	-7.415	-4.636	Boiler Canyon/ Deer Gulch	-10	5	20-cm K horizon
br05-ax-12	113.5	13.5	5.615	-8.215	-3.542	Boiler Canyon/ Deer Gulch	N/A	N/A	Cedar Mountain Fm (overturned)
br05-ax11	NA	NA	5.016	-10.087	-2.918	Boiler Canyon/ Deer Gulch	N/A	N/A	nodule drift (cf. AX-5-10)

Figure 5.6: Stable isotopic and percent inorganic carbon values of pedogenic carbonates, North Horn Formation, Axhandle Basin, Utah. (A) $\delta^{13}C$ and $\delta^{18}O$ time series for Boiler Canyon/Deer Gulch section, PS-1 and 2. Error bars represent temporal uncertainty in paleomagnetic correlation of sample site (Talling et al., 1994; Cande and Kent, 1995). (B) $\delta^{13}C$ and $\delta^{18}O$ time series for Axhandle Canyon and Pete's Canyon sections. PS-5. (C) Comparison of pedogenic carbonate stable isotopic series. Colored datapoints denote stratigraphic section from which sample was collected. Samples marked with a letter are interpreted as secondary (i.e. diagenetic) carbonate accumulations, and are included only for comparison with isotopic values from primary (i.e. pedogenic) nodular carbonates.

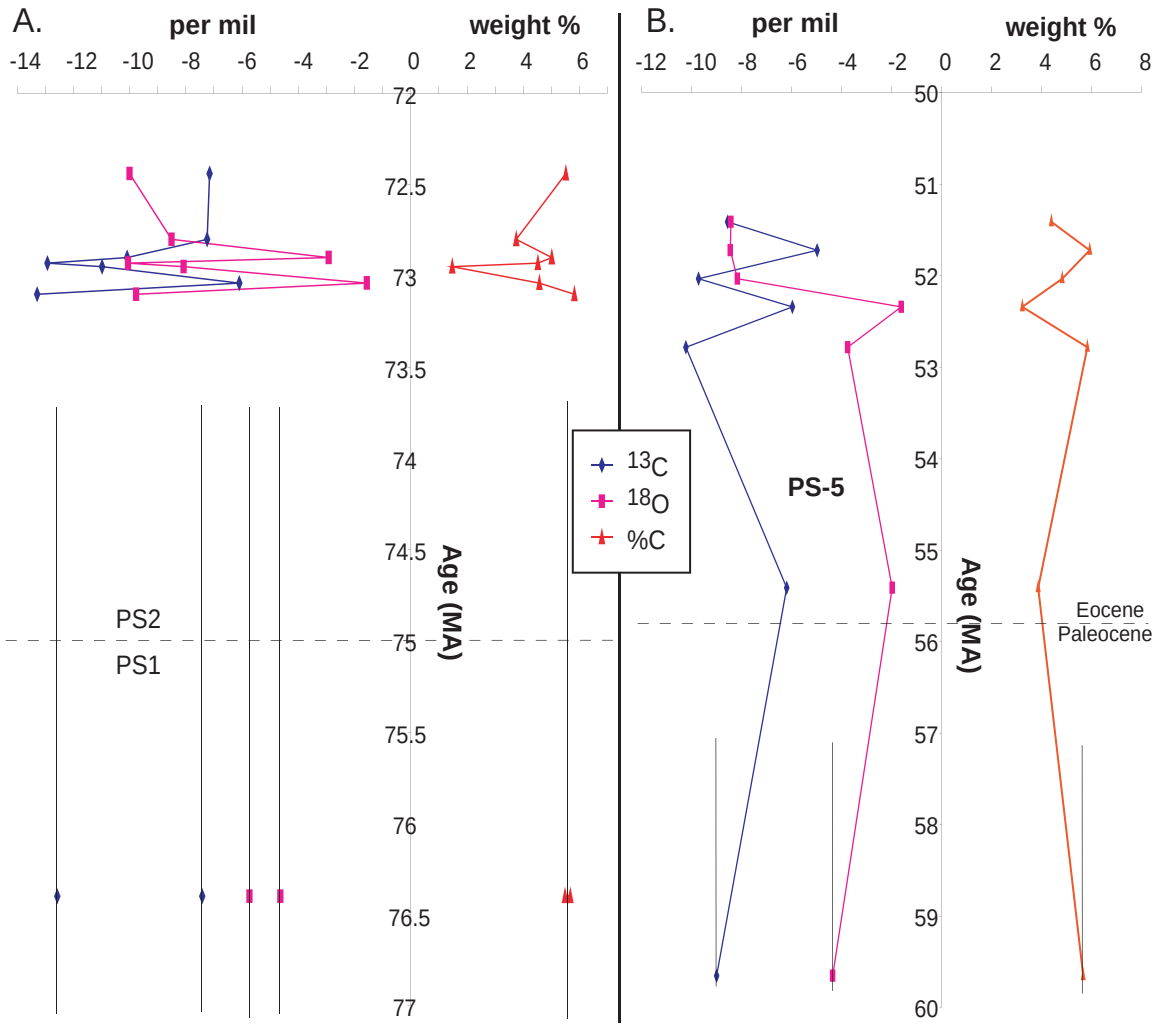
A.
per mil
weight %
-14 -12 -10 -8 -6 -4 -2 0 2 4 6
72 72.5 73 73.5 74 74.5 75 75.5 76 76.5 77
Age (MA)
PS2
PS1
13C
18O
%C
B.
per mil
weight %
-12 -10 -8 -6 -4 -2 0 2 4 6 8
50 51 52 53 54 55 56 57 58 59 60
Age (MA)
PS-5
Eocene
Paleocene

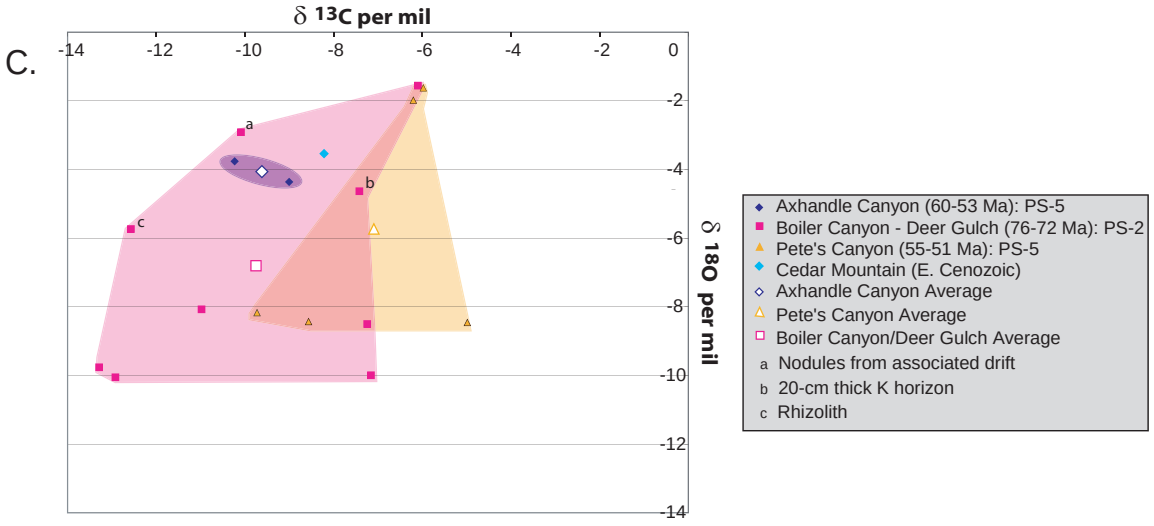
C.
δ 13C per mil
-14 -12 -10 -8 -6 -4 -2 0
-2 -4 -6 -8 -10 -12 -14
δ 18O per mil
a
b
c
Axhandle Canyon (60-53 Ma): PS-5
Boiler Canyon - Deer Gulch (76-72 Ma): PS-2
Pete's Canyon (55-51 Ma): PS-5
Cedar Mountain (E. Cenozoic)
Axhandle Canyon Average
Pete's Canyon Average
Boiler Canyon/Deer Gulch Average
a Nodules from associated drift
b 20-cm thick K horizon
c Rhizolith

This enrichment is ~1‰ for $\delta^{18}O$ and ~2.6‰ δ^{13} C in the well-developed calcic paleosols of Pete's Canyon section. Note that only two calcic paleosols were sampled from Axhandle Canyon, so no meaningful comparison can be made for these samples relative to older samples.

Additional comparisons can be made between primary carbonate nodules and secondary accumulations (Fig. 5.6B). A sample of rhizolithic carbonate was depleted by 2.5 to 5.5‰ $\delta^{13}C$ relative to the mean values of all nodular (i.e. primary) carbonates. In contrast, a sample from a 20 cm thick Bk horizon (coalesced carbonate) yielded values similar to the mean values of the three sampled sections. Finally, a sample from the Cretaceous Cedar Mountain Formation, which is abundantly mottled and recemented with carbonate, was only slightly enriched in $\delta^{18}O$ relative to mean North Horn values, and its δ^{13} C value was nearly identical to the younger samples.

Is the range of isotopic values from this preliminary sample suite within the range obtained from similarly-aged paleosols? Koch *et al*. (2003) analyzed a high-resolution time-series of pedogenic carbonates from three coeval Paleocene-Eocene sections in the Bighorn Basin, north-central Wyoming. Their sampled carbonate nodules were microsampled and values were averaged from 2-4 nodules per profile, such that intra-nodular and intra-soil differences were minimized. The resultant time series exhibits reliable isotopic values for ~57.5 – 52.5 Ma (Figure 5.7). $\delta^{13}C$ values are in the range of -6 to -15.5‰, with the most depleted values occurring at approximately 55 Ma, the Paleocene-Eocene boundary. Koch *et al*.'s (2003) $\delta^{18}O$ values ranged from -6.5 to -10‰, with modest enrichment ~55 Ma. A similar paleosol dataset from southern France (Cojan *et al*., 2000) successfully represents the long-term global isotopic fluctuations recognized in marine deposits at and shortly after the Paleocene-Eocene boundary (Zachos *et al.*, 2001), although the southern France

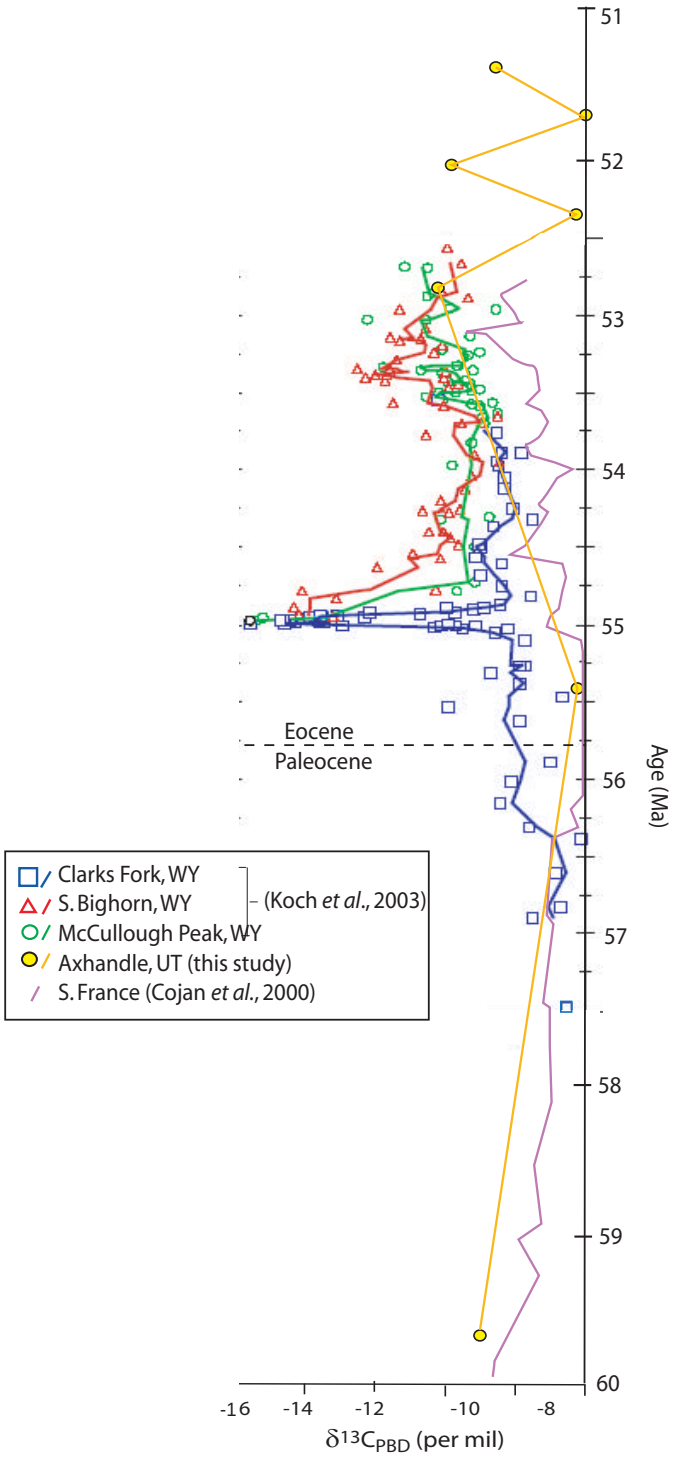

Figure 5.7: Time series of ^{13}C from Late Paleocene-Early Eocene pedogenic carbonates of the western US and southern Spain. Chronology and data from Wyoming adapted from Koch et al., 2003, their Figure 7. Long-term trendline of France data redrafted from Cojan et al., 2000, their Figure 2.

dataset exhibits a narrower range of $\delta^{13}C$ values (-5.5 to -10‰) and a less dramatic excursion at the PETM (note that Koch *et al*., 2003 acknowledge that the greater depletion of their samples relative to Cojan *et al*, 2002 is not understood). Only three Axhandle datapoints coincide with the time range of the Wyoming and French datasets (Fig. 5.7). Yet the $\delta^{13}C$ values for these horizons correspond in magnitude and trends, suggesting that the Axhandle Basin responded to similar humidity trends as existed globally

Because of the multiple, regionally-variant factors affecting $\delta^{18}O$ fractionation, further comparison of our data with the Bighorn Basin and southern France time series is not advisable. Instead, we can directly compare the new data to Mack and Cole's (2005) reported values from Axhandle Basin and their paleoclimate model. They report a mean value $\delta^{18}O_{SMOW}$ of 21.67‰ ($\delta^{18}O_{PDB}$ = -8.97‰) for nodular samples with <5% sparite (n=12, s.d. =0.63). Mack and Cole (2005) state an Early Maastrichtian age for their samples. They were collected from a single interval <200-m-thick of the Lower Redbed member of the North Horn Formation in Boiler Canyon (Gregory Mack, personal communication, 2006), corresponding to stratigraphic sequence PS-2. Recorrelation of the Boiler Canyon paleomagnetic section (Talling *et al.*, 1994) to updated global time scales (Cande and Kent, 1995; Gradstein *et al.*, 2005) places Mack and Cole's (2005) samples in a time interval ~76 – 72 Ma. Our paleosol carbonates sampled from a 41-m-thick portion of the same section (76.4-72.4 Ma) yielded a mean value $\delta^{18}O_{SMOW}$ of 23.40‰ ($\delta^{18}O_{PDB}$ = -7.29‰, n=8, s.d. =3.15), in reasonable agreement with their data. Mack and Cole's (2005) model of $\delta^{18}O$ variations with paleoclimate and latitude reveals that both the new Axhandle isotopic data presented here (Table 5.4) and their original data suggest that the Paleocene-Eocene Axhandle basin was characterized by seasonal precipitation during the winter months (Figure 5.8). The small degree of measured variability in Mack and Cole's

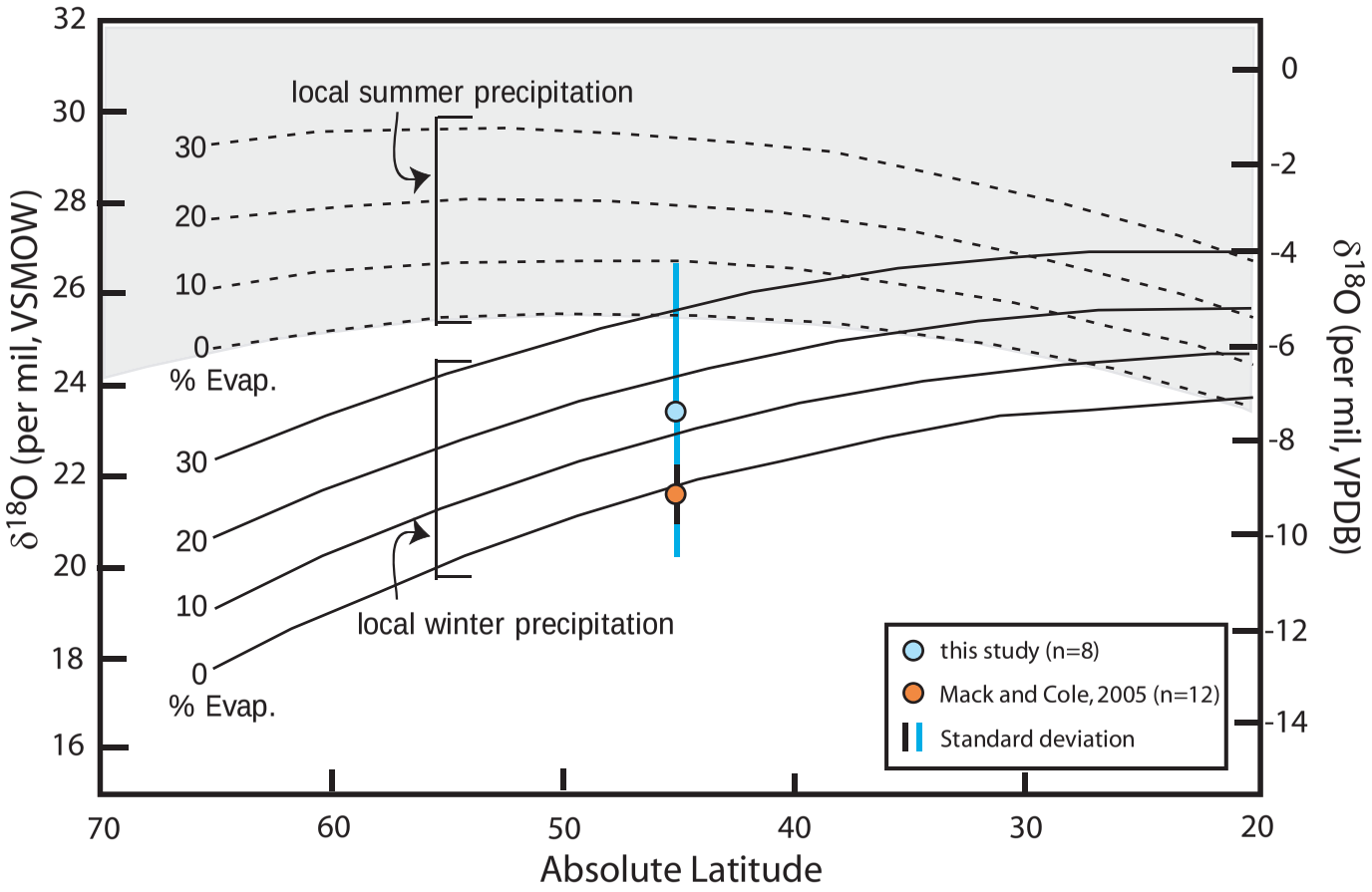

Figure 5.8: Interpreted seasonality of precipitation and evaporative enrichment of Late Cretaceous pedogenic carbonate $\delta^{18}O$ collected from Axhandle Basin (Boiler Canyon section) by comparison to modeled values of Mack and Cole (2005). The modeled $\delta^{18}O$ is a function of absolute latitude. Sampled section and time range (76-72 Ma) for this study are the same as for the Mack and Cole (2005) study. Redrafted from Mack and Cole, 2005, Fig. 1B.

(2005) data implies a more humid climate (i.e. less evaporation) than does the large degree of variability of $\delta^{18}O$ in the suite of samples presented here. However, this difference could alternatively reflect differences in sampling strategy (microsampling by Mack and Cole (2005) versus this study's bulk homogenization of pedogenic carbonates).

Of importance to interpreting the Axhandle Basin isotopic data is the macroscopic lithologic association of the sampled paleosols. Axhandle Canyon PS-5 paleosols developed in deposits in close proximity to units interpreted to have formed at lake margins (Lawton and Weiss, 1999), where groundwater level was likely close to the surface. The lack of preserved carbonate, the abundance of vertic features and generally drab appearance of these paleosol profiles suggest pedogenesis in a poorly-drained setting. In contrast, Boiler Canyon/Deer Gulch samples were obtained from generally well-drained floodplains experiencing episodic sedimentation. The scatter of the isotopic values from PS-2 likely reflects fluctuating groundwater and/or proximity to fluvial channels, perhaps related to autocyclic fluvial avulsion. Comparison of oxygen isotopic values to the modeled and analytical results of Mack and Cole (2005) suggests seasonal precipitation with minimal evaporative enrichment. Paleosols from PS-5 in Pete's Canyon are in association with variable drainage conditions; though oxidation features are more commonly observed, redoximorphic mottling of some paleosol profiles, variable carbonate accumulation stages and interbedded lacustrine limestones imply fluctuating groundwater levels. Where calcic accumulations accompany oxidized profiles (PS-2, uppermost PS-5), soil-drying or falling water table conditions are inferred. In contrast, redoximorphic mottling and iron-oxide nodules (PS-5 in Pete's Canyon) are suggestive of episodic or seasonal soil saturation (Kraus and Aslan, 1993).

IV. Paleoclimate interpretations from Axhandle Basin paleosols

a). Paleocene-Eocene Humidity Spike?

In his 2005 Geology paper, Gregory Retallack reports measurements of calcic horizons in 132 paleosols from the northeast slope of Axhandle Canyon. Based on his studies of Axhandle Canyon, he concluded that modest increase of seasonality of precipitation and a short but dramatic increase in Mean Annual Precipitation accompanied global warming at the end of the Paleocene in Axhandle Basin. Retallack's interpretation of Mean Annual Precipitation and seasonal variability are inferred from measurements of soil carbonate nodule size, depth to Bk horizon, and thickness of Bk horizon. Retallack (2005) converted these measured paleosol attributes to climate characteristics by use of transfer functions based on a global compilation of 807 soils that are younger than 14,000 yrs old, and carbonate accumulation rates from 9 radiocarbon-dated soils in New Mexico (2-10 k.y). Recent reconnaissance of the Axhandle Canyon stratigraphic section with Timothy Lawton (e.g. Lawton and Trexler, 1991; Lawton *et al*., 1993; Talling *et al*., 1994, 1995; Lawton and Weiss, 1999) and consideration of published data raise questions of the nature of the paleosols and inferred paleoclimates of the units measured and reported by Retallack (2005).

Though nodular paleosols are scattered throughout the Paleocene North Horn Formation, the incomplete nature of exposure and the high proportion of channel units lead to the alternative conclusion that in a vertical column at Axhandle Canyon there are fewer paleosols with well-defined Bk horizons than reported by Retallack (2005). Based on his reported chronostratigraphic ties, Retallack's (2005) measured section appears to have been on the order of 400 m thick and within the calcareous siltstone member and lowermost Flagstaff Limestone (PS-5 and 6). Comparing sections of Retallack (2005) and Lawton *et al*. (1993) (not cited by Retallack) results in

uncertainty as to which strata Retallack sampled and how he dealt with multiple offsets in the magnetostratigraphic section of Lawton *et al.* (1993). Retallack's (2005) stated assumption of constant sedimentation rates (see discussion below) is incompatible with his reported temporal record of measurements (Retallack, 2005, Fig. 4), which implies that his 132 paleosols were measured in *at most* 230 m of strata. Further uncertainty exists for paleosol thickness within the sampled Retallack (2005) section. There is an inconsistency of total soil thickness, as the sum of depth to Bk and Bk thickness suggests paleosols account for 100 m of Retallack's section, not counting profile thicknesses below the Bk horizon. In contrast, centimeter-scale stratigraphic measurement by Lawton et al. (1993) reveal that pedogenic units comprise *at most* 130 m of the 500 m total Axhandle Canyon section (Table 5.3). Most difficult to reconcile, the participation of carbonate-bearing paleosols is highly inconsistent, as my reconnaissance and Lawton *et al.* (1993) show that these represent a small fraction of this thickness whereas Retallack's reconnaissance (2005) suggests carbonate-bearing paleosols dominate the section's pedogenic component. In fact, the calcareous siltstone member from which Retallack measured section undergoes a stark lateral transition from north to south. Whereas in Pete's Canyon the unit is extensively pedogenic and distinguished by bright red and purple color banding and mottling, to the south (Axhandle Canyon, where Retallack worked), non-pedogenic conglomerates and sandstones are plentiful and siltstones are rather drab, lacking evidence of well-drained conditions conducive to pedogenic carbonate accumulation.

Retallack's paleoclimatic inferences rely on measurement of the depth to Bk horizons and the thickness of this subhorizon. However, he does not describe diagnostic features of his sampled profiles, other than to report that they all have carbonate nodules and are not eroded, based on observed converging root traces. To obtain an accurate measure of depth to Bk horizon requires that there have been no

post-pedogenic erosional removal of the top part of a paleosol. Yet, we observed that the Axhandle Canyon section contains many coarse-grained channel deposits (some with foresets to 2 m), which locally truncate underlying pedogenic siltstones across erosional surfaces. A correct measurement of primary depth to a Bk horizon may be further obscured in vertic paleosols in which carbonate nodules are translocated by shrink-swell processes (Driese and Mora, 1993). Without explanation of how the upper surfaces of pedogenic units were distinguished from erosive surfaces, criteria for recognizing compound profiles in the Axhandle Canyon section, and criteria to eliminate examples which suffered translocation mixing, the assumption of complete preservation of the soil profile and measurable Bk depths is dubious.

Only two paleosols with distinct Bk subhorizons were recognized in the Axhandle Canyon measured section, at 176 m and 360 m height, and each illustrates additional uncertainties with Retallack's conclusions. The lower paleosol is overlain by an oncolitic limestone, and the Bk horizon is ~30 cm from that upper contact. It is not completely clear whether that nodular horizon (~59.7 Ma) is a Bk calcic nodule horizon or nonpedogenic in origin; the nodular carbonate material in this profile is fossiliferous and sparitic, the latter possibly reflecting diagenetic cementation, replacement of primary micrite or the influence of a fluctuating water table (e.g. PiPujol and Buurman, 1997). Erosive relief occurs at the top of this paleosol unit. The paleosol at 360 m above the base of the section (~ 52.8 Ma) also contains very sparry (possibly diagenetic rather than pedogenic) nodules, concentrated >90 cm from the presumed top of the paleosol. Because part of this horizon and overlying units are obscured with slopewash, a profile thickness cannot be measured. If we interpret these units as well-preserved calcic paleosols, the nodular accumulations are consistent with Retallack's interpretation of greater Bk depth near the Paleocene-Eocene boundary. But it does not seem possible that the variation in Bk depth can be confirmed by data

from as many horizons as Retallack (2005) reported, and we are not satisfied that the Bk depths are well constrained even in the two best examples we found.

Retallack's (2005) association of the Axhandle Basin paleosol data with global paleoclimate is heavily dependent on their ages, and his age model is inconsistent with available magnetic polarity chronology. Retallack applies a linear age-height model for the Axhandle Canyon paleosols whose magnetic polarity data indicate that they span ~ 58 to 49 Ma; he assumes the rate of accumulation was constant and high (27m/m.y.) over this interval. However, his extrapolation of this constant high rate to samples as old as ~64 Ma conflicts with Talling *et al*.'s (1994) data which show that accumulation rate was not constant but instead higher prior to 58 Ma (their Fig. 11 A, see also Figure 6.7).

According to Retallack (2005, his Fig. 4), the calculated mean annual precipitation (MAP) based on depth of Bk horizon for the Axhandle Canyon stratigraphic interval is generally arid (MAP of 327-512 mm/yr for 115 paleosols), with a "humidity spike" represented by 7 paleosols developed under sub-humid conditions (516-810 mm/yr precipitation, beginning at 55.6 ± 0.5 Ma and concluded by 55 Ma). Note that the large MAP ranges reported result in near-overlap of arid vs. sub-humid MAP conditions. The MAP for the remaining 10 measured paleosols is not reported. The Upper Redbed Member (Lawton et al., 1993) of the North Horn Formation (upper PS-5) in Axhandle Canyon is interpreted by Retallack as supportive evidence of an abrupt humidity spike at the Paleocene-Eocene boundary. In Axhandle Canyon, the Upper Redbed, a sandy siltstone, is ~15 m thick and occurs between 50.78 and 49.71 Ma (Talling *et al*., 1994, recorrelated to Cande and Kent, 1995, C23n.1n to C22n). Thus, the Upper Redbed interval post-dates the Paleocene-Eocene boundary by a full 5 million years. Furthermore, whatever its age and climatic significance, the Upper Redbed is not a short-lived interval and thus not reflective of a

humidity “spike”. For example, just 5-6 km NNE in the Pete’s Canyon paleomagnetic section, the redbed unit is much thicker (~120 m) and of longer duration (53.3 to <50.8 Ma, C23n.1n – C24n.3n). In fact, farther west in the Axhandle Canyon, the redbed thickens to 120 m (Lawton and Weiss, 1999).

The oxidized nature of the Upper Redbed member may be related to greater humidity, as Retallack (2005) interprets, although it should be noted that the original interpretation for the reddish coloration was recycling of detritus from the red-colored Jurassic Twist Gulch Formation (Lawton and Weiss, 1999). The Upper Redbed is interpreted as evidence of a humidity “spike” based on limited exposure (the unit pinches out between Pete’s and Axhandle Canyons), but wasn’t as short-lived as Retallack suggests nor is it coincident with the Paleocene-Eocene boundary. A detailed along-strike assessment of paleosol development in the calcareous siltstone member is necessary to determine whether fossil soils responded to increased local or global humidity.

b) Local versus global paleoclimatology:

Despite our misgivings about the use of field measurements of calcic paleosols to record increased humidity for the Axhandle Basin at the Paleocene-Eocene boundary, comparison of carbon stable isotopic values obtained thus far from Axhandle Basin with well-calibrated and high-resolution studies (Cojan *et al*., 2000; Koch *et al*., 2003; Fig. 5.7) suggests that great potential exists to resolve local versus global paleoclimate from the Axhandle Basin paleosol record. In Pete’s Canyon for the time interval of interest, uppermost Paleocene through Lower Eocene strata can be redundantly sampled within the well-calibrated magneto-stratigraphy; chronostratigraphic constraint in Pete’s Canyon is excellent for units younger than 60.9 Ma (Talling *et al.*, 1994). This section is better suited for sampling than is the Axhandle Canyon section examined by Retallack (2005) because drainage conditions

were better and paleosols with carbonate accumulations are more abundant, both of which are necessary for a detailed stable isotopic timeseries of primary pedogenic carbonates. However, given the lateral facies changes from north to south, a robust assessment of Paleocene-Eocene paleoclimate requires detailed paleosol measurement and sampling from all the available paleomagnetic sections.

Based on available data, a qualitative assessment of local paleoclimate variations can be discerned from the Axhandle Basin paleosols. The lateral changes in lithofacies and paleosol characteristics suggest that paleosols are strongly influenced by their "microclimate", that is the drainage conditions dictated by adjacent sedimentary systems (e.g. fluvial channels, floodplains, and lakes). Axhandle Canyon paleosols developed in deposits in close proximity to units interpreted as marginal lacustrine (e.g. Lawton and Weiss, 1999) where groundwater level was likely close to the surface. The lack of preserved carbonate, the abundance of vertic features and generally drab appearance of the paleosol profiles suggest humid-environment pedogenesis. Boiler Canyon/Deer Gulch samples were obtained from generally well-drained floodplains experiencing episodic overflow sedimentation from adjacent fluvial channels (e.g. interbedded sheet sandstones). The scatter of the isotopic values from this series likely reflects variable drainage conditions as the spatial relationship between soils and channels changed through time. Comparison of oxygen isotopic values to the modeled and analytical results of Mack and Cole (2005) suggests winter season precipitation with minimal evaporative enrichment (Fig 5.8). The association of paleosols in Pete's Canyon with interbedded lacustrine limestones implies temporal variation in drainage and/or microclimate. This variability is also apparent from the paleosol characteristics themselves, such as oxidation features in association with larger calcic nodules in some horizons and redoximorphic mottling associated with few or no carbonate accumulations in other horizons. Thus, the paleosols reveal that a

semi-arid (e.g. net water deficit) microclimate was common in northern sections of the basin, but redoximorphic and lacustrine intervals (especially in southern sections) indicate that semi-aridity was interrupted by wet intervals. Also, we note that enrichment of stable isotopes across the Paleocene-Eocene epoch boundary and perhaps long-term enrichment into the early Eocene suggest increasing aridification during PS-5 and PS-6, not humidification as suggested by Retallack (2005).

Summing the spatial variations among sections along the eastern margin of Axhandle Basin with the results of the preliminary suite of stable isotopic analyses, the regional paleoclimate was apparently semi-arid with winter-season precipitation. However, the degree of variability reflected in the isotopic data may not be solely a consequence of fluctuating precipitation between the 3 sampled sections or through time. Rather, isotopic variation may reflect differences in moisture attributable to soil microclimate, that is, the proximity of the paleosols to fluvial channels or lake deposits. For example, the southern (Axhandle Canyon) section is closest to the axis of stacked paleochannels (Big Mountain and Coal Canyon Members, PS-4, lower PS-5), which Talling et al. (1995) interpreted as structurally pinned by the developing thrust belt. Lacustrine delta deposits of PS-5 are also concentrated in southern exposures of the North Horn Formation. These lithofacies and the noncalcareous, reduced paleosols of Axhandle Canyon suggest a high water table, in contrast to better drained (arid?) conditions to the north. The scatter of isotopic values from all sections, particularly for Boiler Canyon samples, also suggests a high degree of microclimate variability.

Conclusions:

A sequence stratigraphic framework is established for the nonmarine Upper Cretaceous-Eocene Axhandle Basin deposits. This framework allows us to qualitatively assess the importance of tectonic and climatic variation across stratigraphic unconformities and intervening intervals of distinct lithofacies. Based on

paleomagnetic dating of thrust events and observed progressive rotations and/or angular unconformities at certain stratigraphic levels, boundaries between PS- 1 and PS-2, as well as between PS-2 and PS-3 are direct consequences of marginal uplift of the east flank of the basin (Talling *et al.,* 1995). Similarly, the PS-5 to PS-6 transition may also be ultimately related to tectonism; though this sequence boundary occurred during a period of local tectonic quiescence, the base-level lowering that resulted in regional inundation and deposition of the Flagstaff limestone has been interpreted as a response to Sevier thrusting (Stanley and Collinson, 1979; Lawton and Weiss, 1999). Conversely, the genetic mechanism(s) responsible for the remaining sequence boundaries (PS 3-4, PS 4-5) is uncertain. The boundaries coincide with major valley incision in the southern sector of the basin and contemporaneous well-drained floodplains with multiple disconformities and paleosols to the north. Minor marginal uplift may have occurred during PS-4 between 69 – 58 Ma (based on minor stratal rotation and paleocurrent reversal), but the timing is not well resolved. The ultimate cause (tectonic base-level lowering and/or climatically induced increased discharge) of the valley incision is not known. A lack of local tectonism throughout PS-2 (75-72 Ma), PS-5 and into PS-6 (<58 Ma) provides the opportunity to assess the degree of climatic variability through time; it is during these intervals that a "pure" climatic signal stands the best chance of being preserved and discerned.

Paleosols within the proposed stratigraphy reflect primarily local humidity variations, but also suggest that global climatology may be isotopically recorded by pedogenic carbonates. Increased local humidity across the Paleocene-Eocene boundary is dismissed. However, the proposed sequences and local complexities documented here provide an interpretive framework for future high-resolution paleoclimate studies, and inform subsequent assessment of nonmarine systems tract models using the well-documented Axhandle strata as a test case.

Acknowledgements:

My appreciation goes to Timothy Lawton (NMSU) for guidance and insights in the field, as well as for supplemental geological materials. Correspondence with Greg Mack (NMSU) was also helpful for comparison with a previous sample suite and interpretation of oxygen isotopic values. Thanks also to Art Kasson (Cornell) for timely stable isotopic analyses.

References:

Anderson, D.S. and Cross, T.A., 2001, Large-scale cycle architecture in continental strata, Hornelen basin (Devonian), Norway: Journal of Sedimentary Research, v. 21, p. 255-271.

Barrell, J, 1917, Rhythms and the measurements of geologic time: Geological Society of America Bulletin 28, p 745-904

Blisniuk, P.M., Stern, L.A., Chamberlain, C.P., Idleman, B., and Zeitler, P.K., 2005, Climatic and ecologic changes during Miocene surface uplift in the Southern Patagonian Andes: Earth and Planetary Science Letters, 230, p. 125-142.

Bloom, A.L., 1998, Geomorphology: A systematic analysis of Late Cenozoic landforms, 3rd ed., Englewood Cliffs, NJ, Prentice-Hall 492 p.

Bown, T.M., and Kraus, M.K., 1986, Integration of channel and floodplain suites in aggrading fluvial systems. I: Developmental sequence and lateral relations of lower Eocene alluvial paleosols, Willwood Formation, Bighorn Basin, Wyoming: Journal of Sedimentary Petrology 57, p. 587-601.

Bown, T.M., and Kraus, M.J., 1993, Time-stratigraphic reconstruction and integration of paleopedologic, sedimentologic, and biotic events (Willwood Formation, Lower Eocene, Northwest Wyoming, USA): Palaios, Vol. 8, p. 68-80.

Brown, L.F., and Fisher, W.L., 1977, Seismic-stratigraphic interpretation of depositional systems: examples from Brazil rift and pull-apart basins in Peyton C.E., ed., Seismic Stratigraphy –Applications to Hydrocarbon Exploration: American Association of Petroleum Geologists Memoir 26, p. 213-248.

Capo, R.C. and Chadwick, O.A., 1999, Sources of strontium and calcium in desert soil and calcrete, Earth and Planetary Science Letters, v. 170, p. 61-72.

Cande, S.C., and Kent, D.V., 1995, A new geomagnetic polarity timescale for the late Cretaceous and Cenozoic: Journal of Geophysical Research, v. 100, p. 6093– 6095.

Cerling, T. E., and Quade, J., 1993, Stable carbon and oxygen isotopes in soil carbonates: in Stuart, P.K., Lohmann, K.C., McKenzie, J., and Savin, S., eds., Climate Change in Continental Isotopic Records, American Geophysical Union, Geophysical Monograph 78, 374 pp.

Cerling, T.E., Harris, J.M., MacFadden, B.J., Leakey, M.G., Quade, J., Eisenmann, V., and Ehleringer. J.R., 1997, Global vegetation change through the Miocene/Pliocene boundary: Nature, 389, p. 153-158.

Cojan, I., Moreau, M.-G., and Stott, L.E., 2000, Stable carbon isotope stratigraphy of the Paleogene pedogenic series of southern France as a basis for continental-marine colleration: Geology, Vol. 28, p. 259-262.

Currie, B. S., 1997: Sequence stratigraphy of nonmarine Jurassic-Cretaceous rocks, central Cordilleran foreland-basin system: Geological Society of America Bulletin, v.9., p. 1206-1222.

Dalrymple, M., Prosser, J., and Williams, B., 1998, A dynamic systems approach to the regional controls on deposition and architecture of alluvial sequences, illustrated in the Statfjord Formation (United Kingdom, Norther North Sea) in Shanley, K.M., and McCabe, P.W., eds., Relative roles of eustasy, climate and tectonism in continental rocks: SEPM Special Publication No. 59, p. 65-81.

Davis, W.M., 1902, Base level, grade, and peneplain: Journal of Geology, p. 77-111

DeCelles, P.G. and Giles, K.A., 1996, Foreland basin systems: Basin Research, v.8, p. 105-123.

Deutz, P., Montañez, I.P., and Monger, H.C., 2002, Morphology and stable and radiogenic isotope composition of pedogenic carbonates in late Quaternary relict soils, New Mexico, U.S.A.: an integrated record of pedogenic overprinting: Journal of Sedimentary Research, v.72, p. 809- 822.

Driese, S.G., and Mora, C.I., 1993, Physico-chemical environment of pedogenic carbonate formation in Devonian vertic paleosols, central Appalachians, USA: Sedimentology, Vol. 40, p. 199-216.

Fricke, H.C., and O'Neill, J.R., 1999, The correlation between $^{18}O/^{16}O$ ratios of meteoric water and surface temperature: its use in investigating terrestrial climate change over geologic time: Earth and Planetary Science Letters, Vol. 170, p. 181-196.

Frostick, L. E. and Steel, R. J, 1993, Tectonic signatures in sedimentary basin fills: an overview in Frostick, L. E. and Steel, R. J (eds) Tectonic controls and signatures in sedimentary successions Special Publication of the International Association of Sedimentologists, 20, p. 1-9

Gingerich, P.D., 2003, Mammalian responses to climate change at the Paleocene-Eocene boundary: Polecat Bench record in the northern Bighorn Basin, Wyoming *in* Wing, S.L., Gingerich, P.D., Schmitz, B., and Thomas, E, eds., Causes and Consequences of Globally Warm Climates in the Early Paleogene: Geological Society of America Special Paper 369, p. 463-478.

Gradstein, F.M., Ogg, J.G., Smith, A.G. et al., 2005, A Geologic Time Scale 2004: Cambridge University Press, 610 p.

Jervey, M.T., 1988, Quantitative geological modeling of siliciclastic rock sequences and their seismic expressions, in C.K. Wilgus et al., eds., Sea level changes: an integrated approach: SEPM Special Publication 42, p. 47-69.

Koch, P.L., Clyde, W.C., Hepple, R.P., Fogel, M.L., Wing, S.L., and Zachos, J.C., 2003, Carbon and oxygen isotope records from paleosols spanning the Paleocene-Eocene boundary, Bighorn Basin, Wyoming: in Wing, S.L., Gingerich, P.D., Schmitz, B., and Thomas, E, eds., Causes and Consequences

of Globally Warm Climates in the Early Paleogene: Geological Society of America Special Paper 369, p. 49-64.

Kraus, M.J., 1987, Integration of channel and floodplain suites, II. Vertical relations of alluvial paleosols: Journal of Sedimentary Petrology, Vol. 57, p. 602-612.

Kraus, M.J., and Aslan, A., 1993, Eocene hydromorphic paleosols: significance for interpreting ancient floodplain processes: Journal of Sedimentary petrology, Vol. 63, p. 453-463.

Kraus, M. J., 1999, Paleosols in clastic sedimentary rocks: their geologic applications: Earth Science Reviews v. 47, p. 41-70.

Kraus, M.J., 2002, Basin-scale changes in floodplain paleosols: Implications for interpreting alluvial architecture: Journal of Sedimentary Research, vol. 72, p. 500-509.

Lal, R., and Kimble, J.M., 2000, Pedogenic carbonates and the global Carbon cycle in Lal, R., Kimble, J.M., Eswaran, H., and Stewart, B.A, eds., Global Climate Change and Pedogenic Carbonates, Lewis Publishers, p. 1-14.

Lawton, T.F., and Trexler, J.H., 1991, Piggyback basin in the Sevier orogenic belt, Utah: Implications for development of the thrust wedge: Geology, Vol. 19, p. 827-830.

Lawton, T.F., P.J. Talling, R.S. Hobbs, J.H. Trexler, Jr., M.P. Weiss, and D.W. Burbank, 1993, Structure and stratigraphy of Upper Cretaceous and Paleogene strata (North Horn Formation), Eastern San Pitch Mountains, Utah – Sedimentation at the front of the Sevier Orogenic Belt: U.S. Geological Survey Publication 1787-II.

Lawton, T.F. and Weiss, M.P., 1999, Geologic map of the Wales quadrangle, Juab and Sanpete Counties, Utah: Utah Geological Survey Micellaneous Publication 99-2.

Latorre, C., Quade, J., and McIntosh, W.C., 1997, The expansion of C4 grasses and global climate change in the late Miocene: Stable isotope evidence from the Americas: Earth and Planetary Science Letters, v.146, p. 83-96.

Leeder, M. R., 1993, Tectonic controls upon drainage basin development, river channel migration and alluvial architecture: implications for hydrocarbon reservoir development and characterization in North, C.P. and Prosser, D.J., eds., Characterization of Fluvial and Aeolian Reservoirs, Geological Society Special Publication No. 73, p. 7-22.

Legarreta, L., Uliana, M.A., Laratonda, C.A. and Meconi, G.R., 1993, Approaches to nonmarine sequence stratigraphy- theoretical models and examples from Argentine basins in Eschard, R., and Doligez, B., eds. Subsurface Reservoir Characterization from Outcrop Observations: Proceedings of the 7th IFP Exploration and Production Research Conference, p. 125-143

Legarreta, L. and Uliana, M.A., 1998, Anatomy of hinterland depositional sequences: Upper Cretaceous fluvial strata, Neuquen Basin, West-Central Argentina: in Shanley, K.M., and McCabe, P.W., eds., Relative roles of eustasy, climate and tectonism in continental rocks: SEPM Special Publication No. 59, p. 83-92.

Liu, B., Phillips, F.M., and Campbell, A.R., 1996, Stable carbon and oxygen isotopes of pedogenic carbonates, Ajo Mountains, southern Arizona: implications for paleoenvironmental change: alaeogeography, Palaeoclimatology, Palaeoecology Vol. 124, p. 233-246.

Machette, M.N., 1985, Calcic soils of the southwestern United States in: Weide, D.L., ed., Soils and Quaternary Geology of the Southwestern United States: Geological Society of America Special Paper, 203, p. 10-21.

Mack, G.H. and Cole, D.R. 2005, Geochemical model of $\delta^{18}O$ of pedogenic calcite versus latitude and its application to Cretaceous paleoclimate: Sedimentary Geology Vol. 174, p. 115-122.

Martinsen, O.J., Ryseth, A., Helland-Hansen, W., Flesche, F., Torkilsden, G., and Idil, S., 1999, Stratigraphic base level and fluvial architecture: Ericson sandstone (Campanian), Rock Springs Uplift, SW Wyoming, USA: Sedimentology, v.46, p.235-259.

McCarthy, P.J., and Plint, A.G., 1998, Recognition of interfluve sequence boundaries: Integrating paleopedology and sequence stratigraphy: Geology, Vol. 26, p. 387-390.

Pendall, E.G., Harden, J.W., Trumbore, S.E., and Chadwick, O.A., 1994, Isotopic approach to soil carbonate dynamics and implications for paleoclimate interpretations: Quaternary Research, v. 42, p. 60-71.

PiPujul, M.D., and Buurman, P., 1997, Dynamics of iron and calcium carbonate redistribution and paleohydrology in middle Eocene alluvial paleosols of the southeast Ebro basin margin (Catalonia, northeast Spain): Palaeogeography, Palaeoclimatology, Palaeoceanography, Vol. 134, p. 87-107.

Plint, A.G., McCarthy, P.J., and Faccini, U., 2001, Nonmarine sequence stratigraphy: Updip expression of sequence boundaries and systems tracts in a high-resolution framework, Cenomanian Dunvegan Formation, Alberta foreland basin, Canada: American Association of Petroleum Geologists Bulletin, v.85, p. 1967-2001.

Quirk, D.G., 1996, 'Base profile': a unifying concept in alluvial sequence stratigraphy in Howell, J.A. and Aitken, J.F., eds, High Resolution Sequence Stratigraphy: Innovations and Applications, Geological Society Special Publication No. 104, p. 37-49.

Retallack, G.J., 2001, Soils of the Past: an Introduction to Paleopedology, 2nd edition: Blackwell Science, 404 p.

Retallack G. J., 2005, Pedogenic carbonate proxies for amount and

seasonality of precipitation in paleosols: Geology, v.33, no. 4, p. 333-336.

Ruskin, B.G., and Jordan, T.E., 2006, Climate change across nonmarine sequence boundaries: paleopedology and lithofacies of Iglesia Basin, northwestern Argentina, in press, Journal of Sedimentary Research

Schumm, S.A., 1993, River response to base level change: Implications for sequence stratigraphy: Journal of Geology, Vol. 101, p. 279-294.

Shanley, K.W., and McCabe, P.J., 1994, Perspectives on the Sequence Stratigraphy of Continental Strata: American Association of Petroleum Geologists Bulletin, v. 78, p 544-568.

Sloss, L.L., 1962, Stratigraphic models in exploration: Journal of Sedimentary Petrology, Vol. 32, p. 415-422

Sloss, L.L., 1991, The tectonic factor in sea level change: a counter veiling view: Journal of Geophysical Research, Vol. 96, p. 6609-6617.

Soil Survey Staff, 2003, Keys to Soil Taxonomy, 9th Edition: United States Department of Agriculture, Natural Resources Conservation Service, 332 p.

Stanley, K.O., and Collinson, J.W., 1979, Depositional history of Paleocene-lower Eocene Flagstaff Limestone and coeval rocks, central Utah: American Association of Petroleum Geologists Bulletin, Vol. 63, p. 311-323.

Talling, P.J., and Burbank, D.W., 1993, Assessment of uncertainties in magnetostratigraphic dating of sedimentary strata: in Aissaoui, D,M., McNeill, D.F, and Hurley, N.F., eds., Applications of paleomagnetism to sedimentary geology: SEPM Special Publication No. 49, p. 59-70.

Talling, P.J., D.W. Burbank, T.F. Lawton, R.S. Hobbs, and S.P. Lund, 1994, Magnetostratigraphic chronology of Cretaceous-to-Eocene thrust belt evolution, central Utah, USA: Journal of Geology, v. 102, p. 181-196.

Talling, P.J., Lawton, T.F., Burbank, D.W., Hobbs, R.S., 1995, Evolution of the latest Cretaceous- Eocene nonmarine deposystems in the Axhandle piggyback basin of central Utah: GSA Bulletin, v. 107, p. 297-315.

Tucker, G.E., and Slingerland, R., 1996, Predicting sediment flux from fold and thrust belts: Basin Research 8, p. 329-349.

Utah Geological Survey, 1999, Redefining the Lower Cretaceous stratigraphy within the central Utah foreland basin: Utah Geological Survey Special Study 99, 21 p.

Vail, P. R., F. Audemard, S. A. Bowman, P. N. Eisner, and G. Perez-Cruz. 1991. The stratigraphic signatures of tectonics, eustacy and sedimentology; an overview, p. 617-659, *in* G. Einsele, W. Ricken, and A. Seilacher, (eds.), Cycles and events in stratigraphy.

Van Wagoner, J.C., H. W. Posamentier, R. M. Mitchum, P. R. Vail, T. F. Sarg, T. S. Loutit, and J. Hardenbol. 1988. An overview of the fundamentals of sequence stratigraphy and key definitions, p. 39-45. In C. K. Wilgus, B. S. Hastings, C. G. St.G Kendall, H. Posamentier, C. A. Ross, and J. C. Van Wagoner, (eds.), Sea-Level Changes-- An Integrated Approach, Society of Economic Paleontologists and Mineralogists Special Publication, 42.

Van Wagoner, J.C., 1995, Sequence stratigraphy and Marine to Nonmarine Facies Architecture of Foreland Basin Strata, Book Cliffs, Utah, U.S.A., in Van Wagoner, J.C., and Bertram, G.T., eds., Sequence Stratigraphy of Foreland Basin Deposits - Outcrop and Subsurface Examples from the Cretaceous of North America: American Association of Petroleum Geologists Memoir 64, p. 137-223.

Wang, Y. Cerling, T. E. ; Quade, J. ; Bowman, J. R. ; Smith, G. A. ; Lindsay, E. H. , 1993, Isotopes of paleosols and fossil teeth as paleoindicators: in Stuart, P.K., Lohmann, K.C., McKenzie, J., and Savin, S., eds., Climate Change in Continental Isotopic Records: American Geophysical Union, Geophysical Monograph 78, p. 241-248.

Weissmann, G.S., Mount, J.F., and Fogg, G.E., 2002, Glacially driven cycles in accumulation space and sequence stratigraphy of a stream-dominated alluvial fan, San Joachin Valley, California, U.S.A.: Journal of Sedimentary Research, Vol. 72, p. 240-251.

Wheeler, H.E., 1964, Base level, lithosphere surface and time-stratigraphy: Geological Society of America Bulletin, Vol. 75, p. 599-609

Working Group on the Origin and Nature of Paleosols, 1971, Criteria for the recognition and classification of paleosols: in Yaalon, D.H., ed., Paleopedology-Origin, Nature, and Dating of Paleosols, p. 153-158, International Society of Soil Science.

CHAPTER 6: ASSESSMENT OF NONMARINE SYSTEMS TRACT AND SEQUENCE GENESIS MODELS UTILIZING TEST BASINS IN THE ANDEAN AND SEVIER FORELANDS

Introduction:

Sequence stratigraphy has become a powerful method of organizing the stratal record into genetically related, and in some cases predictable, successions. The method emphasizes physical correlation of chrono-stratigraphic surfaces and facies details. Stratigraphic analyses of seismic, borehole and outcrop data following the sequence concept have successfully predicted facies architecture in marginal marine settings. In recent years, sequence stratigraphy has become a commonplace component of basin analysis in a variety of settings, including nonmarine deposystems.

Application of sequence stratigraphic concepts to a stratigraphic dataset (whether subsurface or surficial), requires that key surfaces can be determined and interpreted relative to changing base level. Systems tracts are subdivisions of sequences into contemporaneous depositional systems defined by their position within a sequence, bounding surfaces, and lithofacies stacking patterns (Brown and Fisher, 1977). Stratal geometries and lithologies are often characteristic of a particular systems tract, and systems tracts are often named in reference to the phase of the base level cycle during which they were deposited (e.g. “lowstand”, “transgressive” and “highstand”; see Van Wagoner *et al.*, 1988). Whereas unraveling the exact contributions of the agents affecting base level can be challenging, interpretation of base level cyclicity from stratigraphic response can lead to a more complete understanding of the spatial variability of the depositional system (Olsen *et al.,* 1995).

Research leading to development or refinement of base level concepts within continental deposystems presents exciting opportunities to benefit industry,

community, and science. Determining stratal architecture in the subsurface has applications to hydrocarbon and mineral deposit exploration as well as determination of groundwater aquifers and flow paths. The socioeconomic impact of predicting potential oil reservoir characteristics or forecasting contaminant transport is strong motivation for further study. Correlations between changes in relative sea level and age-equivalent alluvial deposits have also been attempted in an effort to holistically integrate regional stratigraphic sequences with global-scale events. However, these motivations presuppose detailed understanding of the causative factors of sequence generation.

An important task of this dissertation is to document the nature of nonmarine stratigraphic sequences and their boundaries, including complexities and trends, and to suggest the relative role of extrinsic mechanisms on sequence formation. By using well-calibrated field and laboratory datasets from entirely nonmarine systems, it is possible to quantify the magnitude of individual extrinsic forcings (e.g. tectonic movements, climatic variability), and to suggest plausible degrees of interaction between these mechanisms. Models for sequence genesis can then be formulated and tested. The test of any general stratigraphic model, however, is how well it conforms to what is preserved in the geologic record. The reverse case is not applicable; real-world examples should not be forced into existing models if the preserved features do not agree with the models. Therefore, it is necessary to critically assess previously proposed sequence models against reasonably well-understood depositional systems.

The Andean and Sevier foreland basins chosen as test cases provide excellent opportunity to assess generalities of nonmarine sequence stratigraphy and lead to insights forming the basis for refinements to existing models. The Axhandle and Iglesia Basins are both entirely nonmarine wedgetop basins, located in proximal positions of extensive foreland basin systems (Sevier and Central Andean forelands,

respectively; Figure 6.1). Each basin is characterized by abundant unconformities and growth strata, both key elements for construction of sequence stratigraphic frameworks (through combination of seismic and outcrop interpretation for Iglesia, see chapter 2; through outcrop measurements in Axhandle Basin, see chapter 5). Chronostratigraphic constraint is excellent for both cases (Talling *et al.,* 1995; Ré *et al.*, 2003; this study), as is knowledge of the local and regional tectonic activity. Outcrop belts cover limited portions of the wedgetop basins (proximal for Axhandle, axial to distal for Iglesia), but lateral and vertical continuity is sufficient in both test basins to describe depositional system evolution through time and space, requisite conditions for identification of systems tracts (e.g. Posamentier and Allen, 1999). Pedogenic facies are an important volumetric component of the basins' interfluvial deposits, thereby providing constraints on syndepositional paleoclimate variations (chapters 3 and 5). Table 6.1 summarizes the observable characteristics of the proposed sequence boundaries for Axhandle and Iglesia basins as well as which extrinsic factors were measurably changing during sequence boundary generation (as discussed in chapters 2, 3 and 5).

Base level and alluvial architecture

To accumulate sediment at a given location, there must be less energy available to transport sediment away from that location than there was energy available to deliver sediment to that location. The net sum of all the features acting across a landscape in such an energy balance is expressed in the concept of base level, a potential surface separating the realms of deposition (below that surface) and erosion (above that surface). Interpreting base level cyclicity from the stratigraphic record incorporates description of bed geometries, erosive or flooding surfaces, grain size transitions, and evidence for surface elevation change and sediment transport.

Systems tract characterization of base level cycles has resulted in terminology

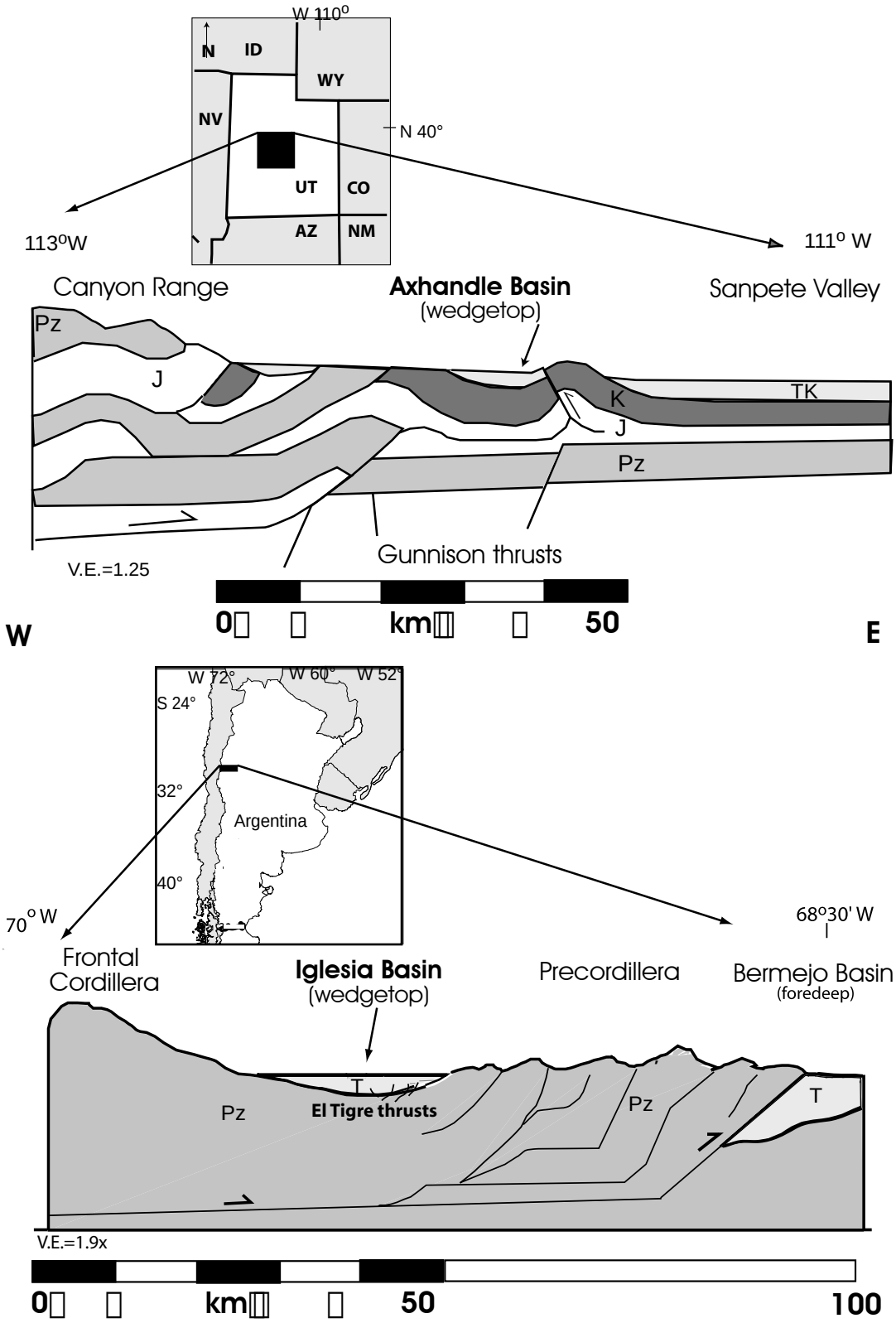

Figure 6.1: Schematic west-east cross sections through the Sevier and Central Andean forelands, illustrating regional structures and the wedgetop test basins.

Table 6.1: Summary of Axhandle and Iglesia Basin nonmarine stratigraphic sequences and interpretations of extrinsic forcing mechanisms concurrent with sequence development.

Axhandle Basin sequence summary

Proposed Sequence	Age (MA)	Nature of basal contact; *Internal hiatuses*	Interpreted Forcing(s)
PS-6	<50	Disconformity (east)	Climate
PS-5	<60.9 - 50	Incised valley; *intense pedogenesis to north; Multiple flooding episodes.*	Climate; Tectonism
PS-4	<68.7 - <60.9	Incised valley; *multiple paleosol horizons >5 MA paleomagnetic gap*	Climate; Tectonism
PS-3	71.3 - 68.7(?)	Angular unconformity (east)	Climate; Tectonism
PS-2	75 - 71.3	Angular unconformity	Climate
PS-1	83 - 75	angular unconformity; *progressive bed rotation*	Tectonism

Iglesia Basin sequence summary

Proposed Sequence	Age (MA)	Outcrop nature of basal contact; *Internal hiatuses*	Interpreted Forcing(s)
7	<5.2	Paleosols, minor erosion; *progressive bed rotation, paleosols*	Tectonism
6	6.6 -5.2	Conformible (lithofacies chage); *intense pedogenesis to north; Multiple flooding episodes.*	Climate (?); Tectonism
5	6.9 -6.6	Paleosol horizons, minor erosion; *progressive bed rotation, channels.*	Climate; Tectonism
4	7.7-6.9	Conformible (lithofacies change); *progressive bed rotation, paleosols.*	Climate;
3	8.7-7.7	Disconformity (lithofacies change); *progressive bed rotation, paleosols.*	Climate; Tectonism
2	<9.0-8.7	Incised valley, >4 Ma hiatus; *progressive bed rotation, channels*	Tectonism

entrenched in the sequence stratigraphic literature, but their application is often inconsistent with the original definitions (Van Wagoner, 1995). Systems tracts have been applied to a variety of depositional settings with reference to either rock properties or to interpreted "relative base level" (e.g. eustatic sea level plus tectonic subsidence or uplift). Interest in the fluvial response to eustatic variation resulted in transfer of systems tract terminology to marginal-marine and even nonmarine realms, the topic of this chapter. However, the terminology should not lead to an uncritical interpretation that certain rock properties are evidence of a particular position of sea level or a portion of the base level curve (Van Wagoner, 1995).

Systems tract interpretations based on rock properties versus those made from inferred base level curves may be fundamentally different. Thus, consistency of usage is advisable. For the nonmarine foreland basins explored herein, I attempt to bridge these interpretations by critically assessing published general models of systems tracts and sequence genesis against observed features of stratigraphic sequences and their interpreted causes. More fundamentally, I analyze whether systems tract concepts are valid for nonmarine depositional systems, whereby base level cyclicity is not tied to eustasy, but instead driven by myriad autocyclic and allocyclic processes (discussed in Chapter 1).

General models for nonmarine sequence formation

For nonmarine sequences, models including systems tract concepts have been proposed as a means to characterize base level cycles, based upon information about gross-scale stratigraphic architecture (e.g. Legarreta *et al.*, 1993; Wright and Marriott, 1993; Van Wagoner, 1995; Currie, 1997; Dalrymple et al., 1998; Legarreta and Uliana, 1998; Plint *et al.*, 2001 among others; Table 6.2). These models do not appeal to a particular forcing mechanism, and though they were formulated from a variety of basin settings (discussed below), each purports to be generally applicable to

Table 6.2: Features of general systems tract models for nonmarine systems considered in text. (1) Legarreta et al., 1993; Legarreta and Uliana, 1998; (2) Wright and Marriott, 1993; (3) Van Wagoner, 1995; (4) Currie, 1997; (5) Dalrymple et al, 1998; (6) Plint et al., 2001. Each text box includes an identical base level curve, constructed as base level elevation versus time (progressing forward to right). The segment of base level history corresponding to text is marked by broad gray bar. Sequence boundary onset is marked by SB and bar crossing base level curve.

1) Legarreta *et al*, 1993; Legaretta and Uliana,1998	2) Wright and Marriott, 1993
Aggradational Widespread suspended load deposits. Increased frequency of paleosols (upward maturing?) Landscape stability/reduced surface gradient (decelerating accommodation capacity) 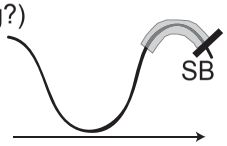	***Highstand*** Reduced accommodation allows well-developed floodplain soils. Higher rates of floodplain reworking, increased channel density. Low-gradient floodplains may develop shallow lakes. 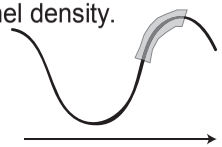
Backstepping Stepwise migration of coarsest facies toward basin margins. Mixed bedload and suspended load deposits. Upward fining grainsize (decreasing net:gross) Depositional response to increased accommodation potential (depositional area expands) 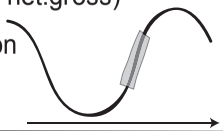	***Transgressive*** Multi-storey sandbodies, floodplain reworking, hydromorphic soils. Increased accommodation enhances floodplain storage (isolated channels, weakly developed, well-drained soils) 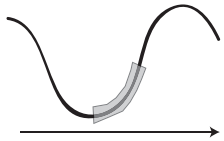
Forestepping Upward coarsening channel fill complexes. Dominated by bedload transport Spatially restricted (near incised surface) Basinward shift of proximal deposits concurrent with marginal incision. Localized decrease in A/S ratio 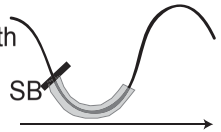	***Lowstand*** Coarse-grained fluvial deposits/ Restricted low-sinuosity (braided) deposits Mature, well-drained soils on terraces 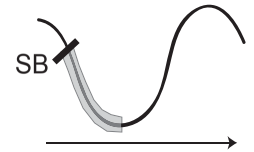

Table 6.2 (Continued)

3) Van Wagoner, 1995	4) Currie, 1997
Highstand Muddy levee, crevasse splay, and lake margin deposits Broad interfluves. Interbedded single-story sandstone (low net:gross) 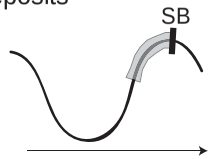	***Aggradational*** Abundant fine grained overbank and lacustrine deposits. Isolated, lenticular channels (anastamosing) transition to braided channel sandstones and conglomerates Increasingly mature paleosols as flood-plain aggradation decreases. 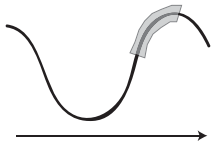
Transgressive Thinner, single-story sandstone, moderate to low net:gross Mudstones dominate strata along with crevasse splays, coals, lakes, soils. Aggradational and upward-fining 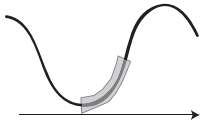	***Transitional*** Transitional from braided (laterally continuous) to meandering (isolated) channels. Increasing preservation of overbank sediment and paleosols. Coarse to fine grained. 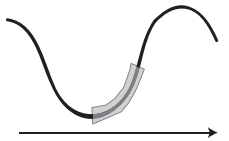
Lowstand Multi-story, high net:gross, laterally continuous sandstones, filling up-dip end of incised valley. Braided crossbedded sands. No overbank accommodation. Upward fining. 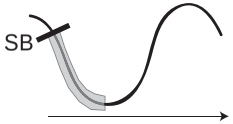	***Degradational*** Coarse grained, braided channel sandstones and conglomerates. Laterally-continuous channel forms fill incised valleys. Thick paleosols adjacent to incised valleys. 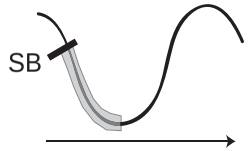

Table 6.2 (Continued)

5) Dalrymple *et al.*, 1998	6) Plint *et al.*, 2001
Unconfined SEP* Low Rate of aggradation lowered. Increased channel amalgamation. If elevation ~unchanged, extensive sheet sands deposited. **SEP: Stream Equilibrium Profile* 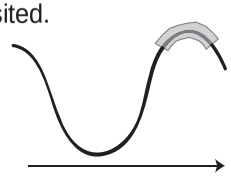	***Paleosol Dominated - Low Accommodation - Late Highstand*** Blocky mudstones representing moderate to well-developed paleosols. Interstratified crevasse splay sands or thin wetland units. The upper part of each sequence, followed by fluvial enrichment, sedimentary bypass and polygenetic pedogenesis. 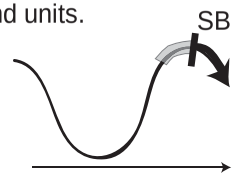
SEP High Rate of aggradation increases Channels more isolated within fine-grained floodplains. During low accommodation, soils develop. Minimal pedogenesis during high rates of aggradation. 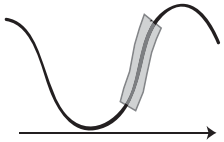	***Lacustrine Dominated - High Accommodation - Late Transgressive/ Early Highstand*** Widespread lacustrine-wetland facies and mud-enclosed ribbon channel sandstones, blanket interfluves and anastamosed rivers. 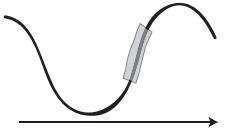
Confined SEP Low Sequence boundary or incised valley, with amalgamated channel sands within incised valley. Correlative floodplain soils (low preservation potential due to lateral channel switching/reworking). 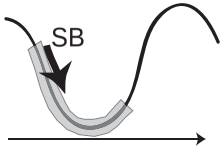	***Channel Dominated - Low Accommodation - Early transgressive*** Meandering multi-storey channels and valley fill. Scarce preservation of flood-plain mudstones, reflecting prolonged fluvial reworking 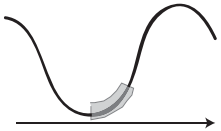

nonmarine systems. Though the terminology of the different systems tract (ST) models varies markedly, each presents a three-component base level cycle: essentially falling, turnaround and rising stages. The main caveats of each model are discussed below.

For basins with no obvious or very minimal connectivity with the marine realm, Legarreta *et al*. (1993) and Legarreta and Uliana (1998) generated a theoretical model of the deposits expected during a base level transit cycle (Table 6.2(1)). They attribute sequence boundary genesis to long-term base level fall. The erosive boundary is overlain by an upward coarsening succession during the first systems tract ("forestepping"). As accommodation increases ("backstepping ST") and then diminished ("aggradational ST"), a fining-upward succession accumulates. These workers consider their model applicable to sequences between 0.5- 3.0 Ma (equivalent to 3rd order marine sequences of Vail *et al.,* 1991). Shorter-duration sequences may be impacted by climatic or orbital cyclicity too complex to be generalized by their model.

The fluvial sequence model of Wright and Marriott (1993; Table 6.2 (2)) emphasized the role of floodplains as sediment sink, especially during the transgressive phase of a base level cycle. These workers approximate sea level with base level, and though their model is located "somewhere" in the fluvial system, ties to sea level change are emphasized throughout. Though base level is the main control emphasized, Wright and Marriott (1993) agree with the hierarchy of potential sequence controls outlined by Schumm (1975), namely, that tectonic change is the major control of sequence architecture, followed by climate and then geomorphic thresholds. Because of these superimposed lower-order mechanisms leading to complex interactions, Wright and Marriott (1993) acknowledge that their base level model may not necessarily apply to most river systems.

Through detailed analysis of the continuous exposures of the Late Cretaceous Book Cliffs foreland basin deposits, west-central Utah, Van Wagoner (1995) proposed a nonmarine systems tract model for high-frequency sequences (200-300 ky durations; Table 6.2(3)). The considered strata can in many cases be correlated laterally to marine surfaces with sequence significance (e.g. transgressive, maximum flooding, downlap), facilitating interpretation of a base level cycle. For the alluvial portions of the Blackhawk Formation (Desert member) and Lower Castlegate Sandstone, Van Wagoner (1995) outlined the alluvial architectural features expected during the creation and reduction of accommodation space. Additionally, Van Wagoner (1995) discussed the role of variable discharge. For example, discharge may be minimal during the highstand systems tract, increasing during the lowstand ST, and decreasing discharge during the transgressive ST. Climatic variability (perhaps resulting in glacioeustatic fluctuations) is one of the more likely means of changing discharge rates.

It should be noted that the Van Wagoner (1995) model's transgressive and highstand systems tracts feature many of the same characteristics (Table 6.2(3)). Both systems tracts contain single-storey, low "net:gross" (e.g. ratio of sand-sized grains to finer grained sediment) sandstones and feature widespread deposition of overbank and floodplain sediments (e.g. soils, mudstones, and lake deposits). Distinction is made chiefly on rate of base level rise, on coal deposits in the transgressive systems tract, and perhaps on the aspect ratio (width:depth) of alluvial channels (e.g. narrow for highstand phase, unspecified for transgressive). However, as will be discussed, rate of base level change cannot be "measured" independent of the sediments found in the systems tract, so this criteria is not useful for comparative purposes. The overlap of features makes distinction between transgressive and highstand phases very difficult.

For their model of alluvial sequences, Dalrymple *et al.* (1998) reject ties to eustatic fluctuation, instead emphasizing complex feedback loops affecting fluctuations of a so-called "Stream Equilibrium Profile" (Table 6.2(5)). The Stream Equilibrium Profile (SEP) is a 2-dimensional hypothetical stream profile, essentially an instantaneous graded stream, integrating all possible extrinsic and intrinsic controls. In three dimensions, the SEP is the "most efficient" depositional surface. These workers equate the ground water table with ultimate base level for continental environments, while stressing that accumulation is controlled by the SEP cyclicity. Two different sequences are recognized: confined and unconfined. The former sequence is bounded below by an incised valley surface (created by the SEP Low) and the upper boundary may be another valley incision or an unconfined surface. This latter sequence is essentially the same, except that it included amalgamated channel sand sheets at its base.

Similar in general fining-upward succession to the previous models, the alluvial systems tract model of Currie (1997) makes predictions about fluvial architecture as accommodation space changes in the nonmarine basin (Table 6.2(4)). The initial coarse deposits of a sequence are likely to be of low sinuosity, either confined to the incised valley, or in the case of more regional, but lower amplitude erosion, the sandstones may be sheetlike. Upsection, channel deposits will become more lenticular and anastamosed. A fining-upward succession with isolated sand bodies and amalgamated fluvial sheet sands was also described in a nonmarine sequence model by Olsen *et al.* (1995), not explicitly considered here. Currie (1997) also predicts that as accommodation space is created, sedimentation rates (or more appropriately, accumulation rates for time-averaged sections) may correspondingly increase. This model is formulated specifically for a foreland basin system.

The role of paleosols in stratigraphic sequence models was fully explored by Plint *et al.* (2001), who broadly defined three systems tracts on the basis of facies changes (Table 6.2(6)). These are the channel-dominated, low accommodation space systems tract, overlain by a lake-dominated, high accommodation succession, and finally, a paleosol-dominated, low accommodation systems tract. Paleosol characteristics (microscopic, macroscopic and geochemical trends) were studied in detail for all members of the Dunvegan Formation, British Columbia (e.g. McCarthy *et al*, 1999), the coastal plain of the Late Cretaceous Western Interior seaway for which the systems tract model was formulated. This particular system obviously has a marine component, chiefly expressed during the low-accommodation systems tract as coastal valleys are filled to the maximum marine flooding surface. However, the response of paleosols to changing accommodation and thus sedimentation rates is an important feature to consider, as most alluvial systems contain significant pedogenic intervals.

In Table 6.2 systems tracts are aligned as closely as possible by common intervals in the hypothetical base level cycles depicted by the authors (*sensu* Van Wagoner, 1995; see above). Note that these authors interpret similar architectural elements to represent markedly different positions in the base level cycle (e.g. single-story sand bodies, floodplain sediments and paleosols are related to both rising and highstand segments of the base level cycles). The result is eye-opening: rock property characterizations appear to have no known relationship to base level. Clearly, little consensus exists as to when stages of the base level cycle begin and end. Additional inconsistencies arise in the placement of the sequence boundary. Though all the modelers agree that base level fall diminishes accommodation space and may lead to erosion, they differ in whether the sequence boundary is generated at the beginning, middle or end of the falling hemicycle. Similar controversy exists for marginal marine

and lacustrine environments (e.g. Posamentier and Allen, 1999). This distinction may be important when attempting to quantify how the variation of aggradation rate relates to dynamics of base level change.

Though general and detailed aspects of the proposed nonmarine systems tract models differ significantly, common elements of the three systems tracts can still be identified and highlighted. During falling and low base level, as accommodation space is lost, each model predicts that coarse-grained channelized deposits will fill incised valleys. As base level rises and accommodation space is created, finer-grained sediments are broadly deposited on floodplains with isolated fluvial sandstones. Minimal pedogenesis occurs on the interfluves. Finally, when base level reaches its highstand position, there may be accommodation space available but the rate of accommodation space creation is reduced, well-developed soils are common before base level again drops, and a sequence boundary is formed.

The lack of spatial scale and temporal specificity complicate quantitative comparisons of natural depositional systems with these generalized models. Some models include relative spatial terms such as ‘proximal’ or ‘distal’. Other depositional landscape relationships, such as “channel” versus “overbank” or “floodplain” are mentioned. Posamentier and Allen (1999) suggest caution, however, in assigning systems tracts because not all systems tracts need be observable in all parts of a given basin.

In contrast to models referencing position in a conceptual base level cycle, other workers have formulated a more quantitative systems tract scheme for nonmarine strata, categorizing facies by their Accommodation/ Sediment supply (A/S) ratio (e.g. Frostic and Steel, 1993; Martinsen *et al.*, 1999; Anderson and Cross, 2001). The features of these models are summarized in Table 6.3. These ratio-dependent models are not directly compared to the test basins because the accommodation and

Table 6.3: Summary of alluvial deposition models based on comparison of accommodation space (A) and sediment suppy (S). The ratio between these quantities is designated A/S.

Frostic and Steel, 1993
A>S: Fining upward succession
A<S: coarsening upward succession
Martinsen *et al.*,1998
A/S >1: Sediment cannot fill available space. Flooding possible.
A/S = 1: Expanded succession with high filling probability
0<A/S<1: Sediments always fill available space; Some sediment may bypass system
A/S<0: No accumulation. Sediment bypass and/or erosion occurs
Abrupt decrease in A/S: Sequence boundary generation
Abrupt increase in A/S: Expansion surface generation
Gradual increase in A/S: Expansion zones
Anderson and Cross, 2001
Maximum A/S: distal facies, rise-to-fall turnaround
Increasing A/S. Proximal to distal facies (contracting alluvial/ braidplain, expanding lakes); Base level rise
Minimum A/S: proximal facies (maximum extent of alluvial fans; lacustrine facies may disappear); fall to rise turnaround
Decreasing A/S: decreasing facies diversity (expanding alluvial/braidplain facies, contracting lakes); distal to proximal vertical facies succession; base level fall

sediment supply fluxes are not quantified and even qualitative comparisons may be nonunique for different parts of the basin system. However, some general principles and caveats of the A/S ratio classifications are discussed following systems tract assessments.

The methodology for assessment of the models by comparison to the Axhandle and Iglesia basin strata is as follows:

1. Comparison of lithofacies features and stratigraphic architecture of individual models with preserved stratigraphic architecture and lithofacies of test basins, prior to consideration of the test basins' proposed sequence stratigraphic framework. Fence diagrams integrating multiple measured stratigraphic sections and regional facies patterns are utilized to summarize and account for lateral as well as vertical trends in lithologic characteristics.
2. Prediction of sequence boundary genesis in test basin strata based on characteristics of individual published models.
3. Comparison of stratigraphic position and lithologic features surrounding sequence boundaries predicted by the models versus sequence boundaries observed in the test basins.
4. Appraisal of model's general validity based on proportion of shared characteristics with test basin as well as success predicting stratigraphic position and features of actual sequence boundaries.
5. Suggestions for model refinement.

Assessment of Axhandle Basin

Documentation of the Late Maastrictian – Early Eocene stratigraphy in the Axhandle wedgetop basin (central Utah) is very complete, due to nine detailed stratigraphic sections and three magnetostratigraphic sections along the eastern range of the Gunnison Plateau (Lawton *et al.,* 1993; Talling *et al.,* 1994, 1995; Lawton and

Weiss, 1999). On the basis of these data, five stratigraphic sequence boundaries were proposed (Chapter 5,) separating six stratigraphic sequences. Large-scale features and sequence boundaries are presented chronologically in Figure 6.2.

For comparison with previously published models of nonmarine systems tracts, I consider two cross-sections through Axhandle strata (Figure 6.2), one in the vicinity between Axhandle and Pete's Canyons (i.e. through the stacked channel complex), and the other between Pete's Canyon and Boiler Canyon/Deer Gulch. These intervals, integrating 2-3 km distances, are chosen as extremes in the lateral (north to south) facies variability documented along the basin margin. Depositional interpretations are those of Lawton and Weiss (1999; see also Chapter 5). All sedimentary units are considered proximal with respect to the periodically thrusted and uplifted eastern basin margin (the San Pitch Mountains), as discussed by Talling *et al.,* (1995).

Table 6.4 (parts 1-3) illustrates a model-based base level and systems tract history for the preserved stratigraphic members of the Axhandle Basin. Each stratigraphic member is assigned to the most appropriate systems tract based on broad rock properties (e.g. grain size, distribution, lithofacies), and then assessment is made of the presence or absence of individual systems tract elements. Figure 6.3 represents graphic rendition of predicted base level and sequence boundary formation in comparison among the six published models as well as to sequence boundaries interpreted directly from the Axhandle stratigraphic sections**.**

One outcome of the systems tract assessment is that all the models suggest that the base level dynamics for the lower half of the North Horn Formation of the Northern section differs from that of the Southern section, though they are only separated by 4-5 km. In general, the models predict a long-term base level rise for the northern section. Some models include fluctuations during deposition of the younger members (e.g. Calcareous Siltstone, Wales Tongue, Upper Redbed and Flagstaff

Figure 6.2: Large-scale stratigraphic features, chronostratigraphic correlation and proposed sequence boundaries of Axhandle Basin (modified from Talling *et al*., 1995). Locations of integrated sections utilized in assessment of nonmarine systems tract models are shown as grey boxes.

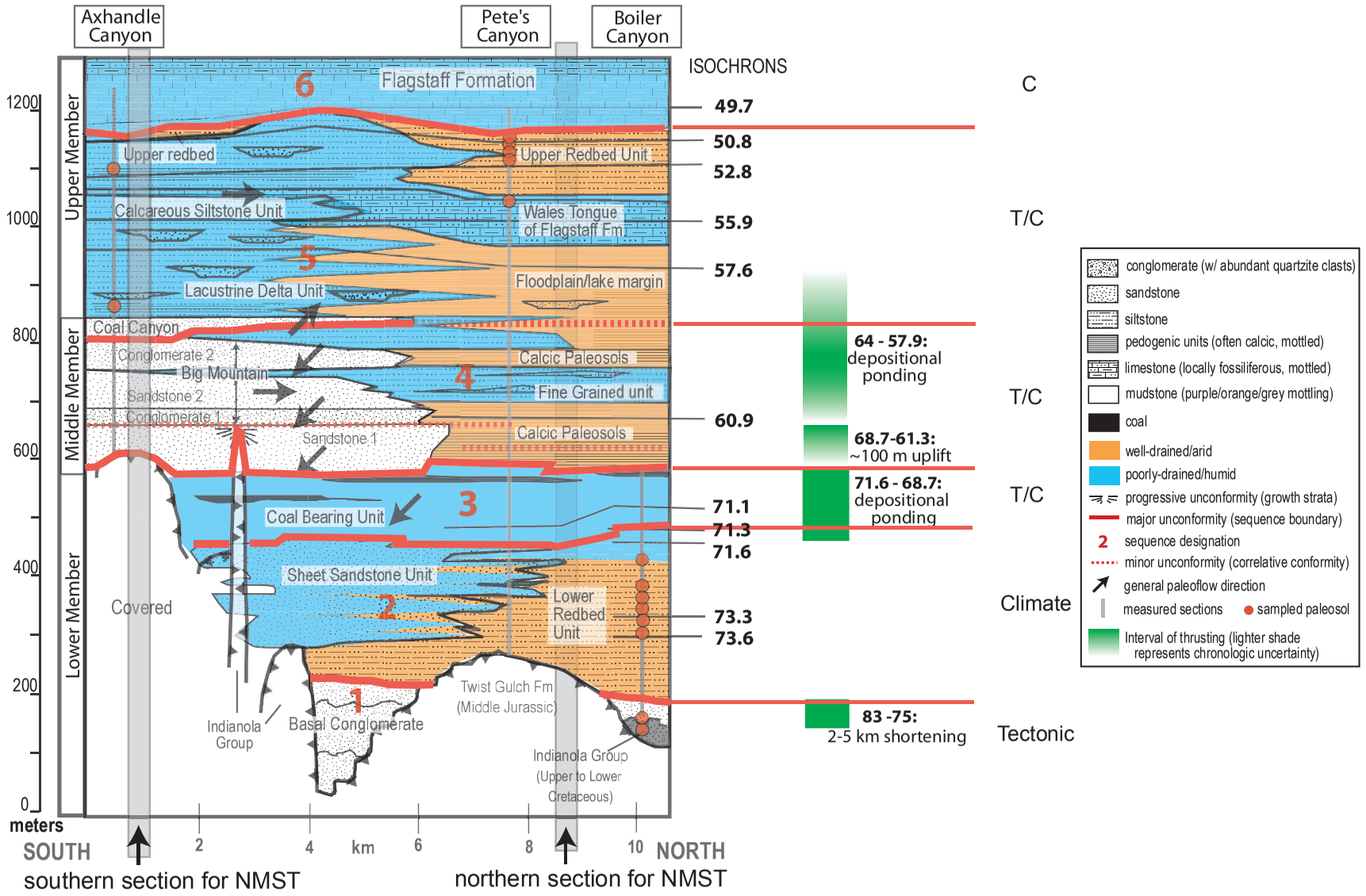
Axhandle Canyon
Pete's Canyon
Boiler Canyon
ISOCHRONS
Upper Member
Middle Member
Lower Member
Flagstaff Formation
Upper redbed
Upper Redbed Unit
Calcareous Siltstone Unit
Wales Tongue of Flagstaff Fm
Floodplain/lake margin
Lacustrine Delta Unit
Coal Canyon
Conglomerate 2
Big Mountain
Sandstone 2
Conglomerate 1
Sandstone 1
Calcic Paleosols
Fine Grained unit
Calcic Paleosols
Coal Bearing Unit
Sheet Sandstone Unit
Covered
Lower Redbed Unit
Twist Gulch Fm (Middle Jurassic)
Indianola Group
Basal Conglomerate
Indianola Group (Upper to Lower Cretaceous)
49.7
50.8
52.8
55.9
57.6
60.9
71.1
71.3
71.6
73.3
73.6
64 - 57.9: depositional ponding
68.7-61.3: ~100 m uplift
71.6 - 68.7: depositional ponding
83 -75: 2-5 km shortening
C
T/C
T/C
T/C
Climate
Tectonic
meters
SOUTH
NORTH
km
southern section for NMST
northern section for NMST
conglomerate (w/ abundant quartzite clasts)
sandstone
siltstone
pedogenic units (often calcic, mottled)
limestone (locally fossiliferous, mottled)
mudstone (purple/orange/grey mottling)
coal
well-drained/arid
poorly-drained/humid
progressive unconformity (growth strata)
major unconformity (sequence boundary)
sequence designation
minor unconformity (correlative conformity)
general paleoflow direction
measured sections
sampled paleosol
Interval of thrusting (lighter shade represents chronologic uncertainty)

Table 6.4: Comparison of systems tract models with observed stratigraphy of Axhandle Basin, central Utah, USA. Each model's systems tract characteristics are numbered and referenced at right if present in Axhandle stratigraphy. Resultant predicted base level curve reflects portions of curve represented by individual model's systems tracts.

Nonmarine Systems Tract Model	Axhandle Basin			
Legarreta *et al*, 1993; Legarreta and Uliana,1998	**N Section Members**	**Systems Tract designation**	**Model elements**	**Base Level Cycle**
Aggradational	Flagstaff Limestone	Aggradational	1,3	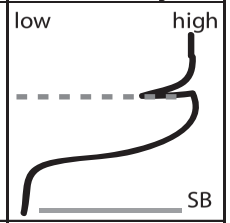
1. Widespread suspended load deposits.	Upper Redbed	Aggradational	3	
2. Increased frequency of paleosols (upward maturing?)	Wales Tongue	Aggradational	1,3	
3. Landscape stability/reduced surface gradient	Calcareous Siltstone	Aggradational/Forestepping	1,2,3/7?	
(decelerating accommodation capacity)	Coal-bearing	Aggradational	1,2,3	
Backstepping	Lower Redbed	Backstepping/Aggradational	4,5,6/2,3	
4. Stepwise migration of coarsest facies toward basin margins	Basal Conglomerate 2	Forestepping	8,9	
5. Mixed bedload and suspended load deposits	Basal Conglomerate 1	Forestepping	8,9	
6. Upward fining grainsize (decreasing net:gross)	**S Section Members**	**Systems Tract designation**	**Model elements**	**Base Level Cycle**
Depositional response to increased accommodation potential	Flagstaff Limestone	Aggradational	1,3	
(depositional area expands)	Upper Redbed	Aggradational	3	
Forestepping	Wales Tongue	Aggradational	1,3	
7. Upward coarsening channel fill complexes.	Calcareous Siltstone	Backstepping	5,6	
8. Dominated by bedload transport	Coal Canyon	Forestepping	7,8,9,10	
9. Spatially restricted (near incised surface)	Big Mountain	Forestepping	7,8,9,10	
10. Basinward shift of proximal deposits concurrent with	Coal-bearing	Aggradational	1,2,3	
marginal incision. Localized decrease in A/S ratio	Sheet Sandstone	Backstepping	4,6	

Nonmarine Systems Tract Model	Axhandle Basin			
Wright and Marriott, 1993	**N Section Members**	**Systems Tract designation**	**Model elements**	**Base Level Cycle**
Highstand	Flagstaff Limestone	Highstand	3	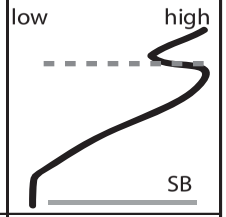
1. Reduced accommodation: well-developed floodplain soils.	Upper Redbed	Transgressive ?	5,6	
2. Higher rates of floodplain reworking, increased channel density.	Wales Tongue	Highstand	3	
3. Low-gradient floodplains may develop shallow lakes.	Calcareous Siltstone	Highstand	1,2,3	
	Coal-bearing	Transgressive	5,6	
Transgressive	Lower Redbed	Transgressive	6	
4. Multi-storey sandbodies	Basal Conglomerate 2	Lowstand	7,8	
5. Floodplain reworking, hydromorphic soils	Basal Conglomerate 1	Lowstand	7,8	
6. Increased accommodation enhances floodplain storage	**S Section Members**	**Systems Tract designation**	**Model elements**	**Base Level Cycle**
(isolated channels, weakly developed, well-drained soils)	Flagstaff Limestone	Highstand	3	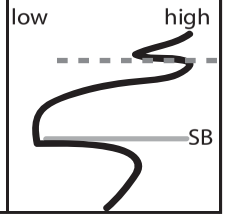
	Upper Redbed	Transgressive ?	5,6	
Lowstand	Wales Tongue	Highstand	3	
7. Coarse-grained fluvial deposits.	Calcareous Siltstone	Transgressive	5,6	
8. Restricted low-sinuosity (braided) deposits	Coal Canyon	Lowstand	7,8,9	
9. Mature, well-drained soils on terraces	Big Mountain	Lowstand	7,8,9	
	Coal-bearing	Transgressive	5,6	
	Sheet Sandstone	Transgressive	4	

Table 6.4 (Continued)

Nonmarine Systems Tract Model	Axhandle Basin			
Van Wagoner, 1995	**N Section Members**	**Systems Tract designation**	**Model elements**	**Base Level Cycle**
Highstand	Flagstaff Limestone	Highstand	1,2	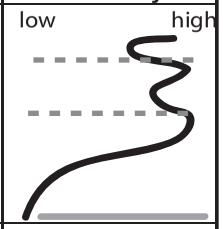
1. Muddy levee, crevasse splay, and lake margin deposits	Upper Redbed	Transgressive	4,6	
2. Broad interfluves.	Wales Tongue	Highstand	1,2	
3. Interbedded single-storey sandstone (low net:gross)	Calcareous Siltstone	Transgressive	4,5	
	Coal-bearing	Highstand	1,2,3	
Transgressive	Lower Redbed	Transgressive	4,5,6	
4.Thinner, single-story sandstone, moderate to low net:gross	Basal Conglomerate 2	Lowstand	7,9,10	
5. Mudstones dominate strata + crevasse splays, lakes, soils.	Basal Conglomerate 1	Lowstand	7,9,10	
6. Aggradational and upward-fining	**S Section Members**	**Systems Tract designation**	**Model elements**	**Base Level Cycle**
	Flagstaff Limestone	Highstand	1,2	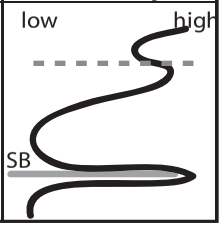
	Upper Redbed	Transgressive	4,6	
Lowstand	Wales Tongue	Highstand	1,2	
7. Multi-story, high net:gross, laterally continuous sandstones	Calcareous Siltstone	Transgressive	4,5,6	
8. Filling updip end of incised valley.	Coal Canyon	Lowstand	7,8,9	
9. Braided crossbedded sands.	Big Mountain	Lowstand	7,8,9	
10. No overbank accommodation	Coal-bearing	Highstand	1,2,3	
11. Upward fining	Sheet Sandstone	Lowstand	7,9,11	

Nonmarine Systems Tract Model	Axhandle Basin			
Currie, 1997	**N Section Members**	**Systems Tract designation**	**Model elements**	**Base Level Cycle**
Aggradational	Flagstaff Limestone	Aggradational	1	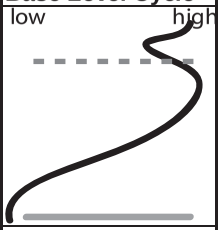
1. Abundant fine grained overbank and lacustrine deposits	Upper Redbed	Transitional	5,6	
2. Isolated, lenticular channels (anastamosing) transition to braided channels and conglomerates.	Wales Tongue	Aggradational	1	
3. Increasingly mature paleosols as flood-plain aggradation decreases.	Calcareous Siltstone	Aggradational	1,3	
Transitional	Coal-bearing	Transitional	4,5,6	
4. Transitional from braided (laterally continuous) to meandering (isolated) channels.	Lower Redbed	Transitional	4,5,6	
5. Increasing preservation of overbank sediment and paleosols	Basal Conglomerate 2	Degradational	7	
6. Coarse to fine grained.	Basal Conglomerate 1	Degradational	7	
	S Section Members	**Systems Tract designation**	**Model elements**	**Base Level Cycle**
	Flagstaff Limestone	Aggradational	1	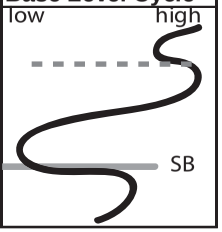
	Upper Redbed	Transitional	5,6	
Degradational	Wales Tongue	Aggradational	1	
7. Coarse grained, braided channel sandstones and conglomerates	Calcareous Siltstone	Transitional	4,5,6	
8. Laterally-continuous channels fill incised valleys	Coal Canyon	Degradational	7,8,9	
9. Thick paleosols adjacent to incised valleys	Big Mountain	Degradational	7,8,9	
	Coal-bearing	Transitional	4,5,6	
	Sheet Sandstone	Transitional	6	

Table 6.4 (Continued)

Nonmarine Systems Tract Model	Axhandle Basin			
Dalrymple *et al.*, 1998	**N Section Members**	**Systems Tract designation**	**Model elements**	**Base Level Cycle**
Unconfined SEP* Low	Flagstaff Limestone	SEP High	NA	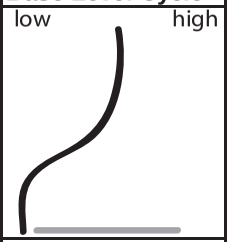
Rate of aggradation lowered.	Upper Redbed	SEP High	4,5, (6?)	
1. Increased channel amalgamation.	Wales Tongue	SEP High ?	NA	
2. If elevation ~unchanged, extensive sheet sands deposited.	Calcareous Siltstone	SEP High	4,5,6	
** SEP: Stream Equilibrium Profile*	Coal-bearing	SEP High	4,6	
SEP High	Lower Redbed	SEP High	4,5	
Rate of aggradation increases	Basal Conglomerate 2	Confined SEP Low	7	
4. Channels more isolated within fine-grained floodplains.	Basal Conglomerate 1	Confined SEP Low	7	
5. During low accommodation, soils develop.	**S Section Members**	**Systems Tract designation**	**Model elements**	**Base Level Cycle**
6. Minimal pedogenesis during high rates of aggradation.	Flagstaff Limestone	SEP High	NA	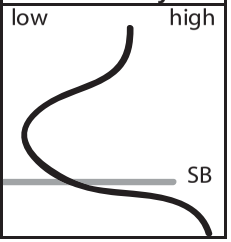
	Upper Redbed	SEP High	4,5,(6?)	
Confined SEP Low	Wales Tongue	SEP High ?	NA	
7. Sequence boundary or incised valley, with amalgamated channel sands within incised valley.	Calcareous Siltstone	SEP High	4,5	
8. Correlative floodplain soils (low preservation potential due to lateral channel switching/reworking).	Coal Canyon	Confined SEP Low	7,8	
	Big Mountain	Confined SEP Low	7,8	
	Coal-bearing	SEP High	4,6	
	Sheet Sandstone	Unconfined SEP Low	1,2	

Nonmarine Systems Tract Model	Axhandle Basin			
Plint *et al.*, 2001	**N Section Members**	**Systems Tract designation**	**Model elements**	**Base Level Cycle**
Late Highstand-Lowstand-Early Transgressive	Flagstaff Limestone	Late Transgressive- Early Highstand	4	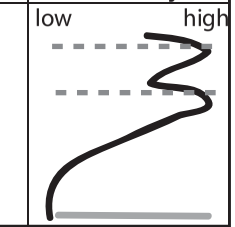
1. Blocky mudstones representing moderate to well-developed paleosols.	Upper Redbed	Late Highstand-Lowstand-Early Transgressive	1,2	
2. Interstratified crevasse splay sands or thin wetland units.	Wales Tongue	Late Transgressive- Early Highstand	4	
3. The upper part of sequence, followed by fluvial enrichment, sedimentary bypass and polygenetic pedogenesis	Calcareous Siltstone	Late Highstand-Lowstand-Early Transgressive	1,2,3	
Late Transgressive - Early Highstand	Coal-bearing	Late Transgressive- Early Highstand	4,5	
4. Widespread lacustrine-wetland facies.	Lower Redbed	Late Transgressive- Early Highstand	5,6	
5. mud-enclosed ribbon channel sandstones	Basal Conglomerate 2	Early Transgressive	7,8	
6. Blanket interfluves and anastamosed rivers.	Basal Conglomerate 1	Early Transgressive	7,8	
	S Section Members	**Systems Tract designation**	**Model elements**	**Base Level Cycle**
Early Transgressive	Flagstaff Limestone	Late Transgressive- Early Highstand	1	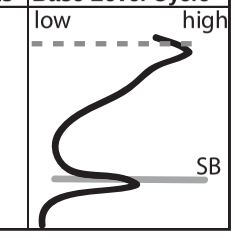
7. Meandering multi-storey channels and valley fill	Upper Redbed	Late Highstand-Lowstand-Early Transgressive	1,2	
8. Scarce preservation of flooplain mudstones, reflecting prolonged fluvial reworking.	Wales Tongue	Late Transgressive- Early Highstand	1	
	Calcareous Siltstone	Late Transgressive- Early Highstand	1,2,3 ?	
	Coal Canyon	Early Transgressive	1,2	
	Big Mountain	Early Transgressive	1,2	
	Coal-bearing	Late Transgressive- Early Highstand	1,2,3	
	Sheet Sandstone	Early Transgressive	1	

Limestone). This is commonly due to uncertain systems tract assignment of the Upper Redbed member and its distinction from the readily-classifiable lacustrine units below and above. For the southern section, base level predictions are quite varied, though nearly all of them predict that there is a long-term rise in base level from the lower to upper parts of the formation. In the lower part, there is significant disparity, though all lead to the interpretation that the base of the Big Mountain unit represents a sequence boundary. Contrasting systems tract assignments for the basal sheet sandstone are common.

Overall, the generalized nonmarine systems tract models (Fig. 6.3, six columns on right) predict only two of the lithologic transitions interpreted as sequence boundaries in Axhandle Basin strata (Fig. 6.3, second column from left), but also suggest the presence of several uninterpreted sequence boundaries. The incised valley sequence boundary (coinciding with the Coal Canyon and Big Mountain members) is successfully predicted by all the models. Plint *et al.*'s (2001) model alone identifies the sequence boundary at the base of the Flagstaff Limestone (PS 5-6 boundary, Chapter 3). Models by Van Wagoner (1995) and Plint *et al.* (2001) predict an additional base level turnaround occurring within the Calcareous Siltstone member of PS-4 (northern section), a possibility suggested by paleomagnetic hiatus and abundant paleosols (e.g. Talling *et al.,* 1995; Chapter 5). Interestingly, four of the models indicate an uninterpreted sequence boundary below the Upper Redbed Member of PS-5.

Assessment of Iglesia Basin

Sequence stratigraphy of Miocene-Early Pliocene strata of Iglesia Basin (northwestern Argentina) based on seismic interpretation and field observation was previously addressed (Chapters 2 and 3). Stratigraphic characteristics compiled from eight measured sections and three paleomagnetic sections in the Iglesia Group are

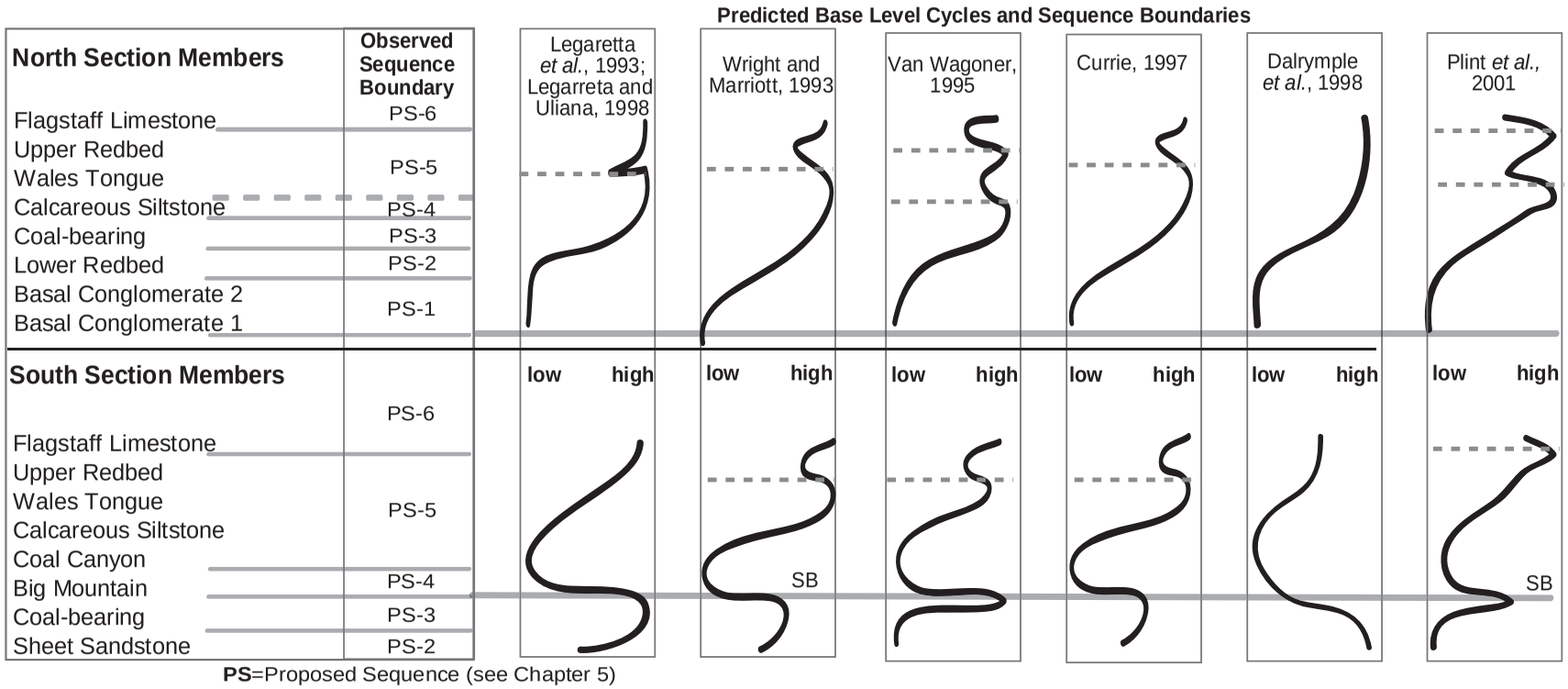

Figure 6.3: Graphic representation of model-predicted base level and sequence boundary location in comparison to sequence boundaries interpreted from Axhandle Basin stratigraphy. Solid gray bars (at right) represent sequence boundaries generated by base level fall to lowstand conditions. Dashed gray lines are potential sequence boundaries generated by base level fall, but not reaching lowstand conditions.

summarized in Figure 6.4. The Frontal Cordillera to the west is considered the dominant headwaters because, by analogy with modern climate and supported by clast provenance and imbrication measurements, most of the water influx was likely from the Frontal Cordillera catchments. But the eastern margin uplands (Precordillera) were episodically a sedimentary source, at least to the eastern portion of the basin and during sequence 2 deposition (Ré *et al*., 2003). Details of the sequence framework as well as the lithofacies characteristics of Iglesia Basin outcrops are discussed in chapters 2 and 3.

For comparison of Iglesia Basin stratigraphic characteristics with the general models (Table 6.2), I utilized the most complete composite section (Figure 6.4) so as to account for lateral facies variations and take advantage of a continuous outcrop belt in the modern day basin center. Unlike the informal member designations for the Axhandle Basin's North Horn Formation, the only suitable subdivisions for Iglesia Group strata are the eleven sequences, as strata were described with respect to the sequence framework. However, sequence bounding surfaces were not considered in the initial systems tract designations. Also, only limited outcrops of seismic sequence 1 (21-13.8 Ma) and sequences 8 and higher (<5 Ma) have been recognized. The former is dominantly volcaniclastic facies, which are not appropriate for comparison to the alluvial facies models of Table 6.2. The youngest sequences are inadequately understood both in lateral or vertical succession. Therefore, only sequences 2 through 7 (9.0 – 5 Ma) are considered.

Table 6.5 (parts 1-3) summarizes the results of the model comparisons to Iglesia Basin strata. As with the first test basin, each stratigraphic "sequence" was assigned the most appropriate systems tract(s) based on the presence or absence of the individual model's systems tract elements. Predicted base level cycles are sketched as appropriate to each model's systems tract position. These curves are compared directly

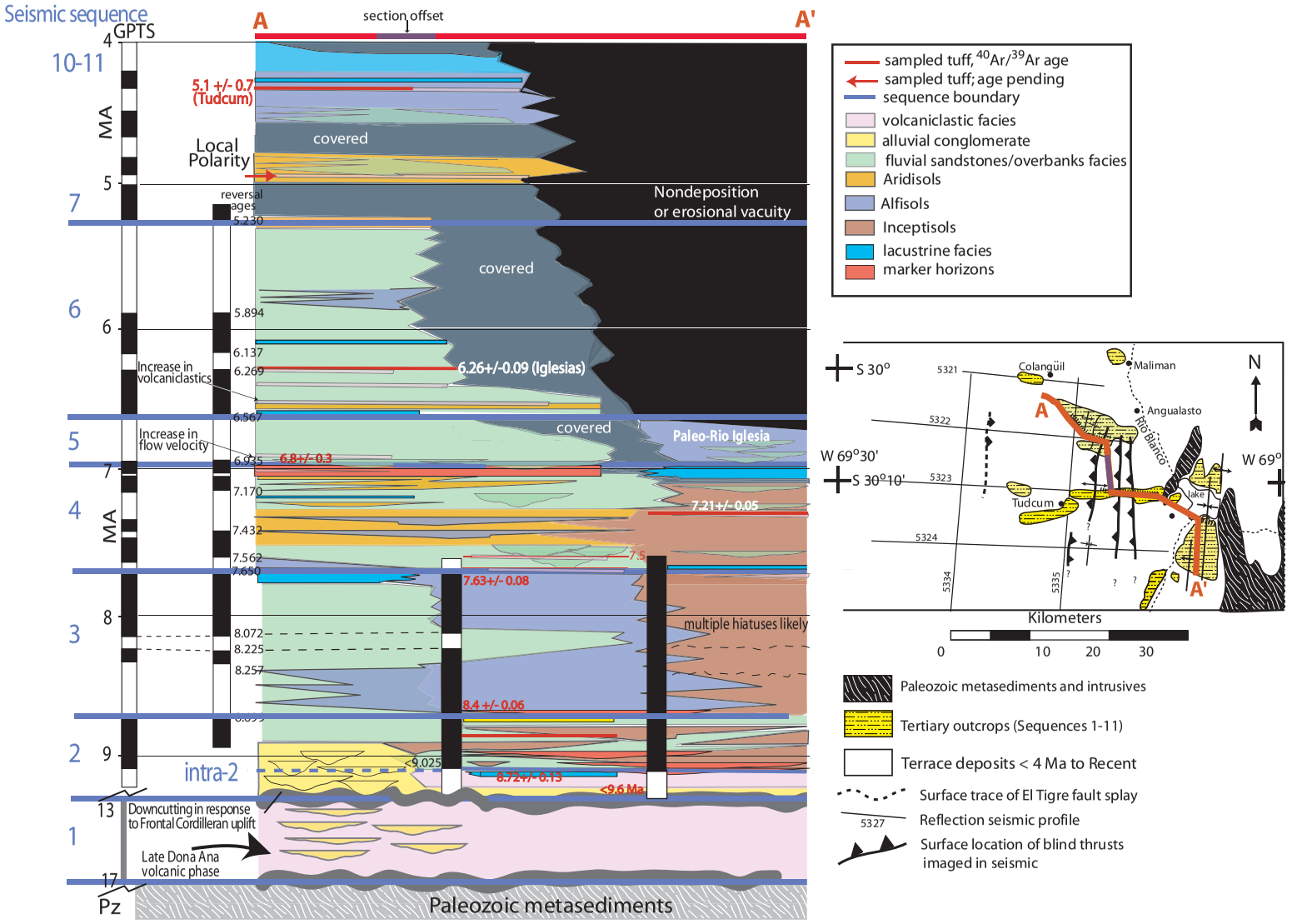

Figure 6.4: Large-scale stratigraphic features, chronostratigraphic correlation and proposed sequence boundaries of Iglesia Basin.

Table 6.5: Comparison of systems tract models with observed stratigraphy of Iglesia Basin, northwestern Argentina. Each model's systems tract characteristics are numbered and referenced at right if present in Iglesia stratigraphy. Resultant predicted base level curve reflects portions of curve represented by individual model's systems tracts.

Nonmarine Systems Tract Model	Iglesia Basin			
Legarreta *et al*, 1993; Legarreta and Uliana,1998	**Sequence**	**Systems Tract designation**	**Model elements**	**Base Level Cycle**
Aggradational	**7**	Aggradational	1,2,3	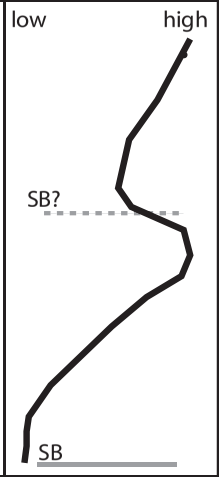
1. Widespread suspended load deposits.				
2. Increased frequency of paleosols (upward maturing?)				
3. Landscape stability/reduced surface gradient (decelerating accommodation capacity)	**6**	Aggradational/Backstepping	3,5	
Backstepping				
4. Stepwise migration of coarsest facies toward basin margins	**5**	Backstepping	5, 6, (10?)	
5. Mixed bedload and suspended load deposits				
6. Upward fining grainsize (decreasing net:gross)				
Depositional response to increased accommodation potential (depositional area expands)	**4**	Aggradational	2,3,5	
Forestepping				
7. Upward coarsening channel fill complexes.	**3**	Backstepping	2,5,6	
8. Dominated by bedload transport				
9. Spatially restricted (near incised surface)				
10. Basinward shift of proximal deposits concurrent with marginal incision. Localized decrease in A/S ratio	**2 and Intra-2**	Forestepping	6,(7?),8,10	

Nonmarine Systems Tract Model	Iglesia Basin			
Wright and Marriott, 1993	**Sequence**	**Systems Tract designation**	**Model elements**	**Base Level Cycle**
Highstand	**7**	Transgressive/ Highstand	(1?), 3,6	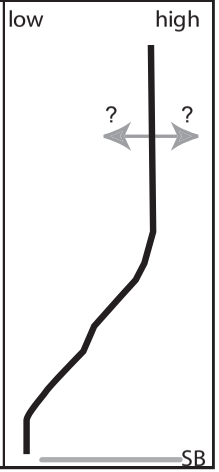
1. Reduced accommodation: well-developed floodplain soils.				
2. Higher rates of floodplain reworking, increased channel density.				
3. Low-gradient floodplains may develop shallow lakes.	**6**	Transgressive/ Highstand	2,3,5	
Transgressive				
4. Multi-storey sandbodies	**5**	Transgressive/ Highstand	2,4,6	
5. Floodplain reworking, hydromorphic soils				
6. Increased accommodation enhances floodplain storage (isolated channels, weakly developed, well-drained soils)	**4**	Transgressive/ Highstand	1,3,6	
Lowstand				
7. Coarse-grained fluvial deposits.	**3**	Transgressive	3,4,5,6	
8. Restricted low-sinuosity (braided) deposits				
9. Mature, well-drained soils on terraces				
	2 and Intra-2	Lowstand	3,4,7,8	

Table 6.5 (Continued)

Nonmarine Systems Tract Model	Iglesia Basin			
Van Wagoner, 1995	**Sequence**	**Systems Tract designation**	**Model elements**	**Base Level Cycle**
Highstand	**7**	Highstand	1,3	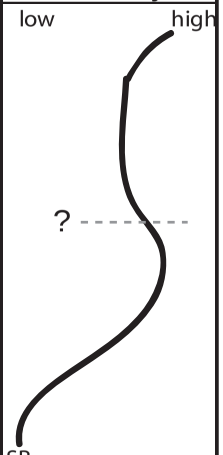
1. Muddy levee, crevasse splay, and lake margin deposits 2. Broad interfluves. 3. Interbedded single-storey sandstone (low net:gross)	**6**	Transgressive	4,5	
Transgressive				
4.Thinner, single-story sandstone, moderate to low net:gross 5. Mudstones dominate strata + crevasse splays, lakes, soils. 6. Aggradational and upward-fining	**5**	Transgressive	4,6	
	4	Transgressive/ Highstand	3,4,6	
Lowstand				
7. Multi-story, high net:gross, laterally continuous sandstones 8. Filling updip end of incised valley. 9. Braided crossbedded sands. 10. No overbank accommodation	**3**	Transgressive	4,5,6	
11. Upward fining	**2 and Intra-2**	Lowstand	7,(8?),9,11	

Nonmarine Systems Tract Model	Iglesia Basin			
Currie, 1997	**Sequence**	**Systems Tract designation**	**Model elements**	**Base Level Cycle**
Aggradational	**7**	Aggradational	1,(3?)	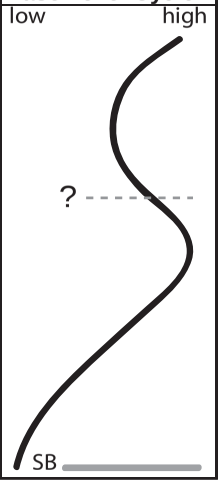
1. Abundant fine grained overbank and lacustrine deposits 2. Isolated, lenticular channels (anastamosing) transition to braided channels and conglomerates. 3. Increasingly mature paleosols as flood-plain aggradation decreases.	**6**	Transitional	2,3	
Transitional				
4. Transitional from braided (laterally continuous) to meandering (isolated) channels. 5. Increasing preservation of overbank sediment and paleosols 6. Coarse to fine grained.	**5**	Transitional	4,6	
	4	Aggradational	2,3	
Degradational				
7. Coarse grained, braided channel sandstones and conglomerates 8. Laterally-continuous channels fill incised valleys 9. Thick paleosols adjacent to incised valleys	**3**	Transitional	4,5,6	
	2 and Intra-2	Degradational	7,8	

Table 6.5 (Continued)

Nonmarine Systems Tract Model	Iglesia Basin			
Dalrymple *et al.*, 1998	**Sequence**	**Systems Tract designation**	**Model elements**	**Base Level Cycle**
Unconfined SEP* Low	**7**	SEP High	4,5	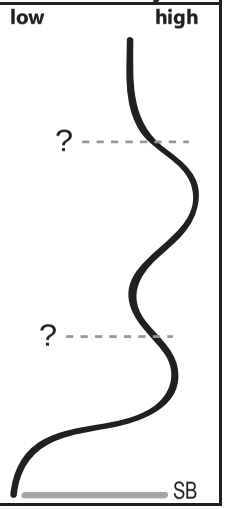
Rate of aggradation lowered. 1. Increased channel amalgamation. 2. If elevation ~unchanged, extensive sheet sands deposited. ** SEP: Stream Equilibrium Profile*	**6**	SEP High/ Unconfined SEP Low	2, 4, 5	
SEP High	**5**	Unconfined SEP Low/ SEP High	1,2,6	
Rate of aggradation increases 4. Channels more isolated within fine-grained floodplains. 5. During low accommodation, soils develop. 6. Minimal pedogenesis during high rates of aggradation.	**4**	SEP High	4,5	
Confined SEP Low	**3**	SEP High/ Unconfined SEP Low	2,4,5	
7. Sequence boundary or incised valley, with amalgamated channel sands within incised valley. 8. Correlative floodplain soils (low preservation potential due to lateral channel switching/reworking).	**2 and Intra-2**	Confined SEP Low	(5), 7	

Nonmarine Systems Tract Model	Iglesia Basin			
Plint *et al.*, 2001	**Sequence**	**Systems Tract designation**	**Model elements**	**Base Level Cycle**
Late Highstand-Lowstand-Early Transgressive	**7**	Late Highstand-Lowstand-Early Transgressive	1,2	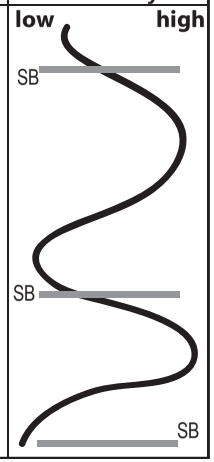
1. Blocky mudstones representing moderate to well-developed paleosols. 2. Interstratified crevasse splay sands or thin wetland units. 3. The upper part of sequence, followed by fluvial enrichment, sedimentary bypass and polygenetic pedogenesis	**6**	Late Transgressive- Early Highstand	2,5,6	
Late Transgressive - Early Highstand	**5**	Late Transgressive- Early Highstand/ Early Transgressive	8, 5	
4. Widespread lacustrine-wetland facies. 5. mud-enclosed ribbon channel sandstones 6. Blanket interfluves and anastamosed rivers.	**4**	Late Highstand-Lowstand-Early Transgressive	1,2,3	
Early Transgressive	**3**	Late Transgressive- Early Highstand	2,4,5,6	
7. Meandering multi-storey channels and valley fill 8. Scarce preservation of flooplain mudstones, reflecting prolonged fluvial reworking.	**2 and Intra-2**	Early Transgressive	7,8,(2)	

to the observed Iglesia sequence boundaries in Figure 6.6.

In assigning systems tracts to Iglesia sequences based on the general lithologic and architectural features of the six models, several uncertainties were recognized. As already mentioned, Van Wagoner's (1995) alluvial model contains significant overlap between transgressive and highstand systems tracts. Similar lack of distinction between these phases of the base level cycle occurred when using the model of Wright and Marriott (1993). The difficulty was due to Iglesia strata exhibiting characteristics of both tracts. A shortcoming of the Dalrymple *et al.* (1998) model is the lack of specified systems tract for lacustrine facies. Perhaps such units are implicit in the "fine-grained floodplains" of the Unconfined SEP Low (e.g. highstand) systems tract. A final poor fit of Iglesia rock properties to the models is with the model of Legarreta *et al.* (1993), who describe upward-coarsening and thickening, laterally restricted channel fill complexes during the forestepping systems tract. The only incised valley channel fill of Iglesia Basin (sequence 2) is upward fining and thinning and is aerially extensive, at least in the basin central outcrop belt.

The predicted base level cycles for Iglesia Basin (Figure 6.5) are quite varied between models. Because sequence 2 consists of incised valley fill and coarse grained deposits, the lowstand-equivalent systems tract of each model is appropriate. Iglesia Basin sedimentary units fine upward, and as this is a frequent lithofacies characteristic of the models' rising base level, it is not surprising that rising base level is a common interpretation for sequences 2 and 3. Above sequence 3, however, multiple interpretations emerge. Four of the models suggest continued base level rise, although with variable turnaround points. The remaining two models (Dalrymple *et al*., 1998; Plint *et al*., 2001) predict a falling base level between sequences 3 and 4, although they differ as to the extent of the fall (e.g. Plint et al.'s 2001 model suggests a return to early transgressive conditions, compared with rising base level for Dalyrmple et al.,

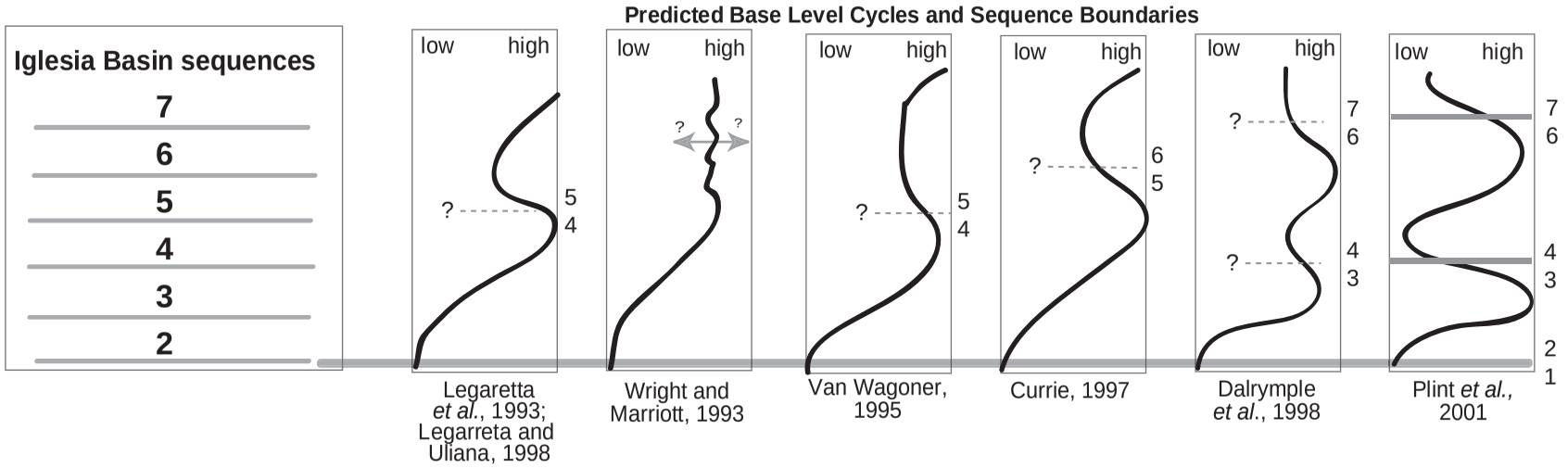

Figure 6.5: Graphic representation of model-predicted base level and sequence boundary location in comparison to sequence boundaries interpreted from Iglesia Basin stratigraphy. Solid gray bars (at right) represent sequence boundaries generated by base level fall to lowstand conditions. Dashed gray lines are potential sequence boundaries generated by base level fall, but not reaching lowstand conditions.

1998). The models also differ on the overall number of base level cycles or partial cycles present in the six sequences. At most, there are two complete predicted cycles (Plint et al., 2001). Four other models achieve highstand conditions twice, but none involves a cycle or cycles which return to lowstand facies. The remaining model (Wright and Marriott, 1993) includes elements in both the transgressive- and highstand-equivalent systems tracts observed in the younger Iglesia Basin sequences, such that a clear systems tract assignment was not possible. It may be that this duality of systems tract characteristics represents higher frequency base level fluctuations. However, the number of such cycles cannot be determined.

Also wide-ranging are the models' predictions of sequence boundary position for Iglesia strata. Each model suggests that a boundary be present somewhere below sequence 2, because it occupies incised valleys and is the coarsest bedload material in the central basin. Assuming that sequence boundaries are generated after base level turn-around (e.g. beginning of falling stage or during maximum rate of fall; see Table 6.2) whether or not the lowstand systems tract is preserved, several sequence boundaries can be identified. Two models (Legarreta et al., 1993; Van Wagoner, 1995) identify the 4-5 sequence boundary on the basis of lithofacies. Another two models (Dalrymple et al., 1998; Plint et al., 2001) agree on the assignment of sequence boundaries between sequences 3 and 4 as well as 6 and 7. The criteria of Currie (1997) locate the 5-6 sequence boundary. As addressed above, uncertain systems tract assignments for the model of Wright and Marriott (1993) leads to a lack of distinct base level falls and thus no sequence boundaries are determined.

Discussion of models' validity:

The difficulties and methodology for recognizing nonmarine sequence boundaries have been discussed elsewhere in this dissertation (see chapters 1-3 and 5). The best potential for their recognition and interpretation comes from integration

of lithologic and chronologic data, keeping in mind the spatial complexities of the foreland system (e.g. proximal unconformities may become laterally conformable), paleosol evidence for changes in fluvial sedimentation, and lithofacies variations on a vertical and lateral scale resolvable in seismic and outcrop. Integrated analyses in Axhandle and Iglesia wedgetop basins have clearly identified stratigraphic boundaries and intervals consistent with the definition of sequences (Mitchum, 1977). Nonetheless, the general systems tract models locate only 2 of the 5 Axhandle Basin sequence boundaries (only one is unanimously predicted). While five of the six well-studied boundaries in Iglesia Basin are predicted, only the oldest sequence boundary (related to valley incision) is forecast by all models on the basis of genetically related lithofacies characteristics (systems tracts).

I propose five possible explanations for the incongruity between general (idealized) systems tract models and the preserved Axhandle and Iglesia Basin stratigraphies.

1: Spatially variable preservation potential of the systems tracts may bias the record in a way that makes application of the models misleading. Van Wagoner (1995), synthesizing his own observations and those of Legarreta *et al.* (1993) and Shanley and McCabe (1995), predicted that most nonmarine sequences are fining-upward with upward decreasing net: gross ratios. This would imply greater proportions in ascending direction of transgressive and highstand deposits in a given sequence in a given stratigraphic column. Additionally, since lowstand deposition occurs chiefly in incisions resulting from base level fall, these deposits may have a higher preservation potential than broadly-deposited highstand strata, which are susceptible to erosion during the next drop of base level. Thus, lowstand deposits should dominate proximal deposits, whereas thin transgressive and highstand systems tracts may dominate more distal deposits (Van Wagoner, 1995). The fining-upward

assumption holds in general for Iglesia Basin, but the spatial distribution of coarse lowstand deposits does not. Iglesia Basin lowstand deposits are not restricted to proximal positions, nor are they confined to paleovalleys. Furthermore, the abundance of proximally-located fine-grained facies accumulated during times of increasing accommodation space (i.e. transgressive and highstand ST) in the Axhandle Basin argues against Van Wagoner's (1995) assertions. In the northern section, only the basal conglomerates are assigned to the lowstand-equivalent systems tract. Clearly some spatial biasing in preservation has occurred, but how does this relate to base level dynamics and the creation or removal of accommodation space?

Proximal versus distal preservation can be conceptually addressed by considering the basin accommodation zone model of Posamentier and Allen (1999). In this model, foreland and passive margin deposits are divided into two zones based on the rates of basin subsidence versus sea-level (i.e. base level) fall (Figure 6.6). Zone A (proximal to thrusts in foreland basins) always subsides faster than base level falls, so accommodation space always exists. Lowstand deposits therefore are rarely preserved. Zone B (distal to thrusts) is the part of the basin which periodically subsides slower than the rate of base level fall, such that lowstand deposition may occur. For passive margins, the zones are reversed (e.g. proximal to land, subsidence is slower than seaward areas). Comparison to Figure 6.1 shows that because of the basin-bounding structures, the subsidence profile of the Iglesia basin is more like Posamentier and Allen's (1999) "passive margin" profile, whereas the Axhandle study area is more like their "foreland" case. Thus, it is suggested that the outcrops of Axhandle are mostly in Zone A and Iglesia outcrops are mostly in Zone B, relative to the Sevier and Precordillera thrust belts. Certainly some adjustments must be made to this simple subdivision because of the structural complexities of each basin.

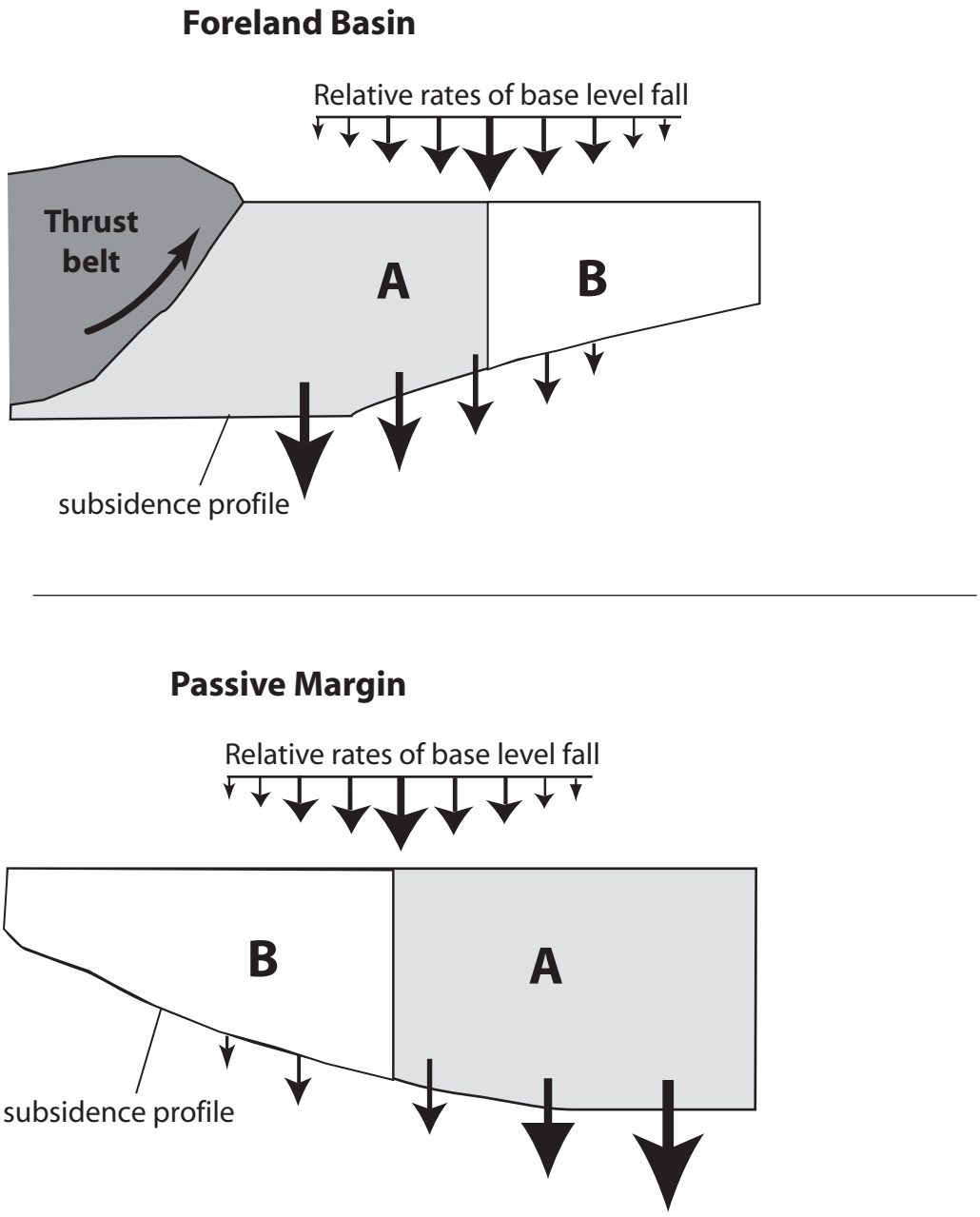

Figure 6.6: Two-part zonation of foreland and passive margin depositional basins by comparison of subsidence profile and rate of base level fall (modified from Posamentier and Allen, 1999). In Zone A, rates of subsidence are always greater than the rate of base level fall. In Zone B, the rate of base level fall is periodically greater than basin subsidence. Arrow sizes represent relative magnitudes of subsidence and falls.

However, these local-scale structural features may partly explain the disparities between model predictions and the stratigraphy observed in the test basins through their role on the basins' subsidence profiles and resultant accommodation space.

2: An explanation for disparity between model-predicted and observed sequence boundaries may be the models' shared premise that sequence boundaries form via valley incision. The proposed sequence stratigraphies (see Table 6.1) recognize that tectonic tilting, regional lacustrine flooding and episodic accumulation rates (e.g. drop in sediment supply) can also result in unconformable contacts (sequence boundaries). Schumm (1977) cautioned that base level fall need not result in fluvial incision, but rather changes in channel geometry. Ethridge *et al.* (1998) raised similar concerns, that base level cyclicity may only affect the downstream portion of the fluvial system and valley incision alone is unlikely to provide sediment for the entire sequence. Again, we are confronted with spatial biasing, as all the models exist "somewhere" unspecified in the fluvial system, so upstream versus downstream effects are not addressed in the models. We are left with 2-dimensional assessments of what may or may not be changing in the entire deposystem. Still, Olsen *et al.* (1995) suggested that alluvial deposition responds only to *local* accommodation space changes, regardless of whether that space is generated by upstream or downstream controls or by intrabasinal subsidence. As such, local outcrop-based assessments may still be useful in documenting local changes in accommodation space, if not of basin-scale base level cycles.

3: The sequence boundary disparity may reflect the simplistic lithologic assemblages of the models. For example, most of the models equate the coarsest grained deposits with valley fill; this is not the case for the braided alluvial fan deposits of the Basal Conglomerates for Axhandle Basin. Several models do not explicitly include carbonate deposits within their systems tracts, resulting in implicit

grouping of Axhandle Basin's Flagstaff Limestone and Wales Tongue Member as "stable landscape" or "floodplain" deposits. Similarly, important intervals of paludal limestone occurring at the 2-3 and 3-4 sequence boundaries in Iglesia Basin (Chapter 2 and Appendix v) may have base level significance, but are difficult to classify in several of the systems tract models.

4: Sequence boundary prediction may be poor because of diachronism of deposition. Though boundaries separating marine systems tracts (*sensu* Brown and Fisher, 1977) may be correlative and perhaps genetically related, they are also likely to reflect significant sedimentary hiatuses, particularly where expressed as lithofacies changes or pedogenic intervals. Thus, the boundaries between systems tracts are not time lines, nor are the sediments within systems tracts always coeval (Posamentier and Allen, 1999). This diachronism may account for variation in base level dynamics between sections (e.g. north and south sections of Axhandle Basin).

5: Finally, and perhaps most important in assessing whether systems tract models are generally applicable, is the role of extrinsic variability and feedbacks in creating stratigraphic architecture and generating sequence boundaries. As summarized in Table 6.1 and discussed in Chapters 2, 3 and 5, tectonism, climate variability or both likely affected sequence development of Axhandle and Iglesia Basins. Feedback relationships between extrinsic factors and intrinsic sedimentation processes are complex (see Figure 1.4) and are difficult to document or quantify in ancient alluvial settings. But it is this superposition of variables, spatially as well as temporally, that is arguably the greatest factor preventing uniform sequence stratigraphic predictions.

There is another alternative to the perceived disparities in sequence boundary position: It is possible that the test basins do not contain the number of sequences previously interpreted. This is to say that, on the basis of the lithofacies and

architectures included in the models, the Axhandle and Iglesia Basins outcrops may truly represent only 2-3 base level cycles capable of generating regional sequence boundaries. In the case of Axhandle Basin, this possibility is distinct; interpreted outcrops are only along the eastern basin margin. Talling *et al.* (1991) found it difficult to correlate to scant exposures on the western Gunnison Plateau, but perhaps these outcrops should be reassessed in light of the sequence framework proposed here. For the Iglesia Basin, repeated interpretation of basin-scale seismic lines has proved that at least eleven sequences do exist in the subsurface (Beer *et al.,* 1990; Fernandez-Seveso, 1993; Chapter 2). But it is acknowledged that locating the sequence boundaries in outcrops proves difficult. However, as discussed in Chapters 2 and 3, the outcrops do reveal impressive lateral and vertical lithologic transitions of the nature described in the models, and most of the boundaries are predicted by at least one of the models. Still, the fact that only one or two theoretical base level cycles are represented over a range of six empirically based sequence boundaries, suggests that base level dynamics may be very different in the basin center (where strata are exposed) and against the western Iglesia Basin margin (where most seismic sequence boundaries are most clearly interpreted).

One major problem in nearly all stratigraphic sequence architectural models is a lack of independent constraint on the rate of aggradation; hence there is much room for circular reasoning. Accommodation potential cannot be measured for the geologic record. However, with high resolution chronostratigraphic data, one can measure stratigraphic thicknesses and assess aggradation rates, with the implicit assumption that changing aggradation rates reflect variable potential to (at least locally) accumulate sediment. In the absence of the chronologic data, if one thinks that a particular nonmarine architectural style or lithology is indicative of a high rate or a low rate of aggradation, then recognition of that architectural element becomes a

motivation to identify it as indicative of “highstand,” “lowstand,” or transitional, which may not be correct. A fundamental shortcoming is that, in the absence of independent knowledge of the combination of extrinsic (e.g. tectonic subsidence and uplift, discharge, weathering and erosion) and intrinsic (autogenic) variation that actually controls nonmarine base level cycles, the existing models rely on analogy to systems tracts in marine depositional systems for which base level and its fluctuations and resultant sequences are better understood and can be semi-quantitatively measured (e.g. flooding surfaces, maximum transgressive surfaces, condensed sections, paleobathymetry, etc.).

Still, the general features of accommodation versus sedimentation (i.e. aggradation) rates have been explored for nonmarine systems (see Table 6.3) and should also be compared against well calibrated test basins. Frostic and Steel (1993) stated that fining-upward or coarsening-upward stratigraphic successions reflect whether accommodation space was being generated (i.e. rising base level) or destroyed (i.e. falling base level). The A/S ratio comparisons of Martinsen *et al.* (1999) incorporate discussion of sequence generation as well as the concept of expansion zones and surfaces, whereby the A/S ratio gradually or abruptly increases, respectively. These workers favor a simple, two systems tract model (A>S or A<S) because of the “lesser variability” in nonmarine strata compared with marine deposition. The third A/S ratio characterization (Anderson and Cross, 2001) also incorporates a hypothetical stratigraphic base level cycle and generalizes facies as proximal (i.e. alluvial fans; high energy deposition) or distal (i.e. floodplains; low depositional energy). Base level fall hemicycles conceptually represent down-gradient movement of sedimentary environments, represented vertically by distal to proximal facies successions. The reverse is true for stratigraphic base level rises (e.g. proximal to distal vertical successions). These base level cycles can be symmetric or

asymmetric and nested within larger scale cycles, akin to the stacking patterns discussed for marine parasequences, which are shallowing-upward successions bounded by flooding surfaces (Van Wagoner *et al.* 1990). Each of these models represents a conceptual attempt to limit marine systems tract terminology and concentrate on stratigraphic rather than eustatic base level. Again, I believe usage of these A/S characterizations must be qualified as only appropriate for interpreting local changes in accommodation.

The Iglesia and Axhandle basins each possess a detailed framework of magnetic polarity chronology (Figures 6.2 and 6.4), such that one can examine the variability of paleosol development and architecture of nonmarine facies as a function of measured aggradation. One finds in both basins that intervals of minimum aggradation rate create erosion and formation of a prominent sequence-bounding unconformity. But the rate of accumulation varies even when it is net positive (see Figure 6.7), and some intervals of abundant, well developed paleosols are times of comparatively slow accumulation and others are times of rapid aggradation. Thus paleosols are not simple indicators of times of high or low aggradation rate. For example, geographic position on the floodplain, strongly affects paleosol development (e.g. Bown and Kraus, 1987; Kraus, 1987, 1999). Therefore, the spatial and temporal characteristics of pedogenic facies are valuable sources of information about sedimentary response to base level change, even though they are not simple measures of aggradation rate.

Summary:

Assessment of these nonmarine systems tract models raises a number of questions about their general validity, at least as applied to a whole basin's base level dynamics. The most universal critique of the models is their lack of specificity of position within an alluvial deposystem. Several models, while seemingly rejecting the

Figure 6.7: Sediment accumulation rates for Axhandle and Iglesia Basins, as determined by preferred magnetostratigraphic correlations to global geomagnetic polarity time scale (Cande and Kent, 1995). The Axhandle curve is modified from Talling *et al*. (1994). The black curve represents compacted average rates, while grey bars illustrate ranges possible due to errors in magnetostratigraphic correlation. The Iglesia Basin curve shows compacted average accumulation rates based on magnetostratigraphy by Ré *et al*. (2003) and new radiometric ages for seismic sequences 2 through 7. The grey envelope represents the range of values for temporally equivalent sections in the central to eastern Iglesia Basin. Time intervals with abundant paleosol development are shown as horizontal boxes.

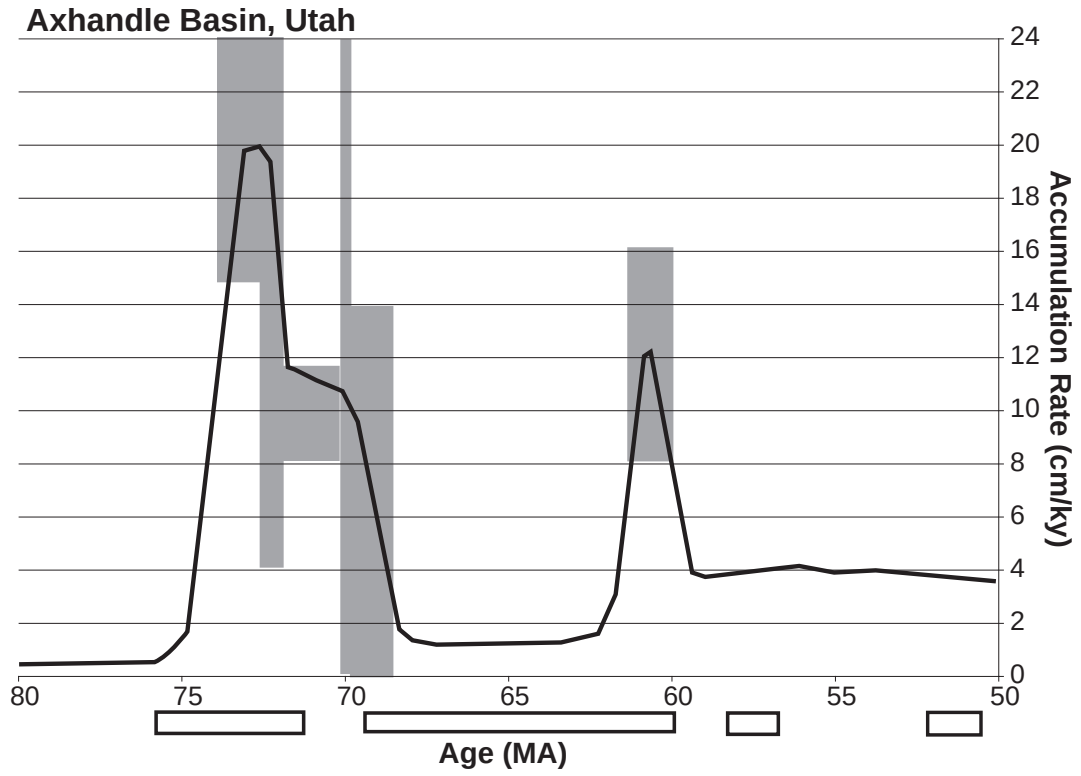
Axhandle Basin, Utah
24
22
20
18
16
14
12
10
8
6
4
2
0
Accumulation Rate (cm/ky)
80
75
70
65
60
55
50
Age (MA)

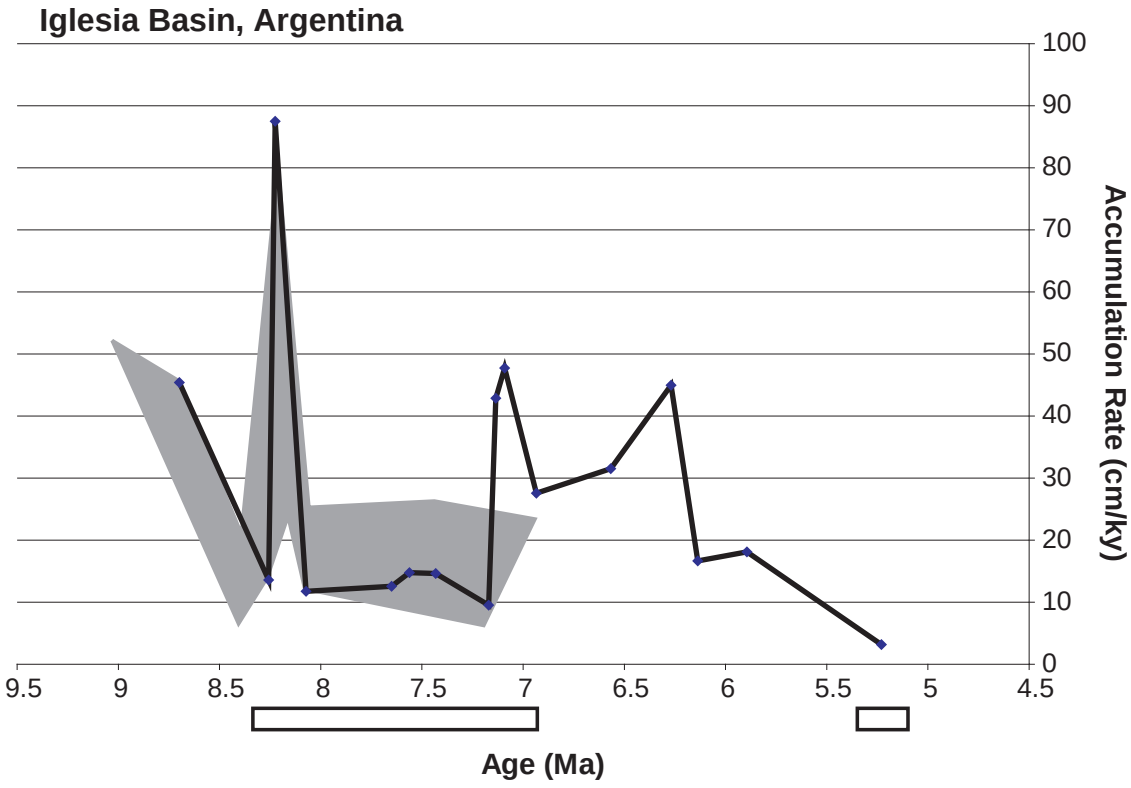
Iglesia Basin, Argentina
100
90
80
70
60
50
40
30
20
10
0
Accumulation Rate (cm/ky)
9.5
9
8.5
8
7.5
7
6.5
6
5.5
5
4.5
Age (Ma)

marine nomenclature, still allow for ties to a distant (e.g. Van Wagoner, 1995) or not-so-distant (Plint *et al.*, 2001) marine system and base level changes triggered by eustasy. These models' lithologic characteristics, while surely well-documented in the basins for which the models were formulated, omit certain lithologies (e.g. limestones) or contain overly generalized facies characteristics which could be applied to more than one systems tract. The premise that valley incision and the coarsest-grained sediments initiate a sequence is highly debatable and certainly not generally applicable to many ancient alluvial basins. Finally, though the models attempt to remain conceptual to allow for system complexity and feedback relationships, the lack of distinction between extrinsic (tectonism vs. climate) forcings is a major failing of the models. The test basins chosen have significant data in support of either tectonic, climatic or both variables affecting sequence genesis. I suspect that other nonmarine basins for which the systems tract model(s) might be applied also provide much evidence to assess relative variability of extrinsic variables. I would suggest that the role of each extrinsic variable continue to be explored via scaled analog modeling (e.g. Paola, 2000; Milana and Tietze, 2002; Hickson, 2005), whereby the complexities of the sediment system can be better understood when certain variables can be controlled or removed. Of course, field measurements continue to provide invaluable documentation of local to regional sedimentary response to base level change. I propose that we use these field insights, the sequence stratigraphic model, and well-scaled experimental sedimentation facilities to better understand basin-scale base level effects before systems tract assignment is routinely or blindly applied to nonmarine stratigraphic successions.

References:

Anderson, D.S. and Cross, T.A., 2001, Large-scale cycle architecture in continental strata, Hornelen basin (Devonian), Norway: Journal of Sedimentary Research, v. 21, p. 255-271.

Beer, J.A., Allmendinger, R.W., Figueroa, D.E., and Jordan, T.E. 1990, Seismic stratigraphy of a non-marine piggyback basin, Central Andes: American Association of Petroleum Geologists Bulletin, v.74, p.1183-1202.

Bown, T.M., and Kraus, M.K., 1987, Integration of channel and floodplain suites in aggrading fluvial systems. I: Developmental sequence and lateral relations of lower Eocene alluvial paleosols, Willwood Formation, Bighorn Basin, Wyoming: Journal of Sedimentary Petrology 57, p. 587-601.

Brown, L.F., and Fisher, W.L., 1977, Seismic-stratigraphic interpretation of depositional systems: examples from Brazil rift and pull-apart basins in Peyton C.E., ed., Seismic Stratigraphy –Applications to Hydrocarbon Exploration: American Association of Petroleum Geologists Memoir 26, p. 213-248.

Currie, B. S., 1997: Sequence stratigraphy of nonmarine Jurassic-Cretaceous rocks, central Cordilleran foreland-basin system: Geological Society of America Bulletin, v.9., p 1206-1222.

Dalrymple, M., Prosser, J., and Williams, B., 1998, A dynamic systems approach to the regional controls on deposition and architecture of alluvial sequences, illustrated in the Statfjord Formation (United Kingdom, Norther North Sea) *in* Shanley, K.M., and McCabe, P.W., eds., Relative roles of eustasy, climate and tectonism in continental rocks: SEPM Special Publication No. 59, p. 65-81.

Ethridge, F.G., Wood, L., and Schumm, S.A., 1998, Cyclic variables controlling sequencedevelopment: Problems and perspectives in relative role of eustasy, climate, and tectonism in continental rocks: SEPM, Spec. Pub. 59, p. 17-29

Fernández-Seveso, F., 1993, Sismoestratigrafia de la Cuenca Iglesia: Informe de actividades en la Universidad de Cornell, Informe interno No. 10.408: 20 pp.

Frostick, L. E. and Steel, R. J, 1993, Tectonic signatures in sedimentary basin fills: an overview in Frostick, L. E. and Steel, R. J (eds) Tectonic controls and signatures in sedimentary successions Special Publication of the International Association of Sedimentologists, 20, p. 1-9.

Hickson, T.A., Sheets, B.A., Paola, C, and Kelberer, M., 2005, Experimental test of tectonic controls on three-dimensional alluvial facies architecture: Journal of Sedimentary Research, Vol. 75, p. 710-722.

Kraus, M.J., 1987, Integration of channel and floodplain suites, II. Vertical relations of alluvial paleosols: Journal of Sedimentary Petrology, Vol. 57, p. 602-612.

Kraus, M. J., 1999, Paleosols in clastic sedimentary rocks: their geologic applications: Earth Science Reviews v. 47, p. 41-70.

Lawton, T.F., P.J. Talling, R.S. Hobbs, J.H. Trexler, Jr., M.P. Weiss, and D.W. Burbank, 1993, Structure and stratigraphy of Upper Cretaceous and Paleogene strata (North Horn Formation), Eastern San Pitch Mountains, Utah – Sedimentation at the front of the Sevier Orogenic Belt: *U.S. Geological Survey* Publication 1787-II.

Lawton, T.F. and Weiss, M.P., 1999, Geologic map of the Wales quadrangle, Juab and Sanpete Counties, Utah: Utah Geological Survey Miscellaneous Publication 99-2.

Legarreta, L., Uliana, M.A., Laratonda, C.A. and Meconi, G.R., 1993, Approaches to nonmarine sequence stratigraphy- theoretical models and examples from Argentine basins *in*. Eschard, R., and Doligez, B., eds. Subsurface Reservoir Characterization from Outcrop Observations: Proceedings of the 7th IFP Exploration and Production Research Conference, p. 125-143

Legarreta, L. and Uliana, M.A., 1998, Anatomy of hinterland depositional sequences: Upper Cretaceous fluvial strata, Neuquen Basin, West-Central Argentina: *in* Shanley, K.M., and McCabe, P.W., eds., Relative roles of eustasy, climate and tectonism in continental rocks: SEPM Special Publication No. 59, p. 83-92.

Martinsen, O.J., Ryseth, A., Helland-Hansen, W., Flesche, F., Torkilsden, G., and Idil, S., 1999, Stratigraphic base level and fluvial architecture: Ericson sandstone (Campanian), Rock Springs Uplift, SW Wyoming, USA: Sedimentology, v.46, p.235-259.

McCarthy, P.J., Faccini, U.F., and Plint, A.G., 1999. Evolution of an ancient coastal plain: palaeosols, interfluves and alluvial architecture in a sequence stratigraphic framework, Cenomanian Dunvegan Formation, Alberta and British Columbia, Canada. Sedimentology, 46

Milana, J.P. and Tietze, K.W., 2002, Three-dimensional analogue modeling of an alluvial basinmargin affected by hydrological cycles: depositional processes, profiles and sequences: Basin Research, v. 14, p. 237-264.

Mitchum, R.M., Jr., 1977, Seismic stratigraphy and global changes of sea level, Part II: Glossary of terms used in seismic stratigraphy *in* Payton, C.E., ed., Seismic stratigraphy – Applications to hydrocarbon exploration: AAPG Memoir 26, p. 205-212.

Olsen, T., Steel, R., Hogseth, K., Skar, T., and Roe, S-L, 1995, Sequential architecture in a fluvial succession: sequence stratigraphy in the Upper Cretaceous Mesaverde Group, Price Canyon, Utah: Journal of Sedimentary Research, Vol. B65, p. 265- 280.

Paola, C., 2000, Quantitative models of sedimentary basin filling: Sedimentology, Vol. 47, p. 121-178.

Plint, A.G., McCarthy, P.J., and Faccini, U., 2001, Nonmarine sequence stratigraphy: Updip expression of sequence boundaries and systems tracts in a high-resolution framework, Cenomanian Dunvegan Formation, Alberta foreland basin, Canada: American Association of Petroleum Geologists Bulletin, v.85, p. 1967-2001.

Posamentier, H.W. and Allen, G.P., 1999, Siliciclastic sequence stratigraphy: Concepts and Applications, SEPM Concepts in Sedimentology and Paleontology 7, 210 p.

Ré, G.H., Jordan, T.E., and Kelley, S., 2003,Cronologia y paleogeografia del Teriario de la cuenca intermontana de Iglesia septentrional, Andes de San Juan, Argentina: Revista de la Asociación Geológica Argentina, v. 58, p. 31-48.

Schumm, S.A., 1975, Episodic erosion: a modification of the geomorphic cycle *in* Melhorn, W.N. and Flemal, R.C., eds., Theories of Landform Development, Publications in Geomorphology, State University of New York, Binghamton, p. 69-85.

Schumm, S.A., 1977, The Fluvial System: New York, Wiley, 338p.

Shanley, K.W., and McCabe, P.J., 1995, Sequence stratigraphy of Turonian-Santonian strata, Kaiparowits Plateau, Southern Utah, USA: Implications for regional correlation and foreland basin evolution: *in* Van Wagoner, J.C., and Bertram, G.T., eds., Sequence Stratigraphy of Foreland Basin Deposits - Outcrop and Subsurface Examples from the Cretaceous of North America: American Association of Petroleum Geologists Memoir 64, p.103-136.

Talling, P.J., D.W. Burbank, T.F. Lawton, R.S. Hobbs, and S.P. Lund, 1994, Magnetostratigraphic chronology of Cretaceous-to-Eocene thrust belt evolution, central Utah, USA: *Journal of Geology*, v. 102, p. 181-196.

Talling, P.J., Lawton, T.F., Burbank, D.W., Hobbs, R.S., 1995, Evolution of the latest Cretaceous-Eocene nonmarine deposystems in the Axhandle piggyback basin of central Utah: GSA Bulletin, v. 107, p. 297-315.

Vail, P.R., Audemard, F., Bowman, S.A., Eisner, P.N. and Perez-Cruz, G. 1991, The stratigraphic signatures of tectonics, eustacy and sedimentation: an overview,

in A. Seilacher and G. Eisner (eds.), Cycles and Events in Stratigraphy, II, Tubingen: Springer-Verlag

Van Wagoner, J.C., H. W. Posamentier, R. M. Mitchum, P. R. Vail, T. F. Sarg, T. S. Loutit, and J. Hardenbol. 1988. An overview of the fundamentals of sequence stratigraphy and key definitions, p. 39-45. *In* C. K. Wilgus, B. S. Hastings, C. G. St.G Kendall, H. Posamentier, C. A. Ross, and J. C. Van Wagoner, (eds.), Sea-Level Changes-- An Integrated Approach, Society of Economic Paleontologists and Mineralogists Special Publication, 42.

Van Wagoner, J.C., Mitchum, R.M., Campion, K.M., and Rahmanian, V.D., 1990, Siliciclastic sequence stratigraphy in well logs, cores, and outcrops: American Association of Petroleum Geologists Methods in Exploration 7, 63 p.

Van Wagoner, J.C., 1995, Sequence stratigraphy and Marine to Nonmarine Facies Architecture of Foreland Basin Strata, Book Cliffs, Utah, U.S.A., *in* Van Wagoner, J.C., and Bertram, G.T., eds., Sequence Stratigraphy of Foreland Basin Deposits - Outcrop and Subsurface Examples from the Cretaceous of North America: American Association of Petroleum Geologists Memoir 64, p. 137-223.

Wright, V.P. and Marriott, S.B., 1993, The sequence stratigraphy of fluvial depositional systems: the role of floodplain sediment storage: Sedimentary Geology, Vol. 86, p. 203-210.

CHAPTER 7: MIOCENE CARBONATES OF THE CENTRAL SIERRAS PAMPEANAS: RECONSIDERATION OF MARGINAL MARINE UNITS AND LOS LLANOS FORMATION

Introduction:

The Miocene "Paranense" epeiric seaway of South America has been the subject of considerable debate concerning its geographic extent, interconnectedness and chronology of flooding. During the Miocene, portions of Argentina, Bolivia, Brazil, Colombia, Equador, Paraguay, Uruguay and Venezuela were inundated with seaways, variously called the Amazonian, Caribbean, and Paranense (e.g. Ramos and Alonso, 1995). Hernández *et al.* (2005) suggest at least two periods of transgression over portions of Bolivia and Argentina, the first between 15-13 Ma and a later episode between 10 and 5 Ma (cf. 11.8 – 10 Ma, Lundberg *et al.,* 1998).

The Miocene Paraná Formation is exposed near Entre Ríos, Argentina and is continuous in the subsurface to the north, while the correlative Puerto Madryn Formation is exposed in northeastern Argentina. These two units are comprised of transgressive sequences with reef and platform limestones containing bivalves and gastropods. These rock types and fossils have been interpreted as evidence of littoral marine conditions, and suggest Atlantic throughflow into the Chaco Plain and eastern Patagonia (Martinez, 1988; Hernández *et al.,* 2005). However, it is more dubious whether other so-called "Paranense" deposits within the Argentine craton (e.g. Ramos and Alonso, 1995; Pérez *et al.,* 1996; Bertolino *et al.,* 2001; Dávila, 2002; Figure 7.1) are of marine origin. The identity of these sparse and thin outcrops is especially suspect where interbedded with Andean foreland sediments widely interpreted as lacustrine and playa lakes deposits. In such nonmarine closed drainage basin environments, carbonate genesis is a possibility, especially where salinity conditions approach those of restricted marine settings. Similar controversy regarding

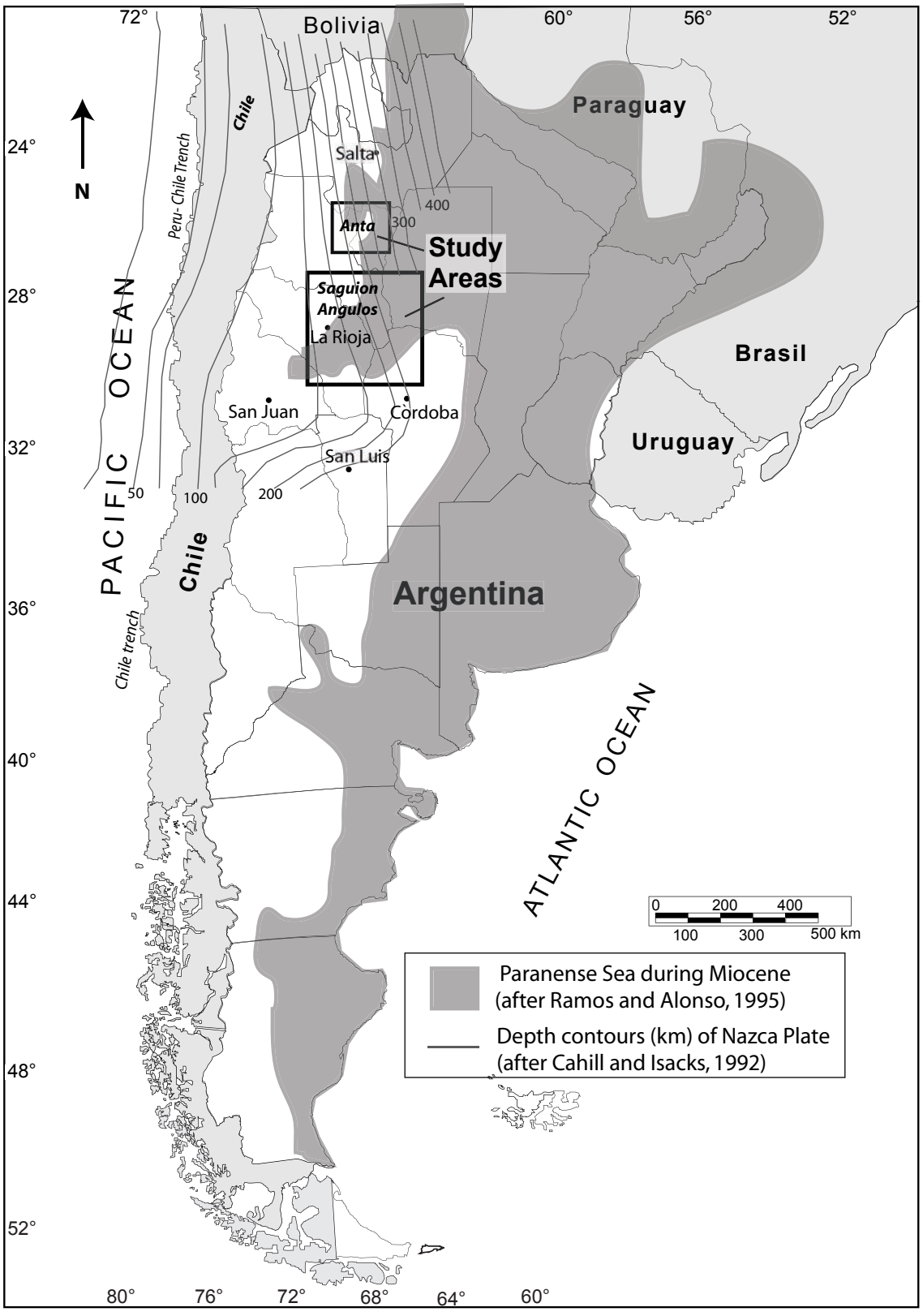

Figure 7.1: Map of study areas and proposed extent of Miocene marine incursion.

depositional environment exists for Miocene deposits in western Amazonia (S 2° - 5°, W 70° - 74°) wherein units once thought to be fluvio-lacustrine have been suggested to contain evidence of occasional marine influence (e.g. Hoorn, 1993; Vonhof *et al.*, 2003). Conflicting datasets exist for each area and much circular reasoning exists as interpretations have become entrenched in the literature.

Constraint of a Miocene sea level datum is of interest not only for historical geographic reconstruction, but also for interpreting lithospheric dynamics. The potential marine units considered in this study are located above the "Central Chile Flat-slab", the portion of the Nazca oceanic plate between about S 27° and S 33° subducting subhorizontally beneath the continental South American plate. At ~100 km inboard of the Chilean trench, the Nazca plate transitions from a typical subduction angle of 20-30° to become subhorizontal for ~450 km under the continent before returning to a steeper angle (Barazangi and Isacks, 1976). The region over the flat-slab is associated with fault-bounded basement blocks in the Andean foreland (10 to <5 Ma) forming the ranges of the Sierras Pampeanas (e.g. Jordan and Allmendinger, 1986; Jordan *et al*., 1989; Coughlin *et al*., 1998). The long-wavelength topographic response to the presumably-enhanced coupling due to thinned lithosphere above a more shallow and subparallel plate comprised of oceanic lithosphere is debated: does flat-slab subduction cause regional uplift (e.g. the Sierras Pampeanas region is presently well above sea level) or subsidence (c.f. the western U.S. Laramide province contemporaneous with Late Cretaceous-Early Tertiary flat-slab subduction, e.g. Cross and Pilger, 1978). As a means of assessing elevation change through time, a temporally-constrained regional datum was sought, in particular the Middle Miocene marginal-marine deposits of the Parana epeiric seaway. However, the scattered nature and minimal documentation of units with interpreted marine origin within the central Sierras Pampeanas required field reassessment and reconnaissance of their extent.

During a 2002 field campaign in Argentina, outcrops known to contain Upper Cenozoic limestones as well as cases previously interpreted as marginal marine deposits were surveyed and sampled. Additional study sites were selected based on LANDSAT remote sensing interpretation of possible limestone exposures. The goals were: 1) to better constrain the Miocene paleoshoreline, whose position has been speculated based on scant exposures of presumed marginal-marine rock (e.g. Ramos and Alonso, 1995; Perez *et al.*, 1996; Hernández *et al.*, 2005), and 2) to determine to what extent, if any, the Paranense Sea inundated the Central Sierras Pampeanas province. Stable isotopic data were collected from three such localities (Saguión Formation ESE of Salinas Grandes in Córdoba Province, Anta Formation in the Santa Maria Valley of Salta Province, and del Abra and del Buey Formations within the Famatina Ranges, La Rioja Province). Both of these goals, if achieved, would aid in the establishment of a regional landscape datum (i.e. sea level) for use in subsequent modeling of long wavelength topography in response to flat-slab subduction.

As part of the field surveillance of Upper Cenozoic limestones in the Central Sierras Pampeanas, we also assessed the lithofacies and pedogenic components of the Neogene (?) Los Llanos Formation. This formation contains intervals of carbonate-bearing paleosols tens of meters in thickness, which implies a period of landscape stability. In the absence of a Paranense sea level datum, it is plausible that regionally continuous paleosols of Los Llanos Formation could provide a surface for comparison of relative structural offset among basement uplifts of the Sierras Pampeanas, as proposed by Fisher *et al.* (2002). We also suggest that this Formation be redefined, on the basis of uncertain correlation among drastically different lithofacies and questionable stratigraphic relationships. A model of lithologic variation as a function of landscape position is also suggested.

Miocene "Paranense" Units- assessing marine versus freshwater deposition:

On the basis of mineralogy and sedimentary structures, it is challenging to differentiate a marginal or restricted marine setting from lacustrine environments. Lithologically, these environments are very similar; carbonates as well as fine-grained siliciclastic rocks accumulate in both nonmarine and marine systems. Certain minerals such as phosphates and iron silicates (e.g. chamosite and glauconite) are predominantly found in shallow marine rocks (Johnson and Baldwin, 1986). There are not, however, distinctly-lacustrine mineralogies. Also, there are no diagnostic structures unique to lakes, because features common in lacustrine environments (e.g. laminated bedding, soft-sediment deformation, tool marks and trace fossils) also may be found on tidal flats and marginal marine settings (Allen and Collinson, 1986; Boggs, 1995). Lithofacies associations may be useful if the surrounding units can be confidently interpreted as continental or marine.

Paleontologic constraints are generally the best indicator between nonmarine and marine settings because some fauna (e.g. corals, echinoderms, articulate brachiopods, bryozoans and cephalopods) are diagnostic of a narrow range of salinity conditions ("stenohaline" organisms). However, certain biota may be adapted to various temperature and salinity ranges that overlap environments. For example, the presence of foraminifera, often presented as evidence of marine conditions, is not a unique indicator of either salinity or water depth, the parameters used to define shallow epicontinental seaways (Heckel, 1972; Johnson and Baldwin, 1986). Numerous species of Quaternary foraminifera have adapted to highly variable changes in the salinity of Australian and Canadian lakes (e.g. Cann and De Deckker, 1981; Patterson and McKillop, 1991; Boudreau *et al.,* 2001). Foraminiferal assemblages in shallow marine conditions also can adapt to variable salinity (e.g. shallow versus deep shelf; Sellwood, 1986; Walsh, 2002). Without constraints of the salinity tolerances of

a particular species throughout its fossil record, the presence (or absence) of foraminifera is not a robust indicator of marine or freshwater conditions.

The ratios of stable isotopes of carbon and oxygen provide a means of assessing the depositional origin of carbonates in the geologic record. Modern marine carbonates are almost always characterized by $\delta^{13}C$ values near zero (-2‰ to 2‰ versus Peedee Belemnite standard is a common range; Ghosh *et al.*, 2001). The $\delta^{18}O$ isotopic composition of seawater throughout the Cenozoic is well known. During the Miocene, the epoch of interest for this study, seawater $\delta^{18}O$ was enriched by 2.5 to 3‰ relative to the present (Zachos *et al.*, 2001). Fields of isotopic values for various carbonate environments, continental and marine, have been assembled (after Milliman, 1974; Hudson, 1977; Talbot, 1990, 1994; Ghosh *et al.*, 2001). Although the range of values for freshwater limestones is rather large (reflecting isotopic fractionation due to variability of influx and biologic content, e.g. Hudson, 1977), a lighter (*i.e.* less negative) $\delta^{18}O$ signature for marine carbonates compared with freshwater carbonates is generally the case.

Because C and O isotopic ratios are affected by mixing of water from different sources, it can be difficult to interpret a unique depositional setting. Sources of water input with distinctive isotopic fractionation values (e.g. precipitation, continental runoff and open marine environments) are challenging to constrain in the geologic record (Vonhof *et al.*, 2003). Nonetheless, we can qualitatively address the likelihood of a marine versus continental paleoenvironment based on comparison of the Sierras Pampeanas data to compiled isotopic results from well constrained depositional systems.

Methods:

A review was conducted of published descriptions of outcrops in the Sierras Pampeanas with marginal marine characteristics. Remote sensing was also employed

to locate additional outcrops of carbonate or evaporitic lithology. I used Landsat Thematic Mapper imagery bands 7, 4 and 2 to maximize discrimination of evaporite and carbonate units (Sabins, 1997). Geologic maps of Catamarca, La Rioja, Cordoba and Salta Provinces were referenced for units described as "calizas" (limestones) or containing carbonate (e.g. Guerrero *et al.,* 1993, Martínez *et al.,* 1995; SEGEMAR, 1999, 2000, 2002). Guided by the spectral and previously-interpreted lithologic characteristics, field reconnaissance of potentially marine outcrops was conducted during May and June, 2002, and samples were collected from three key formations: the Saguion Formation, Córdoba; Del Buey Formation, Sierra de Famatina La Rioja; and Anta Formation, Salta). The approximate extent of the study areas and sample localities are depicted in Figures 7.1 and 7.2.

In the laboratory, carbonate samples were crushed and homogenized with a mortar and pestle to fine sand size fraction (<0.25 mm). These powders were analyzed for stable isotopic ratios at the University of Colorado Institute of Arctic and Alpine Research Stable Isotope Lab with a dual inlet mass spectrometer (precision better than 0.1‰). Thin sections were prepared by Spectrum Petrographics (Vancouver, WA) and studied with a binocular microscope under plain- and cross-polarized light at magnifications 4x to 40x.

Review of Miocene units interpreted as marginal marine:

In the following section, I describe published and observed lithofacies characteristics of three formations from the Central Sierras Pampeanas Province that have been interpreted as marginal facies of the Miocene Paranense seaway.

A. Saguión Formation:

Marginal marine facies have been described within the siliciclastic Miocene-Pliocene Saguión Formation, southeast of Salinas Grandes basin in Córdoba Province (Bertolino *et al.,* 2001; Figure 7.2). This marine interpretation was made on the basis

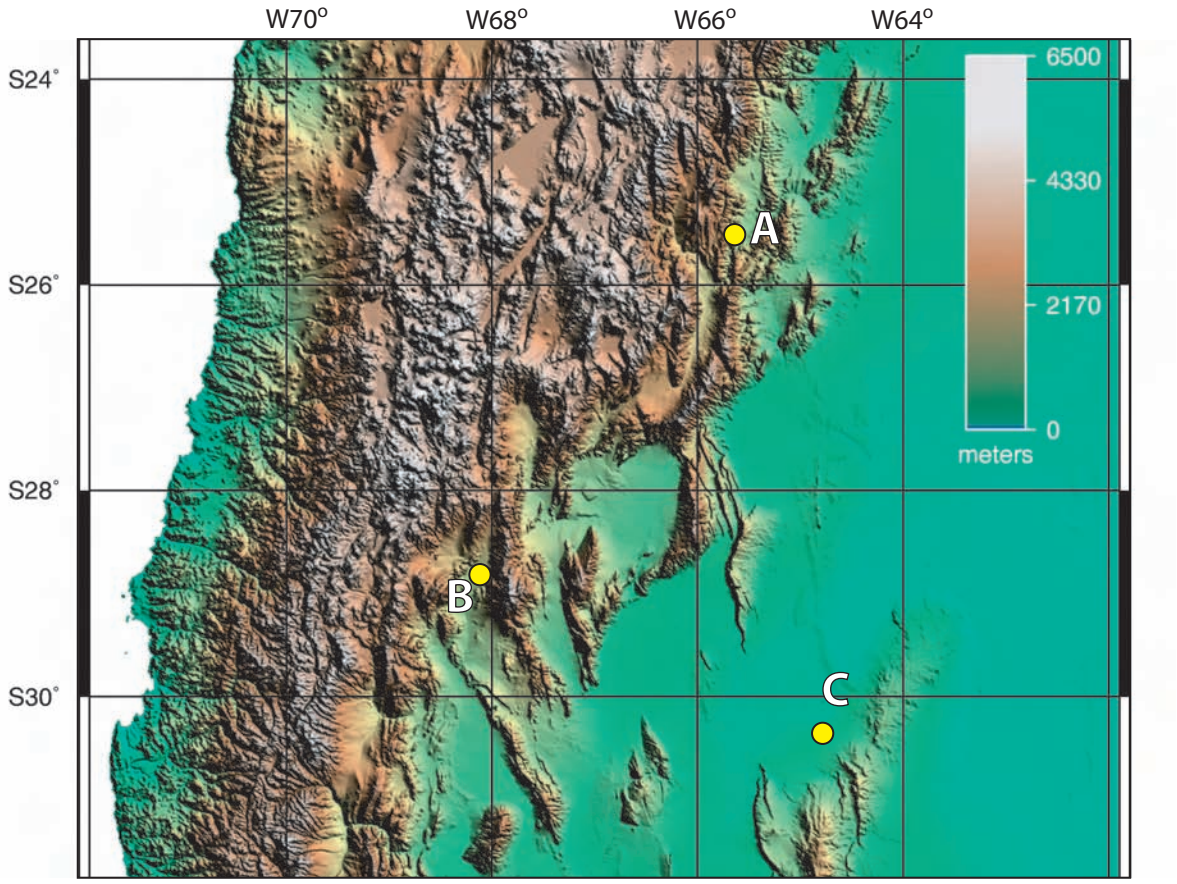

Figure 7.2: Sample localities of Miocene rocks previously intepreted as marginal marine within Sierras Pampeanas Province, Argentina. Localities of units described in text: A) Quebrada La Yesera (Anta Formation); B) Famatina (Angulos Group); C) Salinas Grandes (Saguion Formation).

of a 10-15 meter-thick succession of bioturbated sandstone and siltstone, and greenish micritic stromatolites in the lower (El Simbolar) member of the Saguión Formation (Figure 7.3). Bertolino *et al.* (2001) interpreted specific trace fossils and the stromatolites as evidence of deposition on intertidal flats. These units were revisited with Bertolino in May, 2002. Near the Saguión river valley (S 30º 34', W 64º33'), buff-colored stromatolitic units 2-3 m thick are interbedded with reddish fine sandstone. However, these sandstones are relatively free from bioturbation. The stromatolitic facies is well laminated, undulatory, and structured as laterally linked hemispheroids, collectively suggestive of a low-energy depositional environment. Algal components vary from 5-mm laminae to friable layers up to 3 cm thick. The stromatolites, however, are also interbedded with gypsum and other evaporites, which also appear on the modern ground surface. Whether the interbedded salts are primary saline lake deposits can not be determined.

Samples from Arroyo Saguión (MAS-1, MAS-2) were analyzed for micromorphic characteristics. Under cross-polarized light and 10x magnification, mudstone laminations are found to be >30% muscovite, with subrounded to angular quartz grains often clustered in diffuse bands subparallel to laminated carbonate groundmass. Minor amounts of chlorite are also present. The majority of the carbonate is micritic in form, with only minor evidence for secondary sparite replacement of the laminated matrix. Micritic calcite was utilized for isotopic analyses (see below).

B. Angulos Group:

The Angulos Group is an assemblage of Lower to Middle Miocene synorogenic strata east of the Sierra de Famatina (S 27°-31°, ~W 67° 30', Figure 7.2) basement uplift in of the Sierras Pampeanas (Dávila and Astini, 2003). The three formations that comprise the Angulos Group are, in ascending order, the Del Abra,

Figure 7.3: Stromatolitic facies of Saguión Formation (El Simbolar Member), Córdoba Province, Argentina. Unit is 3 m in total thickness with variable parting but many laminations reveal linked hemispheroidal algal structure.

Del Buey, and El Durazno Formations. Several thin limestones (10 cm or less) appear in the upper Del Abra Formation (an upward-fining colluvial-alluvial sequence; Dávila and Astini, 2003). At least one regionally extensive meter-thick limestone with bivalve fragments is found within the fluvio-lacustrine Del Buey Formation, time correlative with the Middle Miocene Paranense Sea (Dávila, 2002).

Carbonate samples were collected from the members of the Angulos Group exposed in the Durazno River valley within Sierra Famatina near S 28˚ 40', W 67˚ 42'). The most laterally continuous limestone bed (Del Buey Formation) was locally observed to be 70 cm thick, nodular to laminar in structure with trace fossils and shell fragments present on bedding surfaces. Dávila and Astini (2003) correlated the bed for >5 km along-strike. The unit is interbedded with siltstones and fluvially-crossbedded sandstones.

A thin section of a thin upper Del Abra Formation limestone (SO1) revealed few framework grains (<5%) within a micritic matrix (90-95%), with some amorphous hematite accumulations. Framework grains included subhedral twinned and zoned plagioclase with edges altering to clay, anhedral micas, and sparry calcite, the latter confined to elongate zones and suggestive of fossil forms.

C. Anta Formation:

In the Salta Province of Northern Argentina, the Miocene Anta Formation (~13 – 16.5 Ma; Galli *et al.*, 1996) has been proposed to record marine influences from the Paranense Sea. This interpretation was made on the basis of several oolitic limestones and lithologic correlation with formanifera- and mullusc-bearing units (Rio Salí and San José Formations) to the south and west (Hernández *et al*., 2005). Exposures of Anta Formation were observed at two localities (Figure 7.4): within the Quebrada de la Yesera (S 25° 59'20" W 65°45'04") and near the village of Alemania (S 25°36'06" W 65°35'54").

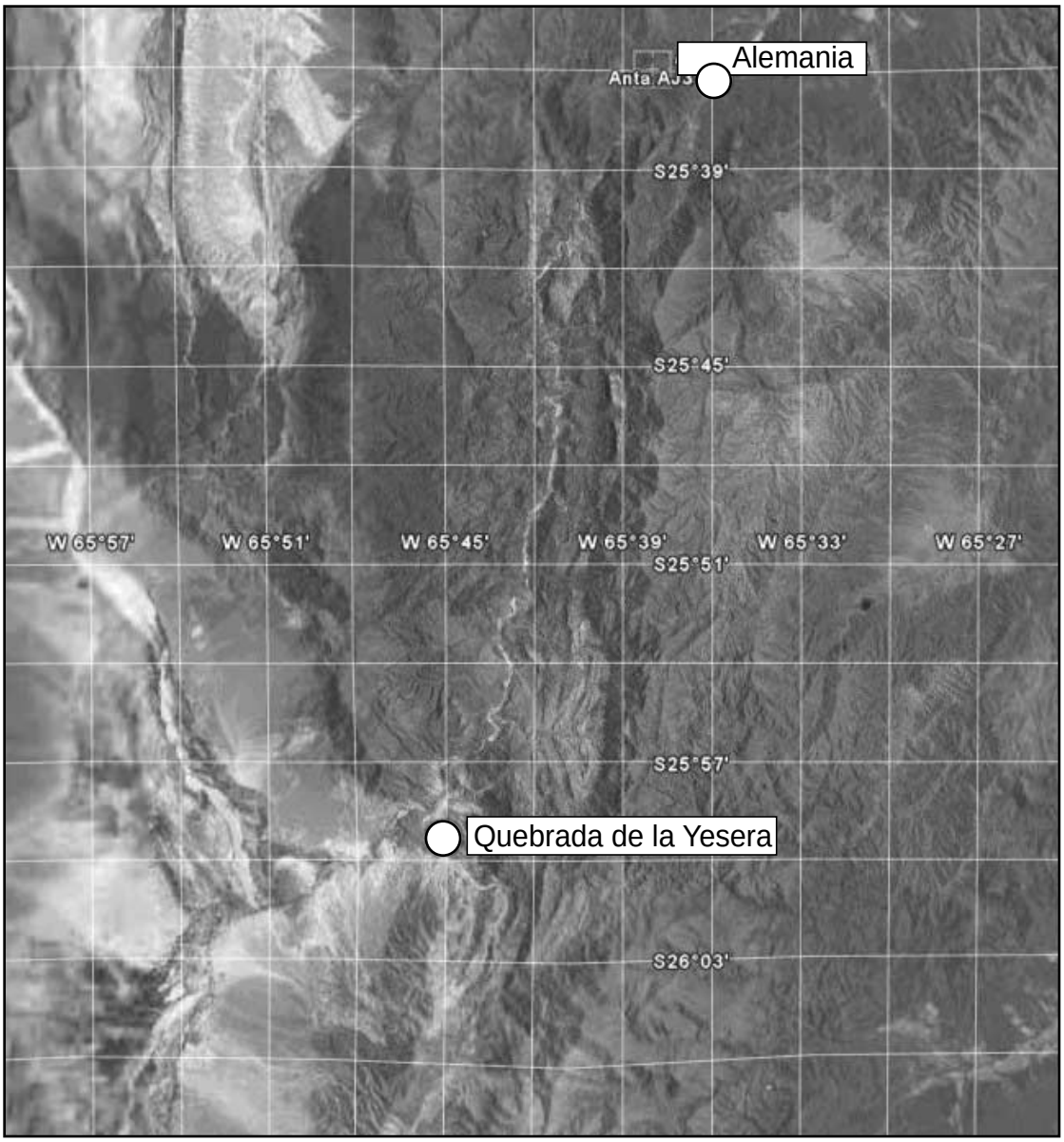

Figure 7.4: Locations of sampled Anta Formation limestone units, Salta Province, northern Argentina. Image modeified from Google Earth (2006).

At the Quebrada de la Yesera locality, the Anta Formation unconformably overlies red mudstones of the Paleogene Lumbrera Formation. Five limestone beds occur within approximately 40 m of well-laminated red and grey mudstones and sandstones (Figure 7.5). The first carbonate bed (sample AJ-1) is ~20 cm thick, overlying a quartz pebble conglomerate exhibiting trough crossbedding which grades upward into pedogenic mudstone (Figure 7.6A). This has been interpreted as the first inundation surface of the Miocene Sea over the Paleogene Lumbrera Formation (R. Hernández, personal communication, 2002). The overlying 3 meters consist of coarse, crossbedded or rippled sandstone, some with mudcracks, and then approximately 10 m of red mudstone. Thin rippled sandstone underlies the next limestone bed (AJ-2), which is oolitic with nuclei of well rounded quartz grains. Three additional limestones (each <1 m thick) are interbedded in the overlying 20 m of mudstone.

The Anta Formation also is exposed northeast of the Quebrada de la Yesera locality, near the town of Alemania (S 25˚36' W 65˚ 36', Fig. 7.4). The studied outcrop initiates with the uppermost several tens of meters of the Paleogene Lumbrera Formation. The observed strata consist of highly bioturbated and/or pedogenic siltstones and fine sandstones. Units are multicolored (green, gray, purple and red), reflecting a range of post depositional redoximorphic conditions. Upsection, beds are generally silty, less pedogenic, and capped with secondary gypsum beds. The overlying Anta Formation consists of 100 -150 m of massive red crossbedded sandstone with thin interbeds of slightly pedogenic siltstone. The siliciclastic Anta strata include a tuff dated 14.5±1.4 Ma (Reynolds *et al.*, 1994). Approximately 100 meters from the base of the Anta Formation a 1-m thick limestone was sampled (Fig. 7.6B), exhibiting laminations suggestive of algal accretion, as well as some carbonate intraclasts and oolites.

Figure 7.5: Miocene Anta Formation exposures in Quebrada de la Yesera, Salta Province, Argentina. Outcrop thickness is approximately 30 m, consisting of rippled sandstones, laminated mudstones and at least five limestone beds (each <1 m thick), containing oolites and/or fossils.

Figure 7.6: (A) Stratigraphically lowest limestone bed of Anta Formation, Quebrada de la Yesera, Salta Province (S 25^{o} 59'20" W 65^{o}45'04"). This limestone (~20 cm thick, sample AJ1) lies above 3-4 m of crossbedded quartz pebble conglomerate grading into pedogenic red and grey mudstone. (B) Anta Formation limestone near Alemania, Salta Province (S 25^{o} 36'06" W 65^{o}35'54"). This limestone (1 m thick, sample AJ3) exhibits algal laminations, limestone intraclasts and oolitic components. It is positioned >100 m from the top of the Lumbrera Formation amid an interval of massive crossbedded sandstone and laminated mudstone. A tuff dated 14.5±1.4 Ma is stratigraphically above the limestone by several tens of meters.

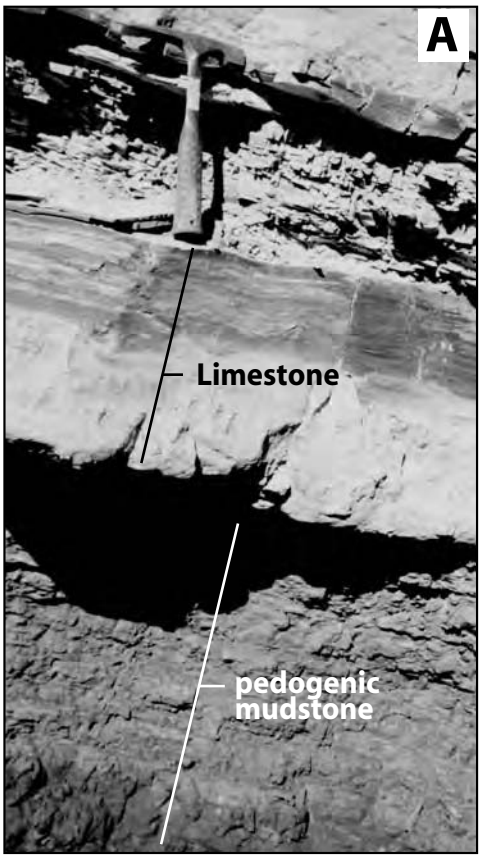
A
Limestone
pedogenic
mudstone

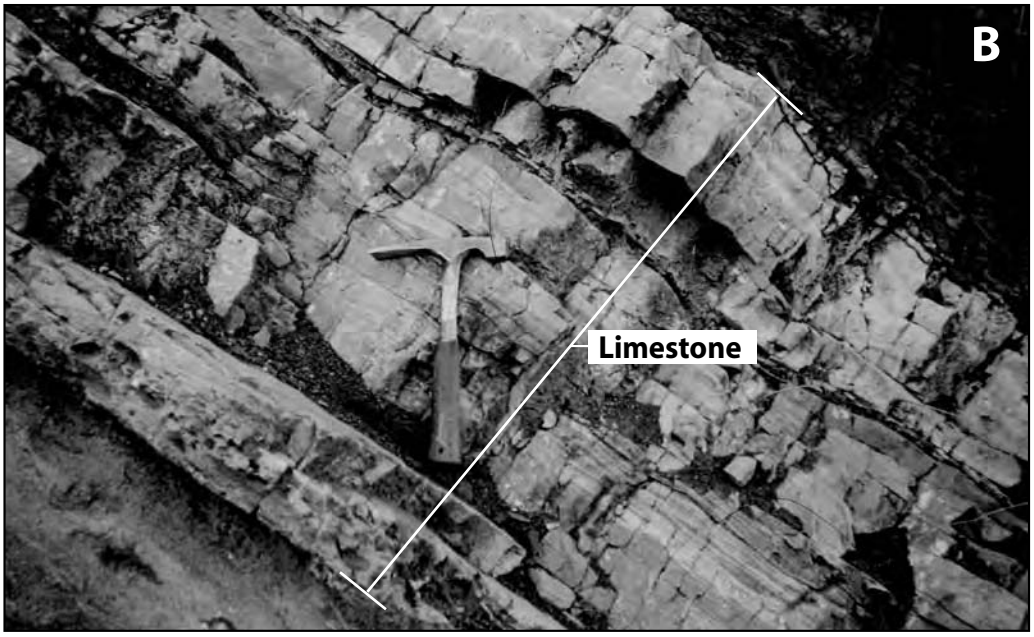
B
Limestone

These outcrops of Anta Formation as well as another nearby exposure exhibit paleontological and palynological features suggestive of lacustrine rather than marine deposition. At Quebrada de la Yesera, freshwater fish have been documented (Cione and Casciotta., 1995), suggesting a freshwater input into an overall saline environment (Stark and Anzótegui, 2001). The Anta Formation is lithologically similar at Río Piedras, consisting of claystones, interbedded tuffs, and at least seven oolitic limestones (Quattrocchio *et al.,* 2003). Grains from the limestones include analcime, a sodic aluminosilicate of the zeolite group, which suggests deposition in an alkaline and saline playa lake (Quattrocchio *et al.,* 2003). The pollen content of the section also corresponds to saline lake depositional environments (Quattrocchio *et al.,* 2003).

Stable Isotopic Results:

Carbon and Oxygen isotopic results from the Anta, Del Abra, Del Buey, and Saguión Formation are summarized in Table 7.1 and compared to isotopic fields defined for various carbonate-precipitating environments (Fig 7.7). Note that all of the samples are characterized by negative values for both isotopic systems (Fig. 7.7).

Three samples from Miocene limestones of the Angulos Group at Sierra de Famatina yield comparable isotopic values. Isotopic values of two Del Buey Formation samples (ED21 and S02) exhibited the least depleted carbon signals (-0.26 to -0.68 ‰). The $\delta^{18}O$ values of the two samples are similar (-8.19 and -7.94‰). These values compare favorably with those compiled by Milliman (1974) and Talbot (1990) for a wide variety of lacustrine limestones from the geologic record. Though carbon values are close to zero per mil, a marine isotopic signature is not apparent from the depleted $\delta^{18}O$ values. One Del Abra Formation carbonate (with a laboratory precision duplicate; S01 and S01D) has a very similar $\delta^{18}O$ signature to the Del Buey limestone (-7.89‰ average) and a somewhat more depleted $\delta^{13}C$ value (-2.21‰

Table 7.1: Stable isotopic values for sampled Miocene limestones of central Sierras Pampeanas province, Argentina. Values are per mil relative to Peedee belemnite standard (PDB).

Sample ID	Formation	Locality	$\delta^{13}C_{PDB}$	$\delta^{18}O_{PDB}$
AJ1	Anta	Quebrada La Yesera, Salta Prov.	-6.72	-3.55
AJ3	Anta	Alemania, Salta Prov.	-6.22	-1.45
ED21	del Buey	Sierra de Famatina, La Rioja Prov.	-0.68	-7.94
SO2	del Buey	Sierra de Famatina, La Rioja Prov.	-0.26	-8.19
SO1	del Abra	Sierra de Famatina, La Rioja Prov.	-2.27	-7.97
SO1D	del Abra	Sierra de Famatina, La Rioja Prov.	-2.15	-7.81
Mas1	Saquion	Saquion River, Cordoba Prov.	-3.63	-7.50
Mas2	Saquion	Saquion River, Cordobo Prov.	-4.23	-6.81

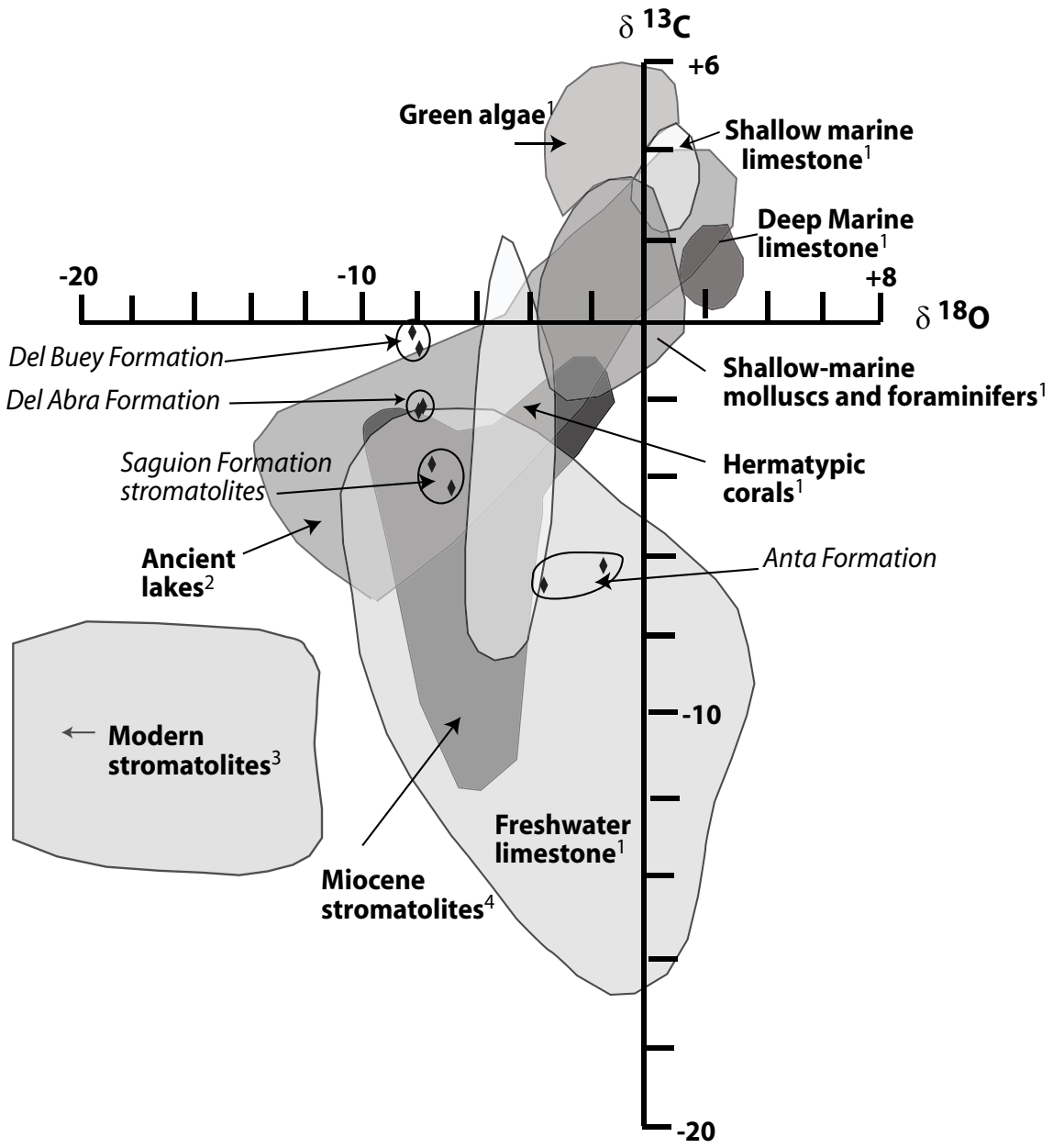

Figure 7.7: Comparison of isotopic signatures of Tertiary carbonate samples with environmental fields defined by: 1. Milliman, (1977); 2. Talbot (1990), 3. Ghosh et al., (2001) and 4. Talbot (1994). Units are per mil relative to Peedee belemnite standard.

average). A freshwater origin is also inferred for this formation based on comparison with the isotopic fields summarized in Fig. 7.7.

The stromatolitic accumulations from the Saguión Formation exhibit values of $\delta^{13}C$ -3.63‰ to -4.23‰ and $\delta^{18}O$ -6.81‰ to -7.51‰. These values are comparable with values for stromatolites from another Miocene lake (Talbot, 1994) as well as values typical of freshwater limestones (Milliman, 1974). Though the Saguión data lie close to the field defined for hermatypic corals (i.e. requiring shallow, warm, low-energy saline water), lack of fossil evidence from in the Saguión Formation precludes this interpretation.

Isotopic analyses of two of the Anta Formation oolitic limestones from Salta Province also suggest that lacustrine deposition is a possibility. These carbonates yield the least depleted $\delta^{18}O$ values (-1.45 to -3.55‰) of all sampled units, which in itself may suggest mixing with a marine-sourced water. However, the carbon signatures are much more depleted (-6.22 to -6.72 ‰), placing the Anta Formation samples firmly in the "freshwater limestone" field (Milliman, 1974).

By comparison of our sample data with other isotopic compilations, all samples from the Sierras Pampeanas limestones yield $\delta^{13}C$ and $\delta^{18}O$ values suggestive of nonmarine depositional environments. However, nonmarine carbonate isotopic values can be significantly affected by evaporation, residence time, continentality, vegetation of their catchment, as well as by altitude and latitude (e.g. Talbot, 1990; Mack and Cole, 2005). Therefore, these isotopic values do not entirely preclude the possibility that the bodies of water which precipitated the limestones may have received influx from a marine source, which would tend to mix the isotopic systems and drive values toward zero per mil. This could be the case for the Anta and Del Buey Formation samples, which exhibit the least depleted oxygen and carbon values, respectively. It is also noteworthy that the Anta Formation $\delta^{13}C$ values (-6.22 to -

6.72‰) are quite similar, even though the sampled units were collected 45 km apart. Could this suggest a well-mixed system receiving a large fraction of isotopically "uniform" seawater? Similarly, both isotopic systems agree within 0.42 ‰ for Del Buey samples, perhaps suggesting a high percentage of marine-sourced water. Conversely, as these samples were collected from one bed only several km apart, they may instead represent precipitation from an isotopically homogeneous ("well-mixed") lake. Talbot (1990) showed that several per mil natural variability is expected for closed-lake carbonate $\delta^{18}O$ values because of changes in water balance.

Potential Miocene carbonates in addition to those above were sought out based on Landsat Thematic Mapper signatures and/or map descriptions of possible limestones or calcretes. We field-checked mapped Tertiary outcrops within Catamarca, Córdoba and La Rioja Provinces described as containing carbonates, including "calchaquense" strata east of Sierra Ancasti, (Martínez, 1995) and Los Chivatos Formation "sandy carbonates" around the flanks of Sierra Brava (SEGEMAR, 2002). Of particular note was the mapped description of the Miocene-Pliocene Los Llanos Formation (equivalent with Los Chivatos Formation; see below), described as containing calcareous siltstones and limestones (e.g. Guerrero *et al.*, 1993). This formation is described below.

Discussion:

Doubts about a marine origin for these Neogene units in the Sierras Pampeanas arise from four criteria. First, the facies associations of the calcareous deposits do not suggest a transgressive sequence following Walther's Principle. Limestones are restricted to meter thick beds amid much thicker successions of alluvial to fluvial strata. They are not laterally traceable into deeper water facies. We acknowledge that Tertiary outcrops are mainly restricted to margins of basement uplifts, for which the contemporaneous basinal deposits would be buried by thick Quaternary alluvium.

However, seismic reflection and borehole analyses have shown that the Tertiary strata may exceed a kilometer in several intermontane basins of the Sierras Pampeanas (e.g. Salinas Grandes and Salinas de Mascasin, Alvarez *et al.,* 1989; La Rioja basin, Fisher *et al.,* 2002; Figure 7.8). Well cuttings of the Tertiary section from the Salina de Mascasin (SW of Sierra de los Llanos) encountered alternating conglomerates, sandstones and siltstones, but no carbonates or marine lithofacies. Secondly, the lithologic features of the proposed carbonates (bioturbated mudstones, algal bioherms, oolithic and laminar carbonates) are not uniquely diagnostic of a "littoral" or marginal marine origin, although they have been interpreted as such. These features are commonly found in modern and ancient lacustrine settings (Dean and Fouch, 1983; Allen and Collinson, 1986). Third, the fossil assemblages do not unequivocally support marine conditions. Freshwater fish collected in the Anta Formation make a marine origin for at least some of the limestone beds particularly suspect. Other fossils collected from the "Paranense" deposits are foraminifera, which have been shown to be present in lacustrine systems and tolerant of variable water salinity. Without supporting data to confirm the range of paleotemperatures and paleosalinities these species can endure, marine influence cannot be assured based on foram presence alone. Finally, based on ^{13}C and ^{18}O isotopic values, a lacustrine origin is interpreted as more likely than marginal marine deposition.

If the Sierras Pampeanas Neogene carbonate horizons are not of marine origin, what is their environmental significance? The extensive Del Buey Formation limestone and carbonate units of the Anta and Saguíon Formations are lithologically unique compared to the Tertiary stratigraphy of their areas. However, these limestones appear amid laminar and often pedogenic silt-and-mudstones interpreted as lacustrine deposits (e.g. Dávila and Astini, 2003; Quattrocchio *et al.***,** 2003). It is suggested that these Middle Miocene lacustrine intervals in the northern and central

Sierras Pampeanas were formed under a climate that was more humid than in earlier Neogene times. For example, cessation of eolian deposits at 14 Ma in Bermejo Basin, west-central Argentina, has been interpreted as climate change from arid to less arid (Jordan *et al.,* 2001). Similar lithologic as well as paleontologic shifts 15-10 Ma from arid to humid conditions have been suggested in northwestern Argentina (Hernández *et al.*, 1996; Starck and Azótegui, 2001). Whether these sedimentary systems were responding to local climate changes driven by Andean orogeny or global changes is still debated (e.g. Alonso *et al.*, in review). However, they are of the same age as a major episode of global oceanic cooling, beginning ~14 Ma, marking the end of the so-called "Mid-Miocene Climatic Optimum" (Zachos *et al.,* 2001).

Given our observations and summary of available datasets, it seems that although parts of eastern and southern Argentina were certainly inundated during the Miocene, we find no evidence that marine conditions entered the Sierras Pampeanas of central Argentina. Until more substantive proof of marine deposition can be found, we reject correlation of the Saguión, Anta, and Del Buey Formations with the Paranense seaway.

Los Llanos Formation: Facies and Degree of Pedogenesis

An alternative datum against which to measure Neogene uplift or subsidence may exist in the Estratos de Los Llanos. Unlike sea level, which is an absolute datum roughly equivalent with the geoidal projection about the earth, any other datum above sea level implies a land surface whose original form can be estimated even if its paleoeleveation is unknown. One category of potential data is subhorizontal depositional surfaces with relationship to the landscape discernible over regions larger than individual Quaternary depositional basins. A unit that contains lithologically distinct horizons and is widespread in the Central Sierras Pampeanas is the Neogene Estratos de Los Llanos, hereafter referred to as Los Llanos Formation. Coira and

Koukharsky (1979) recognized that the Los Llanos Formation locally exhibits features of intense pedogenesis, and we have found up to 40 m of stacked paleosols in various outcrops of Los Llanos Formation in La Rioja Province, Argentina. These pedogenic features may provide a suitable regional datum to assess the development of relative relief during the late Neogene.

Pedogenesis requires a period of landscape stability, plus temporally and spatially punctuated sedimentary deposition (Birkeland, 1999). Though soils can form on hillslopes, their thickness and degree of development are hindered on slopes due to mass wasting and erosive overland flow. In contrast, thick intervals of stacked soils ("compound" pedosequences, *sensu* Kraus, 1987) indicate prolonged soil formation in a depositional system with episodic sedimentation. However, neither pedogenic nor lithologic features are consistent from outcrop to outcrop. Thus, as a prerequisite for evaluating the suitability of Los Llanos Formation as a regional subhorizontal datum, we assessed its facies characteristics over an area ~23,000 km^2 (Fig. 7.8), within which pedogenic features and lithologies vary markedly.

A. General stratigraphy

The Neogene Los Llanos Formation is a regionally extensive, lithologically variable unit which unfortunately lacks adequate age constraint. In general, the Cenozoic stratigraphic organization of the basins between the Sierras Pampeanas has suffered confusion by various terminologies and conflicting age assignments, leading to uncertain regional correlations (discussed by Pascual and Bondesio, 1981; Reynolds *et al.*, 1997). A particular source of confusion is the Los Llanos Formation, which has alternatively been called "Estratos de Los Llanos" (Bodenbender, 1911), Los Chivatos Formation (Ramos, 1982), San Roque Formation (Flores, 1969; Rivarola and di Paola, 1993; corresponding to Lower Los Llanos Formation), Las Mulitas Formation (Flores and Roque, 1972; Upper Los Llanos Formation), or "Estratos Calchaqueños" (Gerth,

1914). The unit's lithology is described as variously colored (white, gray or pink) calcareous-cemented conglomeratic and quartz-rich sandstone, mudstone, oolitic limestone and gypsum interbeds, with facies interpretations ranging from fanglomerates to fluvial and playa lake environments (Caminos, 1968; Rivarola and di Paola, 1993). The unit is said to be 190– 350 m in boreholes and continuous in the subsurface from south of La Rioja city (S 29° 25', W 66° 50') to east of San Juan city (S 31° 30', W 68° 35') to San Luis City (S 33°19', W 66°21'; Caminos, 1968; Pascual and Bondesio, 1981). One mutual feature of these varied descriptions of Los Llanos Formation is an important participation of carbonate and gypsum, as pedogenic nodules, diagenetic concretions or discrete beds of "calcrete" (Guinazú, 1962).

The age assignment has varied between Cretaceous and Pliocene, with lack of consensus in part because of scarcity of fossil content and the disparate nature of outcrops (see discussion below). The type locality near Sierra de los Llanos (Fig. 7.8) was initially correlated as Cretaceous (Bodenbender, 1911). A mammalian fossil found in an outcrop south of Sierra de las Minas was interpreted to be Middle-Miocene or Early Pliocene (Pascual, 1954; Guinazú, 1962). Near San Luis, outcrops of Las Mulitas Formation have yielded several mammalian specimens interpreted to range from 11 – 5 million years in age (Pascual and Bondesio, 1981). Outcrops near Sierra Velasco including dinosaur fossils were considered Los Llanos Formation by Hünicken *et al*., (2001), but lack of lithologic description prohibits comparison to other Los Llanos outcrops. From the available paleontological evidence, a Middle Miocene-Early Pliocene age is preferred.

B. Facies relationships from field observations:

Assessment of facies variation of the Neogene Los Llanos Formation outcrops was conducted during June 2002. The approximate extent of the study area is depicted in Fig. 7.8. Detailed lithologic measurements were conducted at outcrops along the

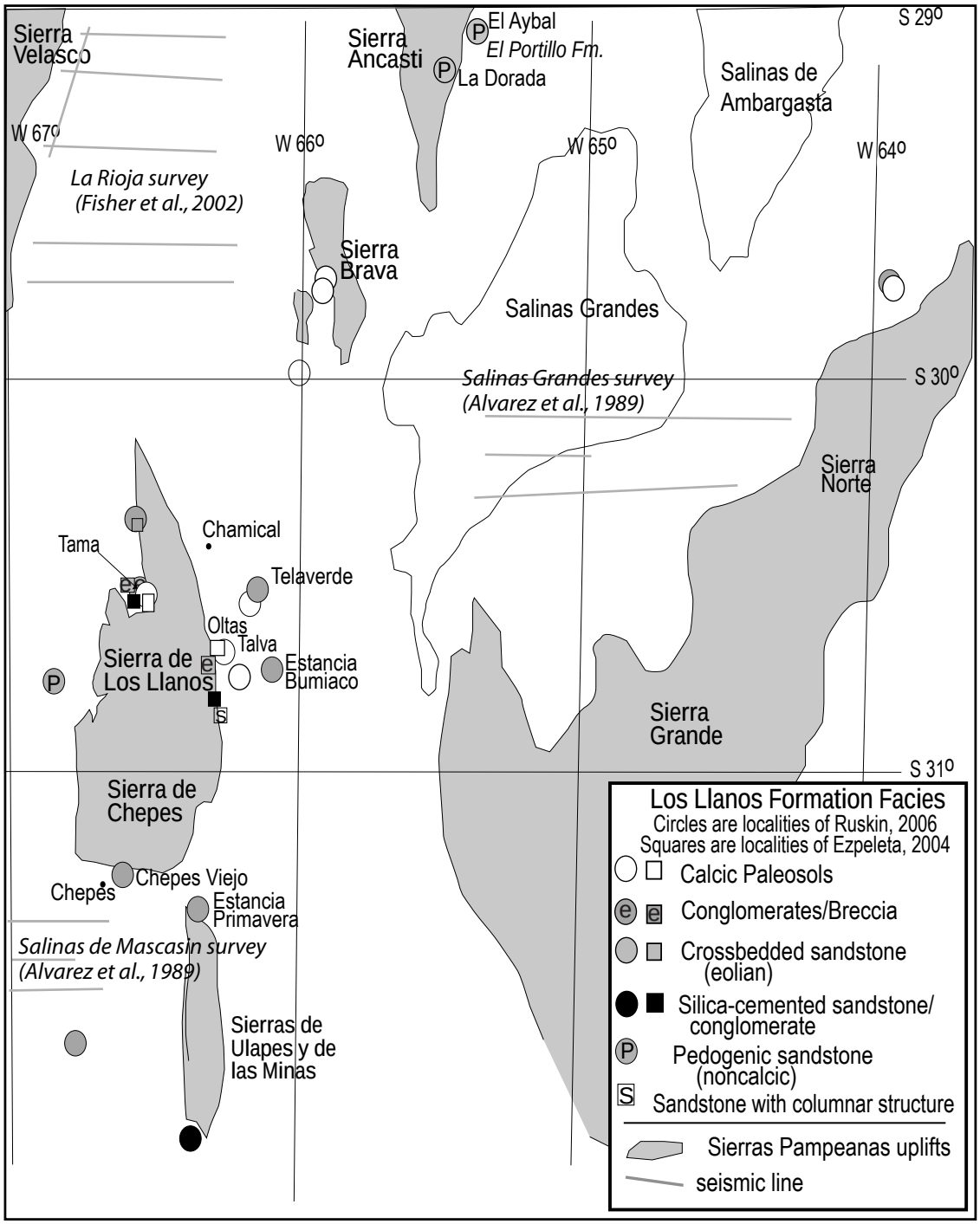

Figure 7.8: Los Llanos Formation sample sites and lithofacies, central Sierras Pampeanas

flanks of the Sierra de los Llanos basement uplift by Miguel Ezpeleta for his undergraduate thesis at Universidad Nacional de Córdoba, Argentina (Ezpeleta, 2004). Fieldwork by Ruskin assessed additional outcrops in the basins between the Pampean uplifts, including pedogenic facies to the East and Northeast of Sierra de los Llanos. These observations lead to some qualifications and concerns with Ezpeleta's stratigraphic and paleoclimatic conclusions (as summarized in Ezpeleta *et al.,* 2004 and Dávila *et al.,* 2004).

On the basis of outcrop observation and subsequent petrography of samples from the west and east flanks of Sierra de Los Llanos, Ezpeleta (2004) defined eight distinct facies for Los Llanos Formation. The limited exposures do not exceed 40 m thickness in this region. Interpretation of paleoenvironments allowed Ezpeleta to integrate the facies into two associations, called the Lower and Upper Members.

The Lower Member, ~15 m thick consists of three facies. The component facies are: 1) Thin and discontinuous clast-supported fine conglomerate with sand matrix (Figure 7.9B); 2) Poorly sorted oligomictic breccias (up to 0.6 m thick) with clasts of metamorphic and granitic basement; and 3) Cross-stratified fine to medium grained subarkosic sandstone (sometimes cemented with calcite) with paleocurrents from foreset measurements directed to the SE (Fig. 7.9A). The former two facies are interpreted as ephemeral and spatially restricted debris flows proximal to the Sierra de los Llanos. The latter and finer-grained facies is interpreted as eolian in origin, based on its structures and grain textures. Together, the Lower Member represents a change from poorly-developed fluvial to widespread eolian deposition (Ezpeleta, 2004).

An Upper Member, comprised of five facies, reaches ~9 m in thickness. Observed facies are: 4) poorly sorted clast-supported fine conglomerates with intense carbonate and silica cementation, internal chaotic fabric, calcic or silicic rhizoliths and carbonate nodules to 8 cm in diameter; 5) Silicified sandstone beds (to 1 m thick),

Figure 7.9: Los Llanos Formation, south of Tama, west flank of Sierra de los Llanos, La Rioja Province (S 30°32'45", W 66°31'32"). (A) Crossbedded sandstone and gypsum-cemented conglomerate. Foresets are 3-5 m in height, and gypsic nodules and laminations are common upsection. (B) Base of section, exhibiting gradation from red Permian conglomerates below (containing quartz clasts and granitic pebble lenses) and grey Tertiary (?) conglomerate above. Bedding is roughly perpendicular, the contact is nonerosive, but color change is noticeable. Grey conglomerate is 5 m thick, with sharp upper contact with crossbedded sandstones (photo A). It is uncertain where the Tertiary Los Llanos Formation begins. (C) Top of section, but ~300 m north of outcrop in Photo A. Here, sandstone is laminated and friable, with abundant gypsum interbeds and nodules. The gypsum has ductily deformed and in some cases tightly folded the sandstone, suggesting syndepositional deformation. Gypsum is more abundant upsection, perhaps leaching downward from conglomeratic capstone. Up to 3 m of erosive relief exist at top of the sandstone.


A


B


C

whose lower portions are intensely red in coloration and clay-rich,and whose upper portions are more sandy, and mottled white and red. The unit also includes silicic columns up to 70 cm in height; 6) Pink to white, intensely mottled sandstone (beds 0.8-1.5 m thick), with chalcedony cementation and some calcic nodules and rhizoliths; 7) Pinkish siltstone-claystone, lacking lamination, but containing ped structure (Figure 7.10B); and 8) regolith formed on top of the granitic to metamorphic basement (<1 m thick). These facies are interpreted to represent various stages of soil formation affecting alluvial parent materials (Ezpleleta, 2004).

In general, the outcrops visited and facies described by Ezpeleta (2004) correspond with those reconnoitered by Ruskin, although with some differences. Ruskin did not observe facies 5 (silicified columnar sandstone) or 8 (basement regolith), although both facies are thin (<1 m) and likely to represent local weathering or diagenetic conditions, rather than characteristic features of the Los Llanos Formation.

It not clear from Ezpeleta's (2004) description what is the nature of the contact between Lower and Upper Members of Los Llanos Formation. Facies 4 is described as having a smooth or slightly undulatory base (Ezpeleta, 2004). However, along-strike assessment of this conglomerate indicates up to 3 m of erosion into the underlying cross-bedded dune sandstones (Fig. 7.9A, near Tama, S 30° 32.2', W 66° 31.7'; facies 3 above). The conglomerate reaches 10 m thickness progressing south along the Sierra de los Llanos flank. It is plausible that this erosive surface represents the contact between the poorly-developed fluvial and eolian Lower Member and the pedogenic alluvial Upper Member. However, both members overlie Permian redbeds, initiate with ~5 m of conglomerate and exhibit pedogenetic alteration upsection. As will be discussed below, the members may be equivalent, but differ in lithology because of different climatic conditions on opposite sides of the Sierra de Los Llanos.

Figure 7.10: (A) Brecciated facies along western flank of Sierra de los Llanos, near Alcanzar (S 30°20'27" W 66°33'07"). Outcrop is 1-1.5 m thick, associated with nearby sandy conglomerates. Breccia is calcareously cemented, but does not appear pedogenic. Similar facies is also seen 2 km to south (near El Alto estancia), and is in contact with granitic basement. (B) Blocky ped structures in Los Llanos Formation, paleosol facies SW of Sierra Brava, La Rioja Province (S 29°46'16" W 65°53'55"). Outcrop is calcareously cemented, mottled red and white, and some peds approach 15 cm in length. Nearby outcrops contain rhizoliths and continuous K horizons.

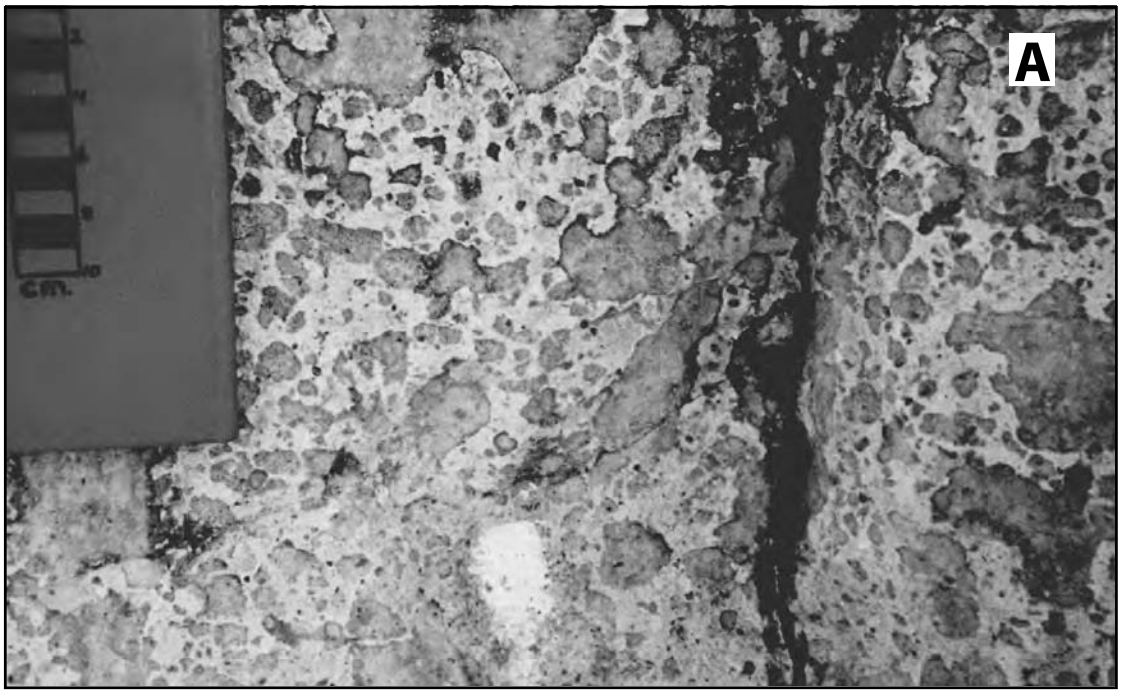
A
cm.

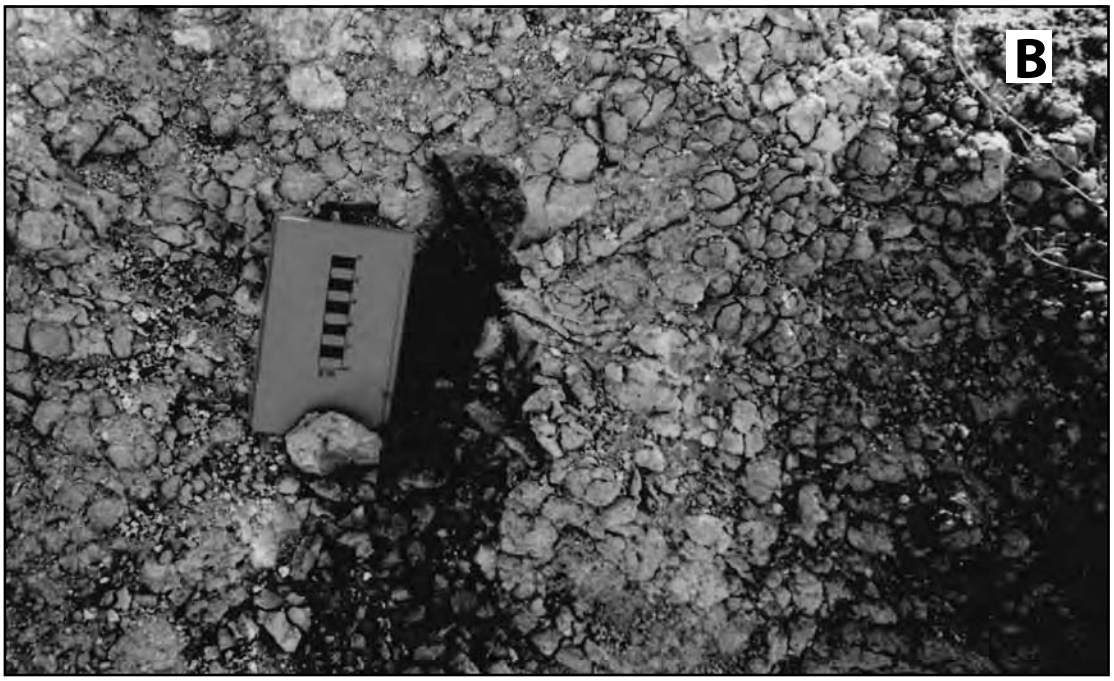
B

In addition, it is uncertain how Ezpeleta's (2004) oligomictic breccia relates to the eolian cross-bedded sandstone. The brecciated unit was witnessed in contact with igneous-metamorphic basement rocks near Alcanzar (S 30° 20' to 30° 22', W 66° 33, Fig. 7.10A), but not in association with crossbedded sandstone. Similarly, a 15 m thick outcrop of sandy breccias with gypsic, quartz and carbonate clasts occurs west of Tama. Ezpleta (2004) suggests lateral transition of facies from proximal debris to distal alluvial fan deposits to explain the grain size variation from north to south along the western flank of Sierra de Los Llanos. However, the brecciated unit cannot be traced east to the Lower Member facies 3 dunes, so it is again uncertain whether it correlates with conglomerates below or above the crossbedded sandstones. A generalized stratigraphic section for Los llanos outcrops near Tama is shown in Figure 7.11A.

An important addition to facies description of Los Llanos Formation is the spatial and vertical extension of compound calcareous paleosol facies northeastward between the Sierra de Los Llanos and Sierra Brava (Fig. 7.8). These correspond in general to Ezpeleta's (2004) Upper Member, which he described only along the eastern flank of Sierra de Los Llanos, near Oltas. Additional outcrops exhibit variable degrees of pedogenesis (described below).

Exposures of Los Llanos Formation SW of Sierra Brava (S 29°30' - 30°, W 66° - 66°15') are the thickest and most intensely pedogenic outcrops observed (Figure 7.12). The outcrops appear as 35-40 m-high cliff faces of sandstone and carbonate which overlie red Permian mudstones and sandstones (Coira and Koukharsky, 1979). The Los Llanos section (Fig. 7.11B) begins with a conglomerate and grades upsection into fine, reddish sandstones interbedded on the 2-3 meter scale with accumulations of nodular or massive carbonate (estimated as 0.3 – 0.6 m thick), which stand out as resistant ledges from the cliff face. Subvertical carbonate accumulations interpreted as

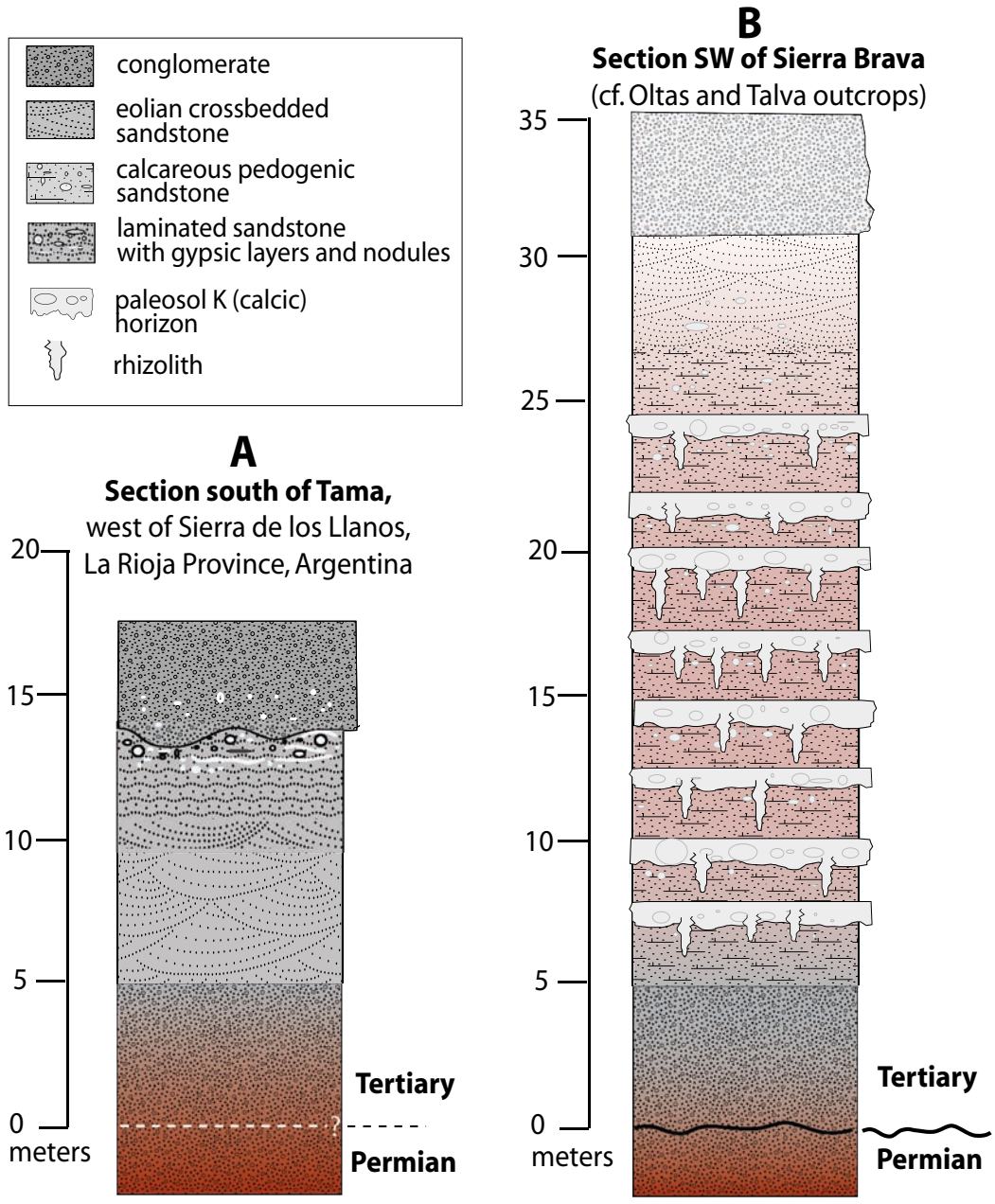

Figure 7.11: Generalized stratigraphic sections for Neogene Los Llanos Formation, La Rioja Province, Argentina. (A) Fluvial-eolian section south of Tama, west of Sierra de los Llanos. (B) Pedogenic section southwest of Sierra Brava. See Figure 7.8 for localities.

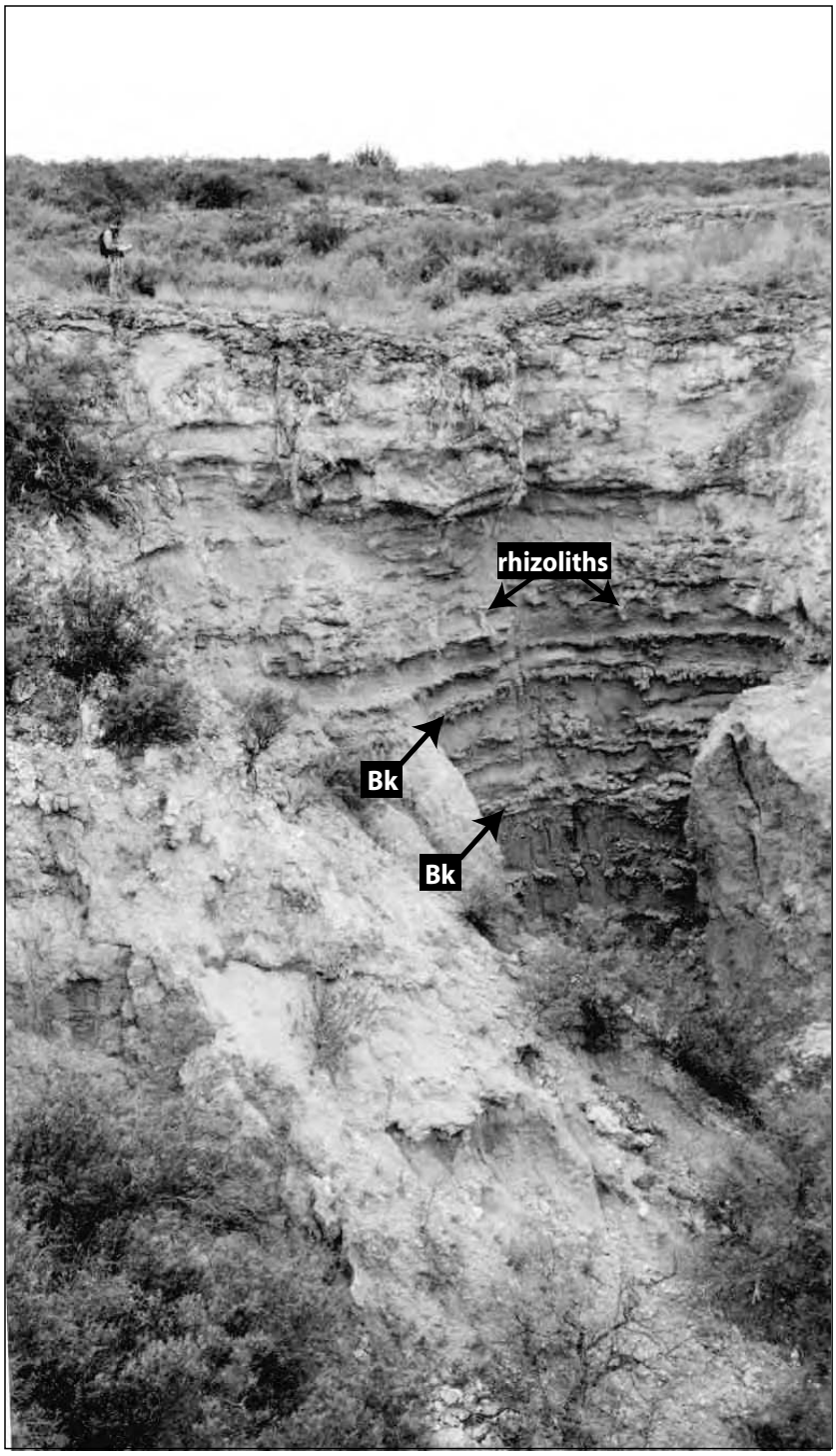

Figure 7.12: Pedogenic facies of Los Llanos, SW Sierra Brava. Resistant layers are cemented with carbonate (horizontal layers are Bk paleosol horizons or "calcretes"; subvertical accumulations are rhizoliths).

root casts (rhizoliths) or casts of burrows are also present, becoming more widely spaced upsection**.** Additionally, sandstone grain size appears to coarsen upsection (pebble lenses become more common) and coloration transitions from pink at base to white upsection. Nodular carbonates are sometimes present within clayey intervals with ped structures. At the top of the section occur cross-bedded sandstones and conglomeratic lenses.

The portion of Los Llanos Formation preserved south of Oltas, Argentina (S 30°42' W 66°14', Figs. 7.8 and 7.13A) also shows evidence of multiple pedogenic events, but with different characteristics than those near Sierra Brava. These outcrops form cliffs exceeding 30 meters high and are continuous over a distance of ~2 kilometers. At the base of the outcrop, calcium carbonate-cemented resistant sandstone beds <20 cm thick are preserved. Unlike at Sierra Brava, a basal unconformity is not observed. Paleosols are weakly developed in this portion of the outcrop. Upsection, the outcrop is relatively homogeneous pink-white sandstone, with some surficial secondary carbonate cementation. The carbonate layers are not of the thickness or lateral extent as those at Sierra Brava to the Northeast. The top of the section consists of more massive, friable sandstone, without carbonate cement. This portion of the section, however, has locally well-developed rounded ped structures 2-20 cm in diameter.

Between the impressive compound calcic paleosols at Sierra Brava and Oltas, there also exist isolated butte-like outcrops near Talva (Figs. 7.8 and 7.13B). These exposures are 20-25 m in height, consisting of interbedded pinkish-white, friable sandstone and ledges of carbonate (nodular and massive) approaching 1 m in thickness. We did not study these exposures in detail, but in general, they reflect a degree of pedogenesis similar to that witnessed at Sierra Brava. However, a significant difference is a lack of rhizoliths at Talva.

Figure 7.13: Pedogenic facies of Los Llanos Formation. (A) Exposures south of Oltas, east flank of Sierra de los Llanos (S 30°42'09" W 66°14'13"). Butte-like exposures are 30-m in height, and outcrop is fairly continuous for 2 km to south. White to pink sandstone are separated by accumulations of carbonate nodules (Bk horizons) or massive carbonates (K horizon). Unlike similar facies SW of Sierra Brava (Figure 7.11), this outcrop has minimal rhizolithic structures and doesn't coarsen upward. Ped structure is most pronounced upsection. To the south, sandstones are crossbedded (3-5 m in height). (B) Butte-like exposure of Los Llanos Formation SE of Talva, La Rioja Province (S 30°46'15" W 66°11'04"). Outcrop is 20-25 m high, with massive pink sandstone interbedded with carbonate horizons up to 1 m thick. Sandstone is calcareous cemented and friable.

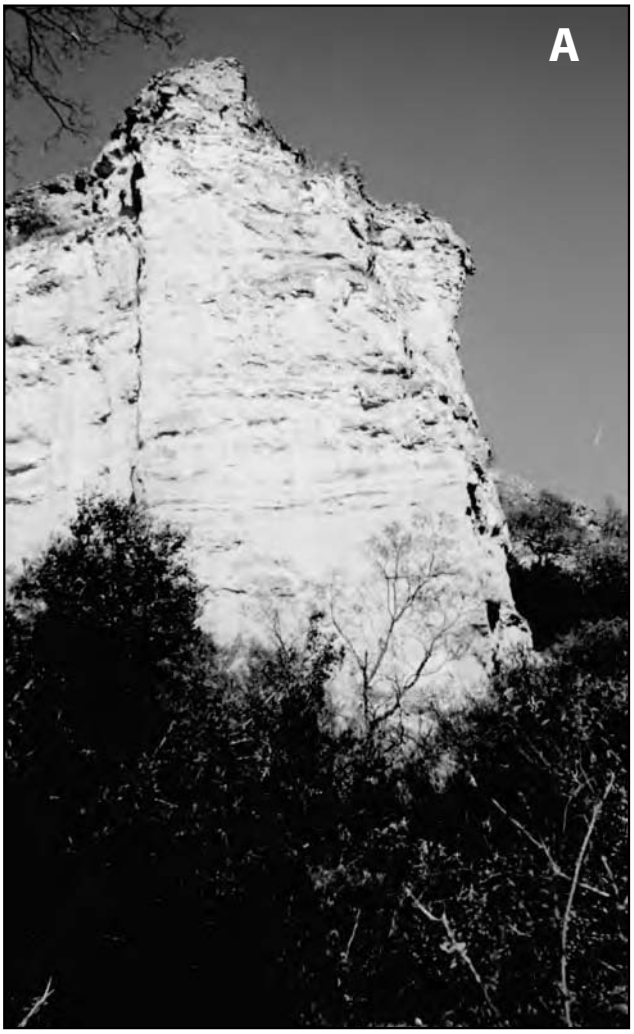
A


B

Additional pedogenic outcrops were discovered to the east of Sierra de los Llanos, although not exhibiting the thickness or degree of calcic cementation as the butte-like exposures described above. Well-developed compound (stacked) paleosols appear along Route 79 NE between Chamical and Sierra Brava (S 30°, W 65° 59'), north of the road. Between Loma Alta and Santa Cruz, La Rioja Province (S 30° 33', W66° 07', Rio Colorado drainages) isolated paleosols with friable sand matrices, blocky ped structure, and carbonate as filamentous, nodular and rhizoconcretionary forms are also exposed.

Based on the most complete sections south of Tama and SW of Sierra Brava, a generalized stratigraphic column is presented in Fig. 7.11. The chronologic scheme (Lower and Upper Members) of Ezpeleta (2004) is rejected in favor of lateral lithofacies variations in response to (a) eolian sandstone (dune) deposits west of Sierra de Los Llanos that were minimally altered by pedogenesis and (b) Intense and episodic pedogenesis east and northeast of Sierra de Los Llanos, affecting sandstones contemporaneous with the eolian dunes but with a greater degree of fluvial input. It is plausible that the Sierra de Los Llanos formed a topographic barrier to these different climatic regimes. These regional lithofacies distinctions are shown in Figure 7.14.

C. Differential pedogenesis:

Exposures of compound paleosols and sandstones encountered east of Sierra de los Llanos imply regional pedogenesis on a stable landscape. The carbonate layers at Oltas, Talva and Sierra Brava represent "calcic" Bk or K soil horizons, stage III –IV of soil carbonates (Machette, 1985), which accumulated in a semi-arid to arid environment over an estimated range of 10^4 to 10^5 years (Retallack, 1998; Hanneman and Wideman, in press). Elsewhere, the calcic accumulations are laterally continuous, forming impermeable barrier to percolation and channeling water above the horizon (Liu *et al.* 1994). Each calcic horizon, therefore, defines the top of a truncated soil

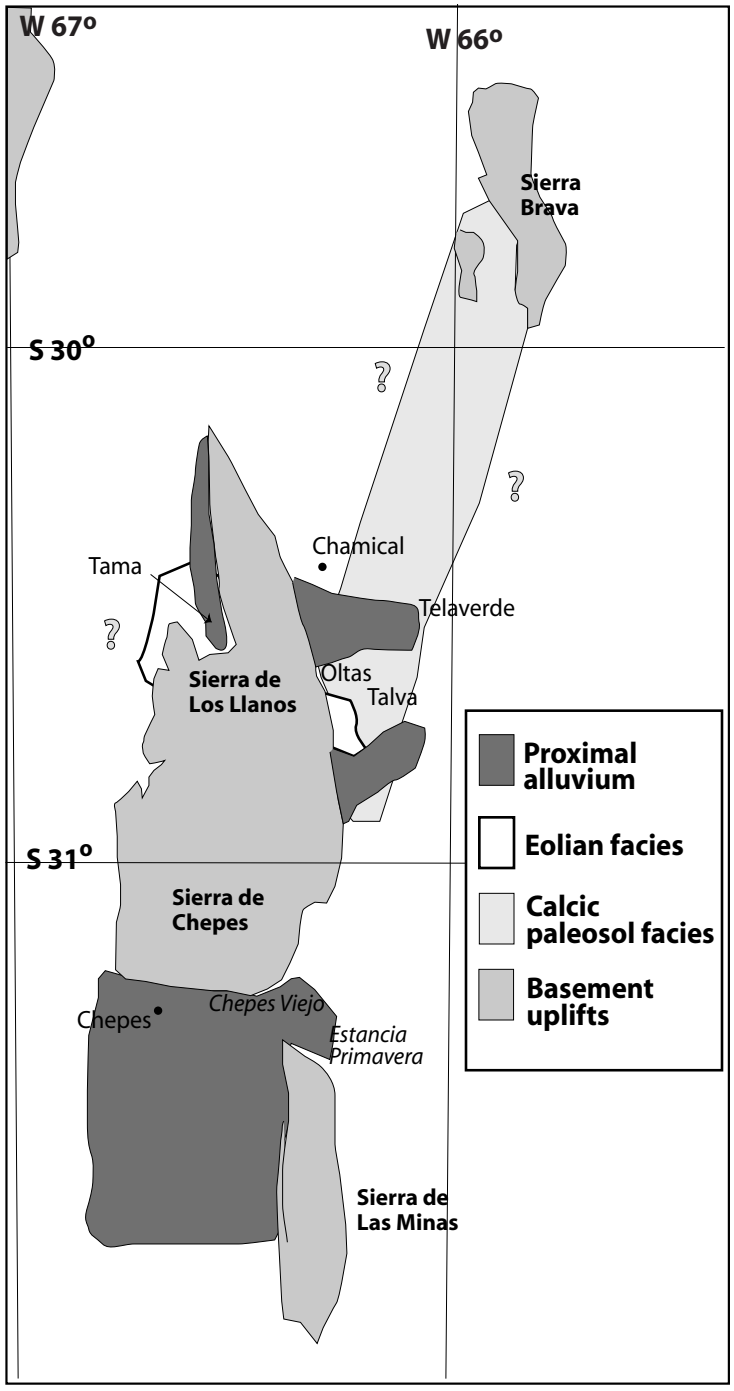

Figure 7.14: Distribution of proximal alluvial, eolian and pedogenic facies of Los Llanos Formation in the vicinity of Sierra de Los Llanos.

profile, and implies repeated periods of low sedimentation rates permitting soil formation and subsequent increases in sedimentation, resulting in soil profile truncation. At the top of the Sierra Brava sections, coarser sandstones and conglomeratic lenses are seen, along with crossbedded paleochannels. It is interpreted that, over time, the rate of sedimentation exceeded that of pedogenesis, such that these primary sedimentary structures were retained rather than pedogenically overprinted. At Oltas, however, the long-term (e.g. timescale represented by the outcrop) rate of pedogenesis probably exceeded sedimentation rates resulting in cumulative rather than composite paleosol formation (Kraus, 1987; 1999). The similar calcic paleosol outcrops near Talva imply that environmental conditions (e.g. climate, sedimentation rate, landscape stability) were conducive to regional soil formation in between the ranges of Sierra Brava and Los Llanos. Local differences in soil properties probably reflect fluctuations in sediment supply and drainage in relation to the Pampean ranges.

Stratigraphic Summary:

Comparing the best-expressed stratigraphic sections of Los Llanos Formation, west of Sierra de los Llanos (Fig. 7.11A, "Lower Member" of Ezpeleta, 2004) and SW of Sierra Brava Fig. 7.11B, comprising the majority of Ezpeleta's pedogenic "Upper Member"), it is suggested that two distinct facies associations are stratigraphically correlated. Both sections overlie Permian units and contain basal conglomerates. Crossbedded, presumed eolian sandstones occur on both flanks of Sierra de Los Llanos (Tama and Oltas exposures). At Oltas, however, Los Llanos outcrops are thicker and more strongly pedogenic than those west of the range. Despite the pedogenic component, Ezpeleta includes the cross-bedded Oltas exposures in his Lower Member. It is plausible that differences in sediment supply, erosion and/or accommodation cause the differences in thickness on either side of the range.

The varied lithologies assigned to Los Llanos Formation (described above) suggest two possible interpretations for the formation. First, facies differences may reflect simple environmental gradation away from the mountain front, with coarsest deposits closest to the ranges. In this hypothetical case, pedogenic alteration affected finer-grained deposits slowly deposited where sedimentation was slow in the intermontane basins and eolian facies were confined to the western basin, perhaps because of topographic control on winds (directed to the SE from Paleocurrent measurements, but blocked by the Sierra de Los Llanos). A second alternative, equally likely, is that the mapped "Los Llanos" outcrops exhibit pronounced lithologic differences because of miscorrelation of units of very different ages (e.g Pleistocene Cruz de Eje Formation conglomerates are also exposed near Telaverde and could also be the quartz-rich conglomerates at Estancia Bumiaco, Estancia Primavera, Chepes as well as south and west of Sierra de Las Minas). We also found through reconnaissance that many mapped "outcrops" were simply unlithified or poorly-lithified (presumed Recent) gravels. Units of uncertain relative age and stratigraphic relationship with the above-described eolian and pedogenic facies of Los Llanos Formation have been loosely termed "Estratos de Los Llanos" in the past, but such correlation is not supported by this study.

On the basis of regional Miocene-Pliocene paleosol formation interpreted from outcrops between Sierra Brava and Sierra de Los Llanos, it is reasonable that a sub-horizontal datum representing a stable landscape can be reconstructed at least in this region of the Sierras Pampeanas. Fisher *et al.*, (2002) suggested that thin, but continuous bright reflectors observed in La Rioja basin seismic reflection profiles (~60-100 km north of Sierra de Los Llanos; see Fig. 7.8) may be correlative with pedogenically-modified Tertiary sediments near Sierra Brava. The cumulative paleosols represent an interval (temporally undefined) of low-relief and tectonically

undisturbed conditions within the intermontane basin. Caveats to using Los Llanos paleosols as a datum, however, are multiple: At present, the unit lacks temporal constraints (it may range from Late Cretaceous to Pleistocene), and it is unknown at what elevation a regionally extensive soil may have formed. However, if a paleohorizontal original depositional surface could be reconstructed for the Los Llanos carbonate-bearing paleosols, *relative* uplift of Pampean ranges since the deposition of Los Llanos Formation could still be assessed.

Seismic reflection and geophysical well log data from basins surrounding Sierra de Los Llanos suggest that Los Llanos Formation paleosols may be a regional rather than local feature. In seismic profiles from La Rioja, Salinas de Mascasin and Salinas Grandes (Figure 7.15), high amplitude and moderately continuous reflectors demarcate the base of the Tertiary section (Alvarez *et al.*, 1989; Fisher *et al.*, 2002). Three Salinas Grandes profiles were reprocessed by Passakorn Pananont (2004, unpublished data), clearly illustrating the high-amplitude response at the base of the Tertiary section (correlated to line drawing interpretations by Alvarez *et al.*, 1989). In two west-east seismic lines of the Salina de Mascasin survey (lines 02187 and 02189), the basal Cenozoic reflectors dip steeply toward the east and can be projected to outcrops south of Sierra de la Huerta and northeast of Sierra de Guayaguas (southeastern Sierra del Valle Fertil) mapped as Los Llanos Formation equivalents ("Estratos Calchaqueños" in Castro de Machuca and Bastias, 1983; San Roque Formation in Ragona *et al.*, 1995; Fig. 7.15). Furthermore, over 200 m of Los Llanos Formation was lithologically and geophysically logged in a well from Mascasin (Alvarez *et al.*, 1989; Fig. 7.15). The formation initiates with a sandy interval 20 meters thick associated with a very high sonic log signal. Similar relatively-high velocity sonic signatures appear in fine-grained intervals of strata 80-90 m and 105-130 m above the base of the Tertiary. It is possible that high amplitude basal Tertiary

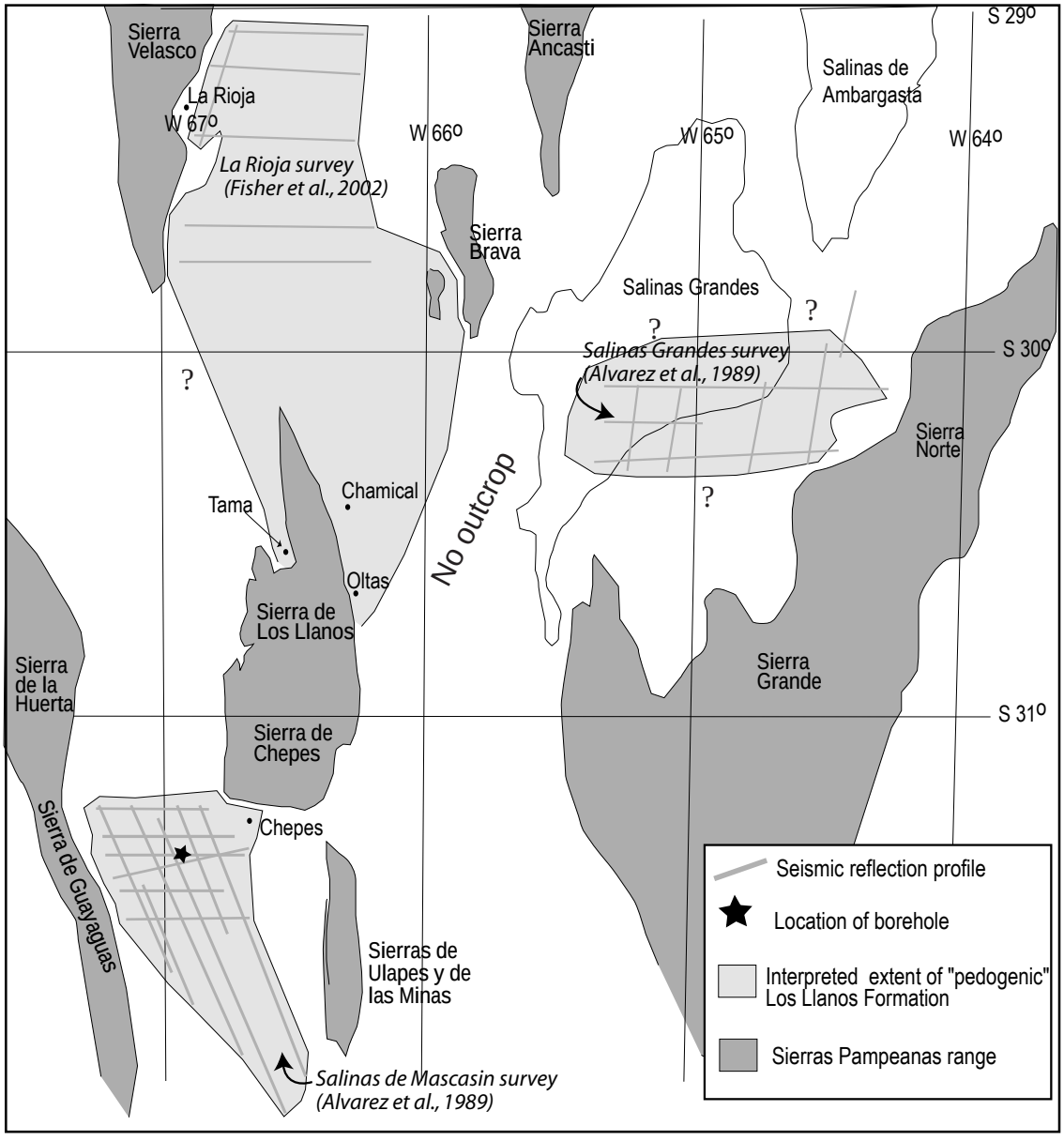

Figure 7.15: Postulated extent of pedogenic Los Llanos Formation from seismic and surface data.

seismic reflectors and corresponding high sonic velocity signals represent the intervals of stacked pedogenic carbonate horizons observed in Los Llanos Formation outcrops. For example, Hanneman *et al.* (1994) recognized that 10-16 m thick intervals of calcic paleosols in the West-Central United States appear in seismic reflection data as high amplitude continuous reflectors. Well cuttings combined with geophysical well logs (resistivity, density, and velocity depth profiles) confirmed that high velocity-high density intervals corresponded with pedogenic carbonates, the K horizons (<1 m thick each) of field-recognized paleosols (Hanneman *et al.,* 1994).

It is postulated that Los Llanos Formation contains a basal pedogenic facies in the intermontane basins surrounding Sierra de Los Llanos. This is supported by consistent high amplitude basal Tertiary reflectors, which can be related to Los Llanos outcrops flanking SW Sierra Brava and SE Sierra del Valle Fertíl (Alvarez *et al.,* 1989; Fisher *et al.,* 2002) as well as lithologic and geophysical response from the central Salinas Mascasin basin. Though the seismic profiles of Salinas Grandes (Alvarez *et al.,* 1989) cannot be confidently projected above the mute zone or into outcrops, reprocessing of three profiles of this survey (Pananont, unpublished data) supports the premise that units of similar acoustic response to the Los Llanos pedogenic facies are present in the subsurface of Salinas Grandes. On the basis of these data, the postulated extent of pedogenic Los Llanos is shown in Fig. 7.15.

In order to utilize the stacked calcic paleosol facies of Los Llanos as a regional datum, the stratigraphic interval must be reconstructed from seismic reflection profiles to remove post-depositional deformation. Though details of pedogenesis vary among the observed Los Llanos outcrops, the interval of interest (consisting of numerous cycles of advanced-stage carbonate accumulation) is remarkably consistent between Sierra Brava and Sierra de Los Llanos. The well-log signature from the Mascasin borehole suggests similar thickness of the lithologically distinct interval in the basin

SW of Sierra de Los Llanos. This consistency of thickness and stage of the calcic horizons implies that pedogenesis occurred on a regionally stable landscape with similar overall rates of accumulation (episodic and low to support soil formation) and long periods of semi-aridity (e.g. Retallack, 1998; Hanneman and Wideman, in press). Further, observed onlap of the formation against Paleozoic basement of Sierra de Los Llanos and potentially Sierra Brava and Sierra del Valle Fertíl could permit assessment of post depositional uplift of these ranges relative to a restored paleohorizontal landscape position for Los Llanos Formation.

Summary:

Field reconnaissance and isotopic analysis of outcrops in the central Sierras Pampeanas strongly suggests that the Miocene Parana seaway did not inundate the region to the extent previously inferred. No distinct marine facies or isotopic signatures were recognized for the Saguión Formation ESE of Salinas Grandes in Córdoba Province, Anta Formation in the Santa Maria Valley of Salta Province, or del Abra and del Buey Formations within the Famatina Ranges, La Rioja Province). Instead, lacustrine deposition, perhaps related to concurrent global climate change, is inferred from these formations. Assessment of the lithofacies and pedogenic components of the Neogene (?) Los Llanos Formation results in a more accurate stratigraphic section and landscape model for this previously poorly-defined formatiun. Furthermore, seismic and well log data suggest the regional presence of stacked paleosol carbonates between S 29°-32° and W 64°-67°, which could provide a surface for comparison of post-Los Llanos relative structural relief among several basement uplifts of the Sierras Pampeanas (Brava, Los Llanos and Valle Fertíl).

Acknowledgements:

Fieldwork in Argentina was supported by NSF Pilot Study 0125274 to T.E. Jordan. Many thanks to our Argentine coworkers for their hospitality and thoughtful

discussions of the themes of this paper: Ricardo Alonso, Luis Alvarez, Ricardo Astini, Silvana Bertolino, Federico and Soledad Dávila, and Roberto Hernández. Federico Martina greatly assisted Ruskin with fieldwork and logistics. Bruce Vaughn (INSTAAR) coordinated isotopic analysis. Debra Hanneman (Whitehall Geogroup, Inc.) provided article preprints. Thanks to Passakorn Pananont (Mahidol University, Thailand) for seismic reprocessing of profiles which were kindly provided by YPF-Repsol.

References:

Allen, P.A., and Collinson, J.D., 1986, Lakes *in* Reading, H.G., ed., Sedimentary Environments and Facies, 2nd Ed., Blackwell Scientific Pub., Oxford, p. 63-94.

Alonso, R., Carrapa, B., Coutand, I., Haschke, M., Hilley, G., Schoenbohm, L., Sobel, E.R., Strecker, M.R., Trauth, M.H., and Villanueva, A., 2006, Tectonics, climate, and landscape evolution of the Southern Central Andes: The Argentine Puna Plateau and adjacent regions between 22 and 28° S lat: *in review*

Alvarez, L.A., Bolatti, N.D., Fernandez-Seveso, F., and Perez, M.A., 1989, Interpretacion del subsuelo en los bolsones de Sierras Pampeanas en base de a la informacion geofisica disponible y geologia de superficie: Comisión Geológica No. 3, Departamiento Geologico Cuyo., 21 p.

Barazangi, M. and Isacks, B.L., 1976, Spatial distribution of earthquakes and ubduction of the Nazca plate beneath South America: Geology, Vol. 4, p. 686-692.

Bertolino, S.R., Poire, D.G., and Carignano, C.,2001, Primer registro de sedimentitas marinas terciarias aflorantes en las Sierras Pampeanas de Córdoba, Argentina: Revista de la Asociación Geológica Argentina, 55, p. 121-124.

Birkeland, P. W., 1999, Soils and Geomorphology, 3rd Edition, Oxford University Press, 432 pp.

Bodenbender, G, 1911, Constitución geológica de la parte meridional de La Rioja y regiones limítrofes. República Argentina, Academia Nacional de Ciencias, Boletin 19, p 5-221.

Boudreau, R.E.A., Patterson, R.T., Dalby, A.P., and McKillop, W.B., 2001, Non-marine occurrence of the foraminifer *Cribroelphidium gunteri* in northern Lake Winnipegosis, Manitoba, Canada: Journal of Foraminiferal Research, Vol. 31, p. 108-119.

Caminos, R., 1968, Descripción geológica de las hojas 21f y 21g, Sierra de las Minas y Ulapes, Provincia de La Rioha, San Juan y Córdoba: Serv. Geol. Nac., Buenos Aires.

Cann, J.H., and de Deccker, P., 1981, Fossil quaternary and living foraminifera from athalassic (non-marine) saline lakes, Southern Australia,: Journal of Paleontology, Vol. 55, p. 660-670.

Castro de Machuca, B., and Bastias, H.E., 1983, Geología de un sector del distrito minero “Cerro Blanco” – Sierra de la Huerta, San Juan, Argentina: Segundo Congreso Nacional de Geologia Económica, Actas Tomo II, p. 389- 404.

Cione, A. L., and J. R. Casciotta. 1995, Freshwater teleostean fishes from the Miocene of the Quebrada de la Yesera, Salta, Northwestern Argentina: Neues Jahrbuch für Geologie und Paläontologie Abhandlungen. 196 377–394

Coughlin, T.J., O'Sullivan, P.B., Kohn, B.P., and Holcombe, R.J., 1998, Apatite fission-track thermochronology of the Sierras Pampeanas, central western Argentina: implications for the mechanisms of plateau uplift in the Andes: Geology, Vol. 26, p. 999-1002.

Cross, T.A., and Pilger, R.H., Jr., 1978, Tectonic controls of Late Cretaceous sedimentation: Nature, 274, p. 653-657.

Dávila, F.M., 2002, Composición de los conglomerados sinorogénicos del Terciario de la sierra de Famatina, y su relación con la fragmentación del antepaís andio central 9th Reunión Argentina de Sedimentología, Córdoba.

Dávila, F.M., and Astini, R.A., 2003, Early Middle Miocene broken foreland development in the southern Central Andes: evidence for extension prior to regional shortening: Basin Research, 15, p. 379-396.

Dávila, F.M., Astini, R.A., and Ezpeleta, M., 2004, La Formación Los Llanos: Una unidad clave en la evolución del antepaís fragmentado y en la discussion tectónica vs. paleoclima: X Reunión Argentina de Sedimentología, San Luís, Resumes, p 52-53.

Dean, W.E., and Fouch, T.D., 1983, Lacustrine Environment: *in* Scholle, P.A., Bebout, D.G., and Moore, C.H., eds., Carbonate Depositional Environments, AAPG Memoir 33., p. 97-130.

Ezpeleta, M., 2004, Estratigrafía y paleoambientes de la Formación de Los Llanos (Neógeno), sierra de Los Llanos, provincia de La Rioja (30º30'LS), Argentina". Unpublished thesis,Universidad Nacional de Córdoba, Argentina.

Ezpeleta, M, Dávila, F.M., and Astini, R.A., 2004, Facies y paleoambeintes de la formación Los Llanos (Mioceno?), Sierra de los Llanos (30°30' LS), La Rioja: Una puesta al día sobre su conocimiento: X Reunión Argentina de Sedimentología, San Luís, Resumes, p 59-60.

Fisher, N.D., Jordan, T.E., and Brown, L., 2002, The structural and stratigraphic evolution of the La Rioja basin, Argentina: Journal of South American Earth Sciences, Vol. 15, p. 141-156.

Flores, M.A.,1969, El Bolson de las Salinas en la Provincia de San Luis: Actas de las Cuartas Jornadas Geológicas Argentinas Tomo I., p. 311-327.

Flores, M.A., and Roque, P.C., 1972, Cuenca de San Luis: *in* Geología Regional Argentina; Córdoba, p. 567-579.

Galli, C.I., Hernández, R., and Reynolds, J., 1996, Análisis estratigráfico del Subgrupo Metán (base del Grupo Orán), en el río Piedras, departamento Metán, Salta, Argentina: Boletín de Informaciones Petroleras, 12 (6), p. 99-107.

Gerth, E., 1914, Constitución geológica, hidrogeológica y minerals de aplicación de la provincial de San Luis: Anal. Min. Agric. Nac. X, p. 1-64.

Ghosh, P., Bhattacharya, S.K., and Chakrabarti, A., 2001, Stable isotopic studies of microbial carbonates from Talchir sediments of east-central India: Current Science, Vol 80, p. 1326-1330.

Guerrero, M.A., Lavandaio, E., marcos, O., Caminos, R., Nullo, F.E., Panza, J.L, Fernandez Lima, J.C.R., and Reinoso, 1993, Mapa Geologico de la Provincia de la Rioja, Republica Argenina: Ministerio de Economía y Obras y Servicios Públicos.

Guiñazu, J.R., 1962, Los llamados "Estratos de los Llanos" en la provincia de San Luis y su contenido de rodados de rocas andesítas y restos de mamíferos fósiles: Anales Primeras Jorn. Geol. Arg. Vol. 2, 89.

Hanneman, D.L., Wideman, C.J., and Halvorson, J., Calcic paleosols: their use in subsurface stratigraphy: American Association of Petroleum Geologists Bulletin, v. 78, p. 1360-1371.

Hanneman, D.L., and Wideman, C.J., Calcic pedocomplexes - regional sequence boundary indicators in Tertiary deposits of the Great Plains and Western USA: in press for GSA Special Paper.

Heckel, P.H., 1972, Recognition of ancient shallow marine environments *in* Rigby, J.K., and Hamblin, W.K., eds., Recognition of Ancient Sedimentary Environments: Spec. Pub. Paleont. Miner., 18, p. 226-286.

Hoorn, C., 1993, Marine incursions and the influence of Andean tectonics on the Miocene depositional history of northwestern Amazonia: results of a palynostratigraphic study: Palaeoecology, Palaeoclimatology, and Palaeoceanography, Vol. 105, p. 267-309.

Hudson, J.D., 1977, Stable isotopes and limestone lithification: Journal of the Geological Society, Vol. 133, p. 637-660.

Hünicken, M.; Tauber, A.; Leguizamón, R., 2001, Hallazgo de huevos y nidos de dinosaurios asociados a restos de vegetales silicificados: asignación al

Cretácico de las secuencias portadoras aflorantes en Sanagasta, provincia de La Rioja. 17º Jornadas Argentinas de Paleontología de Vertebrados.

Johnson, H.D. and Baldwin, C.T., 1986, "Shallow Siliciclastic Seas" *in* Reading, H.G. (ed), Sedimentary Environments and Facies, 2nd ed, p. 229-282.

Jordan, T.E., and Allmendinger, R.W., 1986, The Sierras Pampeanas of Argentina: a modern analog of Rocky Mountain foreland deformation: American Journal of Science, Vol. 286, p. 737-764.

Jordan, T.E., Zeitler, P, Ramos, V.a., and Gleadow, A.J.W., 1989, Thermo-chronometric data on the development of the basement peneplain in the Sierras Pampeanas, Argentina: Journal of South American Earth Sciences, Vol. 2, p.207-222.

Jordan, T.E., Schlunegger, F., and Cardozo, N., 2001, Unsteady and spatially variable evolution of the Neogene Andean Bermejo foreland basin, Argentina: Journal of South American Earth Sciences, Vol. 14, p. 775-798.

Kay, S.M., Maksaev, V., Mpodozis, C., Moscoso, R., Nasi, C, and Gordillo, C.E., 1988, Tertiary Andean magmatism in Argentina and Chile between 28-33° S: correlation of magmatic chemistry with a changing Benioff zone: Journal of South American Earth Sciences, Vol. 1, p. 2-38.

Kraus, M.J., 1987, Integration of channel and floodplain suites, II. Vertical relations of alluvial paleosols: Journal of Sedimentary Petrology, Vol. 57, p. 602-612.

Kraus, M. J., 1999, Paleosols in clastic sedimentary rocks: their geologic applications: Earth Science Reviews v. 47, p. 41-70.

Liu, B., Phillips, F.M., Elmore, D., and Sharma, P., 1994, Depth dependence of soil carbonate accumulation based on cosmogenic ^{36}Cl dating: Geology, Vol. 22, p. 1071-1074.

Lundberg, J.G., Marshall, L.G., Guerrero, J., Horton, B., Malabarba, M.C.S.L., and Wesselingh, F., 1998, The stage for neotropical fish diversification: A history of tropical South American rivers *in* Malabarba, L.R., Reis, R.E., Vari, R.P. Lucena, Z.M.S., and Lucena, C.A.S., eds., *Phylogeny and Classification of Neotropical Fishes,* p. 13-48, Porto Alegre, Brazil: EDIPUCRS

Machette, M.N., 1985, Calcic soils of the southwestern United States *in:* Weide, D.L., ed., Soils and Quaternary Geology of the Southwestern United States: Geological Society of America Special Paper, 203, p. 10-21.

Mack, G.H. and Cole, D.R. 2005, Geochemical model of δ^{18}O of pedogenic calcite versus latitude and its application to Cretaceous paleoclimate: Sedimentary Geology Vol. 174, p. 115-122.

Martinez, S., 1988, Los depositos de la “transgression entrerriana” (Mioceno de Argentina, Brasil y Uruguay). Comparacion de sus principales areas fosiliferas a traves de los bivalves y gastropodos: revista de la Asociación Paleontología Argentina, Vol. 25, p.23-29.

Martínez, L. del V., Nullo, F.E, Caminos, R.L., Panza, J.L., Chipulina, M.A., and Zappettini, E.O., 1995, Mapa Geológico de la Provincia de Catamarca, República Argentina: Ministerio de Economía y Obras y Servicios Públicos

Milliman, J.D., 1974, Recent Sedimentary Carbonates 1: Marine Carbonates:Springer New York.

Pascual, R, 1954, Adiciones a la fauna de la formacion de Los Llanos de San Luis y su edad: Rev. Museo Munic. Cienc. Nat. y Tradic. de Mar del Plata, Vol 1 y 2, p. 113-121.

Pascual, R., and Bondesio, P., 1981, Sedimentitas Cenozoicas: Geología de la Provincia de San Luis: VIII congreso Geológico Argentino, p. 117-154.

Patterson, W.T., and McKillop, W.B., 1991, Distribution and possible paleoecological significance of Annectina viriosa, a new species of agglutinated foraminifera from nonmarine Salt Ponds in Manitoba: Journal of Paleontology, Vol. 65, p. 33-37.

Perez, D.J., Ottone, G., and Ramos, V.A., 1996, La ingression marina miocena en la Provincia de San Juan: sus implicancias paleogeográficas: XIII Congreso Geológico Argentino, Bueno Aires, Actas I, p. 385-398.

Quattrocchio, M., Durango de Cabrera, J, and Galli, C., 2003, Formación Anta (Miocene Temprano/Medio), Subgrupo Metán (Grupo Orán), en el río Piedras, Pcia. de Salta. Datos palinológicos: Revista de la Asociación Geológica Argentina, 58, p. 117-127.

Ragona, D. and 23 others, 1995, Mapa geológico de la provincial de San Juan, República Argentina: Ministerio de Economía y Obras y Servicios Públicos.

Ramos, V.A., 1982, Descripción geológica Hoja 20F Chepes, Provincia de La Rioja: Servicio Geológico Nacional, Boletín 171.

Ramos, V.A., and Alonso, R.N., 1995, El mar paranense en la provincial de Jujuy: Revista del Instituto de Geología y Minería 10, p. 73-80.

Retallack, G.J., 1998, Fossil soils and completeness of the fossil record: in Donovan, S.K. and Paul, C.R.C., eds., The Adequacy of the Fossil Record: John Wiley and Sons, United Kingdom, p. 133-164.

Reynolds, J.H., Idleman, B.D., Hernández, R.M., and Naeser, C.W., 1994, Preliminary chronostratigraphic constraints on Neogene tectonic activity in the Eastern Cordillera and Santa Bárbara system, Salta province, NW Argentina: Geological Society of America Abstracts with Programs 28 (7), A-503.

Reynolds, J.H., Ramos, V.A., Jordan, T.E., and Hernández, 1997, Diachronism of regional Neogene stratigraphy in the Andean foreland, NW Argentina; arguments for retiring the Calchaquense and Araucanense terminology: Geological Society of America Abstracts with Programs 29 (6): 228.

Rivarola, D., and Di Paola, E., 1993, Sintesis de la evolucion de los depositos Cenozoicos en el sur de la Sierra de San Luis. Localidades del potrero de los Funes y sector centro norte de las Chacras, Argentina: XII Congreso Geológico Argentino y II Congreso de Exploración de Hidrocarburos Actas I: p. 204-211.

Sabins, F.F.,1997, *Remote Sensing: Principles and Applications, 3rd Edition:* W.H. Freeman and Company, New York.

SEGEMAR, 1999, Carta Geologica 3166-I, Chamical, Edición Preliminar: Instituto de Geologia y Recursos Minerales.

SEGEMAR, 2000, Carta Geologica 2963-III, Villa Ojo de Agua: Instituto de Geologia y Recursos Minerales.

SEGEMAR, 2002, Carta Geologica 2966-IV, Recreo, Edición Preliminar: Instituto de Geologia y Recursos Minerales.

Sellwood, B.W., 1986, "Shallow-marine carbonate environments" *in* Reading, H.G. (ed), 1986, Sedimentary Environments and Facies 2nd ed., p. 283-342.

Starck, D. and Anzótegui, L.M., 2001, The late Miocene climatic change- persistence of a climatic signal through the orogenic stratigraphic record in northwest Argentina: Journal of South American Earth Sciences, v.14, p. 763-774.

Talbot, M.R., 1990, A Review of the palaeohydrological interpretation of carbon and oxygen stable isotopic ratios in primary carbonates: Chemical Geology (Isotope Geoscience Section), v.80, p.261-279.

Talbot, M.R., 1994, Paleohydrology of the late Miocene Ridge basin lake, California: Geological Society of America Bulletin, Vol. 106., p. 1121-1129.

Vonhof, H.B., Wesselingh, F.P., Kaandorp, R.J.G., Davies, G.R., van Hinte, J.E., Guerrero, J., Rasanen, M., Romero-Pittman, L., and Ranzi, a., 2003, Paleogeography of Miocene Western Amazonia: Isotopic composition of molluscan shells constrains the influence of marine incursions.

Walsh, T.R., Permian foramol carbonates from a variable salinity shelf environment; the Elm Creek Limestone (Artinskian) of north-central Texas salinity: PhD dissertation, Texas Tech University, Lubbock, TX, USA, 239 p.

Zachos, J., Pagini, M., Sloan, L., Thomas, E., and Billups, K., 2001, Trends, rhythms, and aberrations in global climate 65 Ma to present: Science, v. 292, p. 686-693.

APPENDIX A:

MIOCENE-PLIOCENE PALEOSOL CHARACTERISTICS AND STABLE ISOTOPIC DATA, IGLESIA BASIN, NORTHWESTERN ARGENTINA

The following tables summarize paleosol data from field measurements and subsequent laboratory analyses. Locations of samples are referenced in stratigraphic sections, Figures 2.18 through Figure 2.22. Further information about field methods and analytical procedures is discussed in Chapter 3.

Table A.1: Iglesia Basin paleosol carbonate stable isotopic values. Ages assigned by linear interpolation to magnetostratigraphy.

Sample	Age (Ma)	Section	$\delta^{13}C$	$\delta^{18}O$	%C
BR05-28	4.6	South Colanguil	-7.596	-6.990	2.10
BR05-29	4.7	South Colanguil	-2.591	-4.686	2.07
BR05-30	4.8	South Colanguil	-6.524	-7.182	2.36
BR04-17	5	Tudcum	-8.503	-8.083	1.03
BR05-33	5	South Colanguil	-8.571	-5.140	1.79
BR05-38	5.11	Angualasto	-9.123	-3.652	1.35
BR05-37	5.12	Angualasto	-6.792	-2.630	1.28
BR05-36	5.14	Angualasto	-6.788	-2.142	1.30
BR05-35	5.15	Angualasto	-6.482	-6.368	2.09
BR04-14	5.18	Angualasto	-6.992	-5.355	0.46
BR04-13	5.19	Angualasto	-4.421	-9.572	0.85
BR04-12	5.2	Angualasto	-2.345	-5.434	0.15
BR04-10	5.22	Angualasto	-7.603	-6.711	0.54
BR04-11	5.22	Angualasto	-8.006	-7.953	0.32
BR03-27	6	Las Flores	-5.515	-10.859	
BR03-33	6.12	Iglesias	-2.944	-6.024	0.51
BR03-32	6.13	Iglesias	-4.278	-7.290	0.52
BR03-29	6.17	Iglesias	-9.459	-9.242	
BR02-SOL5	6.45	Angualasto	-4.597	-7.685	
BR04-35	6.5	Rodeo 1	-13.235	-8.647	0.35
BR04-36	6.5	Rodeo 1	-11.280	-5.298	0.50
BRO3-39	6.5	Rodeo 1	-8.238	-4.662	
BR03-12	6.6	Angualasto	-4.425	-7.399	0.53
BR05-53	6.61	Cuesta del Viento	-4.196	-2.920	0.33
BR05-52	6.62	Cuesta del Viento	-7.916	-2.072	0.51
BR03-25	6.7	Channel	-5.149	-5.539	
BR03-24	6.85	Channel	-3.948	-8.541	
BR03-21	6.87	Channel	-4.408	-8.318	
BR03-22	6.87	Channel	-3.043	-7.761	
BR03-23	6.88	Channel	-4.680	-8.289	
BR05-50	6.89	Angualasto	-10.945	-2.717	0.73
BR04-4	6.9	Angualasto	-5.545	-8.129	0.54
BR05-49	6.9	Angualasto	-8.963	-1.653	0.42
BR05-40	6.92	Rodeo 1	-9.751	-3.571	2.15
BR04-30	6.93	Rodeo1	-7.330	-6.338	0.51
BR04-7	6.93	Angualasto	-6.323	-8.987	0.45
BR05-41	6.93	Rodeo 1	-9.570	-2.008	1.34
BR05-43	6.93	Angualasto	-3.168	-2.096	1.56
BR04-1	6.935	Angualasto	-6.688	-8.160	1.16
BR04-29	6.935	Rodeo 1	-8.231	-7.715	0.45
BR05-42	6.935	Angualasto	-3.207	-2.736	3.06
BR03-10	6.95	Angualasto	-6.824	-4.812	
BR04-3	6.95	Angualasto	-6.914	-7.515	1.07
BR03-9	6.96	Angualasto	-7.386	-6.190	
BR05-47	6.97	Angualasto	-8.006	-3.952	0.83
BR05-48	6.98	Angualasto	-9.739	-2.017	0.85
BR04-28	7	Rodeo 1	-8.023	-6.658	0.42
BR03-49	7.1	Rodeo 1	-8.631	-5.039	
BR03-49 duplicate	7.1	Rodeo 1	-8.594	-5.013	
BR04-54	7.2	South Angualasto	-6.319	-8.157	0.67
BR04-27	7.29	Rodeo 1	-9.142	-7.756	0.64
BR04-26	7.3	Rodeo 1	-8.590	-9.122	0.63
BR04-25	7.31	Rodeo 1	-10.206	-9.603	0.53
BR04-31	7.31	Rodeo 1	-8.987	-6.778	0.54
BR04-24	7.32	Rodeo 1	-8.172	-9.065	0.64
BR04-23	7.33	Rodeo 1	-8.465	-8.986	0.64
BR04-33	7.35	Rodeo 1	-8.271	-6.408	0.55
BR04-32	7.4	Rodeo 1	-9.352	-7.257	0.57
BR04-53	7.4	South Angualasto	-6.764	-8.630	0.57
BR04-52	7.45	South Angualasto	-8.453	-10.256	0.34
BR04-34	7.5	Rodeo 1	-8.373	-7.568	0.57
BR04-50	7.6	South Angualasto	-7.332	-9.211	0.98
BR04-51	7.6	South Angualasto	-9.424	-7.533	0.38
BR03-47	7.65	Rodeo 1	-9.303	-5.405	
22-6-2002 SOL4	7.8	Angualasto	-7.660	-4.750	
22-6-2002 SOL4 Duplicate	7.8	Angualasto	-7.710	-4.600	
BR03-3	7.8	Angualasto	-7.761	-6.030	
BR03-3 duplicate	7.8		-7.701	-6.016	
BR03-4	7.8	Angualasto	-7.908	-6.931	
BR03-45	7.96	Rodeo 1	-6.612	-9.410	0.54
BR03-2	8	Angualasto	-7.208	-5.906	
BR03-2 Duplicate	8	Angualasto	-7.098	-6.454	
BR03-19	8.19	South of Rodeo 2	-4.995	-2.378	
BR03-37	8.21	Rodeo 1	-6.296	-2.685	
BR02-SOL3	8.25	Angualasto	-5.872	-8.753	0.56
BR03-44	8.34	Rodeo 1	-6.428	-6.881	
BR04-41	8.35	Angualasto	-6.818	-8.704	0.74
BR04-20	8.4	Maliman	-6.956	-10.408	0.64
BR04-21	8.5	Maliman	-5.854	-7.998	0.69
BR03-17	8.58	Rodeo 2	-6.439	-7.753	
BR04-22	8.62	Rodeo 1	-7.627	-7.894	0.55
BR03-16	8.7	Rodeo 2	-5.942	-8.780	0.44
BR04-16	8.7	East of Rio Blanco	-5.500	-8.285	0.95
BR04-59	8.75	South of Rodeo 1	-5.877	-4.455	0.56
BR05-39	8.85	Rodeo 1	-3.117	-3.938	1.88
BR04-18	9.03	East of Rodeo 1	-8.043	-8.085	0.79
BR05-44	9.06	Rodeo 2	-6.165	-2.654	1.32
BR03-13	6.3 +/- 0.6	Cerro Blanco	-6.932	-9.096	

Table A.2: Iglesia Basin paleosol characteristics. Gray boxes indicate compound pedogenic intervals. Superscripts: [1]After Machette, 1985; [2] After Retallack 2001, Fig. 3.12; [3]After Retallack 2001, Fig. 5.3. Note that Rodeo 2 section is highly pedogenic but lacks calcic accumulations and therefore was not abundantly sampled. Coloration of Rodeo 2 aquic paleosols (46-90 m in section): 5GY 7/1; 7.5R 5/4. Coloration of Rodeo 2 aquic paleosols (370-460 m in section): 10R 5/4; 7.5R 6/2; 5BG 7/1.

Sample	Age (Ma)	Section	thickness(m)	Texture	Color	Horizons	Carbonate Stage[1]
BR05-28	4.6	South Colanguil	0.7	silt to fine sand	10R 6/2; 5G 7/1	B, Bt	II
BR05-29	4.7	South Colanguil	0.7	silt to fine sand	10R 6/2; 5G 7/1	Bw, Bk	III
BR05-30	4.8	South Colanguil	0.55	fine sand		B,C	II
BR04-17	5	Tudcum	0.45	clay to fine sand	5GY 7/1	B,C	II
BR05-33	5	South Colanguil	0.4	fine sand		B,Bk	II
BR05-38	5.11	Angualasto	0.5	fine to medium sand		Bk, K	II-III
BR05-37	5.12	Angualasto	0.5	silt	10R 6/4	B,Bk	II
BR05-36	5.14	Angualasto	1.2	fine to medium sand	2.5 YR 6/4	Bt, K	III
BR05-35	5.15	Angualasto	1.7	silt to fine sand	10R 6/3	B, C	II
BR04-14	5.18	Angualasto				Bt	II
BR04-13	5.19	Angualasto	3.5	silt to fine sand	2.5YR 5/4; 7.5 YR 7/2	Bk	III
BR04-12	5.2	Angualasto				Bk	III
BR04-10	5.22	Angualasto		clay to silt		Bt, Bk	II-III
BR04-11	5.22	Angualasto	1	silt to fine sand		Bk, C	II
BR03-27	6	Las Flores	1	fine to medium sand		C	I-II
BR03-33	6.12	Iglesias	0.3	clay		B-C	I
BR03-32	6.13	Iglesias	1.85	clay to silt	5B 7/1	Bt,K	I,IV
BR03-29	6.17	Iglesias	1.5	clay to fine sand	10R 5/6;5YR 7/2	Bk,C	III
BR02-SOL5	6.45	Angualasto	0.2	silt		B,C	I
BR04-35	6.5	Rodeo 1	2	silt to fine sand		B,C	II
BR04-36	6.5	Rodeo 1		silt to fine sand		B,C	II
BRO3-39	6.5	Rodeo 1		silt to fine sand		B,C	II
BR03-12	6.6	Angualasto	0.3	clay to fine sand		B,C	II
BR05-53	6.61	Cuesta del Viento	0.25	clay to fine sand	5YR 7/3	Bk, C	III
BR05-52	6.62	Cuesta del Viento	0.3	silt to fine sand	5YR 7/3	Bk, C	II
BR03-25	6.7	Channel	1	fine to medium sand		C	II
BR03-24	6.85	Channel	1.7	fine sand		Bk,C	II-III
BR03-21	6.87	Channel				Bk	III
BR03-22	6.87	Channel	2.6	fine sand		Bk	III
BR03-23	6.88	Channel				Bk,C	III
BR05-50	6.89	Angualasto	0.7	silt to fine sand	10YR 6/2	Bt,C	II
BR04-4	6.9	Angualasto	0.5	clay to silt	10YR 7/2	Bt,Bk	II-III
BR05-49	6.9	Angualasto	0.4	silt to fine sand		Bk,C	III
BR05-40	6.92	Rodeo 1	0.6	silt to medium sand		B, C	II
BR04-30	6.93	Rodeo1	0.6	silt to fine sand	10R 5/3	Bt,C	II
BR04-7	6.93	Angualasto	2	clay to medium sand	5YR 5/6	Bt,C	II
BR05-41	6.93	Rodeo 1	0.5	silt		Bt,C	II
BR05-43	6.93	Angualasto	0.5	medium sand		C	II
BR04-1	6.935	Angualasto	0	fine sand		Bt,C	II
BR04-29	6.935	Rodeo 1	0.6	silt to fine sand	10R 5/3, 10 YR 6/2	Bt,C	II
BR05-42	6.935	Angualasto	0.6	silt to fine sand		Bw,C	II
BR03-10	6.95	Angualasto	1	clay to	7.5 YR 5/6; 5YR 7/1	Bt,C	II
BR04-3	6.95	Angualasto	0.4	fine to medium sand		C	II
BR03-9	6.96	Angualasto	1	fine sand	7.5 YR 5/6; 5YR 7/1	Bt,C	II
BR05-47	6.97	Angualasto	0.6	clay to fine sand		Bt	II
BR05-48	6.98	Angualasto	2	clay to fine sand		B,C	II
BR04-28	7	Rodeo 1	0.6	clay to silt		B	II
BR03-49	7.1	Rodeo 1	0.5	medium sand		Bw-C	II
BR03-49 duplicate	7.1	Rodeo 1	0.5	medium sand		C	II
BR04-54	7.2	South Angualasto	0.15	silt to fine sand	5YR 6/3	Bk	III
BR04-27	7.29	Rodeo 1					
BR04-26	7.3	Rodeo 1					
BR04-25	7.31	Rodeo 1	12 m compound interval.		7.5R 6/2	B,Bk,C	III
BR04-31	7.31	Rodeo 1	Paleosols: 30-50 cm				
BR04-24	7.32	Rodeo 1	Sandstone interbeds: 10-50 cm				
BR04-23	7.33	Rodeo 1					
BR04-33	7.35	Rodeo 1	0.5	silt		Bk	III
BR04-32	7.4	Rodeo 1	0.5	fine to medium sand		B,Bk,C	II
BR04-53	7.4	South Angualasto	0.25	silt to fine sand	5YR 6/3	B,Bk,C	III
BR04-52	7.45	South Angualasto	0.25	clay to silt	5YR 6/3; 5G 7/1	Bt,Bk	III
BR04-34	7.5	Rodeo 1	0.15	silt to fine sand		B,C	II
BR04-50	7.6	South Angualasto	0.5	fine to medium sand		Bk,C	III
BR04-51	7.6	South Angualasto	0.4	silt to fine sand		Bt,Bk	III
BR03-47	7.65	Rodeo 1	0.5	fine to medium sand		C	II
22-6-2002 SOL4	7.8	Angualasto	0.4	clay to silt		Bt,Bk	II-III
22-6-2002 SOL4Dup	7.8	Angualasto	0.4	clay to silt		Bt,Bk	II-III
BR03-3	7.8	Angualasto	1.6	clay to fine sand	10R 4/6; 5Y 7/1	Bk	III
BR03-3 duplicate	7.8						
BR03-4	7.8	Angualasto				Bt,Bk	III
BR03-45	7.96	Rodeo 1	0.3	fine to medium sand		Bk,C	I-III
BR03-2	8	Angualasto	0.4	fine to medium sand		Bk	III
BR03-2 Duplicate	8	Angualasto	0.4	fine to medium sand		Bk	III
BR03-19	8.19	South of Rodeo 2	1	fine to medium sand		C	I
BR03-37	8.21	Rodeo 1	1	sand		Bt,C	II
BR02-SOL3	8.25	Angualasto	0.4	clay to fine sand		B,C	I
BR03-44	8.34	Rodeo 1	0.6	silt to fine sand		B	II
BR04-41	8.35	Angualasto	1	silt to fine sand		Bt	II
BR04-20	8.4	Maliman	1	clay to fine sand		Bt,Bk,C	II
BR04-21	8.5	Maliman	0.6	silt		Bw	II
BR03-17	8.58	Rodeo 2	0.3	clay to silt		B,Bk	II
BR04-22	8.62	Rodeo 1	1	fine to medium sand		B,Bk,C	II
BR03-16	8.7	Rodeo 2	0.7	clay to silt		Bt	II
BR04-16	8.7	East of Rio Blanco	1	silt to fine sand	5YR 6/2	Bk,C	II-III
BR04-59	8.75	South of Rodeo 1	1	clay		B, Bk	II-III
BR05-39	8.85	Rodeo 1	0.5	fine to medium sand		Bw, C	II
BR04-18	9.03	East of Rodeo 1	2	fine to medium sand		Bk,C	II
BR05-44	9.06	Rodeo 2	0.25	silt to fine sand	5YR 8/1	B,C	II
BR03-13	6.3 +/- 0.6	Cerro Blanco	0.5	silt to fine sand	5YR 7/1	B,C	II

Sample	Nodule form	nodule size (cm)	Ped classification[2]	Other features	Classification[3]
BR05-28	ovoid	3	subangular blocky, medium	redoximorphic compound soil succession	aquic Alfisol
BR05-29	ovoid, irregular	4	subangular blocky, medium	redoximorphic compound soil succession	Aridisol
BR05-30		2		multiple reduced bands, some iron oxides	aquic Alfisol
BR04-17	ovoid	4	angular blocky, medium	iron oxide laminations and redoximorphic banding	aquic Alfisol
BR05-33		2		oxidized compound soil succession	Aridisol
BR05-38	irregular	4	subangular blocky, medium		Aridisol
BR05-37	ovoid	3			Aridisol
BR05-36		6			Aridisol
BR05-35	ovoid	2	angular blocky, medium	compound	Alfisol
BR04-14	ovoid	3			Aridisol
BR04-13	coalesced, ovoid	4	angular blocky, medium	oxidized compound paleosols	Aridisol
BR04-12	coalesced, ovoid	4			Aridisol
BR04-10	coalesced,ovoid	5	subangular blocky, medium		Aridisol
BR04-11	ovoid	3			Aridisol
BR03-27	filamentous to ovoid	2	minimal	slightly tuffaceous sandstone with redoximorphic banding	Inceptisol
BR03-33	filamentous	1	minimal	iron oxide spots within pink claystone	Inceptisol
BR03-32	filamentous; laminar	10	subangular blocky, medium	redoximorphic claystone	Aridisol
BR03-29	coalesced	2		Oxidized and mottled	Aridisol
BR02-SOL5	filamentous	1	minimal	redoximorphic banding and mottling; clay films present	Inceptisol
BR04-35	rounded	3		compound interval, with thin sheet sandstone interbeds	Alfisol
BR04-36	rounded	3			Alfisol
BRO3-39	rounded	4	subangular blocky, medium	redoximorphic banding	Alfisol
BR03-12	ovoid	2	minimal	slickensides and dendritic manganese present in B	Aridisol
BR05-53		6			Aridisol
BR05-52		2			Aridisol
BR03-25	rounded	4	subangular blocky, medium	Rather weathered	Inceptisol
BR03-24	ovoid to coalesced	6	minimal	compound interval,tuff+sandstone interbeds. Channel erodes top	Aridisol
BR03-21	coalesed ovoid	3	subangular blocky, fine		Aridisol
BR03-22	coalesced ovoid	3	subangular blocky, fine	slightly oxidized.	Aridisol
BR03-23	coalesced ovoid	2	subangular blocky, medium	clear B-C transition	Aridisol
BR05-50	ovoid, branching	4	subangular blocky, coarse		Aridisol
BR04-4	ovoid	3	subangular blocky, fine	oxidized paleosols 20-40 cm thick, interbedded sheet sandstones	Aridisol
BR05-49	ovoid	2	subangular blocky, medium	carbonates concentrated within 4 cm; gradual B/C boundary	Aridisol
BR05-40	ovoid	4	minor		Inceptisol
BR04-30	ovoid	4	subangular blocky, medium	Upper paleosol of 4-5 SB, compound; laminated clay at base	Aridisol
BR04-7	ovoid	6	subangular blocky, very coarse	Upper paleosol of 4-5 SB, Compound paleosol, gradual B-C	Aridisol
BR05-41	ovoid	3		compound succession, interbedded tabular sands	Alfisol
BR05-43	irregular	5	minor	redoximorphic mottling	Inceptisol
BR04-1	ovoid	3	subangular blocky, medium	Lower paleosol of 4-5 SB, truncated by Holocene terrace	Alfisol
BR04-29	ovoid	5	subangular blocky, coarse	Lower paleosol of 4-5 SB, clear B-C boundary	Alfisol
BR05-42	ovoid	4		compound, oxidized paleosol succession	Alfisol
BR03-10	ovoid	8	subangular blocky, fine-medium	minor color banding,mottling; carbonate filled burrows 50-64 cm	Aridisol
BR04-3	ovoid	4			Inceptisol
BR03-9	ovoid	7	subangular blocky, fine-medium	comound oxidized succession, minor mottling	Alfisol
BR05-47	ovoid	3	subangular blocky, medium		Alfisol
BR05-48	irregular	3		4 compound oxidized paleosols; red and black mottles	Alfisol
BR04-28	ovoid	8			Alfisol
BR03-49	ovoid to rounded	4	none	oxidized interval	Inceptisol
BR03-49 dup.	ovoid to rounded	4	none	oxidized interval	Inceptisol
BR04-54	ovoid	2	minimal		Aridisol
BR04-27					Aridisol
BR04-26				locally eroded (<0.5 m) by coarse sandstone-filled channels	Aridisol
BR04-25	irregular;coalesced	8	minimal		Aridisol
BR04-31				along-strike equivalent of BR04-25	Aridisol
BR04-24					Aridisol
BR04-23					Aridisol
BR04-33	coalesced irregular	5	minimal	laterally wavy, compacted; compound interval	Aridisol
BR04-32	oblate	6	minimal	4 compound paleosols 10-15 cm each, likely compacted.	Aridisol
BR04-53	oblate	4	subangular blocky, medium	compacted; gradual B-C transition	Aridisol
BR04-52	coalesced ovoid	2		redoximorphic mottles	Aridisol
BR04-34	ovoid	2	minimal	likely truncated, gradual B-C, oxidized	Alfisol
BR04-50	coalesced irregular	4	minimal		Aridisol
BR04-51	coalesced irregular	4	subangular blocky, medium		Aridisol
BR03-47	ovoid	3	minimal	oxidized, slightly pedogenic interval, less so upsection	Inceptisol
22-6-2002 SOL4	ovoid	4	subangular blocky, medium	mottled	Aridisol
22-6-2002 SOL4 Dupl	ovoid	4	subangular blocky, medium	mottled	Aridisol
BR03-3	irregular	5		redoximorphic banding	Aridisol
BR03-3 duplicate				compound paleosol interval	Aridisol
BR03-4	irregular	5	subangular blocky, medium		Aridisol
BR03-45	filamentous - coalesced	4	subangular blocky, medium		Aridisol
BR03-2	coalesced	6	none	redoximorphic banding	Aridisol
BR03-2 Duplicate	coalesced	6	none	redoximorphic banding	Aridisol
BR03-19	filamentous	1	subangular blocky, coarse	redoximorphic	aquic Alfisol
BR03-37	ovoid	3	subangular blocky, medium	redoximorphic banding and mottling	aquic Alfisol
BR02-SOL3	filamentous	1	minor	redoximorphic banding/mottling, B horizon slickensides, trace C	Inceptisol
BR03-44	ovoid	2	minimal	redoximorphic banding	aquic Alfisol
BR04-41	irregular	6	subangular blocky, medium	compound interval, paleosols 20 cm -1 m.	Alfisol
BR04-20	ovoid	3			Aridisol
BR04-21	ovoid	3	subangular blocky, medium	mostly oxidized, some mottles	Alfisol
BR03-17	ovoid	1		tuffaceous, with white mottles, minor slickenside development	Aridisol
BR04-22	ovoid	4	none	carbonates concentrated within 15 cm.	Aridisol
BR03-16	ovoid	5	subangular blocky, medium-coa	Top of paleosol has subvertical clay-filled tubules	Aridisol
BR04-16	irregular	5	subangular blocky, fine-medium	mottled	Aridisol
BR04-59	coalesced irregular	5	none	massive reduced B horizon with multiple Bk horizons	Aridisol
BR05-39	irregular	5	angular blocky, medium		Alfisol
BR04-18	irregular	16		redoximorphic compound soil succession, locally eroded	Aridisol
BR05-44	ovoid to irregular	3	none	uniform coloration	Inceptisol
BR03-13	rounded	3	subangular blocky, fine	slightly oxidized. Rip-up clasts present	Alfisol

APPENDIX B:

RADIOMETRIC ($^{40}Ar/^{39}Ar$) DATA FOR IGLESIA BASIN, NORTHWESTERN ARGENTINA

Late Miocene and Early Pliocene extrusive igneous deposits are locally interbedded with sedimentary units in the Iglesia nonmarine foreland basin, San Juan Province, northwestern Argentina. To supplement and confirm the local magnetic polarity stratigraphic correlations (summarized in Ré *et al.,* 2003) as well as to constrain depositional ages in additional outcrop localities, thirteen ignimbrites and one dacite unit were sampled and their plagioclase feldspar minerals radiometrically analyzed by the $^{40}Ar/^{39}Ar$ method at the University of Nevada, Las Vegas. The samples are shown in outcrop on Figure 2.9 and stratigraphically in Figures 2.19-2.23.

Samples were wrapped in Al foil and stacked in sealed 6 mm inside diameter Pyrex tubes with neutron fluence monitors (FC-2, Fish Canyon Tuff sanidine) placed every 5-10 mm along the tubes. Irradiation packages included synthetic K-glass and optical grade CaF_2 to monitor neutron induced argon interference from K and Ca. Sample irradiation was conducted in McMaster Nuclear Reactor at McMaster University, Ontario, Canada. Samples were in-core for 7 hours, surrounded by fuel rods on each side. Correction factors for neutron interference reactions on K and Ca were determined by repeated analysis of K-glass and CaF_2 fragments. Irradiated crystals and CaF_2 and K-glass fragments were placed in a Cu sample tray on motorized stage in a high vacuum extraction line and fused using a 20 W CO_2 laser. Reactive gases were removed by a single MAP and two GP-50 SAES getters before admission to a MAP 215-50 mass spectrometer. Given the relative volumes of the extraction line and mass spectrometer, 76% of the gas is admitted for furnace heating analyses. Mass spectrometer discrimination and sensitivity was monitored by repeated analysis of atmospheric argon aliquots. Measured $^{40}Ar/^{36}Ar$ ratios were 291.10 ±

0.12% for these analyses, and a discrimination correction of 1.01513 (4 AMU) was applied to the measured isotopic ratios. Automated operation of sample stage, laser, extraction line and mass spectrometer as well as final data reduction and age calculations were done using LabSPEC software by Bruce Idleman (Lehigh University).

Isotopic ratios for the analyzed samples are listed sequentially for each step of the furnace heating process on the following pages, as well as graphical representations of the Argon emission spectra and calculated age. Ages (in millions of years, MA) are given (in increasing order of confidence) as total gas, plateau and isochron ages plus or minus a confidence interval of one standard deviation (σ). Total gas ages are the weighted amount of ^{39}Ar released. Plateau ages are calculated from three or more contiguous gas fractions (emission steps) that have ages overlapping within 2σ analytical error and represent a significant proportion of the total released gas. Inverse isochrons were calculated and compared with the mean squared weighted distribution criteria of Wendt and Carl (1991).

The most reliable age ranges for the samples are based on statistical significance as well as stratigraphic relationships. In order of decreasing confidence, age assessment utilized (when available): (1) isochron age, (2) plateau age, (3) total gas age, and (4) lowest step in emission spectrum ("saddle") as maximum age. The preferred ages for the samples are listed in Table B.1. Individual sample analytical data are presented in Tables B.2 through B.9. Argon emission spectra and (when available) isochron age assessments are given for individual samples in Figures B.1 through B.9.

Table B.1: Age summary for $^{40}Ar/^{39}Ar$ radiometric analyses from Iglesia Basin extrusive igneous samples. Stratigraphic positions of samples shown in Figures 2.18 through 2.22.

Sample ID	Lithology	Age Range (MA)	Type	Comments
BR03-15	rhyolite	7.21 ± 0.05	isochron	
BR03-20	rhyolite	<8.03	saddle	highly discordant spectra
BR03-26	rhyolite	6.54 ± 0.03	total gas	
BR03-28	dacite	12.1 ± 0.3	total gas	highly discordant spectra
BR03-33B	rhyolite	6.26 ± 0.09	isochron	
BR03-38	rhyolite	<8.15	saddle	stratigraphically constrained
BR03-46	rhyolite	7.63 ± 0.08	total gas	
BR03-48	rhyolite	<7.5	saddle	stratigraphically constrained
BR04-2	rhyolite	6.8 ± 0.3	pseudo-plateau	average of steps 5-12
BR04-19	rhyolite	8.40 ± 0.06	plateau	
BR04-39	rhyolite	<6.3	saddle	stratigraphically constrained
BR04-40	rhyolite	<6.03	saddle	stratigraphically constrained
BR04-56	rhyolite	8.72 ± 0.13	plateau	

Table B.2: Stepwise analytical data for samples BR03-15 and BR03-20.

Ruskin-Cornell University, BR03-15, plagioclase, 16.82 mg, J = 0.001672 ± 0.18%

4 amu discrimination = 1.01513 ± 0.12%, 40/39K = 0.0001 ± 100.0%, 36/37Ca = 0.000267 ± 3.83%, 39/37Ca = 0.00070 ± 0.63%

step	T (C)	t (min.)	36Ar	37Ar	38Ar	39Ar	40Ar	%40Ar*	% 39Ar rlsd	Ca/K	40Ar*/39ArK	Age (Ma)	1s.d.
1	730	12	2.544	4.157	1.645	3.273	763.672	3.2	1.4	6.08215094	7.4814	22.43	2.63
2	810	12	1.200	10.387	0.383	7.974	379.581	8.3	3.3	6.23817309	3.9564	11.90	0.56
3	890	12	0.338	20.289	0.301	15.404	139.091	31.0	6.5	6.30782645	2.7879	8.39	0.15
4	960	12	0.227	28.668	0.336	21.460	117.307	47.2	9.0	6.39781999	2.5592	7.70	0.06
5	1020	12	0.124	29.180	0.305	22.342	88.227	64.2	9.4	6.25473509	2.5335	7.63	0.06
6	1075	12	0.139	27.543	0.289	21.206	90.644	60.0	8.9	6.22004665	2.5282	7.61	0.09
7	1125	12	0.181	22.845	0.276	17.899	94.888	50.1	7.5	6.11208623	2.5898	7.80	0.10
8	1175	12	0.259	19.536	0.270	15.357	110.308	35.6	6.4	6.09191325	2.5099	7.56	0.11
9	1225	12	0.428	25.647	0.356	20.030	175.36	32.1	8.4	6.13176168	2.7783	8.36	0.13
10	1275	12	0.417	33.188	0.446	25.676	186.69	38.7	10.8	6.19000434	2.7866	8.39	0.09
11	1330	12	0.406	29.662	0.408	22.255	176.198	34.7	9.3	6.38315306	2.6530	7.99	0.13
12	1400	12	0.634	59.957	0.765	45.509	300.658	41.5	19.1	6.30950697	2.6953	8.11	0.13
							Cumulative %39Ar rlsd =		100.0		Total gas age =	8.30	0.06
											Plateau age =	7.66	0.07
											(steps 4-8)		
											Isochron age =	7.21	0.05
											(steps 4-8)		

note: isotope beams in mV, rlsd = released, error in age includes 0.5% J error, all errors 1 sigma
(36Ar through 40Ar are measured beam intensities, corrected for decay for the age calculations)

Ruskin-Cornell University, BR 03-20, plagioclase, 25.31 mg, J = 0.001670 ± 0.18%

4 amu discrimination = 1.01513 ± 0.12%, 40/39K = 0.0001 ± 100.0%, 36/37Ca = 0.000267 ± 3.83%, 39/37Ca = 0.00070 ± 0.63%

step	T (C)	t (min.)	36Ar	37Ar	38Ar	39Ar	40Ar	%40Ar*	% 39Ar rlsd	Ca/K	40Ar*/39ArK	Age (Ma)	1s.d.
1	650	12	5.714	2.233	36.973	4.333	1745.32	4.7	0.9	2.56946353	18.9620	56.24	1.79
2	730	12	1.911	8.506	3.412	11.277	731.651	24.1	2.3	3.76209612	15.6923	46.67	0.33
3	810	12	1.015	17.792	0.873	18.263	460.886	36.5	3.7	4.86064694	9.2300	27.60	0.27
4	890	12	1.183	30.714	0.719	29.362	533.918	36.4	6.0	5.21962136	6.6417	19.90	0.12
5	960	12	0.413	40.779	0.618	39.158	315.522	64.0	8.0	5.19638466	5.1521	15.46	0.06
6	1020	12	0.257	43.671	0.639	43.740	262.811	74.3	8.9	4.98163113	4.4559	13.38	0.04
7	1075	12	0.236	37.298	0.596	41.471	245.934	74.6	8.5	4.48676874	4.4117	13.24	0.06
8	1125	12	0.278	34.283	0.603	41.099	262.051	72.1	8.4	4.16099991	4.5712	13.72	0.05
9	1175	12	0.304	33.145	0.643	43.304	306.395	73.7	8.8	3.8176433	5.1870	15.56	0.06
10	1225	12	0.274	35.460	0.721	51.197	435.637	83.6	10.5	3.45423699	7.1023	21.27	0.06
11	1270	12	0.278	37.560	0.966	69.369	339.535	78.7	14.2	2.69972531	3.8366	11.52	0.04
12	1310	12	0.265	34.999	0.719	49.043	206.483	65.7	10.0	3.55918216	2.6792	8.05	0.06
13	1350	12	0.247	31.161	0.454	29.302	153.503	56.4	6.0	5.3065678	2.8269	8.50	0.06
14	1400	12	0.319	27.343	0.334	18.825	145.027	38.0	3.8	7.25211151	2.7959	8.40	0.17
							Cumulative %39Ar rlsd =		100.0		Total gas age =	15.37	0.04
											no plateau		
											no isochron		

note: isotope beams in mV, rlsd = released, error in age includes 0.5% J error, all errors 1 sigma
(36Ar through 40Ar are measured beam intensities, corrected for decay for the age calculations)

Table B.3: Stepwise analytical data for samples BR03-26 and BR03-28

Ruskin-Cornell University, BR 03-26, plagioclase, 20.55 mg, J = 0.001669 ± 0.17%

4 amu discrimination = 1.01513 ± 0.12%, 40/39K = 0.0001 ± 100.0%, 36/37Ca = 0.000267 ± 3.83%, 39/37Ca = 0.00070 ± 0.63%

step	T (C)	t (min.)	36Ar	37Ar	38Ar	39Ar	40Ar	%40Ar*	% 39Ar rlsd	Ca/K	40Ar*/39ArK	Age (Ma)	1s.d.
1	700	12	1.280	3.550	0.875	4.625	373.591	0.2	1.8	3.89431145	0.1754	0.53	0.42
2	800	12	0.605	1.465	0.315	15.265	209.473	15.8	5.8	0.48641834	2.1603	6.49	0.42
3	900	12	0.611	31.318	0.504	30.322	237.645	27.3	11.5	5.24235126	2.1360	6.42	0.04
4	980	12	0.233	39.299	0.510	37.683	144.590	57.5	14.3	5.29337456	2.1883	6.58	0.03
5	1040	12	0.146	37.922	0.461	36.855	115.212	68.6	14.0	5.22254482	2.1206	6.37	0.03
6	1095	12	0.155	30.402	0.383	30.304	109.311	63.2	11.5	5.09181366	2.2533	6.77	0.03
7	1140	12	0.166	21.984	0.298	22.112	92.104	53.3	8.4	5.04595079	2.1626	6.50	0.07
8	1185	12	0.126	16.510	0.236	16.538	71.334	54.8	6.3	5.06676921	2.2796	6.85	0.09
9	1225	12	0.122	16.067	0.233	15.899	66.562	53.1	6.0	5.12908801	2.1383	6.43	0.09
10	1270	12	0.142	18.527	0.238	17.892	81.235	55.0	6.8	5.25578881	2.4217	7.28	0.10
11	1315	12	0.309	17.845	0.276	17.142	132.775	32.9	6.5	5.28384921	2.4274	7.29	0.10
12	1400	12	0.341	18.786	0.302	18.164	140.131	29.8	6.9	5.24944865	2.1906	6.58	0.19
							Cumulative %39Ar rlsd =		100.0		Total gas age =	6.54	0.03
											no plateau		
											no isochron		

note: isotope beams in mV, rlsd = released, error in age includes 0.5% J error, all errors 1 sigma
(36Ar through 40Ar are measured beam intensities, corrected for decay for the age calculations)

Ruskin-Cornell University, BR 03-28, plagioclase, 13.65 mg, J = 0.001666 ± 0.14%

4 amu discrimination = 1.01513 ± 0.12%, 40/39K = 0.0001 ± 100.0%, 36/37Ca = 0.000267 ± 3.83%, 39/37Ca = 0.00070 ± 0.63%

step	T (C)	t (min.)	36Ar	37Ar	38Ar	39Ar	40Ar	%40Ar*	% 39Ar rlsd	Ca/K	40Ar*/39ArK	Age (Ma)	1s.d.
1	650	12	2.049	5.545	0.593	1.098	606.587	1.7	1.4	25.9427933	9.5698	28.54	5.34
2	730	12	1.367	16.305	0.464	3.124	407.184	2.8	4.1	26.8188939	3.6680	10.99	1.91
3	810	12	1.428	40.069	0.571	7.469	437.579	5.2	9.7	27.5724129	3.0791	9.23	0.62
4	890	12	1.551	57.107	0.581	10.778	484.988	8.8	14.0	27.2292342	4.0049	12.00	0.29
5	960	12	1.370	50.183	0.485	9.922	431.457	9.3	12.9	25.9824478	4.0625	12.17	0.25
6	1020	12	0.858	34.154	0.319	7.729	266.623	8.0	10.1	22.6783996	2.7823	8.34	0.55
7	1075	12	0.474	20.704	0.190	6.191	156.987	13.6	8.1	17.1343483	3.4391	10.31	0.29
8	1125	12	0.461	14.217	0.193	5.266	154.645	15.1	6.9	13.8187921	4.3925	13.15	0.57
9	1175	12	1.052	15.298	0.325	4.404	319.364	5.0	5.7	17.8011534	3.6171	10.84	0.41
10	1225	12	1.667	21.747	0.499	4.237	497.785	3.3	5.5	26.3702242	3.8900	11.65	1.54
11	1270	12	1.479	22.470	0.453	4.124	447.726	4.3	5.4	28.0071861	4.6902	14.04	0.87
12	1310	12	1.043	21.727	0.354	4.073	318.937	4.7	5.3	27.415346	5.1836	15.51	0.87
13	1350	12	0.704	22.253	0.280	4.126	226.798	9.6	5.4	27.7208992	5.2450	15.70	1.63
14	1400	12	0.741	24.660	0.261	4.283	237.973	9.5	5.6	29.6099488	5.2434	15.69	0.47
							Cumulative %39Ar rlsd =		100.0		Total gas age =	12.14	0.25
											no plateau		
											no isochron		

note: isotope beams in mV, rlsd = released, error in age includes 0.5% J error, all errors 1 sigma
(36Ar through 40Ar are measured beam intensities, corrected for decay for the age calculations)

Table B.4: Stepwise analytical data for samples BR03-33B and BR03-38.

Ruskin-Cornell, BR03-33B, plagioclase, 7.84 mg, J = 0.001684 ± 0.93%

4 amu discrimination = 1.01636 ± 0.22%, 40/39K = 0.0001 ± 100.0%, 36/37Ca = 0.000267 ± 3.83%, 39/37Ca = 0.00070 ± 0.63%

step	T (C)	t (min.)	36Ar	37Ar	38Ar	39Ar	40Ar	%40Ar*	% 39Ar rlsd	Ca/K	40Ar*/39ArK	Age (Ma)	1s.d.
1	700	12	0.570	0.106	0.118	0.102	167.233	1.3	0.1	6.28143543	23.7746	70.74	33.63
2	800	12	0.488	3.652	0.168	4.478	157.696	11.1	4.2	4.92746209	3.8818	11.74	0.41
3	900	12	0.224	24.618	0.391	26.712	114.965	49.3	24.8	5.56937813	2.0983	6.36	0.09
4	980	12	0.112	17.343	0.252	19.340	68.168	60.5	18.0	5.41886669	2.0821	6.31	0.14
5	1040	12	0.116	10.822	0.181	12.844	57.778	48.6	11.9	5.09102443	2.1244	6.44	0.10
6	1090	12	0.147	6.711	0.121	8.336	58.627	31.9	7.8	4.86404822	2.1843	6.62	0.13
7	1140	12	0.174	5.876	0.117	6.680	63.095	23.8	6.2	5.31535819	2.1896	6.63	0.17
8	1185	12	0.207	6.489	0.129	6.017	73.512	21.6	5.6	6.51901452	2.5889	7.84	0.85
9	1225	12	0.183	7.926	0.117	6.913	68.361	26.5	6.4	6.93147202	2.5645	7.77	0.19
10	1270	12	0.110	7.569	0.109	7.415	50.319	42.9	6.9	6.16972759	2.8164	8.53	0.16
11	1315	12	0.084	5.357	0.095	4.619	38.441	39.4	4.3	7.01168028	2.9353	8.89	0.29
12	1400	12	0.149	4.704	0.092	4.101	58.321	26.4	3.8	6.93451199	3.5131	10.63	0.66
							Cumulative %39Ar rlsd =		100.0		Total gas age =	7.27	0.10
											Plateau age =	6.43	0.10
											(steps 3-8)		
											Isochron age =	6.26	0.09
											(steps 3-8)		

note: isotope beams in mV, rlsd = released, error in age includes 0.5% J error, all errors 1 sigma
(36Ar through 40Ar are measured beam intensities, corrected for decay for the age calculations)

Ruskin-Cornell, BR03-38, plagioclase, 10.44 mg, J = 0.001689 ± 0.99%

4 amu discrimination = 1.01636 ± 0.22%, 40/39K = 0.0001 ± 100.0%, 36/37Ca = 0.000267 ± 3.83%, 39/37Ca = 0.00070 ± 0.63%

step	T (C)	t (min.)	36Ar	37Ar	38Ar	39Ar	40Ar	%40Ar*	% 39Ar rlsd	Ca/K	40Ar*/39ArK	Age (Ma)	1s.d.
1	800	12	0.154	0.656	0.176	0.484	46.509	6.1	0.4	8.24528671	5.7658	17.48	3.24
2	890	12	0.191	5.322	0.172	4.444	63.462	16.1	3.9	7.28320785	2.2398	6.81	0.25
3	960	12	0.125	11.803	0.157	9.425	62.769	48.9	8.3	7.61686795	3.1751	9.65	0.16
4	1025	12	0.196	33.048	0.376	26.461	122.351	60.7	23.2	7.59629156	2.7780	8.45	0.10
5	1085	12	0.086	20.107	0.219	16.368	66.150	72.0	14.4	7.47133258	2.8387	8.63	0.12
6	1140	12	0.016	13.329	0.170	11.035	56.592	53.9	9.7	7.34607419	2.6811	8.15	0.13
7	1190	12	0.143	12.406	0.175	10.128	67.300	44.7	8.9	7.44992157	2.8974	8.81	0.15
8	1230	12	0.162	13.404	0.190	10.927	75.052	43.3	9.6	7.46068142	2.9096	8.84	0.17
9	1270	12	0.143	11.954	0.168	9.562	64.121	41.7	8.4	7.60375616	2.7246	8.28	0.14
10	1320	12	0.147	10.376	0.144	8.092	67.983	40.4	7.1	7.79943718	3.2032	9.73	0.19
11	1400	12	0.173	8.919	0.157	6.970	73.635	33.9	6.1	7.78342013	3.4005	10.33	0.48
							Cumulative %39Ar rlsd =		100.0		Total gas age =	8.78	0.11
											no plateau		
											no isochron		

note: isotope beams in mV, rlsd = released, error in age includes 0.5% J error, all errors 1 sigma
(36Ar through 40Ar are measured beam intensities, corrected for decay for the age calculations)

Table B.5: Stepwise analytical data for samples BR03-46 and BR03-48.

Ruskin-Cornell University, BR 03-46, plagioclase, 20.60 mg, J = 0.001708 ± 0.85%

4 amu discrimination = 1.01513 ± 0.12%, 40/39K = 0.0001 ± 100.0%, 36/37Ca = 0.000267 ± 3.83%, 39/37Ca = 0.00070 ± 0.63%

step	T (C)	t (min.)	36Ar	37Ar	38Ar	39Ar	40Ar	%40Ar*	% 39Ar rlsd	Ca/K	40Ar*/39ArK	Age (Ma)	1s.d.
1	700	12	1.841	6.432	99.607	4.848	546.766	2.0	2.1	6.85562429	2.3217	7.14	0.46
2	800	12	0.729	13.103	1.164	9.774	238.429	11.7	4.1	6.92741731	2.8576	8.78	0.42
3	900	12	0.281	28.239	0.416	20.940	131.303	41.4	8.9	6.96868704	2.5805	7.93	0.08
4	980	12	0.174	39.878	0.467	29.840	115.968	62.0	12.6	6.90565149	2.3869	7.34	0.09
5	1040	12	0.138	37.452	0.399	28.350	98.559	65.6	12.0	6.82624238	2.2514	6.92	0.08
6	1095	12	0.084	31.407	0.340	24.241	79.582	76.0	10.3	6.69450546	2.4537	7.55	0.08
7	1140	12	0.078	23.502	0.285	18.156	61.850	73.4	7.7	6.68846467	2.3973	7.37	0.11
8	1185	12	0.099	20.312	0.231	15.561	63.992	63.4	6.6	6.74472598	2.5046	7.70	0.17
9	1225	12	0.136	22.027	0.275	16.846	78.022	56.3	7.1	6.75630412	2.5261	7.77	0.11
10	1270	12	0.194	32.179	0.416	24.597	109.536	55.1	10.4	6.75991926	2.4013	7.38	0.11
11	1315	12	0.173	34.900	0.439	26.378	115.007	63.1	11.2	6.83667092	2.6992	8.30	0.11
12	1400	12	0.607	23.073	0.391	16.914	220.775	20.4	7.2	7.04930945	2.5942	7.98	0.13
							Cumulative %39Ar rlsd =		100.0		Total gas age =	7.63	0.08

note: isotope beams in mV, rlsd = released, error in age includes 0.5% J error, all errors 1 sigma
(36Ar through 40Ar are measured beam intensities, corrected for decay for the age calculations)

no plateau
no isochron

Ruskin-Cornell University, BR 03-48, plagioclase, 10.54 mg, J = 0.001705 ± 0.60%

4 amu discrimination = 1.01513 ± 0.12%, 40/39K = 0.0001 ± 100.0%, 36/37Ca = 0.000267 ± 3.83%, 39/37Ca = 0.00070 ± 0.63%

step	T (C)	t (min.)	36Ar	37Ar	38Ar	39Ar	40Ar	%40Ar*	% 39Ar rlsd	Ca/K	40Ar*/39ArK	Age (Ma)	1s.d.
1	700	12	0.928	2.162	3.469	2.755	295.977	8.6	1.0	4.07858656	9.3096	28.41	0.77
2	800	12	0.282	6.338	0.236	6.639	111.108	26.8	2.5	4.9629574	4.4538	13.65	0.32
3	900	12	0.196	14.561	0.295	15.636	94.069	42.0	5.9	4.84106171	2.4972	7.67	0.09
4	980	12	0.090	18.622	0.332	21.472	76.273	69.6	8.1	4.50801604	2.4273	7.45	0.14
5	1040	12	0.092	16.482	0.312	20.960	73.270	67.0	7.9	4.08691227	2.2961	7.05	0.07
6	1095	12	0.103	13.167	0.305	19.984	74.093	62.1	7.5	3.4236909	2.2589	6.94	0.10
7	1140	12	0.092	10.865	0.291	19.515	72.763	68.6	7.3	2.89255738	2.4655	7.57	0.12
8	1185	12	0.133	12.428	0.388	25.739	98.891	65.0	9.7	2.5083043	2.4336	7.47	0.08
9	1225	12	0.175	18.122	0.585	40.807	146.228	68.7	15.3	2.30683113	2.4238	7.44	0.06
10	1270	12	0.191	22.053	0.736	50.625	179.298	72.3	19.0	2.26277428	2.5312	7.77	0.06
11	1315	12	0.191	14.849	0.443	27.920	123.918	57.0	10.5	2.76303059	2.3895	7.34	0.07
12	1400	12	0.118	9.960	0.237	14.496	73.937	55.3	5.4	3.57042934	2.5537	7.84	0.24
							Cumulative %39Ar rlsd =		100.0		Total gas age =	7.84	0.06

note: isotope beams in mV, rlsd = released, error in age includes 0.5% J error, all errors 1 sigma
(36Ar through 40Ar are measured beam intensities, corrected for decay for the age calculations)

no plateau
no isochron

Table B.6: Stepwise analytical data for sample BR04-2.

Ruskin-Cornell, BR-04-2, plagioclase, 15.00 mg, J = 0.00193258 ± 1.1560%

4 amu discrimination = 1.02830 ± 0.31%, 40/39K = 0.0071 ± 56.0%, 36/37Ca = 0.00025397 ± 4.51%, 39/37Ca = 0.00068493 ± 2.07%

step	T (C)	t (min.)	36Ar	37Ar	38Ar	39Ar	40Ar	%40Ar*	% 39Ar rlsd	Ca/K	40Ar*/39ArK	Age (Ma)	1s.d.
1	650	12	1.352	2.860	0.413	2.298	411.28	5.8	0.6	6.20706586	10.084904	34.82	3.26
2	730	12	0.437	9.012	0.222	10.545	167.98	28.0	2.7	4.25981699	4.078489	14.16	0.28
3	810	12	0.324	21.286	0.335	21.490	152.46	44.9	5.4	4.93812958	2.885957	10.03	0.15
4	890	12	0.348	35.425	0.508	33.644	171.173	48.5	8.5	5.2498602	2.263346	7.87	0.12
5	960	12	0.253	43.640	0.572	42.511	148.436	64.6	10.7	5.11813506	1.983702	6.90	0.12
6	1020	12	0.208	41.677	0.578	43.508	138.204	72.1	11.0	4.77541305	1.993491	6.94	0.10
7	1080	12	0.199	34.593	0.542	40.202	129.349	71.2	10.1	4.28904619	1.971609	6.86	0.09
8	1150	12	0.183	28.881	0.529	40.000	128.524	78.6	10.1	3.59817463	2.071236	7.21	0.10
9	1215	12	0.464	26.462	0.702	49.325	225.698	48.6	12.5	2.6727897	2.004720	6.98	0.10
10	1275	12	0.244	29.955	0.771	60.039	180.227	74.5	15.2	2.48553937	1.953471	6.80	0.09
11	1335	12	0.423	25.213	0.529	35.042	186.261	45.1	8.8	3.58561786	1.901076	6.62	0.10
12	1400	12	0.383	16.267	0.307	17.544	141.286	30.8	4.4	4.62213326	1.798891	6.26	0.13
							Cumulative %39Ar rlsd =		100.0		Total gas age =	7.48	0.09

note: isotope beams in mV, rlsd = released, error in age includes J error, all errors 1 sigma — No plateau

(36Ar through 40Ar are measured beam intensities, corrected for decay for the age calculations) — No Isochron

Table B.7: Stepwise analytical data for sample BR04-19.

Ruskin-Cornell, BR04-19, plagioclase, 16.2 mg, J = 0.00188093 ± 0.2653%

4 amu discrimination = 1.03037 ± 0.22%, 40/39K = 0.0051 ± 63.0%, 36/37Ca = 0.00027178 ± 4.66%, 39/37Ca = 0.00067376 ± 0.992%

step	T (C)	t (min.)	36Ar	37Ar	38Ar	39Ar	40Ar	%40Ar*	% 39Ar rlsd	Ca/K	40Ar*/39ArK	Age (Ma)	1s.d.
1	660	12	0.556	0.153	2.676	0.184	163.418	3.4	0.1	5.67450871	30.146412	99.50	17.51
2	720	12	0.515	0.545	7.194	0.618	152.836	4.5	0.3	6.01876773	10.736911	36.07	2.83
3	780	12	0.384	3.064	6.024	0.142	127.857	18.3	0.1	153.800209	7.468851	25.17	1.45
4	840	12	0.202	9.513	0.180	7.683	85.139	46.5	3.9	8.45676076	4.071987	13.77	0.31
5	900	12	0.148	19.399	0.230	16.656	82.692	72.1	8.4	7.95353927	2.806391	9.50	0.08
6	960	12	0.133	24.693	0.294	21.613	84.393	100.0	10.9	7.80172818	2.623636	8.88	0.16
7	1025	12	0.138	29.089	0.339	25.687	92.039	99.3	13.0	7.73282955	2.491569	8.44	0.09
8	1090	12	0.149	27.940	0.352	25.207	96.012	97.1	12.7	7.56844824	2.478246	8.39	0.06
9	1150	12	0.177	22.057	0.293	20.811	93.684	81.8	10.5	7.23622048	2.438279	8.26	0.16
10	1210	12	0.269	26.346	0.370	24.079	128.627	62.0	12.2	7.47076564	2.503117	8.47	0.07
11	1270	12	0.333	26.590	0.362	24.031	146.459	51.9	12.2	7.55520709	2.488313	8.42	0.10
12	1330	12	0.294	17.095	0.251	15.382	118.129	59.2	7.8	7.58858018	2.468772	8.36	0.07
13	1400	12	0.636	17.637	0.269	15.630	140.785	47.1	7.9	7.70522225	2.621859	8.88	0.12
							Cumulative %39Ar rlsd =		100.0		Total gas age =	8.97	0.06
											Plateau age =	8.40	0.06
											(steps 7-12)		
											no isochron		

note: isotope beams in mV, rlsd = released, error in age includes J error, all errors 1 sigma
(36Ar through 40Ar are measured beam intensities, corrected for decay for the age calculations)

Table B.8: Stepwise analytical data for sample BR04-39.

Ruskin-Cornell, BR-04-39, plagioclase, 5.90 mg, J = 0.0020085 ± 1.0849%

4 amu discrimination = 1.03673 ± 0.33%, 40/39K = 0.0071 ± 56.0%, 36/37Ca = 0.00025397 ± 4.51%, 39/37Ca = 0.00068493 ± 2.07%

step	T (C)	t (min.)	36Ar	37Ar	38Ar	39Ar	40Ar	%40Ar*	% 39Ar rlsd	Ca/K	40Ar*/39ArK	Age (Ma)	1s.d.
1	650	12	1.085	1.344	0.297	4.120	338.24	9.7	2.3	1.89786391	7.169406	25.79	1.31
2	730	12	6.470	2.585	1.285	5.035	1898.17	3.0	2.9	2.9879023	11.016232	39.48	4.43
3	810	12	1.541	5.884	0.430	10.178	484.009	10.3	5.8	3.36484247	4.551950	16.42	0.67
4	890	12	0.590	11.120	0.691	43.222	271.442	44.8	24.5	1.49661657	2.452280	8.86	0.13
5	960	12	0.289	8.790	0.230	14.003	110.229	49.3	7.9	3.65392841	2.069703	7.48	0.34
6	1020	12	0.319	7.040	0.215	11.87	111.162	35.1	6.7	3.45126248	1.766620	6.39	0.25
7	1080	12	0.302	6.364	0.192	10.18	103.21	34.3	5.8	3.63892146	1.740864	6.30	0.19
8	1150	12	0.408	13.129	0.323	19.25	151.054	36.7	10.9	3.96978242	1.910936	6.91	0.11
9	1215	12	0.586	14.803	0.502	29.99	220.811	33.0	17.0	2.8723314	1.873814	6.78	0.15
10	1275	12	0.580	9.728	0.359	18.73	206.339	27.2	10.6	3.02254267	2.265668	8.19	0.18
11	1335	12	0.937	6.501	0.304	8.189	296.277	13.7	4.6	4.62240415	3.541455	12.79	0.53
12	1400	12	0.288	1.509	0.081	1.886	91.262	99.6	1.1	4.65876619	2.156450	7.80	1.84
							Cumulative %39Ar rlsd =		100.0		Total gas age =	9.68	0.12

note: isotope beams in mV, rlsd = released, error in age includes J error, all errors 1 sigma
(36Ar through 40Ar are measured beam intensities, corrected for decay for the age calculations)

No Plateau
No Isochron

Table B.9: Stepwise analytical data for sample BR04-56.

Ruskin-Cornell, BR-04-56, plagioclase, 15.00 mg, J = 0.00199325 ± 1.0671%
4 amu discrimination = 1.02830 ± 0.31%, 40/39K = 0.0071 ± 56.0%, 36/37Ca = 0.00025397 ± 4.51%, 39/37Ca = 0.00068493 ± 2.07%

step	T (C)	t (min.)	36Ar	37Ar	38Ar	39Ar	40Ar	%40Ar*	% 39Ar rlsd	Ca/K	40Ar*/39ArK	Age (Ma)	1s.d.
1	650	12	2.240	0.732	7.905	2.899	660.14	2.8	1.6	1.25056305	6.272521	22.42	2.54
2	730	12	0.124	9.094	0.309	4.297	46.698	36.4	2.4	10.5109029	2.675647	9.60	0.47
3	810	12	0.108	22.840	0.144	10.234	53.106	65.2	5.7	11.086029	2.422698	8.69	0.20
4	890	12	0.111	39.590	0.233	17.480	67.877	78.4	9.8	11.2509936	2.374080	8.52	0.16
5	960	12	0.114	52.828	0.308	23.276	79.768	92.9	13.0	11.2747187	2.451201	8.79	0.16
6	1020	12	0.109	55.114	0.325	24.394	81.021	95.9	13.7	11.2233399	2.465174	8.84	0.12
7	1080	12	0.117	45.838	0.275	20.563	74.536	88.7	11.5	11.0729364	2.421301	8.69	0.12
8	1150	12	0.128	41.105	0.263	18.676	72.475	90.8	10.5	10.932415	2.381624	8.54	0.16
9	1215	12	0.187	55.277	0.382	25.339	102.773	75.7	14.2	10.8354684	2.375756	8.52	0.12
10	1275	12	0.215	36.776	0.273	16.391	94.437	57.2	9.2	11.1453082	2.484736	8.91	0.20
11	1335	12	0.232	19.631	0.167	8.687	85.692	42.9	4.9	11.2257695	2.290824	8.22	0.21
12	1400	12	0.316	14.363	0.153	6.259	103.029	19.0	3.5	11.4000412	1.947051	6.99	0.35
							Cumulative %39Ar rlsd = 100.0				Total gas age =	8.85	0.12
note: isotope beams in mV, rlsd = released, error in age includes J error, all errors 1 sigma											Plateau age =	8.72	0.13
(36Ar through 40Ar are measured beam intensities, corrected for decay for the age calculations)											(steps 2-8)		
											Pseudo Isochron age =	8.91	0.06
											(steps 4-7)		

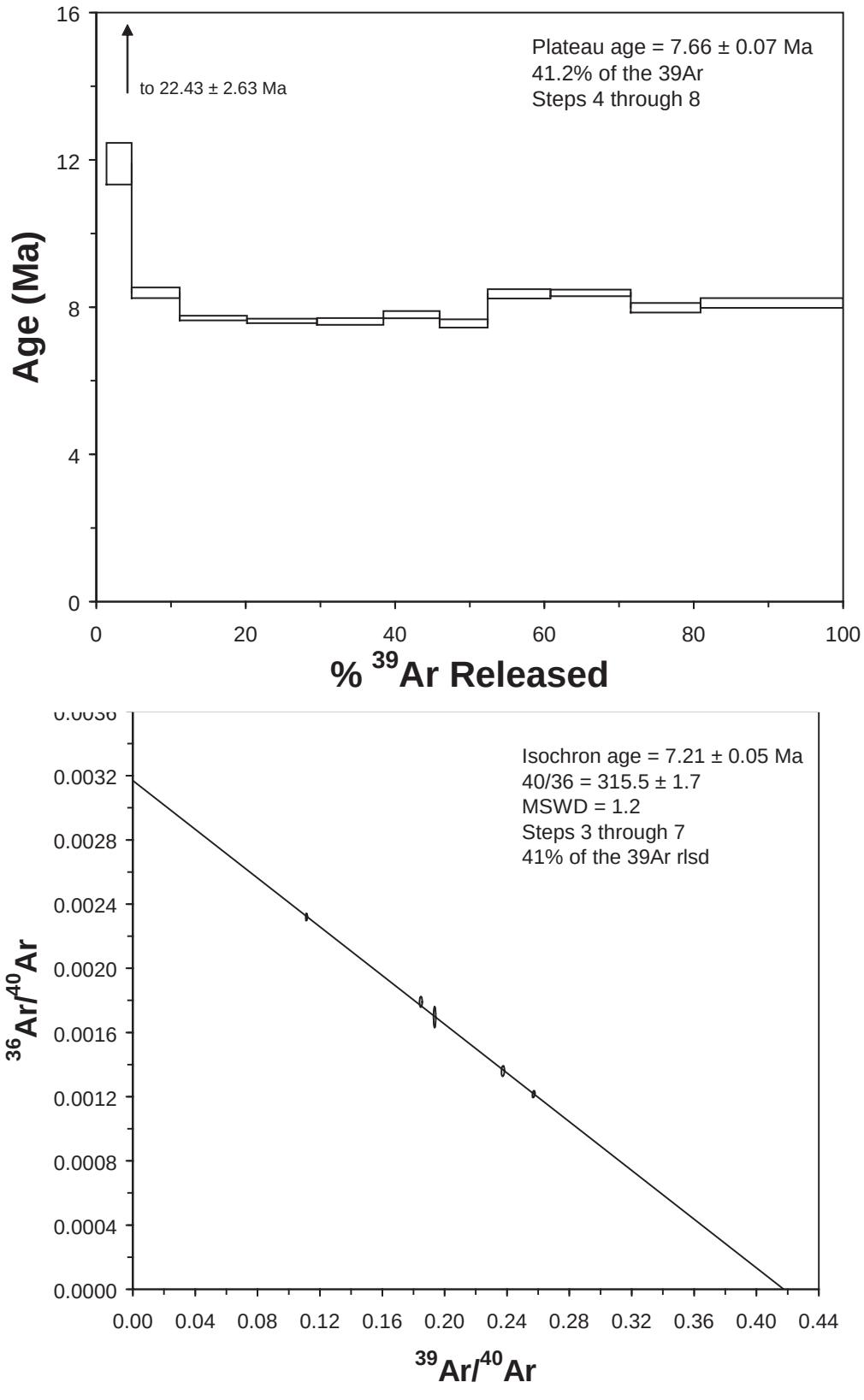

Figure B.1: Emission spectrum and isochron age assessment for sample BR03-15

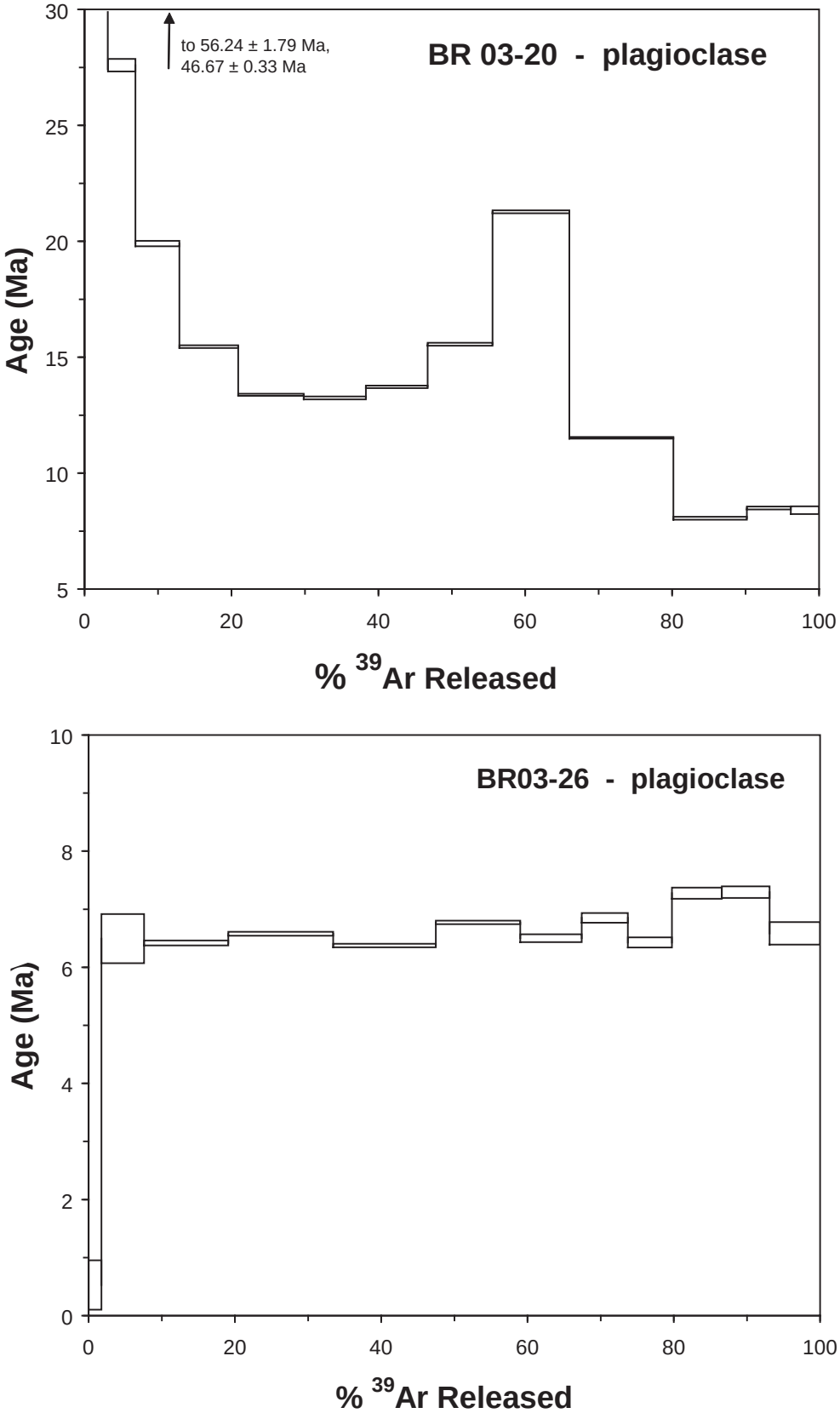

Figure B.2: Emission spectra for samples BR03-20 and BR03-26.

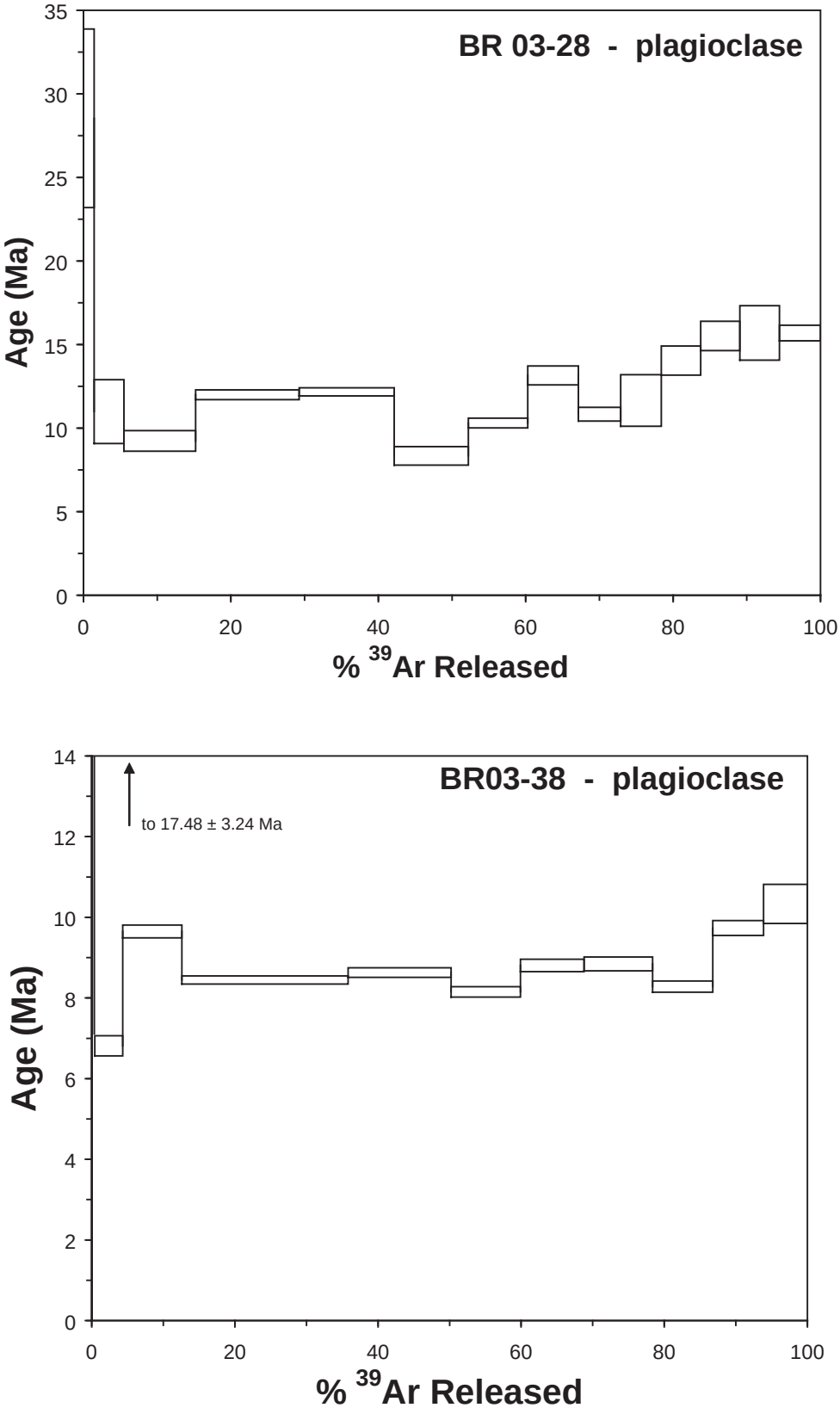

Figure B.3: Emission spectra for samples BR03-28 and BR03-38.

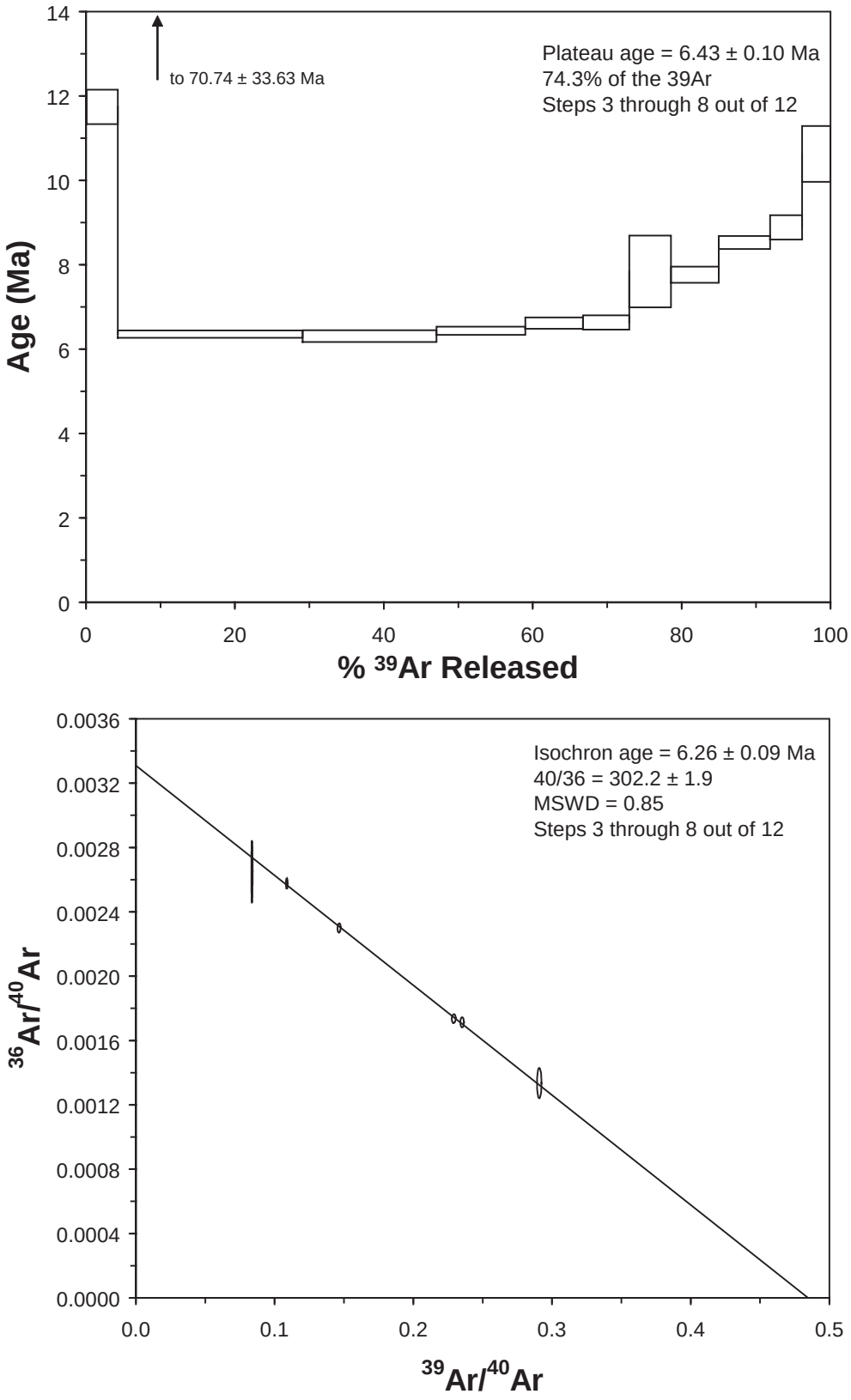

Figure B.4: Emission spectrum and isochron age assessment for sample BR03-33B.

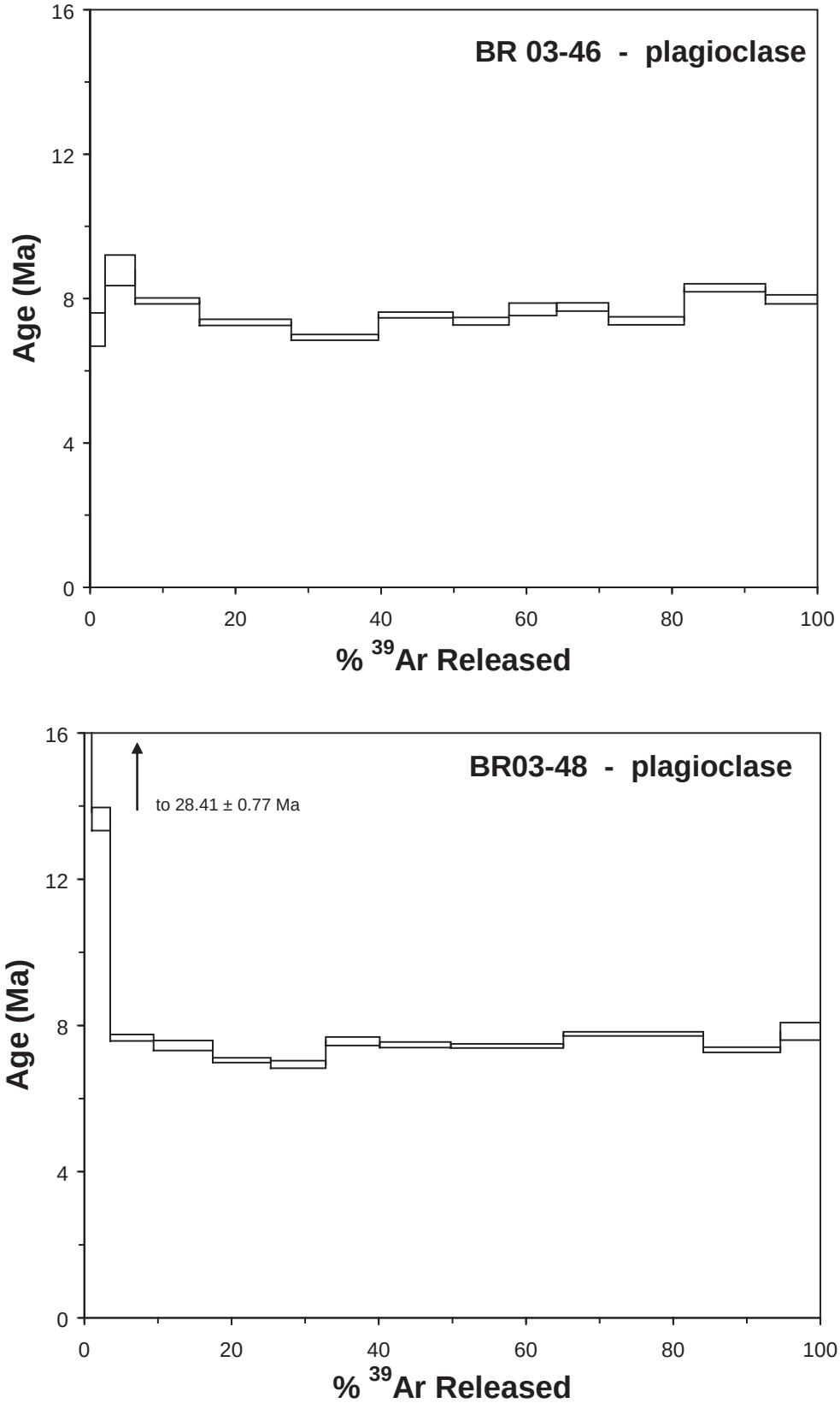

Figure B.5: Emission spectra for samples BR03-46 and BR03-48.

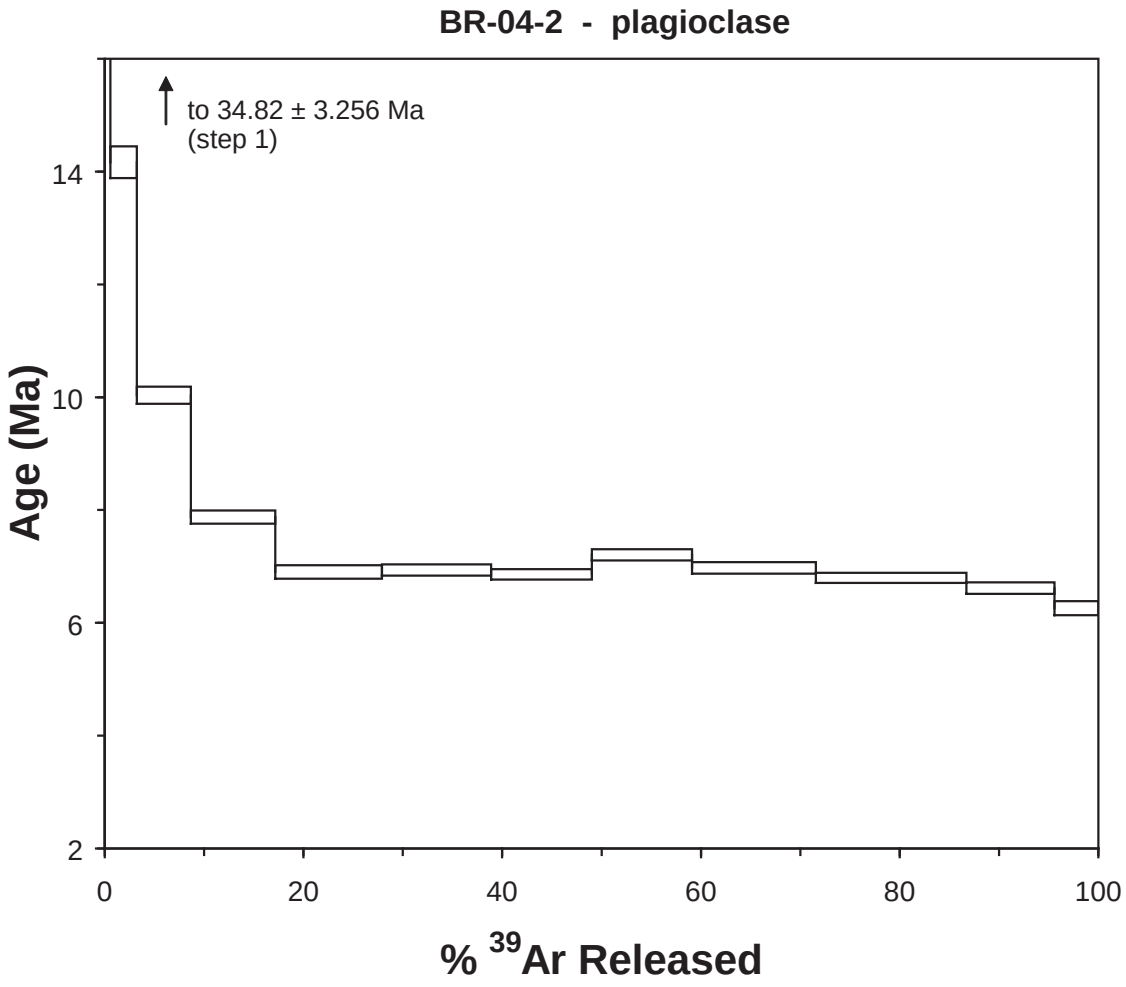

Figure B.6: Emission spectrum for sample BR04-2.

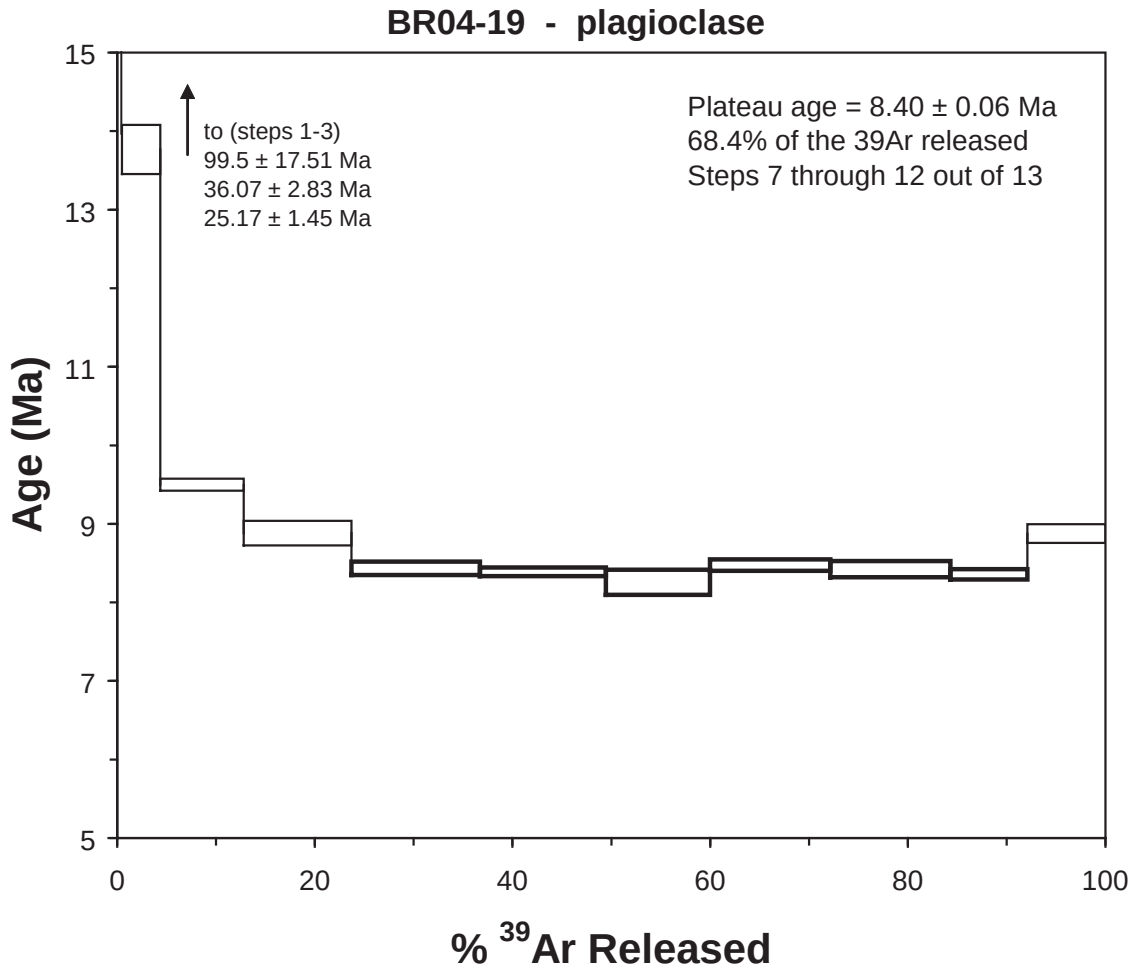

Figure B.7: Emission spectrum for sample BR04-19.

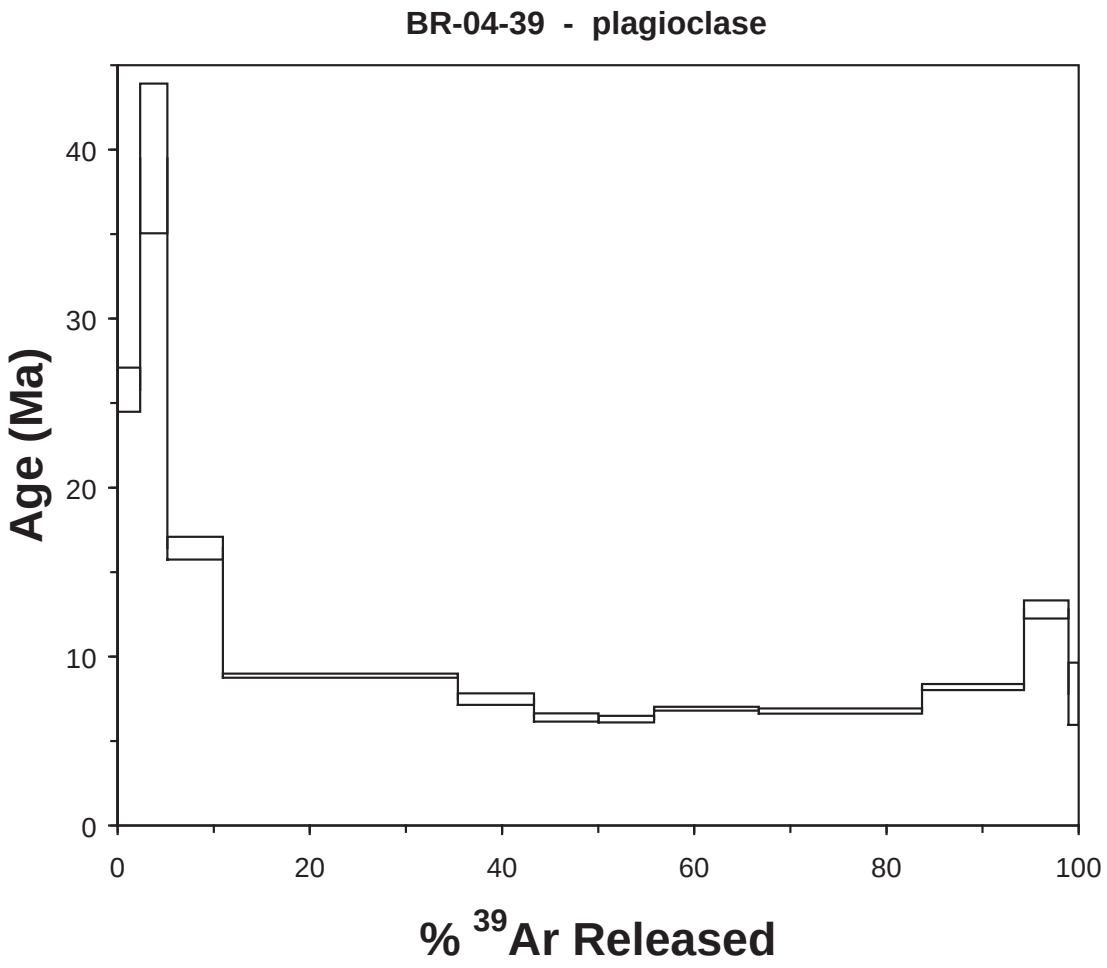

Figure B.8: Emission spectrum for sample BR04-39.

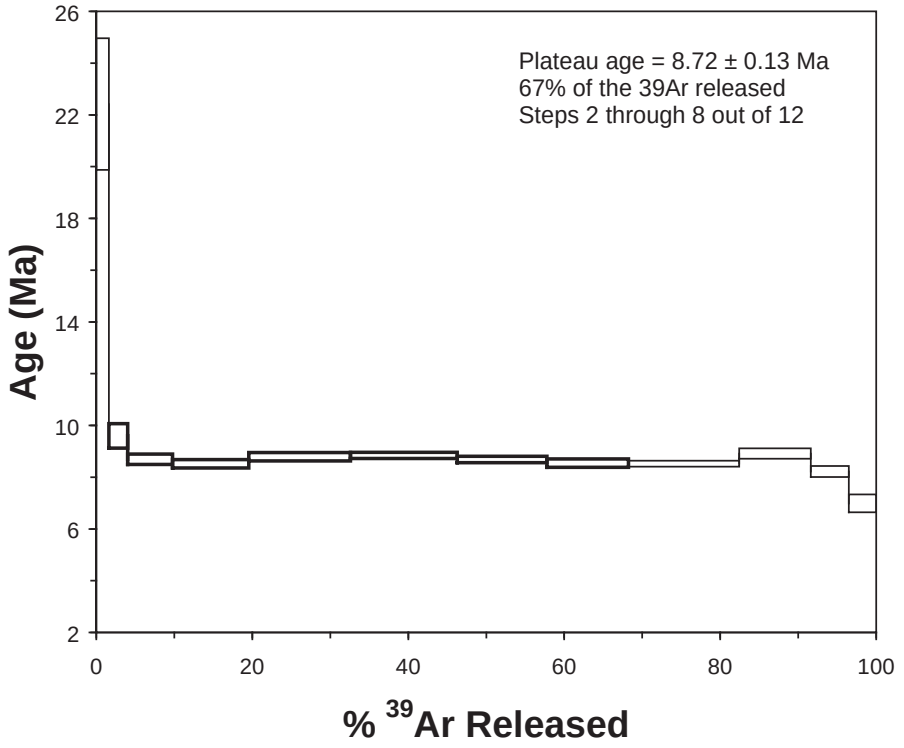

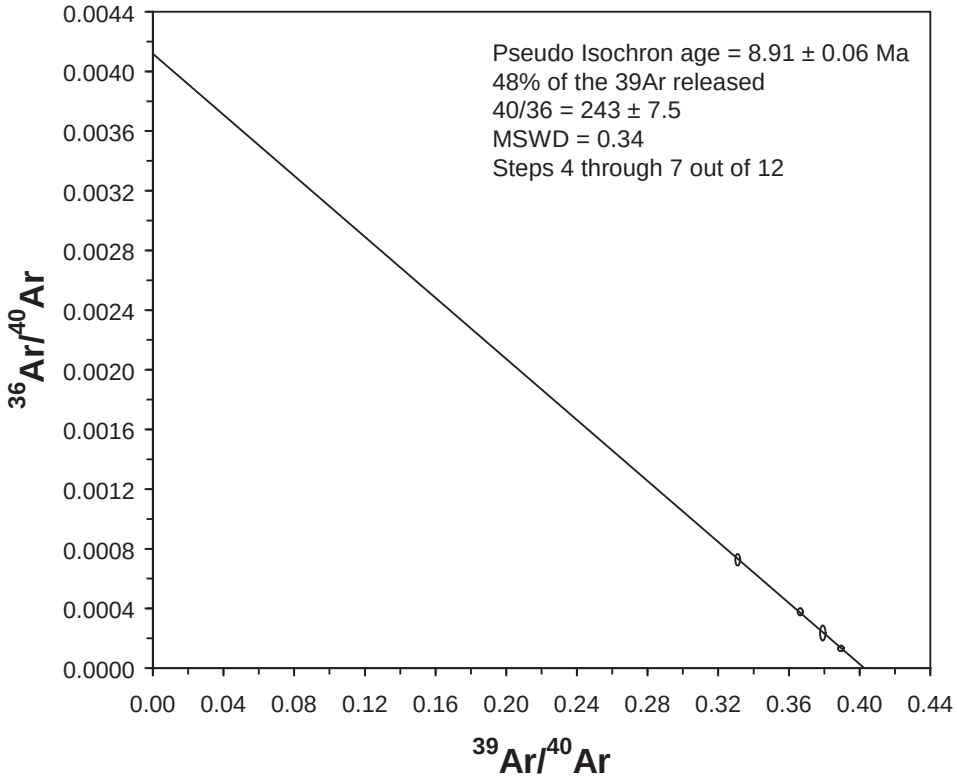

Figure B.9: Emission spectrum and pseudo-isochron age assessment for sample BR04-56.

APPENDIX C:

X-RAY DIFFRACTION DETERMINATION OF IGLESIA BASIN PALEOSOL CLAY MINERALOGY

Clay mineralogy of Miocene-Pliocene paleosols from Iglesia Basin, northwestern Argentina was semiquantitatively determined via X-Ray Diffraction (XRD) analysis. Mineral separates were prepared by gravitational and centrifugal force settling following procedures of Moore and Reynolds (1994). Size accuracy of grain size classes was confirmed by Scanning Electron Microscopy. Fine clay dispersions (grain diameters <0.2 μm) were placed onto glass slides and oven-dried at 90°C for one hour immediately prior to XRD analysis. Analysis was performed at the Cornell Center for Materials Research with a Scintag Theta-Theta Diffractometer. Mineralogy was qualitatively assessed by interpreting diffractograms (after Chen, 1977; Moore and Reynolds, 1994; Bouchet *et al.,* 2000; Poppe *et al.,* 2001) and comparison with lab-run clay standards. When permissible by interpreted mineral assemblages and spectra, proportions of smectite, illite, kaolinite and chlorite were assessed by semi-quantitative means (e.g. by means of various ratios of peak areas from diffractograms), for comparative purposes rather than absolute values (Poppe *et al.,* 2001). The following tables summarize the mineralogic interpretations for 28 paleosols as well as two palustrine carbonates with pedogenic overprinting from Iglesia Basin strata interpolated as 8.77 – 5 Ma in age.

References:

Bouchet, A., Meunier, A., and Sardina, P, Clay Minerals: Crystal structure X-ray diffraction identification, Bull. Centre Rech. Elf Exploration Production, Memoir 23, 136 p.

Chen, P-Y, 1977, Table of key lines in X-ray powder diffraction patterns of minerals in clays and associated rocks: Indiana Geological Survey, 67 p.

Moore, D.M. and Reynolds, R.C., Jr., 1997, X-Ray Diffraction and the Identification and Analysis of Clay Minerals, 2nd Ed: Oxford University Press, New York, 332 p.

Poppe, L.J., Paskevich, V.F., Hathaway, J.C., and Blackwood, D.S., 2001, A Laboratory Manual for X-Ray Powder Diffraction: U.S. Geological Survey Open-File Report 01- 041, http://pubs.usgs.gov/of/of01-041/index.htm

Table C.1: X-Ray diffraction peak intensities and interpreted mineralogy for Iglesia Basin paleosols and palustrine carbonates. Ages are assigned by linear interpolation to magnetostratigraphy (see Figures 2.18 through 2.22).

Sample	**Section**	**Classification**	**Age (Ma)**	**Main peaks (Angstroms)**	**Mineralogy** (uncertain in parentheses)
BR03-6	Tudcum	Alfisol	~5	15.231, 10.029, 7.139, 4.991, 3.552	smectite, illite, kaolinite
BR03-32	Iglesias	Aridisol	6.13	12.661, 10.079, 7.114, 5.015, 3.325	mica-montmorillonite regular 6:4, illite (kaolinite)
BR03-29	Iglesias	Aridisol	6.17	14.679, 10.130, 7.114, 4.978, 3.319	smectite, illite, chlorite
BR03-13	Cerro Blanco	Alfisol	6.3	16.338, 10.130, 7.064, 5.003, 3.540, 3.303	smectite, illite, chlorite
BR03-14	E of Arroyo Iglesia	Inceptisol	6.3	15.231, 10.029, 7.089, 5.003, 3.540	smectite, illite, chlorite
Iglesia 4	Angualasto	palustrine limestone	6.4	14.166, 10.130, 3.034	illite, calcite (chlorite)
Sol 5	Angualasto	Inceptisol	6.45	14.574, 9.883, 4.930, 3.270	smectite
BR03-39	Rodeo 1	Alfisol	6.5	15.006, 10.079, 7.139, 4.966, 3.325, 3.030	smectite, illite, (kaolinite)
BR04-35	Rodeo 1	Alfisol	6.5	14.804, 9.954, 7.087, 4.973, 3.547, 3.328	smectite, illite, chlorite
BR04-36	Rodeo 1	Alfisol	6.5	15.144, 10.120, 7.107, 4.997, 3.543, 3.325	smectite, illite, chlorite
BR03-12	Angualasto	Aridisol	6.6	15.371, 10.316, 5.074, 3.053	smectite, palygorskite, calcite
BR03-25	E of Achango	Inceptisol	6.7	15.231, 10.180, 5.052, 3.030	smectite, illite
BR02Sol 4-5	Angualasto	Aridisol	6.94	16.338, 10.130, 7.064, 5.003, 3.540, 3.303	smectite, illite, kaolinite
BR03-10	Angualasto	Aridisol	6.95	14.574, 9.931, 4.954	smectite, (illite)
BR03-9	Angualasto	Alfisol	6.96	15.006, 10.079, 7.139, 5.003	smectite, illite, kaolinite, calcite
Iglesia 2	Angualasto	palustrine limestone	7.7	13.240, 10.029, 7.114, 3.034	illite, kaolinite, calcite, (smectite)
BR03-3	Angualasto	Aridisol	7.8	14.574, 9.980, 7.114, 3.850, 3.330, 3.030 (2-0.5 micron)	smectite, illite, calcite, (kaolinite)
BR03-4	Angualasto	Aridisol	7.8	14.266, 9.648, 4.954, 2.999	smectite, laumontite
BR03-45	Rodeo 1	Aridisol	7.96	14.266, 10.079, 7.114, 4.978, 3.534, 3.319, 3.039	chlorite, illite
BR03-2	Angualasto	Aridisol	8	15.464, 10.079, 7.139, 5.003, 3.564, 3.034	smectite, illite, kaolinite, calcite (vermiculite)
BR03-19	Rodeo 2	Alfisol	8.19	15.231, 10.029, 7.139, 4.991, 3.540, 3.319	smectite, illite, kaolinite, calcite
BR03-37	Rodeo 1	Alfisol	8.21	14.266, 10.029, 7.089, 4.991, 4.726, 3.325	chlorite, illite
BR02Sol 1	Angualasto	Inceptisol	8.25	14.067, 10.079, 7.114, 5.003, 3.552	smectite, chlorite, illite
BR02Sol 2	Angualasto	Inceptisol	8.25	15.347, 10.029, 7.164. 5.015	smectite, illite, kaolinite
BR02Sol 3	Angualasto	Inceptisol	8.25	15.231, 10.079, 7.139, 4.991, 3.558, 3.330	smectite, illite, kaolinite
BR03-44	Rodeo 1	Alfisol	8.34	12.504, 10.079, 6.185, 3.034, 3.111	Na-montmorillonite, illite, calcite
BR03-16	Rodeo 2	Aridisol	8.75	14.786, 10.284, 5.040, 3.083	smectite, palygorskite
BR03-17	Rodeo 2	Aridisol	8.77	14.574, 10.180, 4.991, 3.319	smectite, illite
BR04-46	Angualasto	Alfisol	uncertain	12.762, 10.102, 7.169, 4.992, 3.577, 3.329, 3.108	smectite, illite, kaolinite
BR04-47	Angualasto	Alfisol	uncertain	15.111, 7.128, 5.043, 3.567, 3.315, 3.037	smectite, illite, kaolinite

Table C.2: Semi-quantitative assessment of clay mineral percentages for subset of Iglesia Basin paleosol samples, following methodology described in Poppe *et al.*, 2001.

Sample	Age (Ma)	% Smectite	% Illite	% Kaolinite	% Chlorite
BR03-6	5	71.2	26.9	1.9	0.0
BR03-13	6.3	71.6	25.9	0.0	2.6
BR03-14	6.3	73.6	22.0	4.4	0.0
Sol 5	6.45	75.5	23.8	0.7	0.0
BR03-39	6.5	77.4	21.5	0.0	1.1
BR04-36	6.5	80.6	17.9	0.0	1.5
BR03-25	6.7	83.5	16.5	0.0	0.0
BR03-10	6.95	40.0	56.9	0.0	3.1
BR03-9	6.96	83.7	16.3	0.0	0.0
BR03-45	7.96	0.0	33.8	0.0	66.2
BR03-2	8	79.6	19.4	1.1	0.0
BR03-19	8.19	40.1	54.3	0.0	5.6
BR03-37	8.21	0.0	37.5	0.0	62.5
Sol 1	8.25	63.8	29.4	0.0	6.8
Sol 2	8.25	75.3	20.2	4.5	0.0
Sol 3	8.25	75.3	22.5	2.2	0.0
BR03-17	8.77	65.2	34.8	0.0	0.0
	Mean:	62.1	28.2	0.9	8.8

APPENDIX D:

IGLESIA BASIN OUTCROP DESCRIPTIONS AND LITHOFACIES INTERPRETATIONS

The northern Iglesia basin margin is not well imaged in seismic: the northernmost profile (5321) exhibits some basement reflections and a thin Tertiary fill, correlated with N-S cross lines as seismic sequence 10. Fieldwork north of line 5321 provided new glimpses of strata in the extreme northern portions of the basin. Tertiary outcrops were located north of line 5321, near the towns of Colangüil and Maliman (see Figure 2.3). Near Maliman (S 29˚59' to 30°, W 69˚11'), a succession of greenish-brown conglomeratic channels and interbedded sheet sandstones up to 60 m thick are exposed. This coarse facies transitions gradually upsection into reddish sands and siltstones, some of which are calcic and oxidized argillic paleosols. Lithologically, the outcrops are reminiscent of 2-3 SB, exposures of which are roughly along-strike 7-10 km to the S in the Angualasto section. Approximately 10 km to the west and SW of Maliman, near the locality of Colangüil, are scant exposures of the youngest seismic sequences. An isolated outcrop (near S 30˚01', W 69˚16') consists of 30 m of cross-bedded coarse-grained arkosic sandstone with occasional conglomeratic lenses (Figure D.1A). Granitic boulders 30-40 cm in diameter are common in the outcrop and surrounding terraces, likely delivered from the Colangűil batholith to the NW (240 ± 10 Ma, Sato and Kawashita, 1988). Some of the sandstone beds are bright orange and form resistant benches from the cliff. The sediments are interpreted to reflect basin-margin alluvial deposits, with braided to unchannelized fluvial facies deposited under high-energy conditions. To the south (S 30° 03', W 69° 16'), similar arkosic sandstones and granitic conglomeratic channels were observed, alternating on the scale of 2-5 m (Figure D.1B). However, the strata are generally finer-grained than those to the north, and pedogenic, chemically reduced siltstones and fine sandstones

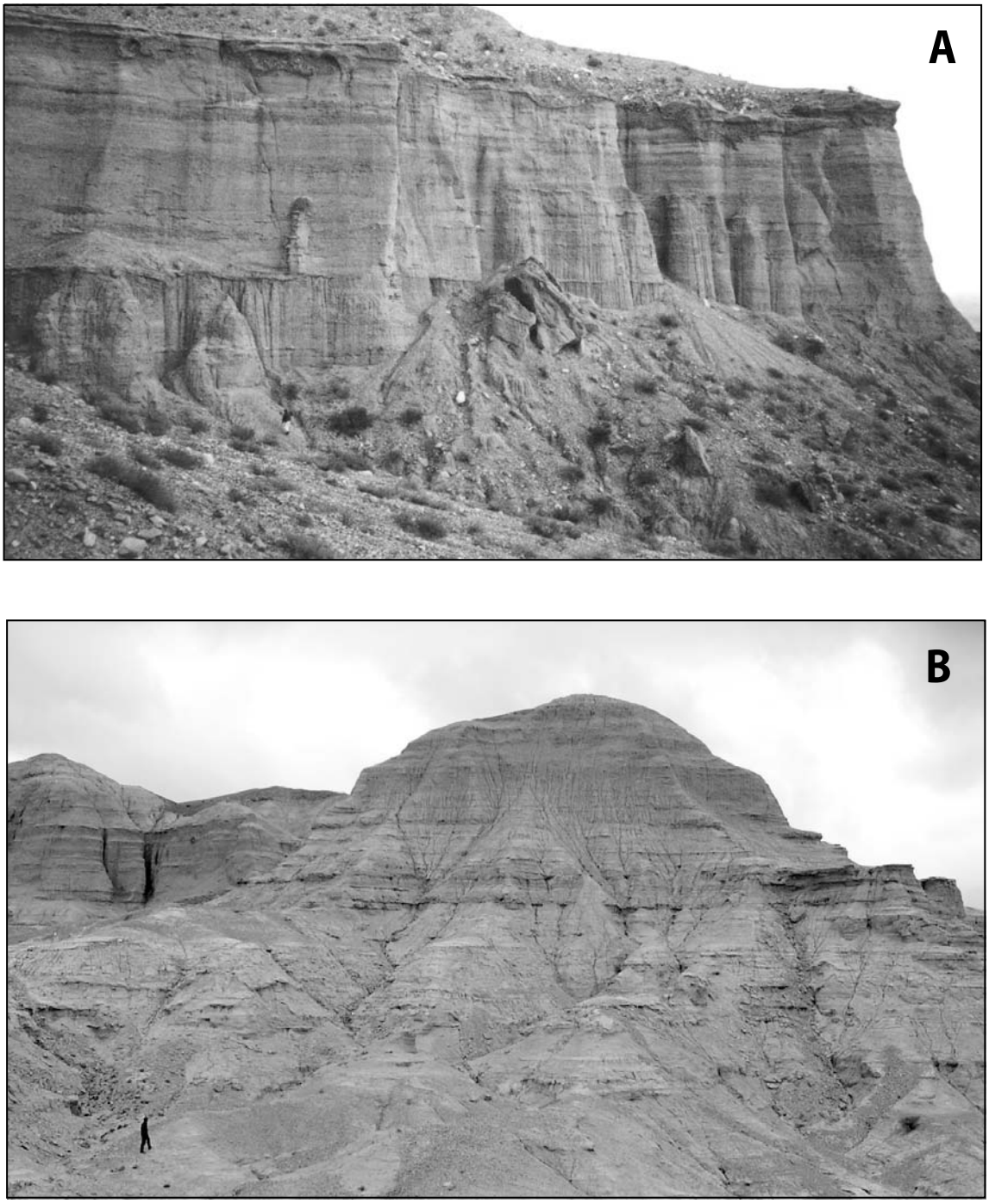

Figure D.1: A: Coarse granitic conglomerates and arkosic sandstones of sequence 10 exposed just SE of Colangüil (Fig. 2.5). B: More distal facies of sequence 10 exposed 5 km south of Colangüil.

are also present, as well as at least two laterally continuous carbonate beds. These exposures likely represent alluvial deposition more distal to those at Colangüil, permitting soils and isolated playa-lakes to accumulate on the ancient floodplains. Both outcrops likely represent sequence 10 or younger.

In contrast to the near-margin deposits near Colangüil, the youngest sequences are of markedly different facies near the basin center. Near Tudcum (Figure 2.3), approximately 260 m of interbedded green-to-brown mudstone, siltstone, and fine pinkish sandstone was measured (Ré et al., 2003). An ash collected from the section yielded a fission-track age of 5.1± 0.8 Ma (error bars providing upper limit of sequence deposition; Ré *et al*, 2003). Redoximorphic paleosols and thin (<15 cm) carbonate units are also present. Interbedded gypsum (several cm thick) is common, resulting in mound-like erosional landforms and bedding contacts, perhaps caused by volume change as a consequence of the gypsum-anhydrite transition. Soft-sediment deformation is also observed, suggesting periodic high rates of water-laden sedimentation. Variable water depths and salinities are suggested by the alternations in oxidation state, ripple marks, and evaporitic intergrowths.

In the canyon walls of the present day basin-center axial drainage (Rio Iglesia, Figure 2.3), strata exhibit evidence of alternating fluvial and floodplain processes during deposition of seismic sequence 4 (Figure D.2). Cycles of repeated lithologies are composed of grey-white mudstone-siltstone associated with thinly bedded, rippled, bench-forming brown sandstones, overlain by red intervals of pedogenic sandstone and capped with laminated redoximorphic silty paleosols. This cycle repeats at least five times in vertical succession and each cycle can be physically correlated over the length of the outcrop belt, approximately 5 km (Fig. D.2). Some ripple marks are unidirectionally oriented on average toward 101° (n=7). Where ripple crests were too eroded to distinguish lee from stoss sides, these were considered bidirectional and are

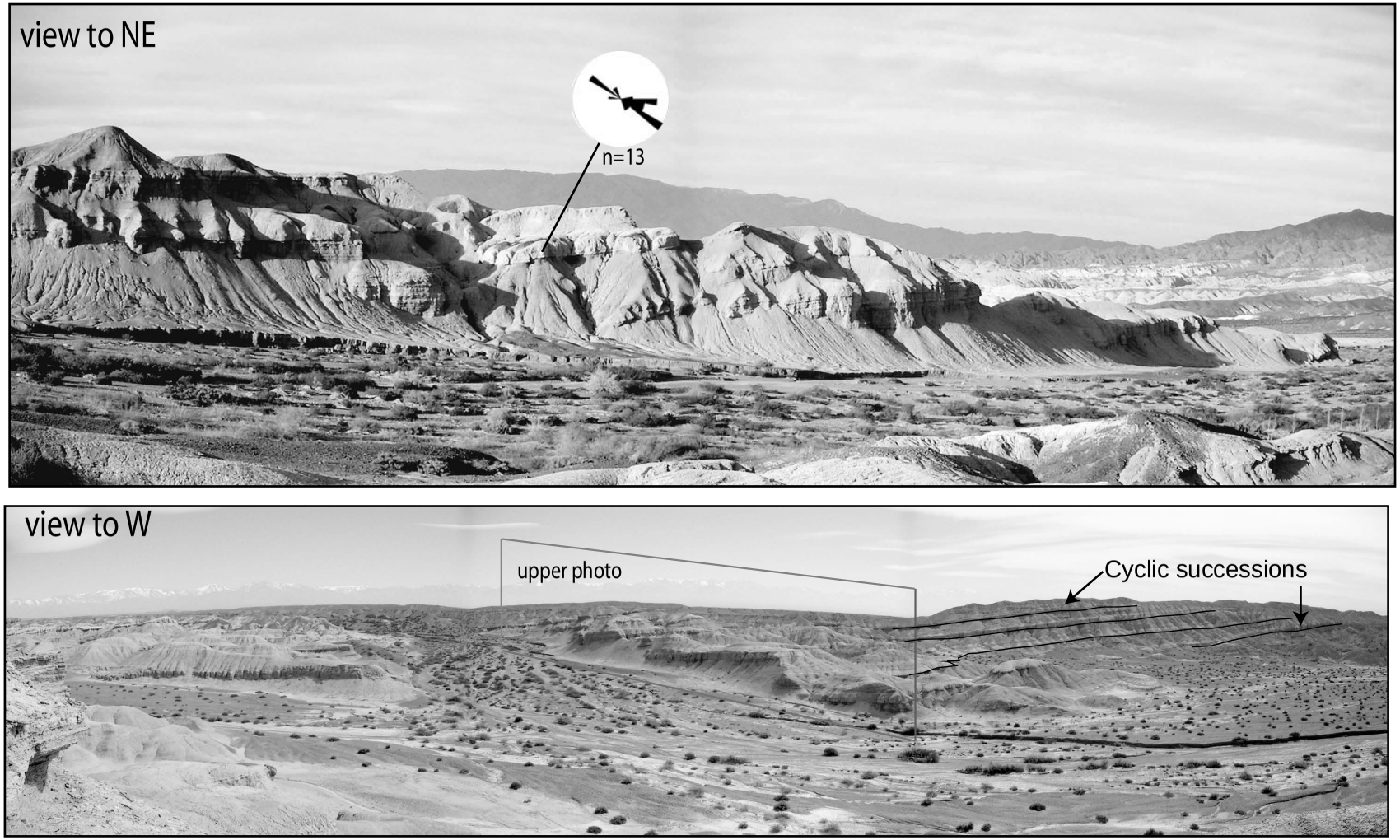

Figure D.2: Repetition of floodplain pedogenic and fluvial avulsion sediments along modern-day Arroyo Iglesia axial drainage (stratigraphic sections in Figure 2.21).

oriented NW-SE (n=6). Interestingly, the paleosols uniformly lack carbonate accumulations and those in the upper cycles are reduced. This interval is interpreted to represent periodic fluvial overflow onto poorly-drained floodplains of the ancestral axial drainage.

The great variety of nonmarine sediments in Iglesia Basin may be summarized in terms of their architectural elements and lithofacies. In Table D.1, the dominant observed lithogies, sedimentary structures and three-dimensional geometries (where discernible) for each observed sequence are listed and classified (after Miall, 1978, 1985). Based on the lithofacies assemblages and major fluvial architectural elements, general depositional interpretations can be made. The general fining upward motif noted by Beer (1989) is supported. Alluvial fan conglomerates are overlain by fluvial sandstones and overbank siltstones, the latter becoming dominant in the youngest sequences. Flow regime is generally low, and correspondingly planar deposits dominate.

In Table D.2, measured paleocurrent directions, general provenance and interpreted environmental energy are summarized, the latter based on lithofacies interpretation, sediment transport energy and rates of accumulation and pedogenesis (Beer, 1989; Ré *et al.*, 2003; this study). As the outcrop belts are in basin-central to distal (with respect to the Frontal Cordillera) positions and the distance from the western margin to the outcrop depocenters was increasing during the interval from Sequence 2 through 7 (see onlap map, Fig. 2.10), the inferred decrease in energy may reflect the natural waning of the sediment transport system or a long-scale decrease in discharge. However, an increase in energy in inferred across the 4-5 Sequence boundary, on the basis of cessation of mature paleosols, and the appearance of trough-crossbedded sandstones, a granitic boulder horizon (5 m above the SB) and abundant soft-sediment deformation features, all suggesting higher rates of sedimentation.

Table D.1: Lithofacies and architectural classification (after Miall, 1977;1985) and interpreted depositional environments for Iglesia Basin stratigraphic sequences.

Sequence	Lithofacies and Code (Miall, 1978)	Sedimentary Structures	Geometries	Architectural Elements (Miall, 1985)	Interpretation
10 or 11	Sand, silt, mud (Fl) massive, crudely bedded gravel (Gm) Pebbly to very coarse sand (Sh)	Fine lamination, very small ripples Horzontal lamination; soft sediment deformation	sheet and lens	Overbank fines (OF) Gravel bars and bedforms (GB)	Proximal: lag deposits or longitudinal bars; distal: overbank and backswamp
9	N/A	N/A	N/A	N/A	N/A
8	Sand,very fine to pebbly (Sh) Sand silt,mud (Fl) Carbonate (P)	Horizontal lamination Fine lamination pedogenic features, rootlets, burrows	sheet, blanket	Laminated sand sheets (LS) Overbank fines (OF)	Planar flow regime fluvial; Overbank deposits
7	Carbonate (P) Silt,mud (Fsc)	pedogenic features Laminated to massive	interbedded with sandy bedforms	Overbank fines (OF) Sandy bedforms (SB)	Overbank and backswamp deposits; paleosols.
6	Very fine to coarse sand (Sh) Carbonate (P)	Horizontal lamination pedogenic features, rootlets, burrows	sheet, blanket	Laminated sand sheets (LS)	Planar flow regime fluvial; backswamp ponds
5	Medium to v. coarse sand (St) Very fine to coarse sand (Sh) carbonate (P)	Groupled trough crossbeds Horizontal lamination; flaser bedding pedogenic features	concave-up erosional bases	Sandy bedforms (SB) Channels (CH)	Planar (lower) flow regime fluvial; overbank deposits
4	Medium to v. coarse sand (St) Silt,mud (Fsc) Sand, silt, mud (Fl) carbonate (P)	Solitary and grouped trough crossbeds Laminated Fine lamination, very small ripples pedogenic features, rootlets, burrows	interbedded with sandy bedforms	Sandy bedforms (SB) Overbank fines (OF)	Lower flow regime fluvial; overbank and waning flood deposits; paleosols.
3	gravel, stratified (Gt) Very fine to coarse sand (Sh) carbonate (P)	Trough crossbeds Horizontal lamination pedogenic features	sheet, crevasse splays	Sandy bedforms (SB)	Channel fills, sheet sands and overbank deposits Palustrine limestones
2	massive, crudely bedded gravel (Gm) gravel, stratified (Gt) Medium to v. coarse sand (St) carbonate (P)	imbricated clasts, graded bedding Trough crossbeds grouped trough crossbeds rootlets, burrows	tabular interbedded bodies multistorey sheets Highly variable erosional bases.	Gravel bars and bedforms (GB) Channels (CH)	proximal to distal alluvial fan; lag and sieve deposits; minor channel fills and palustrine limestones
1	massive, matrix supported gravel (Gms) Ignimbrite*	Graded bedding Graded bedding	sheet	Sediment gravity flows (SG)	Ashfall deposits, flows

Table D.2: Provenance information (after Beer, 1989; Re *et al*., 2003, this study) and interpreted environmental energy for Iglesia Basin stratigraphic sequences.

Sequence	Paleocurrent direction	Dominant provenance	Environmental energy
10 or 11	variable	Frontal Cordillera (Colanguil)	distal* proximal*
9	N/A	*Unknown*	?
8	N/A	*Unknown*	
7	N/A	Frontal Cordillera	
6	variable	Frontal Cordillera	
5	variable, mean to NE (n=20)	Frontal Cordillera (Colanguil)	
4	SE (n=13)	Frontal Cordillera	
3	N/A	Frontal Cordillera	
2	Base: to SE (n=31); Top: N-S (n=8)	Precordillera	
1		Frontal Cordillera	
			Low **High**

**defined by outcrop position (see Appendix D)*

Interestingly, decrease of depositional energy still generally holds for sequences 7 and higher, despite the fact that the basin became restricted to the west of the El Tigre Fault system (Fig 2.3) during deposition of these sequences. The locally coarser (e.g. higher-enegry) alluvial deposits near Colangüil (discussed above) are interpreted t o represent proximity to the Colangüil batholith and northwestern basin margin.

Finally, a note of caution for field geologists conducting reconnaissance with increasing dependence on remote sensory (satellite) images: we noted many disparities between the satellite images and actual outcrops. Images from two NASA satellite missions were utilized for fieldwork: Landsat-4's Thematic Mapper (TM, 30 m ground resolution) and Terra's Advanced Spaceborne Thermal Emission and Reflection Radiometer (ASTER, 15-90 m ground resolution). Because of the dominantly vertical incidence angle direction of the satellites' instruments, many cliff-face outcrops were not recognized because the satellite only recorded their terrace cover. These near-vertical outcrops often reveal the most stratigraphic detail owing to their relatively unweathered surfaces. In contrast, the limited spatial resolution of the satellite instruments means that some areas with similar spectral characteristics to the sedimentary units appear as outcrops when in fact they are not. In Iglesia Basin, most outcrops are covered with several centimeters of smectite derived from weathering, making it difficult to distinguish areas of outcrop from abandoned Recent floodplains. Improved ground resolution and oblique view imagery will likely diminish these concerns, but remote sensing-based mapping should still be "ground-truthed" because of the abovementioned likelihood of misinterpretation and incomplete imaging.

References:

Beer, J.A.., 1989, Magnetic polarity stratigraphy and depositional environments of the Bermejo Basin, and seismic stratigraphy of the Iglesia Basin, Central Andes: Ph.D. Dissertation, Cornell University, Ithaca, NY, 195 p.

Miall, A.D., 1978, Lithofacies types and vertical profile models in braided river deposits: a summary *in* Miall, A.D., ed., Fluvial Sedimentology, Canadian Soc. Petroleum Geology, Memoir 5., p. 597-604.

Miall, A.D., 1985, Architectural-element analysis: a new method of facies analysis applied to fluvial deposits: Earth-Science Reviews, Vol. 22, p. 261-308.

Ré, G.H., Jordan, T.E., and Kelley, S., 2003, Cronologia y paleogeografia del Teriario de la cuenca intermontana de Iglesia septentrional, Andes de San Juan, Argentina: Revista de la Asociación Geológica Argentina, v. 58, p. 31-48.

Sato, A. M., and Kawashita, K., 1988, Edad Rb-Sr de la ultima intrusion del batolito de Colangűil, Provincia de San Juan, *Asociaciacion Geologica Argentina*, Rev. XLIII (3), 415-418.

APPENDIX E:

PALEOMAGNETIC DATA FOR MOGNA AND EL CORRAL FORMATIONS, LOMAS DE LAS TAPIAS, SAN JUAN PROVINCE, ARGENTINA

The following pages (Table E.1) list the data obtained from incremental thermal demagnetization analysis of 137 samples collected from fine-grained Late Miocene-Pliocene strata outcropping at Lomas de Las Tapias, Departamento de Ullúm, San Juan Province, Argentina.

Analysis was conducted at the University of Pittsburgh Paleomagnetic Laboratory, 2004-2006. A three-axis 2-G cryogenic superconducting rock magnetometer (SRM) with an automated sample handler system was utilized in the magnetically shielded lab (maximum field <300 nT). Natural remanent magnetism (NRM) for each sample was recorded first (listed at ambient room temperature, or T=20°), after which was applied a thermal demagnetization sequence (T=200°, 400°, 450°, 500°, 550°, and 600°C) to each sample using a large-capacity furnace with shielded (<4 nT) cooling area. Samples were heated in quartz boats for one hour and cooled for an additional hour prior to analysis.

The magnetometer control scripts and data presentation as Zidjerveld, Equal area, and intensity decay diagrams utilized custom-coded Macintosh software. Well-established Fortran codes from the United States Geological Survey's Paleomagnetics Laboratory were used for subsequent data reduction and formatting.

Sample	Inclination	Declination		Intensity	Moment		Temp (°C)
A1A-1	I=+19.5	D=324.9	R= 30.00	J=2.89,-4	M=2.89,-4	MM=0.05	T20
A1A-1	I=+13.7	D=309.1	R= 30.00	J=2.63,-4	M=2.63,-4	MM=0.05	T200
A1A-1	I=+16.6	D=312.5	R= 30.00	J=1.17,-4	M=1.17,-4	MM=0.05	T400
A1A-1	I=+21.5	D=322.0	R= 30.00	J=9.51,-5	M=9.51,-5	MM=0.05	T450
A1A-1	I=+31.6	D=315.8	R= 30.00	J=7.93,-5	M=7.93,-5	MM=0.05	T500
A1A-1	I=+33.9	D=330.6	R= 30.00	J=5.05,-5	M=5.05,-5	MM=0.05	T550
A1A-1	I=+29.0	D=312.0	R= 30.00	J=2.24,-5	M=2.24,-5	MM=0.05	T600
A1B-1	I=+29.6	D=319.0	R= 30.00	J=4.42,-4	M=4.42,-4	MM=0.05	T20
A1B-1	I=+17.4	D=303.8	R= 30.00	J=5.19,-4	M=5.19,-4	MM=0.05	T200
A1B-1	I=+17.8	D=309.4	R= 30.00	J=2.58,-4	M=2.58,-4	MM=0.05	T400
A1B-1	I=+16.7	D=304.3	R= 30.00	J=2.30,-4	M=2.30,-4	MM=0.05	T450
A1B-1	I=+26.0	D=297.1	R= 30.00	J=1.76,-4	M=1.76,-4	MM=0.05	T500
A1B-1	I=+32.6	D=309.1	R= 30.00	J=1.43,-4	M=1.43,-4	MM=0.05	T550
A1B-1	I=+31.5	D=288.7	R= 30.00	J=9.48,-5	M=9.48,-5	MM=0.05	T600
A1C-1	I=+32.0	D=319.0	R= 30.00	J=3.43,-4	M=3.43,-4	MM=0.05	T20
A1C-1	I=+28.8	D=309.7	R= 30.00	J=3.38,-4	M=3.38,-4	MM=0.05	T200
A1C-1	I=+26.7	D=303.9	R= 30.00	J=1.56,-4	M=1.56,-4	MM=0.05	T400
A1C-1	I= +4.5	D=311.7	R= 30.00	J=1.26,-4	M=1.26,-4	MM=0.05	T450
A1C-1	I=+21.8	D=297.4	R= 30.00	J=1.18,-4	M=1.18,-4	MM=0.05	T500
A1C-1	I=+25.5	D=302.2	R= 30.00	J=8.48,-5	M=8.48,-5	MM=0.05	T550
A1C-1	I=+38.0	D=298.1	R= 30.00	J=5.78,-5	M=5.78,-5	MM=0.05	T600
A1D-1	I=+13.8	D=342.3	R= 30.00	J=1.33,-4	M=1.33,-4	MM=0.05	T20
A1D-1	I=+19.3	D=321.4	R= 30.00	J=1.39,-4	M=1.39,-4	MM=0.05	T200
A1D-1	I=+23.0	D=312.0	R= 30.00	J=6.54,-5	M=6.54,-5	MM=0.05	T400
A1D-1	I=+28.7	D=309.3	R= 30.00	J=4.37,-5	M=4.37,-5	MM=0.05	T450
A1D-1	I=+11.8	D=271.4	R= 30.00	J=7.34,-5	M=7.34,-5	MM=0.05	T500
A1D-1	I=+44.0	D=230.6	R= 30.00	J=5.62,-5	M=5.62,-5	MM=0.05	T550
A1D-1	I=+71.9	D=359.0	R= 30.00	J=1.40,-5	M=1.40,-5	MM=0.05	T600
A2A-1	I=-31.3	D= 4.4	R= 30.00	J=3.14,-4	M=3.14,-4	MM=0.05	T20
A2A-1	I= -0.8	D=352.6	R= 30.00	J=6.46,-5	M=6.46,-5	MM=0.05	T200
A2A-1	I=-32.2	D= 30.1	R= 30.00	J=1.73,-5	M=1.73,-5	MM=0.05	T400
A2A-1	I= +1.8	D= 68.8	R= 30.00	J=2.14,-5	M=2.14,-5	MM=0.05	T450
A2A-1	I=+68.8	D= 0.3	R= 30.00	J=4.32,-5	M=4.32,-5	MM=0.05	T500
A2A-1	I=+33.3	D= 50.7	R= 30.00	J=3.90,-5	M=3.90,-5	MM=0.05	T550
A2A-1	I=+65.0	D=338.7	R= 30.00	J=3.83,-5	M=3.83,-5	MM=0.05	T600
A2B-1	I=-42.9	D=354.4	R= 30.00	J=3.80,-4	M=3.80,-4	MM=0.05	T20
A2B-1	I= -0.5	D=289.4	R= 30.00	J=1.09,-4	M=1.09,-4	MM=0.05	T200
A2B-1	I= -2.5	D=264.2	R= 30.00	J=7.48,-5	M=7.48,-5	MM=0.05	T400
A2B-1	I=+11.6	D=246.4	R= 30.00	J=9.13,-5	M=9.13,-5	MM=0.05	T450
A2B-1	I=+47.3	D=255.7	R= 30.00	J=7.93,-5	M=7.93,-5	MM=0.05	T500
A2B-1	I=+41.5	D=264.2	R= 30.00	J=7.44,-5	M=7.44,-5	MM=0.05	T550
A2B-1	I=+72.7	D=358.7	R= 30.00	J=6.27,-5	M=6.27,-5	MM=0.05	T600
A2-1	I= +5.4	D=340.1	R= 30.00	J=6.24,-4	M=6.24,-4	MM=0.05	T20
A2-1	I=+57.5	D=266.3	R= 30.00	J=3.45,-4	M=3.45,-4	MM=0.05	T200
A2-1	I=+51.7	D=254.1	R= 30.00	J=2.12,-4	M=2.12,-4	MM=0.05	T400
A2-1	I=+52.3	D=240.9	R= 30.00	J=1.61,-4	M=1.61,-4	MM=0.05	T450
A2-1	I=+63.1	D=265.0	R= 30.00	J=2.08,-4	M=2.08,-4	MM=0.05	T500
A2-1	I=+68.2	D=242.7	R= 30.00	J=1.58,-4	M=1.58,-4	MM=0.05	T550
A2-1	I=+77.2	D=330.8	R= 30.00	J=1.28,-4	M=1.28,-4	MM=0.05	T600
A2D-1	I=-17.3	D=335.0	R= 30.00	J=6.87,-4	M=6.87,-4	MM=0.05	T20
A2D-1	I=+45.6	D=266.2	R= 30.00	J=3.93,-4	M=3.93,-4	MM=0.05	T200

A2D-1	I=+47.8	D=260.5	R= 30.00	J=2.18,-4	M=2.18,-4	MM=0.05	T400
A2D-1	I=+40.8	D=246.6	R= 30.00	J=1.89,-4	M=1.89,-4	MM=0.05	T450
A2D-1	I=+58.4	D=273.3	R= 30.00	J=2.51,-4	M=2.51,-4	MM=0.05	T500
A2D-1	I=+59.0	D=260.9	R= 30.00	J=2.03,-4	M=2.03,-4	MM=0.05	T550
A2D-1	I=+70.5	D=257.8	R= 30.00	J=1.14,-4	M=1.14,-4	MM=0.05	T600
A3A-1	I=-54.2	D=338.5	R= 30.00	J=3.36,-4	M=3.36,-4	MM=0.05	T20
A3A-1	I=-68.3	D=335.2	R= 30.00	J=8.20,-5	M=8.20,-5	MM=0.05	T200
A3A-1	I=-52.8	D=358.6	R= 30.00	J=6.36,-5	M=6.36,-5	MM=0.05	T400
A3A-1	I=-60.7	D=337.3	R= 30.00	J=4.83,-5	M=4.83,-5	MM=0.05	T450
A3A-1	I=-73.2	D= 37.8	R= 30.00	J=3.70,-5	M=3.70,-5	MM=0.05	T500
A3A-1	I=+27.8	D=209.7	R= 30.00	J=5.50,-5	M=5.50,-5	MM=0.05	T550
A3A-1	I=+34.6	D=207.4	R= 30.00	J=5.91,-5	M=5.91,-5	MM=0.05	T600
A3B-1	I=-35.0	D=335.5	R= 30.00	J=5.23,-4	M=5.23,-4	MM=0.05	T20
A3B-1	I=-52.6	D=358.1	R= 30.00	J=1.54,-4	M=1.54,-4	MM=0.05	T200
A3B-1	I=+63.0	D=235.9	R= 30.00	J=1.22,-4	M=1.22,-4	MM=0.05	T400
A3B-1	I=+67.8	D=240.5	R= 30.00	J=9.26,-5	M=9.26,-5	MM=0.05	T450
A3B-1	I=-14.9	D= 90.1	R= 30.00	J=7.44,-5	M=7.44,-5	MM=0.05	T500
A3B-1	I=+31.2	D=207.0	R= 30.00	J=7.40,-5	M=7.40,-5	MM=0.05	T550
A3B-1	I=+45.8	D= 95.8	R= 30.00	J=5.73,-5	M=5.73,-5	MM=0.05	T600
A3-1	I=+49.4	D=177.7	R= 30.00	J=3.95,-4	M=3.95,-4	MM=0.05	T20
A3-1	I=-52.9	D= 31.7	R= 30.00	J=2.14,-4	M=2.14,-4	MM=0.05	T200
A3-1	I=-52.1	D= 52.2	R= 30.00	J=1.17,-4	M=1.17,-4	MM=0.05	T400
A3-1	I=-45.3	D= 58.9	R= 30.00	J=8.22,-5	M=8.22,-5	MM=0.05	T450
A3-1	I=-43.1	D= 53.9	R= 30.00	J=6.56,-5	M=6.56,-5	MM=0.05	T500
A3-1	I=-74.6	D=130.1	R= 30.00	J=3.48,-5	M=3.48,-5	MM=0.05	T550
A3-1	I=-30.6	D= 4.5	R= 30.00	J=3.11,-5	M=3.11,-5	MM=0.05	T600
A4A-1	I=+43.0	D=277.9	R= 30.00	J=4.31,-4	M=4.31,-4	MM=0.05	T20
A4A-1	I=+50.4	D=257.7	R= 30.00	J=4.52,-4	M=4.52,-4	MM=0.05	T200
A4A-1	I=+47.9	D=257.4	R= 30.00	J=2.55,-4	M=2.55,-4	MM=0.05	T400
A4A-1	I=+47.7	D=265.5	R= 30.00	J=1.81,-4	M=1.81,-4	MM=0.05	T450
A4A-1	I=+57.1	D=272.8	R= 30.00	J=1.93,-4	M=1.93,-4	MM=0.05	T500
A4A-1	I=+52.1	D=267.3	R= 30.00	J=1.51,-4	M=1.51,-4	MM=0.05	T550
A4A-1	I=+56.7	D=297.3	R= 30.00	J=8.33,-5	M=8.33,-5	MM=0.05	T600
A4B-1	I=+51.1	D=269.5	R= 30.00	J=5.41,-4	M=5.41,-4	MM=0.05	T20
A4B-1	I=+49.1	D=252.2	R= 30.00	J=5.19,-4	M=5.19,-4	MM=0.05	T200
A4B-1	I=+48.7	D=247.4	R= 30.00	J=3.14,-4	M=3.14,-4	MM=0.05	T400
A4B-1	I=+43.4	D=246.2	R= 30.00	J=2.68,-4	M=2.68,-4	MM=0.05	T450
A4B-1	I=+50.2	D=248.1	R= 30.00	J=2.54,-4	M=2.54,-4	MM=0.05	T500
A4B-1	I=+57.3	D=257.2	R= 30.00	J=2.14,-4	M=2.14,-4	MM=0.05	T550
A4B-1	I=+59.2	D=259.2	R= 30.00	J=1.26,-4	M=1.26,-4	MM=0.05	T600
A4-1	I=+48.1	D=263.4	R= 30.00	J=3.04,-4	M=3.04,-4	MM=0.05	T20
A4-1	I=+41.0	D=232.1	R= 30.00	J=3.38,-4	M=3.38,-4	MM=0.05	T200
A4-1	I=+46.0	D=221.6	R= 30.00	J=1.81,-4	M=1.81,-4	MM=0.05	T400
A4-1	I=+45.6	D=228.6	R= 30.00	J=1.39,-4	M=1.39,-4	MM=0.05	T450
A4-1	I=+54.7	D=241.6	R= 30.00	J=1.40,-4	M=1.40,-4	MM=0.05	T500
A4-1	I=+65.2	D=247.8	R= 30.00	J=1.08,-4	M=1.08,-4	MM=0.05	T550
A4-1	I=+47.0	D=254.5	R= 30.00	J=7.81,-5	M=7.81,-5	MM=0.05	T600
A5A-1	I=+41.4	D=306.9	R= 30.00	J=1.96,-4	M=1.96,-4	MM=0.05	T20
A5A-1	I=+55.7	D=256.2	R= 30.00	J=2.17,-4	M=2.17,-4	MM=0.05	T200
A5A-1	I=+57.2	D=263.3	R= 30.00	J=1.33,-4	M=1.33,-4	MM=0.05	T400
A5A-1	I=+56.4	D=265.2	R= 30.00	J=1.17,-4	M=1.17,-4	MM=0.05	T450
A5A-1	I=+64.4	D=263.5	R= 30.00	J=8.20,-5	M=8.20,-5	MM=0.05	T500

A5A-1	I=+63.2	D=241.5	R= 30.00	J=1.00,-4	M=1.00,-4	MM=0.05	T550
A5A-1	I=+57.1	D=269.0	R= 30.00	J=3.89,-5	M=3.89,-5	MM=0.05	T600
A5B-1	I=+18.8	D=249.6	R= 30.00	J=6.40,-4	M=6.40,-4	MM=0.05	T20
A5B-1	I=+27.0	D=227.7	R= 30.00	J=6.71,-4	M=6.71,-4	MM=0.05	T200
A5B-1	I=+27.4	D=233.6	R= 30.00	J=3.45,-4	M=3.45,-4	MM=0.05	T400
A5B-1	I=+24.1	D=238.2	R= 30.00	J=2.90,-4	M=2.90,-4	MM=0.05	T450
A5B-1	I=+30.0	D=235.9	R= 30.00	J=2.36,-4	M=2.36,-4	MM=0.05	T500
A5B-1	I=+33.8	D=248.8	R= 30.00	J=2.22,-4	M=2.22,-4	MM=0.05	T550
A5B-1	I=+40.3	D=259.5	R= 30.00	J=7.93,-5	M=7.93,-5	MM=0.05	T600
A5-1	I=+52.0	D=276.7	R= 30.00	J=2.03,-4	M=2.03,-4	MM=0.05	T20
A5-1	I=+59.9	D=233.3	R= 30.00	J=2.43,-4	M=2.43,-4	MM=0.05	T200
A5-1	I=+50.1	D=227.7	R= 30.00	J=1.36,-4	M=1.36,-4	MM=0.05	T400
A5-1	I=+40.7	D=238.8	R= 30.00	J=1.07,-4	M=1.07,-4	MM=0.05	T450
A5-1	I=+45.0	D=231.3	R= 30.00	J=8.97,-5	M=8.97,-5	MM=0.05	T500
A5-1	I=+41.3	D=238.5	R= 30.00	J=1.23,-4	M=1.23,-4	MM=0.05	T550
A5-1	I=+56.0	D=245.8	R= 30.00	J=4.56,-5	M=4.56,-5	MM=0.05	T600
B1A-1	I=+33.5	D=357.7	R= 30.00	J=1.50,-3	M=1.50,-3	MM=0.05	T200
B1A-1	I=+33.6	D=359.3	R= 30.00	J=5.56,-4	M=5.56,-4	MM=0.05	T450
B1A-1	I=+31.9	D= 4.8	R= 30.00	J=3.80,-4	M=3.80,-4	MM=0.05	T500
B1A-1	I=+31.0	D=355.4	R= 30.00	J=2.87,-4	M=2.87,-4	MM=0.05	T550
B1A-1	I=+20.0	D= 3.8	R= 30.00	J=1.40,-4	M=1.40,-4	MM=0.05	T600
B1B-1	I=+44.8	D=177.9	R= 30.00	J=2.26,-3	M=2.26,-3	MM=0.05	T200
B1B-1	I=+43.8	D=177.7	R= 30.00	J=8.43,-4	M=8.43,-4	MM=0.05	T450
B1B-1	I=+43.1	D=175.5	R= 30.00	J=5.54,-4	M=5.54,-4	MM=0.05	T500
B1B-1	I=+43.4	D=176.7	R= 30.00	J=4.45,-4	M=4.45,-4	MM=0.05	T550
B1B-1	I=+18.4	D=169.7	R= 30.00	J=1.98,-4	M=1.98,-4	MM=0.05	T600
B1-1	I=+14.7	D= 10.1	R= 30.00	J=1.03,-3	M=1.03,-3	MM=0.05	T200
B1-1	I=+11.7	D= 6.1	R= 30.00	J=4.01,-4	M=4.01,-4	MM=0.05	T450
B1-1	I= +8.4	D= 4.3	R= 30.00	J=2.73,-4	M=2.73,-4	MM=0.05	T500
B1-1	I= +5.5	D= 7.4	R= 30.00	J=2.23,-4	M=2.23,-4	MM=0.05	T550
B1-1	I= -6.3	D= 13.4	R= 30.00	J=1.17,-4	M=1.17,-4	MM=0.05	T600
B1D-1	I=+34.2	D=343.6	R= 30.00	J=8.86,-4	M=8.86,-4	MM=0.05	T200
B1D-1	I=+35.7	D=340.8	R= 30.00	J=3.39,-4	M=3.39,-4	MM=0.05	T450
B1D-1	I=+28.5	D=348.0	R= 30.00	J=2.35,-4	M=2.35,-4	MM=0.05	T500
B1D-1	I=+31.2	D=344.0	R= 30.00	J=1.82,-4	M=1.82,-4	MM=0.05	T550
B1D-1	I=+22.2	D= 2.5	R= 30.00	J=1.22,-4	M=1.22,-4	MM=0.05	T600
B2A-1	I=+19.4	D=331.5	R= 30.00	J=6.25,-4	M=6.25,-4	MM=0.05	T200
B2A-1	I=+16.5	D=326.9	R= 30.00	J=3.62,-4	M=3.62,-4	MM=0.05	T450
B2A-1	I=+15.2	D=328.1	R= 30.00	J=2.47,-4	M=2.47,-4	MM=0.05	T500
B2A-1	I=+14.9	D=325.3	R= 30.00	J=2.17,-4	M=2.17,-4	MM=0.05	T550
B2A-1	I= +8.1	D=318.0	R= 30.00	J=1.12,-4	M=1.12,-4	MM=0.05	T600
B2B-1	I=+48.9	D=351.2	R= 30.00	J=9.13,-4	M=9.13,-4	MM=0.05	T200
B2B-1	I=+43.5	D=349.9	R= 30.00	J=5.08,-4	M=5.08,-4	MM=0.05	T450
B2B-1	I=+41.8	D=347.3	R= 30.00	J=3.48,-4	M=3.48,-4	MM=0.05	T500
B2B-1	I=+40.2	D=343.7	R= 30.00	J=2.84,-4	M=2.84,-4	MM=0.05	T550
B2B-1	I=+20.9	D=345.2	R= 30.00	J=1.37,-4	M=1.37,-4	MM=0.05	T600
B2-1	I=+37.6	D=303.7	R= 30.00	J=9.45,-4	M=9.45,-4	MM=0.05	T200
B2-1	I=+35.9	D=305.1	R= 30.00	J=5.66,-4	M=5.66,-4	MM=0.05	T450
B2-1	I=+34.7	D=297.9	R= 30.00	J=4.89,-4	M=4.89,-4	MM=0.05	T500
B2-1	I=+32.0	D=302.5	R= 30.00	J=3.50,-4	M=3.50,-4	MM=0.05	T550
B2-1	I=+20.5	D=289.8	R= 30.00	J=1.52,-4	M=1.52,-4	MM=0.05	T600
B2D-1	I=+44.4	D=323.1	R= 30.00	J=9.13,-4	M=9.13,-4	MM=0.05	T200

B2D-1	I=+39.5	D=319.8	R= 30.00	J=5.49,-4	M=5.49,-4	MM=0.05	T450
B2D-1	I=+48.4	D=313.9	R= 30.00	J=4.26,-4	M=4.26,-4	MM=0.05	T500
B2D-1	I=+39.8	D=316.1	R= 30.00	J=3.51,-4	M=3.51,-4	MM=0.05	T550
B2D-1	I=+35.3	D=313.9	R= 30.00	J=1.63,-4	M=1.63,-4	MM=0.05	T600
B3A-1	I=-78.4	D= 67.0	R= 30.00	J=5.22,-4	M=5.22,-4	MM=0.05	T200
B3A-1	I=-77.5	D= 73.2	R= 30.00	J=2.50,-4	M=2.50,-4	MM=0.05	T450
B3A-1	I=-78.8	D= 70.6	R= 30.00	J=2.32,-4	M=2.32,-4	MM=0.05	T500
B3A-1	I=-82.4	D= 83.3	R= 30.00	J=1.82,-4	M=1.82,-4	MM=0.05	T550
B3A-1	I=-76.7	D=221.4	R= 30.00	J=6.04,-5	M=6.04,-5	MM=0.05	T600
B3B-1	I=-65.0	D= 17.3	R= 30.00	J=4.21,-4	M=4.21,-4	MM=0.05	T200
B3B-1	I=-62.9	D= 39.3	R= 30.00	J=2.02,-4	M=2.02,-4	MM=0.05	T450
B3B-1	I=-61.3	D= 22.8	R= 30.00	J=1.78,-4	M=1.78,-4	MM=0.05	T500
B3B-1	I=-67.4	D= 18.4	R= 30.00	J=1.37,-4	M=1.37,-4	MM=0.05	T550
B3B-1	I=-82.4	D= 27.1	R= 30.00	J=5.94,-5	M=5.94,-5	MM=0.05	T600
B3-1	I=-69.9	D= 74.7	R= 30.00	J=1.01,-3	M=1.01,-3	MM=0.05	T200
B3-1	I=-71.1	D=102.1	R= 30.00	J=4.00,-4	M=4.00,-4	MM=0.05	T450
B3-1	I=-70.9	D= 87.4	R= 30.00	J=3.04,-4	M=3.04,-4	MM=0.05	T500
B3-1	I=-75.8	D= 82.7	R= 30.00	J=2.46,-4	M=2.46,-4	MM=0.05	T550
B3-1	I=-83.2	D= 56.2	R= 30.00	J=1.56,-4	M=1.56,-4	MM=0.05	T600
B3D-1	I=-48.5	D=122.4	R= 30.00	J=9.76,-4	M=9.76,-4	MM=0.05	T200
B3D-1	I=-63.8	D=116.6	R= 30.00	J=4.61,-4	M=4.61,-4	MM=0.05	T450
B3D-1	I=-65.8	D=108.3	R= 30.00	J=3.47,-4	M=3.47,-4	MM=0.05	T500
B3D-1	I=-68.8	D=110.9	R= 30.00	J=2.75,-4	M=2.75,-4	MM=0.05	T550
B3D-1	I=-79.7	D=118.9	R= 30.00	J=1.77,-4	M=1.77,-4	MM=0.05	T600
B4A-1	I=+65.4	D=266.4	R= 30.00	J=3.07,-4	M=3.07,-4	MM=0.05	T200
B4A-1	I=+68.1	D=265.8	R= 30.00	J=1.95,-4	M=1.95,-4	MM=0.05	T450
B4A-1	I=+61.1	D=275.8	R= 30.00	J=1.29,-4	M=1.29,-4	MM=0.05	T500
B4A-1	I=+67.5	D=279.2	R= 30.00	J=1.13,-4	M=1.13,-4	MM=0.05	T550
B4A-1	I= +3.5	D=248.3	R= 30.00	J=3.99,-5	M=3.99,-5	MM=0.05	T600
B4B-1	I=+60.8	D=287.2	R= 30.00	J=1.44,-4	M=1.44,-4	MM=0.05	T200
B4B-1	I=+56.7	D=263.3	R= 30.00	J=9.10,-5	M=9.10,-5	MM=0.05	T450
B4B-1	I=+52.7	D=278.8	R= 30.00	J=7.69,-5	M=7.69,-5	MM=0.05	T500
B4B-1	I=+48.2	D=259.2	R= 30.00	J=5.12,-5	M=5.12,-5	MM=0.05	T550
B4B-1	I=+17.2	D=264.7	R= 30.00	J=2.99,-5	M=2.99,-5	MM=0.05	T600
B4-1	I=+56.9	D=273.2	R= 30.00	J=1.42,-4	M=1.42,-4	MM=0.05	T200
B4-1	I=+53.9	D=279.3	R= 30.00	J=8.97,-5	M=8.97,-5	MM=0.05	T450
B4-1	I=+48.2	D=281.3	R= 30.00	J=7.30,-5	M=7.30,-5	MM=0.05	T500
B4-1	I=+37.2	D=260.8	R= 30.00	J=4.50,-5	M=4.50,-5	MM=0.05	T550
B4-1	I=+37.3	D=293.7	R= 30.00	J=2.88,-5	M=2.88,-5	MM=0.05	T600
B4D-1	I=+37.6	D=265.3	R= 30.00	J=9.69,-5	M=9.69,-5	MM=0.05	T200
B4D-1	I=+37.6	D=265.3	R= 30.00	J=9.69,-5	M=9.69,-5	MM=0.05	T400
B4D-1	I=+38.1	D=257.2	R= 30.00	J=5.03,-5	M=5.03,-5	MM=0.05	T450
B4D-1	I=+30.5	D=259.2	R= 30.00	J=4.61,-5	M=4.61,-5	MM=0.05	T500
B4D-1	I=+38.1	D=257.2	R= 30.00	J=5.03,-5	M=5.03,-5	MM=0.05	T500
B4D-1	I=+26.0	D=255.1	R= 30.00	J=3.75,-5	M=3.75,-5	MM=0.05	T550
B4D-1	I=+38.1	D=257.2	R= 30.00	J=5.03,-5	M=5.03,-5	MM=0.05	T550
B4D-1	I=+15.5	D=244.3	R= 30.00	J=2.75,-5	M=2.75,-5	MM=0.05	T600
B5A-1	I=+57.8	D=329.3	R= 30.00	J=6.02,-5	M=6.02,-5	MM=0.05	T400
B5A-1	I=+56.2	D=323.2	R= 30.00	J=5.55,-5	M=5.55,-5	MM=0.05	T450
B5A-1	I=+47.7	D=311.1	R= 30.00	J=4.23,-5	M=4.23,-5	MM=0.05	T500
B5A-1	I=+45.9	D=322.0	R= 30.00	J=3.53,-5	M=3.53,-5	MM=0.05	T550
B5A-1	I=-39.9	D=243.6	R= 30.00	J=1.30,-5	M=1.30,-5	MM=0.05	T600

B5B-1	I=+55.2	D=302.8	R= 30.00	J=5.25,-5	M=5.25,-5	MM=0.05	T400
B5B-1	I=+47.4	D=300.1	R= 30.00	J=4.42,-5	M=4.42,-5	MM=0.05	T450
B5B-1	I=+54.3	D=286.5	R= 30.00	J=4.44,-5	M=4.44,-5	MM=0.05	T500
B5B-1	I=+61.0	D=315.4	R= 30.00	J=2.69,-5	M=2.69,-5	MM=0.05	T550
B5B-1	I=-61.5	D=242.2	R= 30.00	J=9.60,-6	M=9.60,-6	MM=0.05	T600
B5-1	I=+57.2	D=307.1	R= 30.00	J=2.01,-4	M=2.01,-4	MM=0.05	T400
B5-1	I=+56.3	D=302.6	R= 30.00	J=1.75,-4	M=1.75,-4	MM=0.05	T450
B5-1	I=+54.5	D=303.5	R= 30.00	J=1.38,-4	M=1.38,-4	MM=0.05	T500
B5-1	I=+54.7	D=315.3	R= 30.00	J=9.67,-5	M=9.67,-5	MM=0.05	T550
B5-1	I=+48.7	D=275.8	R= 30.00	J=2.28,-5	M=2.28,-5	MM=0.05	T600
B5D-1	I=+45.3	D=296.5	R= 30.00	J=8.48,-5	M=8.48,-5	MM=0.05	T400
B5D-1	I=+41.8	D=290.0	R= 30.00	J=6.86,-5	M=6.86,-5	MM=0.05	T450
B5D-1	I=+36.4	D=285.2	R= 30.00	J=5.48,-5	M=5.48,-5	MM=0.05	T500
B5D-1	I=+39.2	D=262.2	R= 30.00	J=3.15,-5	M=3.15,-5	MM=0.05	T550
B5D-1	I=-53.4	D=187.0	R= 30.00	J=5.49,-6	M=5.49,-6	MM=0.05	T600
B6A-1	I=-38.4	D=188.6	R= 30.00	J=1.80,-4	M=1.80,-4	MM=0.05	T400
B6A-1	I=-40.1	D=194.4	R= 30.00	J=1.56,-4	M=1.56,-4	MM=0.05	T450
B6A-1	I=-42.4	D=194.1	R= 30.00	J=1.14,-4	M=1.14,-4	MM=0.05	T500
B6A-1	I=-41.9	D=184.6	R= 30.00	J=9.04,-5	M=9.04,-5	MM=0.05	T550
B6A-1	I=-52.9	D=200.7	R= 30.00	J=5.00,-5	M=5.00,-5	MM=0.05	T600
B6B-1	I=-48.7	D=178.7	R= 30.00	J=3.15,-4	M=3.15,-4	MM=0.05	T400
B6B-1	I=-41.7	D=181.6	R= 30.00	J=2.49,-4	M=2.49,-4	MM=0.05	T450
B6B-1	I=-41.2	D=186.3	R= 30.00	J=2.02,-4	M=2.02,-4	MM=0.05	T500
B6B-1	I=-52.5	D=188.8	R= 30.00	J=1.58,-4	M=1.58,-4	MM=0.05	T550
B6B-1	I=-47.7	D=189.6	R= 30.00	J=9.74,-5	M=9.74,-5	MM=0.05	T600
B6-1	I=-46.3	D=166.6	R= 30.00	J=2.56,-4	M=2.56,-4	MM=0.05	T400
B6-1	I=-46.4	D=167.6	R= 30.00	J=2.17,-4	M=2.17,-4	MM=0.05	T450
B6-1	I=-50.7	D=170.8	R= 30.00	J=1.73,-4	M=1.73,-4	MM=0.05	T500
B6-1	I=-56.2	D=167.4	R= 30.00	J=1.51,-4	M=1.51,-4	MM=0.05	T550
B6-1	I=-58.1	D=161.6	R= 30.00	J=8.76,-5	M=8.76,-5	MM=0.05	T600
B6D-1	I=-44.4	D=161.1	R= 30.00	J=3.01,-4	M=3.01,-4	MM=0.05	T400
B6D-1	I=-46.0	D=161.5	R= 30.00	J=2.69,-4	M=2.69,-4	MM=0.05	T450
B6D-1	I=-47.6	D=158.1	R= 30.00	J=2.12,-4	M=2.12,-4	MM=0.05	T500
B6D-1	I=-52.9	D=157.1	R= 30.00	J=1.80,-4	M=1.80,-4	MM=0.05	T550
B6D-1	I=-62.5	D=169.4	R= 30.00	J=1.02,-4	M=1.02,-4	MM=0.05	T600
B7A-1	I=-68.9	D=306.8	R= 30.00	J=4.24,-4	M=4.24,-4	MM=0.05	T400
B7A-1	I=-70.2	D=323.3	R= 30.00	J=3.56,-4	M=3.56,-4	MM=0.05	T450
B7A-1	I=-71.4	D=309.9	R= 30.00	J=2.98,-4	M=2.98,-4	MM=0.05	T500
B7A-1	I=-71.8	D=307.4	R= 30.00	J=2.31,-4	M=2.31,-4	MM=0.05	T550
B7A-1	I=-74.4	D=316.3	R= 30.00	J=1.20,-4	M=1.20,-4	MM=0.05	T600
B7B-1	I=-68.0	D=298.1	R= 30.00	J=3.67,-4	M=3.67,-4	MM=0.05	T400
B7B-1	I=-68.0	D=300.0	R= 30.00	J=3.20,-4	M=3.20,-4	MM=0.05	T450
B7B-1	I=-64.1	D=288.2	R= 30.00	J=2.91,-4	M=2.91,-4	MM=0.05	T500
B7B-1	I=-68.7	D=287.2	R= 30.00	J=2.18,-4	M=2.18,-4	MM=0.05	T550
B7B-1	I=-65.8	D=280.6	R= 30.00	J=8.53,-5	M=8.53,-5	MM=0.05	T600
B7-1	I=-71.7	D=267.3	R= 30.00	J=2.59,-4	M=2.59,-4	MM=0.05	T400
B7-1	I=-78.8	D=277.5	R= 30.00	J=2.19,-4	M=2.19,-4	MM=0.05	T450
B7-1	I=-78.1	D=308.1	R= 30.00	J=1.86,-4	M=1.86,-4	MM=0.05	T500
B7-1	I=-81.6	D=297.5	R= 30.00	J=1.32,-4	M=1.32,-4	MM=0.05	T550
B7-1	I=-81.5	D=314.2	R= 30.00	J=7.30,-5	M=7.30,-5	MM=0.05	T600
B7D-1	I=-63.9	D=298.4	R= 30.00	J=4.16,-4	M=4.16,-4	MM=0.05	T400
B7D-1	I=-67.2	D=303.5	R= 30.00	J=3.64,-4	M=3.64,-4	MM=0.05	T450

B7D-1	I=-66.5	D=293.2	R= 30.00	J=2.98,-4	M=2.98,-4	MM=0.05	T500
B7D-1	I=-67.8	D=310.8	R= 30.00	J=2.20,-4	M=2.20,-4	MM=0.05	T550
B7D-1	I=-71.6	D=324.6	R= 30.00	J=8.63,-5	M=8.63,-5	MM=0.05	T600
B8A-1	I=+43.8	D=330.1	R= 30.00	J=9.99,-5	M=9.99,-5	MM=0.05	T400
B8A-1	I=+31.1	D=323.4	R= 30.00	J=8.90,-5	M=8.90,-5	MM=0.05	T450
B8A-1	I=-16.2	D= 10.9	R= 30.00	J=3.40,-5	M=3.40,-5	MM=0.05	T500
B8A-1	I=-23.1	D=337.6	R= 30.00	J=5.76,-5	M=5.76,-5	MM=0.05	T550
B8A-1	I=-38.1	D=167.3	R= 30.00	J=6.16,-5	M=6.16,-5	MM=0.05	T600
B8B-1	I=+28.3	D= 11.9	R= 30.00	J=1.81,-4	M=1.81,-4	MM=0.05	T400
B8B-1	I=+18.3	D=346.8	R= 30.00	J=1.49,-4	M=1.49,-4	MM=0.05	T450
B8B-1	I= +0.5	D= 1.1	R= 30.00	J=9.69,-5	M=9.69,-5	MM=0.05	T500
B8B-1	I=-47.6	D= 11.4	R= 30.00	J=1.01,-4	M=1.01,-4	MM=0.05	T550
B8B-1	I=-31.3	D= 45.9	R= 30.00	J=5.22,-5	M=5.22,-5	MM=0.05	T600
B8-1	I=-62.1	D=263.6	R= 30.00	J=7.75,-5	M=7.75,-5	MM=0.05	T400
B8-1	I=-67.5	D=173.2	R= 30.00	J=7.70,-5	M=7.70,-5	MM=0.05	T450
B8-1	I=-67.2	D= 93.6	R= 30.00	J=1.16,-4	M=1.16,-4	MM=0.05	T500
B8-1	I=-53.1	D= 93.5	R= 30.00	J=1.48,-4	M=1.48,-4	MM=0.05	T550
B8-1	I=-65.4	D=170.6	R= 30.00	J=1.78,-4	M=1.78,-4	MM=0.05	T600
B8D-1	I=-23.3	D=340.6	R= 30.00	J=6.35,-5	M=6.35,-5	MM=0.05	T400
B8D-1	I=+21.3	D=337.6	R= 30.00	J=8.64,-5	M=8.64,-5	MM=0.05	T450
B8D-1	I=-32.5	D=340.6	R= 30.00	J=5.66,-5	M=5.66,-5	MM=0.05	T500
B8D-1	I=-44.3	D= 94.9	R= 30.00	J=3.41,-5	M=3.41,-5	MM=0.05	T550
B8D-1	I=-54.2	D= 91.4	R= 30.00	J=1.50,-4	M=1.50,-4	MM=0.05	T600
U11A-1	I=+39.6	D=239.2	R= 30.00	J=3.26,-4	M=3.26,-4	MM=0.05	T20
U11A-1	I=+42.6	D=224.4	R= 30.00	J=3.41,-4	M=3.41,-4	MM=0.05	T200
U11A-1	I=+48.9	D=220.6	R= 30.00	J=2.35,-4	M=2.35,-4	MM=0.05	T400
U11A-1	I=+47.9	D=219.6	R= 30.00	J=1.92,-4	M=1.92,-4	MM=0.05	T450
U11A-1	I=+45.0	D=218.6	R= 30.00	J=1.46,-4	M=1.46,-4	MM=0.05	T500
U11A-1	I=+49.3	D=222.4	R= 30.00	J=1.45,-4	M=1.45,-4	MM=0.05	T550
U11A-1	I=+60.1	D=247.9	R= 30.00	J=6.55,-5	M=6.55,-5	MM=0.05	T600
U12B-1	I=+19.1	D=356.1	R= 30.00	J=7.83,-4	M=7.83,-4	MM=0.05	T20
U12B-1	I=+14.7	D=344.5	R= 30.00	J=7.49,-4	M=7.49,-4	MM=0.05	T200
U12B-1	I=+14.9	D=347.4	R= 30.00	J=5.01,-4	M=5.01,-4	MM=0.05	T400
U12B-1	I=+13.6	D=356.6	R= 30.00	J=4.29,-4	M=4.29,-4	MM=0.05	T450
U12B-1	I=+12.3	D=355.6	R= 30.00	J=3.17,-4	M=3.17,-4	MM=0.05	T500
U12B-1	I=+21.8	D=358.6	R= 30.00	J=2.54,-4	M=2.54,-4	MM=0.05	T550
U12B-1	I=+31.7	D=357.8	R= 30.00	J=1.28,-4	M=1.28,-4	MM=0.05	T600
U13B-1	I= -4.8	D=336.5	R= 30.00	J=4.34,-4	M=4.34,-4	MM=0.05	T20
U13B-1	I=-25.2	D=308.1	R= 30.00	J=5.43,-4	M=5.43,-4	MM=0.05	T200
U13B-1	I=-26.1	D=306.6	R= 30.00	J=3.64,-4	M=3.64,-4	MM=0.05	T400
U13B-1	I=-27.7	D=302.4	R= 30.00	J=3.22,-4	M=3.22,-4	MM=0.05	T450
U13B-1	I=-27.6	D=301.3	R= 30.00	J=2.49,-4	M=2.49,-4	MM=0.05	T500
U13B-1	I=-16.8	D=282.6	R= 30.00	J=1.49,-4	M=1.49,-4	MM=0.05	T550
U13B-1	I= +6.8	D=275.6	R= 30.00	J=6.64,-5	M=6.64,-5	MM=0.05	T600
U14-1	I=-38.6	D=333.5	R= 30.00	J=7.93,-4	M=7.93,-4	MM=0.05	T20
U14-1	I=-28.5	D=320.0	R= 30.00	J=5.64,-4	M=5.64,-4	MM=0.05	T200
U14-1	I=-24.8	D=317.6	R= 30.00	J=3.03,-4	M=3.03,-4	MM=0.05	T400
U14-1	I=-25.5	D=317.1	R= 30.00	J=2.66,-4	M=2.66,-4	MM=0.05	T450
U14-1	I=-24.0	D=318.2	R= 30.00	J=1.96,-4	M=1.96,-4	MM=0.05	T500
U14-1	I=-19.6	D=318.2	R= 30.00	J=1.73,-4	M=1.73,-4	MM=0.05	T550
U14-1	I= -0.5	D=312.9	R= 30.00	J=9.57,-5	M=9.57,-5	MM=0.05	T600
U14PB-1	I= -1.0	D=295.4	R= 30.00	J=3.91,-4	M=3.91,-4	MM=0.05	T20

U14PB-1	I=+22.4	D=277.9	R= 30.00	J=2.95,-4	M=2.95,-4	MM=0.05	T200
U14PB-1	I=+20.8	D=265.2	R= 30.00	J=1.43,-4	M=1.43,-4	MM=0.05	T400
U14PB-1	I=+17.5	D=272.9	R= 30.00	J=1.60,-4	M=1.60,-4	MM=0.05	T450
U14PB-1	I=+38.1	D=265.0	R= 30.00	J=1.12,-4	M=1.12,-4	MM=0.05	T500
U14PB-1	I=+42.9	D=241.2	R= 30.00	J=1.14,-4	M=1.14,-4	MM=0.05	T550
U14PB-1	I=+31.6	D=275.1	R= 30.00	J=7.34,-5	M=7.34,-5	MM=0.05	T600
U15A-1	I=+21.6	D=263.3	R= 30.00	J=4.36,-4	M=4.36,-4	MM=0.05	T20
U15A-1	I=+35.4	D=258.6	R= 30.00	J=4.36,-4	M=4.36,-4	MM=0.05	T200
U15A-1	I=+36.1	D=255.8	R= 30.00	J=2.37,-4	M=2.37,-4	MM=0.05	T400
U15A-1	I=+33.9	D=254.5	R= 30.00	J=1.84,-4	M=1.84,-4	MM=0.05	T450
U15A-1	I=+39.8	D=251.0	R= 30.00	J=1.87,-4	M=1.87,-4	MM=0.05	T500
U15A-1	I=+40.0	D=251.6	R= 30.00	J=1.59,-4	M=1.59,-4	MM=0.05	T550
U15A-1	I=+40.4	D=243.7	R= 30.00	J=1.16,-4	M=1.16,-4	MM=0.05	T600
U16-1	I=-36.8	D=264.7	R= 30.00	J=7.43,-4	M=7.43,-4	MM=0.05	T20
U16-1	I=-54.0	D=267.0	R= 30.00	J=2.81,-4	M=2.81,-4	MM=0.05	T200
U16-1	I=-57.1	D=260.7	R= 30.00	J=1.54,-4	M=1.54,-4	MM=0.05	T400
U16-1	I=-57.9	D=263.6	R= 30.00	J=1.24,-4	M=1.24,-4	MM=0.05	T450
U16-1	I=-28.4	D=220.3	R= 30.00	J=6.50,-5	M=6.50,-5	MM=0.05	T500
U16-1	I= +7.3	D=201.9	R= 30.00	J=5.80,-5	M=5.80,-5	MM=0.05	T550
U16-1	I=+38.0	D=186.5	R= 30.00	J=6.10,-5	M=6.10,-5	MM=0.05	T600
U17B-1	I= -4.5	D=321.1	R= 30.00	J=3.29,-4	M=3.29,-4	MM=0.05	T20
U17B-1	I=+41.4	D=290.6	R= 30.00	J=2.49,-4	M=2.49,-4	MM=0.05	T200
U17B-1	I=+44.2	D=291.7	R= 30.00	J=1.39,-4	M=1.39,-4	MM=0.05	T400
U17B-1	I=+41.5	D=295.5	R= 30.00	J=1.15,-4	M=1.15,-4	MM=0.05	T450
U17B-1	I=+43.9	D=284.2	R= 30.00	J=1.47,-4	M=1.47,-4	MM=0.05	T500
U17B-1	I=+55.1	D=267.5	R= 30.00	J=1.13,-4	M=1.13,-4	MM=0.05	T550
U17B-1	I=+49.1	D=290.4	R= 30.00	J=8.04,-5	M=8.04,-5	MM=0.05	T600
U18B-1	I=-57.6	D=197.0	R= 30.00	J=9.66,-4	M=9.66,-4	MM=0.05	T20
U18B-1	I=-66.1	D=193.5	R= 30.00	J=3.98,-4	M=3.98,-4	MM=0.05	T200
U18B-1	I=-72.5	D=181.6	R= 30.00	J=8.12,-5	M=8.12,-5	MM=0.05	T400
U18B-1	I=-71.3	D=214.7	R= 30.00	J=6.72,-5	M=6.72,-5	MM=0.05	T450
U18B-1	I=+76.5	D=203.3	R= 30.00	J=7.21,-5	M=7.21,-5	MM=0.05	T500
U18B-1	I=+67.0	D=310.7	R= 30.00	J=7.89,-5	M=7.89,-5	MM=0.05	T550
U18B-1	I=+48.2	D=216.2	R= 30.00	J=7.73,-5	M=7.73,-5	MM=0.05	T600
U19B-1	I=-42.9	D= 4.1	R= 30.00	J=9.32,-4	M=9.32,-4	MM=0.05	T20
U19B-1	I=-42.1	D= 17.7	R= 30.00	J=4.91,-4	M=4.91,-4	MM=0.05	T200
U19B-1	I=-37.2	D= 25.1	R= 30.00	J=2.19,-4	M=2.19,-4	MM=0.05	T400
U19B-1	I=-48.2	D= 22.4	R= 30.00	J=2.03,-4	M=2.03,-4	MM=0.05	T450
U19B-1	I=-13.2	D= 26.1	R= 30.00	J=6.89,-5	M=6.89,-5	MM=0.05	T500
U19B-1	I= +1.2	D= 42.6	R= 30.00	J=8.13,-5	M=8.13,-5	MM=0.05	T550
U19B-1	I=+64.7	D=329.2	R= 30.00	J=6.43,-5	M=6.43,-5	MM=0.05	T600
U1B-1	I=-25.1	D= 26.3	R= 30.00	J=4.54,-4	M=4.54,-4	MM=0.05	T200
U1B-1	I=-21.7	D= 23.2	R= 30.00	J=2.66,-4	M=2.66,-4	MM=0.05	T400
U1B-1	I=-25.3	D= 13.1	R= 30.00	J=2.21,-4	M=2.21,-4	MM=0.05	T450
U1B-1	I=-25.8	D= 26.7	R= 30.00	J=1.71,-4	M=1.71,-4	MM=0.05	T500
U1B-1	I= -8.2	D=357.3	R= 30.00	J=1.14,-4	M=1.14,-4	MM=0.05	T550
U1B-1	I=+33.1	D=359.7	R= 30.00	J=3.32,-5	M=3.32,-5	MM=0.05	T600
U1PB-1	I=-32.3	D= 59.7	R= 30.00	J=9.40,-5	M=9.40,-5	MM=0.05	T20
U1PB-1	I=-51.0	D=280.7	R= 30.00	J=4.74,-5	M=4.74,-5	MM=0.05	T200
U1PB-1	I=-55.0	D=215.9	R= 30.00	J=1.96,-5	M=1.96,-5	MM=0.05	T400
U1PB-1	I=-56.5	D=219.5	R= 30.00	J=3.19,-5	M=3.19,-5	MM=0.05	T450
U1PB-1	I=-24.7	D=184.6	R= 30.00	J=2.35,-5	M=2.35,-5	MM=0.05	T500

U1PB-1	I=+28.1	D=230.7	R= 30.00	J=3.23,-5	M=3.23,-5	MM=0.05	T550
U1PB-1	I= +5.7	D=226.7	R= 30.00	J=1.34,-5	M=1.34,-5	MM=0.05	T600
U20A-1	I=+63.3	D=281.1	R= 30.00	J=1.80,-4	M=1.80,-4	MM=0.05	T20
U20A-1	I=+63.9	D=218.9	R= 30.00	J=2.11,-4	M=2.11,-4	MM=0.05	T200
U20A-1	I=+56.9	D=235.2	R= 30.00	J=1.04,-4	M=1.04,-4	MM=0.05	T400
U20B-1	I=+71.9	D=180.7	R= 30.00	J=5.56,-4	M=5.56,-4	MM=0.05	T20
U20B-1	I=+57.0	D=192.1	R= 30.00	J=7.01,-4	M=7.01,-4	MM=0.05	T200
U20B-1	I=+60.3	D=168.3	R= 30.00	J=3.54,-4	M=3.54,-4	MM=0.05	T400
U20B-1	I=+59.0	D=168.7	R= 30.00	J=2.67,-4	M=2.67,-4	MM=0.05	T450
U20B-1	I=+69.3	D=177.7	R= 30.00	J=2.22,-4	M=2.22,-4	MM=0.05	T500
U20B-1	I=+75.8	D=169.7	R= 30.00	J=1.71,-4	M=1.71,-4	MM=0.05	T550
U20B-1	I=+82.0	D=132.4	R= 30.00	J=9.44,-5	M=9.44,-5	MM=0.05	T600
U20-1	I=+56.8	D= 24.5	R= 30.00	J=2.43,-4	M=2.43,-4	MM=0.05	T200
U20-1	I=+60.1	D= 20.2	R= 30.00	J=1.13,-4	M=1.13,-4	MM=0.05	T400
U20-1	I=+46.8	D= 17.4	R= 30.00	J=8.45,-5	M=8.45,-5	MM=0.05	T450
U20-1	I=+71.2	D= 39.9	R= 30.00	J=7.30,-5	M=7.30,-5	MM=0.05	T500
U20-1	I=+89.6	D= 8.3	R= 30.00	J=5.34,-5	M=5.34,-5	MM=0.05	T550
U20-1	I=+60.1	D=186.7	R= 30.00	J=2.46,-5	M=2.46,-5	MM=0.05	T600
U20D-1	I=+54.3	D= 50.1	R= 30.00	J=1.27,-4	M=1.27,-4	MM=0.05	T20
U21A-1	I=+53.1	D= 85.1	R= 30.00	J=3.23,-5	M=3.23,-5	MM=0.05	T200
U21A-1	I=+57.0	D= 53.6	R= 30.00	J=2.68,-5	M=2.68,-5	MM=0.05	T200
U21A-1	I=+46.7	D= 58.8	R= 30.00	J=1.83,-5	M=1.83,-5	MM=0.05	T400
U2A-1	I=+33.1	D=242.2	R= 30.00	J=3.35,-4	M=3.35,-4	MM=0.05	T20
U2A-1	I=+49.3	D=197.7	R= 30.00	J=3.70,-4	M=3.70,-4	MM=0.05	T200
U2A-1	I=+52.7	D=199.1	R= 30.00	J=2.27,-4	M=2.27,-4	MM=0.05	T400
U2A-1	I=+48.0	D=195.8	R= 30.00	J=1.92,-4	M=1.92,-4	MM=0.05	T450
U2A-1	I=+46.7	D=191.1	R= 30.00	J=1.55,-4	M=1.55,-4	MM=0.05	T500
U2A-1	I=+39.0	D=188.2	R= 30.00	J=1.63,-4	M=1.63,-4	MM=0.05	T550
U2A-1	I=+43.0	D=180.6	R= 30.00	J=8.73,-5	M=8.73,-5	MM=0.05	T600
U2PA-1	I=+33.5	D=139.6	R= 30.00	J=7.77,-4	M=7.77,-4	MM=0.05	T20
U2PA-1	I=+32.5	D=144.7	R= 30.00	J=6.04,-4	M=6.04,-4	MM=0.05	T200
U2PA-1	I=+28.6	D=148.0	R= 30.00	J=3.22,-4	M=3.22,-4	MM=0.05	T400
U2PA-1	I=+24.6	D=156.4	R= 30.00	J=2.76,-4	M=2.76,-4	MM=0.05	T450
U2PA-1	I=+30.3	D=146.6	R= 30.00	J=2.13,-4	M=2.13,-4	MM=0.05	T500
U2PA-1	I=+31.6	D=146.7	R= 30.00	J=2.04,-4	M=2.04,-4	MM=0.05	T500
U2PA-1	I=+34.4	D=153.1	R= 30.00	J=1.76,-4	M=1.76,-4	MM=0.05	T550
U2PA-1	I=+46.2	D=161.6	R= 30.00	J=1.02,-4	M=1.02,-4	MM=0.05	T600
U3PA-1	I=-55.5	D=292.7	R= 30.00	J=1.32,-3	M=1.32,-3	MM=0.05	T20
U3PA-1	I=-69.8	D=289.0	R= 30.00	J=1.16,-3	M=1.16,-3	MM=0.05	T200
U3PA-1	I=-75.1	D=309.0	R= 30.00	J=6.68,-4	M=6.68,-4	MM=0.05	T400
U3PA-1	I=-75.3	D=296.5	R= 30.00	J=5.68,-4	M=5.68,-4	MM=0.05	T450
U3PA-1	I=-76.6	D=313.2	R= 30.00	J=4.22,-4	M=4.22,-4	MM=0.05	T500
U3PA-1	I=-73.7	D=349.0	R= 30.00	J=2.71,-4	M=2.71,-4	MM=0.05	T550
U3PA-1	I=-68.6	D= 66.2	R= 30.00	J=5.80,-5	M=5.80,-5	MM=0.05	T600
U4P-1	I=+74.0	D=252.0	R= 30.00	J=8.22,-4	M=8.22,-4	MM=0.05	T20
U4P-1	I=+62.6	D=327.9	R= 30.00	J=2.66,-4	M=2.66,-4	MM=0.05	T200
U4P-1	I=+25.3	D=354.0	R= 30.00	J=9.45,-5	M=9.45,-5	MM=0.05	T400
U4P-1	I= +0.9	D= 2.7	R= 30.00	J=7.93,-5	M=7.93,-5	MM=0.05	T450
U4P-1	I= -5.6	D= 14.3	R= 30.00	J=4.09,-5	M=4.09,-5	MM=0.05	T500
U4P-1	I=+27.6	D=333.7	R= 30.00	J=6.30,-5	M=6.30,-5	MM=0.05	T550
U4P-1	I=+51.8	D=349.2	R= 30.00	J=2.11,-5	M=2.11,-5	MM=0.05	T600
U5B-1	I=+11.2	D=283.1	R= 30.00	J=1.81,-4	M=1.81,-4	MM=0.05	T20

U5B-1	I=+34.7	D=244.6	R= 30.00	J=2.55,-4	M=2.55,-4	MM=0.05	T200
U5B-1	I=+36.1	D=244.1	R= 30.00	J=1.61,-4	M=1.61,-4	MM=0.05	T400
U5B-1	I=+37.7	D=245.0	R= 30.00	J=1.34,-4	M=1.34,-4	MM=0.05	T450
U5B-1	I=+36.1	D=244.1	R= 30.00	J=1.61,-4	M=1.61,-4	MM=0.05	T500
U5B-1	I=+36.0	D=229.5	R= 30.00	J=1.09,-4	M=1.09,-4	MM=0.05	T550
U5B-1	I=+56.5	D=233.5	R= 30.00	J=7.23,-5	M=7.23,-5	MM=0.05	T600
U5PA-1	I=-37.3	D=306.9	R= 30.00	J=1.27,-3	M=1.27,-3	MM=0.05	T20
U5PA-1	I=-36.7	D=297.2	R= 30.00	J=1.26,-3	M=1.26,-3	MM=0.05	T200
U5PA-1	I=-36.2	D=296.4	R= 30.00	J=7.94,-4	M=7.94,-4	MM=0.05	T400
U5PA-1	I=-36.0	D=298.0	R= 30.00	J=6.10,-4	M=6.10,-4	MM=0.05	T450
U5PA-1	I=-37.2	D=296.4	R= 30.00	J=4.88,-4	M=4.88,-4	MM=0.05	T500
U5PA-1	I=-35.4	D=289.9	R= 30.00	J=3.11,-4	M=3.11,-4	MM=0.05	T550
U5PA-1	I=-20.8	D=279.2	R= 30.00	J=1.53,-4	M=1.53,-4	MM=0.05	T600
U6A-1	I=+46.4	D=230.6	R= 30.00	J=8.52,-4	M=8.52,-4	MM=0.05	T20
U6A-1	I=+48.1	D=214.6	R= 30.00	J=8.28,-4	M=8.28,-4	MM=0.05	T200
U6A-1	I=+47.5	D=212.7	R= 30.00	J=4.62,-4	M=4.62,-4	MM=0.05	T400
U6A-1	I=+40.5	D=211.9	R= 30.00	J=3.75,-4	M=3.75,-4	MM=0.05	T450
U6A-1	I=+42.3	D=221.2	R= 30.00	J=3.03,-4	M=3.03,-4	MM=0.05	T500
U6A-1	I=+44.1	D=223.8	R= 30.00	J=2.77,-4	M=2.77,-4	MM=0.05	T550
U6A-1	I=+48.9	D=228.2	R= 30.00	J=1.27,-4	M=1.27,-4	MM=0.05	T600
U7-1	I=+75.9	D= 45.6	R= 30.00	J=1.55,-4	M=1.55,-4	MM=0.05	T20
U7-1	I=+42.4	D=246.5	R= 30.00	J=1.32,-4	M=1.32,-4	MM=0.05	T200
U7-1	I=+30.9	D=236.6	R= 30.00	J=6.39,-5	M=6.39,-5	MM=0.05	T400
U7-1	I=+26.7	D=238.2	R= 30.00	J=4.56,-5	M=4.56,-5	MM=0.05	T450
U7-1	I=+23.7	D=245.7	R= 30.00	J=3.71,-5	M=3.71,-5	MM=0.05	T500
U7-1	I=+51.1	D=250.1	R= 30.00	J=4.98,-5	M=4.98,-5	MM=0.05	T550
U7-1	I=+58.7	D=221.9	R= 30.00	J=4.08,-5	M=4.08,-5	MM=0.05	T600
U8-1	I=+57.1	D=292.5	R= 30.00	J=2.11,-4	M=2.11,-4	MM=0.05	T20
U8-1	I=+81.2	D=285.7	R= 30.00	J=2.36,-4	M=2.36,-4	MM=0.05	T200
U8-1	I=+86.4	D= 19.8	R= 30.00	J=1.35,-4	M=1.35,-4	MM=0.05	T400
U8-1	I=+83.4	D=266.5	R= 30.00	J=1.17,-4	M=1.17,-4	MM=0.05	T450
U8-1	I=+83.1	D=260.7	R= 30.00	J=9.62,-5	M=9.62,-5	MM=0.05	T500
U8-1	I=+74.4	D=189.2	R= 30.00	J=1.06,-4	M=1.06,-4	MM=0.05	T550
U8-1	I=+73.7	D=212.4	R= 30.00	J=5.03,-5	M=5.03,-5	MM=0.05	T600
U9B-1	I=-77.3	D=265.4	R= 30.00	J=1.28,-3	M=1.28,-3	MM=0.05	T20
U9B-1	I=-70.9	D=243.7	R= 30.00	J=1.28,-3	M=1.28,-3	MM=0.05	T200
U9B-1	I=-69.2	D=241.0	R= 30.00	J=7.16,-4	M=7.16,-4	MM=0.05	T400
U9B-1	I=-68.3	D=244.6	R= 30.00	J=6.23,-4	M=6.23,-4	MM=0.05	T450
U9B-1	I=-70.6	D=238.2	R= 30.00	J=4.56,-4	M=4.56,-4	MM=0.05	T500
U9B-1	I=-65.8	D=230.2	R= 30.00	J=3.75,-4	M=3.75,-4	MM=0.05	T550
U9B-1	I=-62.6	D=236.2	R= 30.00	J=2.12,-4	M=2.12,-4	MM=0.05	T600
Y9B-1	I=-62.6	D=236.2	R= 30.00	J=2.12,-4	M=2.12,-4	MM=0.05	T600

U1_A-1	I=-11.5	D=350.9	R= 30.00	J=9.24,-5	M=9.24,-5	MM=0.05	T0
U1_A-1	I=+42.2	D=246.5	R= 30.00	J=7.68,-5	M=7.68,-5	MM=0.05	T200
U1_A-1	I=+23.9	D=282.7	R= 30.00	J=3.76,-5	M=3.76,-5	MM=0.05	T400
U1_A-1	I=+63.9	D=267.9	R= 30.00	J=4.71,-5	M=4.71,-5	MM=0.05	T450
U1_A-1	I=+30.3	D=268.8	R= 30.00	J=2.54,-5	M=2.54,-5	MM=0.05	T500
U1_A-1	I=+21.7	D=103.5	R= 30.00	J=1.89,-5	M=1.89,-5	MM=0.05	T550
U1_A-1	I=-22.4	D=302.3	R= 30.00	J=1.92,-5	M=1.92,-5	MM=0.05	T600
U1_-1	I=+40.1	D=335.4	R= 30.00	J=7.48,-5	M=7.48,-5	MM=0.05	T0
U1_-1	I=-31.6	D=307.7	R= 30.00	J=4.10,-5	M=4.10,-5	MM=0.05	T200
U1_-1	I=-24.5	D=267.2	R= 30.00	J=1.41,-5	M=1.41,-5	MM=0.05	T400
U1_-1	I=-51.7	D=249.2	R= 30.00	J=1.18,-5	M=1.18,-5	MM=0.05	T450
U1_-1	I=+46.7	D=321.4	R= 30.00	J=1.30,-5	M=1.30,-5	MM=0.05	T500
U1_-1	I= +1.7	D= 15.0	R= 30.00	J=1.51,-5	M=1.51,-5	MM=0.05	T550
U10A-1	I= -2.2	D=138.4	R= 30.00	J=3.92,-4	M=3.92,-4	MM=0.05	T0
U10A-1	I=-16.4	D=155.6	R= 30.00	J=4.41,-4	M=4.41,-4	MM=0.05	T200
U10A-1	I=-19.2	D=158.6	R= 30.00	J=1.94,-4	M=1.94,-4	MM=0.05	T400
U10A-1	I= -3.8	D=147.7	R= 30.00	J=2.04,-4	M=2.04,-4	MM=0.05	T450
U10A-1	I= -6.7	D=142.7	R= 30.00	J=1.41,-4	M=1.41,-4	MM=0.05	T500
U10A-1	I=-12.3	D=151.0	R= 30.00	J=1.02,-4	M=1.02,-4	MM=0.05	T550
U10A-1	I= -2.7	D=144.5	R= 30.00	J=5.85,-5	M=5.85,-5	MM=0.05	T600
U10-1	I= -5.6	D=173.1	R= 30.00	J=9.80,-4	M=9.80,-4	MM=0.05	T0
U10-1	I= -2.5	D=161.5	R= 30.00	J=6.73,-4	M=6.73,-4	MM=0.05	T200
U10-1	I= -1.3	D=159.2	R= 30.00	J=3.03,-4	M=3.03,-4	MM=0.05	T400
U10-1	I= -0.2	D=162.1	R= 30.00	J=2.83,-4	M=2.83,-4	MM=0.05	T450
U10-1	I= -7.9	D=162.0	R= 30.00	J=1.86,-4	M=1.86,-4	MM=0.05	T500
U10-1	I= +8.2	D=162.0	R= 30.00	J=1.24,-4	M=1.24,-4	MM=0.05	T550
U11B-1	I= -4.8	D=333.6	R= 30.00	J=1.95,-3	M=1.95,-3	MM=0.05	T0
U11B-1	I=+10.2	D=332.5	R= 30.00	J=5.83,-4	M=5.83,-4	MM=0.05	T200
U11B-1	I=+16.3	D=294.5	R= 30.00	J=1.95,-4	M=1.95,-4	MM=0.05	T400
U11B-1	I=+32.1	D=291.0	R= 30.00	J=1.84,-4	M=1.84,-4	MM=0.05	T450
U11B-1	I=+36.6	D=279.2	R= 30.00	J=1.34,-4	M=1.34,-4	MM=0.05	T500
U11B-1	I=+49.0	D=268.3	R= 30.00	J=1.07,-4	M=1.07,-4	MM=0.05	T550
U11B-1	I=+42.8	D=253.5	R= 30.00	J=6.44,-5	M=6.44,-5	MM=0.05	T600
U11-1	I=+44.7	D= 77.1	R= 30.00	J=3.45,-4	M=3.45,-4	MM=0.05	T0
U11-1	I=+20.5	D= 83.0	R= 30.00	J=3.72,-4	M=3.72,-4	MM=0.05	T200
U11-1	I=+31.9	D= 87.2	R= 30.00	J=1.93,-4	M=1.93,-4	MM=0.05	T400
U11-1	I=+34.7	D= 92.9	R= 30.00	J=2.09,-4	M=2.09,-4	MM=0.05	T450
U11-1	I=+39.5	D= 91.6	R= 30.00	J=1.55,-4	M=1.55,-4	MM=0.05	T500
U11-1	I=+31.5	D= 91.2	R= 30.00	J=1.17,-4	M=1.17,-4	MM=0.05	T550
U12A-1	I=+55.1	D=243.9	R= 30.00	J=1.91,-4	M=1.91,-4	MM=0.05	T0
U12A-1	I=+35.3	D=207.1	R= 30.00	J=2.53,-4	M=2.53,-4	MM=0.05	T200
U12A-1	I=+40.2	D=204.6	R= 30.00	J=1.52,-4	M=1.52,-4	MM=0.05	T400
U12A-1	I=+37.8	D=206.0	R= 30.00	J=1.32,-4	M=1.32,-4	MM=0.05	T450
U12A-1	I=+19.0	D=212.1	R= 30.00	J=9.72,-5	M=9.72,-5	MM=0.05	T500
U12A-1	I=+37.8	D=217.5	R= 30.00	J=6.50,-5	M=6.50,-5	MM=0.05	T550
U12A-1	I=+42.9	D=196.2	R= 30.00	J=4.34,-5	M=4.34,-5	MM=0.05	T600
U12-1	I=-20.7	D=103.5	R= 30.00	J=3.68,-4	M=3.68,-4	MM=0.05	T0
U12-1	I=-23.2	D=113.7	R= 30.00	J=3.66,-4	M=3.66,-4	MM=0.05	T200
U12-1	I=-12.9	D=118.3	R= 30.00	J=1.69,-4	M=1.69,-4	MM=0.05	T400
U12-1	I=-26.7	D=122.9	R= 30.00	J=1.99,-4	M=1.99,-4	MM=0.05	T450
U12-1	I=-28.6	D=117.4	R= 30.00	J=1.12,-4	M=1.12,-4	MM=0.05	T500
U12-1	I=-17.6	D=123.6	R= 30.00	J=9.05,-5	M=9.05,-5	MM=0.05	T550

U13A-1	I=-34.6	D=355.3	R= 30.00	J=1.21,-4	M=1.21,-4	MM=0.05	T0
U13A-1	I=-27.2	D=278.7	R= 30.00	J=1.73,-4	M=1.73,-4	MM=0.05	T200
U13A-1	I=-29.0	D=264.5	R= 30.00	J=1.07,-4	M=1.07,-4	MM=0.05	T400
U13A-1	I=-36.4	D=265.1	R= 30.00	J=9.30,-5	M=9.30,-5	MM=0.05	T450
U13A-1	I=-32.5	D=266.1	R= 30.00	J=7.47,-5	M=7.47,-5	MM=0.05	T500
U13A-1	I=-35.6	D=274.6	R= 30.00	J=7.25,-5	M=7.25,-5	MM=0.05	T550
U13A-1	I=-15.1	D=257.7	R= 30.00	J=2.39,-5	M=2.39,-5	MM=0.05	T600
U13-1	I=+32.5	D=175.3	R= 30.00	J=2.34,-4	M=2.34,-4	MM=0.05	T0
U13-1	I=+50.6	D=136.3	R= 30.00	J=2.87,-4	M=2.87,-4	MM=0.05	T200
U13-1	I=+69.4	D=148.9	R= 30.00	J=1.85,-4	M=1.85,-4	MM=0.05	T400
U13-1	I=+51.9	D=137.3	R= 30.00	J=1.63,-4	M=1.63,-4	MM=0.05	T450
U13-1	I=+50.0	D=145.9	R= 30.00	J=1.40,-4	M=1.40,-4	MM=0.05	T500
U13-1	I=+53.2	D=138.6	R= 30.00	J=1.14,-4	M=1.14,-4	MM=0.05	T550
U14_A-1	I=+18.5	D=290.0	R= 30.00	J=1.41,-4	M=1.41,-4	MM=0.05	T0
U14_A-1	I=+60.9	D=235.8	R= 30.00	J=1.92,-4	M=1.92,-4	MM=0.05	T200
U14_A-1	I=+61.2	D=196.2	R= 30.00	J=1.21,-4	M=1.21,-4	MM=0.05	T400
U14_A-1	I=+70.0	D=223.4	R= 30.00	J=8.24,-5	M=8.24,-5	MM=0.05	T450
U14_A-1	I=+79.7	D=207.0	R= 30.00	J=8.00,-5	M=8.00,-5	MM=0.05	T500
U14_A-1	I=+83.5	D=321.5	R= 30.00	J=5.79,-5	M=5.79,-5	MM=0.05	T550
U14_A-1	I=+12.4	D= 50.7	R= 30.00	J=3.18,-5	M=3.18,-5	MM=0.05	T600
U14_-1	I= -6.5	D=278.5	R= 30.00	J=1.67,-4	M=1.67,-4	MM=0.05	T0
U14_-1	I=+28.8	D=235.0	R= 30.00	J=1.94,-4	M=1.94,-4	MM=0.05	T200
U14_-1	I=+25.4	D=226.1	R= 30.00	J=1.21,-4	M=1.21,-4	MM=0.05	T400
U14_-1	I=+34.2	D=231.5	R= 30.00	J=9.93,-5	M=9.93,-5	MM=0.05	T450
U14_-1	I=+28.9	D=233.9	R= 30.00	J=6.17,-5	M=6.17,-5	MM=0.05	T500
U14_-1	I=+45.6	D=251.9	R= 30.00	J=8.71,-5	M=8.71,-5	MM=0.05	T550
U14A-1	I=-42.3	D= 18.7	R= 30.00	J=9.46,-4	M=9.46,-4	MM=0.05	T0
U14A-1	I=-42.8	D= 50.5	R= 30.00	J=7.34,-4	M=7.34,-4	MM=0.05	T200
U14A-1	I=-49.8	D= 62.6	R= 30.00	J=3.91,-4	M=3.91,-4	MM=0.05	T400
U14A-1	I=-43.5	D= 44.6	R= 30.00	J=3.35,-4	M=3.35,-4	MM=0.05	T450
U14A-1	I=-44.1	D= 23.9	R= 30.00	J=3.07,-4	M=3.07,-4	MM=0.05	T500
U14A-1	I=-41.4	D= 21.6	R= 30.00	J=2.30,-4	M=2.30,-4	MM=0.05	T550
U14A-1	I=-45.3	D= 22.0	R= 30.00	J=1.11,-4	M=1.11,-4	MM=0.05	T600
U14B-1	I=+45.6	D=184.3	R= 30.00	J=2.51,-3	M=2.51,-3	MM=0.05	T0
U14B-1	I=+35.1	D=197.3	R= 30.00	J=8.47,-4	M=8.47,-4	MM=0.05	T200
U14B-1	I=+44.6	D=189.8	R= 30.00	J=1.82,-4	M=1.82,-4	MM=0.05	T400
U14B-1	I=+23.4	D=189.6	R= 30.00	J=1.23,-4	M=1.23,-4	MM=0.05	T450
U14B-1	I=+35.7	D=188.7	R= 30.00	J=9.48,-5	M=9.48,-5	MM=0.05	T500
U14B-1	I= +1.8	D=173.4	R= 30.00	J=4.29,-5	M=4.29,-5	MM=0.05	T550
U15B-1	I= +8.5	D=292.8	R= 30.00	J=1.33,-4	M=1.33,-4	MM=0.05	T0
U15B-1	I=+14.2	D=292.3	R= 30.00	J=5.60,-5	M=5.60,-5	MM=0.05	T200
U15B-1	I= -3.3	D=296.4	R= 30.00	J=3.26,-5	M=3.26,-5	MM=0.05	T400
U15B-1	I=+13.8	D=299.1	R= 30.00	J=3.57,-5	M=3.57,-5	MM=0.05	T450
U15B-1	I=+22.9	D=306.2	R= 30.00	J=2.56,-5	M=2.56,-5	MM=0.05	T500
U15B-1	I= +0.5	D=282.6	R= 30.00	J=1.97,-5	M=1.97,-5	MM=0.05	T550
U15B-1	I=-50.8	D=305.1	R= 30.00	J=5.33,-6	M=5.33,-6	MM=0.05	T600
U15-1	I= -7.2	D=355.9	R= 30.00	J=1.47,-4	M=1.47,-4	MM=0.05	T0
U15-1	I=-16.2	D= 28.1	R= 30.00	J=5.76,-5	M=5.76,-5	MM=0.05	T200
U15-1	I=-21.5	D= 25.6	R= 30.00	J=2.75,-5	M=2.75,-5	MM=0.05	T400
U15-1	I= -1.7	D= 46.1	R= 30.00	J=3.44,-5	M=3.44,-5	MM=0.05	T450
U15-1	I=+13.7	D= 60.5	R= 30.00	J=3.11,-5	M=3.11,-5	MM=0.05	T500
U15-1	I= -7.4	D= 41.4	R= 30.00	J=2.41,-5	M=2.41,-5	MM=0.05	T550

U16A-1	I=+42.1	D=250.3	R= 30.00	J=6.73,-4	M=6.73,-4	MM=0.05	T0
U16A-1	I=+42.8	D=224.1	R= 30.00	J=4.66,-4	M=4.66,-4	MM=0.05	T200
U16A-1	I=+38.9	D=215.6	R= 30.00	J=2.44,-4	M=2.44,-4	MM=0.05	T400
U16A-1	I=+43.5	D=220.1	R= 30.00	J=2.01,-4	M=2.01,-4	MM=0.05	T450
U16A-1	I=+45.1	D=213.5	R= 30.00	J=2.03,-4	M=2.03,-4	MM=0.05	T500
U16A-1	I=+32.9	D=224.8	R= 30.00	J=1.53,-4	M=1.53,-4	MM=0.05	T550
U16A-1	I=+42.6	D=215.2	R= 30.00	J=9.86,-5	M=9.86,-5	MM=0.05	T600
U16B-1	I= +3.7	D= 0.5	R= 30.00	J=1.98,-4	M=1.98,-4	MM=0.05	T0
U16B-1	I=-21.6	D=306.2	R= 30.00	J=1.09,-4	M=1.09,-4	MM=0.05	T200
U16B-1	I=-24.3	D=313.5	R= 30.00	J=2.61,-5	M=2.61,-5	MM=0.05	T400
U16B-1	I=-24.6	D=301.4	R= 30.00	J=2.85,-5	M=2.85,-5	MM=0.05	T450
U16B-1	I= +2.8	D=311.9	R= 30.00	J=2.24,-5	M=2.24,-5	MM=0.05	T500
U16B-1	I=-30.3	D= 12.0	R= 30.00	J=1.67,-5	M=1.67,-5	MM=0.05	T550
U17A-1	I=-61.2	D=112.9	R= 30.00	J=1.20,-4	M=1.20,-4	MM=0.05	T0
U17A-1	I=-40.6	D= 33.0	R= 30.00	J=8.44,-5	M=8.44,-5	MM=0.05	T200
U17A-1	I=-25.3	D= 32.7	R= 30.00	J=4.45,-5	M=4.45,-5	MM=0.05	T400
U17A-1	I=-12.8	D= 29.0	R= 30.00	J=3.64,-5	M=3.64,-5	MM=0.05	T450
U17A-1	I= -1.9	D= 37.5	R= 30.00	J=3.49,-5	M=3.49,-5	MM=0.05	T500
U17A-1	I= +5.2	D= 50.9	R= 30.00	J=3.58,-5	M=3.58,-5	MM=0.05	T550
U17A-1	I=+27.4	D= 52.3	R= 30.00	J=9.51,-6	M=9.51,-6	MM=0.05	T600
U17-1	I=-45.4	D=324.7	R= 30.00	J=1.99,-4	M=1.99,-4	MM=0.05	T0
U17-1	I=+29.5	D=265.1	R= 30.00	J=4.82,-5	M=4.82,-5	MM=0.05	T200
U17-1	I=+34.2	D=254.4	R= 30.00	J=1.89,-5	M=1.89,-5	MM=0.05	T400
U17-1	I=+39.0	D=256.1	R= 30.00	J=2.79,-5	M=2.79,-5	MM=0.05	T450
U17-1	I=+45.1	D=309.2	R= 30.00	J=1.60,-5	M=1.60,-5	MM=0.05	T500
U17-1	I=+16.0	D=235.4	R= 30.00	J=1.81,-5	M=1.81,-5	MM=0.05	T550
U18A-1	I=+32.9	D=142.9	R= 30.00	J=4.60,-4	M=4.60,-4	MM=0.05	T0
U18A-1	I=+28.0	D=142.1	R= 30.00	J=1.86,-4	M=1.86,-4	MM=0.05	T200
U18A-1	I=+19.1	D=119.8	R= 30.00	J=9.75,-5	M=9.75,-5	MM=0.05	T400
U18A-1	I=+24.3	D=114.0	R= 30.00	J=7.45,-5	M=7.45,-5	MM=0.05	T450
U18A-1	I= +2.8	D=109.8	R= 30.00	J=7.75,-5	M=7.75,-5	MM=0.05	T500
U18A-1	I= -6.4	D=115.8	R= 30.00	J=9.62,-5	M=9.62,-5	MM=0.05	T550
U18A-1	I=-30.3	D= 95.2	R= 30.00	J=3.64,-5	M=3.64,-5	MM=0.05	T600
U18-1	I=+17.8	D= 37.7	R= 30.00	J=3.07,-4	M=3.07,-4	MM=0.05	T0
U18-1	I=-15.7	D=351.2	R= 30.00	J=7.34,-5	M=7.34,-5	MM=0.05	T200
U18-1	I=-61.1	D=226.5	R= 30.00	J=2.42,-6	M=2.42,-6	MM=0.05	T400
U18-1	I=-16.0	D=339.6	R= 30.00	J=6.11,-5	M=6.11,-5	MM=0.05	T450
U18-1	I= -8.3	D=328.9	R= 30.00	J=4.86,-5	M=4.86,-5	MM=0.05	T500
U18-1	I=-24.6	D= 12.3	R= 30.00	J=1.36,-5	M=1.36,-5	MM=0.05	T550
U19_A-1	I=-38.8	D=175.9	R= 30.00	J=2.50,-4	M=2.50,-4	MM=0.05	T0
U19_A-1	I=-29.6	D=184.5	R= 30.00	J=7.23,-5	M=7.23,-5	MM=0.05	T200
U19_A-1	I=+40.7	D=189.3	R= 30.00	J=1.28,-5	M=1.28,-5	MM=0.05	T400
U19_A-1	I=+61.8	D= 58.5	R= 30.00	J=1.42,-5	M=1.42,-5	MM=0.05	T450
U19_A-1	I=+54.1	D= 88.3	R= 30.00	J=1.12,-5	M=1.12,-5	MM=0.05	T500
U19_A-1	I=+40.9	D=199.8	R= 30.00	J=9.18,-6	M=9.18,-6	MM=0.05	T550
U19_A-1	I=+50.9	D= 67.6	R= 30.00	J=1.34,-5	M=1.34,-5	MM=0.05	T600
U19_B-1	I=-39.9	D=188.8	R= 30.00	J=2.81,-4	M=2.81,-4	MM=0.05	T0
U19_B-1	I=-41.9	D=186.5	R= 30.00	J=1.08,-4	M=1.08,-4	MM=0.05	T200
U19_B-1	I=+27.8	D=237.6	R= 30.00	J=5.73,-5	M=5.73,-5	MM=0.05	T400
U19_B-1	I=+61.8	D=230.9	R= 30.00	J=4.94,-5	M=4.94,-5	MM=0.05	T450
U19A-1	I=-39.7	D=149.3	R= 30.00	J=3.64,-4	M=3.64,-4	MM=0.05	T0
U19A-1	I=-41.7	D=144.2	R= 30.00	J=1.77,-4	M=1.77,-4	MM=0.05	T200

U19A-1	I=-49.3	D=129.9	R= 30.00	J=6.30,-5	M=6.30,-5	MM=0.05	T400
U19A-1	I=-52.4	D=118.2	R= 30.00	J=4.96,-5	M=4.96,-5	MM=0.05	T450
U19A-1	I=-48.5	D=122.0	R= 30.00	J=3.79,-5	M=3.79,-5	MM=0.05	T500
U19A-1	I= -6.1	D=165.0	R= 30.00	J=1.50,-5	M=1.50,-5	MM=0.05	T550
U19A-1	I= +0.7	D=196.9	R= 30.00	J=2.45,-5	M=2.45,-5	MM=0.05	T600
U19-1	I=+48.9	D=143.8	R= 30.00	J=2.18,-4	M=2.18,-4	MM=0.05	T0
U19-1	I=+26.3	D=143.5	R= 30.00	J=5.77,-5	M=5.77,-5	MM=0.05	T200
U19-1	I=-24.7	D=285.5	R= 30.00	J=9.50,-8	M=9.50,-8	MM=0.05	T400
U19-1	I=+35.7	D=152.0	R= 30.00	J=2.11,-5	M=2.11,-5	MM=0.05	T450
U19-1	I=+29.5	D=160.0	R= 30.00	J=1.71,-5	M=1.71,-5	MM=0.05	T500
U19-1	I=-10.9	D=173.1	R= 30.00	J=1.22,-5	M=1.22,-5	MM=0.05	T550
U1A-1	I=-37.5	D=340.8	R= 30.00	J=3.45,-4	M=3.45,-4	MM=0.05	T0
U1A-1	I=-31.5	D= 6.4	R= 30.00	J=1.66,-4	M=1.66,-4	MM=0.05	T200
U1A-1	I=-37.8	D= 22.5	R= 30.00	J=8.69,-5	M=8.69,-5	MM=0.05	T400
U1A-1	I=-37.8	D= 12.6	R= 30.00	J=8.23,-5	M=8.23,-5	MM=0.05	T450
U1A-1	I=-37.5	D= 6.5	R= 30.00	J=7.39,-5	M=7.39,-5	MM=0.05	T500
U1A-1	I=-46.2	D= 23.4	R= 30.00	J=5.37,-5	M=5.37,-5	MM=0.05	T550
U1A-1	I=-12.9	D= 14.3	R= 30.00	J=1.41,-5	M=1.41,-5	MM=0.05	T600
U1-1	I=-36.4	D=359.4	R= 30.00	J=5.76,-4	M=5.76,-4	MM=0.05	T0
U1-1	I=-31.0	D= 17.2	R= 30.00	J=3.86,-4	M=3.86,-4	MM=0.05	T200
U1-1	I=-32.0	D= 27.3	R= 30.00	J=1.94,-4	M=1.94,-4	MM=0.05	T400
U1-1	I=-32.6	D= 31.1	R= 30.00	J=1.63,-4	M=1.63,-4	MM=0.05	T450
U1-1	I=-31.4	D= 26.9	R= 30.00	J=1.41,-4	M=1.41,-4	MM=0.05	T500
U1-1	I=-34.8	D=298.1	R= 30.00	J=8.23,-5	M=8.23,-5	MM=0.05	T550
U2_B-1	I=+54.7	D=225.6	R= 30.00	J=8.13,-4	M=8.13,-4	MM=0.05	T0
U2_B-1	I=+44.4	D=205.4	R= 30.00	J=8.64,-4	M=8.64,-4	MM=0.05	T200
U2_B-1	I=+50.2	D=215.8	R= 30.00	J=4.40,-4	M=4.40,-4	MM=0.05	T400
U2_B-1	I=+39.3	D=207.8	R= 30.00	J=4.06,-4	M=4.06,-4	MM=0.05	T450
U2_B-1	I=+46.6	D=212.0	R= 30.00	J=3.10,-4	M=3.10,-4	MM=0.05	T500
U2_B-1	I=+49.8	D=215.3	R= 30.00	J=2.13,-4	M=2.13,-4	MM=0.05	T550
U2_B-1	I=+44.1	D=210.0	R= 30.00	J=1.02,-4	M=1.02,-4	MM=0.05	T600
U2_-1	I=+33.8	D=254.1	R= 30.00	J=7.03,-4	M=7.03,-4	MM=0.05	T0
U2_-1	I=+40.1	D=220.0	R= 30.00	J=7.34,-4	M=7.34,-4	MM=0.05	T200
U2_-1	I=+42.1	D=228.2	R= 30.00	J=3.90,-4	M=3.90,-4	MM=0.05	T400
U2_-1	I=+45.9	D=235.5	R= 30.00	J=3.69,-4	M=3.69,-4	MM=0.05	T450
U2_-1	I=+23.3	D=226.0	R= 30.00	J=2.68,-4	M=2.68,-4	MM=0.05	T500
U2_-1	I=+51.7	D=231.2	R= 30.00	J=1.97,-4	M=1.97,-4	MM=0.05	T550
U20B-1	I=+50.7	D=136.9	R= 30.00	J=1.53,-4	M=1.53,-4	MM=0.05	T0
U20B-1	I=+68.0	D= 78.4	R= 30.00	J=1.71,-4	M=1.71,-4	MM=0.05	T200
U20B-1	I=+58.4	D= 71.6	R= 30.00	J=8.88,-5	M=8.88,-5	MM=0.05	T400
U20B-1	I=+56.8	D= 32.8	R= 30.00	J=6.75,-5	M=6.75,-5	MM=0.05	T450
U20B-1	I=+48.4	D= 19.0	R= 30.00	J=4.78,-5	M=4.78,-5	MM=0.05	T500
U20B-1	I=+48.6	D= 32.7	R= 30.00	J=4.06,-5	M=4.06,-5	MM=0.05	T550
U20B-1	I=-37.9	D=263.6	R= 30.00	J=1.34,-5	M=1.34,-5	MM=0.05	T600
U20D-1	I= -0.4	D= 0.1	R= 30.00	J=1.83,-4	M=1.83,-4	MM=0.05	T0
U20D-1	I=+54.5	D=352.8	R= 30.00	J=1.36,-4	M=1.36,-4	MM=0.05	T200
U20D-1	I=+65.4	D=289.1	R= 30.00	J=5.45,-5	M=5.45,-5	MM=0.05	T450
U20D-1	I=+70.7	D=264.6	R= 30.00	J=6.35,-5	M=6.35,-5	MM=0.05	T500
U20D-1	I=+75.8	D=187.8	R= 30.00	J=3.89,-5	M=3.89,-5	MM=0.05	T550
U21B-1	I=+43.0	D=208.5	R= 30.00	J=3.59,-4	M=3.59,-4	MM=0.05	T0
U21B-1	I=+39.8	D=197.6	R= 30.00	J=5.97,-4	M=5.97,-4	MM=0.05	T200
U21B-1	I=+36.5	D=179.6	R= 30.00	J=2.58,-4	M=2.58,-4	MM=0.05	T400

U21B-1	I=+43.8	D=195.6	R= 30.00	J=1.67,-4	M=1.67,-4	MM=0.05	T450
U21B-1	I=+29.0	D=206.6	R= 30.00	J=1.11,-4	M=1.11,-4	MM=0.05	T500
U21B-1	I=-45.2	D=354.0	R= 30.00	J=5.53,-5	M=5.53,-5	MM=0.05	T550
U21B-1	I=+50.0	D=290.8	R= 30.00	J=4.44,-5	M=4.44,-5	MM=0.05	T600
U2B-1	I=-37.8	D= 19.4	R= 30.00	J=6.25,-4	M=6.25,-4	MM=0.05	T0
U2B-1	I=-38.8	D= 23.4	R= 30.00	J=4.47,-4	M=4.47,-4	MM=0.05	T200
U2B-1	I=-48.3	D= 30.7	R= 30.00	J=2.04,-4	M=2.04,-4	MM=0.05	T400
U2B-1	I=-48.2	D= 24.5	R= 30.00	J=1.71,-4	M=1.71,-4	MM=0.05	T450
U2B-1	I=-41.8	D= 32.1	R= 30.00	J=1.52,-4	M=1.52,-4	MM=0.05	T500
U2B-1	I=-35.9	D= 33.8	R= 30.00	J=1.06,-4	M=1.06,-4	MM=0.05	T550
U2B-1	I=-35.6	D= 31.2	R= 30.00	J=4.27,-5	M=4.27,-5	MM=0.05	T600
U2-1	I=-50.7	D=351.1	R= 30.00	J=3.04,-4	M=3.04,-4	MM=0.05	T0
U2-1	I=-67.2	D= 6.2	R= 30.00	J=1.65,-4	M=1.65,-4	MM=0.05	T200
U2-1	I=-64.6	D= 53.1	R= 30.00	J=7.39,-5	M=7.39,-5	MM=0.05	T400
U2-1	I=-71.1	D= 66.1	R= 30.00	J=7.49,-5	M=7.49,-5	MM=0.05	T450
U2-1	I=-57.2	D= 72.0	R= 30.00	J=6.97,-5	M=6.97,-5	MM=0.05	T500
U2-1	I=-54.4	D=113.5	R= 30.00	J=3.11,-5	M=3.11,-5	MM=0.05	T550
U3_B-1	I=+57.2	D=295.5	R= 30.00	J=5.09,-4	M=5.09,-4	MM=0.05	T0
U3_B-1	I=+78.4	D=273.9	R= 30.00	J=5.55,-4	M=5.55,-4	MM=0.05	T200
U3_B-1	I=+75.1	D=300.8	R= 30.00	J=2.97,-4	M=2.97,-4	MM=0.05	T400
U3_B-1	I=+66.7	D=260.8	R= 30.00	J=3.07,-4	M=3.07,-4	MM=0.05	T450
U3_B-1	I=+68.7	D=262.9	R= 30.00	J=2.29,-4	M=2.29,-4	MM=0.05	T500
U3_B-1	I=+71.5	D=257.5	R= 30.00	J=1.67,-4	M=1.67,-4	MM=0.05	T550
U3_B-1	I=+75.6	D=275.3	R= 30.00	J=1.19,-4	M=1.19,-4	MM=0.05	T600
U3_-1	I=+12.5	D=101.8	R= 30.00	J=2.03,-4	M=2.03,-4	MM=0.05	T0
U3_-1	I=+23.9	D=102.9	R= 30.00	J=3.81,-4	M=3.81,-4	MM=0.05	T200
U3_-1	I=+25.1	D=120.5	R= 30.00	J=2.01,-4	M=2.01,-4	MM=0.05	T400
U3_-1	I=+15.7	D=121.8	R= 30.00	J=1.97,-4	M=1.97,-4	MM=0.05	T450
U3_-1	I=+16.4	D=134.9	R= 30.00	J=1.37,-4	M=1.37,-4	MM=0.05	T500
U3_-1	I= +1.7	D=136.9	R= 30.00	J=8.65,-5	M=8.65,-5	MM=0.05	T550
U3A-1	I= +0.5	D=199.0	R= 30.00	J=2.72,-4	M=2.72,-4	MM=0.05	T0
U3A-1	I=+38.6	D=207.1	R= 30.00	J=2.44,-4	M=2.44,-4	MM=0.05	T200
U3A-1	I=+56.1	D=212.3	R= 30.00	J=1.13,-4	M=1.13,-4	MM=0.05	T400
U3A-1	I=+56.0	D=213.1	R= 30.00	J=1.10,-4	M=1.10,-4	MM=0.05	T450
U3A-1	I=+50.4	D=218.7	R= 30.00	J=9.55,-5	M=9.55,-5	MM=0.05	T500
U3A-1	I=+58.3	D=232.8	R= 30.00	J=8.17,-5	M=8.17,-5	MM=0.05	T550
U3A-1	I=+68.4	D=206.0	R= 30.00	J=3.68,-5	M=3.68,-5	MM=0.05	T600
U3-1	I=+28.6	D=271.0	R= 30.00	J=2.95,-4	M=2.95,-4	MM=0.05	T0
U3-1	I=+48.8	D=257.0	R= 30.00	J=3.39,-4	M=3.39,-4	MM=0.05	T200
U3-1	I=+50.8	D=258.3	R= 30.00	J=1.85,-4	M=1.85,-4	MM=0.05	T400
U3-1	I=+46.9	D=248.5	R= 30.00	J=1.72,-4	M=1.72,-4	MM=0.05	T450
U3-1	I=+48.1	D=255.4	R= 30.00	J=1.63,-4	M=1.63,-4	MM=0.05	T500
U3-1	I=+50.1	D=243.7	R= 30.00	J=9.80,-5	M=9.80,-5	MM=0.05	T550
U3-1	I=+61.0	D=196.0	R= 30.00	J=8.36,-5	M=8.36,-5	MM=0.05	T550
U4_A-1	I=+13.7	D=316.5	R= 30.00	J=5.08,-4	M=5.08,-4	MM=0.05	T0
U4_A-1	I=+33.6	D=293.0	R= 30.00	J=3.09,-4	M=3.09,-4	MM=0.05	T200
U4_A-1	I=+33.3	D=288.7	R= 30.00	J=1.19,-4	M=1.19,-4	MM=0.05	T400
U4_A-1	I=+36.5	D=273.3	R= 30.00	J=1.10,-4	M=1.10,-4	MM=0.05	T450
U4_A-1	I=+39.7	D=271.7	R= 30.00	J=8.11,-5	M=8.11,-5	MM=0.05	T500
U4_A-1	I=+43.4	D=274.5	R= 30.00	J=6.79,-5	M=6.79,-5	MM=0.05	T550
U4_A-1	I=+50.4	D=244.5	R= 30.00	J=2.88,-5	M=2.88,-5	MM=0.05	T600
U4_-1	I=-56.8	D= 92.6	R= 30.00	J=1.64,-4	M=1.64,-4	MM=0.05	T0

U4_-1	I=-66.3	D=123.0	R= 30.00	J=6.57,-5	M=6.57,-5	MM=0.05	T200
U4_-1	I=-67.4	D=185.0	R= 30.00	J=3.29,-5	M=3.29,-5	MM=0.05	T400
U4_-1	I=-59.5	D=186.6	R= 30.00	J=3.23,-5	M=3.23,-5	MM=0.05	T450
U4_-1	I=-68.8	D= 40.5	R= 30.00	J=1.15,-5	M=1.15,-5	MM=0.05	T500
U4_-1	I=-70.0	D=144.1	R= 30.00	J=1.54,-5	M=1.54,-5	MM=0.05	T550
U4A-1	I= -3.7	D=313.8	R= 30.00	J=7.75,-5	M=7.75,-5	MM=0.05	T0
U4A-1	I=+51.6	D=255.3	R= 30.00	J=5.23,-5	M=5.23,-5	MM=0.05	T200
U4A-1	I=+73.0	D=126.5	R= 30.00	J=2.57,-5	M=2.57,-5	MM=0.05	T400
U4A-1	I=+77.1	D=115.6	R= 30.00	J=3.35,-5	M=3.35,-5	MM=0.05	T450
U4A-1	I=+27.5	D=140.5	R= 30.00	J=3.19,-5	M=3.19,-5	MM=0.05	T500
U4A-1	I=+36.5	D=234.9	R= 30.00	J=3.10,-5	M=3.10,-5	MM=0.05	T550
U4A-1	I=+58.5	D=302.1	R= 30.00	J=2.64,-5	M=2.64,-5	MM=0.05	T600
U4B-1	I=+10.2	D=289.0	R= 30.00	J=1.50,-4	M=1.50,-4	MM=0.05	T0
U4B-1	I=+29.0	D=243.0	R= 30.00	J=1.08,-4	M=1.08,-4	MM=0.05	T200
U4B-1	I=+25.7	D=241.8	R= 30.00	J=5.20,-5	M=5.20,-5	MM=0.05	T400
U4B-1	I=+20.3	D=246.0	R= 30.00	J=4.99,-5	M=4.99,-5	MM=0.05	T450
U4B-1	I=+14.4	D=254.2	R= 30.00	J=3.99,-5	M=3.99,-5	MM=0.05	T500
U4B-1	I=+24.8	D=248.5	R= 30.00	J=2.67,-5	M=2.67,-5	MM=0.05	T550
U5_B-1	I=+34.4	D=302.6	R= 30.00	J=2.41,-4	M=2.41,-4	MM=0.05	T0
U5_B-1	I=+46.1	D=265.6	R= 30.00	J=2.56,-4	M=2.56,-4	MM=0.05	T200
U5_B-1	I=+49.0	D=258.3	R= 30.00	J=1.46,-4	M=1.46,-4	MM=0.05	T400
U5_B-1	I=+47.3	D=274.6	R= 30.00	J=1.06,-4	M=1.06,-4	MM=0.05	T450
U5_B-1	I=+52.7	D=274.6	R= 30.00	J=8.46,-5	M=8.46,-5	MM=0.05	T500
U5_B-1	I=+50.8	D=283.7	R= 30.00	J=7.04,-5	M=7.04,-5	MM=0.05	T550
U5_B-1	I=+55.6	D=281.1	R= 30.00	J=4.75,-5	M=4.75,-5	MM=0.05	T600
U5_-1	I=+61.1	D=238.8	R= 30.00	J=1.61,-3	M=1.61,-3	MM=0.05	T0
U5_-1	I=+60.0	D=234.3	R= 30.00	J=1.36,-3	M=1.36,-3	MM=0.05	T200
U5_-1	I=+61.0	D=238.3	R= 30.00	J=5.33,-4	M=5.33,-4	MM=0.05	T400
U5_-1	I=+52.5	D=229.7	R= 30.00	J=4.52,-4	M=4.52,-4	MM=0.05	T450
U5_-1	I=+55.2	D=233.9	R= 30.00	J=3.89,-4	M=3.89,-4	MM=0.05	T500
U5_-1	I=+57.2	D=230.9	R= 30.00	J=2.58,-4	M=2.58,-4	MM=0.05	T550
U5A-1	I=+14.5	D=293.9	R= 30.00	J=2.34,-4	M=2.34,-4	MM=0.05	T0
U5A-1	I=+30.2	D=256.2	R= 30.00	J=2.07,-4	M=2.07,-4	MM=0.05	T200
U5A-1	I=+35.0	D=262.1	R= 30.00	J=8.48,-5	M=8.48,-5	MM=0.05	T400
U5A-1	I=+34.0	D=261.1	R= 30.00	J=7.59,-5	M=7.59,-5	MM=0.05	T450
U5A-1	I=+24.9	D=252.3	R= 30.00	J=6.62,-5	M=6.62,-5	MM=0.05	T500
U5A-1	I=+28.8	D=259.0	R= 30.00	J=5.20,-5	M=5.20,-5	MM=0.05	T550
U5A-1	I=+36.2	D=232.7	R= 30.00	J=2.32,-5	M=2.32,-5	MM=0.05	T600
U5-1	I=+37.8	D=331.7	R= 30.00	J=2.75,-4	M=2.75,-4	MM=0.05	T0
U5-1	I=+32.7	D=240.3	R= 30.00	J=2.05,-4	M=2.05,-4	MM=0.05	T200
U5-1	I=+30.5	D=249.8	R= 30.00	J=9.61,-5	M=9.61,-5	MM=0.05	T400
U5-1	I=+23.4	D=221.3	R= 30.00	J=8.93,-5	M=8.93,-5	MM=0.05	T450
U5-1	I=+30.2	D=227.5	R= 30.00	J=8.96,-5	M=8.96,-5	MM=0.05	T500
U5-1	I=+28.1	D=224.0	R= 30.00	J=5.61,-5	M=5.61,-5	MM=0.05	T550
U6_A-1	I=-19.4	D=257.9	R= 30.00	J=4.49,-4	M=4.49,-4	MM=0.05	T0
U6_A-1	I=-36.7	D=270.6	R= 30.00	J=2.88,-4	M=2.88,-4	MM=0.05	T200
U6_A-1	I=-54.0	D=263.5	R= 30.00	J=1.54,-4	M=1.54,-4	MM=0.05	T400
U6_A-1	I=-62.0	D=275.0	R= 30.00	J=1.20,-4	M=1.20,-4	MM=0.05	T450
U6_A-1	I=-61.8	D=302.4	R= 30.00	J=9.33,-5	M=9.33,-5	MM=0.05	T500
U6_A-1	I=-58.2	D=304.3	R= 30.00	J=7.58,-5	M=7.58,-5	MM=0.05	T550
U6_A-1	I=-61.2	D=311.3	R= 30.00	J=4.51,-5	M=4.51,-5	MM=0.05	T600
U6_-1	I=-13.5	D=248.3	R= 30.00	J=5.98,-4	M=5.98,-4	MM=0.05	T0

U6_-1	I= +0.6	D=239.9	R= 30.00	J=2.59,-4	M=2.59,-4	MM=0.05	T200
U6_-1	I=-59.7	D=188.8	R= 30.00	J=5.62,-5	M=5.62,-5	MM=0.05	T400
U6_-1	I=-67.9	D=155.6	R= 30.00	J=5.81,-5	M=5.81,-5	MM=0.05	T450
U6_-1	I=-76.4	D=111.9	R= 30.00	J=4.80,-5	M=4.80,-5	MM=0.05	T500
U6_-1	I=-40.5	D= 89.3	R= 30.00	J=4.04,-5	M=4.04,-5	MM=0.05	T550
U6B-1	I=+32.1	D=248.9	R= 30.00	J=3.69,-4	M=3.69,-4	MM=0.05	T0
U6B-1	I=+33.0	D=220.1	R= 30.00	J=4.93,-4	M=4.93,-4	MM=0.05	T200
U6B-1	I=+33.5	D=213.3	R= 30.00	J=2.54,-4	M=2.54,-4	MM=0.05	T400
U6B-1	I=+30.3	D=208.3	R= 30.00	J=1.56,-4	M=1.56,-4	MM=0.05	T450
U6B-1	I=+31.1	D=214.4	R= 30.00	J=2.19,-4	M=2.19,-4	MM=0.05	T450
U6B-1	I=+31.9	D=217.0	R= 30.00	J=1.85,-4	M=1.85,-4	MM=0.05	T500
U6B-1	I=+31.6	D=223.2	R= 30.00	J=1.48,-4	M=1.48,-4	MM=0.05	T550
U6B-1	I=+26.9	D=218.6	R= 30.00	J=5.39,-5	M=5.39,-5	MM=0.05	T600
U6-1	I=+43.1	D=226.0	R= 30.00	J=3.01,-4	M=3.01,-4	MM=0.05	T200
U6-1	I=+43.1	D=263.6	R= 30.00	J=2.13,-4	M=2.13,-4	MM=0.05	T200
U6-1	I=+25.1	D=231.5	R= 30.00	J=1.76,-4	M=1.76,-4	MM=0.05	T400
U6-1	I=+43.1	D=226.0	R= 30.00	J=3.01,-4	M=3.01,-4	MM=0.05	T400
U6-1	I=+40.2	D=233.7	R= 30.00	J=1.38,-4	M=1.38,-4	MM=0.05	T500
U6-1	I=+35.2	D=218.6	R= 30.00	J=9.23,-5	M=9.23,-5	MM=0.05	T550
U7A-1	I=-18.9	D=242.5	R= 30.00	J=1.50,-4	M=1.50,-4	MM=0.05	T0
U7A-1	I=-35.9	D=240.3	R= 30.00	J=1.53,-4	M=1.53,-4	MM=0.05	T200
U7A-1	I=-33.8	D=226.3	R= 30.00	J=7.02,-5	M=7.02,-5	MM=0.05	T400
U7A-1	I=-42.3	D=212.7	R= 30.00	J=5.67,-5	M=5.67,-5	MM=0.05	T450
U7A-1	I=-36.4	D=223.3	R= 30.00	J=4.96,-5	M=4.96,-5	MM=0.05	T500
U7A-1	I=-49.1	D=193.9	R= 30.00	J=3.74,-5	M=3.74,-5	MM=0.05	T550
U7A-1	I=-52.6	D=148.7	R= 30.00	J=1.54,-5	M=1.54,-5	MM=0.05	T600
U7B-1	I=-57.5	D=345.4	R= 30.00	J=4.29,-4	M=4.29,-4	MM=0.05	T0
U7B-1	I=-50.3	D= 2.9	R= 30.00	J=3.28,-4	M=3.28,-4	MM=0.05	T200
U7B-1	I=-35.0	D= 14.2	R= 30.00	J=1.43,-4	M=1.43,-4	MM=0.05	T400
U7B-1	I=-30.5	D=358.1	R= 30.00	J=1.33,-4	M=1.33,-4	MM=0.05	T450
U7B-1	I=-28.8	D= 8.8	R= 30.00	J=1.16,-4	M=1.16,-4	MM=0.05	T500
U7B-1	I=-22.5	D= 7.5	R= 30.00	J=6.69,-5	M=6.69,-5	MM=0.05	T550
U8A-1	I=+53.8	D=248.2	R= 30.00	J=3.29,-4	M=3.29,-4	MM=0.05	T0
U8A-1	I=+53.3	D=222.4	R= 30.00	J=3.24,-4	M=3.24,-4	MM=0.05	T200
U8A-1	I=+54.4	D=218.8	R= 30.00	J=1.64,-4	M=1.64,-4	MM=0.05	T400
U8A-1	I=+44.1	D=214.1	R= 30.00	J=1.49,-4	M=1.49,-4	MM=0.05	T450
U8A-1	I=+52.6	D=206.5	R= 30.00	J=1.18,-4	M=1.18,-4	MM=0.05	T500
U8A-1	I=+46.8	D=216.2	R= 30.00	J=8.93,-5	M=8.93,-5	MM=0.05	T550
U8A-1	I=+41.0	D=220.4	R= 30.00	J=3.73,-5	M=3.73,-5	MM=0.05	T600
U8B-1	I=+66.7	D=282.7	R= 30.00	J=1.56,-4	M=1.56,-4	MM=0.05	T0
U8B-1	I=+46.8	D=228.5	R= 30.00	J=1.37,-4	M=1.37,-4	MM=0.05	T200
U8B-1	I=+32.1	D=236.0	R= 30.00	J=6.74,-5	M=6.74,-5	MM=0.05	T400
U8B-1	I=+35.9	D=233.9	R= 30.00	J=6.19,-5	M=6.19,-5	MM=0.05	T450
U8B-1	I=+37.4	D=236.2	R= 30.00	J=3.76,-5	M=3.76,-5	MM=0.05	T500
U8B-1	I=+46.1	D=234.0	R= 30.00	J=4.47,-5	M=4.47,-5	MM=0.05	T550
U9A-1	I=-28.4	D=338.9	R= 30.00	J=2.06,-4	M=2.06,-4	MM=0.05	T0
U9A-1	I=-43.5	D=348.2	R= 30.00	J=2.92,-4	M=2.92,-4	MM=0.05	T200
U9A-1	I=-43.8	D=341.8	R= 30.00	J=1.39,-4	M=1.39,-4	MM=0.05	T400
U9A-1	I=-38.2	D=336.6	R= 30.00	J=1.33,-4	M=1.33,-4	MM=0.05	T450
U9A-1	I=-45.0	D=341.9	R= 30.00	J=1.03,-4	M=1.03,-4	MM=0.05	T500
U9A-1	I=-33.9	D=353.3	R= 30.00	J=7.40,-5	M=7.40,-5	MM=0.05	T550
U9A-1	I=-37.6	D=336.3	R= 30.00	J=3.45,-5	M=3.45,-5	MM=0.05	T600
U9-1	I=+45.9	D=211.2	R= 30.00	J=7.75,-4	M=7.75,-4	MM=0.05	T0
U9-1	I=+45.5	D=198.4	R= 30.00	J=7.19,-4	M=7.19,-4	MM=0.05	T200
U9-1	I=+42.3	D=202.8	R= 30.00	J=3.68,-4	M=3.68,-4	MM=0.05	T400
U9-1	I=+36.9	D=197.8	R= 30.00	J=3.48,-4	M=3.48,-4	MM=0.05	T450
U9-1	I=+32.7	D=195.6	R= 30.00	J=2.69,-4	M=2.69,-4	MM=0.05	T500
U9-1	I=+40.8	D=190.3	R= 30.00	J=1.82,-4	M=1.82,-4	MM=0.05	T550
U9-1	I=+40.8	D=190.3	R= 30.00	J=1.82,-4	M=1.82,-4	MM=0.05	T550

APPENDIX F

PALUSTRINE CARBONATES OF IGLESIA BASIN, NORTHWESTERN ARGENTINA: OUTCROP CHARACTERISTICS AND STABLE ISOTOPIC DATA

Carbonate beds interpreted as palustrine are abundant in central basin outcrops of Iglesia Basin at approximately 8.9 - 8.3 Ma and also 7.85 - 7.7 Ma. These units also occur with greater frequency in the youngest seismic sequences (5 - 4.3 Ma) in comparison with the majority of the underlying stratigraphic interval. It should be noted that there is often difficulty in distinguishing palustrine beds from pedogenic "caliche" or "calcretes" on the basis of macroscopic texture or fabric. Therefore, lateral and vertical facies associations must be considered for proper classification and given the similarities and pedogenic component of each, a continuum between these terms exists (Esteban and Klappa, 1983). Caliche typically exhibits a transition zone downsection into less-calcareous sediments, whereas the units we distinguish as palustrine have sharp basal contacts and are not clearly a part of a single soil profile. In the case of the lithofacies transition at ~8.7 Ma (2-3 sequence boundary), palustrine beds are associated with oxidized conglomeratic paleochannels and aquic Inceptisols. At the 3-4 sequence boundary (~7.7 Ma) and the young, depositionally-ponded sequences, palustrine units are also pedogenically overprinted, but associated with different depositional environments. Sequence 3 and 4 consist of fluvial sheet and channel sands with overbank paleosols exhibiting variable oxidation state (discussed above). In the case of the young sequences (outcropping in the westernmost sub-basin), deposition is interpreted as a playa lake setting, based on the abundance of calcareous fine-grained sediments interbedded with gypsum and generally reduced paleosols.

The presence of freshwater carbonates is in itself indicative of semi-arid climate and a low input of siliciclastics and biogenic/pedogenic alteration of the thin palustrine units is suggestive of occasional drying leading to subaerial exposure (e.g. Cecil, 1990; De Wet *et al.*, 1998). Association between freshwater carbonates with periods of low siliciclastic input is an important clue to the hiatal nature of the 3-4 sequence boundary, where palustrine beds are temporally clustered (see above).

Several other localized carbonate beds in Iglesia strata are worth mention because of their relation to local or regional discharge. In the vicinity of the 5-6 sequence boundary, a 10-cm thick carbonate is associated with a silicified interval approximately 0.5 m below. The opaline quality of the interval and its continuity along-strike suggests pervasive throughflow and recementation of surrounding rocks. In addition, outcrops near Rodeo 2 section (eastern section) and Iglesias (southwesternmost part of outcrop belt) are also strongly pedogenic and exhibit evidence of modern groundwater flow such as karstic topography, caves, gypsum crusts, and abundant mottling. These associations are important with respect to the following isotopic interpretations.

The Carbon and Oxygen isotopic compositions of palustrine carbonates depend on salinity, temperature, and overturn rates during carbonate precipitation as well as the identity and abundance of organic influxes (e.g. fluvial, groundwater, authigenic and biological precipitates, etc) to the shallow-water systems (Anderson and Arthur, 1983; Chivas *et al.*, 1993; De Wet, 1998). $\delta\ ^{13}C$ composition reflects various sources of bicarbonate, such as organic respiration and decay, atmospheric exchange, and subsequent pedogenic and diagenetic modifications (De Wet *et al.*, 1998). The $\delta^{18}O$ composition responds to temperature and water composition, driven to more negative (depleted) values by pedogenesis or diagenesis, and toward less negative (enriched) values by evaporation or aridity (De Wet *et al.*, 1998).

Following the same analytical and data reporting standards as for the paleosol carbonates for Iglesia Basin (See Chapter 3 and Appendix A), isotopic ratios for 34 palustrine carbonates spanning 8.9 to 4.75 Ma are presented in Table F.1. Iglesia basin values are quite scattered, which is not surprising given the number of variables to shallow-water systems (see above) which can't be adequately constrained. However, it is noteworthy that the $\delta^{13}C$ values are less variant than the $\delta^{18}O$ time series. $\delta^{13}C$ values fluctuate about a mean of -5.86‰ (s.d. 1.41‰), the only major departure occurring at 6.15 Ma ($\delta^{13}C$ = -9.9‰). This sample was taken from an oxidized carbonate bed, such that the isotopic value may reflect subsequent diagenetic fractionation. Conversely, the $\delta^{18}O$ time series appears to oscillate between enriched (more positive) and depleted (more negative) states through time. The series is greatly enriched at the Intra-2 sequence boundary (~9.0 Ma), and thereafter seems to follow a long-term trend toward depletion lasting until 6.35 Ma. Then, from 6.35 until 4.75, oxygen isotopic values follow a semi-linear trend toward enrichment.

Temporal trends in $\delta^{13}C$ and $\delta^{18}O$ values for lake limestones have been shown to reflect residence time and allow inferenced about hydrologic inputs (e.g. Talbot, 1990, 1994). Hydrologically open lakes are characterized by fairly stable $\delta^{13}C$ and $\delta^{18}O$ (or fixed $\delta^{18}O$ with variable $\delta^{13}C$), whereas covariant $\delta^{13}C$ and $\delta^{18}O$ isotopic time series suggest closed systems, the values constrained by hydrologic balance between influx and evaporative loss (Talbot, 1990; Li and Ku, 1997). The Iglesia Basin palustrine isotopic time series (Figure F.1) does not show covariation between series, nor is the $\delta^{18}O$ fixed. In contrast, $\delta^{13}C$ values appear fairly stable while $\delta^{18}O$ values fluctuate. As such, we cannot assess hydrologic closure or lack thereof for Iglesia palustrine carbonates. However, it is important to note that minimal thickness and local extent of the units, as well as characteristics which imply periodic subaerial exposure suggest that the bodies of water which evaporated the carbonate were

ephemeral and likely hydrologically isolated on fluvial floodplains. Furthermore, assessment of isotopic dynamics for lake deposits tens of meters thick (e.g. Talbot, 1990) may not be appropriate for comparison to thin palustrine units.

Considered spatially (Figure F.2), most sampled limestone isotopic values cluster between about -4 to -8‰ for both isotopic series. Several explainable departures are evident for the oxygen values, however. The least negative $\delta\ ^{18}O$ values are associated with samples from the eastern basin margin and from younger sequences deposited in the restricted western sub-basin (<5.2 Ma for northern outcrop belt); both areas are associated with evaporitic deposits, the former likely due to modern run-off and the latter a result of depositional ponding leading to increased salinity. In contrast, the most negative $\delta^{18}O$ values come from carbonates associated with pedogenic or diagenetically modified sections, where gypsum, iron oxide or silica crusts are observed on surrounding strata. Both of these associations are in accord with isotopic fractionation in response to lake evaporation or post-depositional alteration (De Wet *et al.*, 1998).

References:

Anderson, T.F, and Arthur, M.A., 1983, Stable isotopes of oxygen and carbon and their application to sedimentologic and paleoenvironmental problems, *in* Arthur, M.A., Anderson, T.F., Kaplan, I.R., Veizer, J. and Land, L.S., eds., Stable Isotopes in Sedimentary Geology, SEPM Short Course, No.10, Dallas.

Cecil, C.B., 1990, Paleoclimate controls on stratigraphic repetition in chemical and siliciclastic rocks: Geology, Vol. 18, p.533-536.

Chivas, A.R, Cali, J. A., Chapman, A., Shelley, J. M.G., and De Dekker, P., 1993, Coupled stable-isotope and trace-element measurements of carbonates as paleoclimatic indicators: *in* Stuart, P.K., Lohmann, K.C., McKenzie, J., and Savin, S., eds., Climate Change in Continental Isotopic Records, American Geophysical Union, Geophysical Monograph 78, 374 pp.

De Wet, C.B., Yocum, D.A., and Mora, C.I., 1998, Carbonate lakes in closed basins: sensitive indicators of climate and tectonics: an example from the Gettysburg Basin (Triassic), Pennsylvania, USA, in Shanley, K, W. and McCabe, P.J., eds., Relative Role of Eustasy, Climate and Tectonism in Continental Rocks: SEPM Special Publication, No. 59, p. 191-212.

Esteban, M and Klappa, C.F., 1983, Subaerial exposure environment, *in* Scholle, P.A., Bebout, D.G., and Moore, C.H., *eds.* "Carbonate Depositional Environments, American Association of Petroleum Geologists Memoir 33, p.1-96.

Li, H-C., and Ku, T.L., 1997, $\delta\ ^{13}C$ and $\delta\ ^{18}O$ covariance as a paleohydrological indicator for closed-basin lakes: Palaeogeography, Palaeoclimatology, Palaeoecology, v.133, p. 69-80.

Talbot, M.R., 1990, A Review of the palaeohydrological interpretation of carbon and oxygen stable isotopic ratios in primary carbonates: Chemical Geology (Isotope Geoscience Section), v.80, p.261-279.

Talbot, M.R., 1994, Paleohydrology of the late Miocene Ridge basin lake, California: Geological Society of America Bulletin, Vol. 106., p. 1121-1129.

Table F.1: Stable isotopic values for palustrine carbonates of Iglesia Basin. Ages are assigned by linear interpolation with magnetostratigraphic correlation (see Figures 2.18 through 2.22 and Figure 3.4).

Sample ID	Lithology	Age (Ma)	Section	$\delta^{13}C_{PDB}$	$\delta^{18}O_{PDB}$
BR05-31	calcareously cemented sandstone	4.75	Angualasto	-6.53	-2.27
BR05-32	calcareously cemented sandstone	4.9	Angualasto	-5.70	-4.05
BR05-51	calcareously cemented sandstone	5	Angualasto	-5.24	-3.09
BR04-9	carbonate cemented sandstone	5.23	Angualasto	-4.25	-5.50
23-6-2002 IGLESIA 5	calcareously cemented sandstone	6	Angualasto	-3.78	-7.16
BR03-36	oxidized limestone	6.15	Iglesias	-9.90	-8.63
BR03-30	calcareous sandstone	6.35	Iglesias	-6.44	-10.93
23-6-2002 IGLESIA 4	calcareously cemented sandstone	6.4	Angualasto	-4.89	-5.14
23-6-2002 IGLESIA 4 Duplicate	calcareously cemented sandstone	6.4	Angualasto	-4.82	-5.30
BR04-5	limestone	6.5	Angualasto	-6.86	-9.19
BR04-48	marl of sequence 3	7.7	Angualasto	-4.02	-6.99
21-6-2002 IGLESIA 2	carbonaceous sandstone	7.7	Angualasto	-7.31	-6.49
BR04-45	calcareous sandstone = Iglesia 2	7.7	Angualasto	-7.06	-9.00
BR03-8	calcareous sandstone = Iglesia 2	7.7	Angualasto	-6.14	-4.63
IGLESIA 3	vuggy calcareous sandstone	7.75	Angualasto	-6.72	-3.82
IGLESIA 3 Duplicate	vuggy calcareous sandstone	7.75	Angualasto	-6.69	-3.71
BR03-5 Duplicate	vuggy calcareous sandstone	7.75	Angualasto	-5.95	-6.49
BR03-5	vuggy calcareous sandstone = Iglesia 3	7.75	Angualasto	-6.03	-6.42
BR03-7	vuggy calcareous sandstone = Iglesia 3	7.75	Angualasto	-7.00	-6.71
BR04-44	vuggy calcareous sandstone = Iglesia 3	7.75	Angualasto	-7.42	-9.30
BR04-43	vuggy calcareous sandstone 3	7.8	Angualasto	-4.12	-7.07
BR04-42	vuggy calcareous sandstone 1	7.85	Angualasto	-4.25	-7.20
20-6-2002 IGLESIA 1	carbonate cemented sandstone	8.3	Angualasto	-4.12	-5.25
BR03-1	calcareously cemented sandstone	8.35	Angualasto	-6.91	-5.77
BR03-1 Duplicate	calcareously cemented sandstone	8.35	Angualasto	-7.08	-5.25
BR03-18	oxidized limestone	8.37	Rodeo 2	-5.85	-3.30
BR03-43	calcareously cemented sandstone	8.69	Rodeo 1	-5.87	-7.26
BR05-46	calcareously cemented sandstone	8.7	Rodeo 2	-5.76	-1.75
BR05-45	calcareously cemented sandstone	8.71	Rodeo 2	-8.33	-1.32
BR03-42	calcareously cemented sandstone	8.78	Rodeo 1	-5.63	-6.00
BR03-41	calcareously cemented sandstone	8.79	Rodeo 1	-4.45	-6.66
BR04-58	calcareously cemented ss = BR03-41	8.79	Rodeo 1	-4.39	-6.41
BR04-57	calcareously cemented sandstone	8.82	Rodeo 1	-5.75	-7.58
BR03-40	vuggy carbonate	8.9	Rodeo 1	-3.87	-6.57

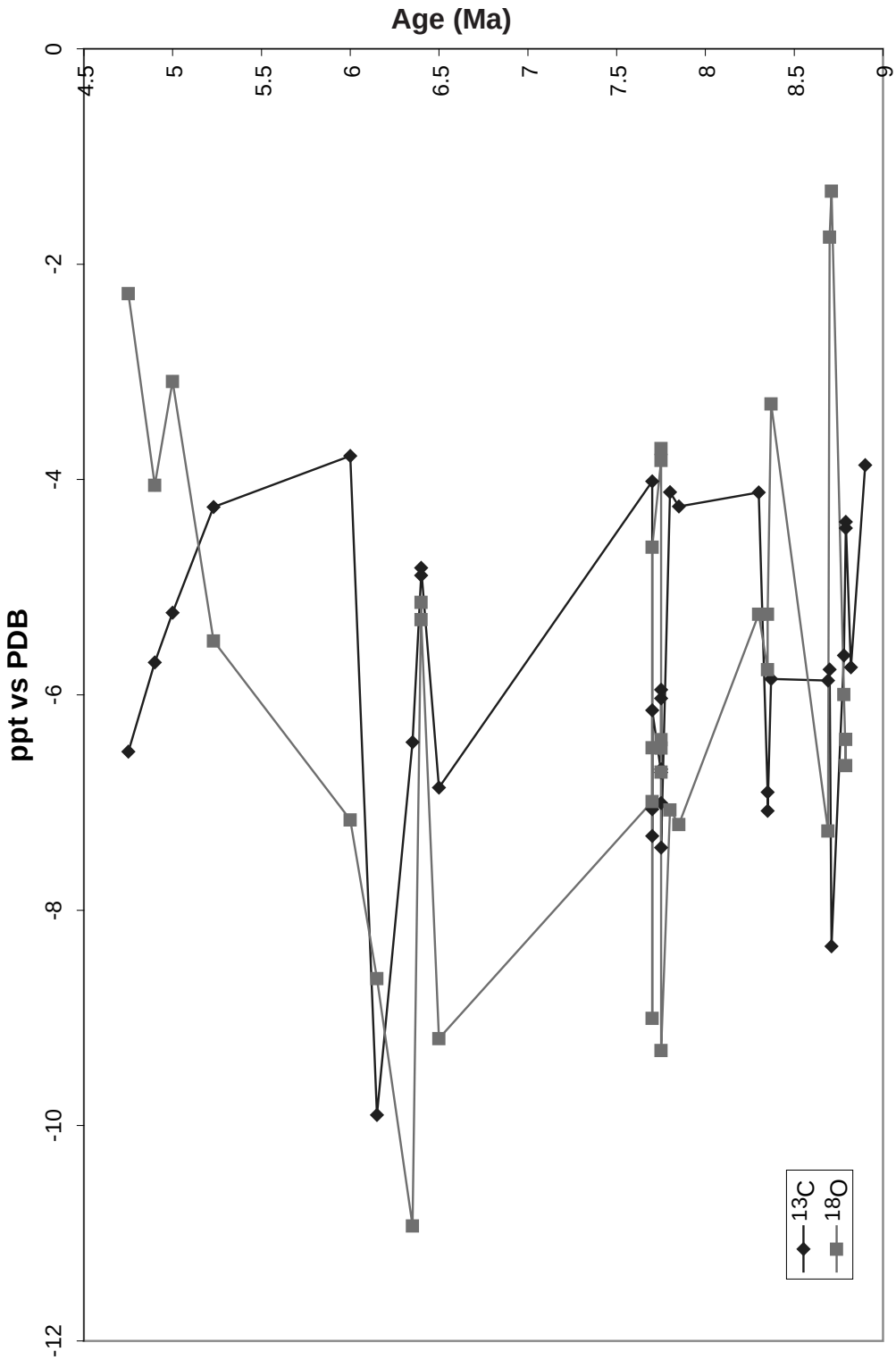

Figure F.1: Isotopic time series for Iglesia Basin palustrine carbonates

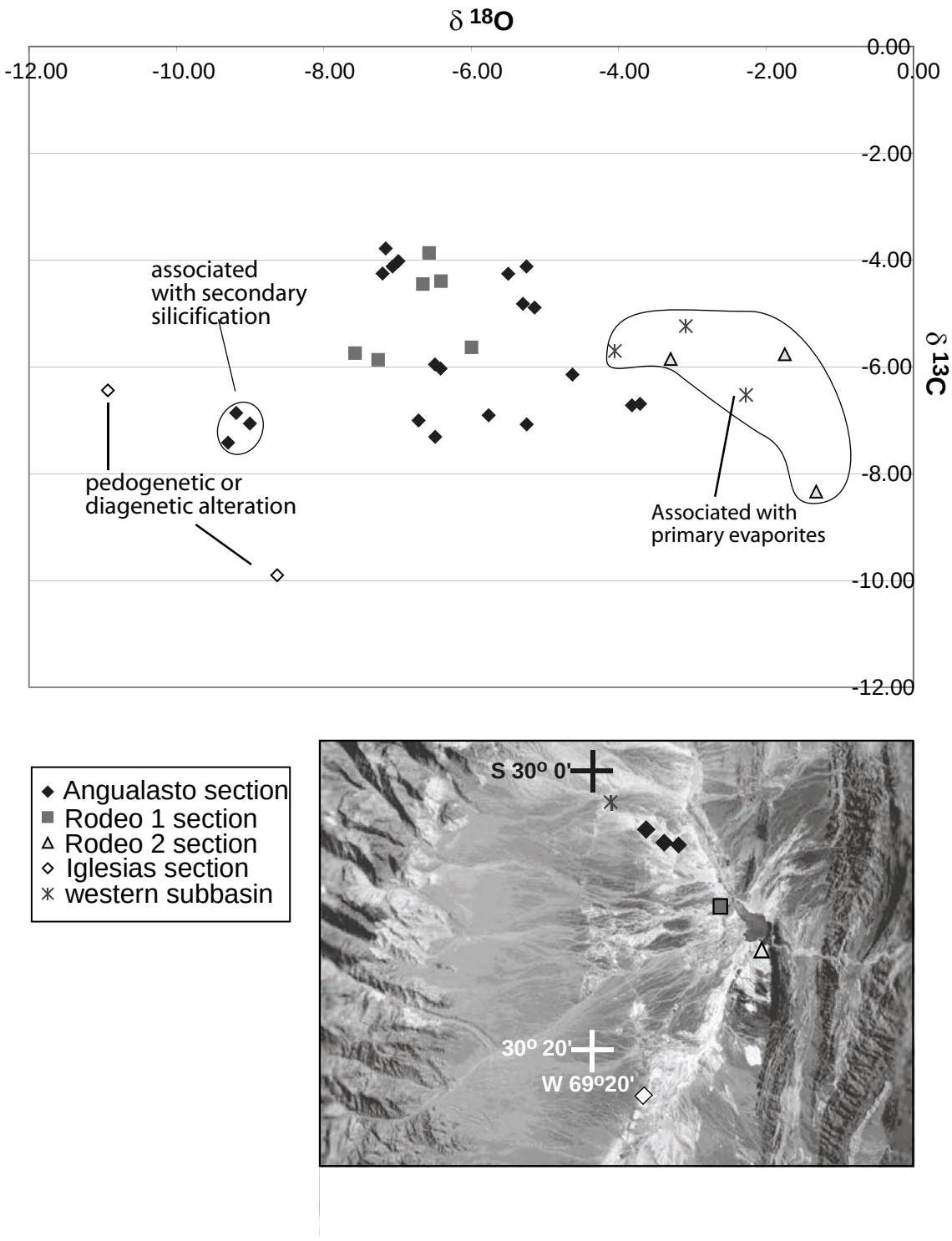

Figure F.2: Iglesia Basin palustrine carbonate isotopic values grouped by geographic position.

APPENDIX G:

CARBONATES EAST OF CARACOL THRUST SHEET, CENTRAL PRECORDILLERA, NORTHERN SAN JUAN PROVINCE, ARGENTINA

Intense pedogenic sandstones with large carbonate accumulations are observed in three intermontane valleys of the central Precordillera fold-thrust belt (Caracol, Rio Blanco and Los Blanquitos; Jordan *et al.*, 1993). In a quebrada east of Sierra Caracol (S 30°13.500' W 68° 57.336'), these paleosols and associated carbonates were measured and sampled.

Within Miocene sandstones (24< x < 11.9 Ma; Jordan *et al.,* 1993) near kilometer marker 258 of Route 150 between Jachal and Rodeo), laterally continuous purple and green pedogenic profiles can be traced across the narrow canyon of the Río Jáchal (Figure G.1). These beds are not accessible within the river canyon but are observed to be steeply dipping (~70° W) and contain horizons of resistant carbonate. The profiles also outcrop in a narrow drainage on the south side of the road, where ~10 m of interbedded pedogenic sands, pebble lenses and carbonate beds outcrop below Quaternary terraces and debris. Paleosols have a purplish hue (7.5R 4.4; Munsell Color, 1973), have a crumbly ped structure and are very weathered. Profiles appear to be composite, based on multiple carbonate (Bk) horizons.

Observed carbonate structures include (1) discrete micritic Stage II-III nodules as Bk horizons (Machette, 1985), (2) larger and more coalesced Stage IV "calcrete" beds (30-40 cm thick), (3) small botryoidal forms (<10 cm), (4) massive sparitic rounded forms (40-50 cm), and (5) vesicular cements.

The macroscopic textures of the larger carbonates (forms 2 through 5 above) suggest post-depositional alteration. Only the nodular Stage II-III paleosols are closely associated with paleosol profiles. The vesicular and botryoidal appearance of some

beds matches the appearance of modern and ancient travertine deposits (cf. Crystal Geyser, central Utah; Mammoth Hot Springs, NE Wyoming). Similar carbonate structures are associated with pedogenic facies of the Early Cretaceous Cedar Mountain Formation in central Utah. For those carbonates, Woods *et al.* (2003) described three potential sources of the structures: (1) pedogenic modification of lacustrine deposits, (2) deposition or modification by spring deposits and (3) erosion/redeposition of preexisting soil carbonates. For the Caracol carbonates, the first option is least likely, as there are not lacustrine units associated with these strata. Furthermore, though some of the massive carbonate may be supplied by groundwater leaching through surrounding paleosols, their forms do not match those typical of pedogenic carbonate accumulations (e.g. Machette, 1985). Though Stages V and VI of accumulation may include pisolithic forms, the observed concretionary structures are too large and lack the concentric internal structure of pisoliths. Furthermore, sparitic carbonate is often associated with precipitation from groundwater whereas pedogenic carbonates are generally micritic (e.g. Garzione *et al.,* 2006). It is suggested therefore that the vesicular, bulbous and massive carbonate accumulations east of Sierra Caracol have been altered or chiefly deposited by spring deposits.

Three carbonate samples were collected from the exposure for isotopic analysis, two from unique Bk horizons and one from a massive nodular accumulation (18 cm by 16 cm) removed from a coalesced carbonate bed. Samples were powdered and analyzed at Cornell University Stable Isotope Laboratory. Values of ^{13}C and ^{18}O are reported as parts per thousand (per mil.; ‰) relative to the Peedee belemnite standard (PDB; Table G.1).

For the three analyses, $\delta^{13}C$ values vary between -4.29 and -8‰, while $\delta^{18}O$ values are less depleted and more similar between samples, ranging from -1.74 to -1.99‰. The range of $\delta^{13}C$ values is similar to those obtained from other Miocene

paleosols and calcretes of the Andean foreland (see Chapters 3 and 4). However, the uniformity of $\delta^{18}O$ values from unassociated units may indicate isotopic homogenization via diagenesis (e.g. Pendall *et al.,* 1994; Wang and Cerling, 1994; Liu *et al.,* 1996).

Thus, on the basis of macroscopic form and isotopic composition, there is evidence for significant groundwater or hydrothermal alteration of syntectonic strata in the Central Precordillera. Through nodular Stage II or III carbonates from paleosol profiles may have been initially deposited pedogenically, their $\delta^{18}O$ values reveal an open system and post-pedogenic fractionation. Furthermore, the massive carbonate nodules and beds (40-50 cm diameter) documented by Jordan *et al.* (1993) are probably not pedogenic in origin. Finally, the botryoidal and vesicular accumulations almost certainly represent diagenetic processes.

References:

Garzione, C.N., Molnar, P., Libarkin, J.C., and MacFadden, B.J., 2006, Rapid late Miocene rise of the Bolivian Altiplano: Evidence for removal of mantle lithosphere: Earth and Planetary Science Letters, Vol. 241, p. 543-556.

Jordan. T.E, Drake, R.E., and Naeser, C.W., 1993b, Estratigrafia del Cenozoico Medio en la Precordillera a la latitude del Rio Jachal, San Juan Argentina: XII Congreso Geológico Argentino, Actas Tomo II, p. 132-141.

Liu, B., Phillips, F.M., and Campbell, A.R., 1996, Stable carbon and oxygen isotopes of pedogenic carbonates, Ajo Mountains, southern Arizona: implications for paleoenvironmental change: Palaeogeography, Palaeoclimatology, Palaeoecology Vol. 124, p. 233-246.

MacBeth Division of Kollmorgen Instruments Corp., Munsell Soil Color Charts, 1973 edition. Baltimore, MD.

Machette, M.N., 1985, Calcic soils of the southwestern United States *in:* Weide, D.L., ed., Soils and Quaternary Geology of the Southwestern United States: Geological Society of America Special Paper, 203, p. 10-21.

Pendall, E.G., Harden, J.W., Trumbore, S.E., and Chadwick, O.A., 1994, Isotopic approach to soil carbonate dynamics and implications for paleoclimate interpretations: Quaternary Research, v. 42, p. 60-71.

Wang, Y., and Cerling, T. E., 1994. A model of fossil tooth and bone diagenesis: Implications for paleodiet reconstruction from stable isotopes. *Palaeogeography, Palaeoclimatology, Palaeoecology*, 107: 281-289

Woods, K. L., Scalise, R.L., Beagle, P., Maxson, J., Schubel, K., and Swanson, B., 2003, Spring deposits within the palustrine carbonates of the Cedar Mountain Formation, UT. Geological Society of America Abstracts with Programs, Vol. 35, no. 7.

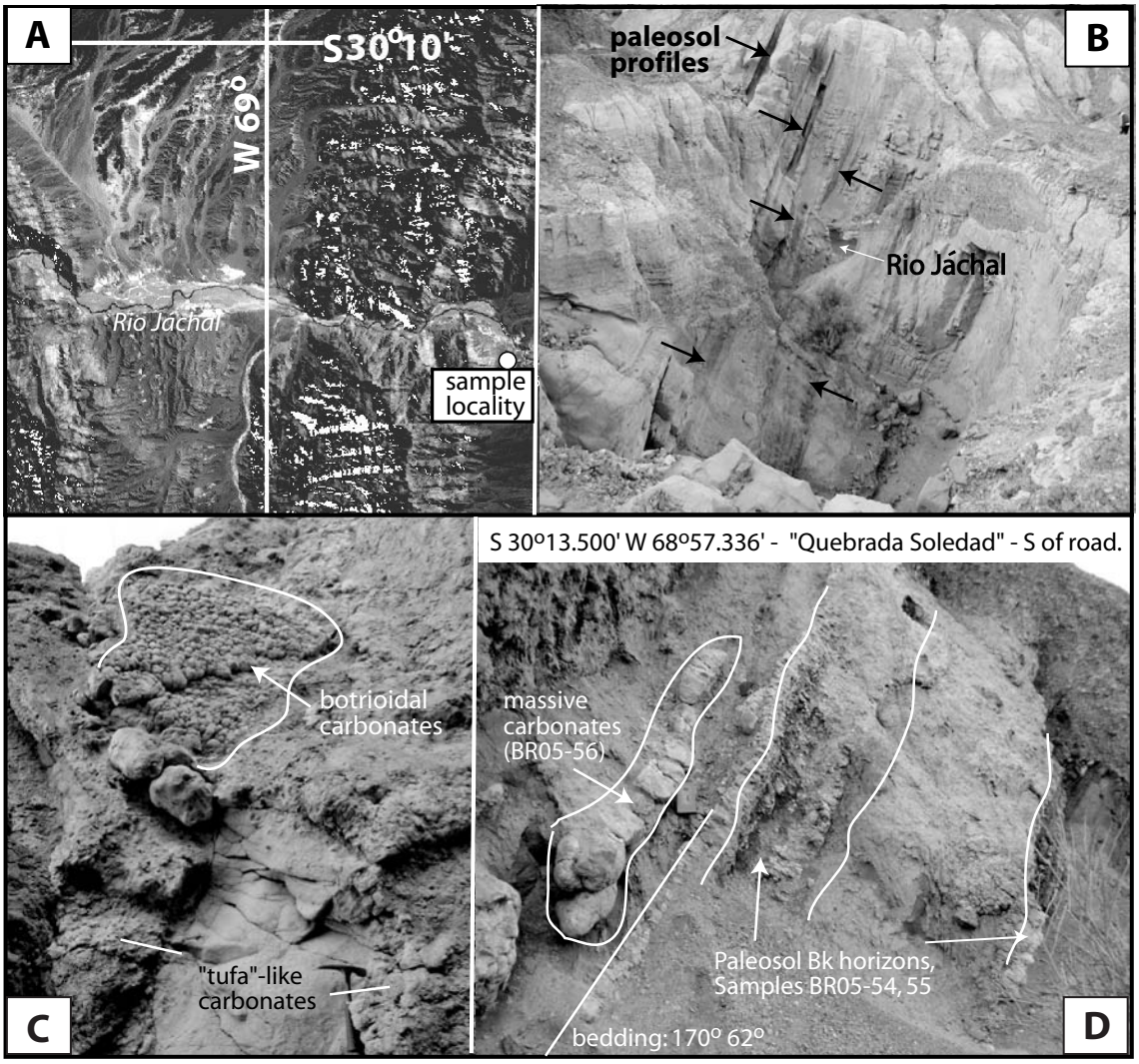

Figure G.1: A) Location of sampled nodular carbonates, south side of Rio Jachal river canyon. B) Oxidized paleosol profiles in steeply tilted Tertiary strata exposed in Rio Jachal canyon. C) and D) Examples of carbonate morphologies in quebradas south of Rio Jachal canyon, along-strike with profiles shown in B).

Table G.1: Isotopic values and estimated age range for nodular carbonates east of Caracol thrust sheet, western Precordillera, San Juan Province, Argentina.

Sample ID	Location	Lithology	Age range (Ma)	Mean Age (Ma)	$\delta^{13}C$ (PDB)	$\delta^{18}O$ (PDB)
BR05-54	S 30° 13.500' W 68° 57.336'	paleosol carbonate	11.9<x<24	~18	-7.999	-1.744
BR05-55	S 30° 13.500' W 68° 57.336'	paleosol carbonate	11.9<x<24	~18	-5.568	-1.987
BR05-56	S 30° 13.500' W 68° 57.336'	nodular limestone	11.9<x<24	~18	-4.289	-1.845

APPENDIX H:

MODERN CLIMATOLOGY, SAN JUAN, ARGENTINA

For the purposes of better understanding current features of the modern climate regional to Iglesia Basin (e.g. mean temperature and precipitation, seasonality, interannual variability), station data and modeled regional climatology for portions of San Juan Province, Argentina were compiled (e.g. Montgomery *et al.,* 2001; New *et al.,* 2002; International Water Management Institute Climatology 1961-1990, NOAA station data).

Montgomery *et al.* (2001) report mean annual precipitation rates of between 200 and 400 mm/year for the geographic position of Iglesia Basin. This compares well with a 10' summary of station data, whereby the Iglesia valley receives approximately 300 mm/year precipitation (New *et al.,* 2002). Stations in closest proximity to Iglesia Basin (San Juan Airport at S 31. °5, W 68.7°, 630 m elevation, San Jose de Jáchal at S30.25°, W68.75°, 1165 m elevation; Uspallata, S 32.60°, W 69.33°, 1891 m elevation, Figure H.1) are utilized to illustrate spatial variability of the precipitation field. Both San Juan and Jáchal are outside the immediate rainshadow of the High Andes and receive somewhat more precipitation annually than Uspallata in northern Mendoza Province (at similar geographic position as Iglesia Basin with respect to the Frontal Cordillera of the Andes).

The city of San Juan experiences a seasonal climate with superimposed decadal variation in mean annual precipitation. Precipitation near San Juan City is seasonal, with 90% of annual rainfall occurring between October and March, the austral summer (Perucca and Paredes, 2004). During the period 1876-2005, San Juan mean annual precipitation (MAP) fluctuated decadally (15-20 year period) between minima of <100 mm/year to maxima of ~1000 mm/year (Figure H.2). During the

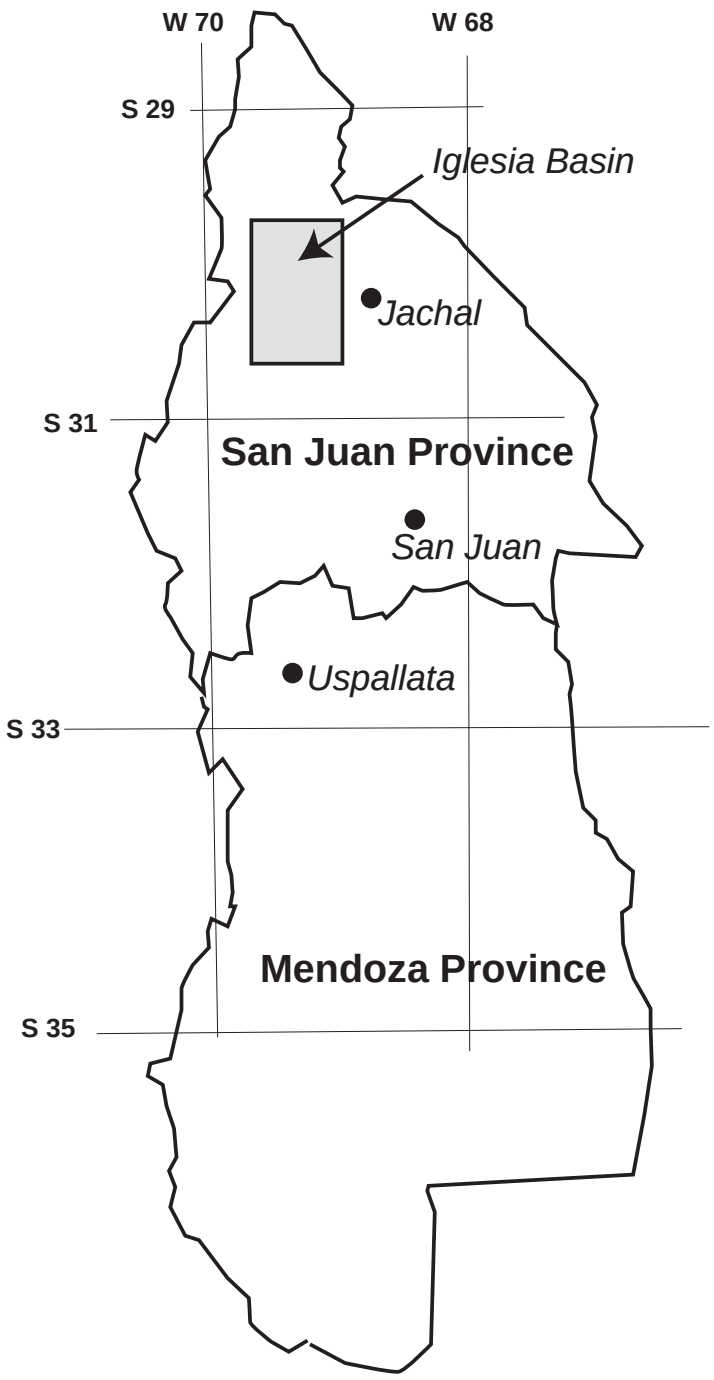

Figure H.1: Location map of text-referenced weather stations in closest proximity to Iglesia Basin (grey box) within San Juan and Mendoza Provinces, Argentina

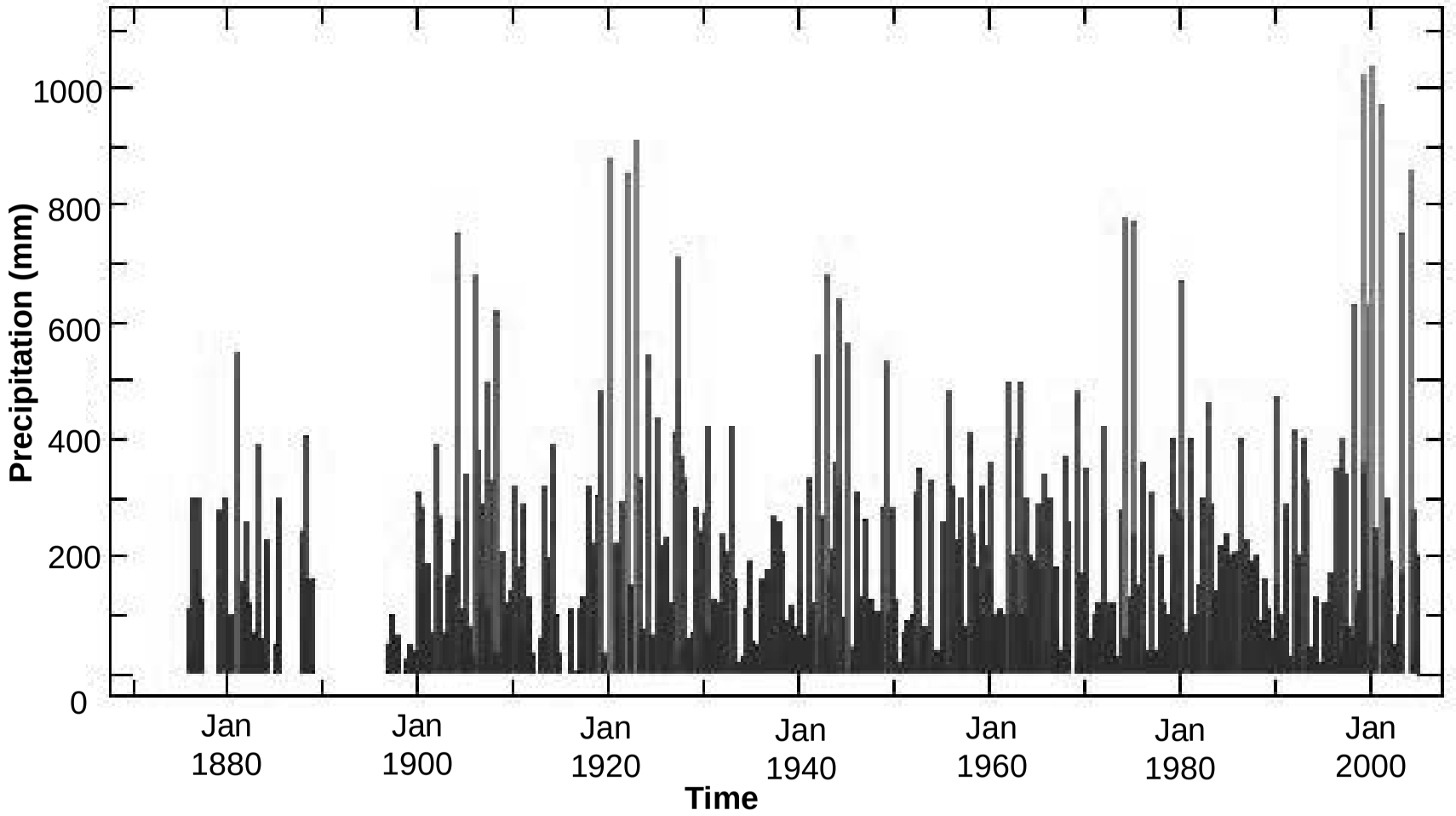

Figure H.2: NOAA Climatology: San Juan Airport, Argentina - 1876-2005

period 1981-1990, the MAP at San Juan city was 92.3 mm/year (reported by the Servicio Meteorologico Nacional de Argentina). Station data compiled for the period 1994-2003 from San Juan Aerodrome (Table H1, Figures H.3 and H.4) show wide inter-annual fluctuations in MAP, from 38 mm/year to 618 mm/year. Mean annual temperatures (MAT) for this period were less variant, averaging 18°C.

Monthly temperature and precipitation at San Juan airport (1994-2003) reveal seasonality. Maximum temperatures occur during December-February (~25°C) and minimum temperatures correspond with June and July (~8°C; Fig. H.3). Mean monthly precipitation varied markedly during this time period, although most large precipitation events occurred during the austral summer (Fig. H.4).

San Jose de Jáchal (S30.25°, W68.75°, 1165 m elevation) is located in the east-central Precordillera, approximately 30 km east of the Iglesia Basin's eastern margin (Fig. H.1). Records of precipitation were obtained for the period 1961-1981 as well as for 1993-94 (Figure H.5). Like San Juan, Jáchal also receives the majority of its MAP during the austral summer months, wherein ~150 mm/month is common and occasionally single months exceed 300 mm of precipitation. Annual precipitation rarely exceeded 1000 mm during the time interval considered.

Uspallata (S 32.60°, W 69.33°, 1891 m elevation) is actually in northern Mendoza province (Figure H.1), but is considered as geographically analogous to Iglesia Basin, as both locations are in the rain shadow of the high Andes and have similar relief between mountains to the west and valley floor (>2000 m). A record of precipitation for Uspallata (Figure H.6) spans 1967-1990. Summer-season precipitation is distinct, with most years receiving >200 mm in a single month. Interannual variation in MAP is significant, however: annual values range from as little as 300 mm/year to well over 1000 mm/year.

Table H.1: Meteorological data for San Juan airport, San Juan, Argentina, 1994-2003. S 31.4º W 68.41º, elevation: 597 msl.

		month												
Temp		j	f	m	a	m	j	jy	a	s	o	n	d	Tmean (C)
Year	1994	27.1	24.2	22.6	16.8	14.4	11	8.7	11.9	16.4	19.2	24.5	28.5	18.78
	1995	26.5	24	22.9	17.5	13.4	9.6	8	10.1	15	19.2	24	28.7	18.24
	1996	26.6	25.1	23.4	17	14.8	7.5	7.9	13	14.4	20.5	24.7	25.6	18.38
	1997	27.4	25.3	23.9	19.9	14.4	8.7	10.1	12.2	15.8	19.1	22.9	25.6	18.78
	1998	27.2	22	21.8	16.5	13.1	9.9	10.1	12	13.4	21.5	23.2	25.5	18.02
	1999	25.9	27.2	21.7	15.4	13.1	8.3	7.5	10.7	17.3	18.9	21.8	24.7	17.71
	2000	27.5	25.5	22.1	18.5	11.8	10.1	7.4	11.1	14	19.9	21.6	26.1	17.97
	2001	28	28.5	23	16.4	11.2	9.3	8.8	12.1	14.1	19.9	22.4	26.4	18.34
	2002	26.6	24.9	23.3	17.3	13.3	7	8.5	11.5	16.4	21.2	24.1	25.2	18.28
	2003	28.3	26	23.6	17.2	13.3	11.2	8.8	10.3	16.1	22.4	24.9	25.6	18.98

		month												
Precip		j	f	m	a	m	j	jy	a	s	o	n	d	sum precip (mm)
Year	1994	1.53	24.64	0.25	1.52	0	0	6.1	0	1.02	1.78	0	1.02	37.86
	1995	0	1.78	1.02	0	0	59.9	0	0	39.4	0	105.9	35.05	243.06
	1996	8.13	0	30.99	0	2.03	1.02	0	0.25	5.08	0	0	0	47.5
	1997	130.8	0.25	3.05	56.9	5.33	0	0	0	0.76	0	2.03	24.13	223.25
	1998	0	189	213.1	48.25	0	0	0	0	162	0.25	6.09	0	618.71
	1999	6.09	4.06	20.07	3.05	0	0	2.79	0	0	10.9	6.85	34.8	88.63
	2000	2.03	6.1	90.17	22.86	85.3	46	4.57	0	1.02	17.3	1.78	0	277.11
	2001	9.9	0.76	12.19	4.56	2.28	15.8	0.76	1.52	17	2.53	17.02	10.41	94.69
	2002	7.36	13.71	0.76	9.91	1.52	0	31	0	0	5.08	0	41.92	111.25
	2003	0.51	12.19	10.16	15.74	0	0	0	0	0	0	0	0	38.6

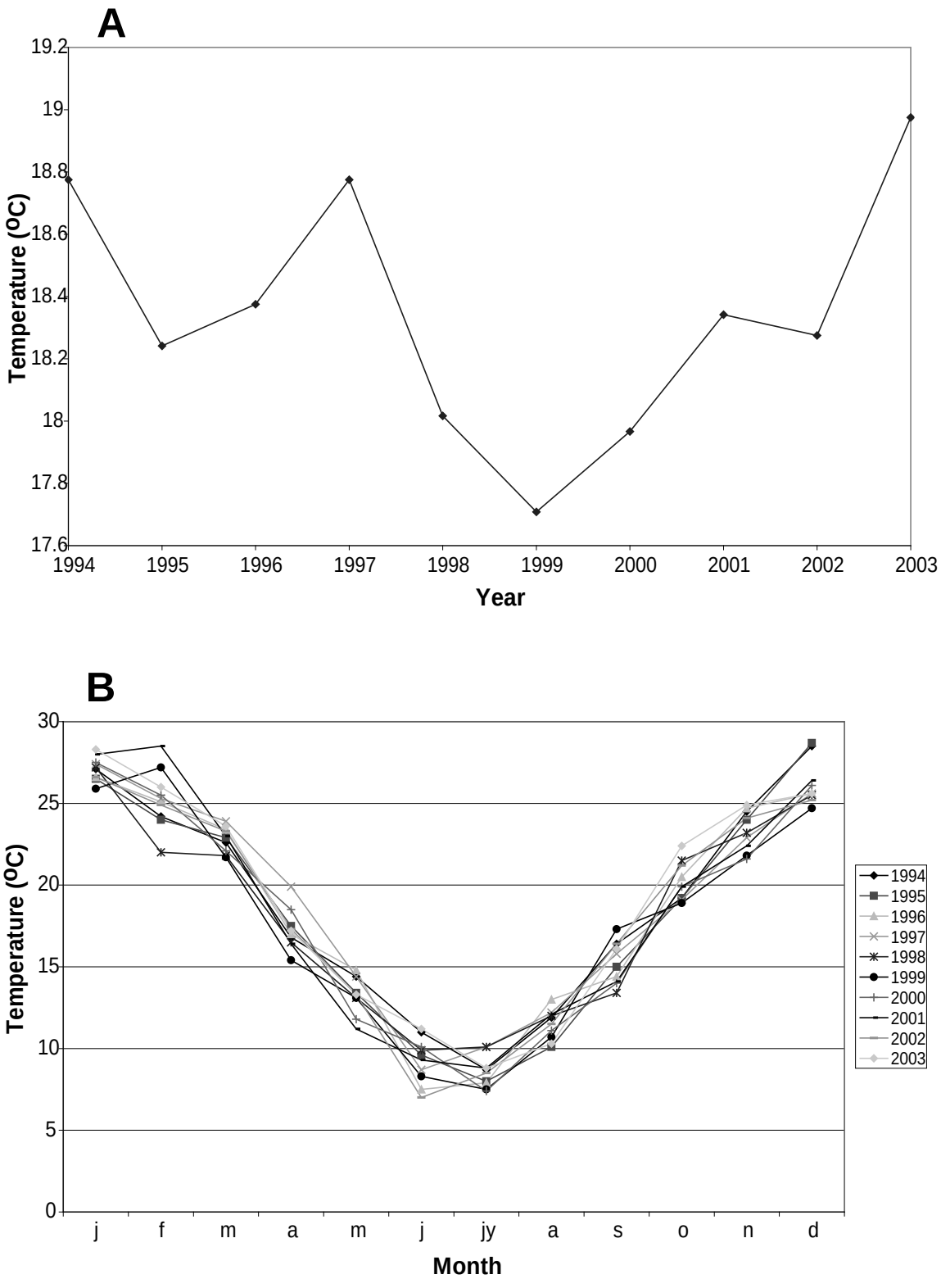

Figure H.3: A) Mean annual temperature at San Juan airport, 1994-2003. B) Mean monthly temperature at San Juan Airport, 1994-2003.

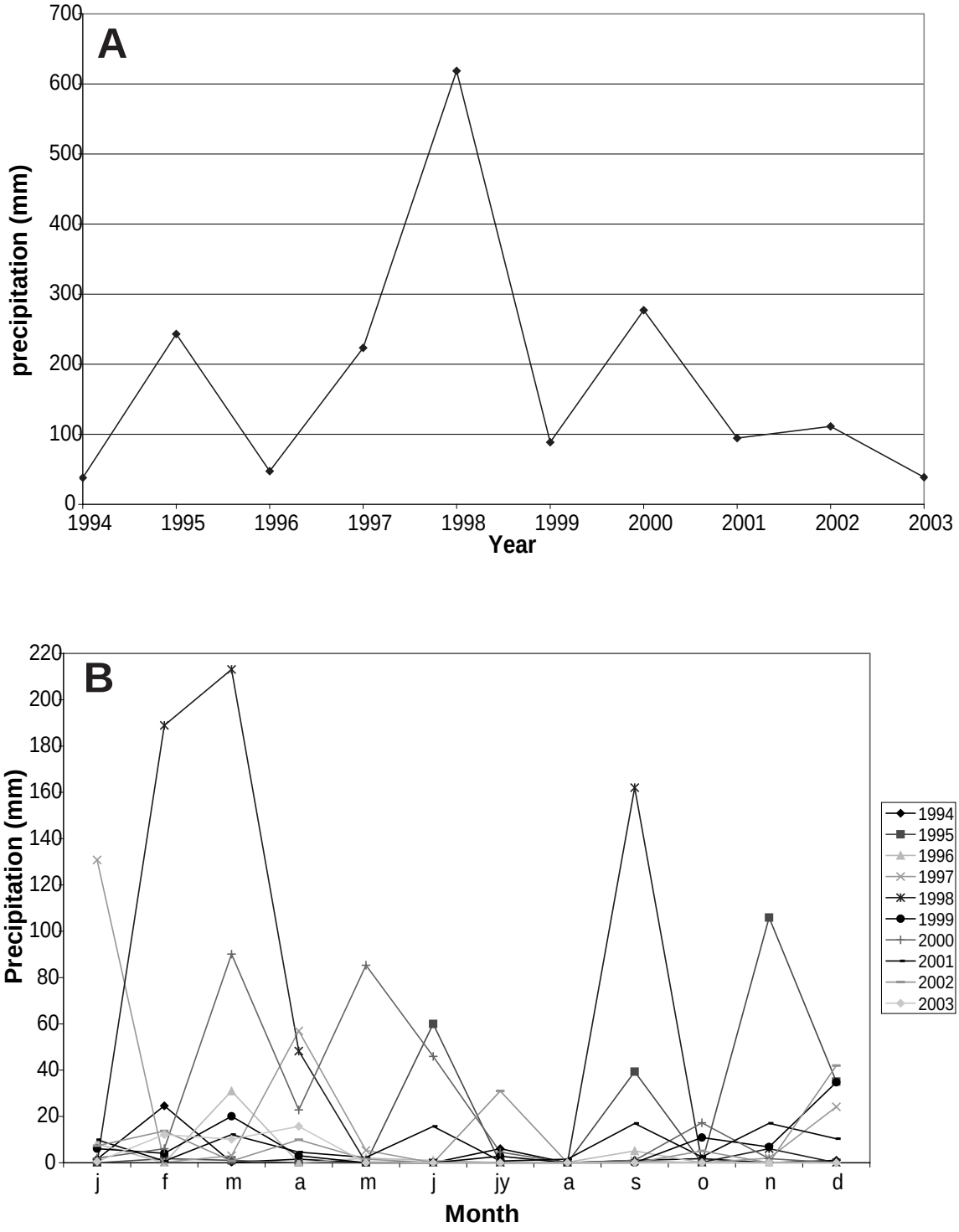

Figure H.4: A) Mean annual precipitation at San Juan airport, 1994-2003. B) Mean monthly precipitation at San Juan airport, 1994-2003.

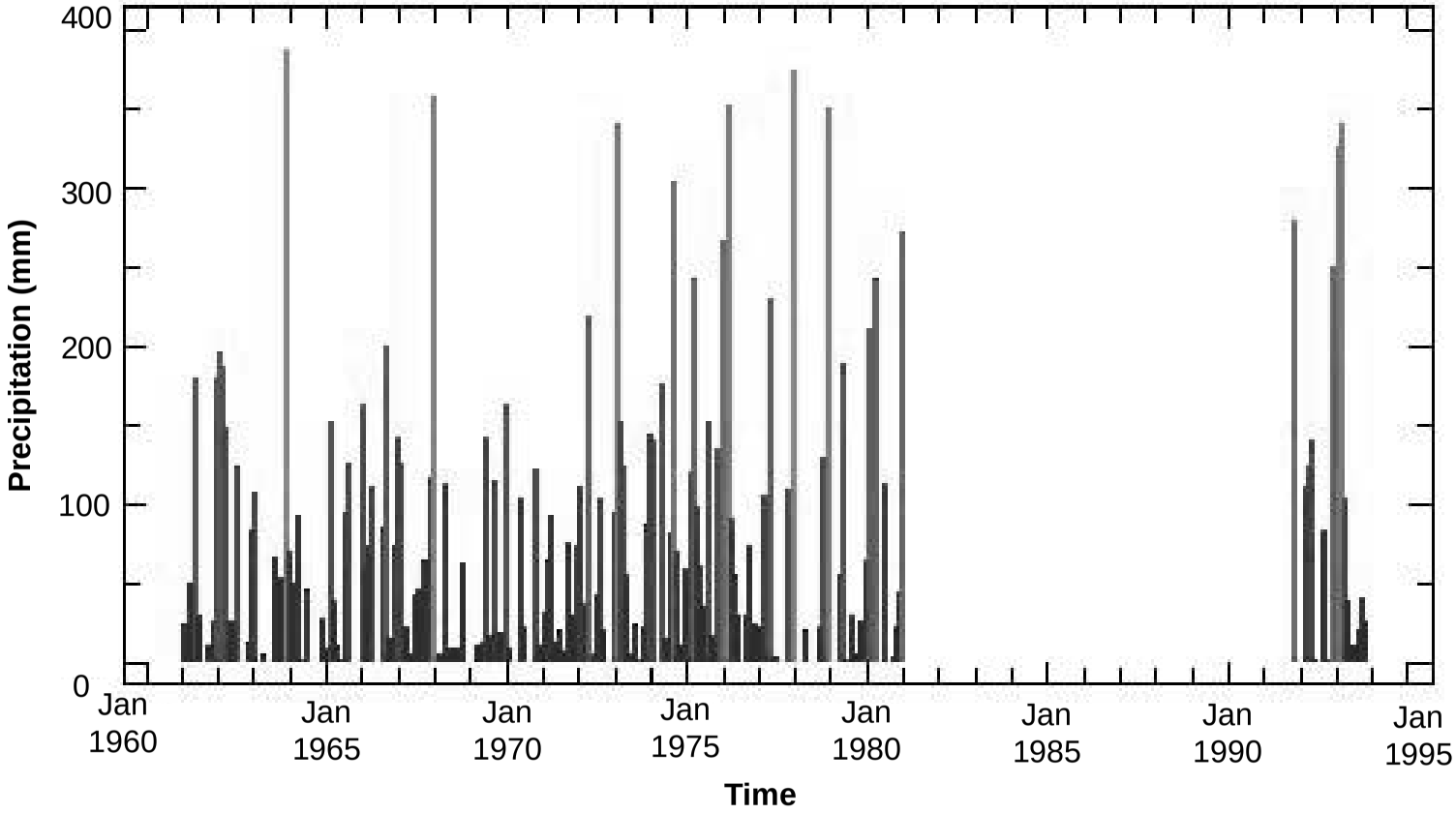

Figure H.5: NOAA Climatology: San Jose de Jachal, Argentina - 1961-1994

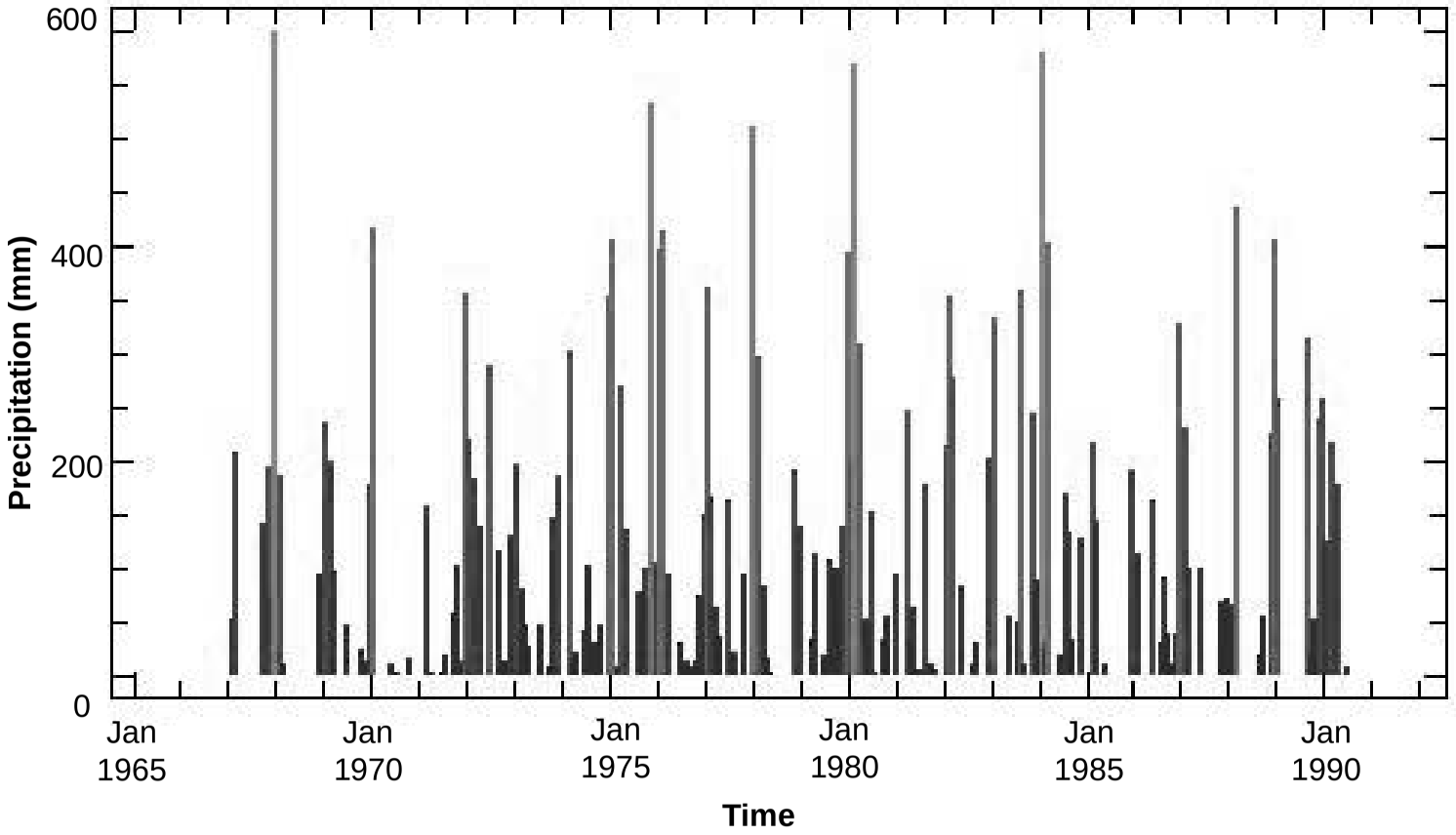

Figure H.6: NOAA Climatology: Uspallata, Argentina - 1967-1990

Within the Iglesia Basin there are no official rain gauges, but climate characteristics can be approximated using regional climate models. The International Water Management Institute's online Water and Climate Atlas (www.iwmi.cgiar.org) provides modeled values of temperature, precipitation, evapotranspiration, etc. For the purposes of characterizing the headwater and intrabasinal climate of Iglesia Basin, mean annual temperature (MAT) and precipitation (MAP) rates were determined for various parts of the basin (Figures H.7 and H.8). The models suggests MAT of 10-13°C and MAP of 50-100 mm/year (data compiled every 5' from 30°0'0"S, 69°0'0" W through 30° 30' S, 69° 30' W). This model also reveals seasonality: Iglesia Basin precipitation is greatest during January and February, with a secondary maximum during June-August (Fig. H.8).

Classification of the local climate of San Juan Province is made by comparison to the Köppen and Trewartha climate classification schemes (McKnight and Hess, 2000). The Köppen climate classification (e.g. Köppen, 1931) is based on the concept that native vegetation best expresses climate. It combines average annual and monthly precipitation and temperatures as well as seasonality of precipitation. The Trewartha scheme (e.g. Trewartha, 1968) is a modified version of the former, with revised vegetative boundary conditions. For dry (semi-arid to arid) climates wherein potential evapotranspiration is greater than precipitation, a precipitation or aridity threshold can be calculated. For the Köppen scheme, one multiplies MAT in °C by 20, then adds 280 if 70% or more of the total precipitation is in the high-sun half of the year (October through March for the Southern Hemisphere), or 140 if 30%-70% of the MAT is received during the applicable period, or 0 if less than 30% of the MAT is so received. The aridity threshold of the Trewartha scheme is equal to ((MAT − 10) + 3*P*) multiplied by 10, with *P* representing the percentage of total precipitation received in the high-sun half of the year. These measured and modeled results permit Iglesia

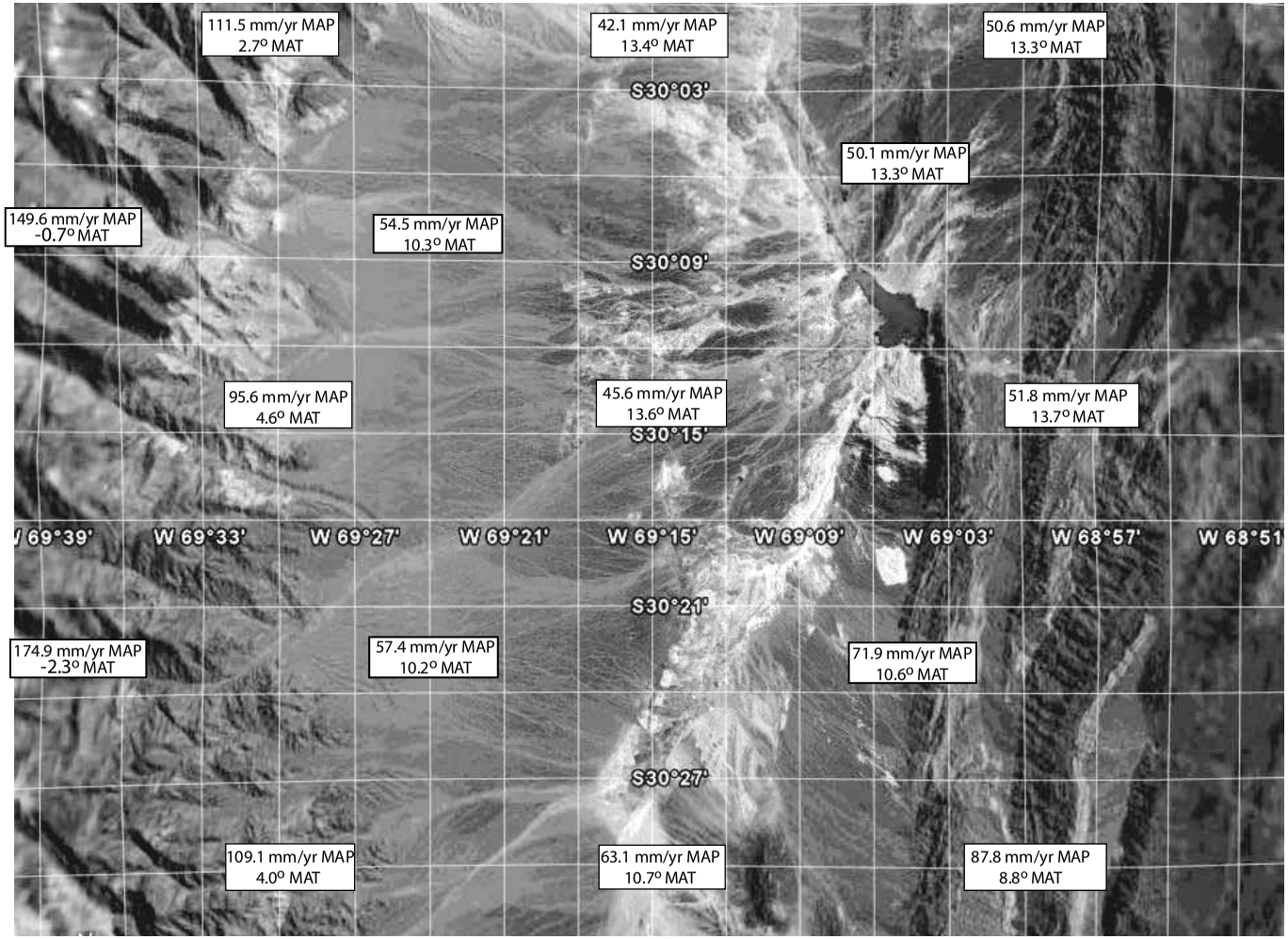

Figure H.7: Climatology 1961-1990 for Iglesia Basin and eastern slope of Frontal Cordillera from International Water Management Institute World Water and Climate Atlas (www.iwmi.cgiar.org/WAtlas/atlas.htm). Mean annual precipitation computed from P50 values.

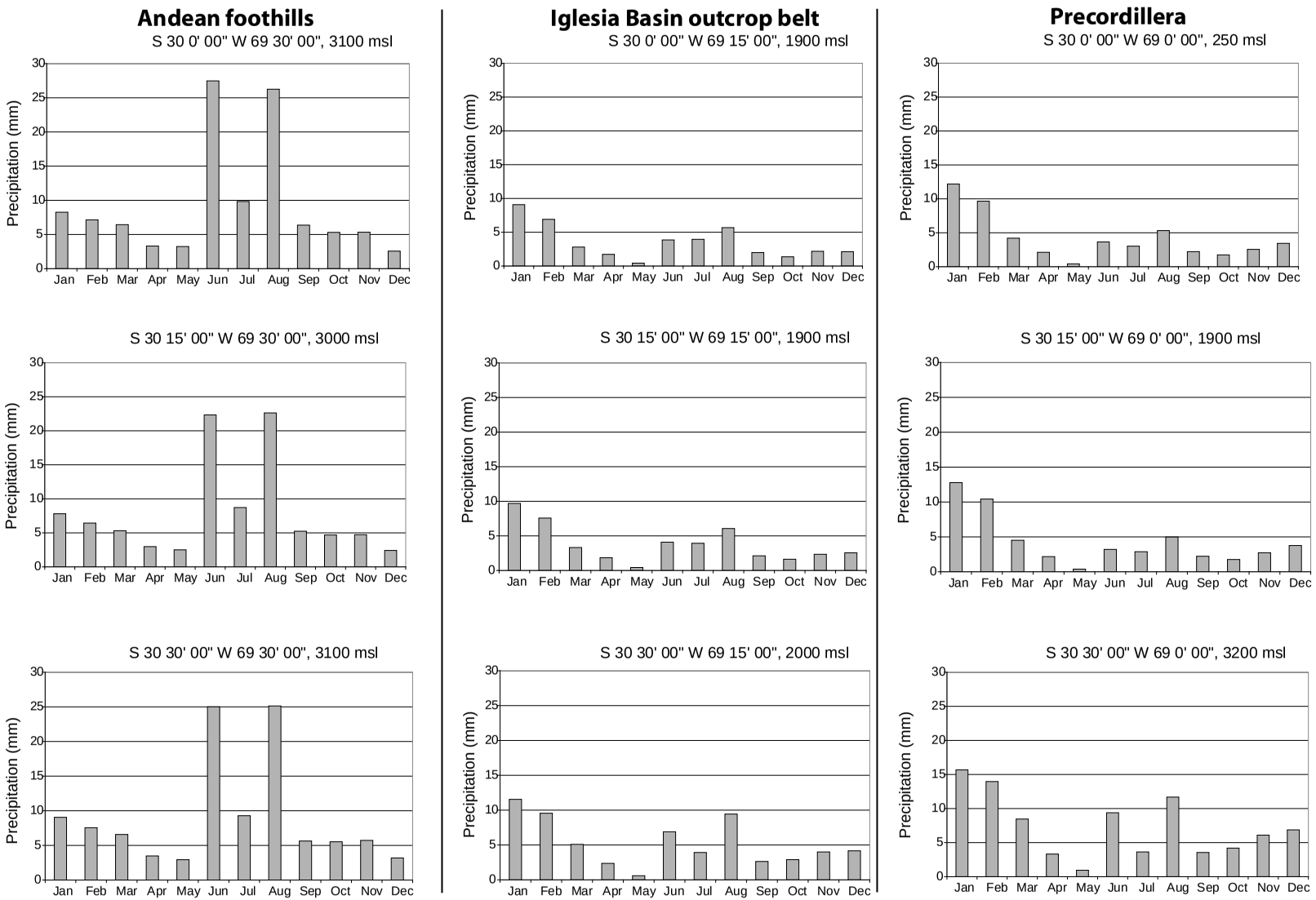

Figure H.8: Monthly precipitation (mm) for Iglesia Basin and margins, from IWMI Climatology 1961-1990

Basin to be considered a “steppe” semi-arid climatic zone by both the Köppen and Trewartha climate classification schemes.

A strong contributor to the climate of western San Juan Province, Argentina is the orographic effect of the adjacent Andes. Climate modeling has shown that a primary control of Central Andean precipitation patterns is the Andean orogen (Lenters and Cook, 1995). The appreciable topography of the Frontal Cordillera (elevations up to 6200 m to west of Iglesia Basin) results in blockage of westerlies containing moisture from the Pacific Ocean, and the air must rise, cool and condense, Thus precipitation is focused on the western slope and the high topography of the Andes and a corresponding rain shadow is formed in the eastern foreland (the Iglesia catchment).

In addition to the rain-shadow setting of the Iglesia Basin, present semi-aridity is also controlled by Hadley Circulation and the Foehn effect. The Hadley cell is thermal circulation which transfers sensible and radiative heat from equatorial to higher latitudes. At its latitudinal position (S 30-31°), Iglesia Basin is located in a zone of high pressure where the Hadley cell drives descent of dry air which hinders precipitation and drives evaporation. Past positions of the sinking air of Hadley circulation have been explored using a general circulation model (GCM) to explore the global effects of changes in the latitudinal sea surface temperature gradient, as well as global climate change (Rind, 1998; Rind and Perlwitz, 2004). If the meridional temperature gradient increased during the late Tertiary (with or without global climate change), the model predicts increased Hadley cell intensity (*i.e.* increased stream function of the zonal mean meridional wind circulation). Also, GCMs suggest that numerous factors influence the poleward extent of Hadley circulation, including topography and seasonality (Cook, 2004; Rind and Pelwitz, 2004). Both of these could have profoundly affected Iglesia Basin climate during uplift of the Andes, as shifts in

the poleward extent of Hadley circulation would impact the regional climate of deposystems on the fringe of the circulation cycle. The orographic precipitation minimum is compounded by the dry adiabatic descent of high-velocity hot air down the leeward slope, the "Foehn Effect". These warm, dry winds, locally called "zonda winds", are frequent during the Austral winter in conjunction with low-pressure systems that approach from the west, and can raise temperatures by up to 15°C while depressing dewpoints by 20°C in a few hours (Puliafito *et al.*, 2002; Seluchi *et al.*, 2002).

Acknowledgement:

Climatologic data for San Juan airport from 1994-2003 was kindly provided with express written consent by TuTiempo Network, S.L (www.tutiempo.net).

References:

Cook, K.H., 2004, Hadley circulation dynamics: seasonality and the role of continents: *in* Diaz, H.F. and Bradley, R.S., eds., The Hadley Circulation: Present, Past and Future Advances in global Change Research Vol. 21, Kluwer Academic Publishers, p. 61-84.

International Water Management Institute World Water and Climate Atlas, 2006: http://www.iwmi.cgiar.org/WAtlas/atlas.htm

Köppen, W., 1931. *Grundriss der klimakunde.* Walter de Gruyter, Berlin

Lenters, J.D. and K. H. Cook, 1995, Simulation and diagnosis of the regional summertime precipitation climatology of South America: *Journal of Climate*, Vol. 8, No. 12, p. 2988-3005.

McKnight, T.L andHess, D., 2000, Climate Zones and Types: Dry Climates (Zone B): *Physical Geography: A Landscape Appreciation*, Upper Saddle River, NJ: Prentice Hall. pp. 212-19,

Montgomery, D.R., G. Balco, S.D. Willett, 2001, Climate, tectonics, and the morphology of the Andes: *Geology*, Vol. 29, No. 7, p. 579-582.

New, M., Lister, D., Hulme, M., and Makin, I., 2002, A high-resolution data set of surface climate over global land areas: Climate Research, Vol. 21, p. 1-25.

Perucca, L.P., and Paredes, J., 2004, Alluvial fan flooding in the Department of Pocito, Province of San Juan, Argentina, Episodes, Vol. 27, No. 3, p. 190-194.

Puliafito, C., Puliafito, S.E., and G.K. Hartmann, 2002, Observations of large stratospheric ozone variations over Mendoza, Argentina: *Atmospheric Chemistry and Physics Discussions*, 2, p. 507-523.

Rind, D., 1998, Latitudinal temperature gradients and climate change: Journal of Geophysical Research, v.103, p. 5943-5971.

Rind, D., and Perlwitz, J., 2004, The response of Hadley Circulation to climate changes, past and future *in* Diaz, H.F., and Bradley, R.S., eds., The Hadley Circulation: Present, Past and Future, Kluwer Academic Publishers, p. 399-435.

Seluchi, M.E., Norte, F.A., Satyamurty, P., and S.Chan Chou, 2002, Analysis of three situations of the Foehn Effect over the Andes (Zonda Wind) using the Eta-CPTEC Regional Model: *Weather and Forecasting*, Vol. 18, No. 3, p. 481-501.

Trewartha, G.T., 1968, *An introduction to climate.* 4th Ed. McGraw-Hill, New York.